


UCID- 19075
Volume 1

BURRO SERIES DATA REPORT
LLNL/NWC 1980 LNG SPILL TESTS

R.P. Koopman, J. Baker, R.T. Cederwall,
H.C. Goldwire, Jr., W.J. Hogan, L.M. Kamppinen,
R.D. Kiefer, J.W. McClure, T.G. McRae, D.L. Morgan,
L.K. Morris, M.W. Spann, Jr., and C.D. Lind

December 1982

CIRCULATION COPY
SUBJECT TO RECALL
IN TWO WEEKS

 Lawrence
Livermore
Laboratory

This is an informal report intended primarily for internal or limited external distribution. The opinions and conclusions stated are those of the author and may or may not be those of the Laboratory.

Work performed under the auspices of the U.S. Department of Energy by the Lawrence Livermore Laboratory under Contract W-7405-Eng-48.

DISCLAIMER

This document was prepared as an account of work sponsored by an agency of the United States Government. Neither the United States Government nor the University of California nor any of their employees, makes any warranty, express or implied, or assumes any legal liability or responsibility for the accuracy, completeness, or usefulness of any information, apparatus, product, or process disclosed, or represents that its use would not infringe privately owned rights. Reference herein to any specific commercial products, process, or service by trade name, trademark, manufacturer, or otherwise, does not necessarily constitute or imply its endorsement recommendation, or favoring of the United States Government or the University of California. The views and opinions of authors expressed herein do not necessarily state or reflect those of the United States Government or the University of California, and shall not be used for advertising or product endorsement purposes.

Best Available Quality

for original report

**call
Reports Library**

x37097

TABLE OF CONTENTS

	<u>Page Number</u>
<u>Volume 1</u>	
Abstract	1
A. Introduction	2
B. Facility and Equipment	2
Facility	2
Instrumentation	6
Data Acquisition System	20
Data Handling	21
C. Test Summary	22
D. Wind Field Data	30
Wind Data	31
General Wind-Field Features	31
Specific Wind-Field Features--Flowlines	34
E. Turbulence Data	39
F. Humidity and Heat Flux Data	138
Humidity	138
Heat Flux	156
G. Gas Concentration Data	167
H. Conclusions	283
I. References	285
<u>Volume 2</u>	
Appendix A. Wind Field Data and Flowlines	
Appendix B. Horizontal Gas Concentration Contours	
Appendix C. Vertical Gas Concentration Contours	

Acknowledgments

The data reported here represent the work of many people from several organizations. We would like to acknowledge the hard work and dedication of the following individuals and organizations:

LLNL/Livermore

Greg Bianchini	I.J. Grettler	Gary Powers
Rex Blocker	David Hipple	Art Rudd
Bruce Borman	Gale Holladay	William Wakeman
Dennis Chakedis	James Lamb	Roland Wallstedt
Donald Ermak	William McCauley	Michael Wolters
Donald Garka	William O'Neal	Richard Zacharias
Cleo Fry	Albert Pierce	

LLNL Nevada

Kenneth Moon
William Pittman
Troy Williams

EG&G Special Measurements Department, LVO

EG&G Scientific Services Department, LVO

EG&G Remote Measurements Department, LVO

JPL FBDR Group

ABSTRACT

During the summer of 1980, the Burro series of liquefied natural gas (LNG) spill experiments were performed at the Naval Weapons Center (NWC), China Lake, California. These experiments involved eight spills of LNG and one of liquid nitrogen, each of approximately 40 m³, onto water. A large array of instruments was used to make measurements of gas concentration, temperature, humidity, heat flux from the ground, and turbulence within the dispersing gas cloud. A separate instrument array made measurements of the wind field both upwind of the spill and over the area in which the gas was dispersing.

This report contains the data from these tests with an explanation of how and where the data was taken and the reliability of the instruments used to take it. It does not include analysis of the data, other than that which is necessary to understand the reliability of the data. Data analysis will be covered in a series of other reports.

A. INTRODUCTION

The Burro series of liquefied natural gas (LNG) spill experiments was performed at the Naval Weapons Center (NWC) at China Lake, California, during the summer of 1980. The tests were conducted jointly by personnel from NWC and LLNL. Nine tests were completed between June 6 and September 17. The first test, Burro 1, was a spill of approximately 40 m³ of liquefied nitrogen (LN₂) onto water, for the purpose of developing a fog correction algorithm for the infrared (IR) gas sensors. The remaining eight tests, Burro 2 through Burro 9, were all nominally 40-m³ spills of LNG onto water, to measure the dispersion of the LNG vapor cloud in the atmosphere under various conditions.

The purpose of this report is to make the data from these tests available in a format that will be most useful to the largest number of people. The data set itself is voluminous, consisting of over six million words of digital data stored in the LLNL data base. Because of the large amount of data, not all of it will be presented here. Some selectivity has been exercised. If the users of this report need data which is not presented here, or data in a format different than that given here, they are advised to contact the authors of this report.

This report is intended to present the data only, and contains little analysis. The analysis of selected data from this set will be published in other reports.

B. FACILITY AND EQUIPMENT

Facility

Since 1973, Dr. C.D. Lind of the NWC has been investigating the fire and explosion hazards of liquefied fuels. As part of this program, a facility was constructed capable of spilling up to 5.7 m³ of liquefied fuels on a water

test basin to study the combustion or dispersion of the vapor produced. This facility has been used for test spills of LNG, liquefied petroleum gas (LPG), gasoline, and LN_2 .

The original 5.7-m^3 facility was expanded in 1980 so that it is capable of safely handling up to 40 m^3 of LNG (1). This expansion consisted of a minor enlargement of the existing water test basin into a more circular basin, the installation of an additional cryogenic liquid storage tank capable of spilling up to 40 m^3 of LNG, the addition of appropriate cryogenic piping and valving to deliver the LNG to either the enlarged test basin or to a newly constructed diked dry test basin, and the installation of associated remote spill control and monitoring systems.

Figure 1 is a site plan showing the layout of the expanded facility. The 40-m^3 tank is located approximately 30 m south of the original 5.7-m^3 tank. The 40-m^3 spill tank is a vacuum-jacketed tank 10.7 m long by 3.5 m in diameter, with a total volume of 52 m^3 ; its design operating pressure is 2.4 bars. The liquid fuel is forced out of the tank through a 20-cm-diameter vertical stainless steel diptube, when the tank is pressurized with gaseous nitrogen (GN_2). A 25-cm-diameter insulated stainless steel spill line runs from the 40-m^3 tank to a junction north of the 5.7-m^3 tank. A 25-cm-diameter line continues from this point to the center of the water test basin, while a 15-cm-diameter insulated stainless steel spill line extends from this point to the edge of the 15 m x 15 m x 0.15 m dry pond.

The water test basin has an average diameter of 58 m, with an average water level about 1.5 m below the surrounding ground level. The average depth of the water is approximately 1 m. The slopes of all but the south bank have also been reduced to provide less turbulent wind flow over the water test basin.

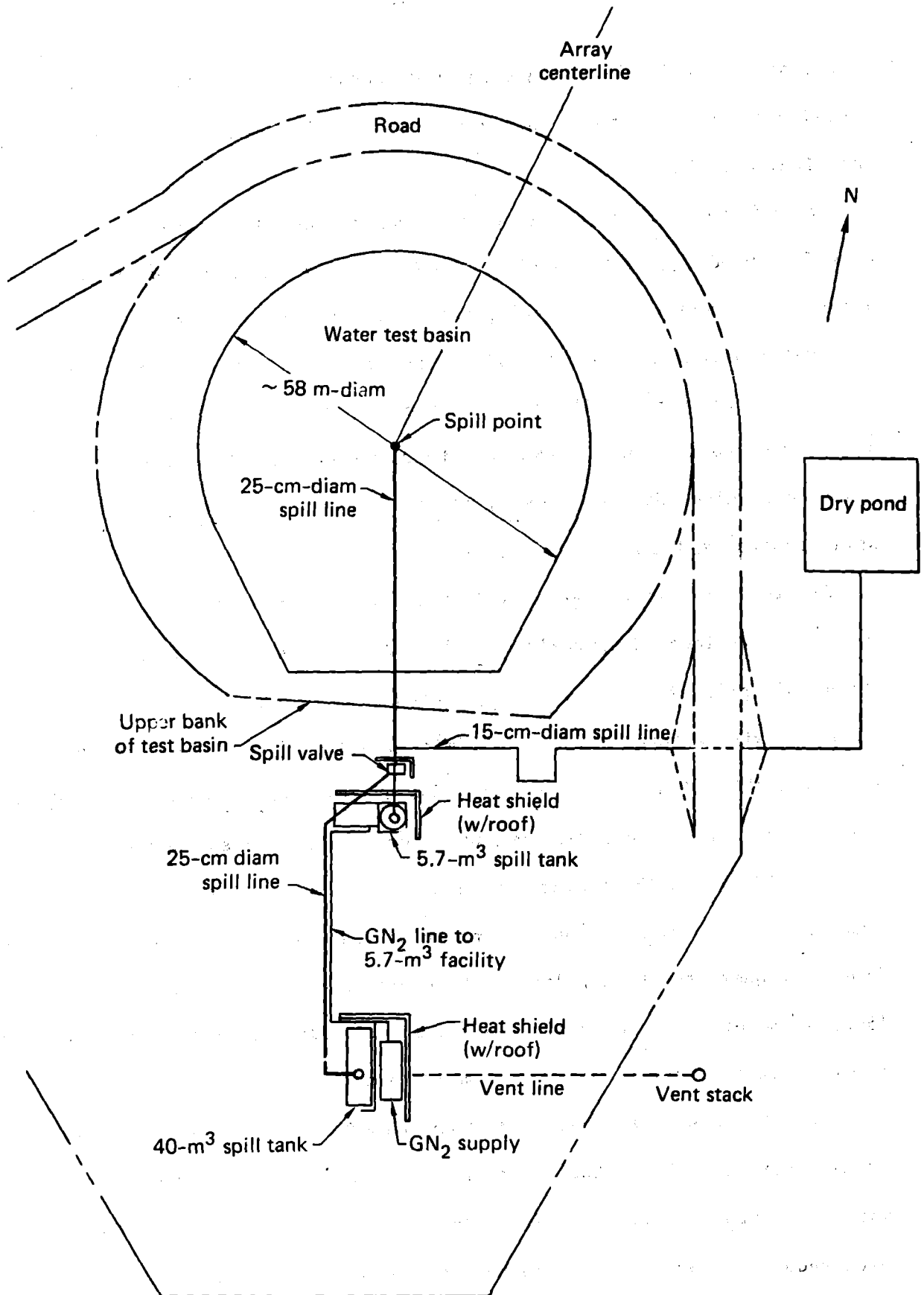


FIG. 1. Site plan of Naval Weapons Center (NWC) spill facility at China Lake.

Large heat-shield structures are used to provide thermal protection for both spill tanks, while a smaller heat shield protects the cool-down and spill valves. The heat shield protecting the 40-m³ tank also provides protection for the GN₂ supply trailer.

Pressurization of the tank prior to a spill is achieved through three stages of pressure reduction from approximately 138 bars at the GN₂ trailer down to the operating pressure of the tank, 2.4 bars. This pressurization is remotely controlled and monitored from the control van.

The control van, located 250 m northwest of the tank, also contains controls for the remote operation of the vent system and the cool-down and spill valves. In addition, remote monitoring of the tank liquid level, tank and spill-line temperatures, tank internal pressure, nitrogen supply pressure, and liquid flow rate is done at the control van.

The tank is loaded from an over-the-road trailer at a loading point 15 m from the tank through a 10-cm-diameter insulated stainless steel loading line. During loading, the tank is vented by means of a 20-cm-diameter vent line and an 18-m-high vent stack.

After the tank is loaded, a sample is taken for later analysis. At this point all personnel are cleared from the spill site and subsequent steps are performed remotely. The remote vent valve is closed, the three stages of pressure regulation are set, and the spill tank is pressurized. The cool-down valve is opened, cooling the spill line; the spill valve is then opened and the test conducted. A "heel" of approximately 1.2 m³ is usually left in the tank after the test.

Instrumentation

Instrument Array. A large array of gas-sensing and wind-measuring instruments was deployed out to 800 m both upwind and downwind of the spill site (2). This array was used to make measurements on both the dispersing gas and the atmosphere into which it was dispersing. A schematic diagram of the array superimposed on the topography around the spill facility is shown in Fig. 2. The array centerline was oriented at 225° (S 45° W), which coincides with the prevailing southwesterly wind direction for the summer season. The acceptance angle for the array was about 50° (from 200° to 250°) and the spacing between stations varied from 13 m close to the pond to 80 m at 800 m downwind. The station locations, including height above sea level, are given in Table 1.

The array was actually made up of three separate arrays, one of 2-m-high cup-and-vane anemometers to map the wind field, one of gas sensors at three heights to track the cloud, and one of propeller bivane anemometers and fast gas sensors at three heights to measure turbulence effects. A typical wind-field station is shown in Fig. 3. Twenty of these were used at China Lake at locations shown in Fig. 2. A turbulence station is shown in Fig. 4. Gas sensor stations were similar to these except that they had no anemometers. There were 25 gas stations and 5 turbulence stations arranged in arcs at 57 m, 140 m, 400 m, and 800 m from the spill point. There was an additional turbulence station, T1, located just upwind of the spill pond, which had bivanes, a humidity sensor and thermocouples, but no gas sensors. The turbulence stations were also distinguished from the gas stations in that they took data at a higher rate (3-5 Hz compared to 1 Hz). Seven of the gas stations had humidity and heat flux sensors in addition to the gas sensors and temperature sensors normally present. The remaining 18 gas stations had gas sensors and thermocouples at three levels. The stations were battery-powered and micro-processor-controlled, with some onboard memory. They communicated with the data-recording trailer by radio telemetry, turning on instruments on command and sending back data when polled.

101/101

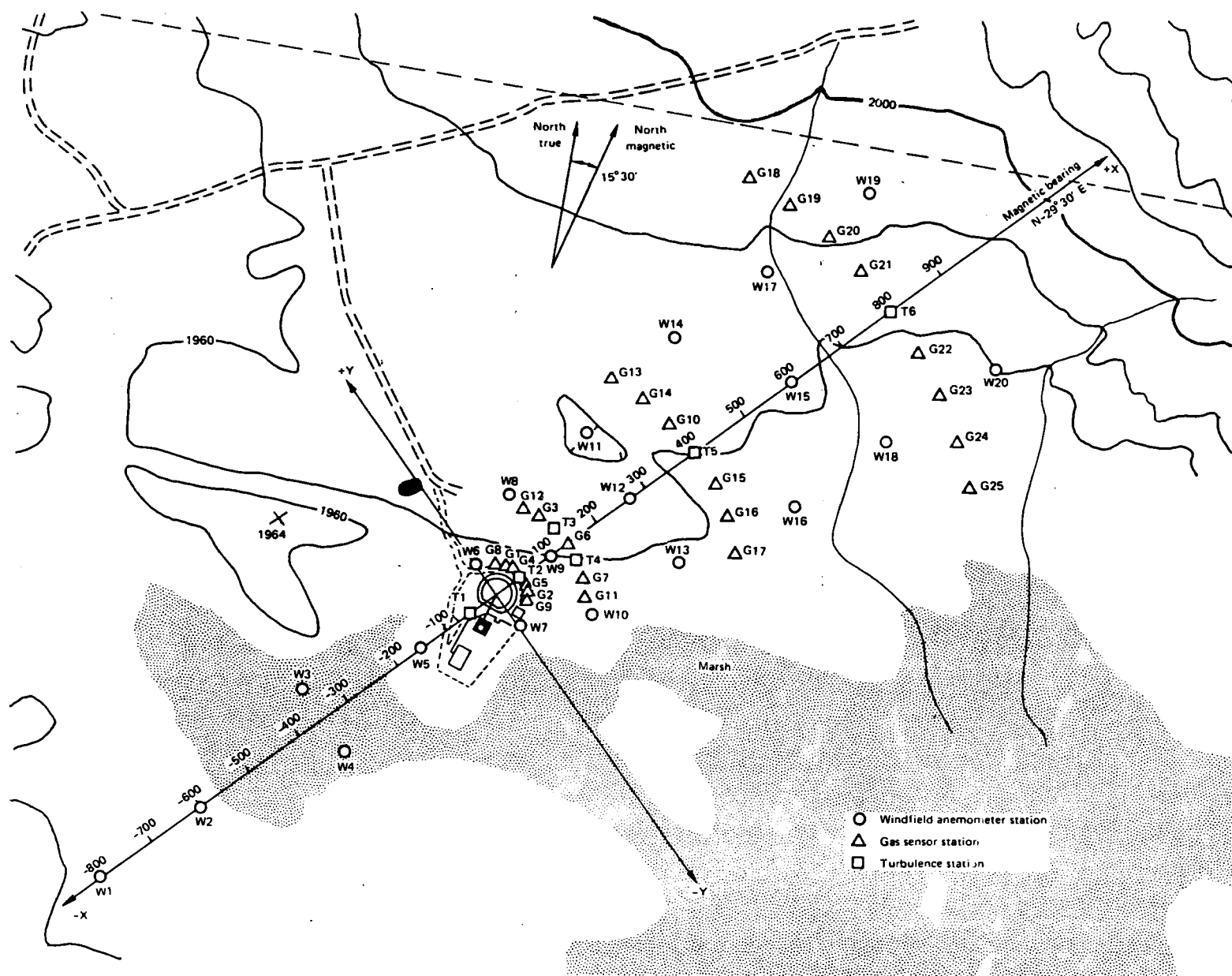


Fig. 2. The instrumentation array for the 1980 LNG dispersion tests at NWC, China Lake.

TABLE 1. Tower Array Coordinates

Tower No.	Foundation I.D.	x (metres)	y (metres)	Elevation (metres)
W1	-800 L	-800	0	595.33
W2	-600 L	-600	0	590.54
W3	-355 J	-350	60	591.24
W4	-355 N	-350	-60	591.24
W5	-150 L	-150	0	590.17
T1	-62 L	-62	0	592.89
G8	57 H	37	38	592.94
G1	57 J	49	28.7	593.13
G4	57 K	55	14.9	593.94
T2	57 L	57	0	593.99
G5	57 M	55	-14.9	593.62
G2	57 N	49	-28.7	593.07
G9	57 P	40	-40.6	592.59
W6	60 J	0	60	593.12
W7	60 N	0	-60	591.91
W9	104 L	104	0	597.02
G12	140 H	112	84	597.89
G3	140 J	127	58	597.77
T3 ^a	140 K	137	30	597.64
G6	140 L	140	0	597.12
T4	140 M	137	-30	595.58
G7	140 N	127	-58	593.53
G11	140 P	112	-84	591.53
W8	159 F	104	120	597.77
W10	159 S	104	-120	591.17
W12	275 L	275	0	594.83
W11	304 J	275	130	595.02
W13	304 N	275	-130	593.30
G13	400 H	360	174	596.59
G14	400 J	382	118	596.27
G10 ^b	400 K	395.5	59.8	595.58
T5 ^a	400 L	400	0	594.01
G15	400 M	395.5	-59.8	593.91
G16	400 N	382	-118	593.98
G17 ^b	400 P	360	-174	594.63
W14	509 J	480	170	596.39
W16	509 N	480	-170	592.65
W15	600 L	600	0	595.11
W17	691 J	670	170	593.33
W18	691 N	670	-170	592.57
G18	800 G	737	312	603.09
G19	800 H	764	236.5	601.44
G20	800 J	784	159	600.49
G21	800 K	796	79.9	598.03

TABLE 1. (Continued)

Tower No.	Foundation I.D.	x (metres)	y (metres)	Elevation (metres)
T6	800 L	800	0	596.02
G22	800 M	796	-79.9	594.40
G23	800 N	784	-159	593.76
G24	800 P	764	-236.5	590.27
G25	800 R	737	-312	591.
W19	900 J	882	180	602.08
W20	900 N	882	-180	593.33
Spill Point	000 L	0	0	590.95

^a T5 and T3 exchanged locations in array for Burro 9 test.

^b G10 and G17 exchanged locations in array for Burro 6, 7, 8, and 9 tests.

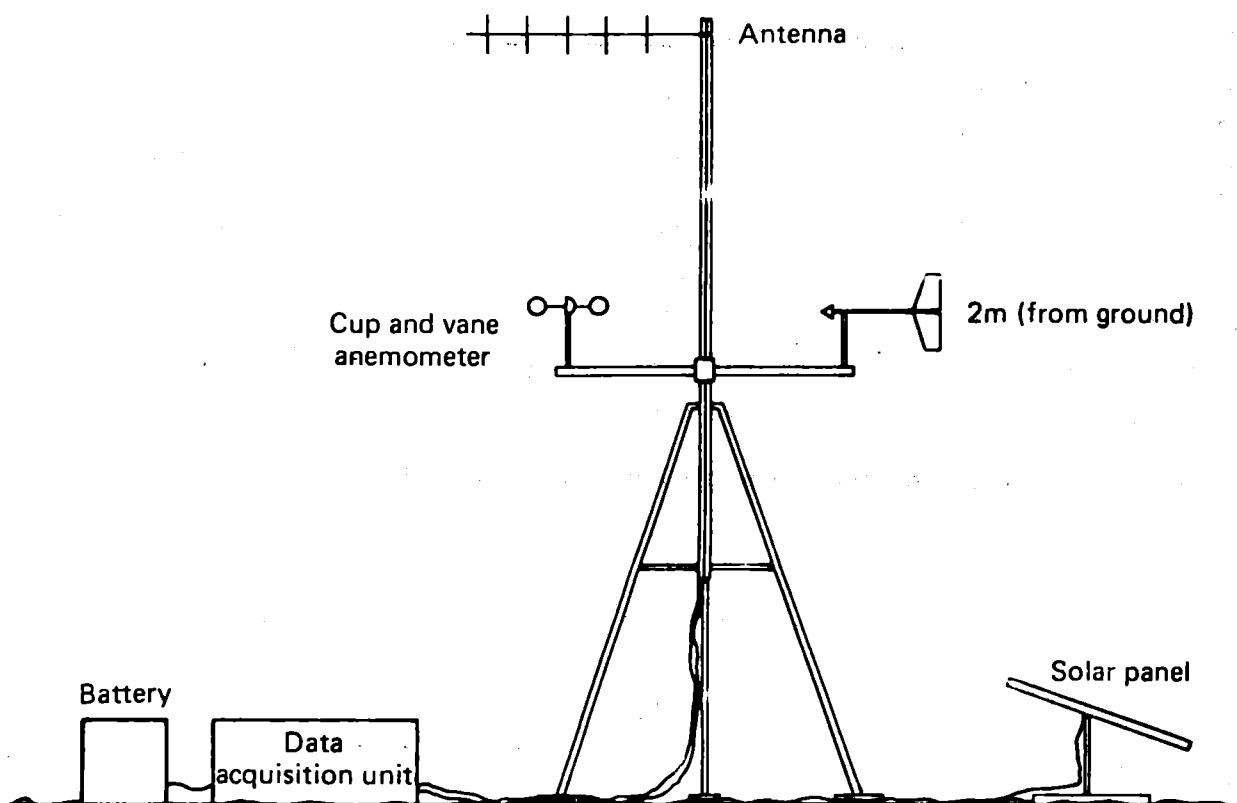


Fig. 3. A wind field anemometer station.

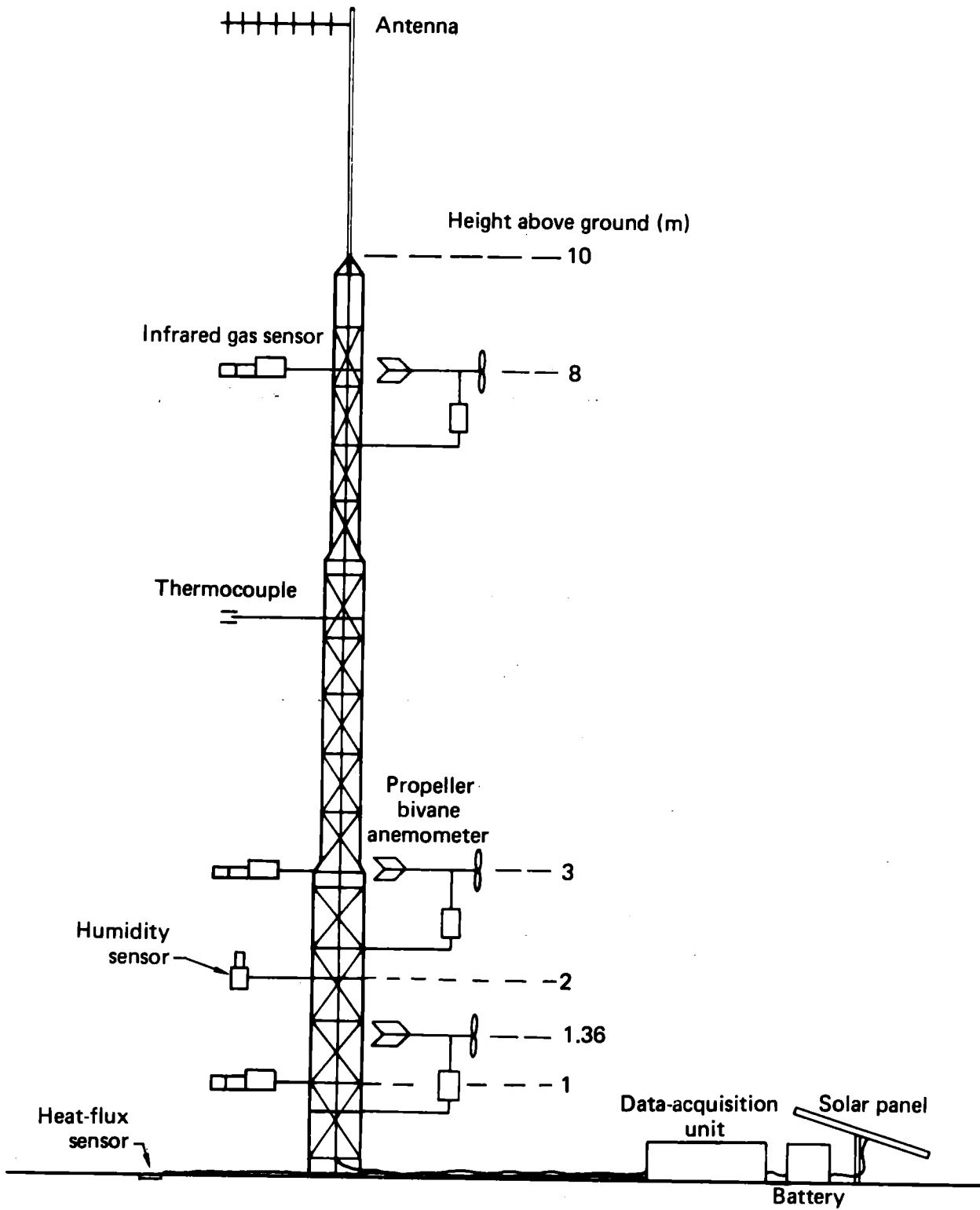


Fig. 4. A turbulence station.

Gas Sensors. A sensor evaluation program (Avocet Series), undertaken in 1978 (3,4) at China Lake, determined that suitable gas sensors for use in the field experiments did not exist. In response to this finding, a fast, portable, differential-IR-absorption sensor that would work in the dense fog associated with LNG spills and detect separately methane and ethane-plus-propane was developed at LLNL (5). A similar sensor was developed by JPL for use in fog-free regions (6). This sensor was faster and detected separately methane, ethane, and propane. Thirty-three of the LLNL sensors were built and deployed on six towers in the first two arcs and on the five downwind turbulence towers. A prototype version of the JPL IR sensor was fielded on the last three tests of the Burro series and data from it agreed well with the LLNL IR sensor close by.

Because the IR sensors were expensive, it was not possible to outfit the entire array (90 sensors) with them. Two inexpensive general hydrocarbon sensors were chosen for the rest of the array. Fifteen stations (45 sensors) were outfitted with IST (International Sensor Technology) solid-state sensors, and four stations (12 sensors) were outfitted with MSA (Mine Safety Appliance) catalytic sensors. The IST sensors had not been evaluated in the field during the Avocet series of tests in 1978, but had been extensively tested in the laboratory during 1979. The IST sensor was selected as a result of this lab testing and because it was capable of measuring gas concentrations as high as 25% and had been successfully temperature-compensated. Unfortunately some problems with it still remained to be discovered in the field. The sensor proved to be sensitive to humidity in the presence of methane, a sensitivity which varied with the methane concentration. Using humidity sensor data (the humidity sensor was not sensitive to hydrocarbon gases) from the field and a laboratory calibration of the IST's for both methane and humidity, we were able

to correct the field data for this effect. The humidity effect was as much as a factor of two for some of the sensors, but on the average was about 10-20% of the reading for gas concentrations of 2-3%, typical for most of the tests.

The IST sensors also showed variable sensitivity to the higher hydrocarbons, ethane and propane. In the worst cases, some sensors were 40 or more times as sensitive to ethane and propane as they were to methane. Nine sensors showed sensitivity ratios of 17 or more, and the average of the remaining 35 sensors was about 6. Knowing the response of each sensor and using the methane/methane ratios measured as a function of time by the IR sensor stations, we were able to correct the IST sensor data for this effect also.

Some of the IST sensors exhibited calibration changes and gain changes during the course of the experiments. The sensors were all recalibrated in the lab after being brought back from China Lake, and these calibrations were generally used with the data. The result of all of the corrections to the IST sensor data is a fairly high residual uncertainty in its accuracy. Our current best estimate is that for concentrations below 5% the uncertainty is 20-30% of the indicated value, and above 5% it is approximately 50% of the value with uncertainties varying greatly from sensor to sensor. For instance, comparison between one IST and one LLNL IR sensor at the same location on Burro 8 and 9 showed agreement to within about 10%.

The LLNL-developed IR gas sensor was considerably more successful. It was developed as a fast, portable, multispecies gas sensor which would work in the fog and it has successfully met our expectations. The gas calibration of the sensor was done in the laboratory before going to China Lake last summer, and several checks in the field have shown that the calibrations are quite stable, and did not change over a four-month period of operation in the extremes of the desert environment.

A schematic drawing of the sensor is shown in Fig. 5. Infrared radiation from the source passes through an optical path open to the atmosphere. If hydrocarbons are present, then absorption occurs, and the amounts of absorption specific to methane, ethane-plus-propane, and fog are detected at the pyro-electric detector. Absorption specific to these species is defined by four narrow bandpass filters between 3.0 and 3.9 μm .

In the absence of fog, two channels serve primarily to determine the methane and ethane gas concentrations. Two other channels are used as reference channels to compensate for shifts in system throughput due to fog, dust on the lenses, or temperature-induced baseline shifts. Relatively little cross-gas sensitivity is experienced within the two main channels. The instruments were calibrated using methane concentrations of 0-50% and ethane concentrations of 0-30%. Expressed as a percentage of the gas sensor reading, the averaged single-gas calibration uncertainties were $\pm 5.5\%$ and $\pm 2.5\%$ for methane and ethane, respectively. If the reference channels were not used for compensation, methane uncertainties did not change markedly, but ethane uncertainties increased to $\pm 6.0\%$ of the sensor reading.

Several methane-ethane gas mixtures were analyzed with the instruments as part of the calibration procedure. Inaccuracies in the ethane results were only slightly larger than those obtained for the ethane-only calibration runs. However, the methane results were consistently found to be too high by about 10% of the reading. These biases are thought to be due to the form of the calibration algorithm employed. By design, the sensor responds to propane essentially as it does to ethane, but with an increased sensitivity of about 40%. Thus 1% propane appears as 1.4% ethane in the ethane-plus-propane channel.

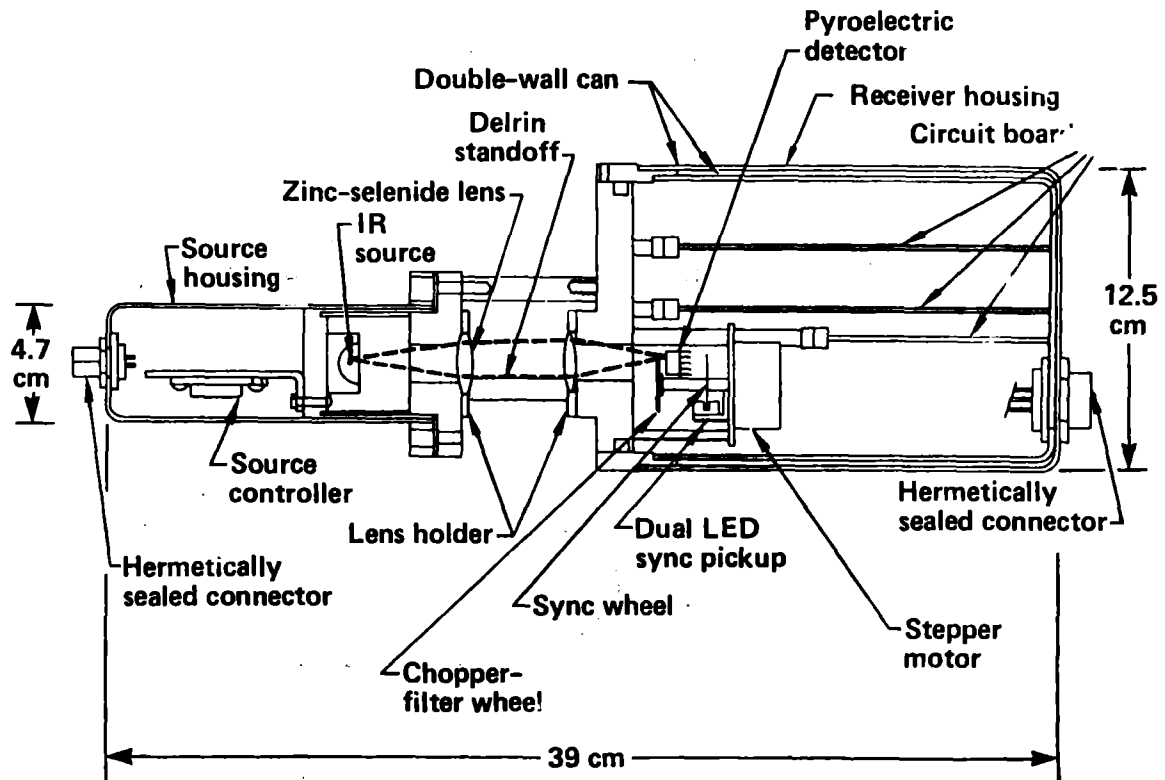


Fig. 5. Schematic drawing of the infrared gas sensors' electro-optical head, showing source housing, receiver housing, and major components.

In the presence of fog, the two bands on either side of the methane and ethane-plus-propane bands are used to correct for the spectral scattering due to fog particles. Reference levels are determined from data acquired before and after the spill. The algorithm developed to make this correction was based on Mie scattering calculations and experimental data. The calculations showed that, for a given particle size distribution, the extinction coefficient in the four absorption bands varies linearly with the total particle number density. However, the ratios of the extinction coefficients in the four absorption bands are functions of the particle size distribution. Consequently, a 40-m³ liquid nitrogen spill (Burro 1) was used to empirically determine the wavelength dependence of the fog attenuation during actual field environmental conditions. This dependence was found to change very little with time or position in the fog, apparently indicating little change in particle size distribution.

When this empirically determined relationship is used together with the fog-free calibration results, the methane and ethane-plus-propane gas concentrations can be determined even in the dense fog. The overall accuracy of the gas concentrations determined in this manner can be estimated by a self-consistency examination of the data from Burro 1 which had fog but no hydrocarbon gas. When little or no fog is present, the results agree with the fog-free determinations, and for the great majority of the data from Burro 1, the results show quite variable fog concentrations but essentially no apparent hydrocarbon. For example, for the period of time that fog was present, the averaged indicated methane and ethane-plus-propane concentrations, for three of the four sensors in the dense fog, indicate 0.1% and 0.9% respectively; however, spikes with peak apparent values as high as 4% and 18% respectively were seen. Since the gas concentrations appeared to vary continuously with

time, this suggests that the character of the fog did deviate substantially on occasions from the averaged character. That these deviations occurred in times of both dense and tenuous fog also supports this supposition. Finally, the specific filter characteristics (i.e., temperature sensitivity), together with the form of the fog calibration algorithm, lead to the largest apparent errors appearing in the ethane results. This is fortunate in the respect that LNG is primarily methane, but it makes accurate determination of ethane specific effects, such as differential boiloff, difficult.

These sensors were used on both the turbulence towers, where they took data at the rate of 3-5 Hz, and on the close-in gas stations, where they took data at 1 Hz. The gas stations in the 57-m arc were the only ones to experience very dense fog.

The MSA sensors are well understood, standard commercial units, operating on the catalytic principle. They work well as long as the gas concentration remains below the stoichiometric mixture (10% for methane). The sensor response is very linear and shows an uncertainty of about 10% of the reading.

Humidity Sensors. These sensors were developed at LLNL specifically for use in a cold cloud of condensed water droplets. The sensitive element is the commercially available Humicap. It is protected from the environment by a porous sintered frit which is heated to 40° C by thermostatically controlled resistors and designed to evaporate any water droplets coming in contact with the frit. The sensitive element cannot tolerate contact with water droplets, and this design assures that it senses only water vapor.

The sensors were calibrated before going to NWC in the early summer of 1980 and again the following winter after returning to Livermore, using a dew point hygrometer and an environmental chamber. They appear to have a nearly linear response over the relative humidity range 10-60% (at the controlled

temperature of 40° C), while marked curvature is seen below 10%. The consistency of the calibration-run data fits is typically $\pm 1/2\%$ or better. Side-by-side comparisons of the instruments show agreement to better than $\pm 2\%$. The amount of long-term sensor drift is not known, but is estimated to be less than $\pm 3\%$. The overall accuracy of the present data is estimated to be about $\pm 4\%$.

Eight of these instruments were mounted on stations throughout the array, including one upwind at station T1.

Anemometers. Two different types of anemometers were used in these tests. The anemometers used for wind field measurements were standard, commercially available (Met-One), two-axis cup-and-vane anemometers located at 20 stations, 2 m above the ground, both upwind and downwind of the spill point. They have a starting threshold of 0.2 m/s and a response distance constant of 1.5 m with an accuracy of $\pm 1\%$ or 0.07 m/s. Data taken by these instruments were averaged for 10 s before being transmitted to the data recording trailer. The data were displayed in realtime and were used to choose optimum test conditions such that the gas cloud would disperse within the array of instruments and would not endanger NWC personnel controlling the spill.

The wind field anemometers were calibrated with respect to three standards from the same batch. The standards were then sent off to NBS for calibration in a wind tunnel, and the results of this calibration were used as the final calibration of the field instruments.

The six turbulence stations used standard, commercially available, Gill bivane anemometers manufactured by R.M. Young Co.. Three of these were mounted vertically on each tower at 1.36 m, 3 m, and 8 m, so that the vertical wind profile could be determined as well as the various parameters related to atmospheric turbulence. These anemometers have a starting threshold of 0.1-0.2 m/s

and a response distance constant of 1.0 m. Factory-supplied calibration curves were used. Data were taken at the rate of 3-5 Hz with these instruments.

Heat Flux Sensors. The heat flux sensors were standard, commercially available heat flux plates manufactured by Hy-Cal Engineering. They consisted of two layers of thermopiles separated by a layer of material of known thermal conductivity, forming a thin rectangular wafer which was buried just below the soil surface. These devices were installed on seven downwind stations along with the humidity sensors.

Temperature Sensors. Standard Chromel-Alumel (type K) thermocouples were collocated with each gas sensor to provide temperature measurements of the gas cloud. The response time of the 10-mil thermocouples was about 0.5 s in a 5-m/s wind, corresponding roughly with the IR gas sensors on the gas stations, which averaged data for 1 s. The thermocouple amplifier drift during the course of an experiment (1°C) did not allow temperature difference data to be used to determine the vertical temperature gradient in the ambient atmosphere ($0.02\text{--}0.2^{\circ}\text{C/m}$ in the lower 15 m). Data from the upwind NWC meteorological tower was used for this determination. However, temperature variations due to the presence of the cloud ($10\text{--}30^{\circ}\text{C}$), were quite accurately determined.

Cameras. Photography was an important diagnostic tool, and cameras were in operation during all experiments except Burro 7. Remotely controlled 16-mm motion picture cameras were used in three locations. The crosswind camera was on top of the control bunker, about 220 m from the spill point. The upwind camera was about 70 m upwind of the spill point (close to T1) and about 1.5 m above ground level. The overhead camera was about 120 m north (downwind) of the spill point and about 45 m above ground level. The cameras were supplied by NWC personnel and operated from the bunker.

Infrared imagers. The EG&G Remote Measurements group provided IR imaging of several spills (Burros 2, 4, 6, and 9), using a helicopter-mounted Infra-metrics dual-band infrared imager. The instrument had two channels--one sensitive to radiation with wavelengths between 4 and 6.5 μm and one sensitive to radiation with wavelengths between 7 and 14 μm . A strong methane IR absorption band between 7 and 8.5 μm should allow the methane cloud to be imaged in the long-wavelength channel, using the ground as a thermal radiation source.

The overflights were successful in imaging the gas cloud as it dispersed downwind. Traces of the cloud were seen, in the 7- to 14- μm channel, as far downwind as 1500 m, where the gas concentration would have been substantially less than 1%. Unfortunately, the cold gas also cooled the ground, changing the source characteristics. Consequently, the observed image was a combination of methane absorption and the cold-ground effect. These two effects will be separated in future work. An attempt was made to measure the size of the LNG pool on the Burro 9 experiment by reducing the imager sensitivity to see through the dense fog and image the LNG pool against the water.

Data Acquisition System.

This flexible and powerful system utilizes UHF radio telemetry for command and data transmission and is designed to acquire data from sensors distributed over an area with a diameter of up to 10 miles (14). Twenty of the portable data acquisition units acquire wind field data from two-axis anemometers. The remaining 31 data acquisition units are used to acquire data from a wide variety of sensors. This network of 51 units can acquire data from up to 700 channels with data rates and channel assignments programmable remotely from the data acquisition trailer. Each of the data acquisition units consist of a Pacific Cyber/Metrix Model PPS-1201 micro-processor, up to 8 K words of RAM,

instrumentation amplifiers, relays to turn on sensors, and a radio transmitter and receiver. Data acquired from the various sensors are packed into one of two 2000-byte buffers in a double buffering scheme. The buffers are filled in 10 seconds to 4 minutes, depending on the data acquisition rate, number of channels, data resolution, and type of data. Each of the three subsystems functions independently and communicates with its own minicomputer in the data-recording trailer. These minicomputers poll the stations in their network requesting that they transmit their full data buffers back to the data-recording trailer at 19.2 K baud. These systems each consist of an LSI-11/23 minicomputer, a 10-megabyte disk unit, and a graphics display video terminal, with a shared magnetic tape unit and a floppy disk unit.

Data Handling.

The data from each LNG spill were transferred from magnetic tape to the MASS storage system (7) at the LLNL Computation Center, for archival preservation. In order to be able to manipulate this large amount of data, i.e. select data from the data base and perform an operation on it, it is necessary to use a data base management system. The data base management system we used is one developed at LLNL, called FRAMIS (8). This is a relational system which was developed mainly for the scientific community, so that it handles numerical input conveniently. The tables produced by FRAMIS are stored on the MASS system, so they are readily available for analysis.

Most of the data manipulation, plotting, and contour generation was done with these data base files using a data analysis system developed at LLNL called MATHSY (9). This is an interactive, array-processing, math and graphics system which has been a powerful tool for the analysis, handling, and display of the large quantities of data involved in this report.

C. TEST SUMMARY

A summary of the test and meteorological conditions for each of the nine Burro series spills is given in this section. Table 2 is a summary of the tests, in which the descriptive atmospheric stability category is based on the Richardson number.

A more complete set of stability indices is listed on the data base summary sheets, one for each test, which are reproduced here. These sheets contain descriptive information for each test, most of which is self-explanatory. The composition of the LNG given in the summary is based on the measured composition in the San Diego Gas and Electric storage tank prior to shipment, corrected for boiloff during shipment and during storage in the NWC tank. Our zero time signal occurs when the valve is fully open. The array centerline stayed fixed at 225° (S 45° W) for the duration of the test series. The average wind direction, its standard deviation (σ_{θ}), the average wind speed, and its standard deviation (σ_{speed}) were taken from the 10-second-averaged wind field data from the 20 anemometer stations averaged over a six-minute period starting at zero time. The average vertical wind profile and u_{*} , the diabatically adjusted (i.e., corrected for non-adiabatic effects of atmospheric stability) friction velocity, are derived from the turbulence tower and wind field data using the following relationship:

$$u(z) = \frac{u_{*}}{k} \left(\ln \frac{z}{z_0} - \psi \right).$$

For neutral-stability tests, $\psi \rightarrow 0$, and $\phi \rightarrow 1$ as $R \rightarrow 0$, therefore

$$u_{*} = \frac{k}{\phi} \frac{\partial u}{\partial (\ln z)} \approx k \left\{ \frac{u_2 - u_1}{\ln(z_2/z_1)} \right\},$$

where $k = 0.4$ (von Karman's constant) and u_2 = wind speed at height z_2 , (space-averaged.)

TABLE 2. Burro Series Test Summary (1980).

Test Name	Date	Spill Volume (m3)	Spill Rate (m3/min)	Averaged Wind Speed (m/s)	Averaged Wind Direction (degrees)	Atmospheric Stability
Burro 2	18 June	34.3	11.9	5.4	221	Unstable
Burro 3	2 July	34.0	12.2	5.4	224	Unstable
Burro 4	9 July	35.3	12.1	9.0	217	Slightly Unstable
Burro 5	16 July	35.8	11.3	7.4	218	Slightly Unstable
Burro 6	5 Aug.	27.5	12.8	9.1	220	Slightly Unstable
Burro 7	27 Aug.	39.4	13.6	8.4	208	Neutral to Slightly unstable
Burro 8	3 Sept.	28.4	16.0	1.8	235	Slightly stable
Burro 9	17 Sept.	24.2	18.4	5.7	232	Neutral

BURRO 1 Summary Sheet

TEST NAME : BURRO 1 (LN-3)
TEST TYPE : DISPERSION (4Ø M3)
MATERIAL : LIQUID NITROGEN
COMPOSITION : Ø% METHANE
: Ø% ETHANE
: Ø% PROPANE
DATE : 6 JUNE 198Ø
VALVE BEGINS TO OPEN : 15:28:27 PDT
VALVE OPEN (ZERO TIME) : 15:28:36 PDT
VALVE BEGINS TO CLOSE : 15:32:1Ø PDT
VALVE CLOSED : 15:32:18 PDT
SPILL RATE : 1Ø.1 M3/MIN*
SPILL VOLUME : 34.9 M3
SPILL DURATION : 2Ø7 SEC*
ARRAY CENTERLINE : 225 DEGREES
AVERAGE WIND DIRECTION : 2Ø7 DEGREES
SIGMA THETA : 22 DEGREES
AVERAGE WIND SPEED : 4.3 M/SEC
SIGMA SPEED : 1.3 M/SEC
UPWIND VERTICAL PROFILE :
AT 1M : 4.Ø5 M/SEC
AT 3M : 4.43 M/SEC
AT ØM : 4.66 M/SEC
U STAR : Ø.2Ø2 M/SEC
PERCENT CLOUD COVER :
TEMPERATURE AT 2M : 2Ø.9 DEGREES C
DELTA T AT 1M : +Ø.5Ø DEGREES C
DELTA T AT 5M : -Ø.38 DEGREES C
DELTA T AT 1ØM : -Ø.3Ø DEGREES C
DELTA T AT 15M : -1.17 DEGREES C
T STAR : -Ø.58 DEGREES C
BAROMETRIC PRESSURE : 942.5 MILLIBARS
UPWIND HUMIDITY : NOT AVAILABLE
DOWNWIND HUMIDITY (G4) : 5.7%
TURBULENT PRANDTL NO. : 1.63
SENSIBLE HEAT FLUX : -141 WATT/M2
MOMENTUM DIFFISIVITY (2M) : Ø.264 M2/SEC
RICHARDSON NO. (2M) : -Ø.378
MONIN-ØBUKHOV LENGTH : -5.29 M

REMARKS:

*NOTE: TANK EMPTY 16SEC BEFORE VALVE CLOSED.

BURRO 2 Summary Sheet

TEST NAME : BURRO 2 (LNG-27)
TEST TYPE : DISPERSION (4Ø M3)
MATERIAL : LNG
COMPOSITION : 91.3% METHANE
: 7.2% ETHANE
: 1.5% PROPANE
DATE : 18 JUNE 198Ø
VALVE BEGINS TO OPEN : 15:59:21 PDT
VALVE OPEN (ZERO TIME) : 15:59:2Ø PDT
VALVE BEGINS TO CLOSE : 16:Ø2:32 PDT
VALVE CLOSED : 16:Ø2:4Ø PDT
SPILL RATE : 11.9 M3/MIN*
SPILL VOLUME : 34.3 M3
SPILL DURATION : 173 SEC*
ARRAY CENTERLINE : 225 DEGREES
AVERAGE WIND DIRECTION : 221 DEGREES
SIGMA THETA : 13.5 DEGREES
AVERAGE WIND SPEED : 5.4 M/SEC
SIGMA SPEED : 1.8 M/SEC
UPWIND VERTICAL PROFILE :
AT 1M : 5.Ø6 M/SEC
AT 3M : 5.59 M/SEC
AT ØM : 5.9Ø M/SEC
U STAR : Ø.248 M/SEC
PERCENT CLOUD COVER :
TEMPERATURE AT 2M : 37.6 DEGREES C
DELTA T AT 1M : +Ø.52 DEGREES C
DELTA T AT 5M : -Ø.71 DEGREES C
DELTA T AT 1ØM : -Ø.53 DEGREES C
DELTA T AT 15M : -1.31 DEGREES C
T STAR : -Ø.57 DEGREES C
BAROMETRIC PRESSURE : 939.5 MILLIBARS
UPWIND HUMIDITY : NOT AVAILABLE
DOWNWIND HUMIDITY (G4) : 7.1%
TURBULENT PRANDTL NO. : 1.4Ø
SENSIBLE HEAT FLUX : -122 WATT/M2
MOMENTUM DIFFISIVITY (2M) : Ø.278 M2/SEC
RICHARDSON NO. (2M) : -Ø.178
MONIN-ØBUKHOV LENGTH : -11.3 M

REMARKS:

*NOTE: TANK EMPTY 18SEC BEFORE VALVE BEGAN TO CLOSE.

BURRO 3 Summary Sheet

TEST NAME : BURRO 3 (LNG-28)
TEST TYPE : DISPERSION (40 M3)
MATERIAL : LNG
COMPOSITION : 92.5% METHANE
: 6.2% ETHANE
: 1.3% PROPANE
DATE : 2 JULY 1980
VALVE BEGINS TO OPEN : 15:08:00 PDT
VALVE OPEN (ZERO TIME) : 15:08:06 PDT
VALVE BEGINS TO CLOSE : 15:10:47 PDT
VALVE CLOSED : 15:10:55 PDT
SPILL RATE : 12.2 M3/MIN
SPILL VOLUME : 34.0 M3
SPILL DURATION : 166.8 SEC
ARRAY CENTERLINE : 225 DEGREES
AVERAGE WIND DIRECTION : 224 DEGREES
SIGMA THETA : 13.3 DEGREES
AVERAGE WIND SPEED : 5.4 M/SEC
SIGMA SPEED : 1.19 M/SEC
UPWIND VERTICAL PROFILE
AT 1M : 5.06 M/SEC
AT 3M : 5.58 M/SEC
AT 8M : 5.94 M/SEC
U STAR : 0.249 M/SEC
PERCENT CLOUD COVER :
TEMPERATURE AT 2M : 33.8 DEGREES C
DELTA T AT 1M : +0.80 DEGREES C
DELTA T AT 5M : -0.70 DEGREES C
DELTA T AT 10M : -0.92 DEGREES C
DELTA T AT 15M : -1.40 DEGREES C
T STAR : -0.65 DEGREES C
BAROMETRIC PRESSURE : 948.0 MILLIBARS
UPWIND HUMIDITY : NOT AVAILABLE
DOWNWIND HUMIDITY (G4) : 5.2%
TURBULENT PRANDTL NO. : 1.46
SENSIBLE HEAT FLUX : -154 WATT/M2
MOMENTUM DIFFUSIVITY (2M) : 0.291 M2/SEC
RICHARDSON NO. (2M) : -0.221
MONIN-OBUKHOV LENGTH : -9.06 M

BURRO 4 Summary Sheet

TEST NAME : BURRO 4 (LNG-29)
TEST TYPE : DISPERSION (40 M3)
MATERIAL : LNG
COMPOSITION : 93.8% METHANE
: 5.1% ETHANE
: 1.1% PROPANE
DATE : 9 JULY 1980
VALVE BEGINS TO OPEN : 14:07:21 PDT
VALVE OPEN (ZERO TIME) : 14:07:27 PDT
VALVE BEGINS TO CLOSE : 14:10:24 PDT
VALVE CLOSED : 14:10:32 PDT
SPILL RATE : 12.1 M3/MIN*
SPILL VOLUME : 35.3 M3
SPILL DURATION : 175 SEC*
ARRAY CENTERLINE : 225 DEGREES
AVERAGE WIND DIRECTION : 217.5 DEGREES
SIGMA THETA : 7.3 DEGREES
AVERAGE WIND SPEED : 9.0 M/SEC
SIGMA SPEED : 1.19 M/SEC
UPWIND VERTICAL PROFILE
AT 1M : 8.37 M/SEC
AT 3M : 9.35 M/SEC
AT 8M : 10.14 M/SEC
U STAR : 0.403 M/SEC
PERCENT CLOUD COVER :
TEMPERATURE AT 2M : 35.4 DEGREES C
DELTA T AT 1M : +0.50 DEGREES C
DELTA T AT 5M : -0.76 DEGREES C
DELTA T AT 10M : -0.50 DEGREES C
DELTA T AT 15M : -1.32 DEGREES C
T STAR : -0.65 DEGREES C
BAROMETRIC PRESSURE : 945.0 MILLIBARS
UPWIND HUMIDITY : 2.9%
DOWNWIND HUMIDITY (G21) : 2.7%
TURBULENT PRANDTL NO. : 1.17
SENSIBLE HEAT FLUX : -150 WATT/M2
MOMENTUM DIFFUSIVITY (2M) : 0.377 M2/SEC
RICHARDSON NO. (2M) : -0.054
MONIN-OBUKHOV LENGTH : -27.1 M
*NOTE: TANK EMPTY 8 SEC BEFORE VALVE BEGAN TO CLOSE

BURRO 5 Summary Sheet

TEST NAME : BURRO 5 (LNG-30)
TEST TYPE : DISPERSION (40 M3)
MATERIAL : LNG
COMPOSITION : 93.6% METHANE
: 5.3% ETHANE
: 1.1% PROPANE
DATE : 16 JULY 1980
VALVE BEGINS TO OPEN : 16:19:30 PDT
VALVE OPEN (ZERO TIME) : 16:19:36 PDT
VALVE BEGINS TO CLOSE : 16:22:40 PDT
VALVE CLOSED : 16:22:48 PDT
SPILL RATE : 11.3 M3/MIN
SPILL VOLUME : 35.0 M3
SPILL DURATION : 190 SEC
ARRAY CENTERLINE : 225 DEGREES
AVERAGE WIND DIRECTION : 218 DEGREES
SIGMA THETA : 11.1 DEGREES
AVERAGE WIND SPEED : 7.4 M/SEC
SIGMA SPEED : 1.13 M/SEC
UPWIND VERTICAL PROFILE
AT 1M : 7.00 M/SEC
AT 3M : 7.79 M/SEC
AT 8M : 8.42 M/SEC
U STAR : 0.330 M/SEC
PERCENT CLOUD COVER :
TEMPERATURE AT 2M : 40.5 DEGREES C
DELTA T AT 1M : +0.62 DEGREES C
DELTA T AT 5M : -0.63 DEGREES C
DELTA T AT 10M : -0.37 DEGREES C
DELTA T AT 15M : -0.96 DEGREES C
T STAR : -0.60 DEGREES C
BAROMETRIC PRESSURE : 941.0 MILLIBARS
UPWIND HUMIDITY (T1) : 5.6%
DOWNWIND HUMIDITY (G4) : 5.9%
TURBULENT PRANDTL NO. : 1.23
SENSIBLE HEAT FLUX : -131 WATT/M2
MOMENTUM DIFFUSIVITY (2M) : 0.327 M2/SEC
RICHARDSON NO. (2M) : -0.079
MONIN-OBUKHOV LENGTH : -25.5 M

BURRO 6 Summary Sheet

TEST NAME : BURRO 6 (LNG-31)
TEST TYPE : DISPERSION (40 M3)
MATERIAL : LNG
COMPOSITION : 92.8% METHANE
: 5.8% ETHANE
: 1.43% PROPANE
DATE : 5 AUG 1980
VALVE BEGINS TO OPEN : 16:05:00 PDT
VALVE OPEN (ZERO TIME) : 16:05:06 PDT
VALVE BEGINS TO CLOSE : 16:07:09 PDT
VALVE CLOSED : 16:07:17 PDT
SPILL RATE : 12.8 M3/MIN
SPILL VOLUME : 27.5 M3
SPILL DURATION : 128.0 SEC
ARRAY CENTERLINE : 225 DEGREES
AVERAGE WIND DIRECTION : 220 DEGREES
SIGMA THETA : 6.72 DEGREES
AVERAGE WIND SPEED : 9.1 M/SEC
SIGMA SPEED : 1.00 M/SEC
UPWIND VERTICAL PROFILE
AT 1M : 9.37 M/SEC
AT 3M : 9.35 M/SEC
AT 8M : 10.16 M/SEC
U STAR : 0.402 M/SEC
PERCENT CLOUD COVER :
TEMPERATURE AT 2M : 39.2 DEGREES C
DELTA T AT 1M : +0.32 DEGREES C
DELTA T AT 5M : -0.63 DEGREES C
DELTA T AT 10M : -0.71 DEGREES C
DELTA T AT 15M : -1.35 DEGREES C
T STAR : -0.57 DEGREES C
BAROMETRIC PRESSURE : 935.0 MILLIBARS
UPWIND HUMIDITY (T1) : 4.8%
DOWNWIND HUMIDITY (G4) : 5.1%
TURBULENT PRANDTL NO. : 1.14
SENSIBLE HEAT FLUX : -132 WATT/M2
MOMENTUM DIFFUSIVITY (2M) : 0.371 M2/SEC
RICHARDSON NO. (2M) : -0.044
MONIN-OBUKHOV LENGTH : -45.8 M

BURRO 7 Summary Sheet

TEST NAME : BURRO 7 (LNG-32)
TEST TYPE : DISPERSION (4Ø M3)
MATERIAL : LNG
COMPOSITION : 87.Ø% METHANE
: 1Ø.4% ETHANE
: 2.6Ø% PROPANE
DATE : 27 AUG 198Ø
VALVE BEGINS TO OPEN : 18:12:15 PDT
VALVE OPEN (ZERO TIME) : 18:12:21 PDT
VALVE BEGINS TO CLOSE : 18:15:Ø9 PDT
VALVE CLOSED : 18:15:17 PDT
SPILL RATE : 13.6 M3/MIN
SPILL VOLUME : 39.4 M3
SPILL DURATION : 174 SEC
ARRAY CENTERLINE : 225 DEGREES
AVERAGE WIND DIRECTION : 2Ø8.4 DEGREES
SIGMA THETA : 5.21 DEGREES
AVERAGE WIND SPEED : 8.4 M/SEC
SIGMA SPEED : 1.16 M/SEC
UPWIND VERTICAL PROFILE
AT 1M : 7.8Ø M/SEC
AT 3M : 8.75 M/SEC
AT 8M : 9.56 M/SEC
U STAR : Ø.372 M/SEC
PERCENT CLOUD COVER :
TEMPERATURE AT 2M : 33.7 DEGREES C
DELTA T AT 1M : +Ø.11 DEGREES C
DELTA T AT 5M : -Ø.34 DEGREES C
DELTA T AT 1ØM : -Ø.32 DEGREES C
DELTA T AT 15M : -Ø.56 DEGREES C
T STAR : -Ø.23 DEGREES C
BAROMETRIC PRESSURE : 94Ø.Ø MILLIBARS
UPWIND HUMIDITY (T1) : 6.7%
DOWNWIND HUMIDITY (G4) : 7.4%
TURBULENT PRANDTL NO. : 1.Ø6
SENSIBLE HEAT FLUX : -41 WATT/M2
MOMENTUM DIFFUSIVITY (2M) : Ø.316 M2/SEC
RICHARDSON NO. (2M) : -Ø.Ø18
MONIN-OBUKHOV LENGTH : -114.Ø M

BURRO 8 Summary Sheet

TEST NAME : BURRO 8 (LNG-33)
TEST TYPE : DISPERSION (4Ø M3)
MATERIAL : LNG
COMPOSITION : 87.4% METHANE
: 1Ø.3% ETHANE
: 2.3Ø% PROPANE
DATE : 3 SEPT 198Ø
VALVE BEGINS TO OPEN : 19:Ø9:16 PDT
VALVE OPEN (ZERO TIME) : 19:Ø9:22 PDT
VALVE BEGINS TO CLOSE : 19:11:Ø3 PDT
VALVE CLOSED : 19:11:1Ø PDT
SPILL RATE : 16.Ø M3/MIN
SPILL VOLUME : 28.4 M3
SPILL DURATION : 1Ø7 SEC
ARRAY CENTERLINE : 225 DEGREES
AVERAGE WIND DIRECTION : 234.8 DEGREES
SIGMA THETA : 5.57 DEGREES
AVERAGE WIND SPEED : 1.8 M/SEC
SIGMA SPEED : Ø.27 M/SEC
UPWIND VERTICAL PROFILE
AT 1M : 1.63 M/SEC
AT 3M : 1.94 M/SEC
AT 8M : 2.4Ø M/SEC
U STAR : Ø.Ø74 M/SEC
PERCENT CLOUD COVER :
TEMPERATURE AT 2M : 33.1 DEGREES C
DELTA T AT 1M : -Ø.23 DEGREES C
DELTA T AT 5M : -Ø.Ø4 DEGREES C
DELTA T AT 1ØM : +Ø.Ø3 DEGREES C
DELTA T AT 15M : +Ø.14 DEGREES C
T STAR : Ø.145 DEGREES C
BAROMETRIC PRESSURE : 941.Ø MILLIBARS
UPWIND HUMIDITY (T1) : 4.7%
DOWNWIND HUMIDITY (G4) : 4.5%
TURBULENT PRANDTL NO. : Ø.623
SENSIBLE HEAT FLUX : 2.2 WATT/M2
MOMENTUM DIFFUSIVITY (2M) : Ø.Ø37 M2/SEC
RICHARDSON NO. (2H) : Ø.121
MONIN-OBUKHOV LENGTH : 16.5 M

BURRO 9 Summary Sheet

TEST NAME	: BURRO 9 (LNG-34)
TEST TYPE	: DISPERSION (40 M3)
MATERIAL	: LNG
COMPOSITION	: 83.1% METHANE
	: 13.9% ETHANE
	: 3.00% PROPANE
DATE	: 17 SEPT 1988
VALVE BEGINS TO OPEN	: 18:37:02 PDT
VALVE OPEN (ZERO TIME)	: 18:37:08 PDT
VALVE BEGINS TO CLOSE	: 18:38:21 PDT
VALVE CLOSED	: 18:38:29 PDT
SPILL RATE	: 18.4 M3/MIN
SPILL VOLUME	: 24.2 M3
SPILL DURATION	: 79 SEC
ARRAY CENTERLINE	: 225 DEGREES
AVERAGE WIND DIRECTION	: 232 DEGREES
SIGMA THETA	: 4.4 DEGREES
AVERAGE WIND SPLED	: 5.7 M/SEC
SIGMA SPEED	: 0.74 M/SEC
UPWIND VERTICAL PROFILE	
AT 1M	: 5.29 M/SEC
AT 3M	: 5.94 M/SEC
AT 8M	: 6.49 M/SEC
U STAR	: 0.252 M/SEC
PERCENT CLOUD COVER	: 15%
TEMPERATURE AT 2M	: 35.4 DEGREES C
DELTA T AT 1M	: -0.03 DEGREES C
DELTA T AT 5M	: -0.08 DEGREES C
DELTA T AT 10M	: -0.13 DEGREES C
DELTA T AT 15M	: -0.27 DEGREES C
T STAR	: -0.10 DEGREES C
BAROMETRIC PRESSURE	: 940.0 MILLIBARS
UPWIND HUMIDITY (T1)	: 11.7%
DOWNWIND HUMIDITY (G4)	: 14.4%
TURBULENT PRANDTL NO.	: 1.05
SENSIBLE HEAT FLUX	: -10.0 WATT/M2
MOMENTUM DIFFUSIVITY (2M)	: 0.212 M2/SEC
RICHARDSON NO. (2M)	: -0.014
MONIN-OBUKHOV LENGTH	: -140. M

One can then solve the wind profile equation for the roughness length, $z_0 = 2.05 \times 10^{-4}$ m, which is approximately constant for the China Lake site. The resulting vertical profile is given in the summary sheets. The percent cloud cover was determined roughly from observation. The temperature and ΔT values listed were measured by Lind on a meteorological tower upwind close to T1. Temperature was measured at 2 m and temperature difference was measured between the 2-m sensor and sensors at 1 m, 5 m, 10 m, and 15 m. T_{\star} was calculated by linear regression using the formula

$$T_{\star} = \frac{\partial T}{\partial (\ln z)} \approx \frac{T_2 - T_1}{\ln(z_2/z_1)} .$$

T_{\star} values did not vary significantly during any test. Barometric pressure was measured by Lind, and relative humidity was measured by LLNL upwind at T1 and at seven locations downwind. Both the upwind value and a value typical of the downwind environment into which the LNG vapor disperses are listed here.

The Richardson number, R , was calculated from the relationship

$$R = \frac{\frac{g}{T} \left\{ \frac{\partial T}{\partial z} + \frac{g}{C_p} \right\}}{\left\{ \frac{\partial u}{\partial z} \right\}^2},$$

where $g = 9.8 \text{ m/s}^2$ and $C_p = 1005 \text{ W s kg}^{-1} \text{ }^{\circ}\text{C}^{-1}$. If it is assumed that $R = z/L$, where L is the Monin-Obukhov length, the inverse turbulent Prandtl number, α , and the parameters ϕ and ψ can be expressed as :

$$\left. \begin{aligned} \alpha &= 1/\phi, \\ \phi &= (1 - 16R)^{-1/4}, \\ \psi &\approx 1.1(-R)^{1/2}, \end{aligned} \right\} \quad \text{for } R \leq 0,$$

and

$$\left. \begin{aligned} \alpha &= 1/\phi, \\ \phi &\approx 1 + 5R, \\ \psi &\approx -5R, \end{aligned} \right\} \quad \text{for } R > 0,$$

according to the theory of Dyer and Businger (10, 11), as modified from Lettau (12) with our approximations.

The sensible heat flux, H , defined to be negative upward, is calculated from:

$$H = \rho C_p k \alpha^2 u_*^2 \left\{ T_* + \frac{gz}{C_p} \right\},$$

where $\rho = 1.13 \times 10^{-3} \text{ g/cm}^3$ ($\pm 1\%$ for $30-40^\circ \text{ C}$).

The diabatically adjusted momentum diffusivity, K_m , and the Monin-Obukhov length are calculated from the formulas

$$K_m = u_* k z / \phi,$$

$$L = \frac{u_*^3 / \kappa}{\frac{g}{T} \left\{ \frac{H}{\rho C_p} \right\}}.$$

where $\alpha = K_h / K_m$, where K_h = heat diffusivity.

D. WIND FIELD DATA

One of the major factors influencing the spread of natural gas from an LNG spill is the wind field. This section of the data report is a description of the local wind field that existed during each of the Burro series LNG experiments.

Wind Data

The data used to obtain the local wind field during the experiments are provided by 20 wind data stations distributed upwind and downwind of the spill pond as shown in Fig. 2. These stations measure the horizontal wind speed and direction at an elevation 2 m above the surface. The data at each station are averaged over an interval of 10 seconds and then transmitted to the data recording trailer.

An example of the wind data is shown in Fig. 6. The arrows indicate the wind direction, and their length is proportional to the wind speed. Arrows of a length corresponding to 1 m/s are shown in the lower left corner of the figure. The stations are located at the bases of the arrows adjacent to the station names. The data from the upwind stations W1 through W4 are not shown but were used in the wind field computations and for field operations.

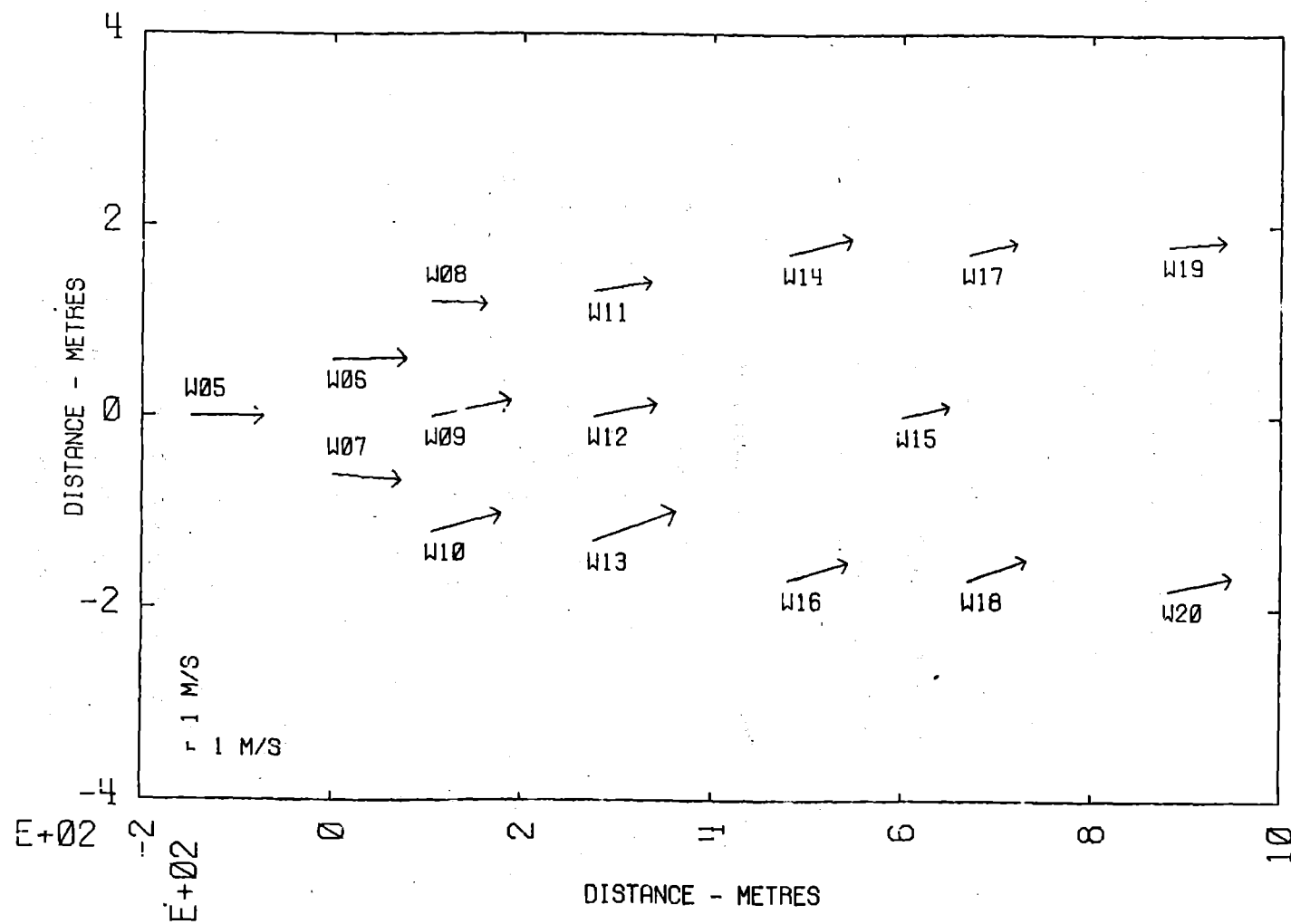
The origin of the coordinate system used in Fig. 6 is shown by the dot between W6 and W7 and is at the center of the spill pond. The horizontal axis at the center of the figure represents the centerline of both the wind and gas station arrays; it is oriented from the southwest (at the left) to the northeast (at the right), corresponding to the most common wind direction at China Lake during the summer months.

General Wind-Field Features

During each of the Burro series of experiments, the wind speed and direction varied significantly with time and position. Some features of this variation are given in Table 3. Columns 2 and 3 of the table contain the full ranges of speed and direction measured at any of the stations during the course of each experiment. Columns 4 and 5 contain the root mean square (RMS) time variances of speed and direction averaged over the stations. These

SITE: CHINA LAKE

TIME: 100 SEC.



WIND MEASUREMENTS AT 2. METRES
ABOVE TOPOGRAPHY

Fig. 6.

TABLE 3. Wind Field Variability During the Burro Series LNG Spill Experiments

Burro	Speed Range (m/s)	Direction Range (degrees)	RMS Variability in		Wind Speed Tendency	Non-Operating Wind Station Numbers (W :)
			Speed	Direction		
2	1.2-10.4	179-261	33%	14 deg	decreasing	1, 19, 20
3	1.0- 9.7	169-293	22%	13 deg	fairly constant	1, 19, 20
4	4.6-13.8	195-240	13%	7 deg	fairly constant	1, 12, 19, 20
5	3.8-11.7	187-247	15%	11 deg	fairly constant	1, 19, 20
6	5.3-12.3	202-244	12%	7 deg	fairly constant	none
7	4.6-12.4	189-226	14%	5 deg	nearly constant	none
8	0.2- 3.1	180-270	15%	6 deg	decreasing	20
9	2.5-8.4	214-249	13%	4 deg	slowly decreasing	20

(Angles for wind direction are measured clockwise from true north to the direction from which the wind is blowing.)

(Input data are 10-second averages of speed and direction)

figures are the same as the values of "sigma speed" and "sigma theta" given earlier in this report except for rounding and the fact that the speed variance has been reexpressed as a percent variance relative to the average speed. The variances of speed and direction over the stations (space variation) when averaged over time were about the same as the time variances for each of the experiments and are not shown. The general tendency of wind speed during each experiment is indicated qualitatively in column 6.

Specific Wind-Field Features--Flowlines

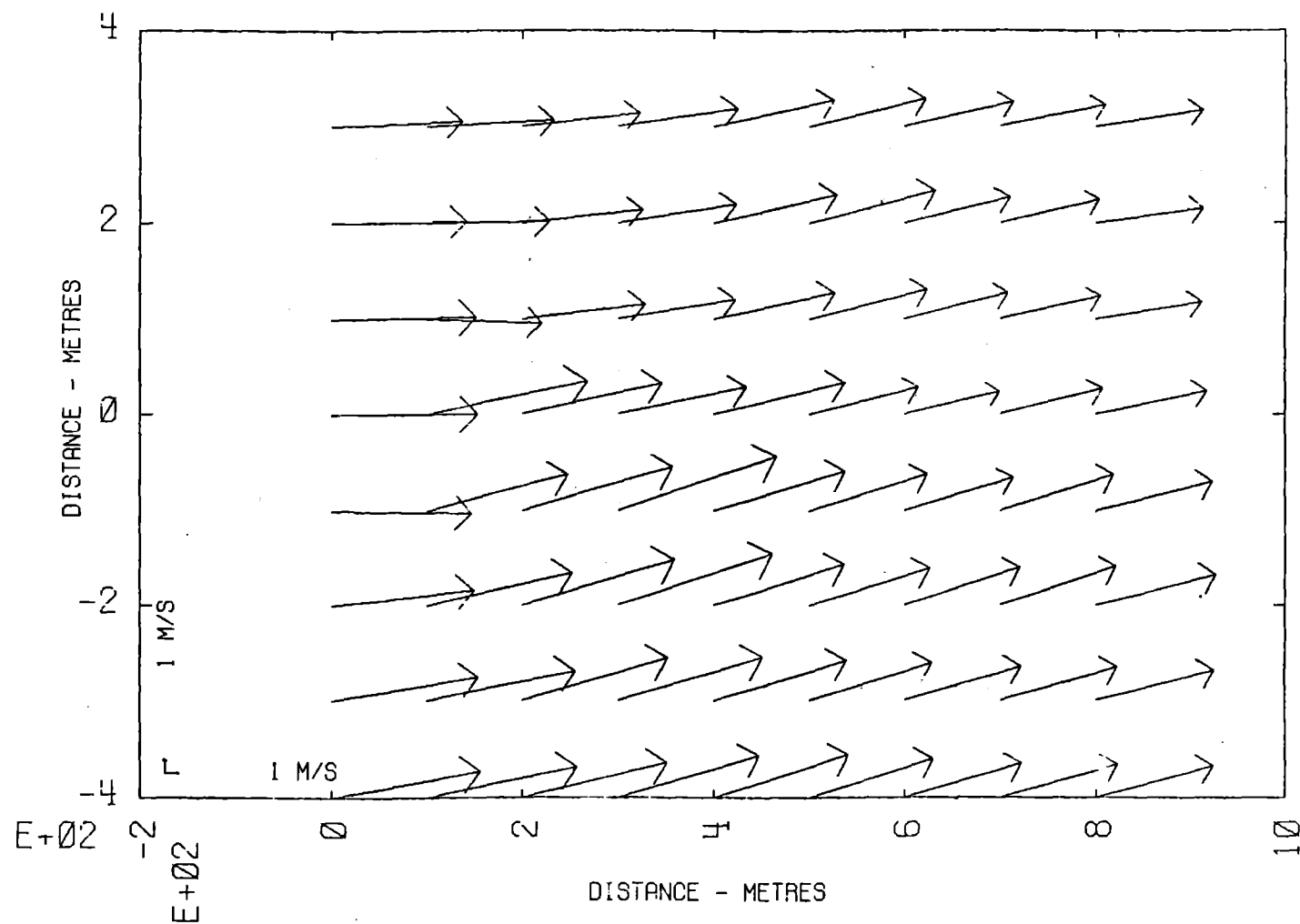
The specific features of the wind field at 60-second intervals for each of the Burro experiments are presented in Appendix 1. Burro 2 through Burro 9 involved spills of LNG. Burro 1 was a test spill of liquid nitrogen. The presentation consists of a series of figures for each Burro experiment. For the most part each series consists of pairs of figures. The first figure of a pair contains the basic data. In the second figure, we present the flowlines (explained below) which are derived from the basic data.

The basic data consists of the 10-second averages of wind speed and direction described earlier. This data is given for the time of the spill (time = 0 s) and for each minute thereafter up to a time which, except for Burro 8, exceeds the duration of the experiment. Each of these figures is similar in format to Fig. 6. Stations not operating are listed in Table 3 and do not appear in the figures.

The wind field data are used to derive (to a good approximation) the values of wind speed and direction on a uniform grid of points in the vicinity of the wind data station array. An example of such a calculation is shown in Fig. 7 where the data depicted in Fig. 6 was employed. At other points within the grid, values of wind speed and direction are determined by interpolation. These calculations are performed using the ATMAS code (13) for all times within the duration of each experiment, and are used to obtain the flowlines.

SITE: CHINA LAKE

TIME: 100 SEC.



MATHW GRID WIND FIELD AT 2. METRES
ABOVE TOPOGRAPHY

Fig. 7

An example of flowlines is shown in Figs. 8 and 9. In Fig. 8 the scale is the same as in Figs. 6 and 7. In Fig. 9 the scale has been expanded by a factor of two. The expanded scale is employed in the concentration contour plots, which are presented later in Appendix 2. The square at the origin of each figure is roughly the size of the spill pond. The center flowline is generated by emitting a pseudo particle (conceptually, using ATMAS) from the center of the spill pond every 2.5 seconds. Each pseudo particle then flows with the calculated wind field. The positions of these particles, marked by X's superimposed on O's, constitute the central flowline. The rightmost particle of the central flowline, which may be seen in Fig. 8, was emitted at the time the spill began (time = 0 seconds), while the leftmost particle was emitted 97.5 seconds after the spill began (2.5 seconds before 100 seconds, the time at which the flowline is shown). Thus the central flowline represents the course of a nondiffusing, horizontal tracer emitted from the center of the spill pond. In a similar manner the other flowlines are generated by emitting pseudo particles from points above (northwest of) and below (southeast of) the center of the spill pond at intervals of 100 metres. The positions of these particles are marked with O's with dots (sometimes invisible in the figures) at their centers. Figure 8 shows the total of five flowlines thereby generated, while Fig. 9 shows the central three of these. Also shown in these figures is the area occupied by the gas sensor array. The border of the area is indicated by dashed lines, and the positions of the individual sensors are indicated by dots. The full array is shown in Fig. 8, while in Fig. 9 the most distant arc of gas sensors falls beyond the right edge.

A wind field whose direction was uniform in time and space would give rise to straight, parallel flowlines. If, in addition, its speed were likewise constant, the particle positions would be equally separated along each flowline.

SITE: CHINA LAKE

TIME: 100 SEC.

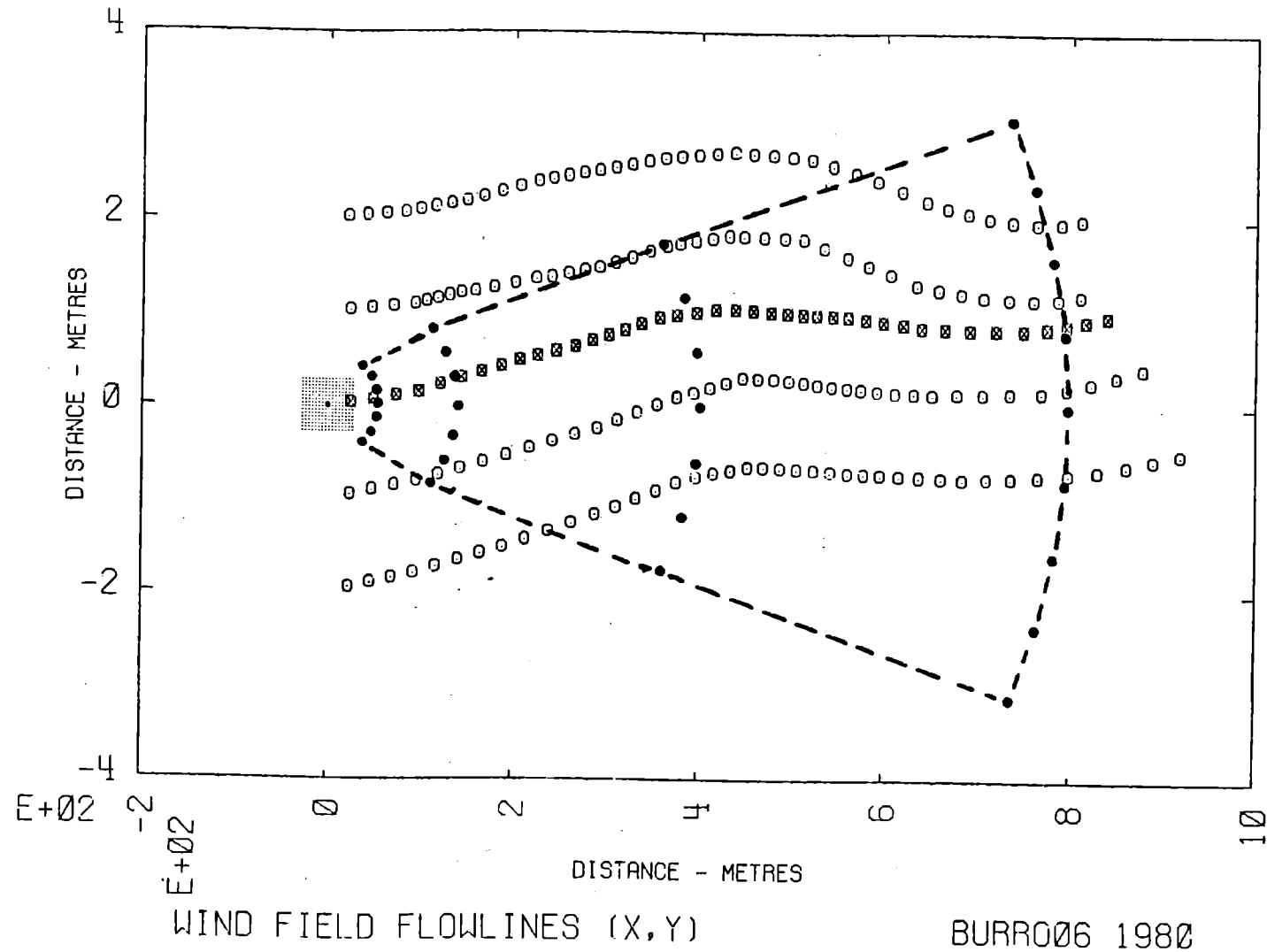


Fig. 8

SITE: CHINA LAKE

TIME: 100 SEC.

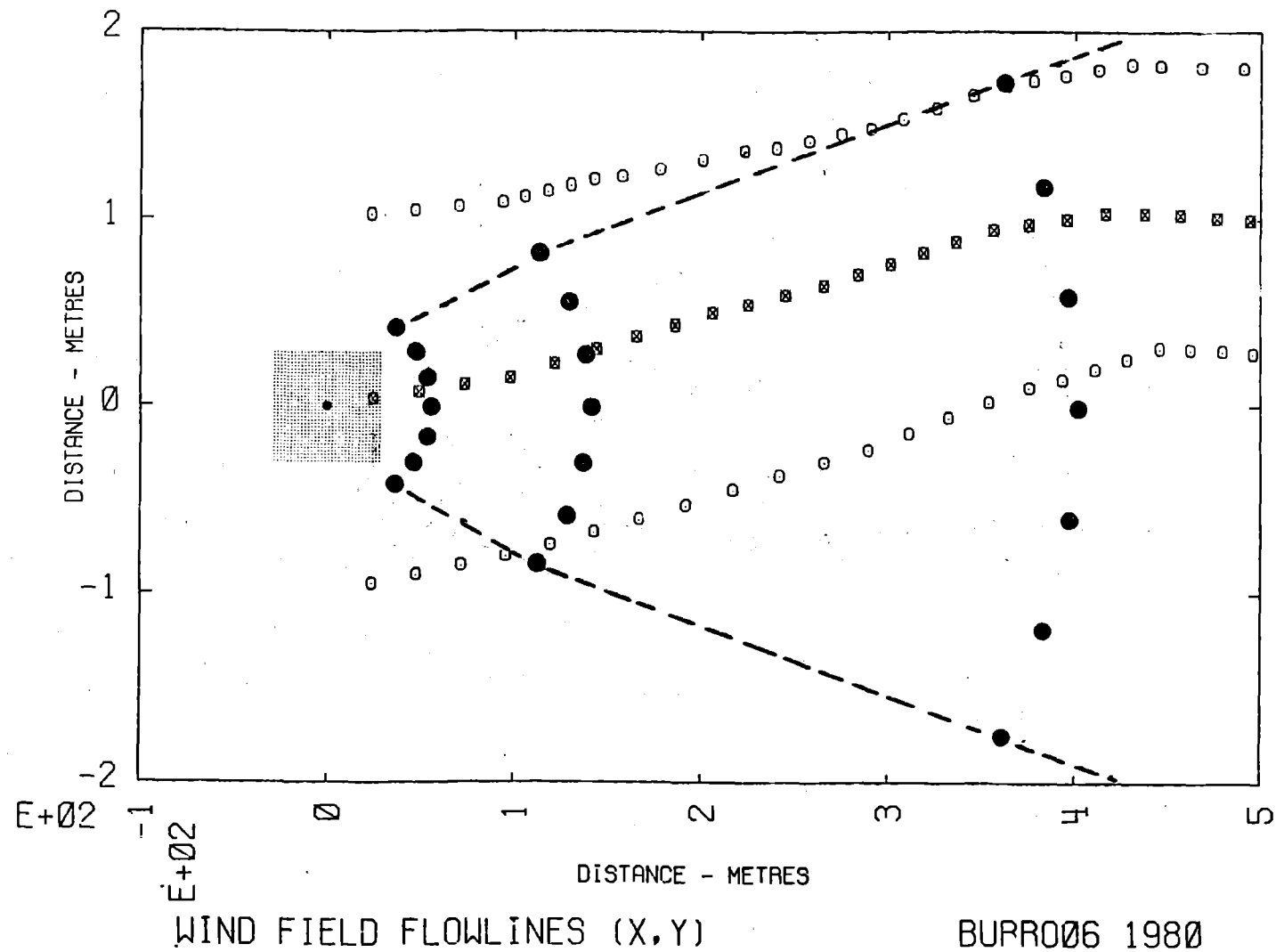
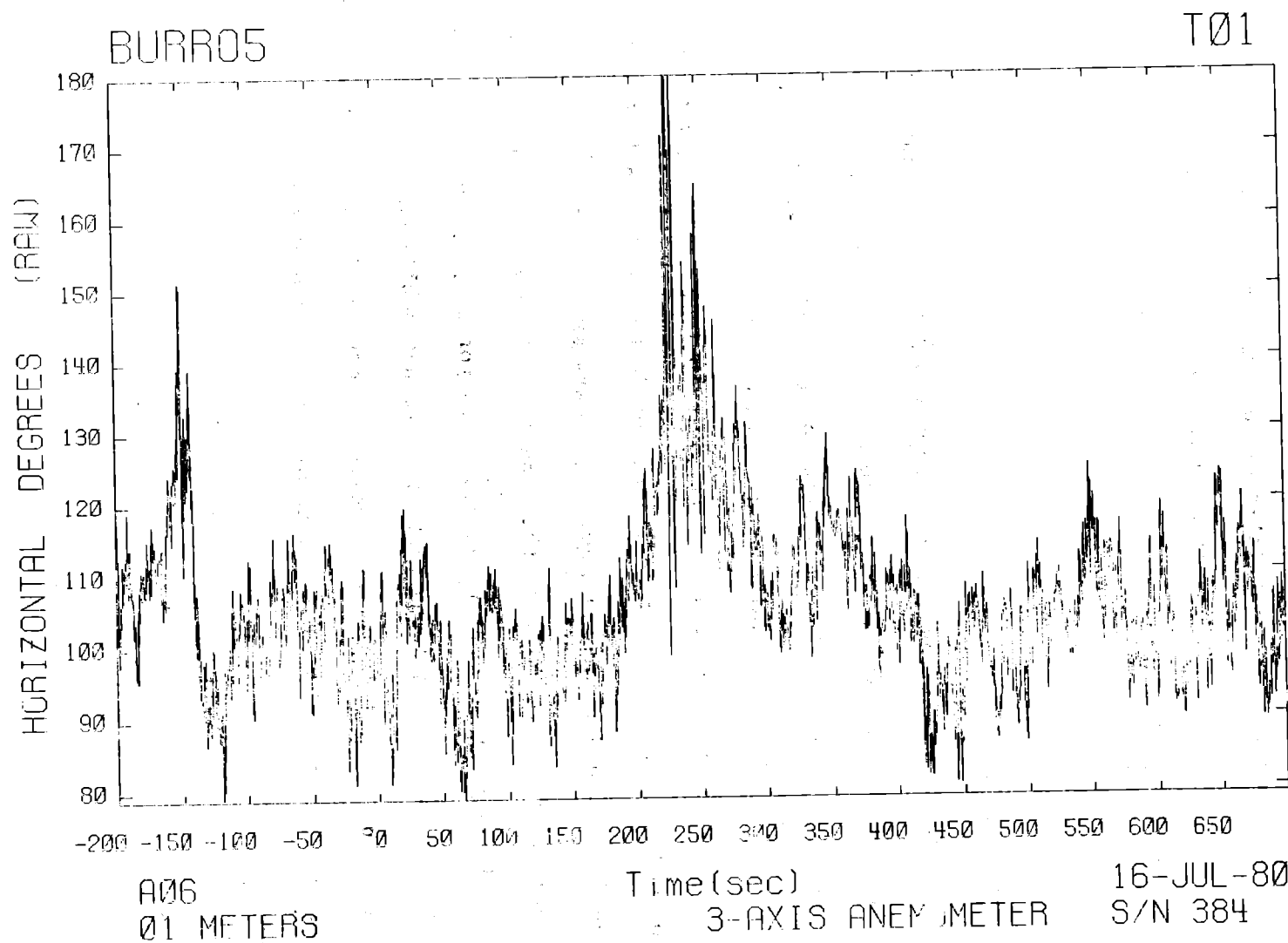


Fig. 9

The flowlines are shown for the Burro experiments in Appendix 1, for one minute after each spill and at intervals of one minute thereafter, up to a time following or near the end of the experiment. The expanded scale of Fig. 9 is employed for all tests.

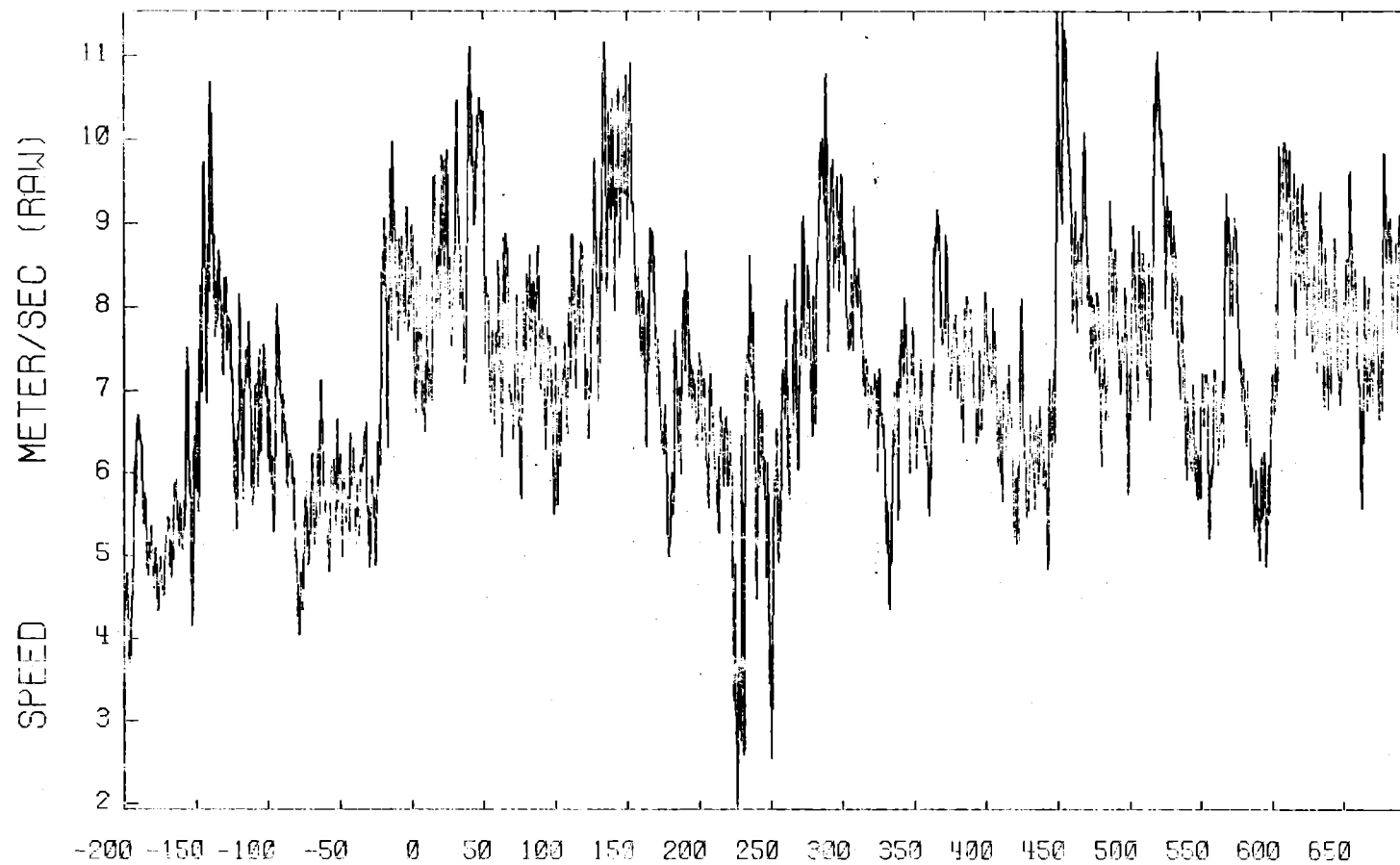
E. TURBULENCE DATA

The turbulence stations collected high-speed (3 - 5 Hz) data from gas sensors, bivariate anemometers, and thermocouples. The gas sensor and thermocouple data are presented in the section on gas concentration after averaging for 10 s. This section contains data from the bivariate anemometers at the 1.36 m, 3 m, and 8 m levels for stations T1 (50 m upwind), and T2 (57 m downwind) for Burros 5, 7, 8, and 9. In addition, for Burro 8 the data from turbulence stations T3, T4, and T5 are included. The data are presented in terms of the horizontal direction in degrees, the wind speed in m/sec, and the vertical direction in degrees, at each position. Data for the stations T3 - T5 are generally available for all the tests but are not published here because of the large quantity of information involved. Vertical direction data at the 3-m level for station T2 on Burro 5 is missing because of problems with the instrument.



BURR05

T01



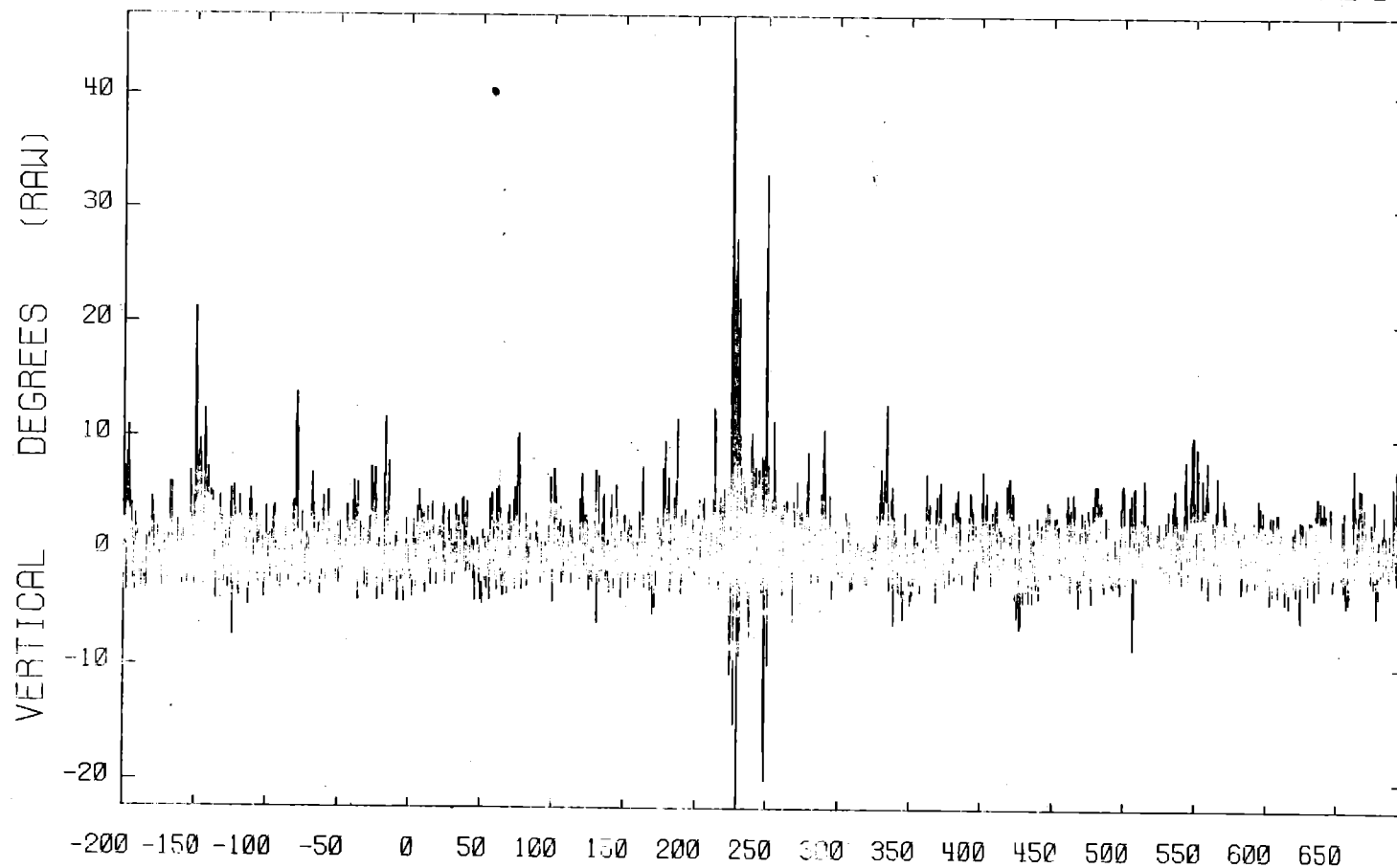
A07
01 METERS

Time(sec)
3-AXIS ANEMOMETER

16-JUL-80
S/N 384

BURR05

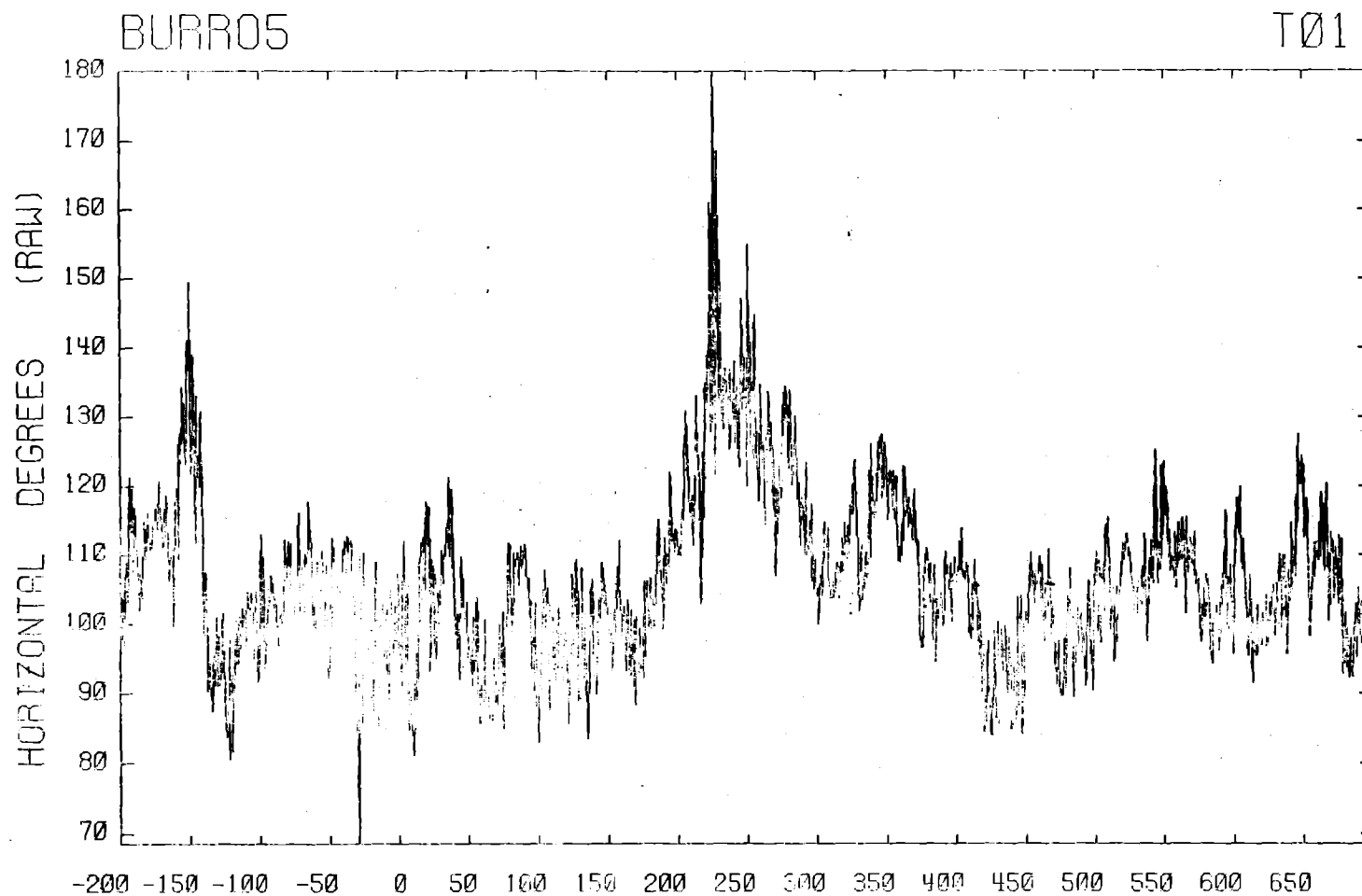
T01



A08
01 METERS

Time(sec)
3-AXIS ANEMOMETER

16-JUL-80
S/N 384



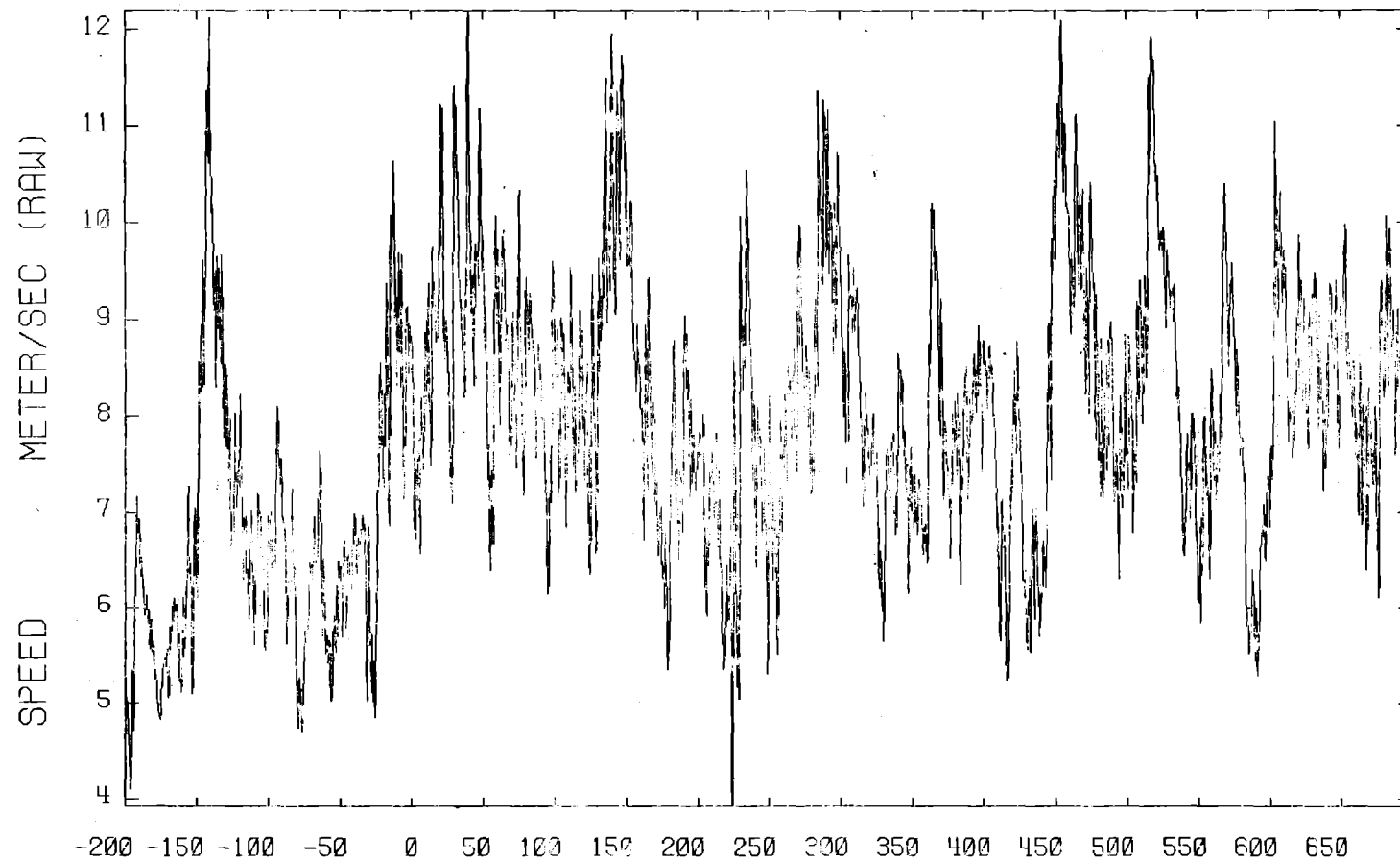
A09
03 METERS

Time(sec)
3-AXIS ANEMOMETER

16-JUL-80
S/N 387

BURR05

T01



A10

03 METERS

Time(sec)

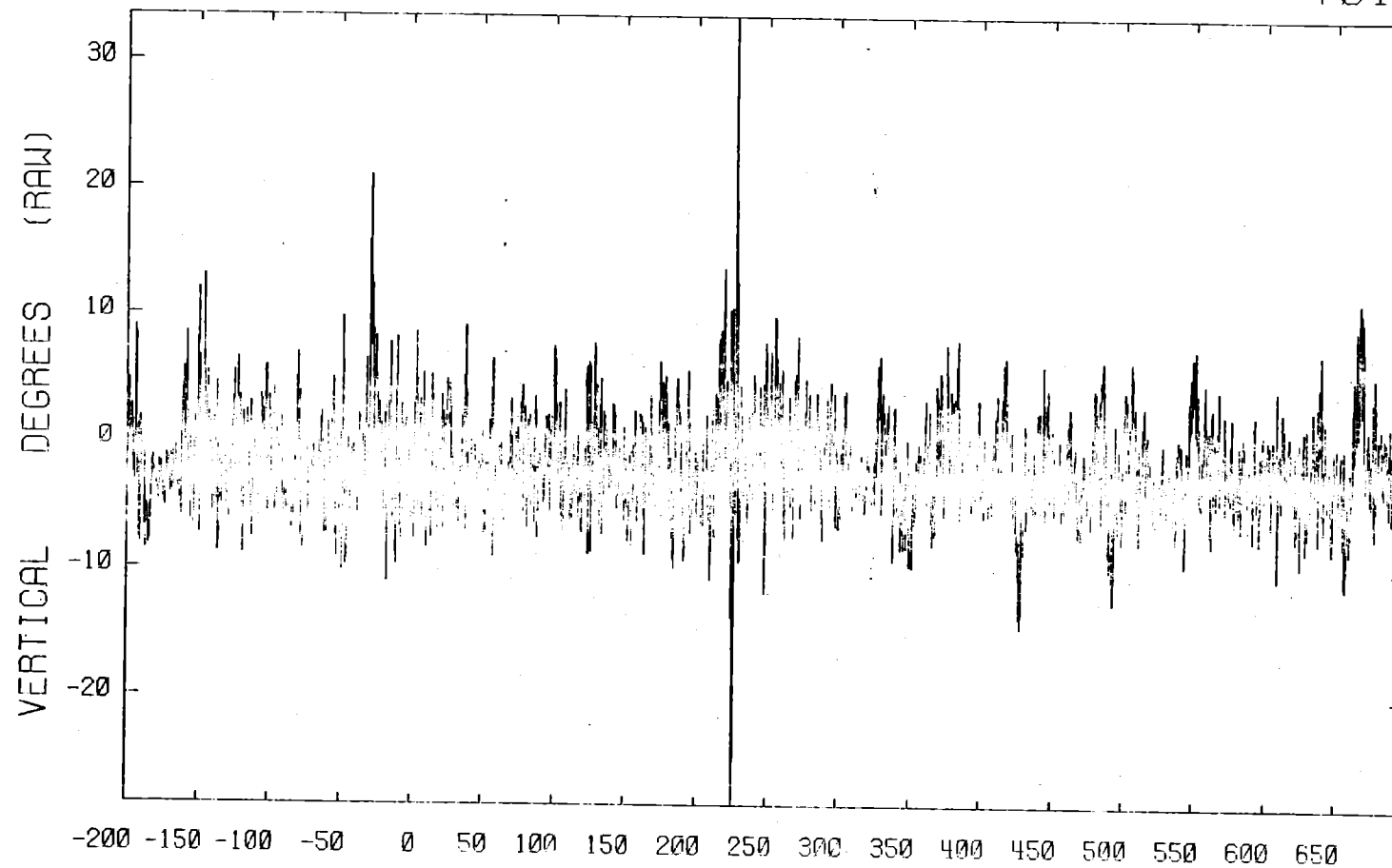
3-AXIS ANEMOMETER

16-JUL-80

S/N 387

BURR05

T01



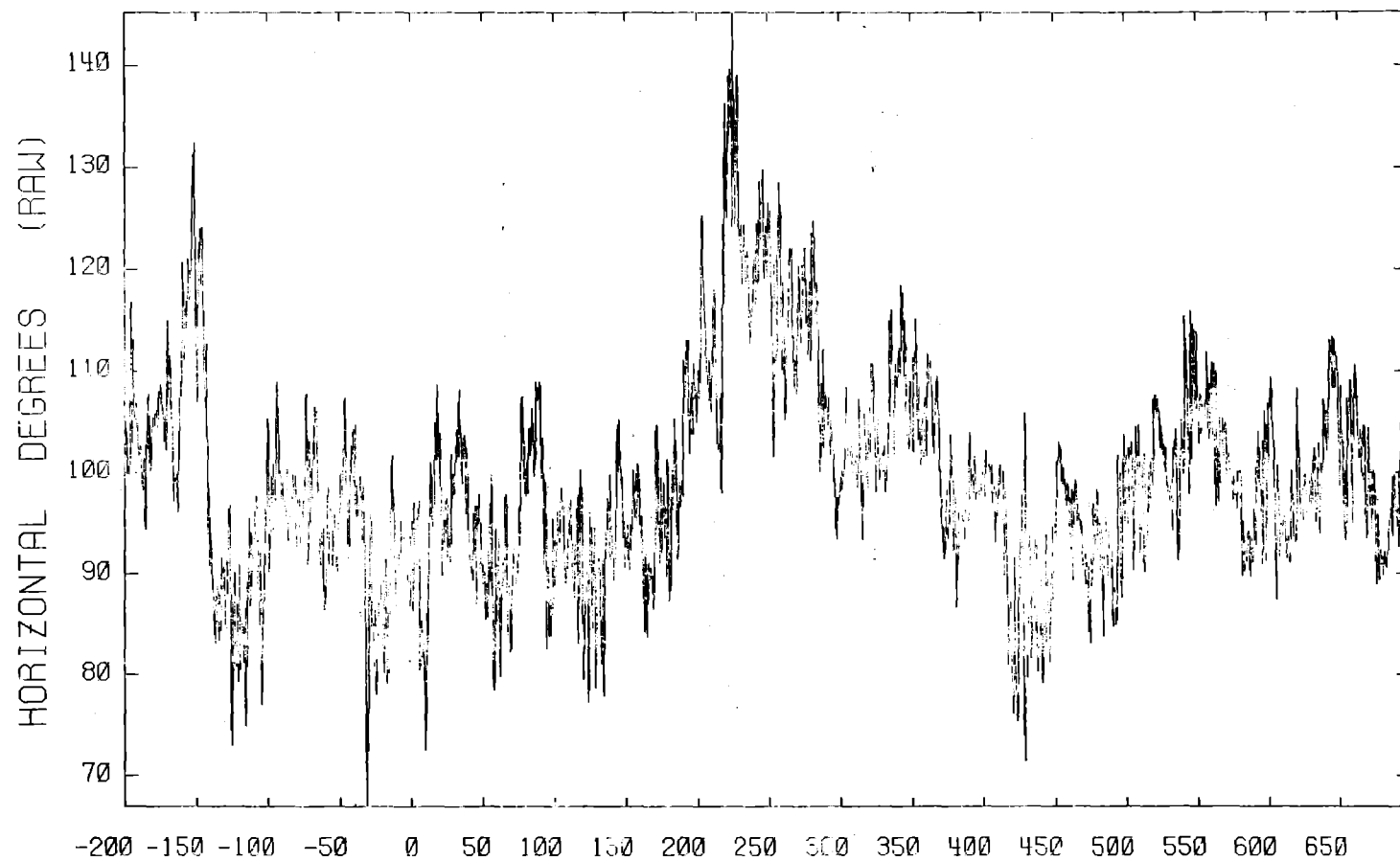
A11
03 METERS

Time(sec)
3-AXIS ANEMOMETER

16-JUL-80
S/N 387

BURR05

T01



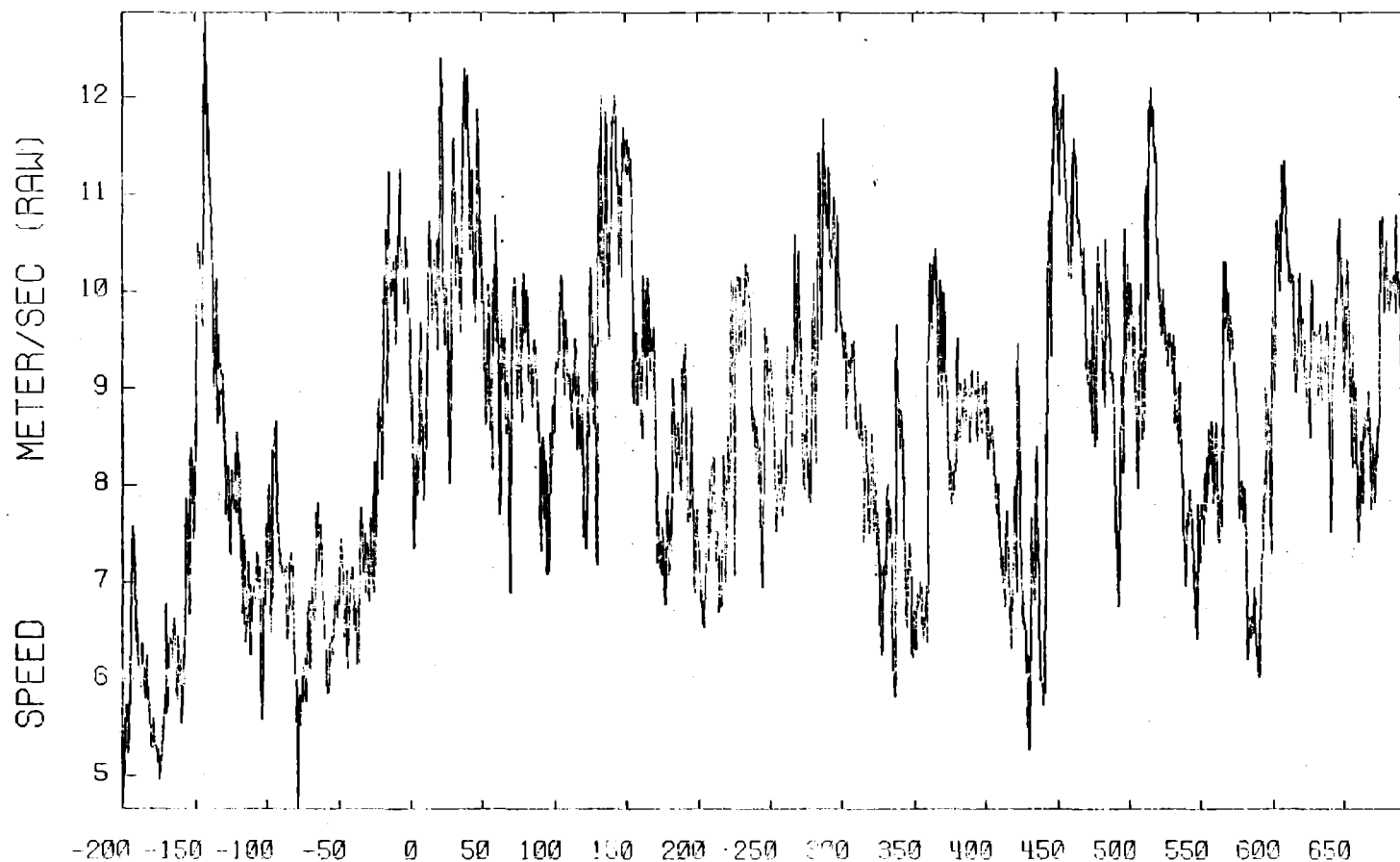
A12
08 METERS

Time(sec)
3-AXIS ANEMOMETER

16-JUL-80
S/N 376

BURR05

T01



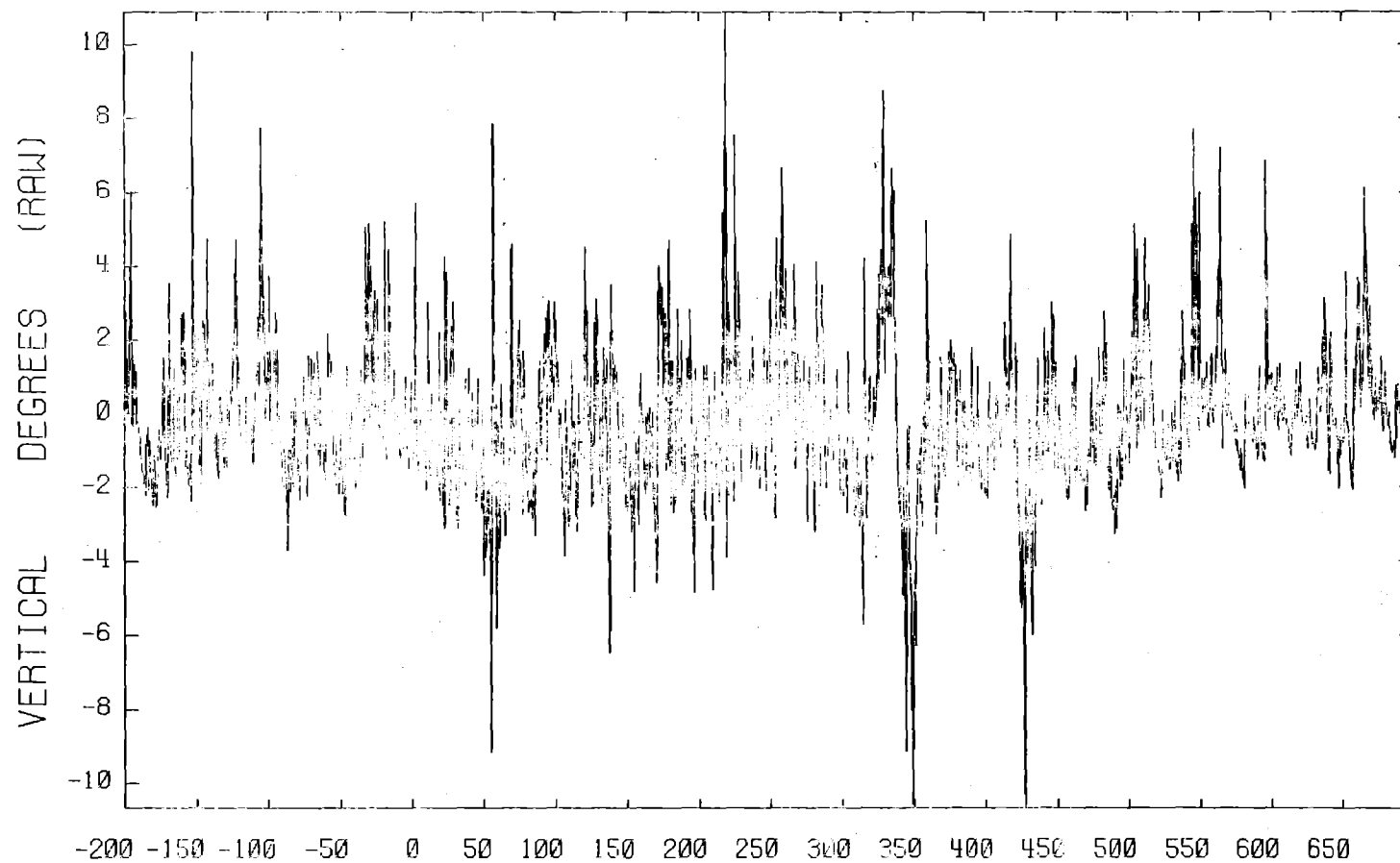
A13
08 METERS

Time(sec)
3-AXIS ANEMOMETER

16-JUL-80
S/N 376

BURR05

T01



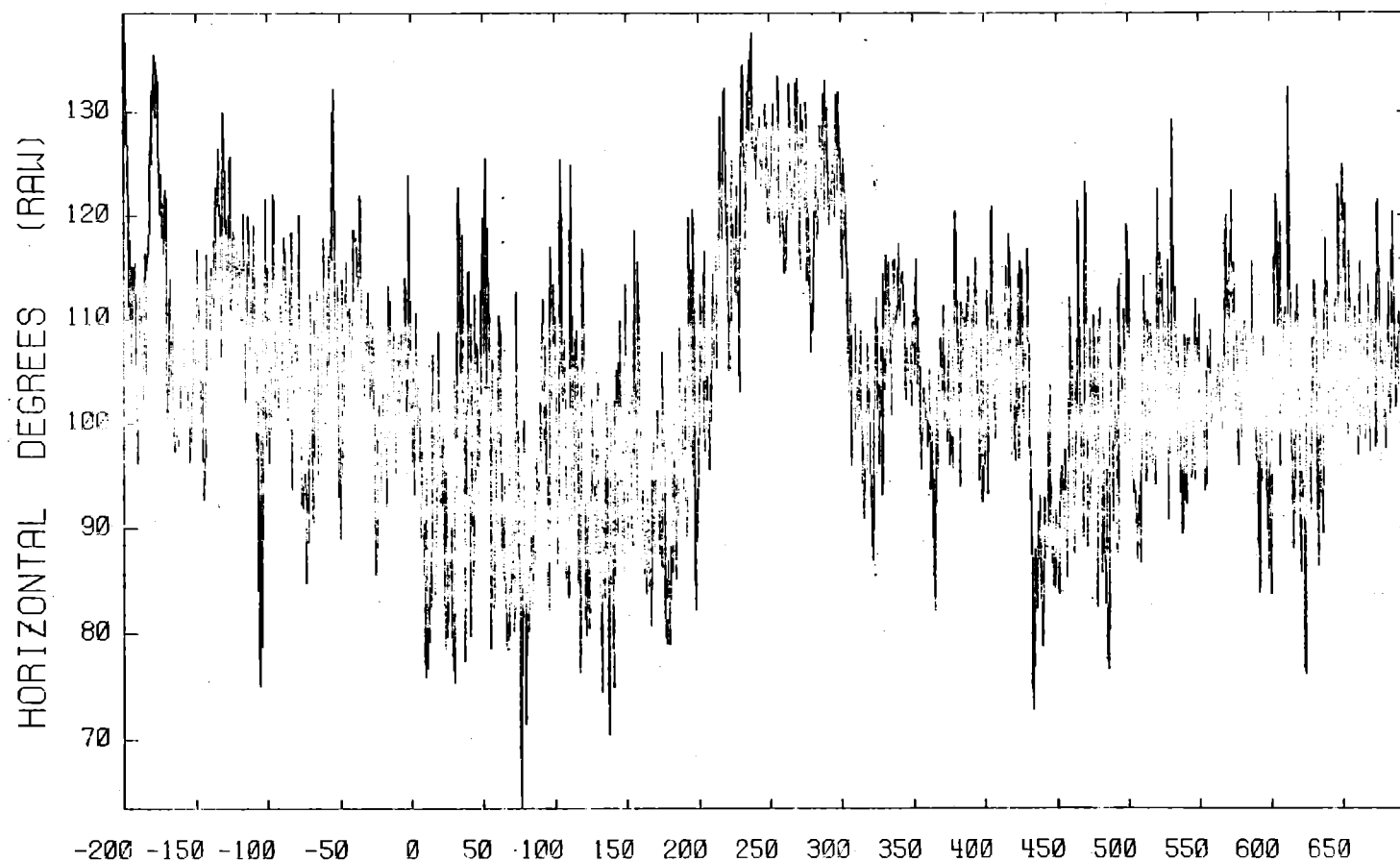
A14
08 METERS

Time(sec)
3-AXIS ANEMOMETER

16-JUL-80
S/N 376

BUR005

T02



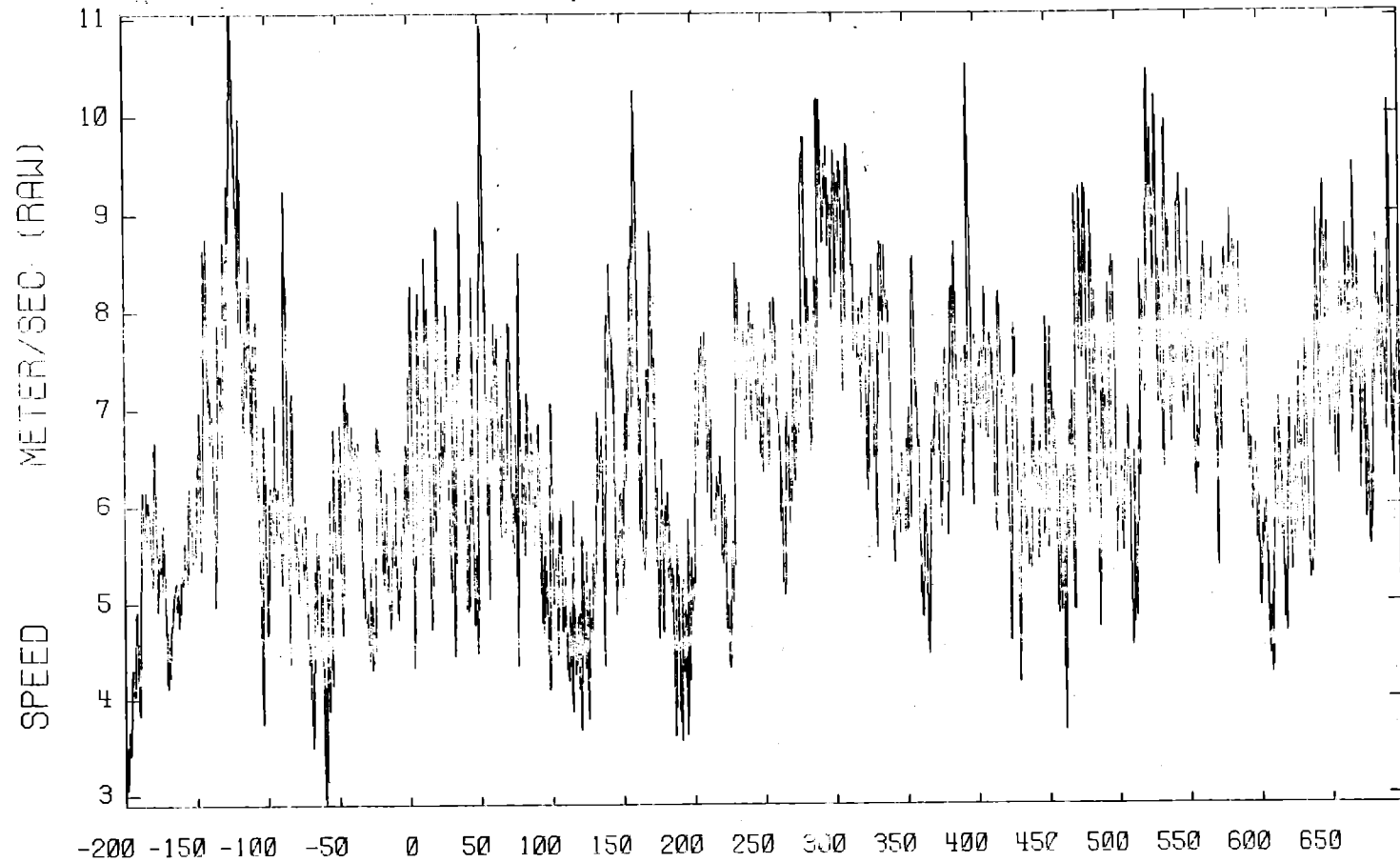
A06
01 METERS

Time(sec)
3-AXIS ANEMOMETER

16-JUL-80
S/N 386

BUR005

T02



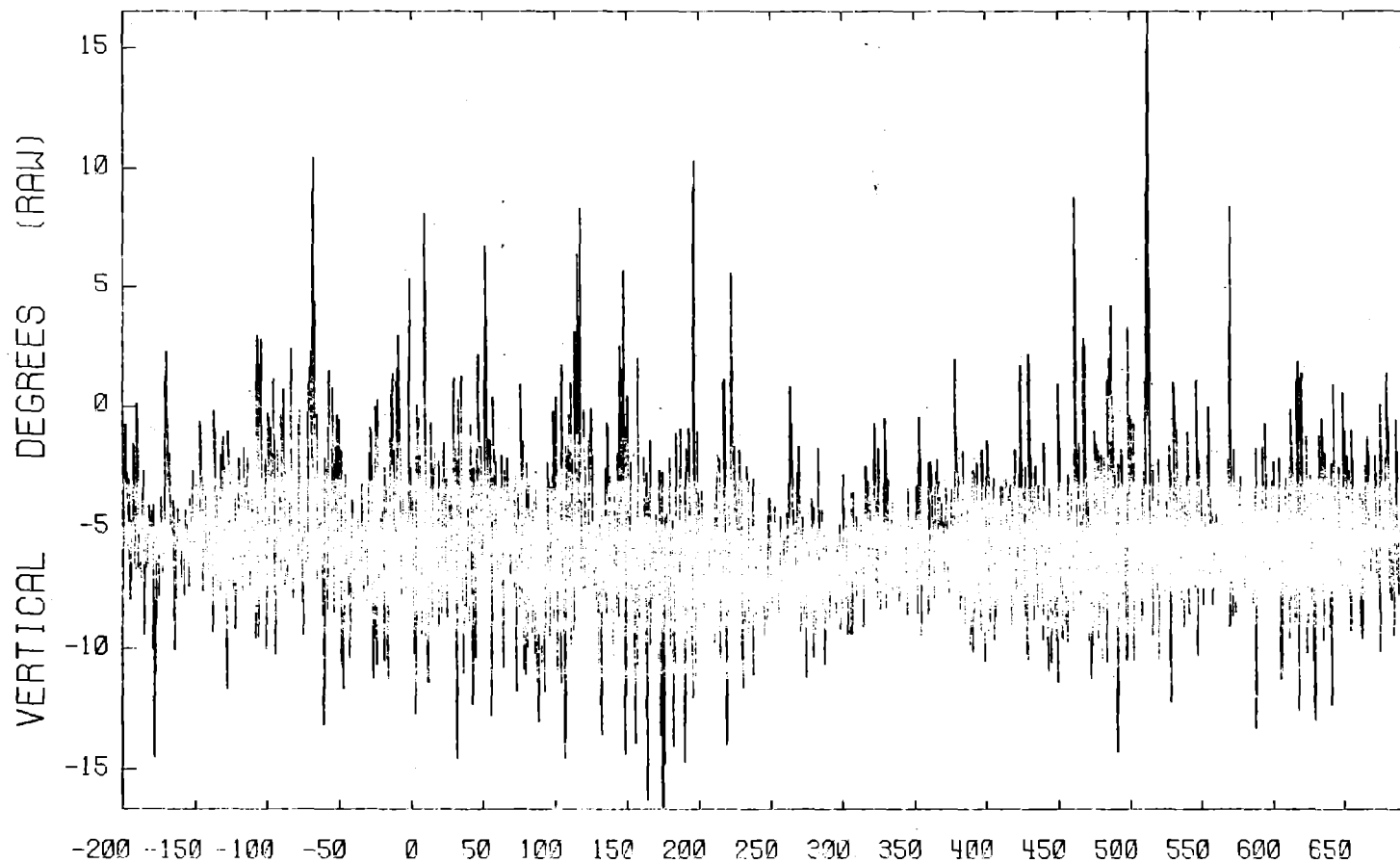
A07
01 METERS

3-AXIS ANEMOMETER

16-JUL-80
S/N 386

BUR005

T02



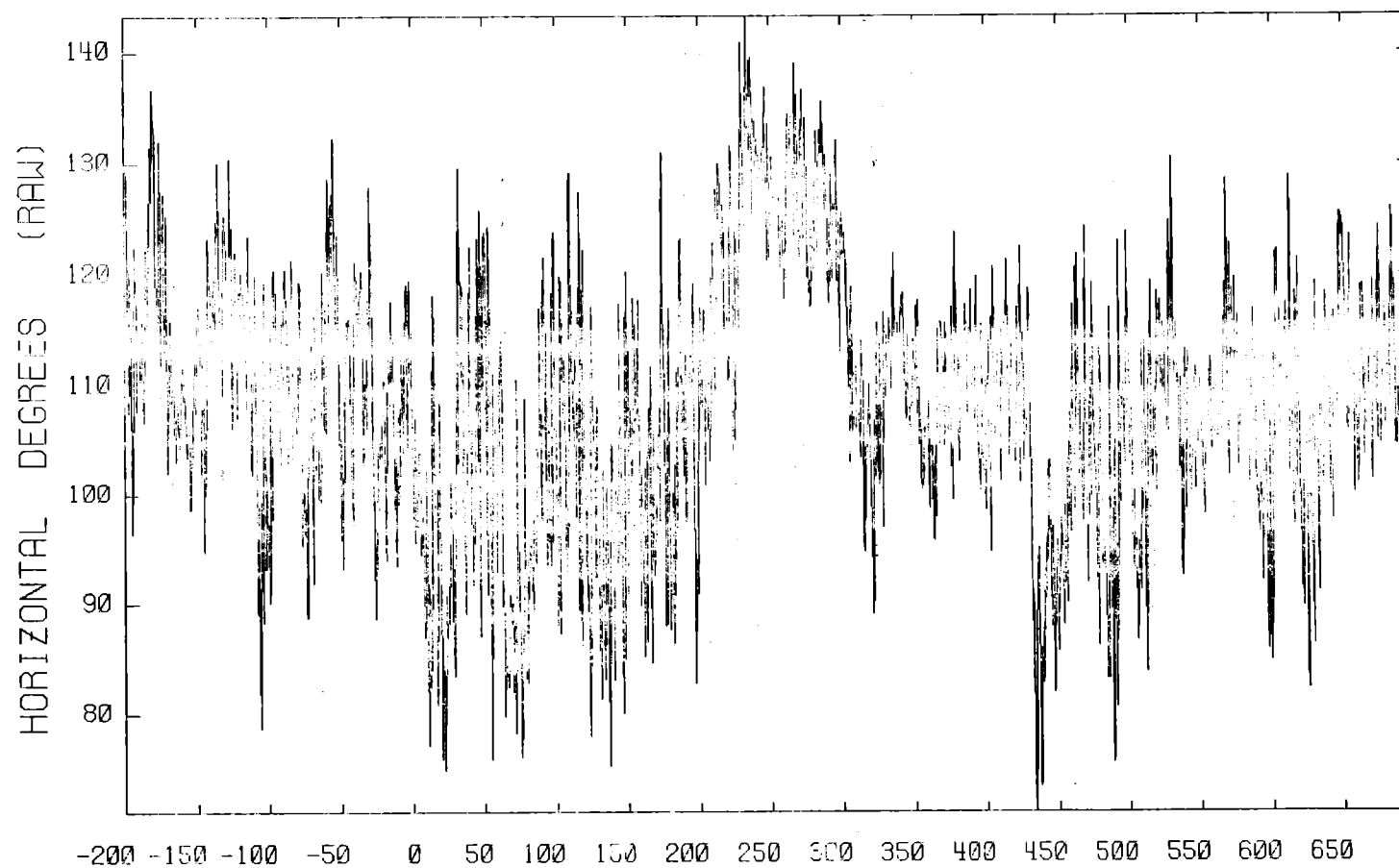
A08
01 METERS

Time(sec)
3-AXIS ANEMOMETER

16-JUL-80
S/N 386

BUR005

T02



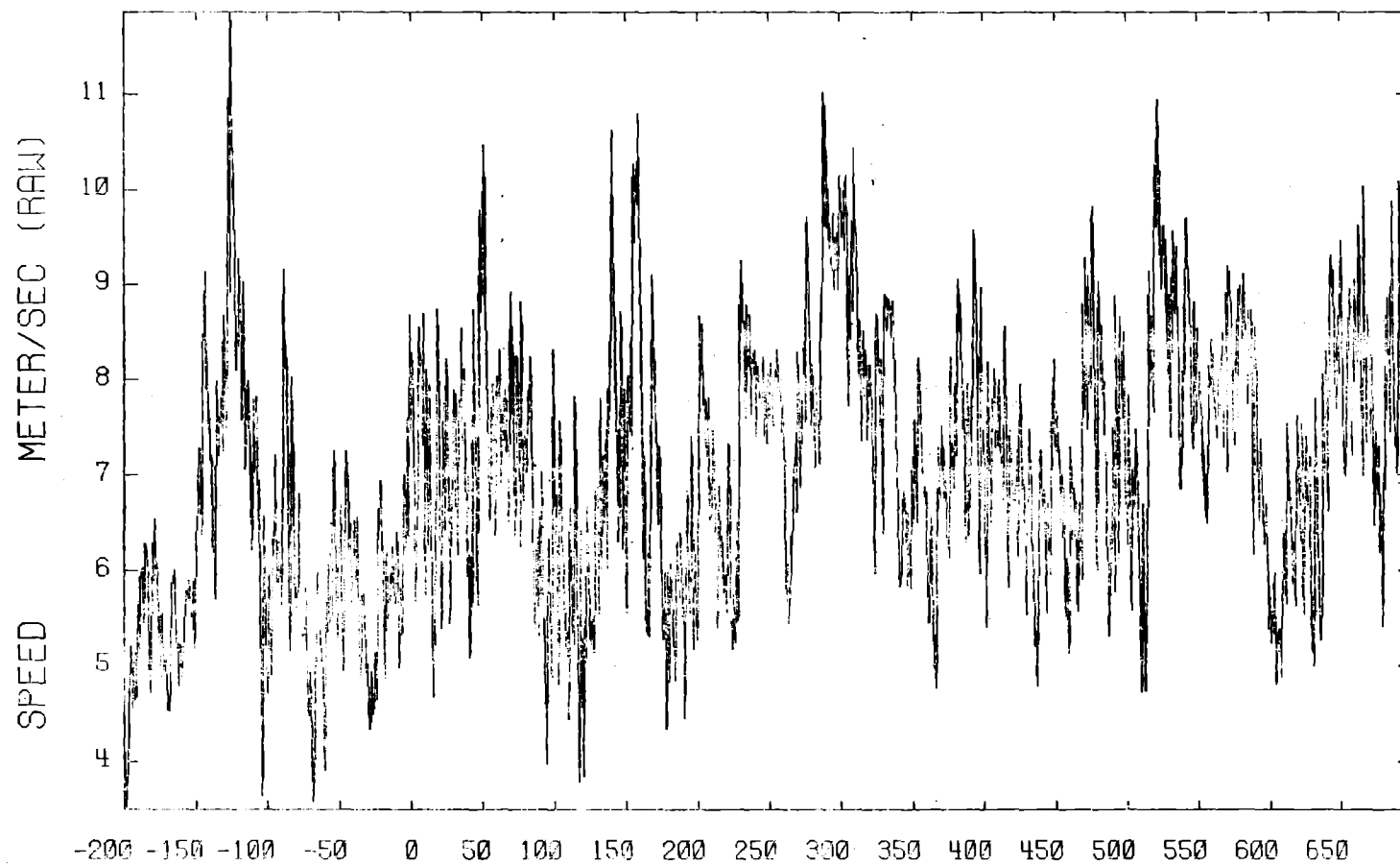
A09
03 METERS

Time(sec)
3-AXIS ANEMOMETER

16-JUL-80
S/N 381

BUR005

T02



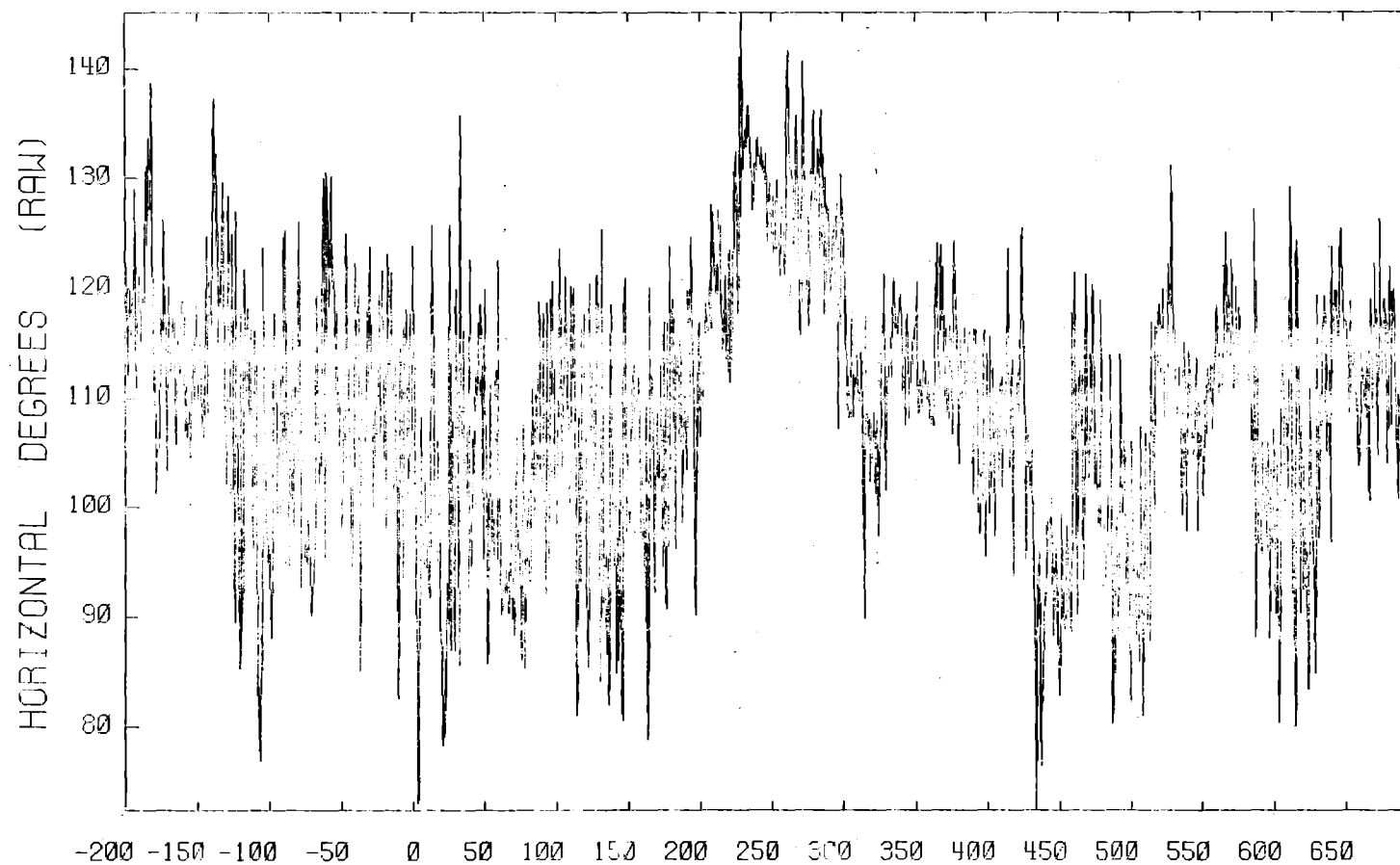
A10
03 METERS

Time(sec)
3-AXIS ANEMOMETER

16-JUL-80
S/N 381

BUR005

T02



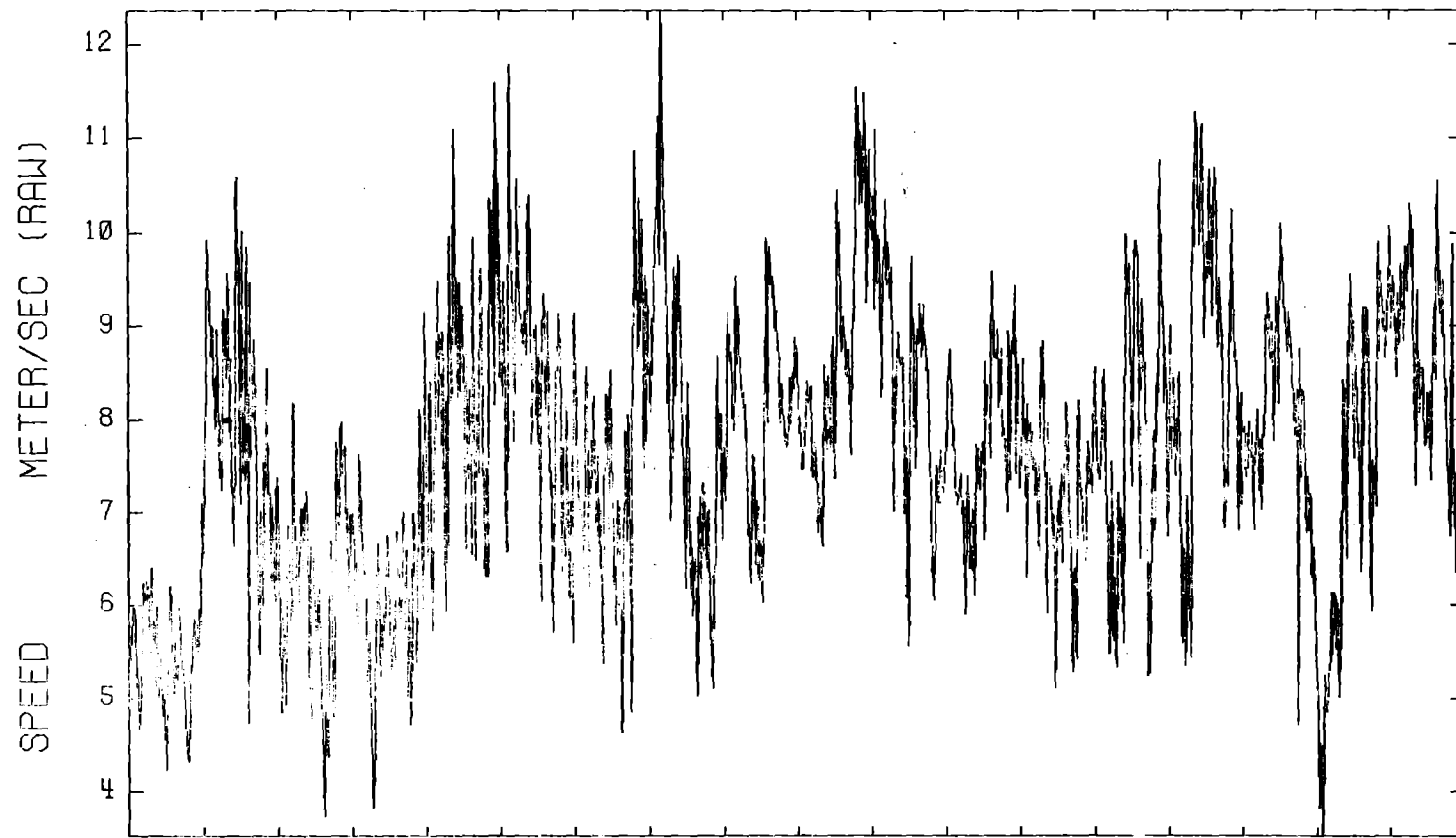
A12
08 METERS

Time(sec)
3-AXIS ANEMOMETER

16-JUL-80
S/N 380

BUR005

T02



-200 -150 -100 -50 0 50 100 150 200 250 300 350 400 450 500 550 600 650

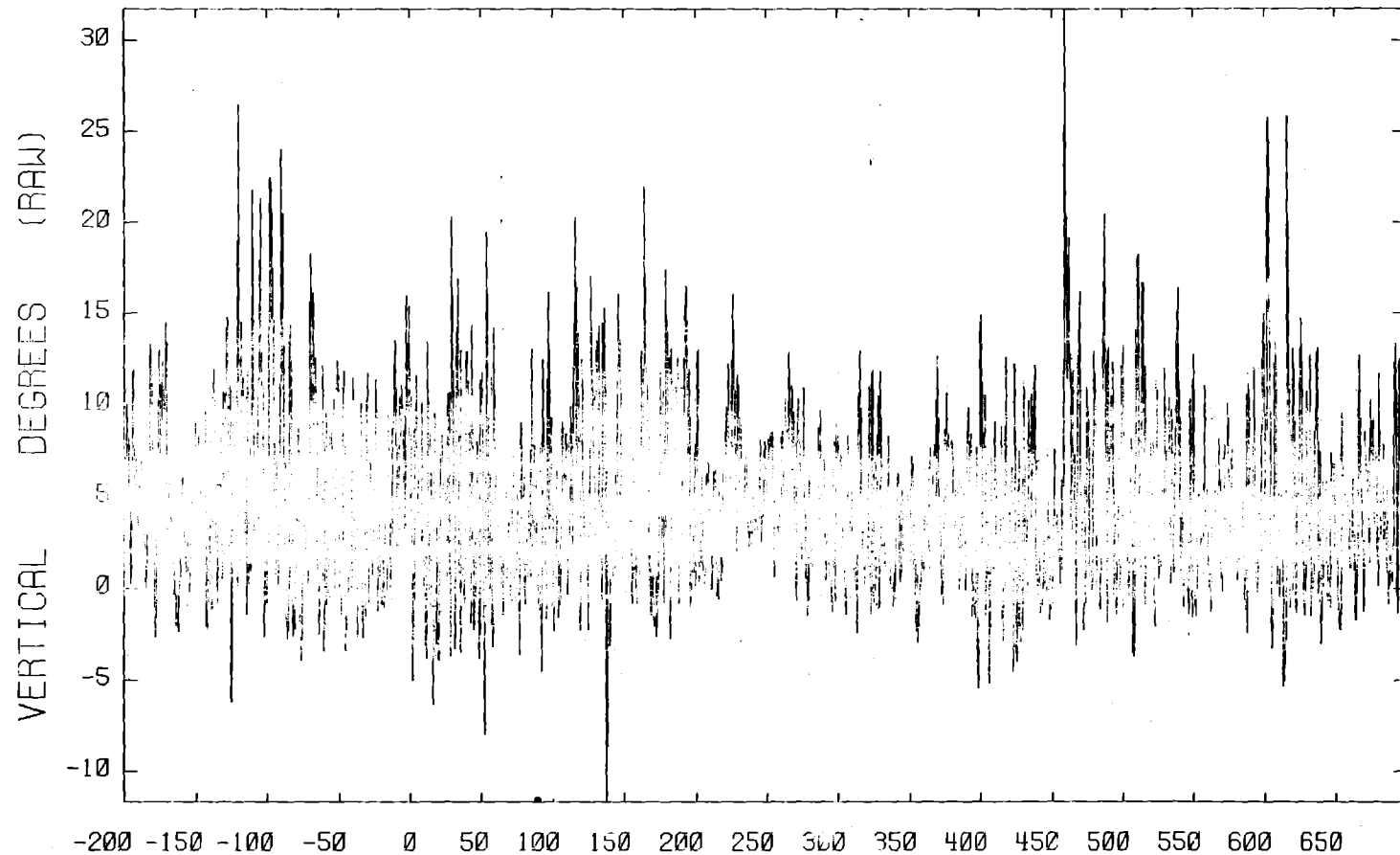
A13
08 METERS

Time(sec)
3-AXIS ANEMOMETER

16-JUL-80
S/N 380

BUR005

T02



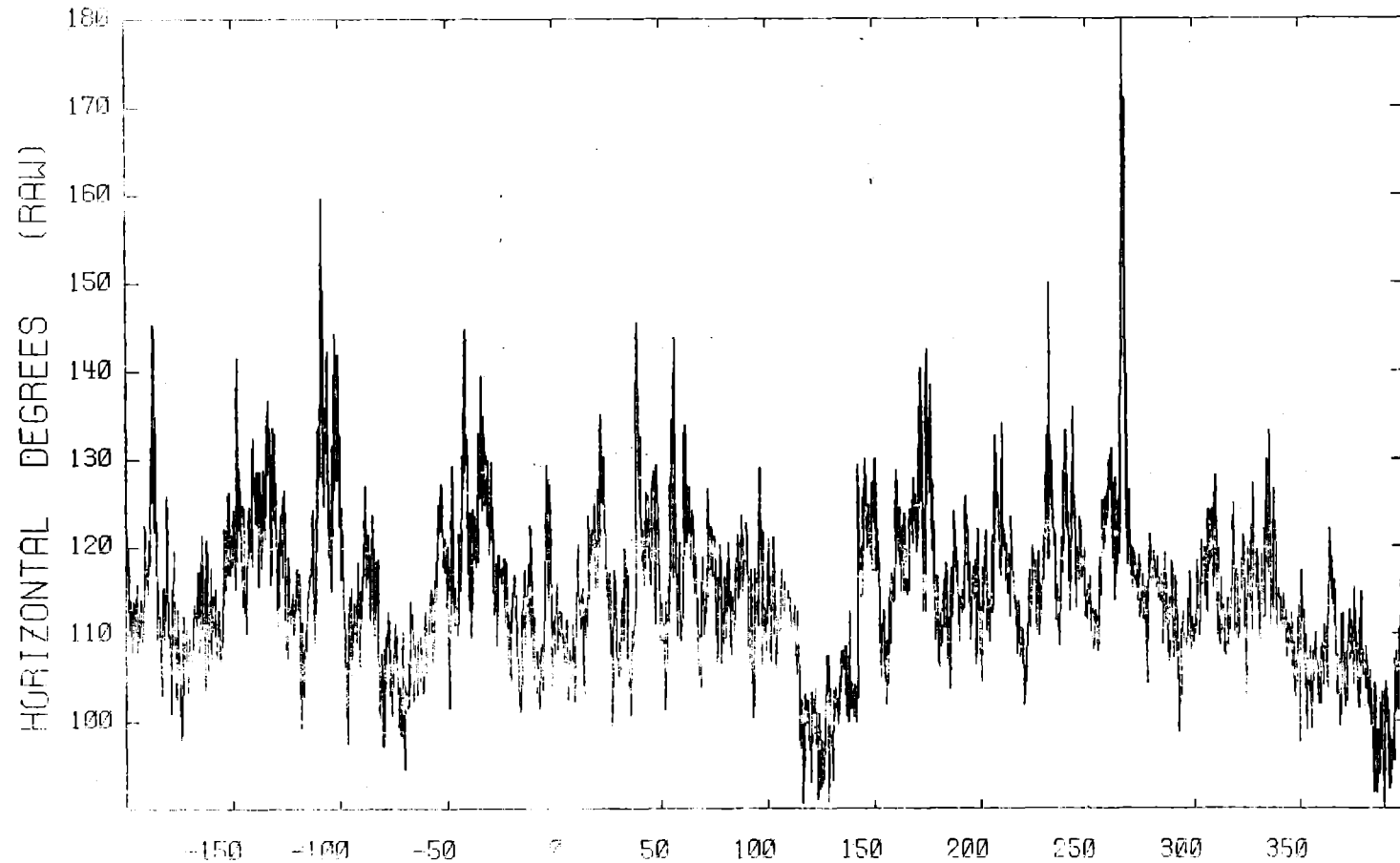
A14
08 METERS

Time(sec)
3-AXIS ANEMOMETER

16-JUL-80
S/N 380

RUR007

T01



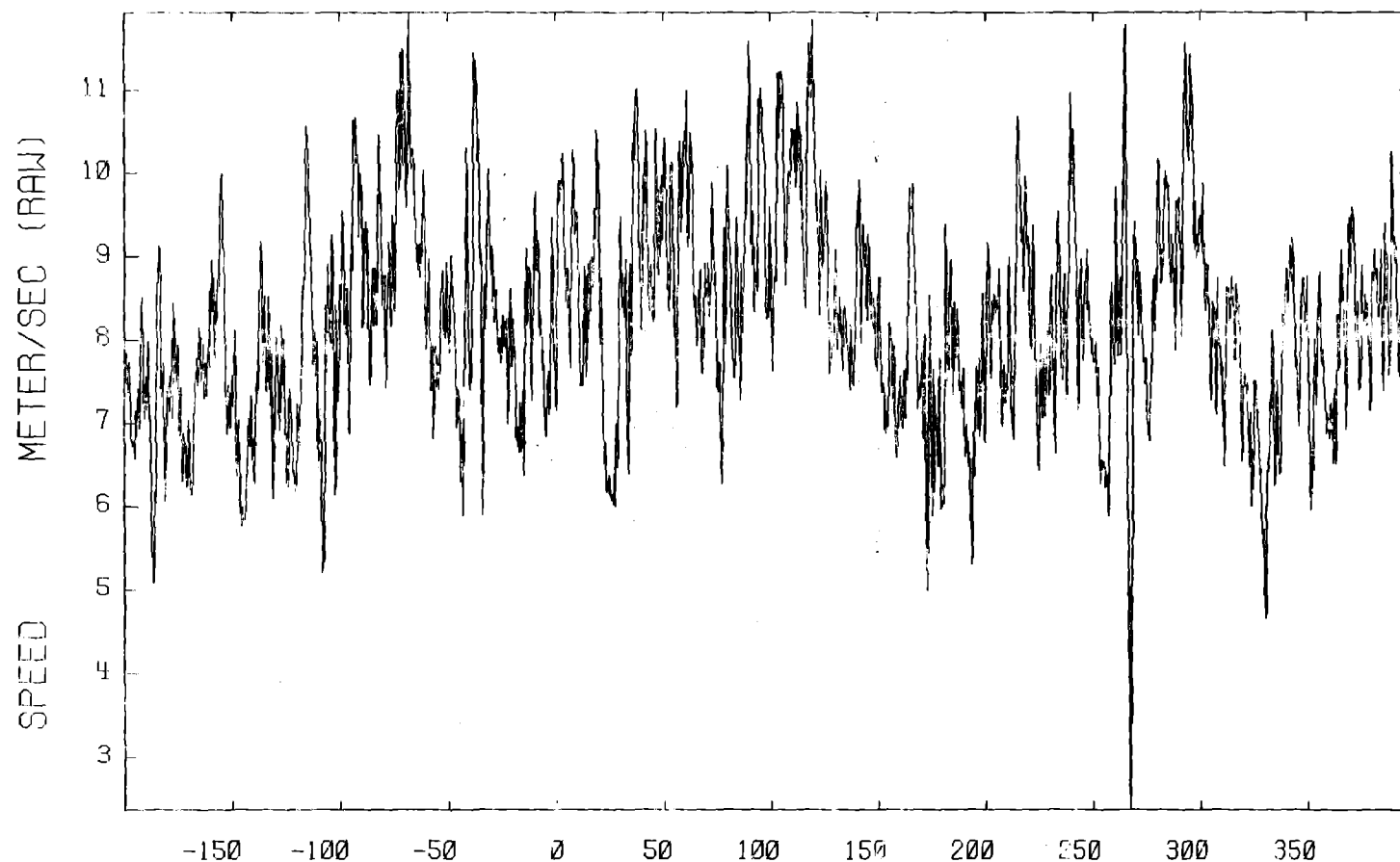
A06
01 METERS

3-AXIS ANEMOMETER

27-AUG-80
S/N 384

BUR007

T01



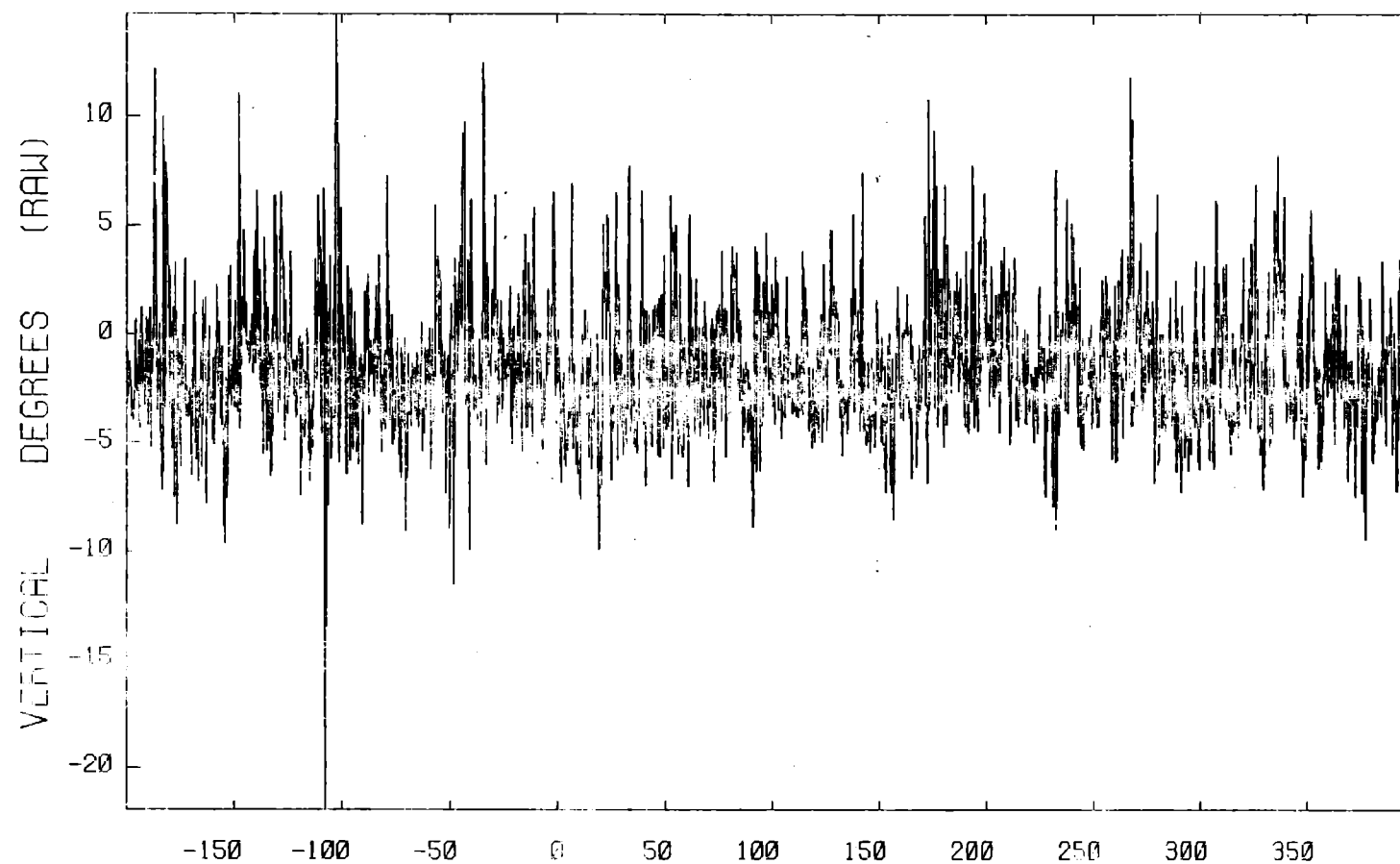
A07
01 METERS

Time(sec)
3-AXIS ANEMOMETER

27-AUG-80
S/N 384

BUR007

T01



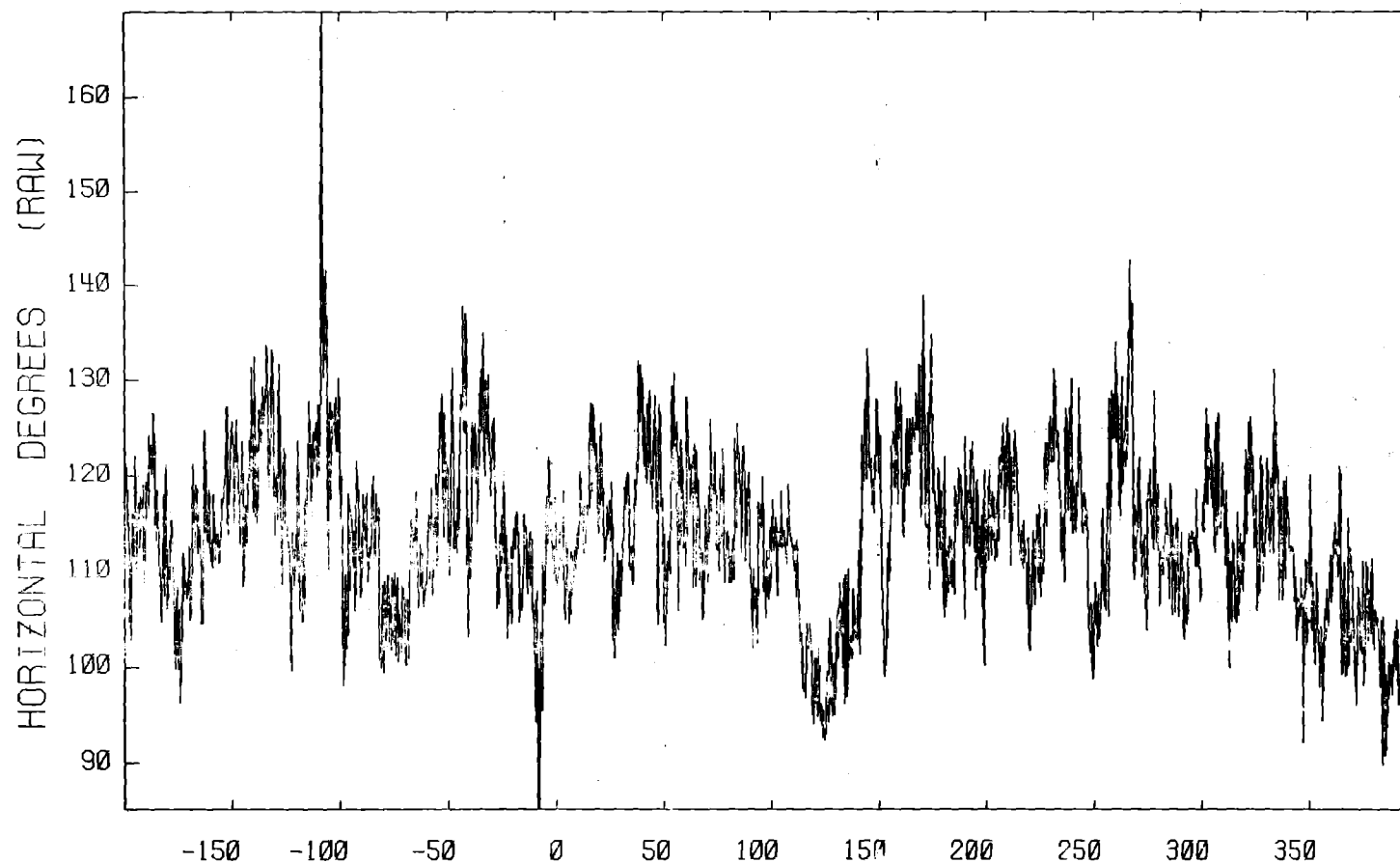
A08
01 METERS

Time(sec)
3-AXIS ANEMOMETER

27-AUG-80
S/N 384

BUR007

T01



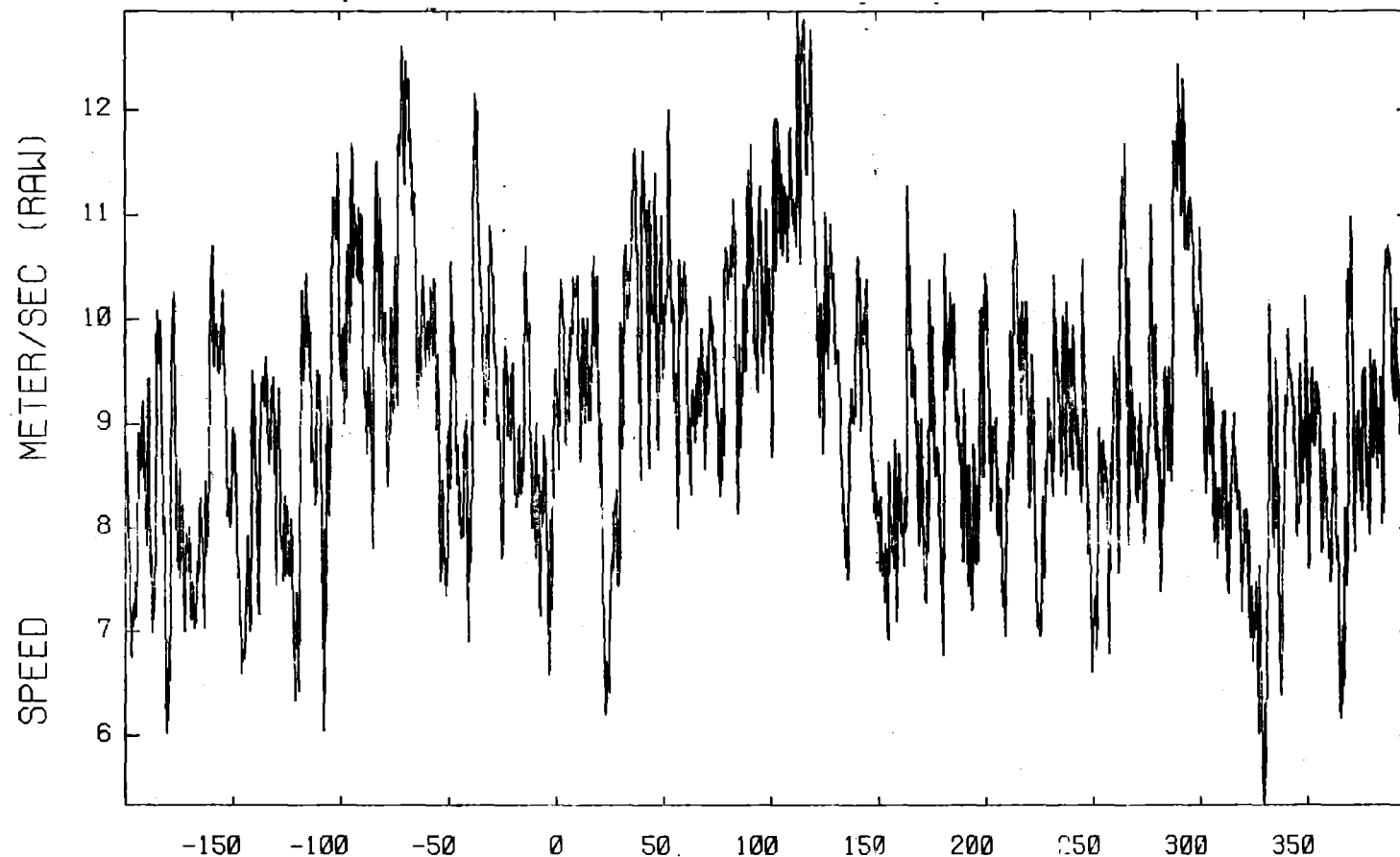
A09
03 METERS

Time(sec)
3-AXIS ANEMOMETER

27-AUG-80
S/N 387

BUR007

T01



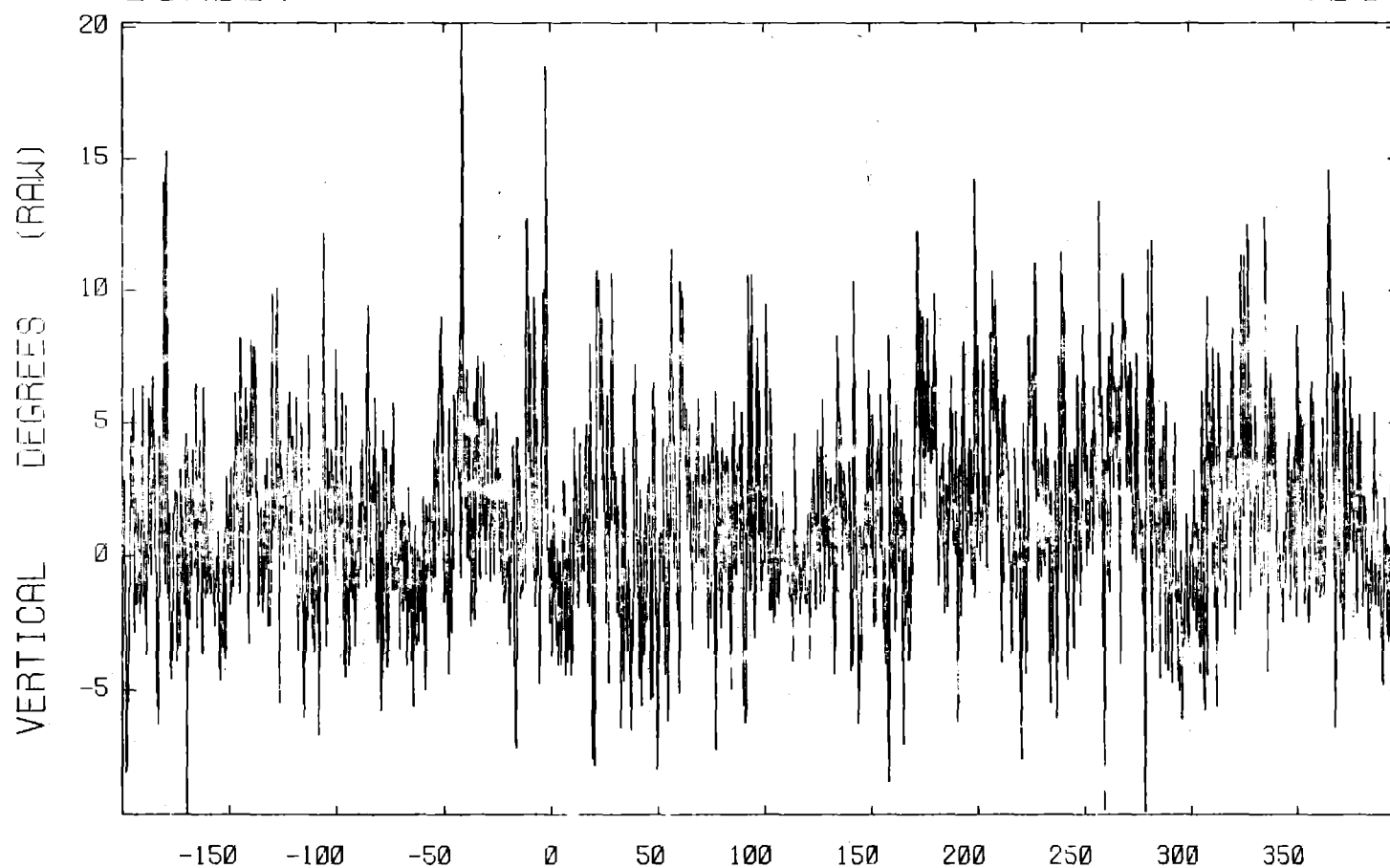
A10
03 METERS

Time(sec)
3-AXIS ANEMOMETER

27-AUG-80
S/N 387

BUR007

T01



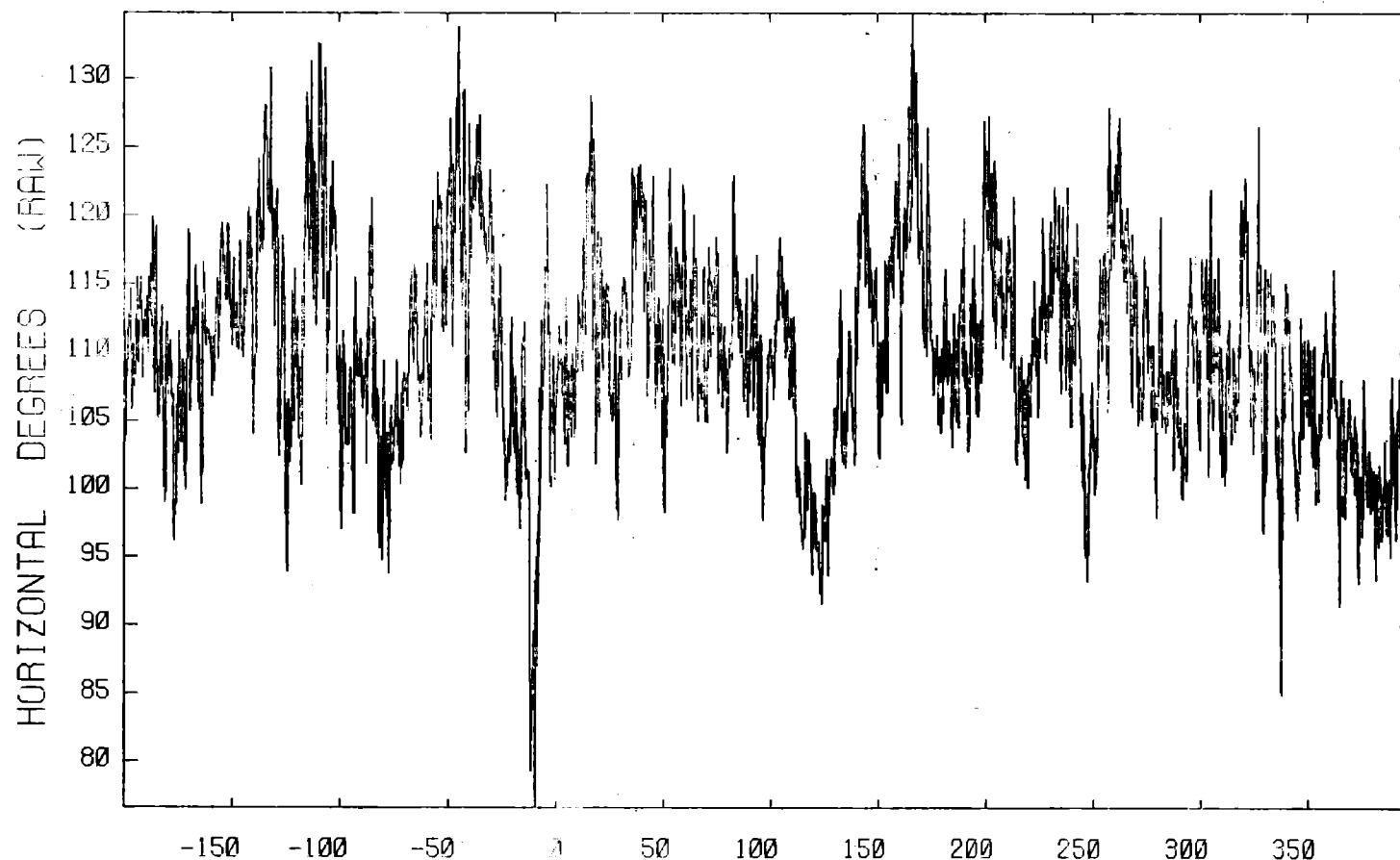
A11
03 METERS

Time(sec)
3-AXIS ANEM METER

27-AUG-80
S/N 387

BUR007

T01



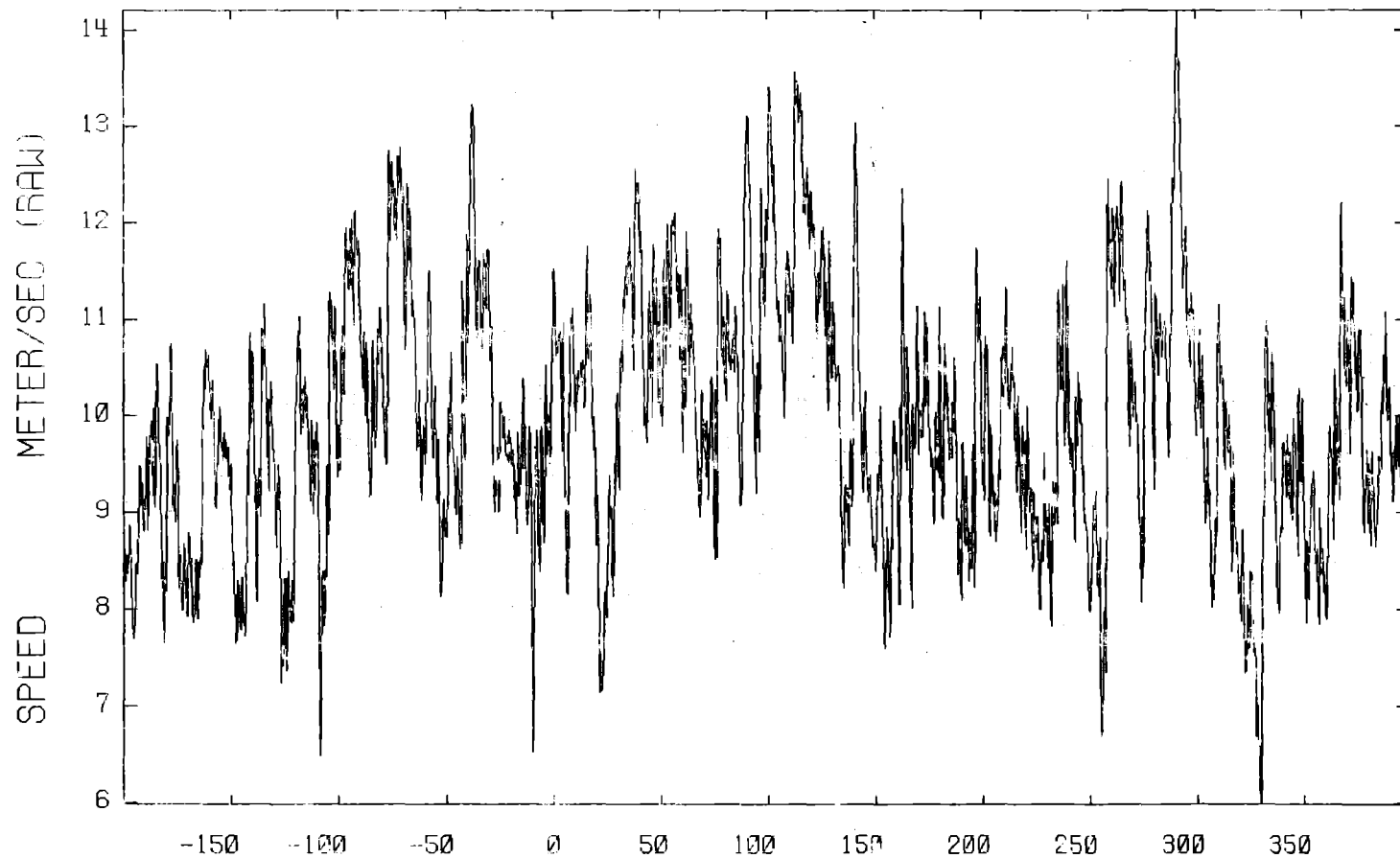
A12
08 METERS

Time(sec)
3-AXIS ANEMOMETER

27-AUG-80
S/N 376

BUR007

T01



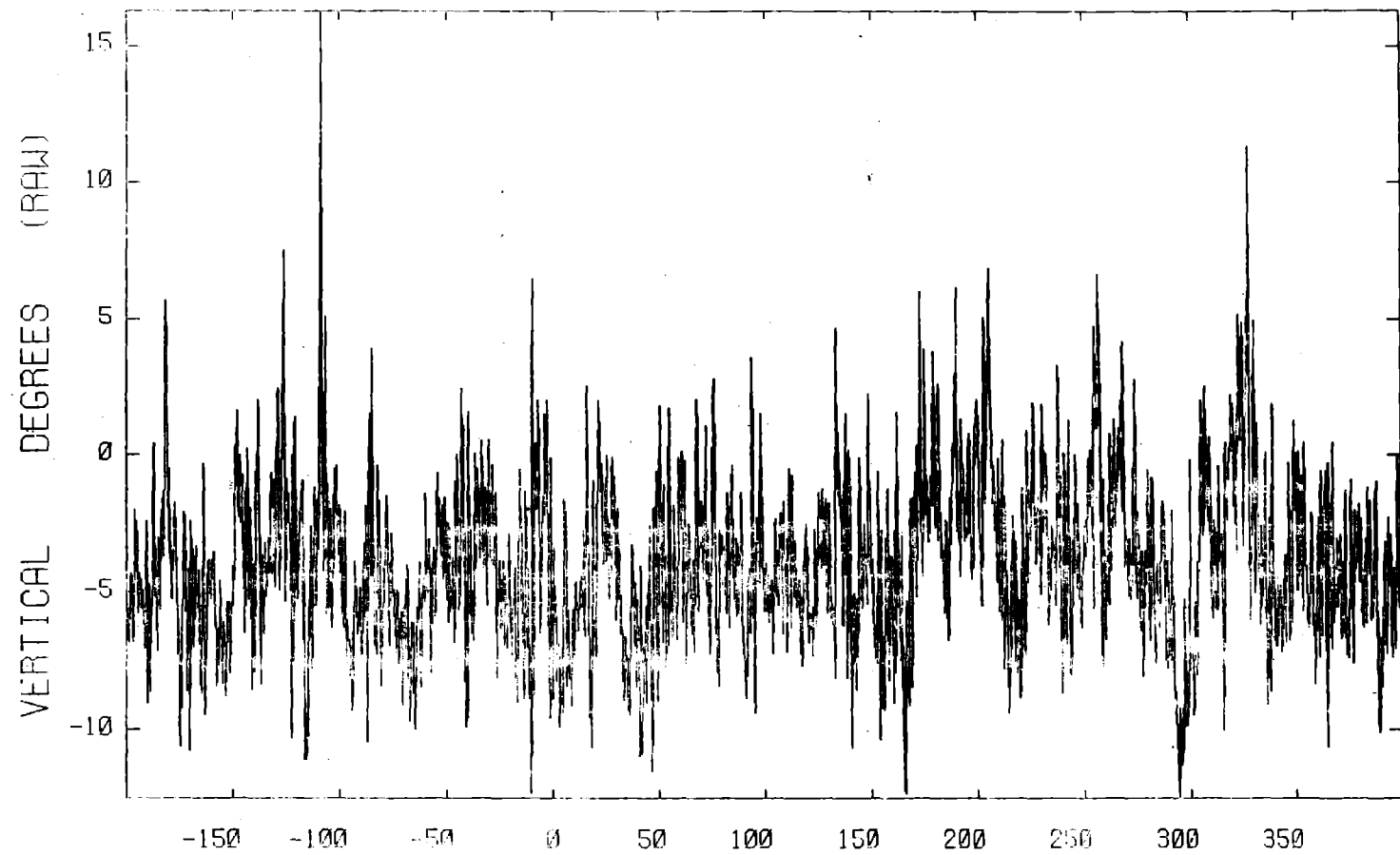
A13
08 METERS

Time(sec)
3-AXIS ANEMOMETER

27-AUG-80
S/N 376

BUR007

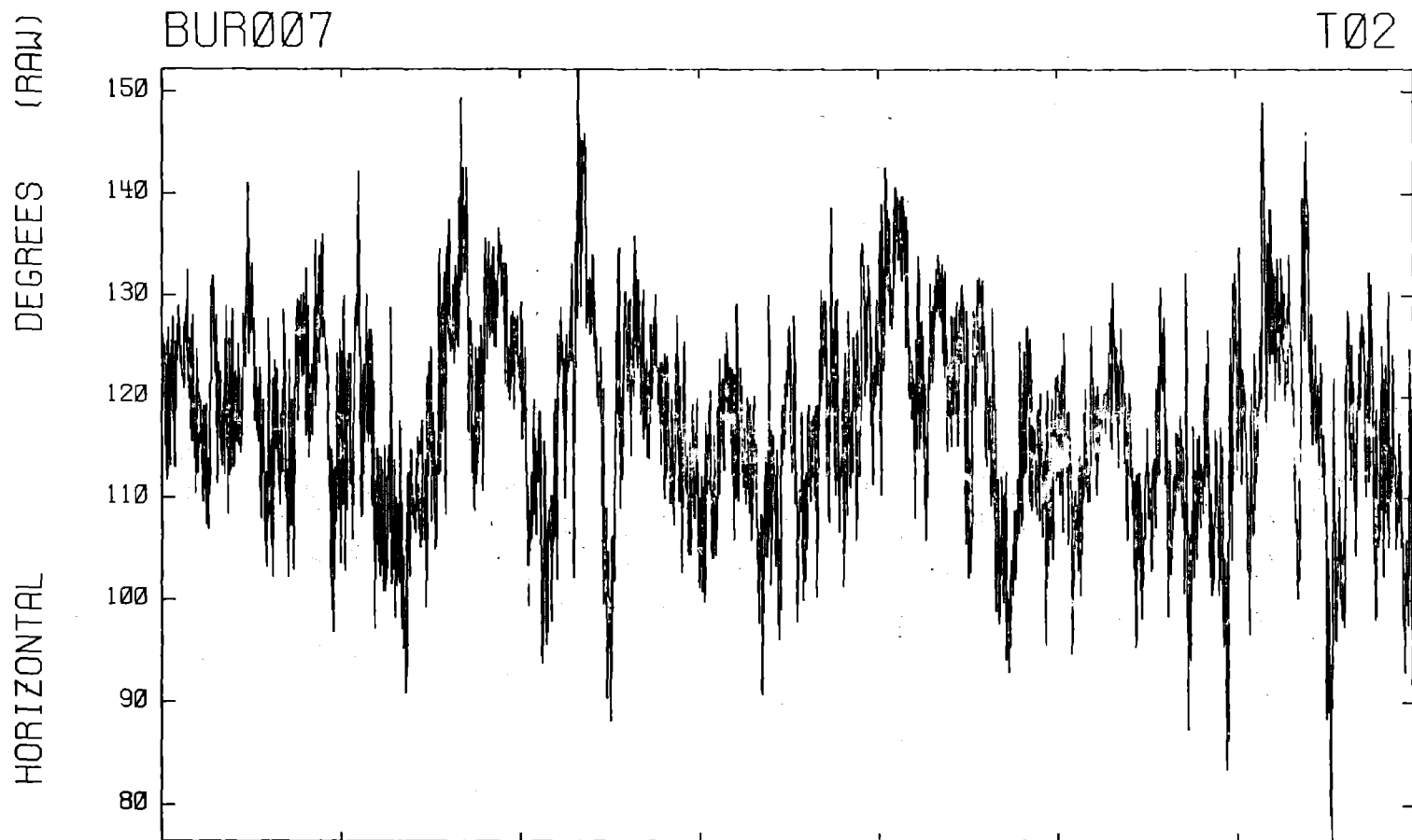
T01



A14
08 METERS

Time(sec)
3-AXIS ANEM METER

27-AUG-80
S/N 376



A06
01 METERS

Time(sec)
3-AXIS ANEMOMETER

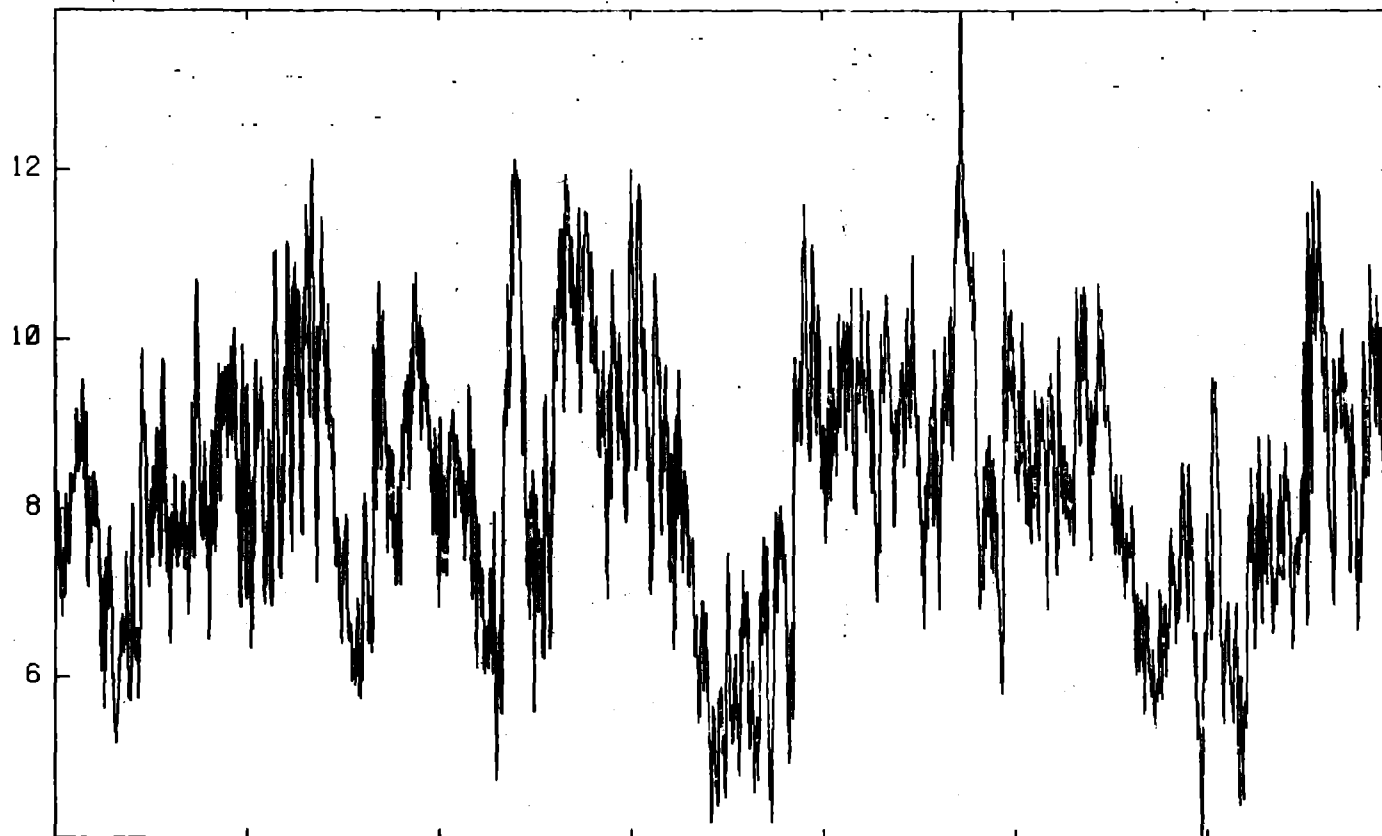
28-AUG-80
S/N 386

METER/SEC (RAW)

SPEED

BUR007

T02



A07
01 METERS

E+02

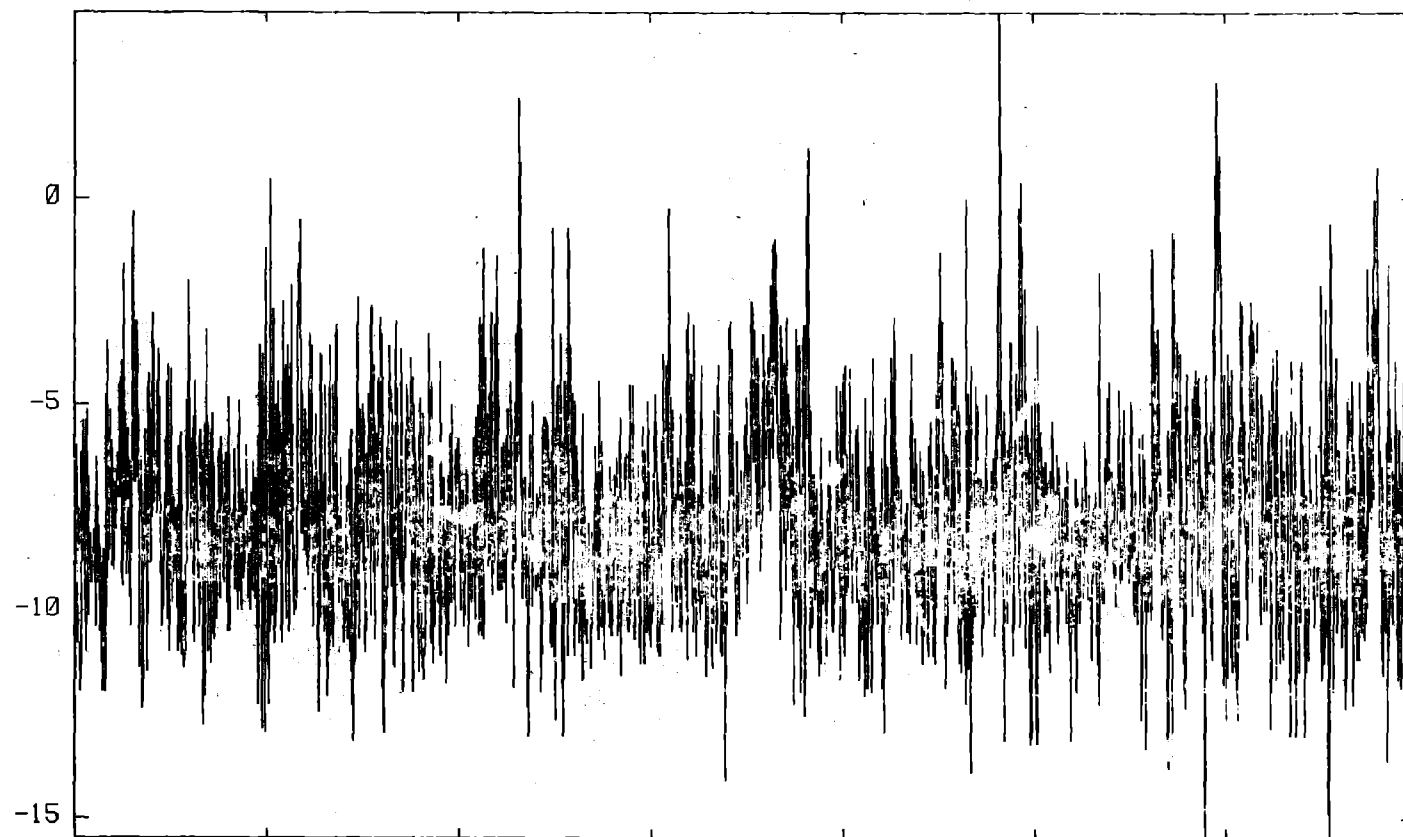
Time(sec)
3-AXIS ANEMOMETER

28-AUG-80
S/N 386

VERTICAL DEGREES (RAW)

BUR007

T02



A08
01 METERS

E+02

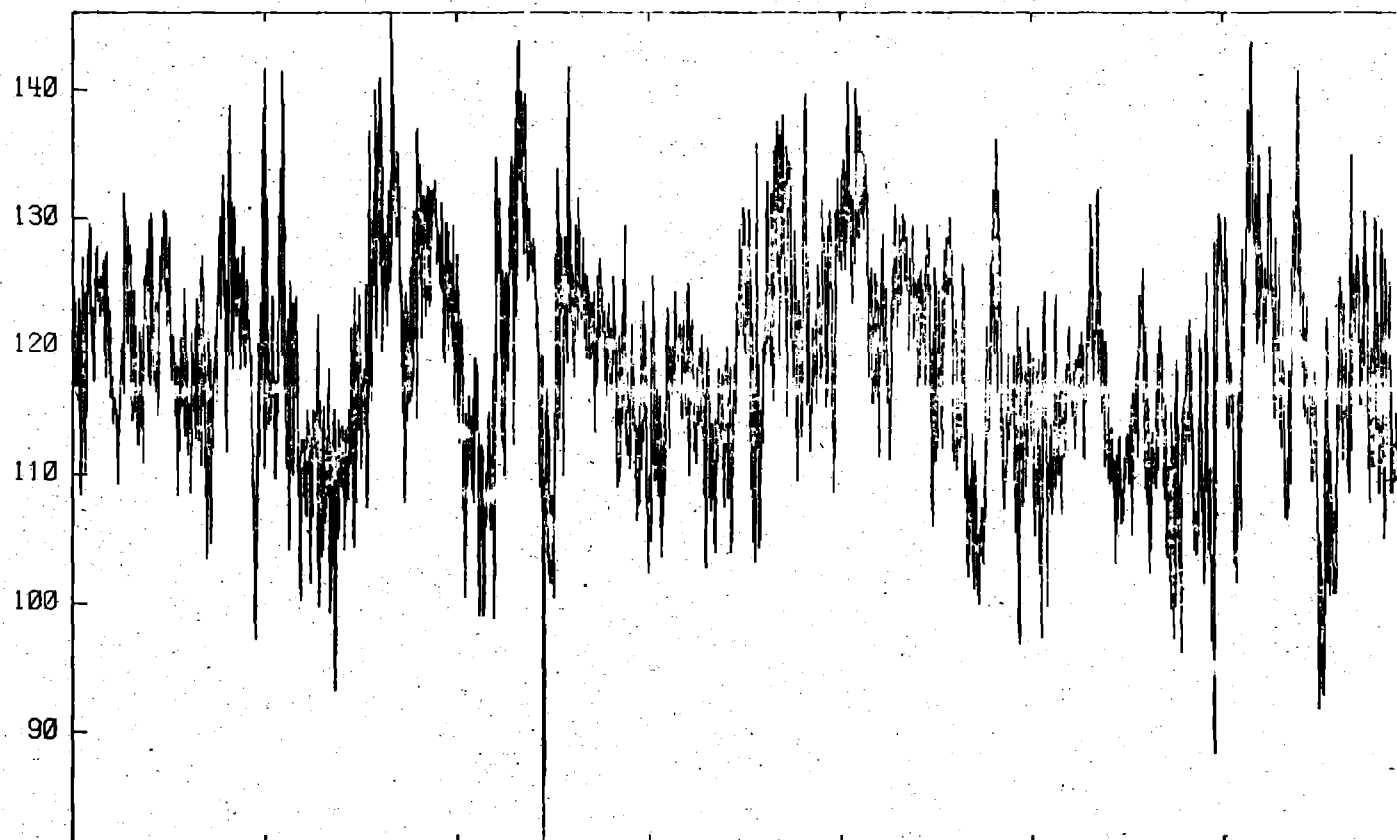
Time(sec)
3-AXIS ANEMOMETER

28-AUG-80
S/N 386

HORIZONTAL DEGREES (RAW)

BUR007

T02



A09
03 METERS

E+02

Time (sec)

3-AXIS INERTIAL METER

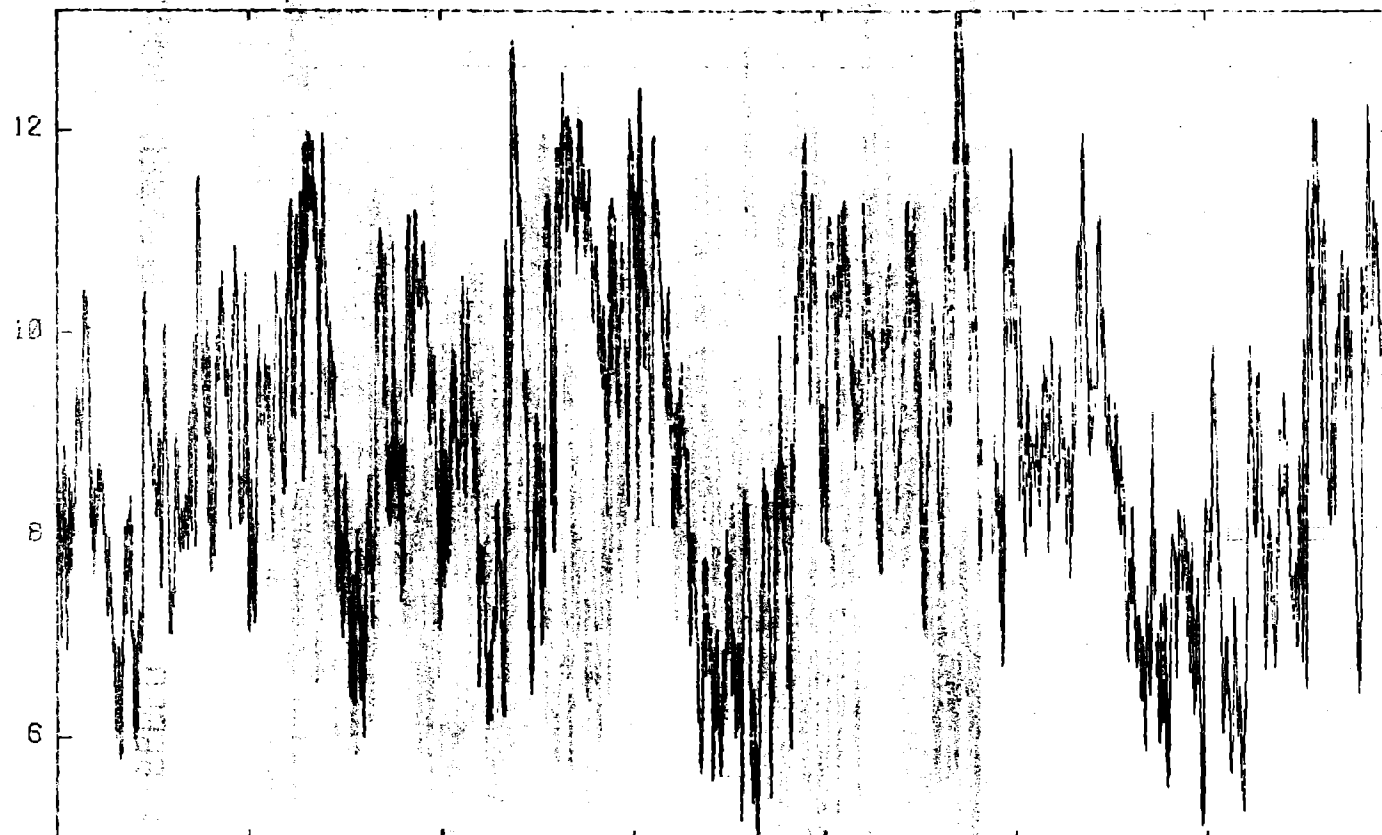
28-AUG-80
S/N 381

METER/SEC (RAW)

SPEED

BUR007

T02



A10

03 METERS

E+02

Time(sec)

3-AXIS ANEMOMETER

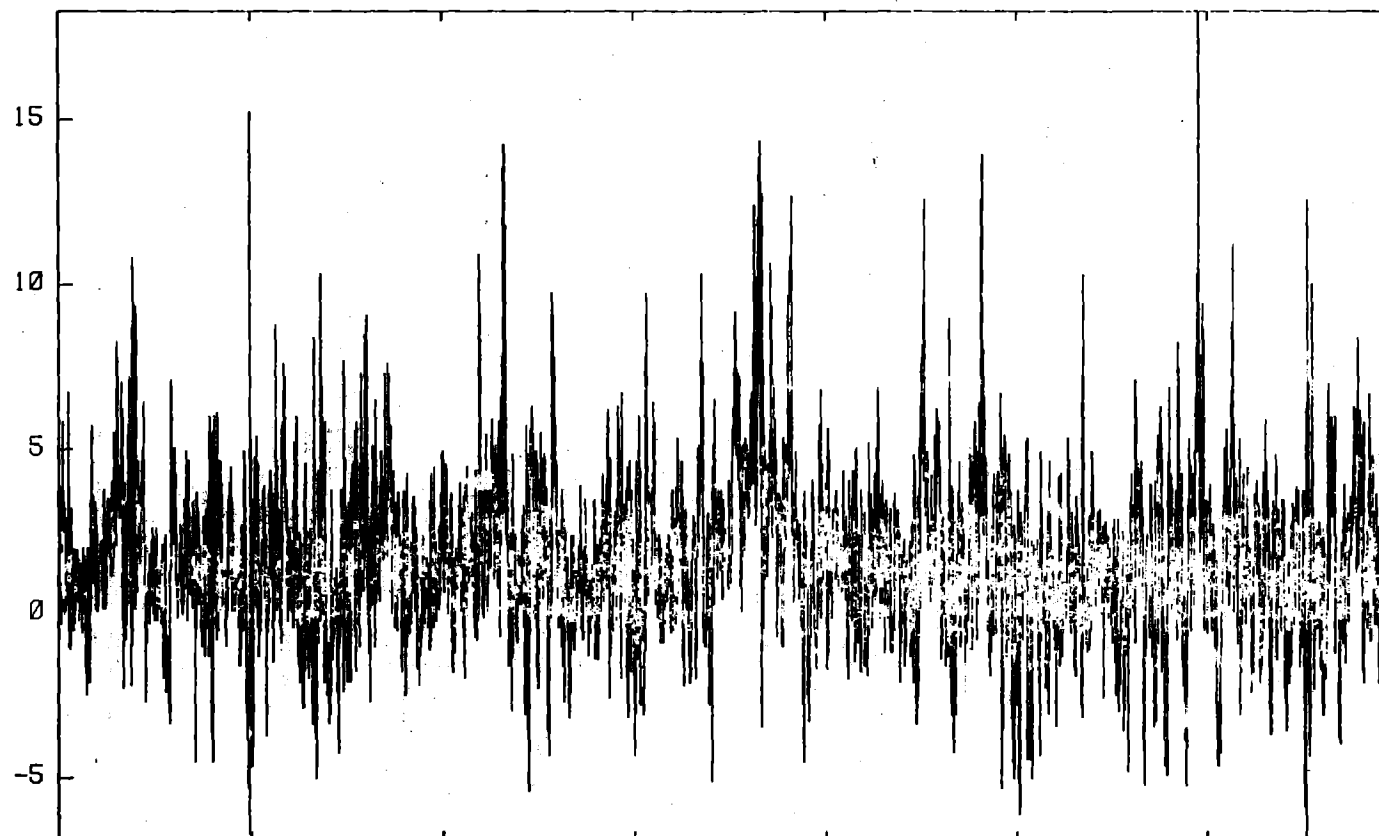
28-AUG-80

S/N 381

VERTICAL (RAW) DEGREES

BUR007

T02



A11
03 METERS

E+02

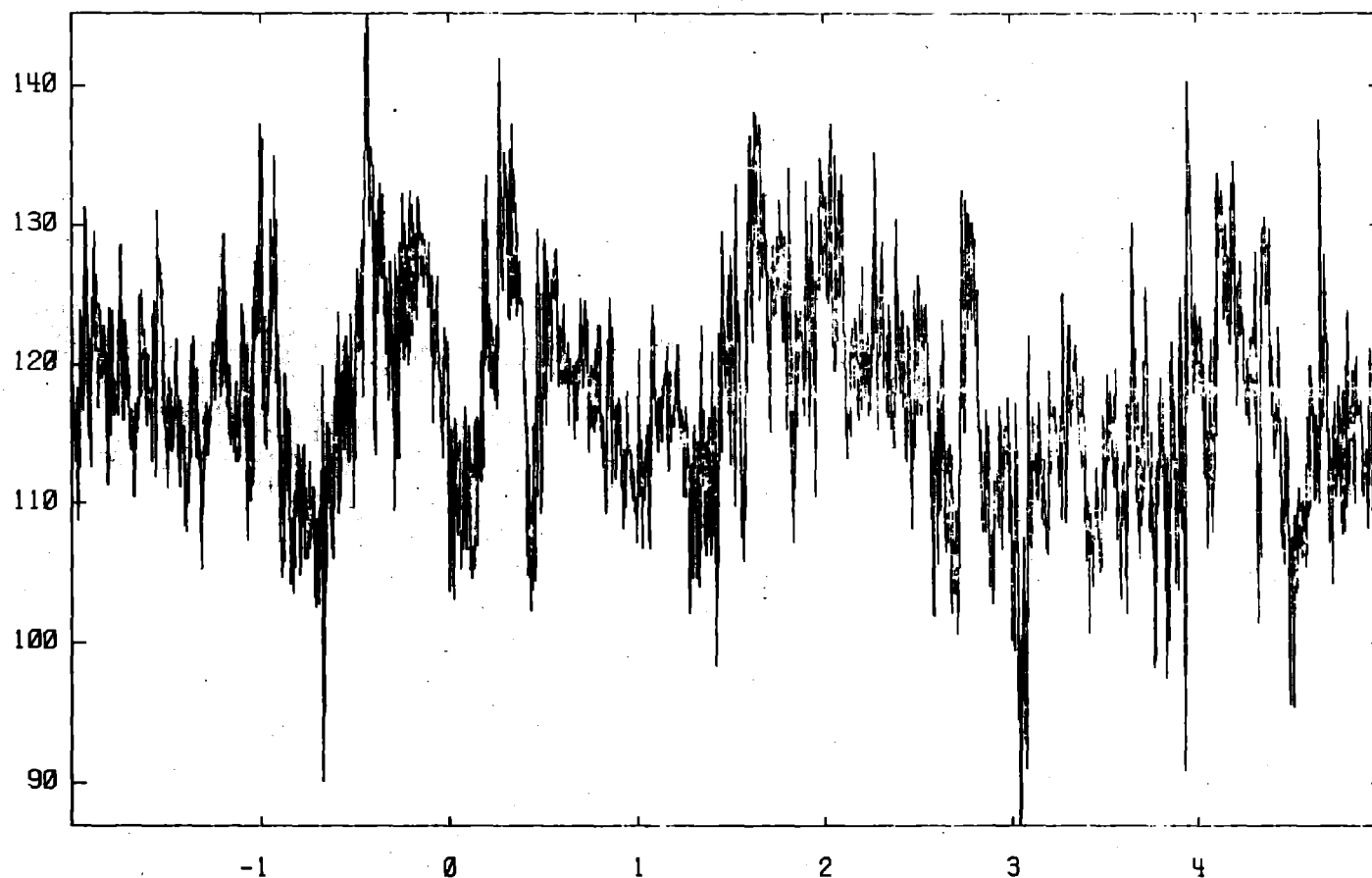
Time(sec)
3-AXIS ANEMOMETER

28-AUG-80
S/N 381

HORIZONTAL DEGREES (RAW)

BUR007

T02



A12
08 METERS

Time(sec)
3-AXIS ANEMOMETER

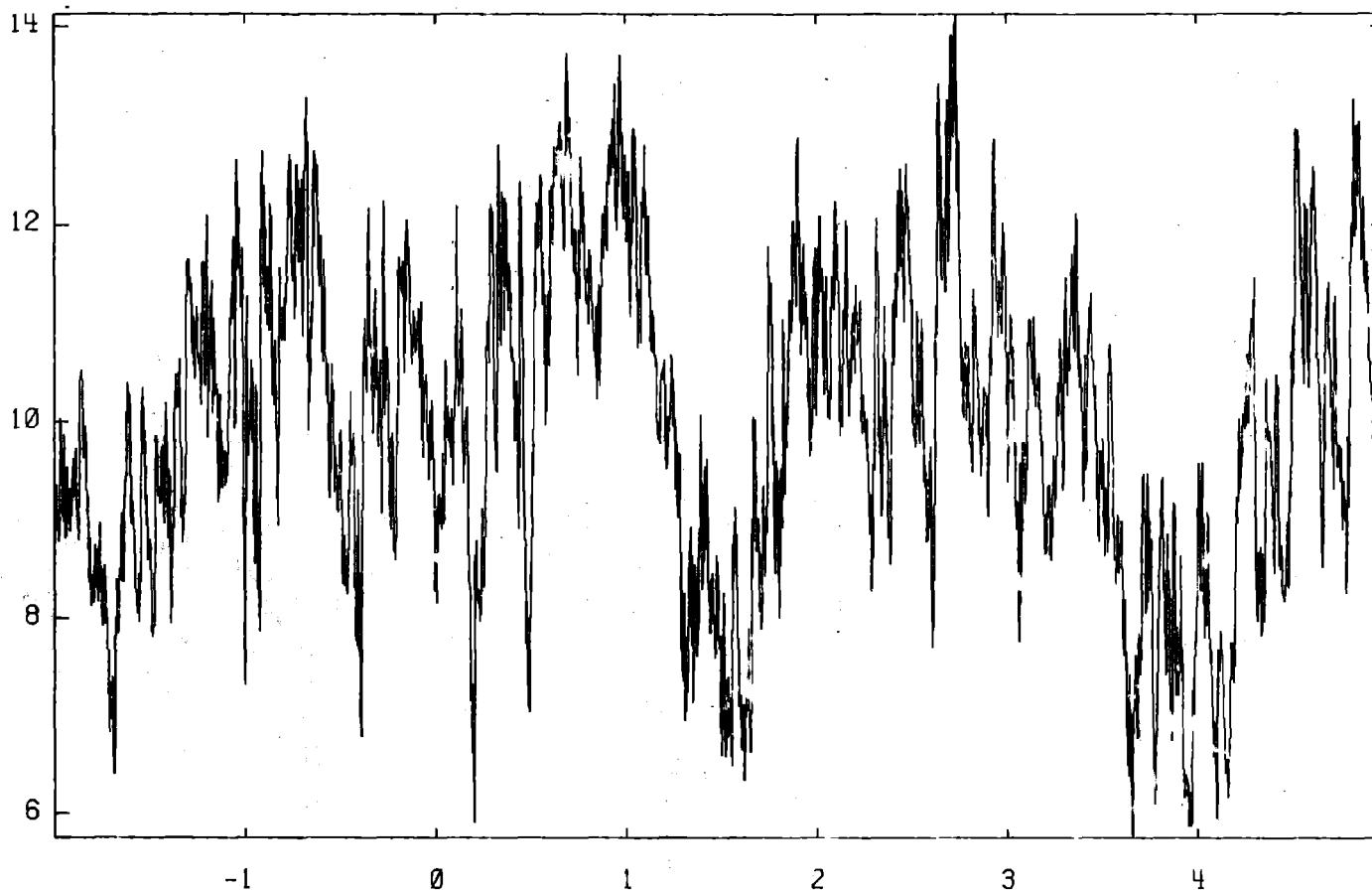
28-AUG-80
S/N 380

METER/SEC (RAW)

SPEED

BUR007

T02



A13
08 METERS

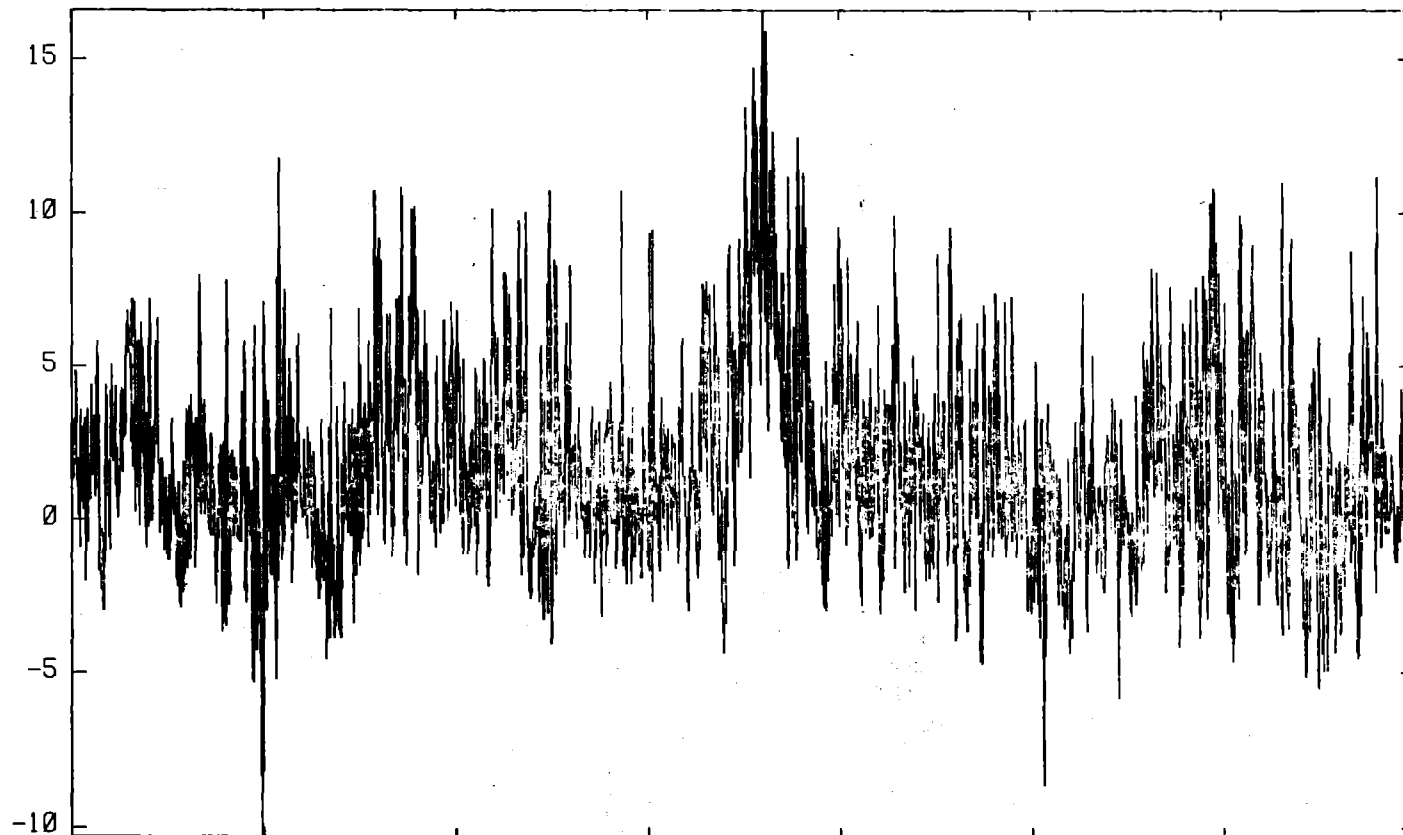
Time (sec)
3-AXIS ANEMOMETER

28-AUG-80
S/N 380

VERTICAL DEGREES (RAW)

BUR007

T02



A14
08 METERS

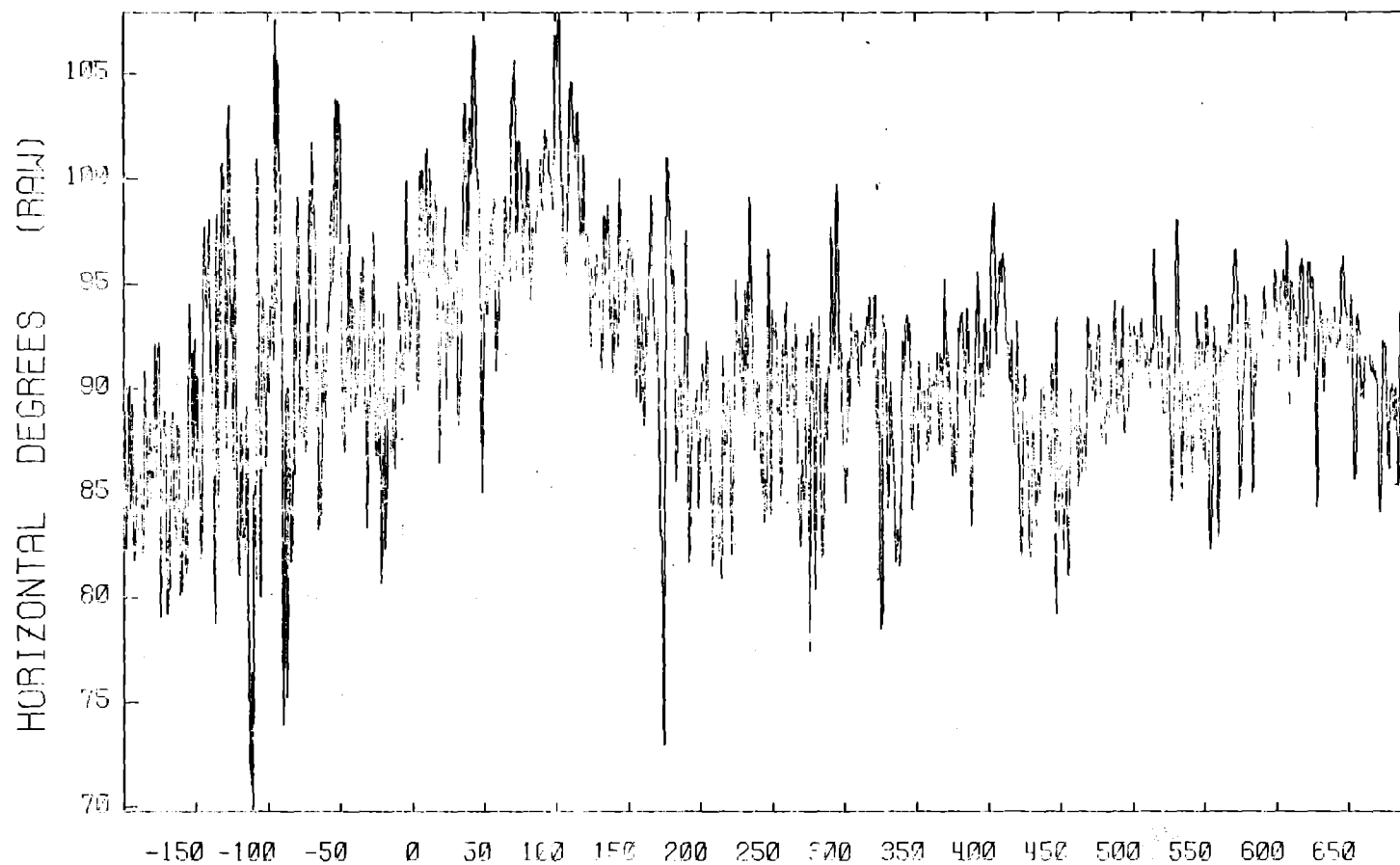
E+02

Time(sec)
3-AXIS ANEMOMETER

28-AUG-80
S/N 380

BURR08

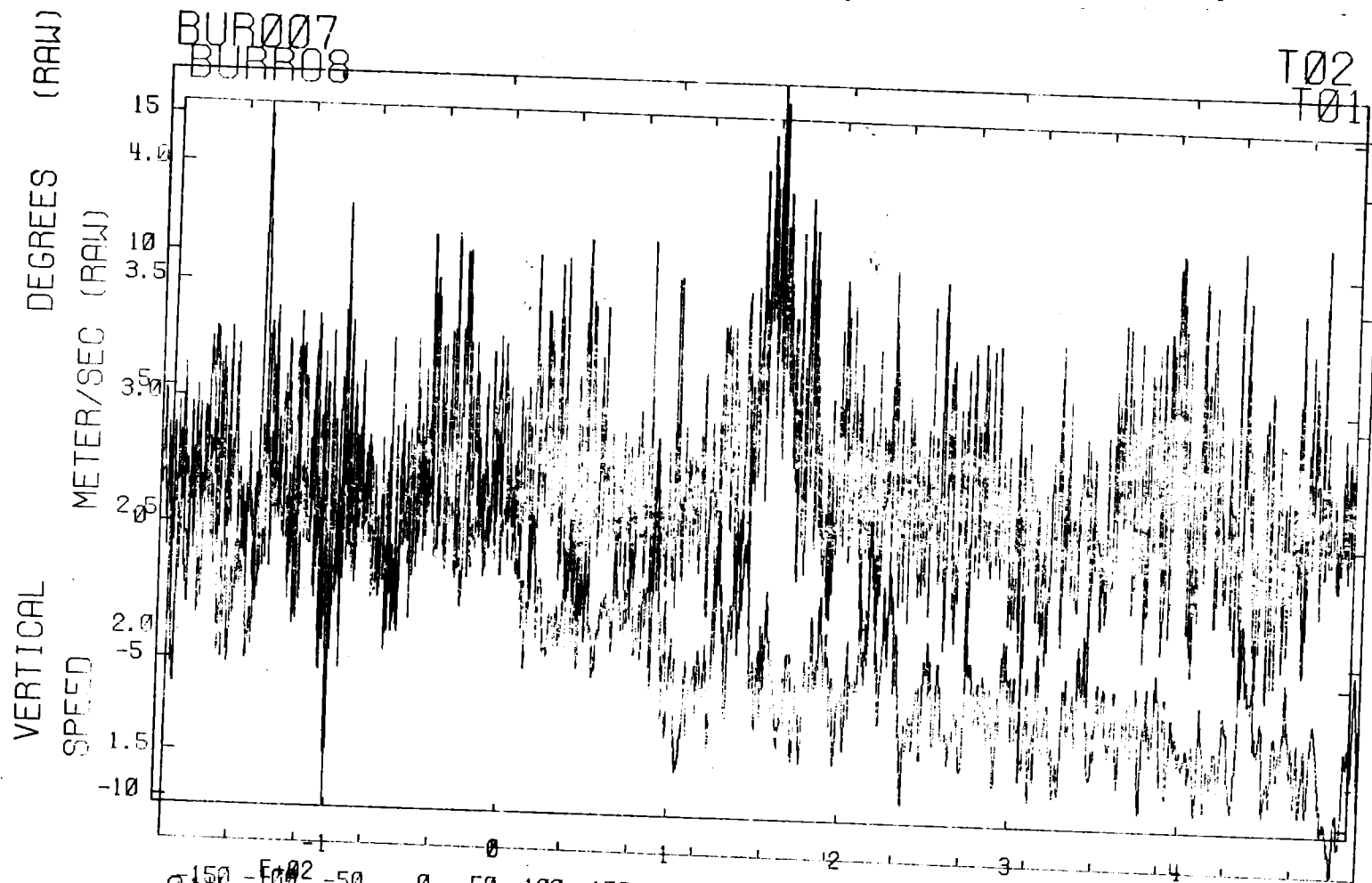
T01



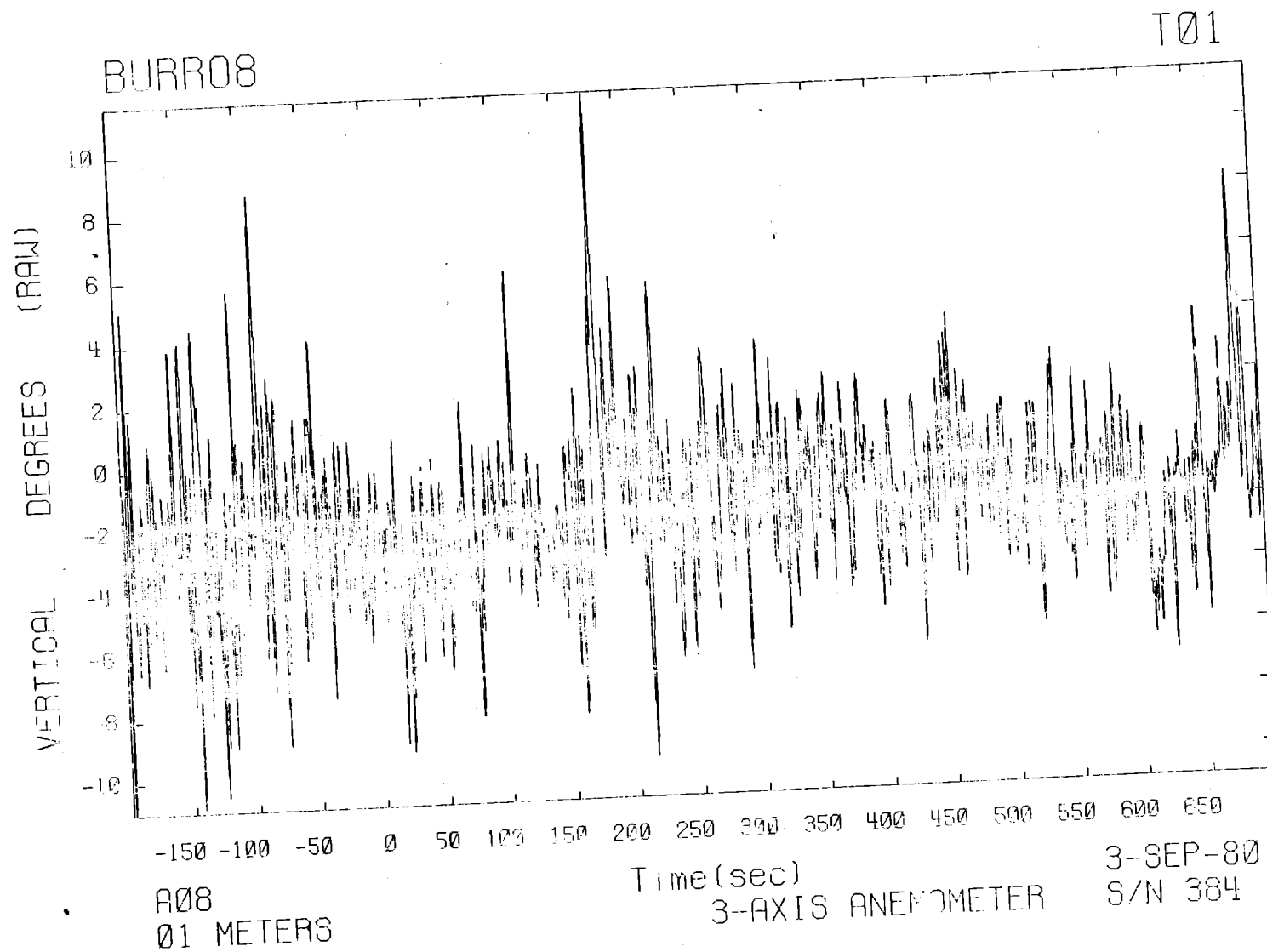
A06
01 METERS

Time(sec)
3-AXIS ANEMOMETER

3-SEP-80
S/N 384

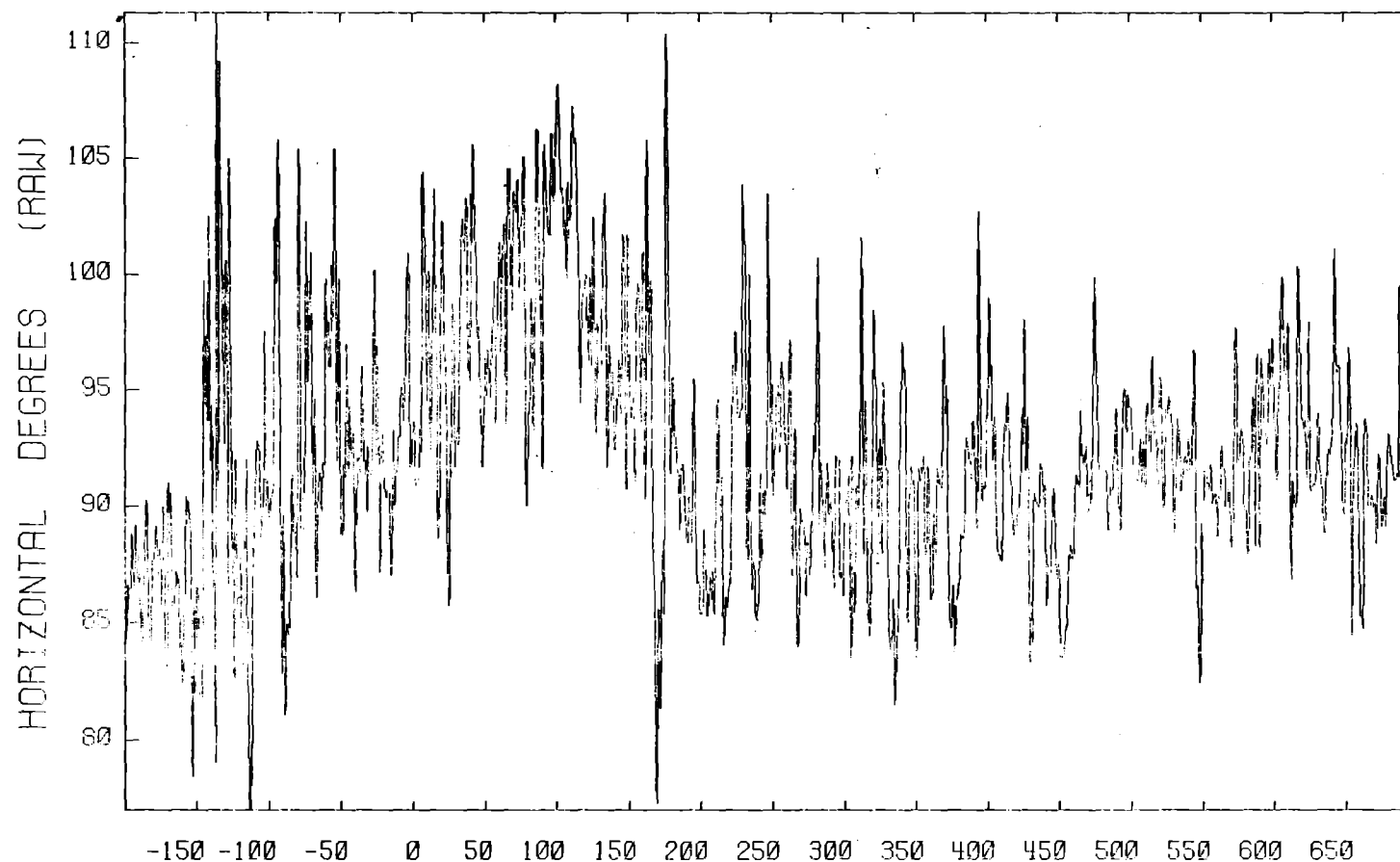


150 -50 0 50 100 150 200 250 300 350 400 450 500 550 600 650
 A14 007 METERS 01 METERS
 Time (sec)
 3-AXIS ANEMOMETER
 28-AUG-80
 S/N 384



BURR08

T01



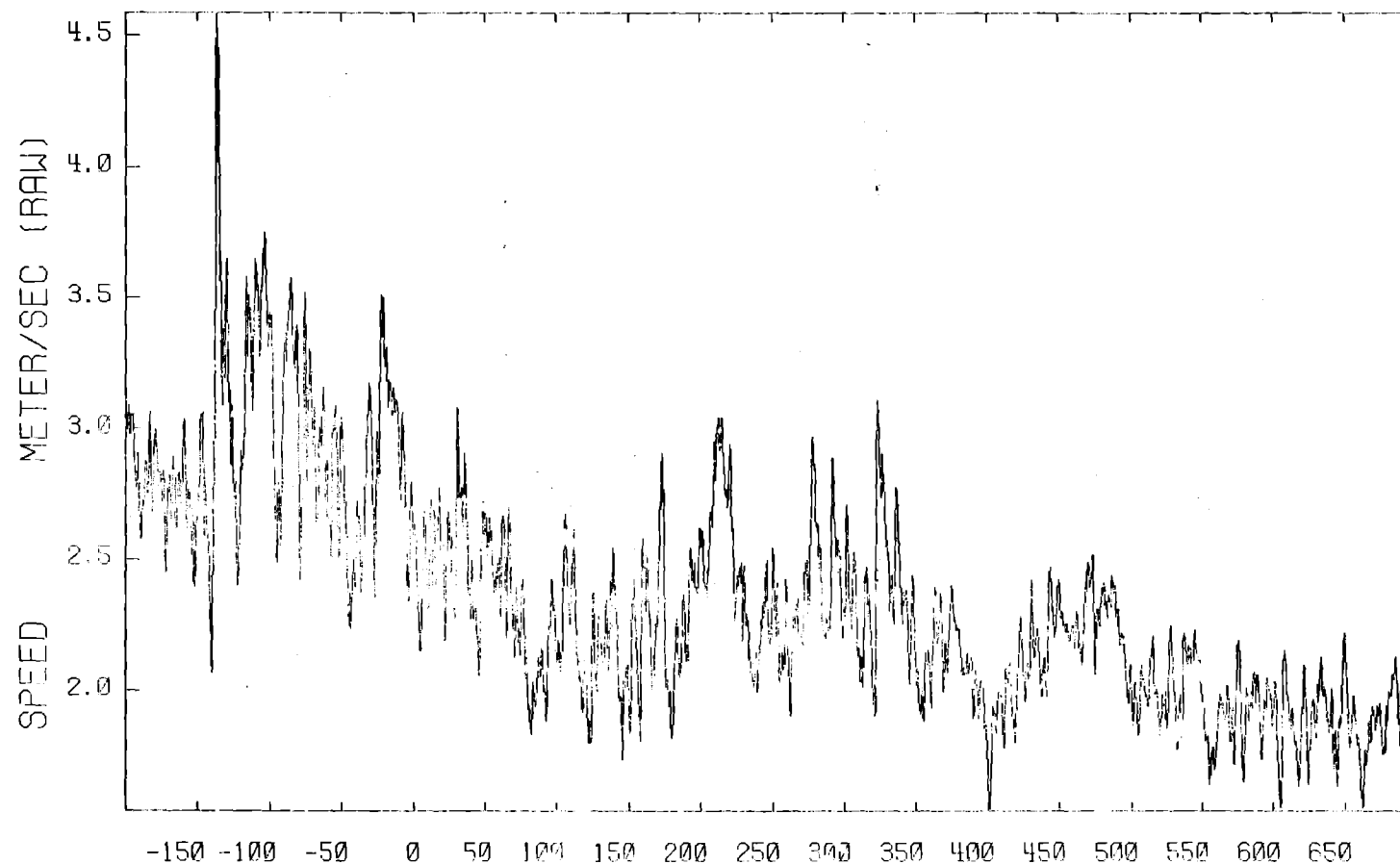
A09
03 METERS

3-AXIS ANEMOMETER

3-SEP-80
S/N 387

BURR08

T01



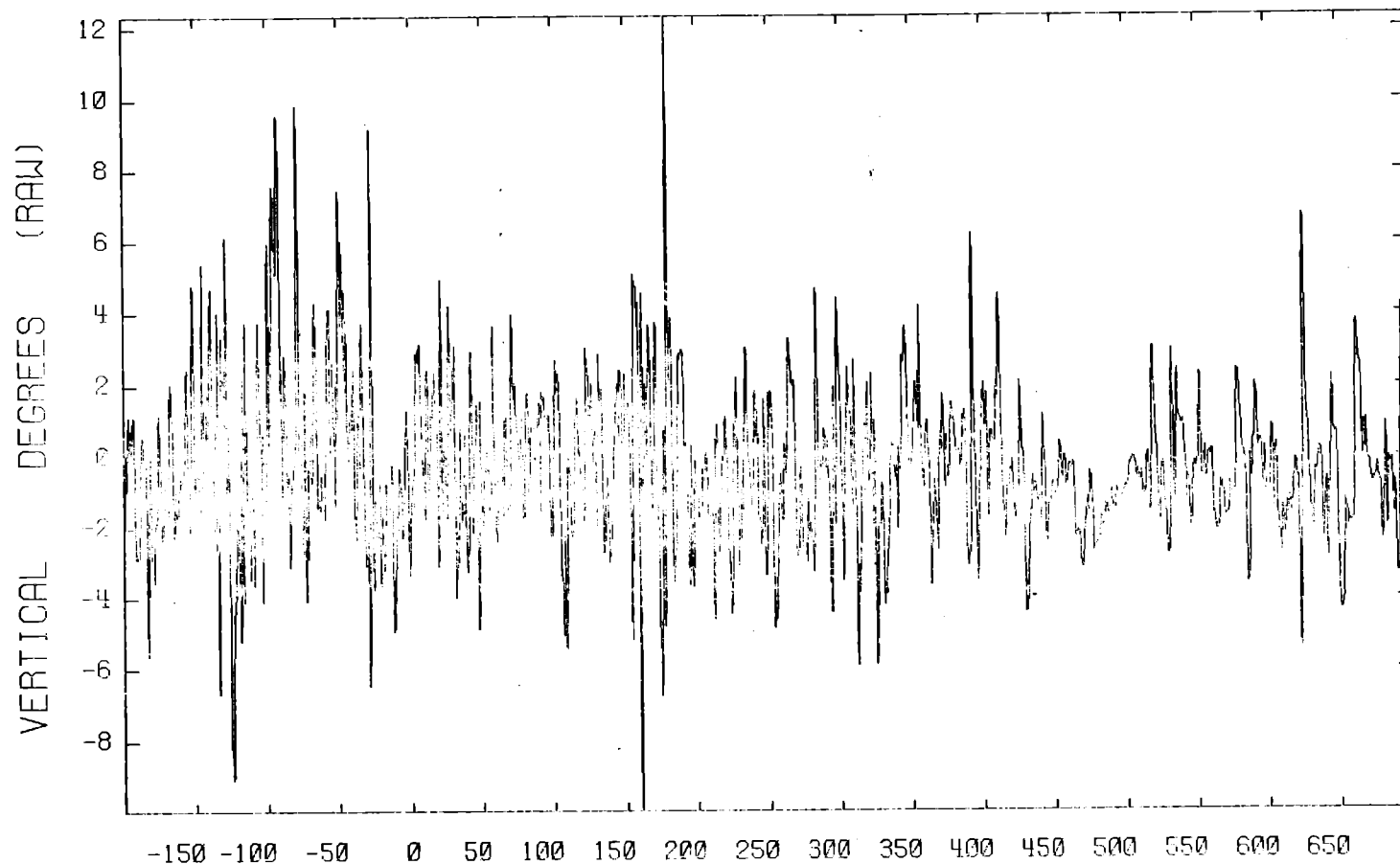
A10
03 METERS

Time(sec)
3-AXIS ANEMOMETER

3-SEP-80
S/N 387

BURR08

T01



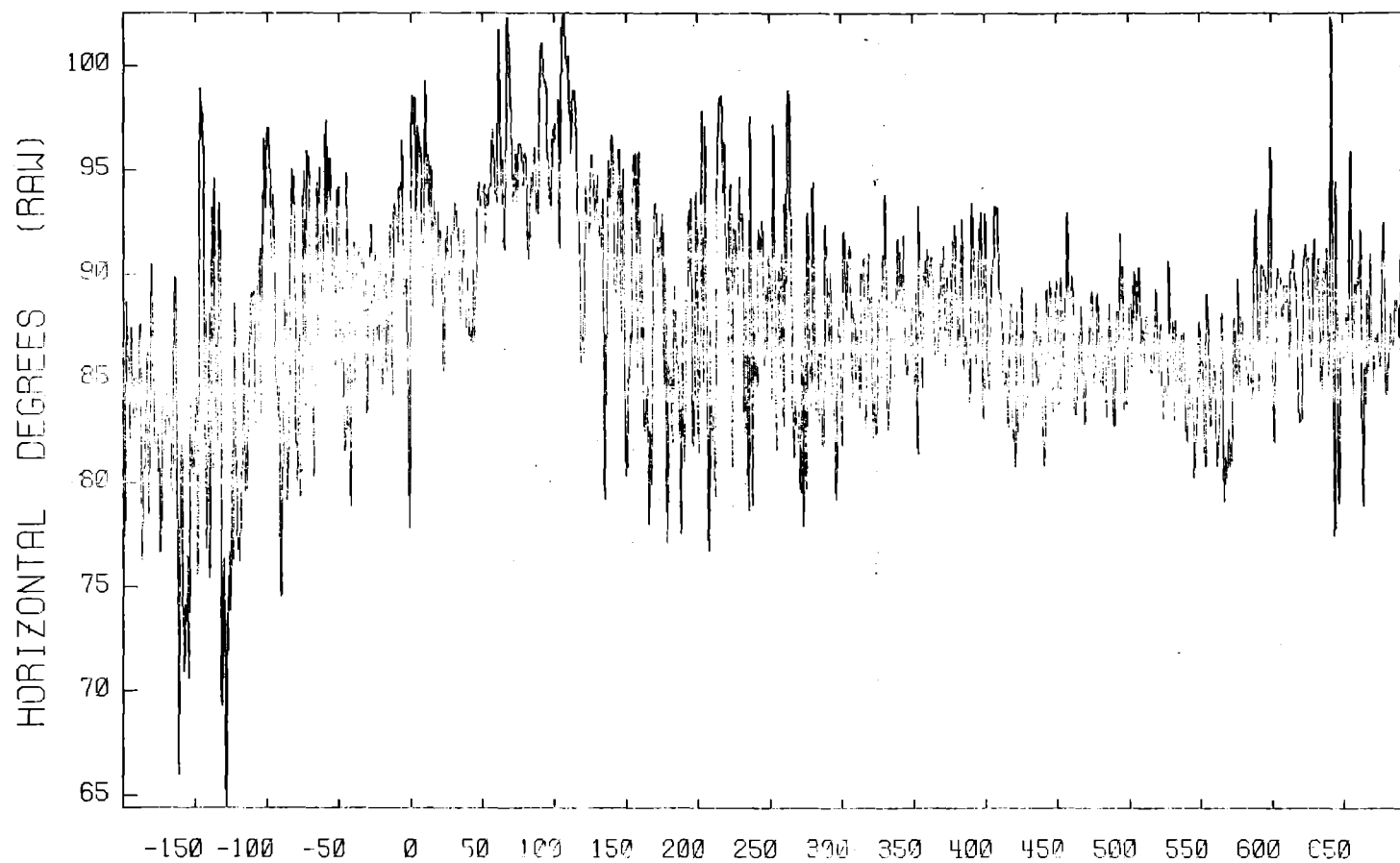
A11
03 METERS

Time(sec)
3-AXIS ANEMOMETER

3-SEP-80
S/N 387

BURR08

T01



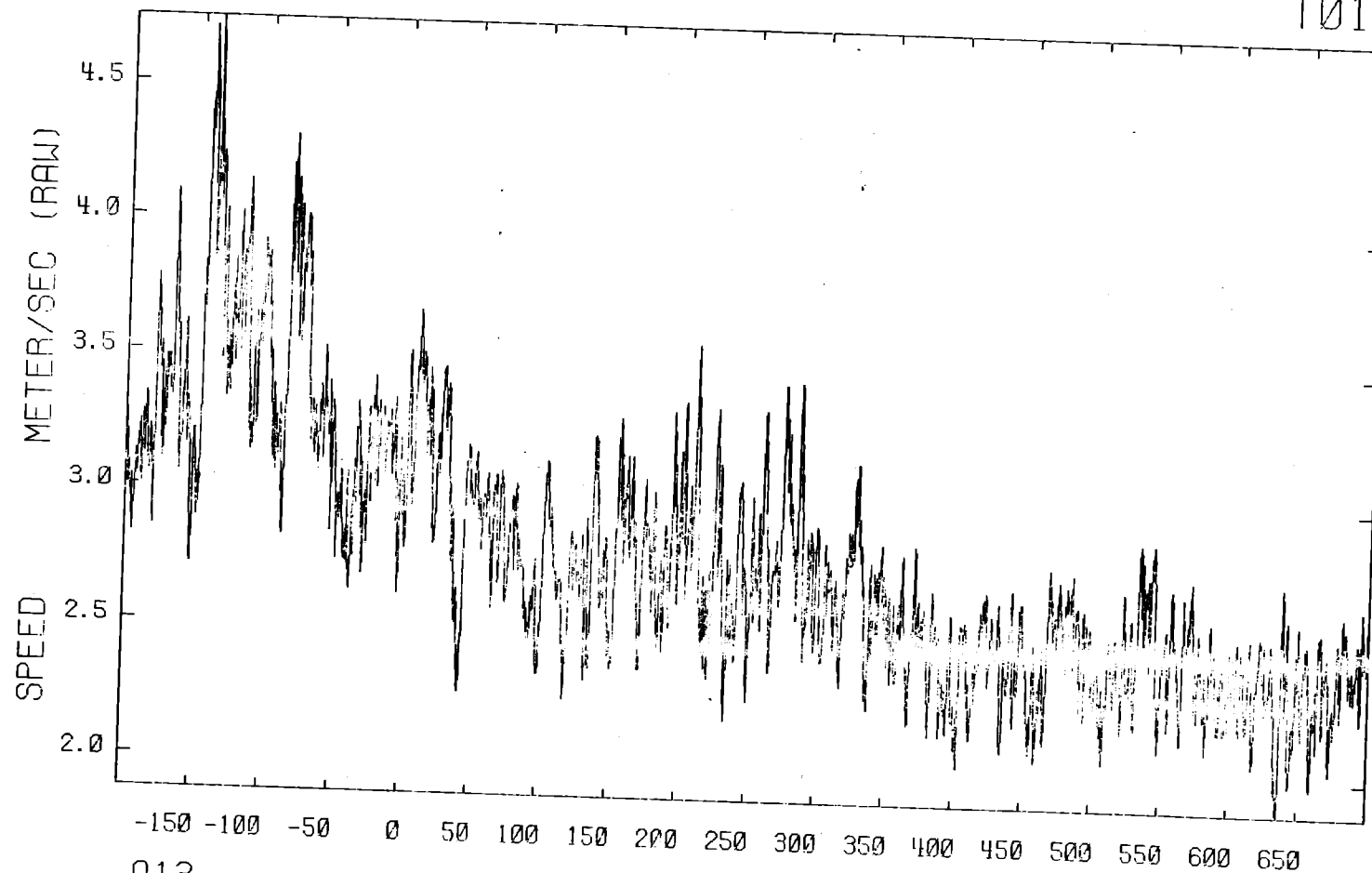
A12
08 METERS

Time(sec)
3-AXIS ANEMOMETER

3-SEP-80
S/N 376

BURR08

T01



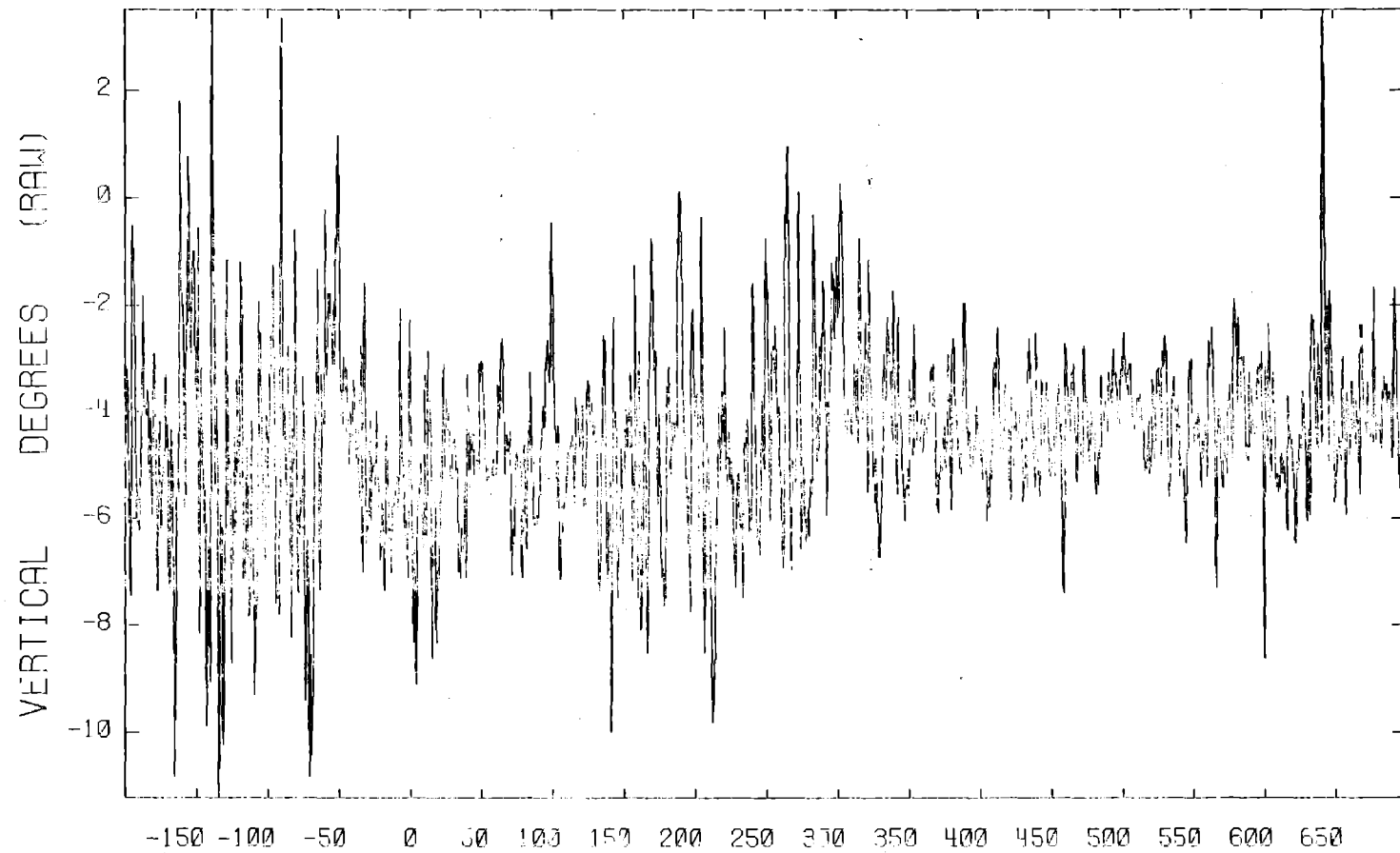
A13
08 METERS

Time(sec)
3-AXIS ANEMOMETER

3-SEP-80
S/N 376

BURR08

T01



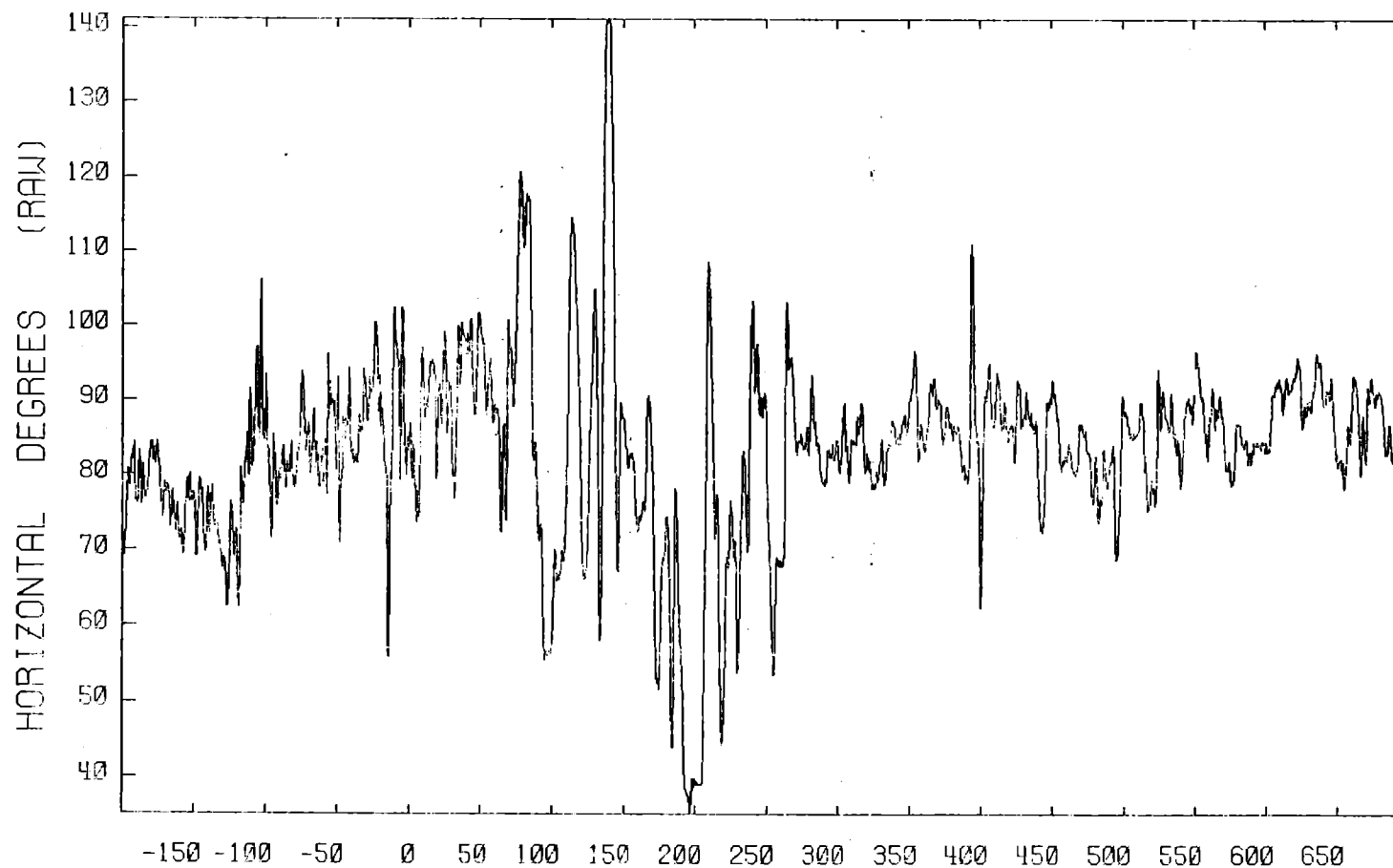
A14
08 METERS

Time(sec)
3-AXIS ANEMOMETER

3-SEP-80
S/N 376

BURR08

T02



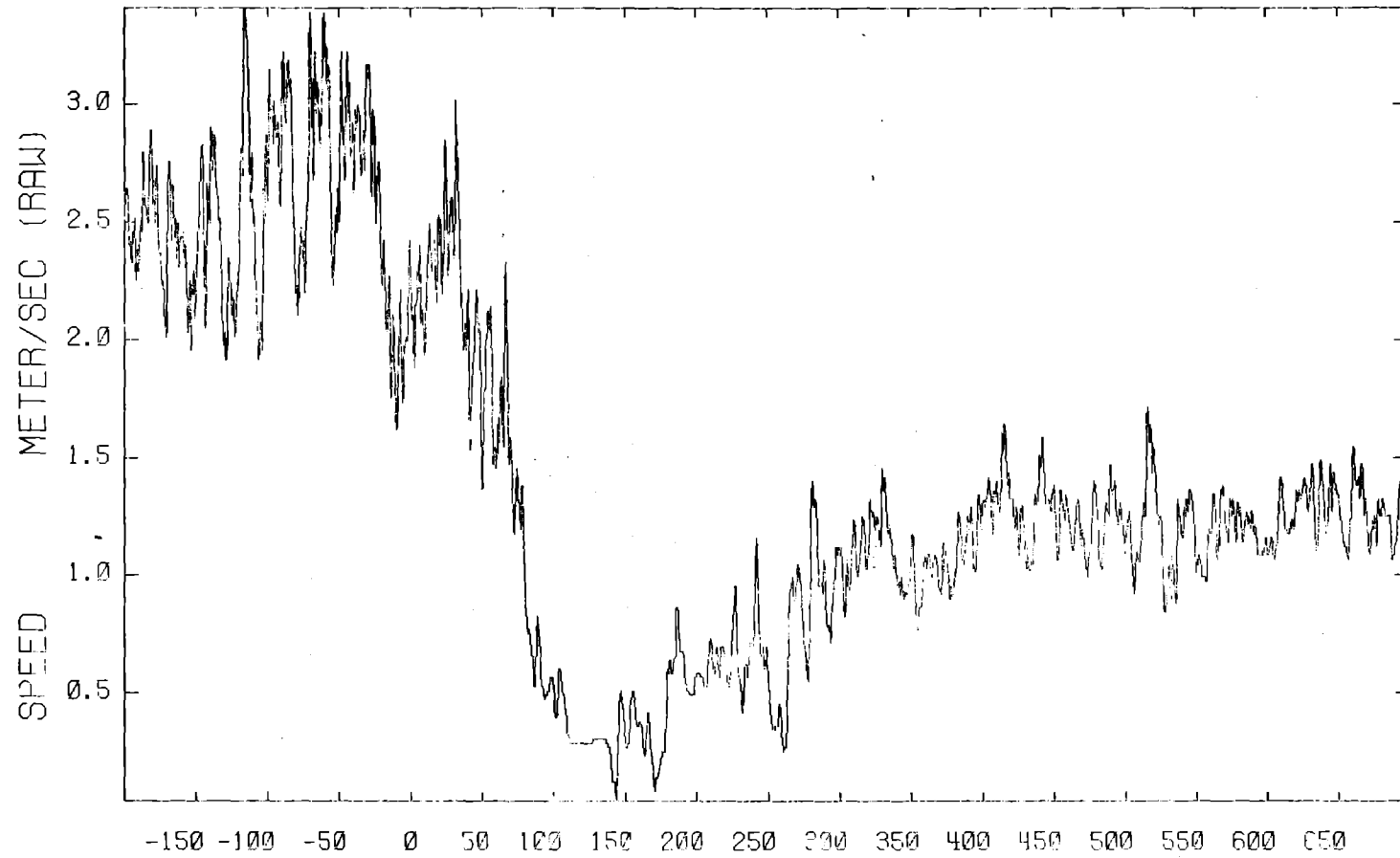
A06
01 METERS

Time(sec)
3-AXIS ANEMOMETER

3-SEP-80
S/N 386

BURR08

T02



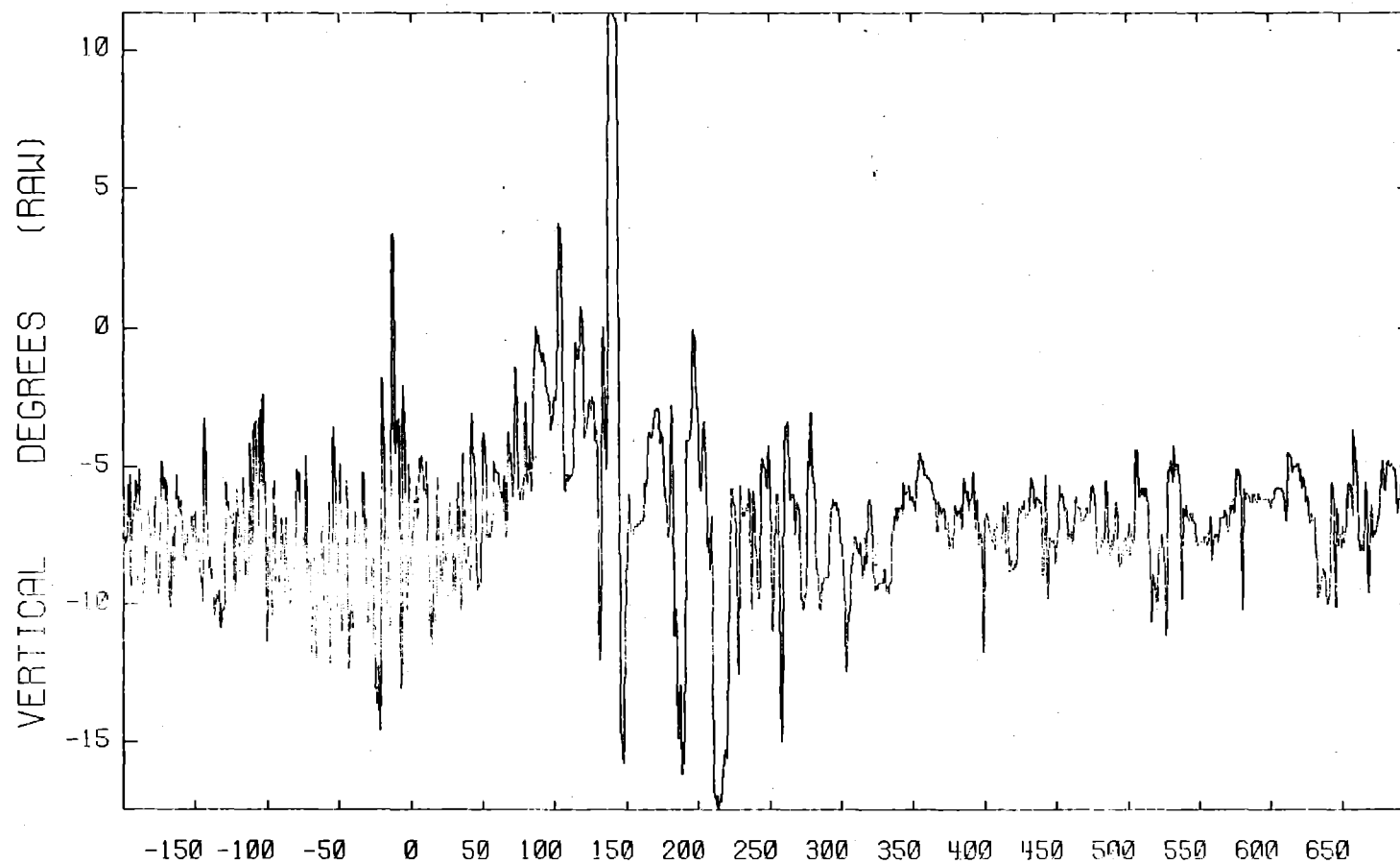
A07
01 METERS

Time(sec)
3-AXIS ANEMOMETER

3-SEP-80
S/N 386

BURR08

T02



A08

01 METERS

Time(sec)

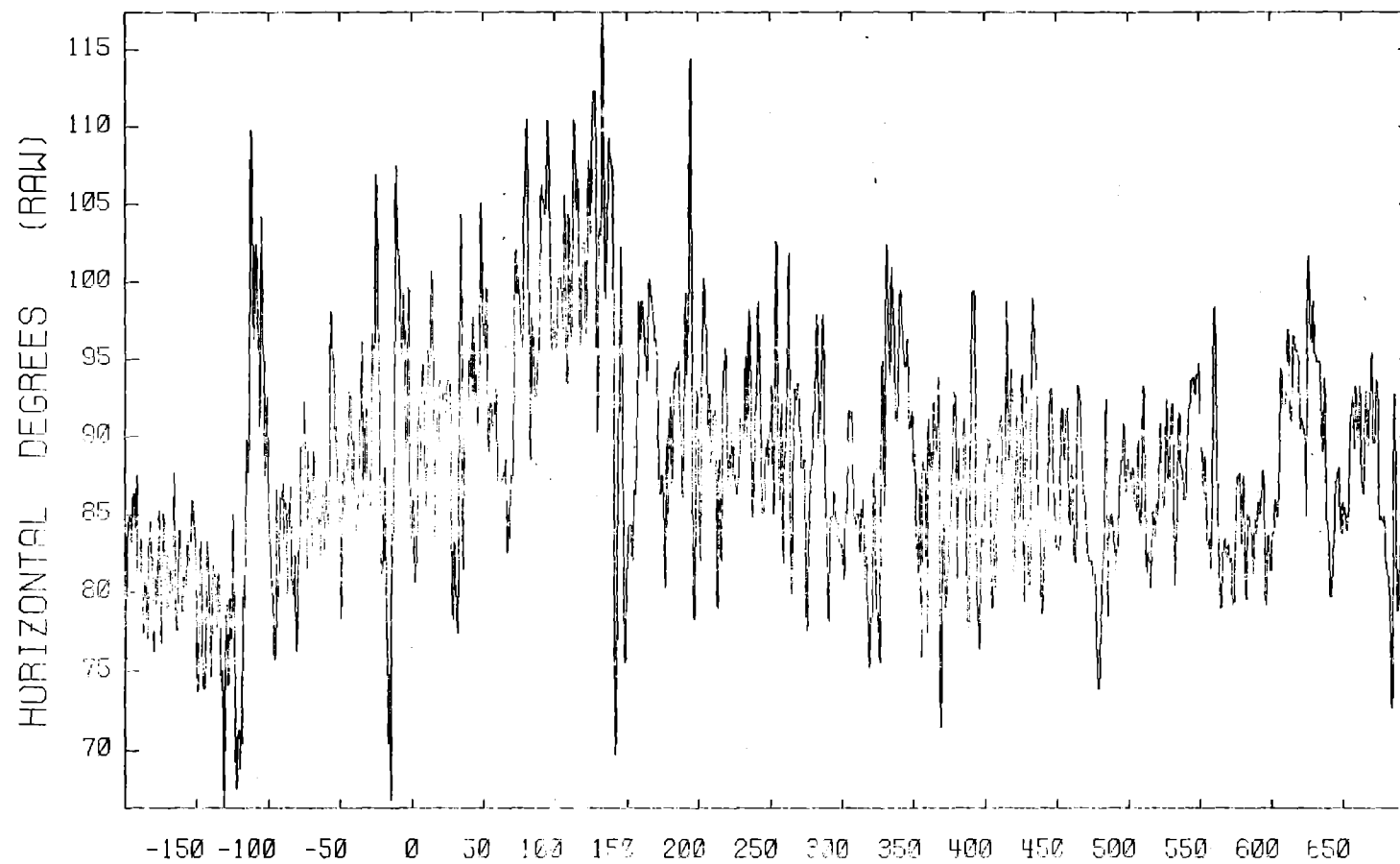
3-AXIS ANEMOMETER

3-SEP-80

S/N 386

BURR08

T02



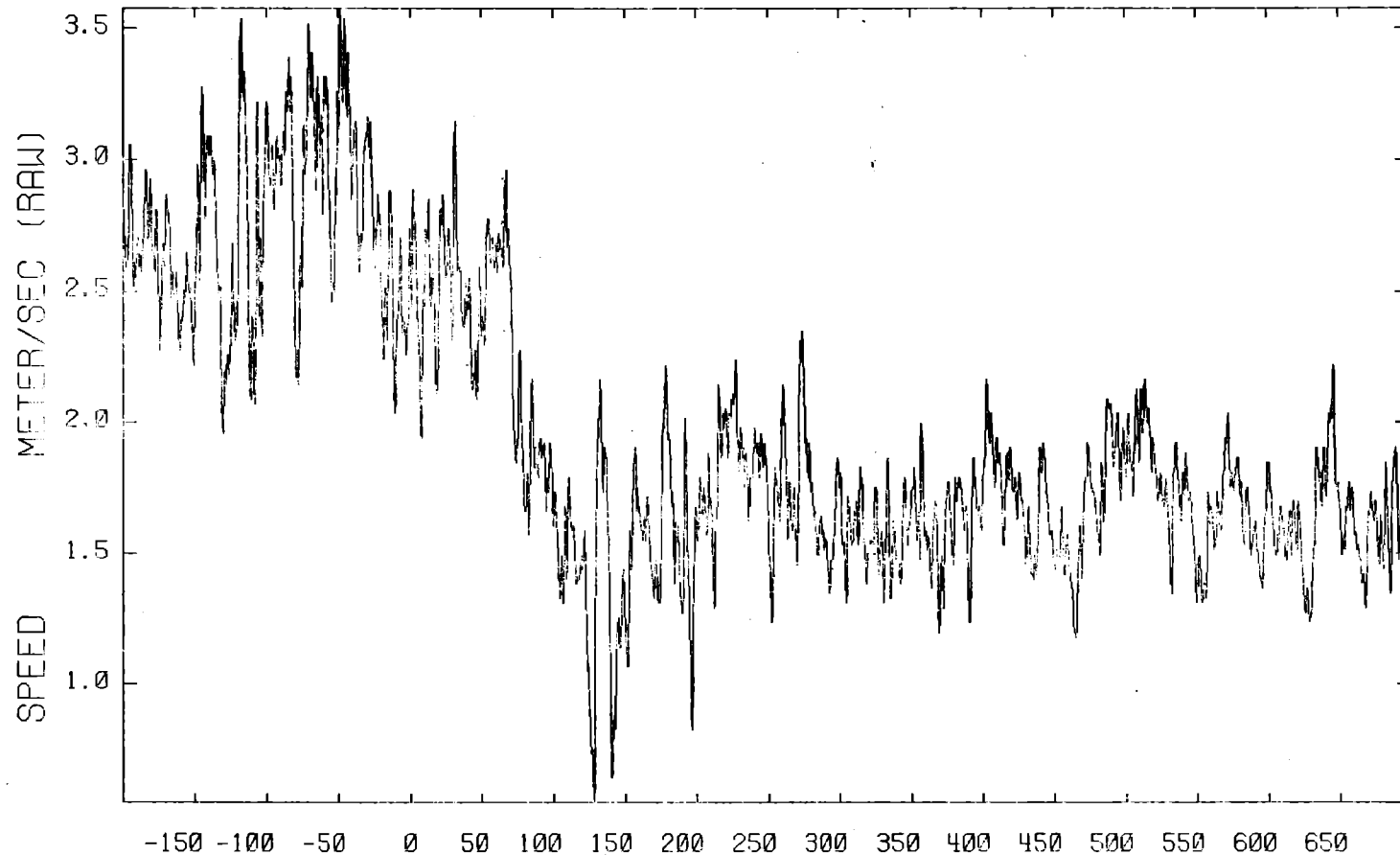
A09
03 METERS

Time(sec)
3-AXIS ANEMOMETER

3-SEP-80
S/N 381

BURR08

T02



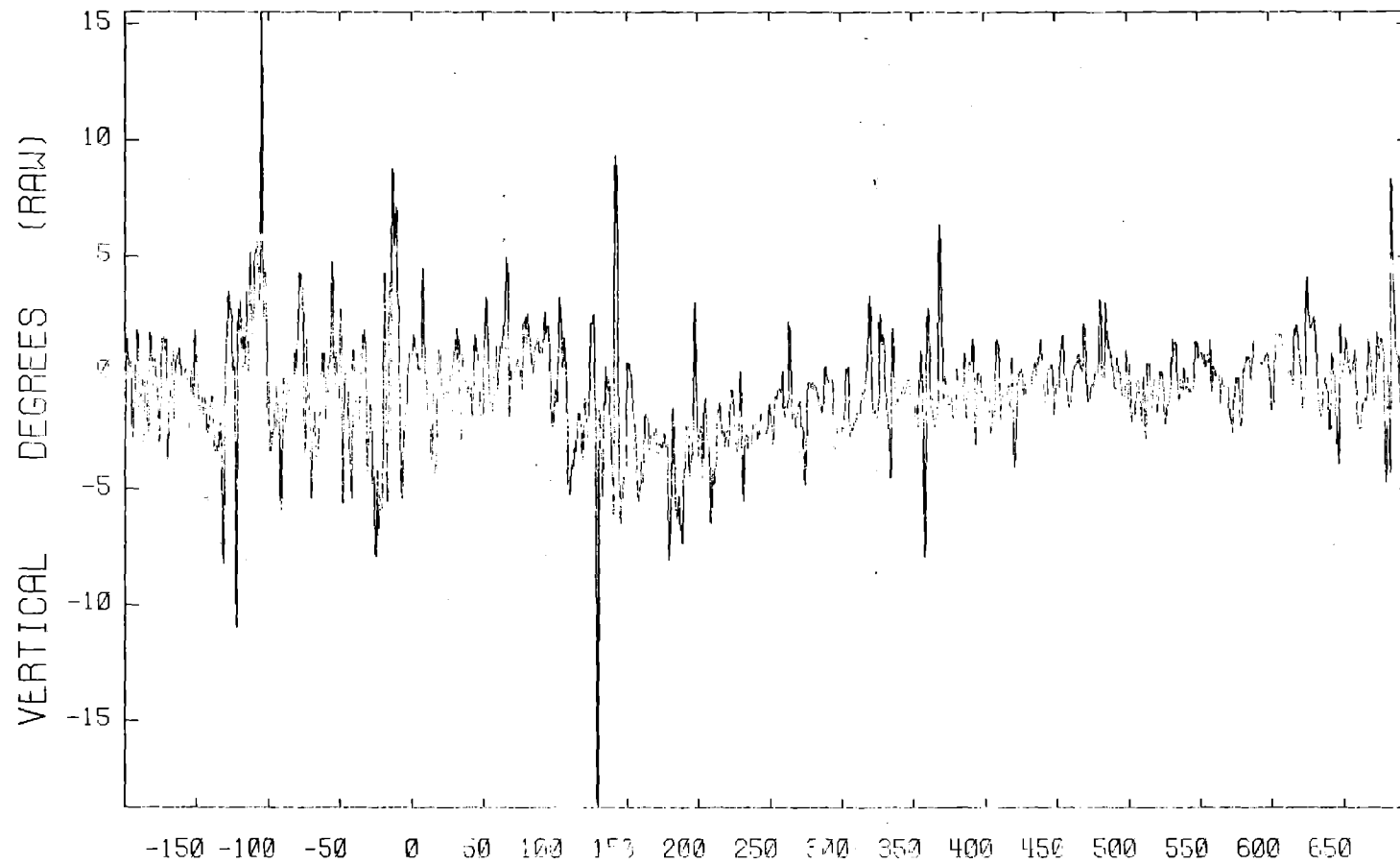
A10
03 METERS

Time(sec)
3-AXIS ANEMOMETER

3-SEP-80
S/N 381

BURR08

T02



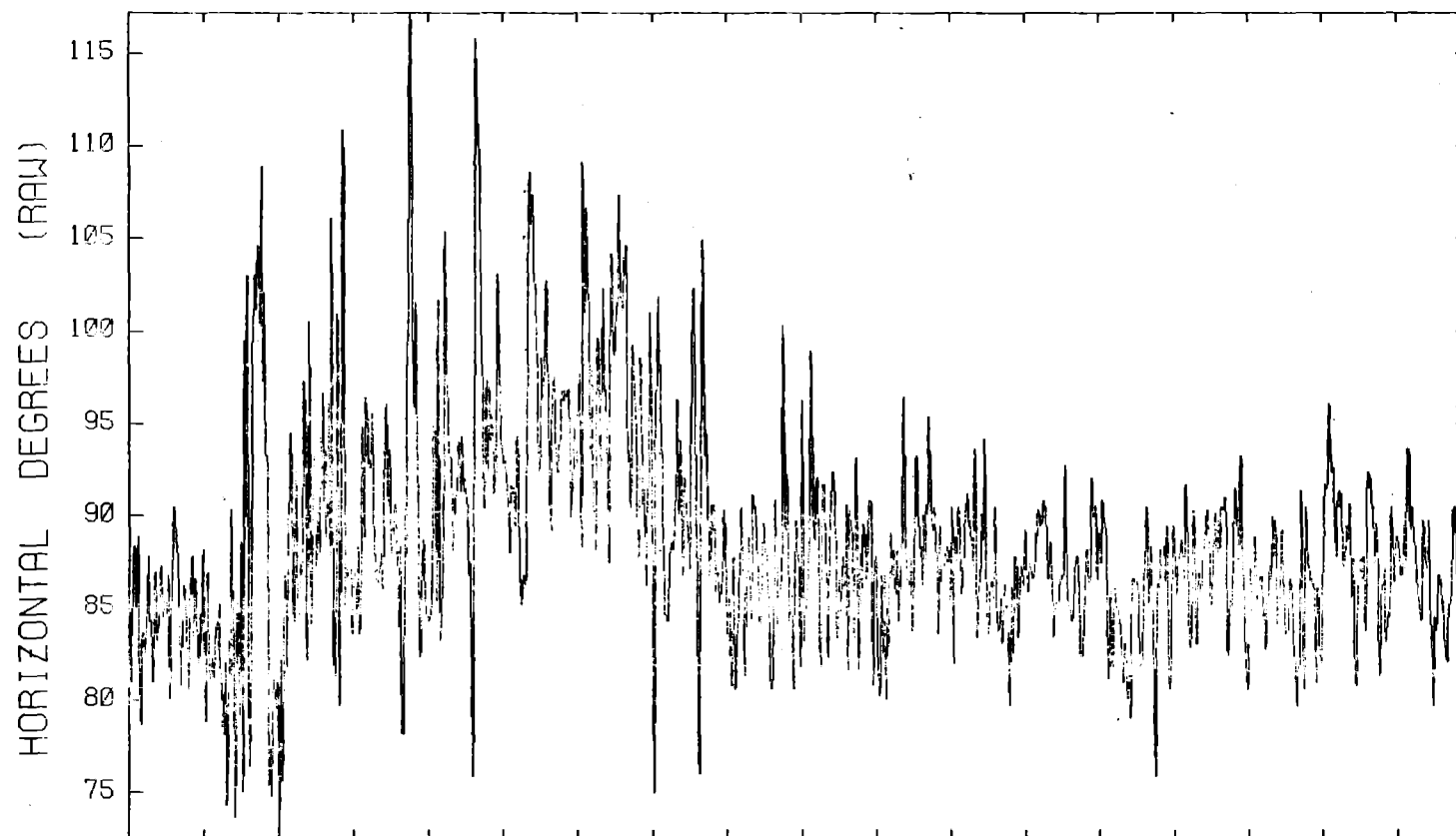
A11
03 METERS

Time(sec)
3-AXIS ANEMOMETER

3-SEP-80
S/N 381

BURR08

T02



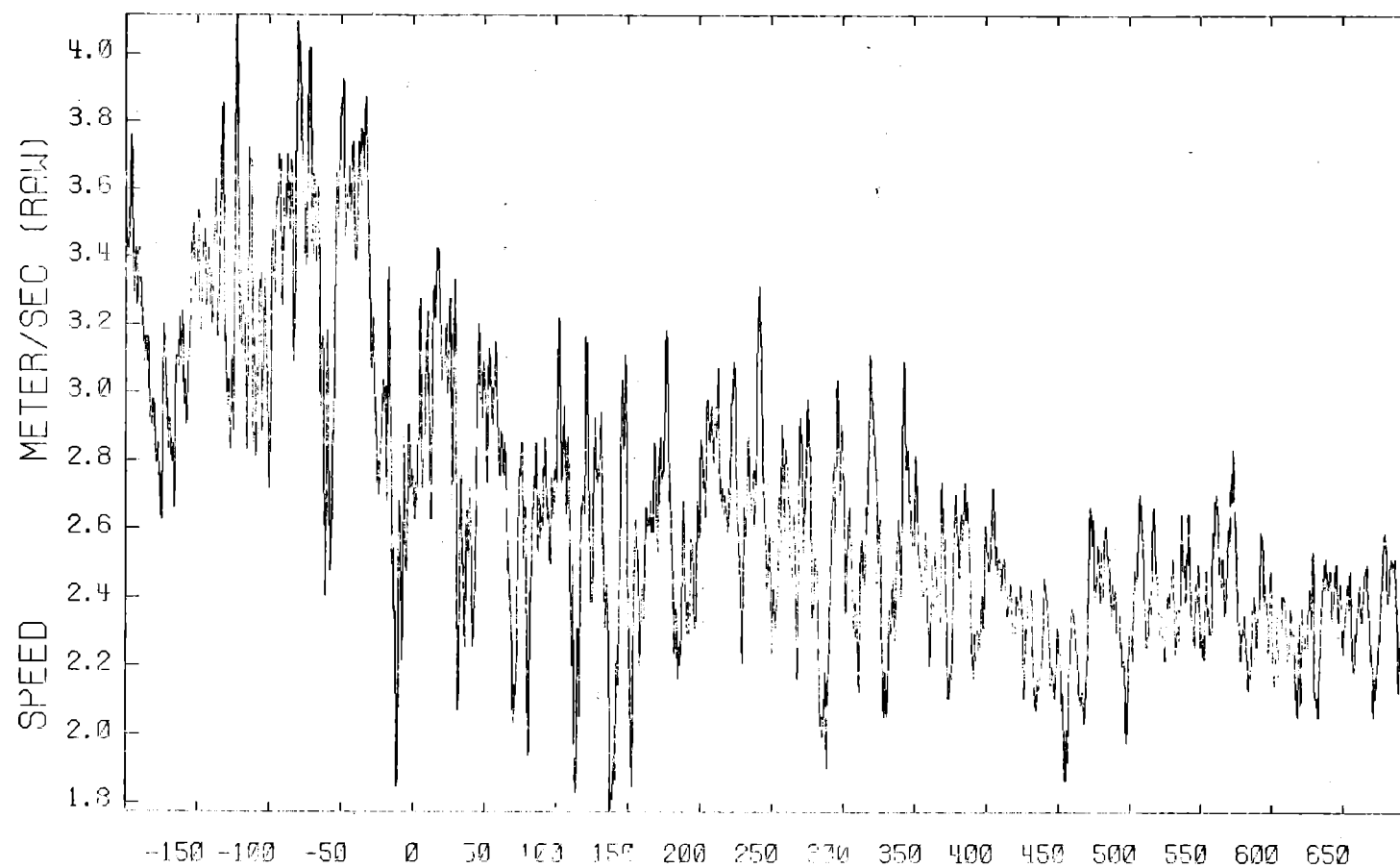
A12
08 METERS

Time(sec)
3-AXIS ANEMOMETER

3-SEP-80
S/N 380

BURR08

T02



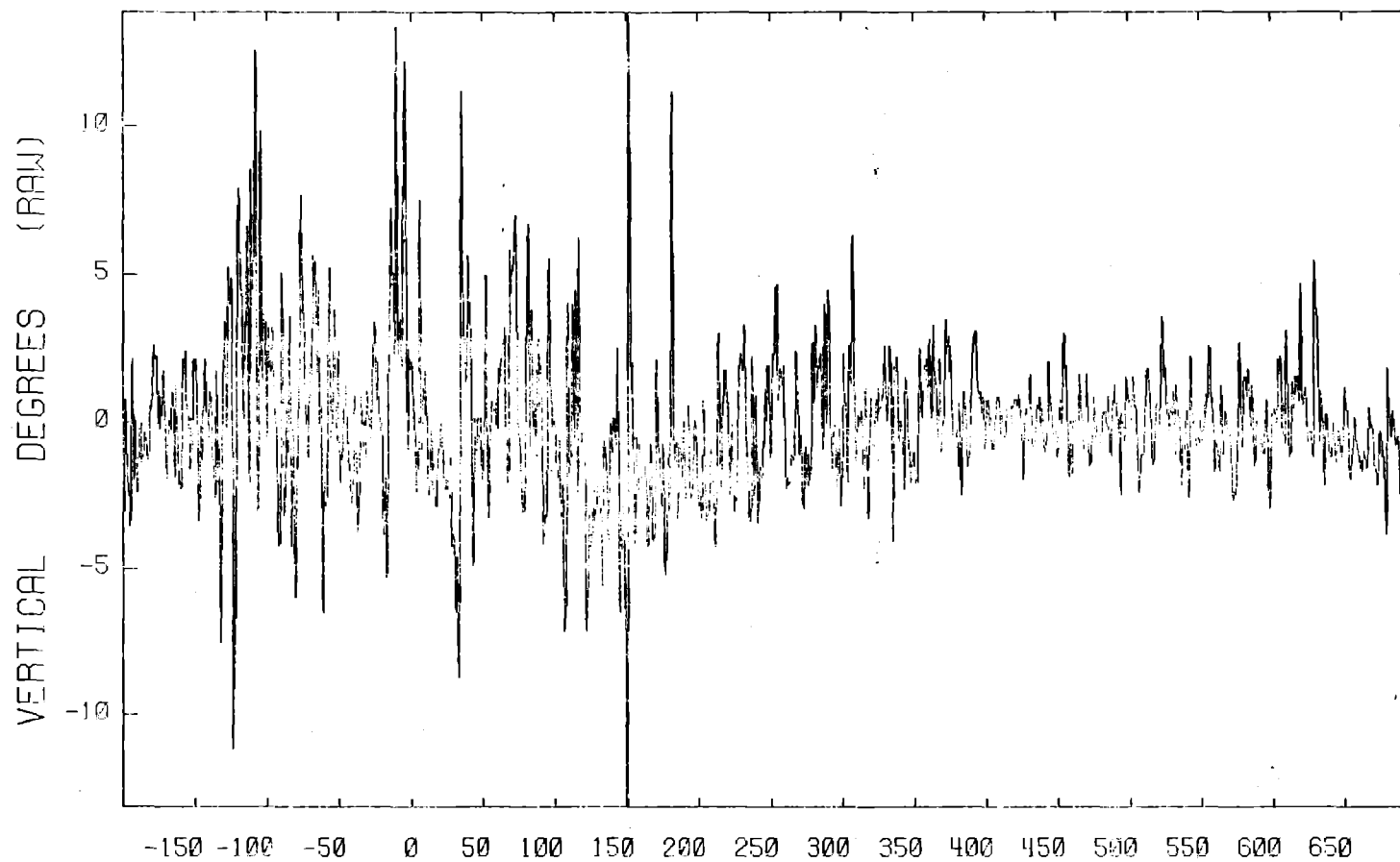
A13
08 METERS

Time(sec)
3-AXIS ANEMOMETER

3-SEP-80
S/N 380

BURR08

T02



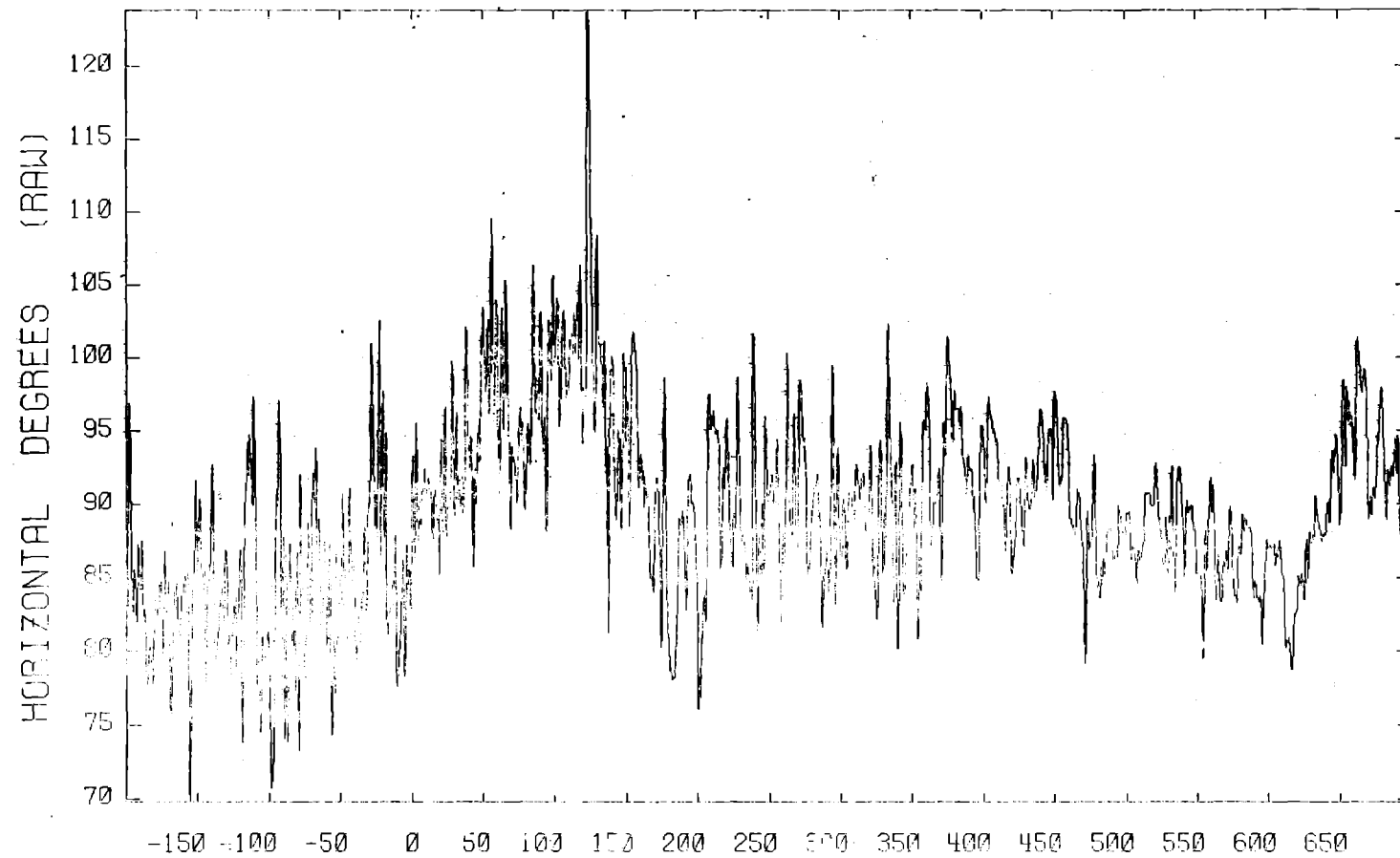
A14
08 METERS

Time(sec)
C AXIS ANEMOMETER

3-SEP-80
S/N 380

BURR08

T03



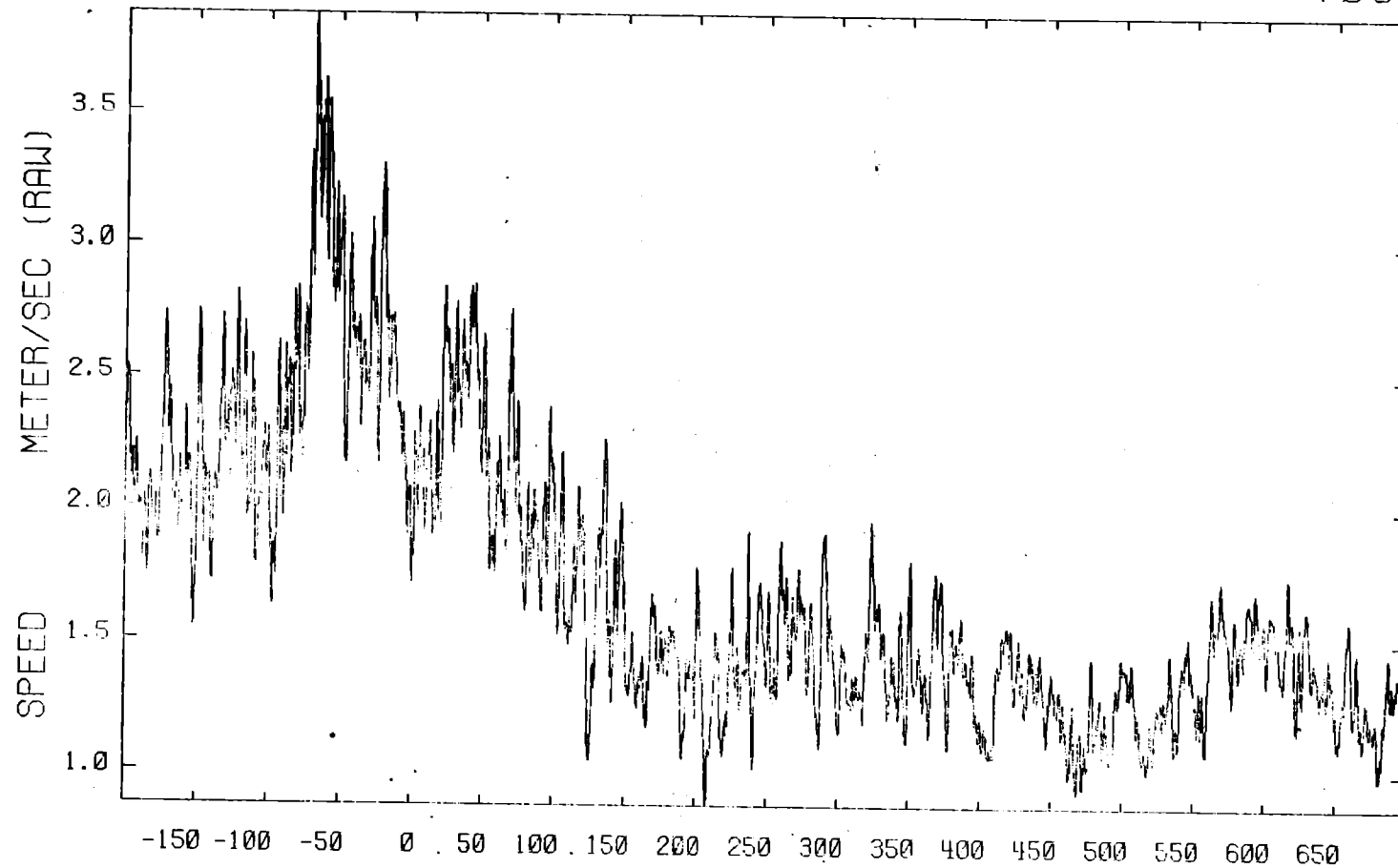
A06
01 METERS

Time(sec)
3-AXIS ANEMOMETER

3-SEP-80
S/N 377

BURR08

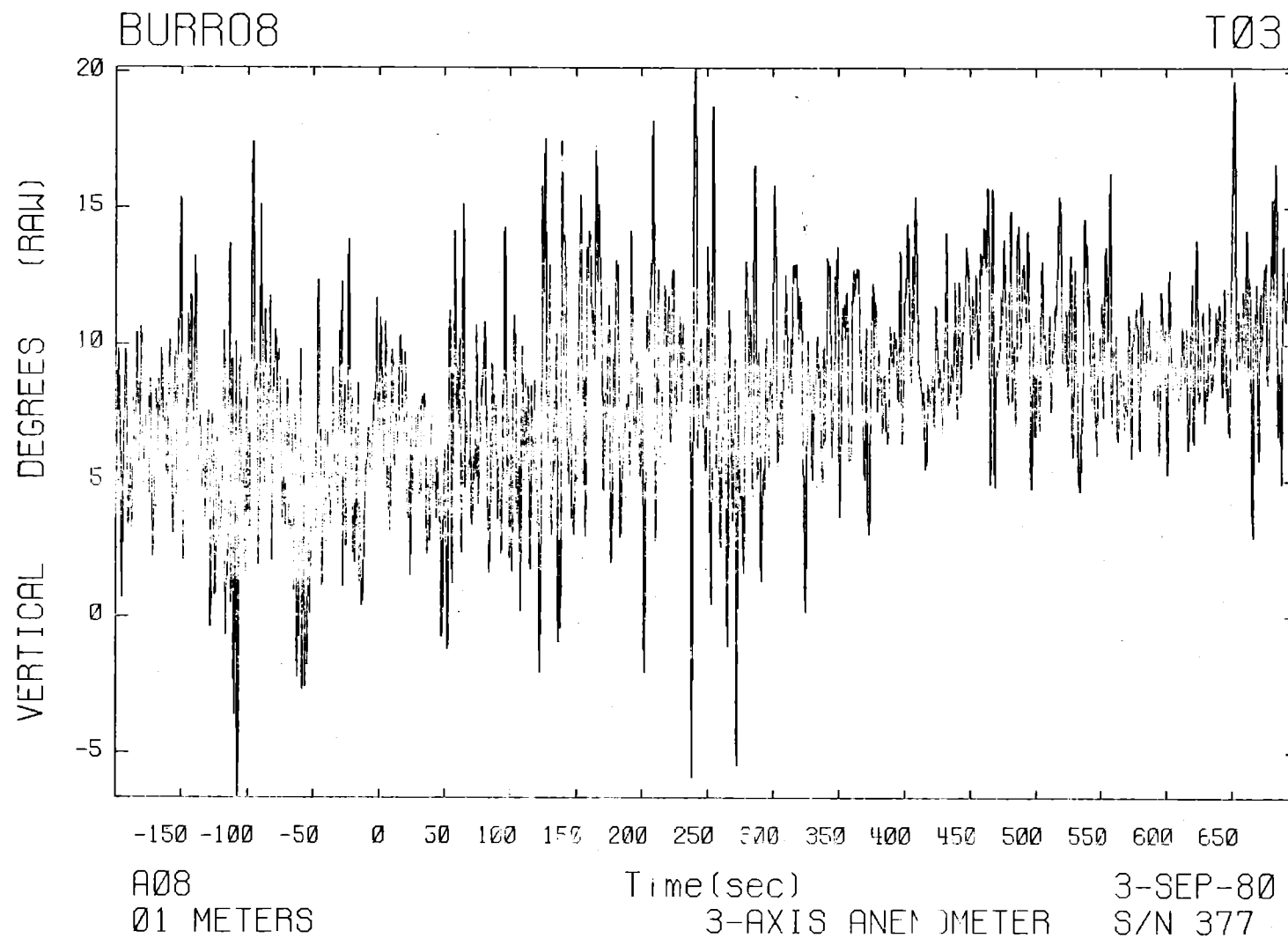
T03



A07
01 METERS

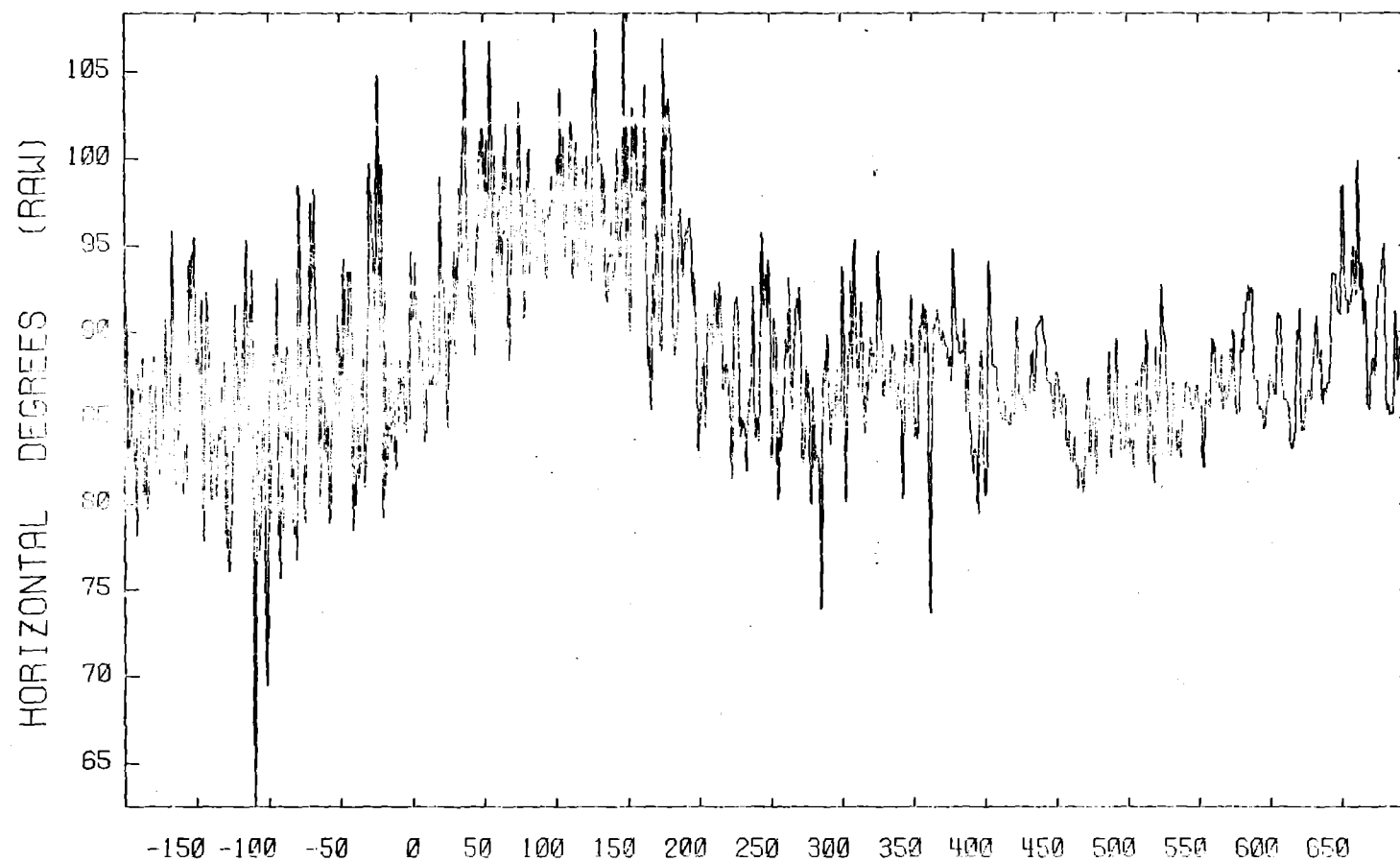
Time(sec)
3-AXIS ANEMOMETER

3-SEP-80
S/N 377



BURR08

T03



A09

03 METERS

Time(sec)

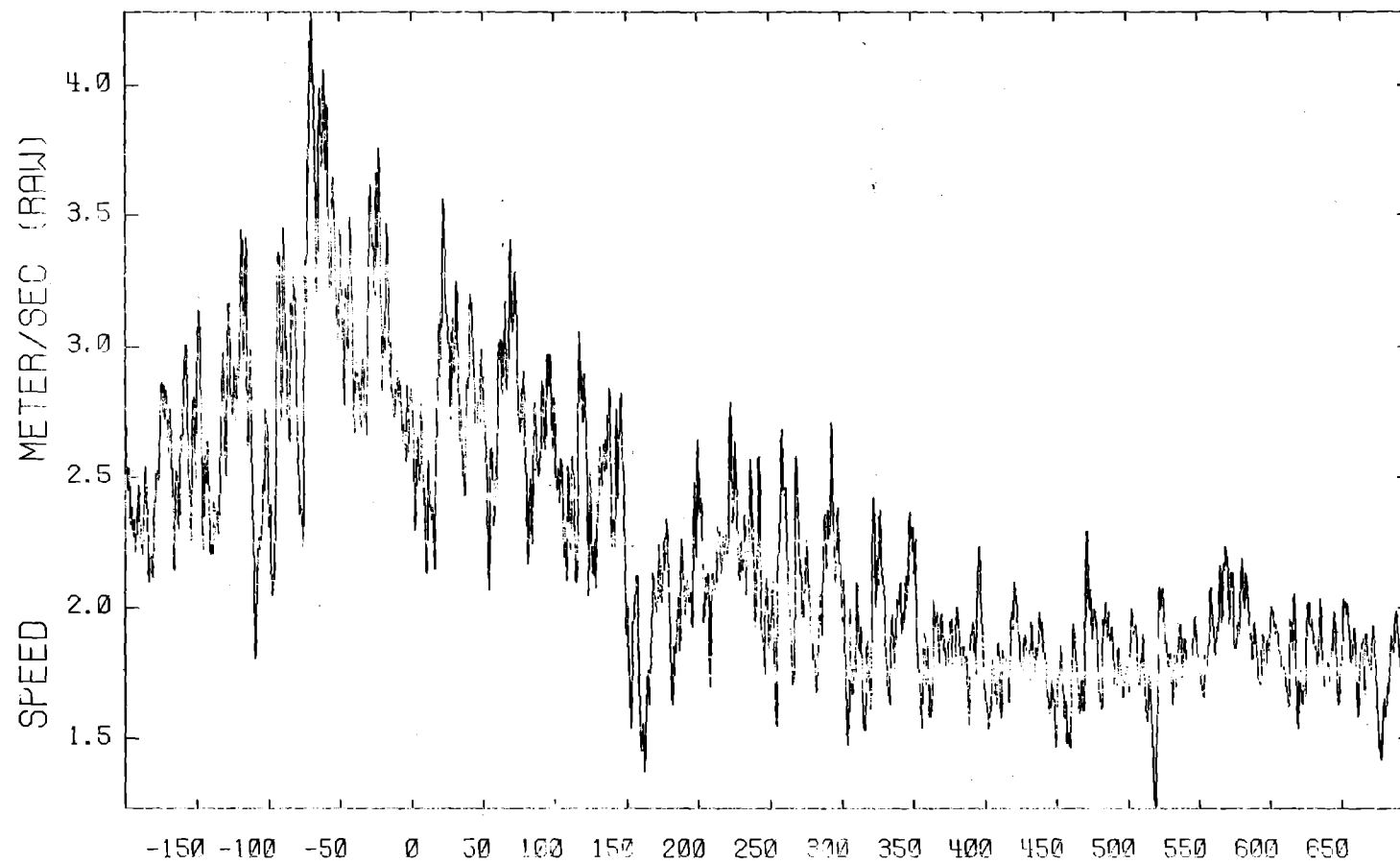
3-AXIS ANEMOMETER

3-SEP-80

S/N 378

BURR08

T03



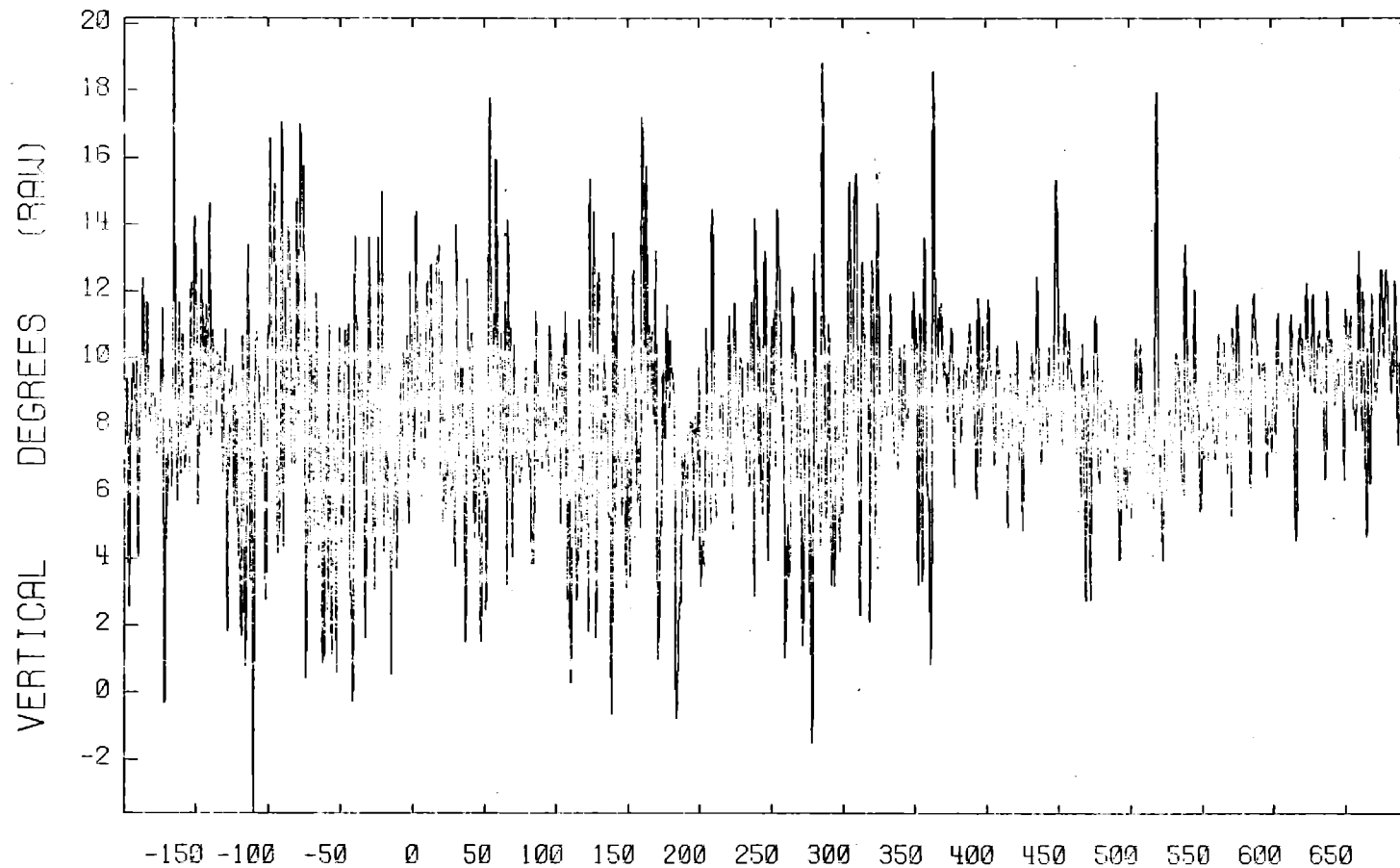
A10
03 METERS

Time(sec)
3-AXIS ANEMOMETER

3-SEP-80
S/N 378

BURR08

T03



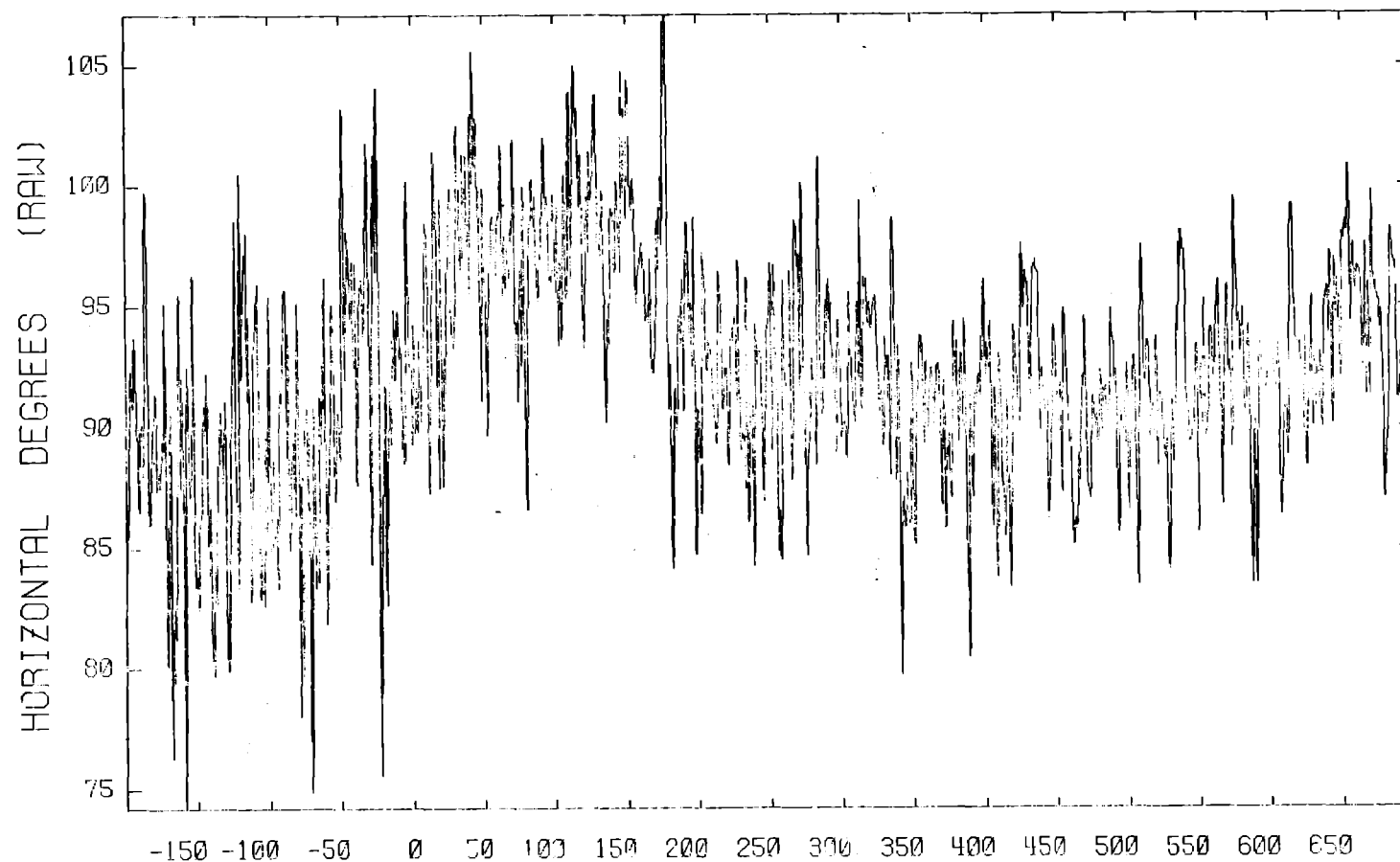
A11
03 METERS

Time(sec)
3-AXIS ANEMOMETER

3-SEP-80
S/N 378

BURR08

T03



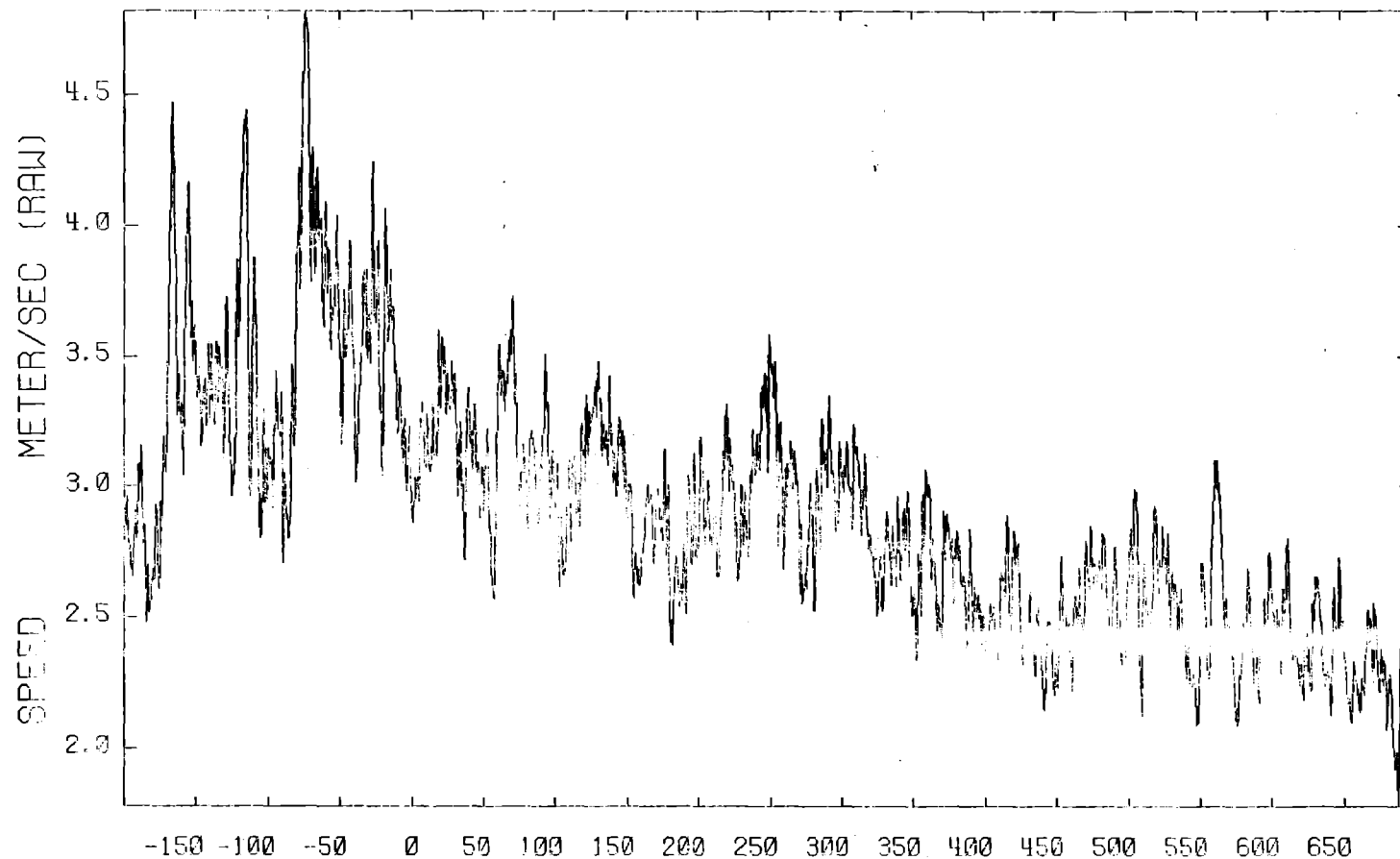
A12
08 METERS

Time(sec)
3-AXIS ANEMOMETER

3-SEP-80
S/N 379

BURR08

T03



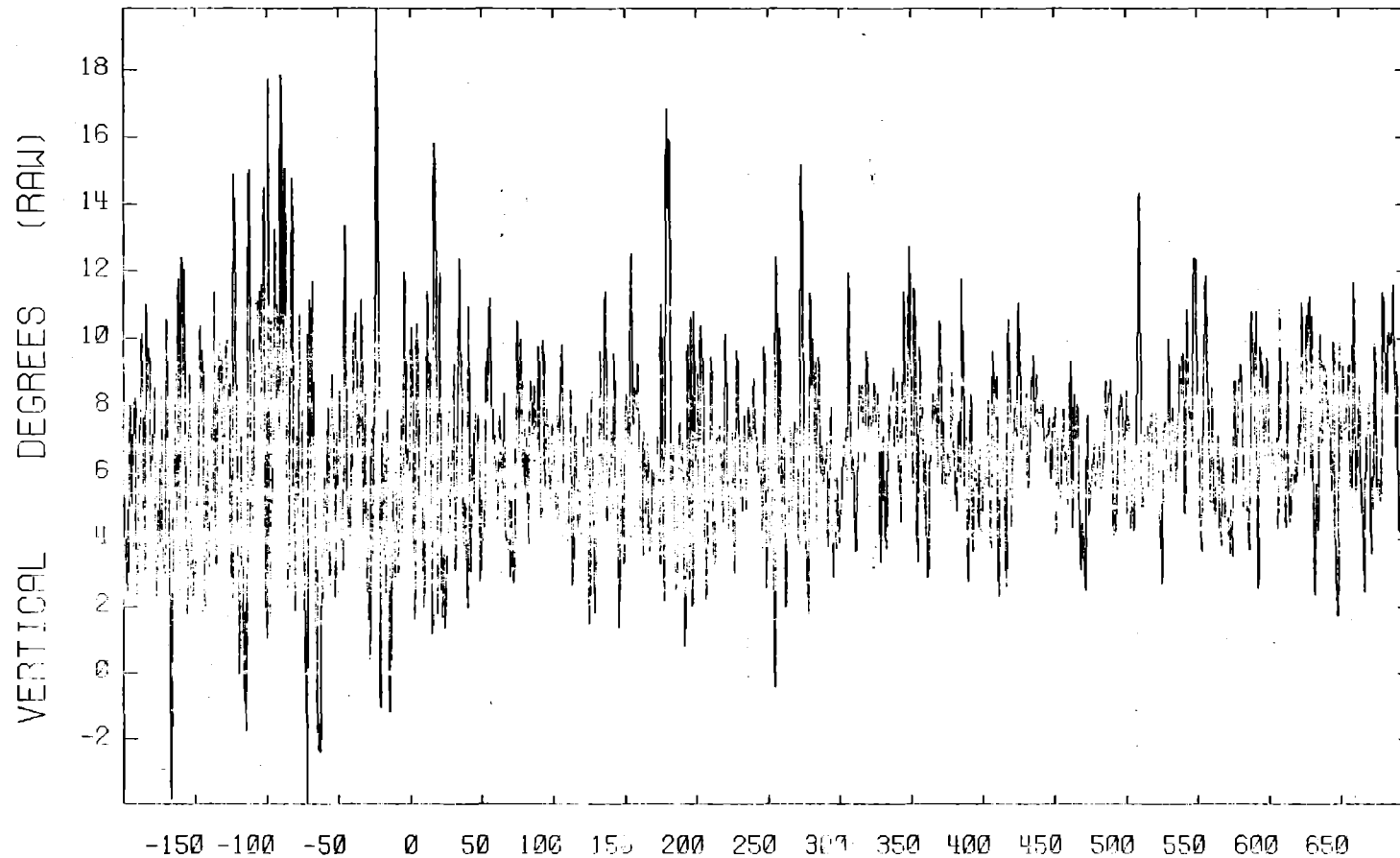
A13
08 METERS

Time(sec)
3-AXIS ANEMOMETER

3-SEP-80
S/N 379

BURR08

T03



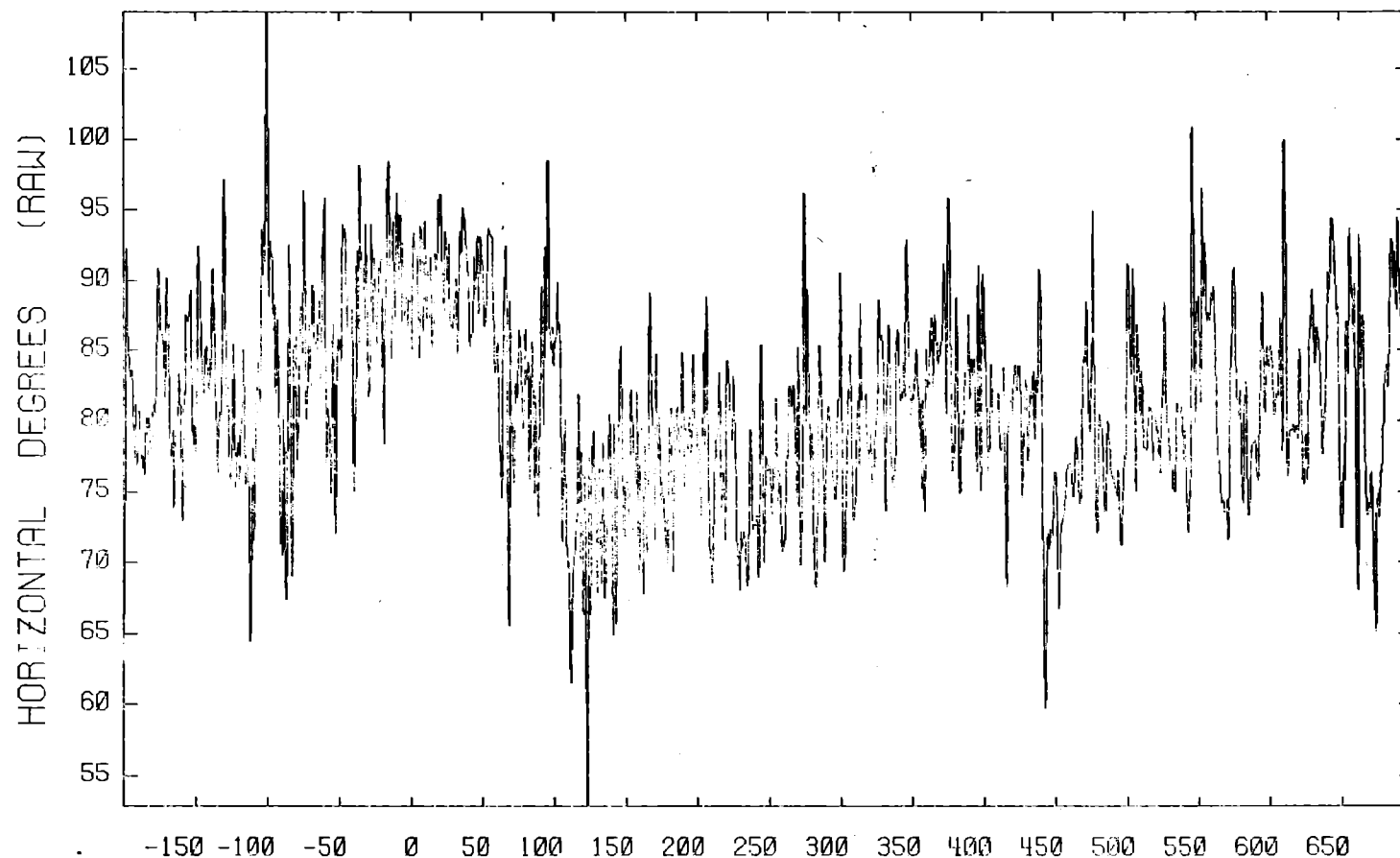
A14
08 METERS

Time(sec)
3-AXIS ANEM METER

3-SEP-80
S/N -----

BURR08

T04



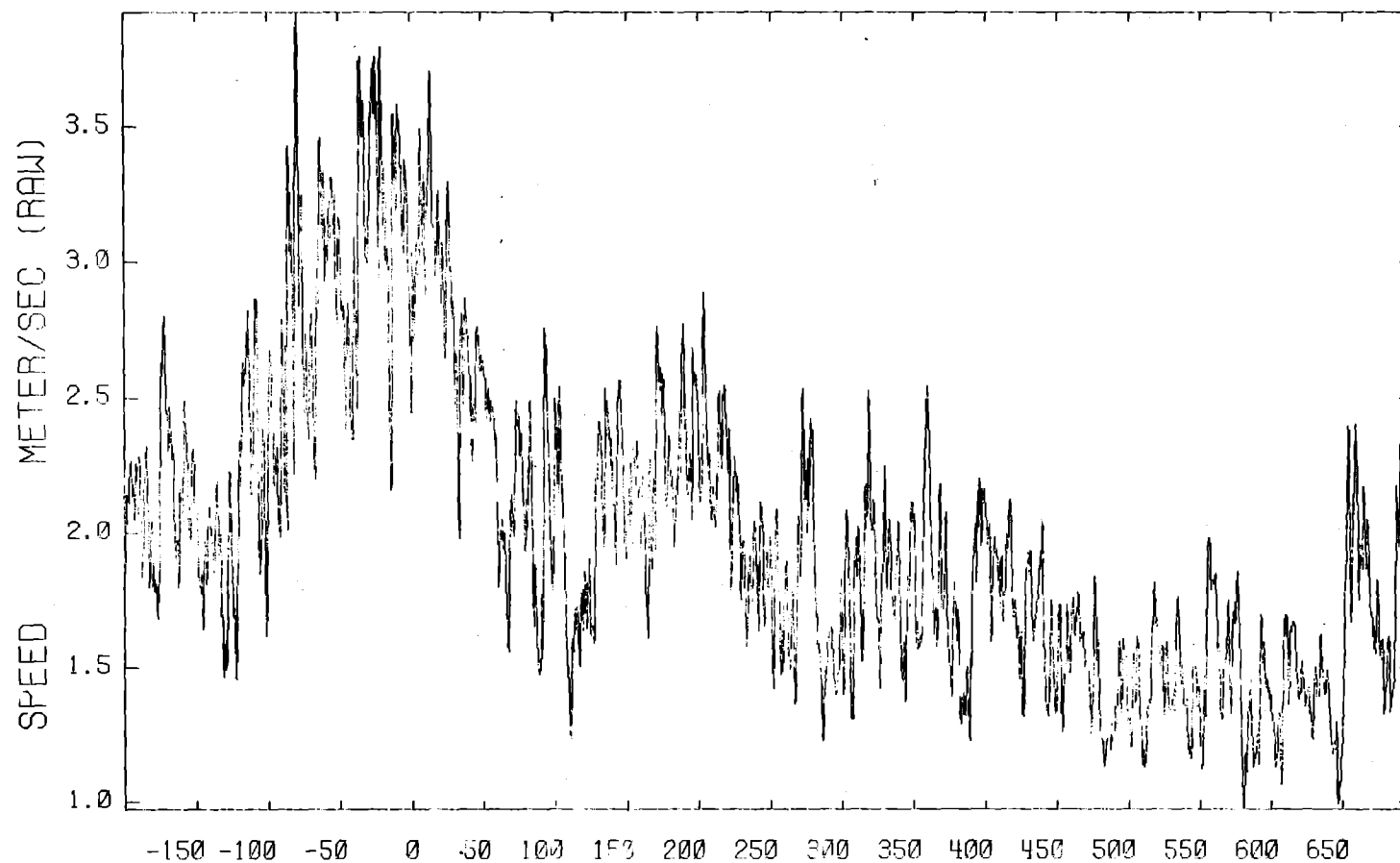
A06
01 METERS

Time(sec)
3-AXIS ANEMOMETER

3-SEP-80
S/N 375

BURR08

T04



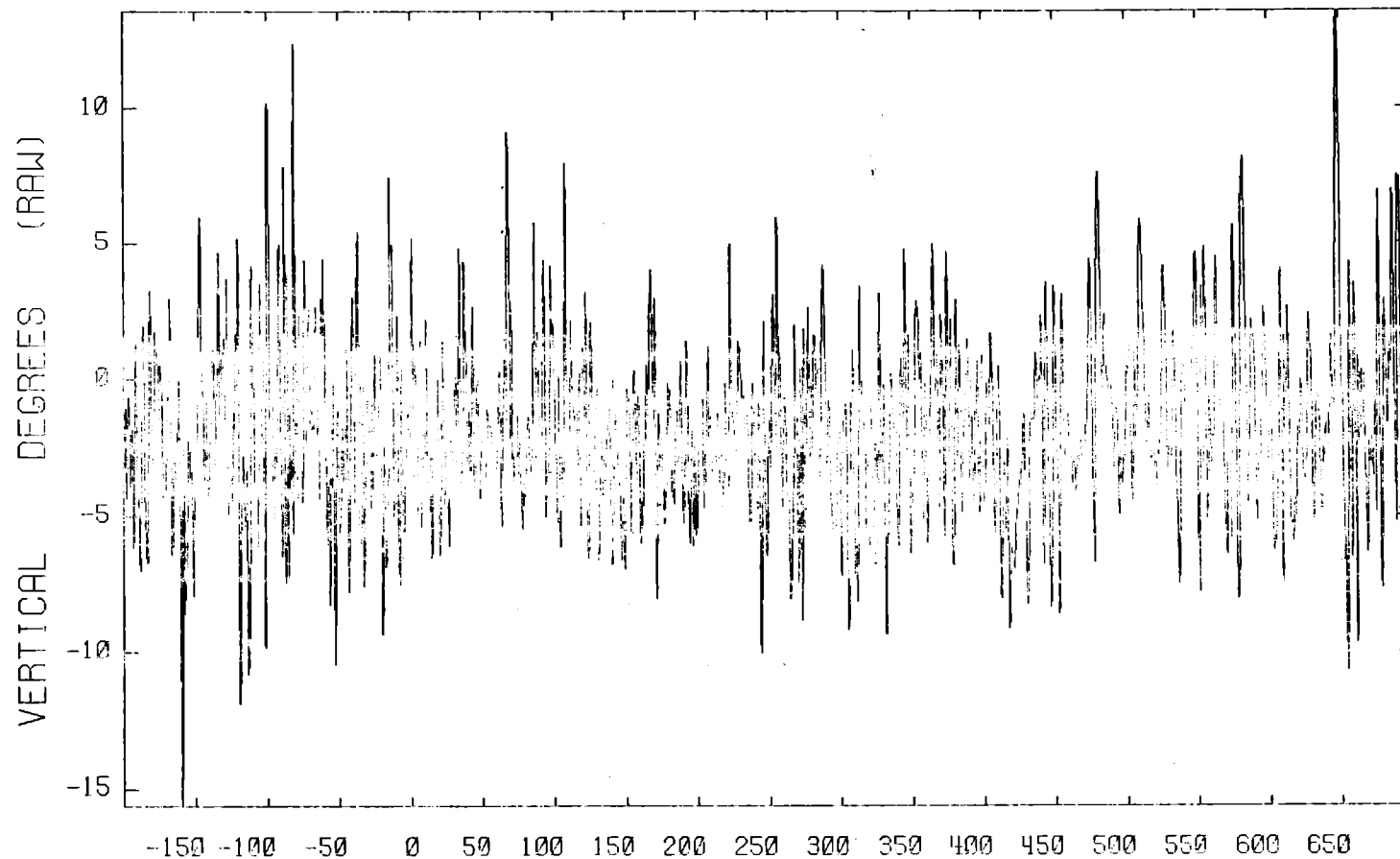
A07
01 METERS

Time(sec)
3-AXIS ANEMOMETER

3-SEP-80
S/N 375

BURR08

T04



A08

01 METERS

Time(sec)

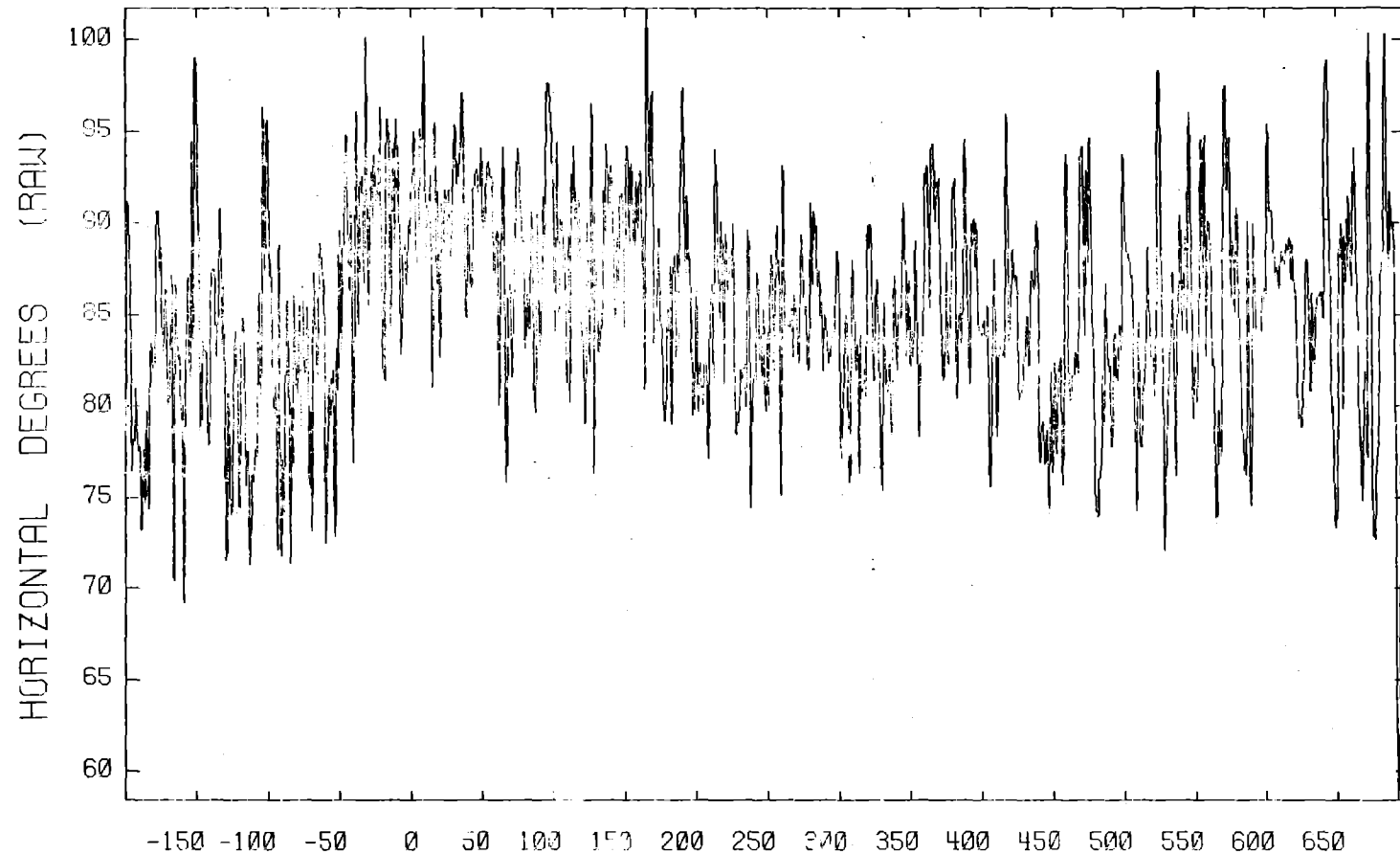
3-AXIS ANEMOMETER

3-SEP-80

S/N 375

BURR08

T04



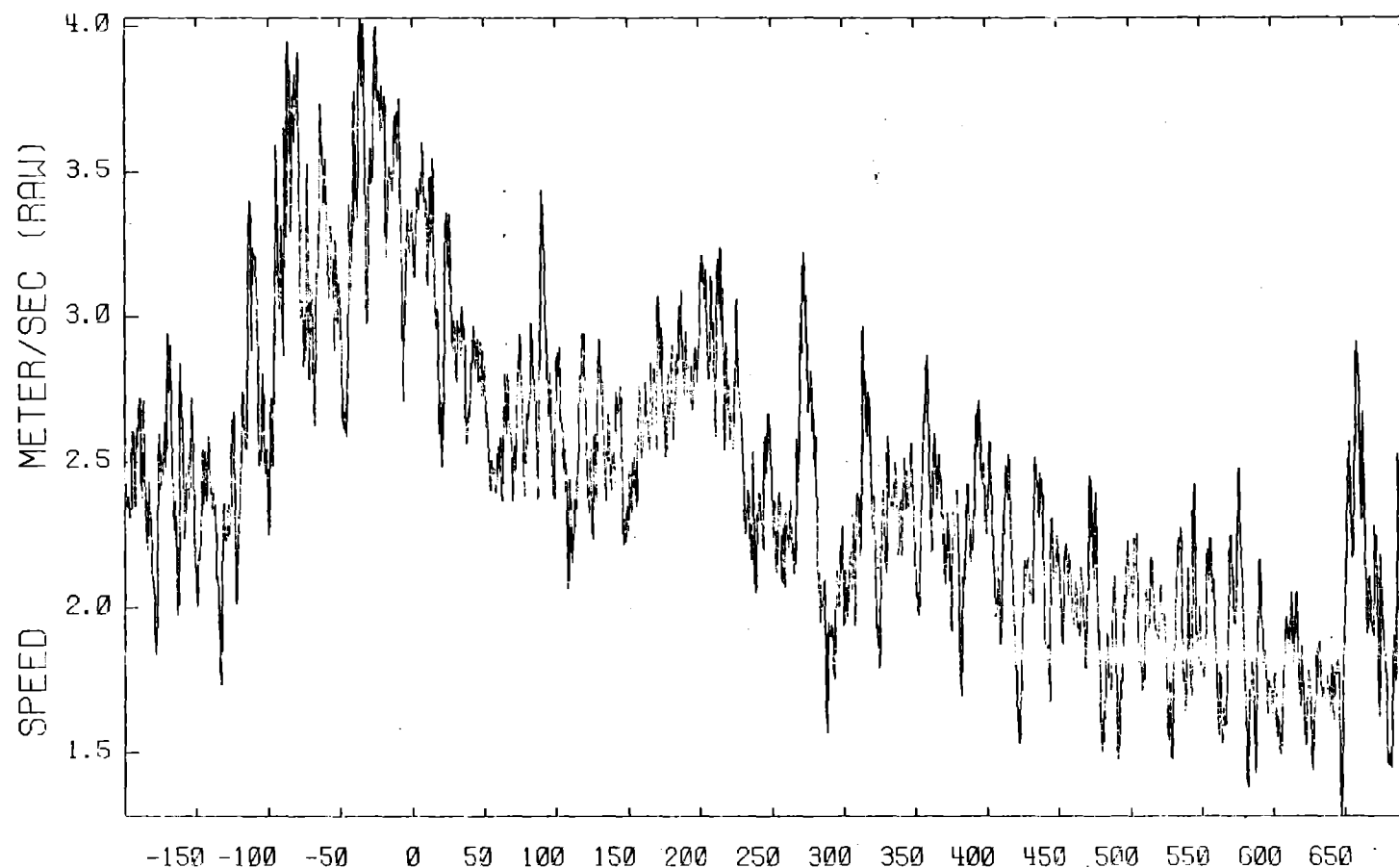
A09
03 METERS

Time(sec)
3-AXIS ANEMOMETER

3-SEP-80
S/N 373

BURR08

T04



A10

03 METERS

Time(sec)

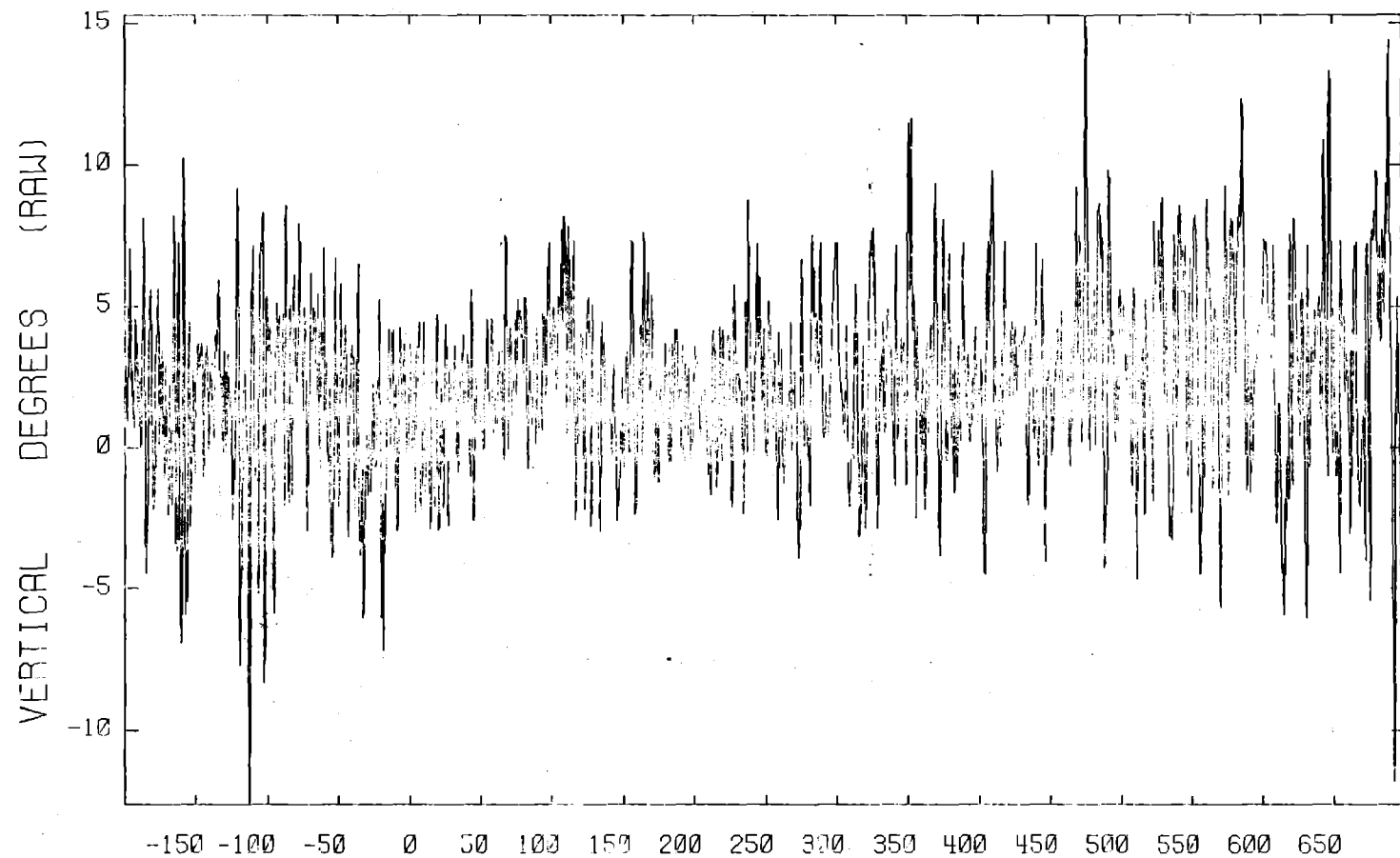
3-AXIS ANEMOMETER

3-SEP-80

8/N 373

BURR08

T04



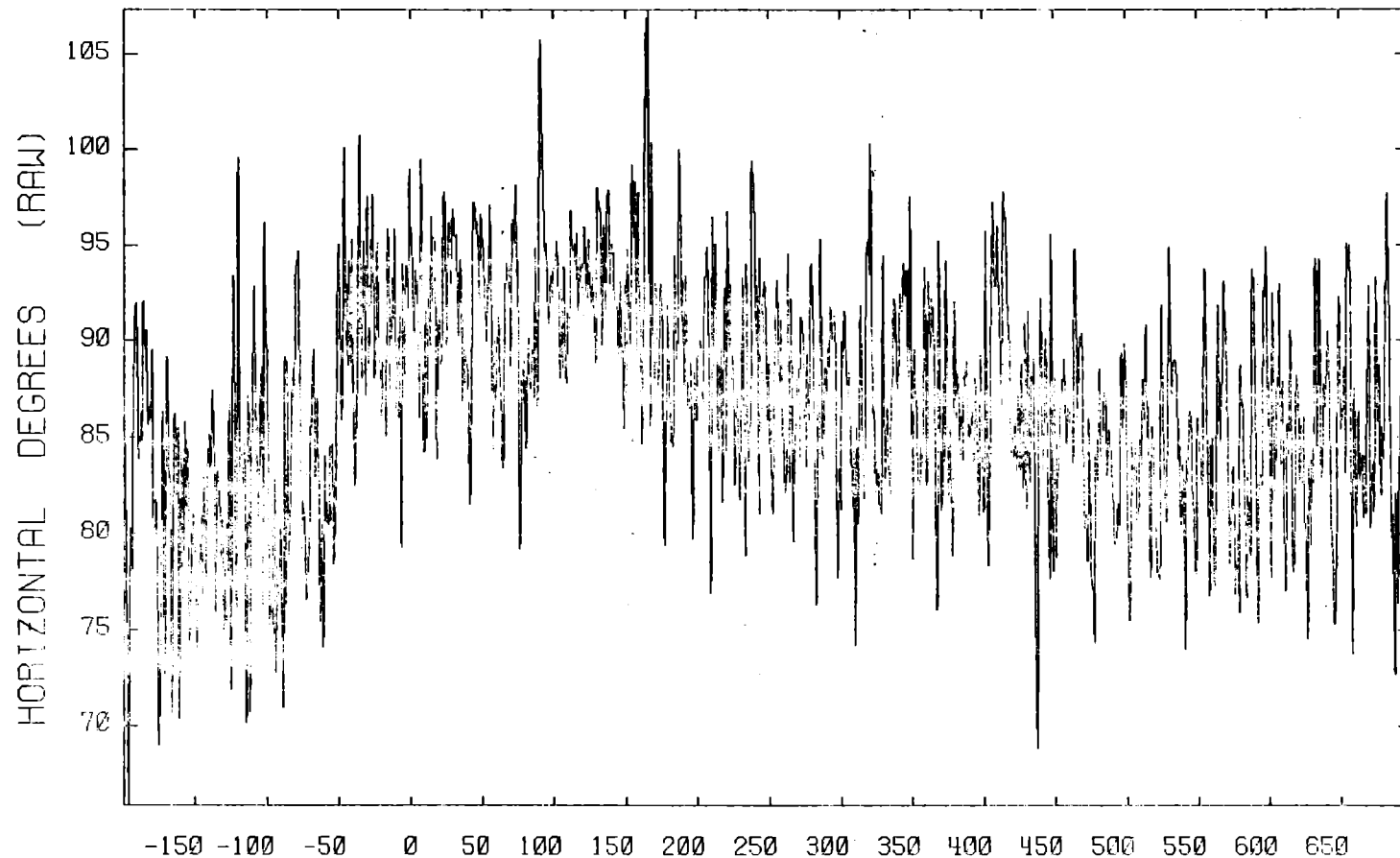
A11
03 METERS

Time(sec)
3-AXIS ANEM METER

3-SEP-80
S/N 373

BURR08

T04



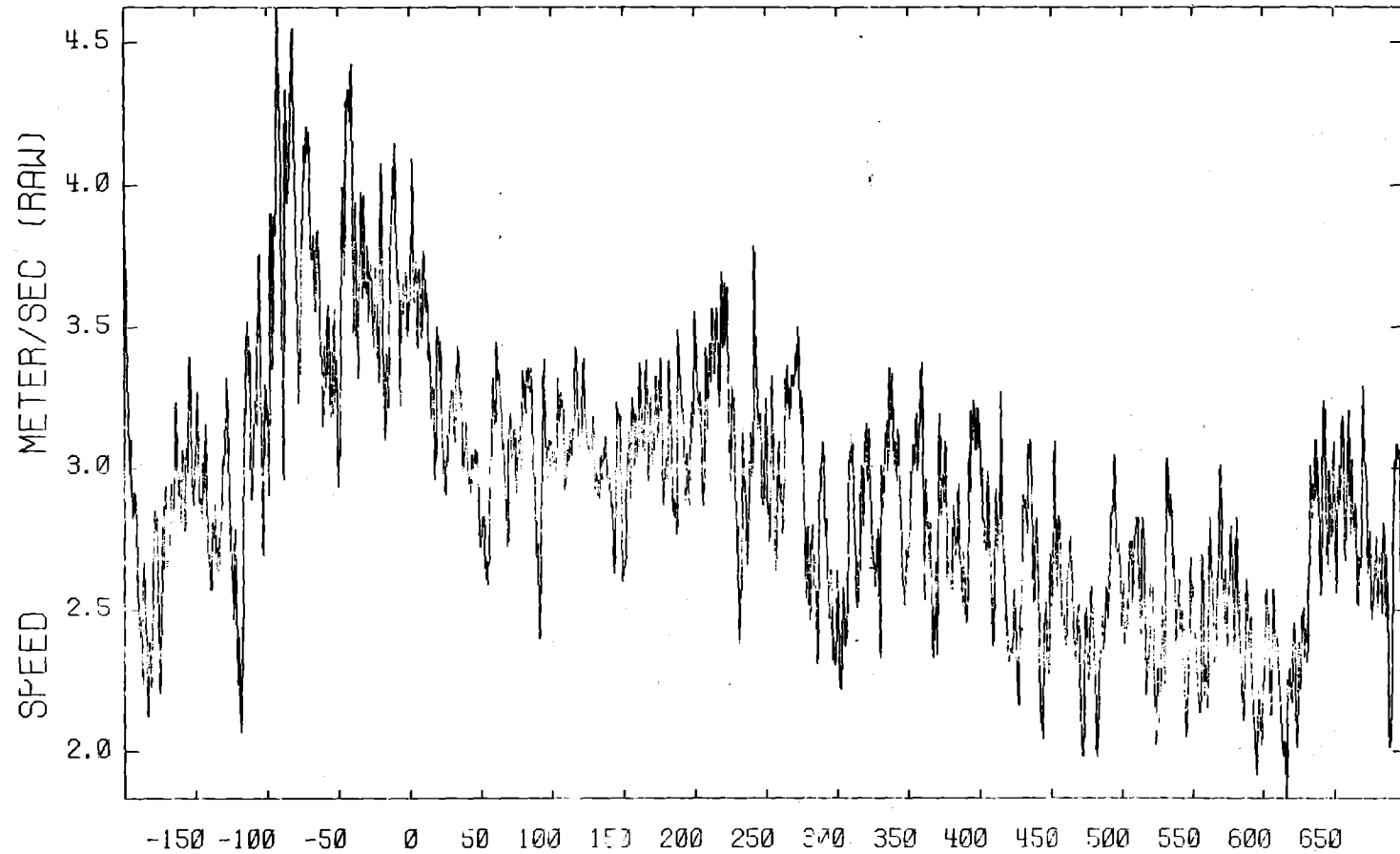
A12
08 METERS

Time(sec)
3-AXIS ANEMOMETER

3-SEP-80
S/N 382

BURR08

T04



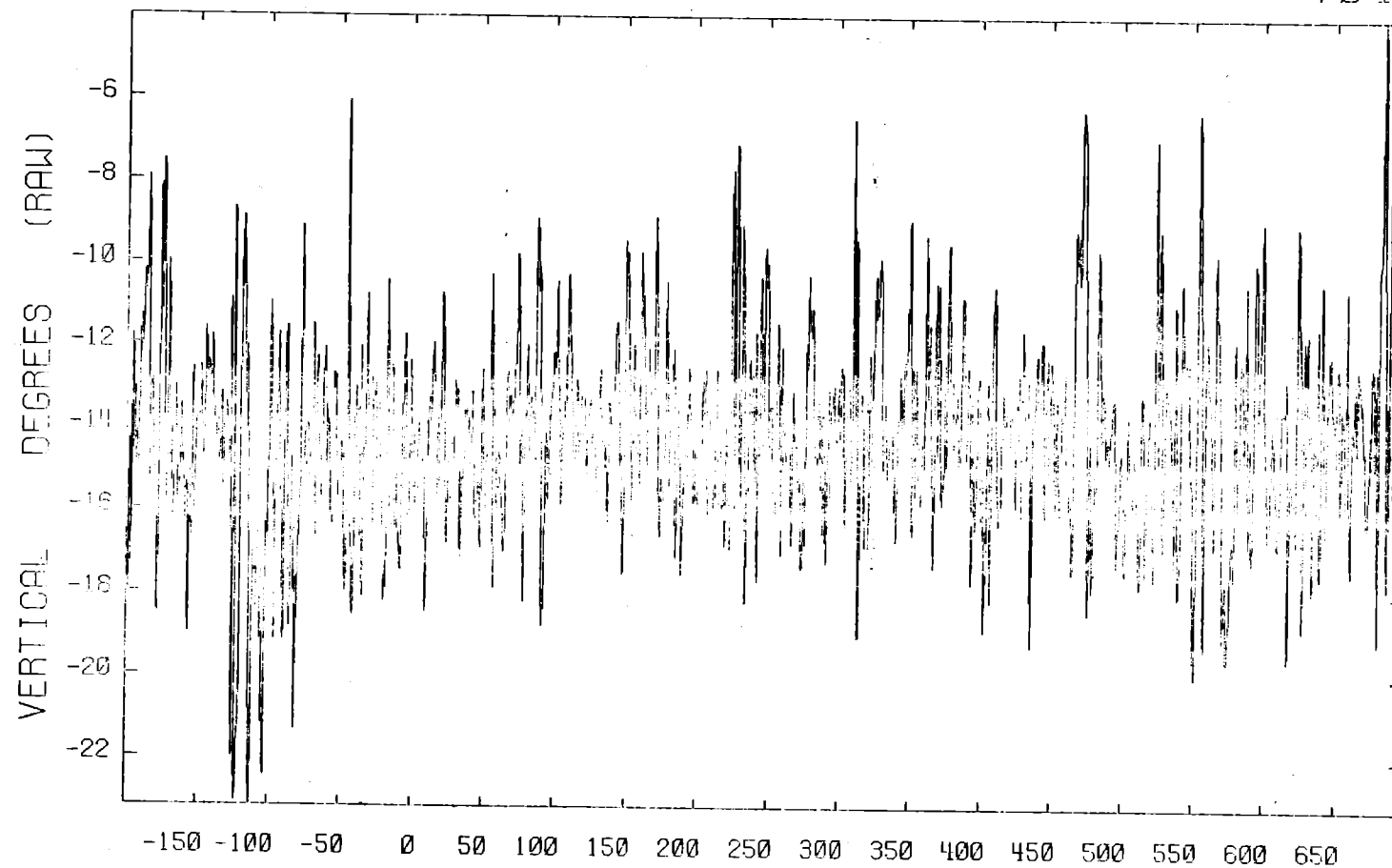
A13
08 METERS

Time(sec)
3-AXIS ANEM METER

3-SEP-80
S/N 382

BURR08

T04



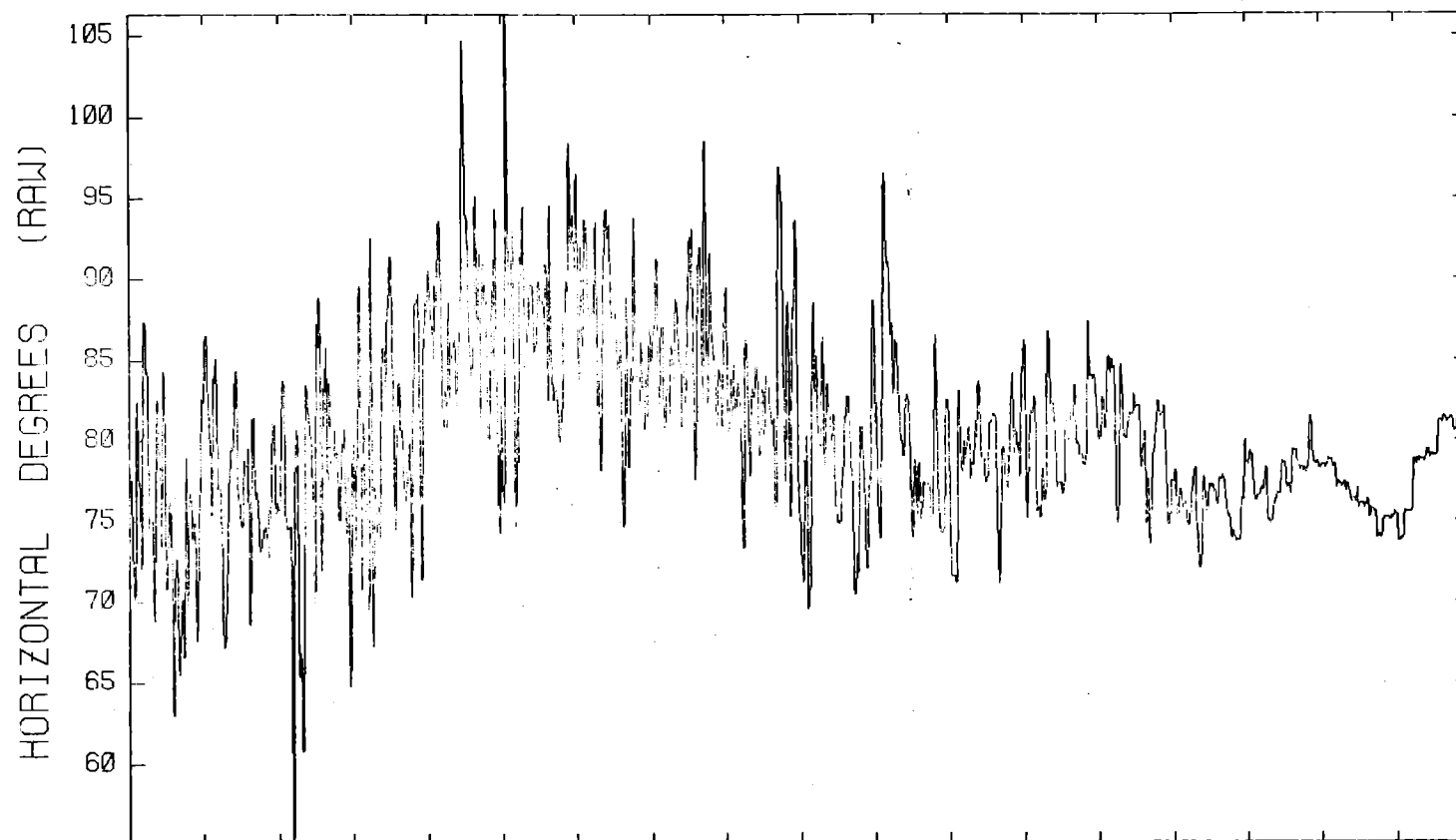
A14
08 METERS

Time(sec)
3-AXIS ANEMOMETER

3-SEP-80
S/N 382

BURR08

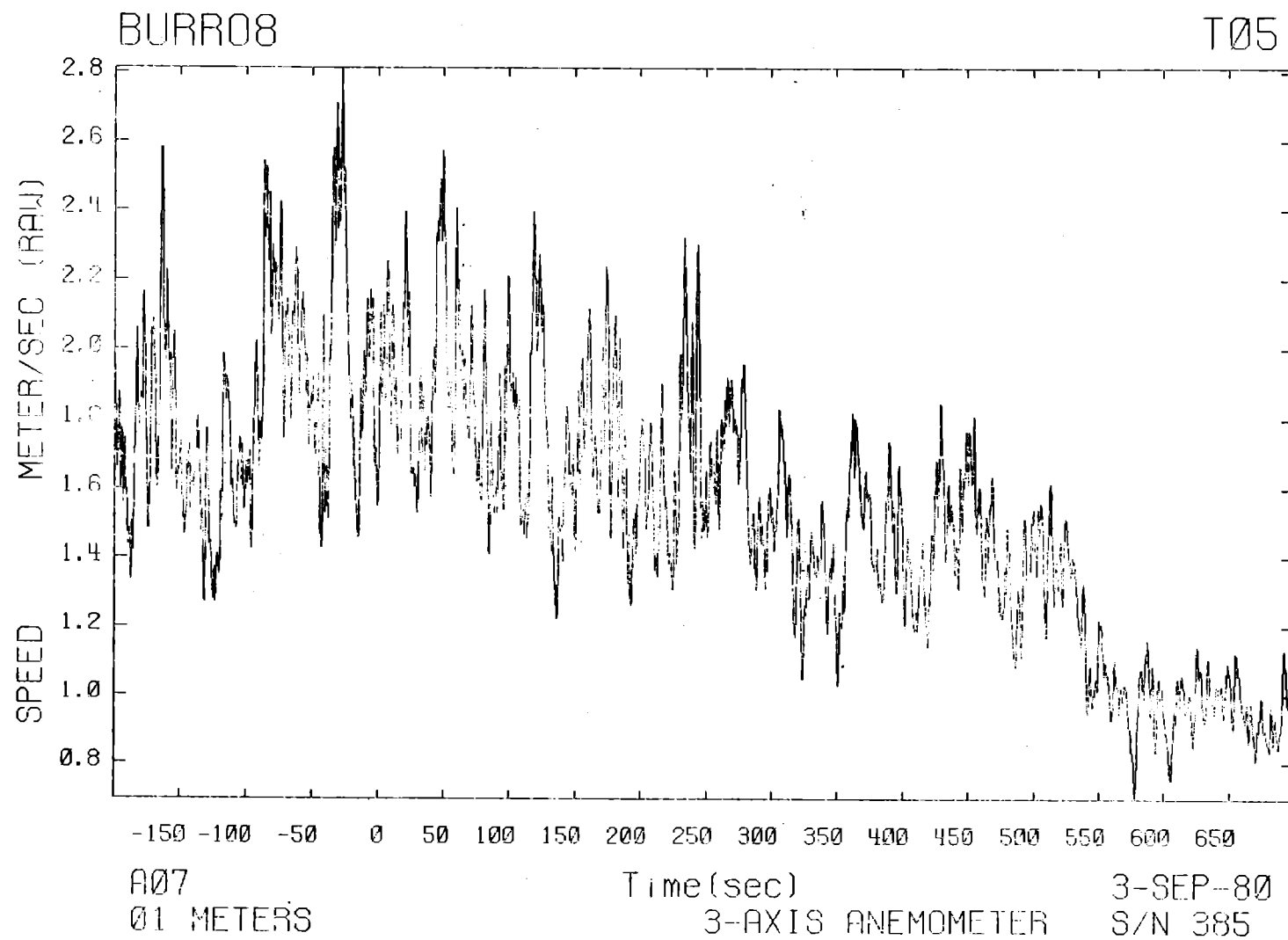
T05



A06
01 METERS

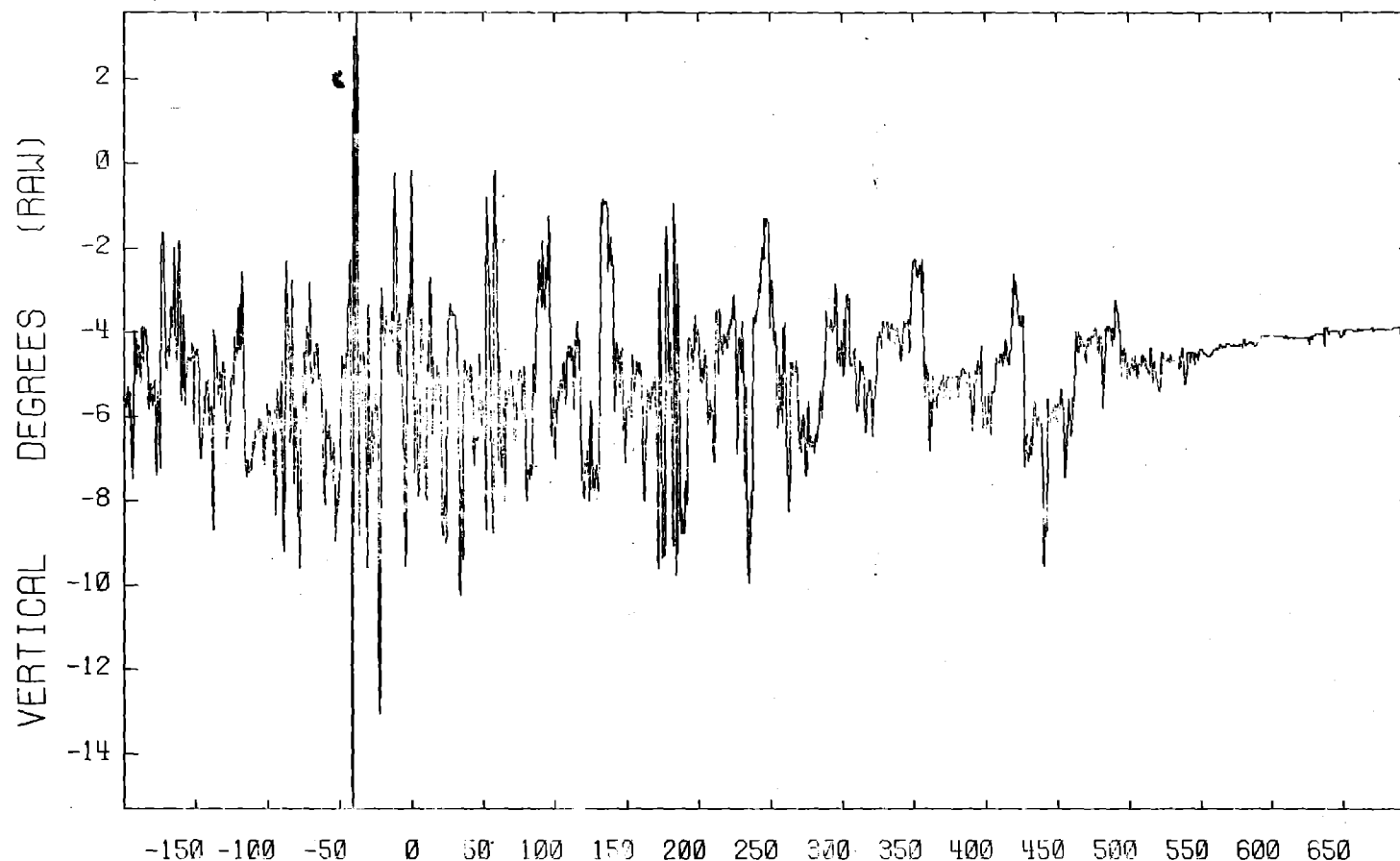
Time(sec)
3-AXIS ANEMOMETER

3-SEP-80
S/N 385



BURR08

T05



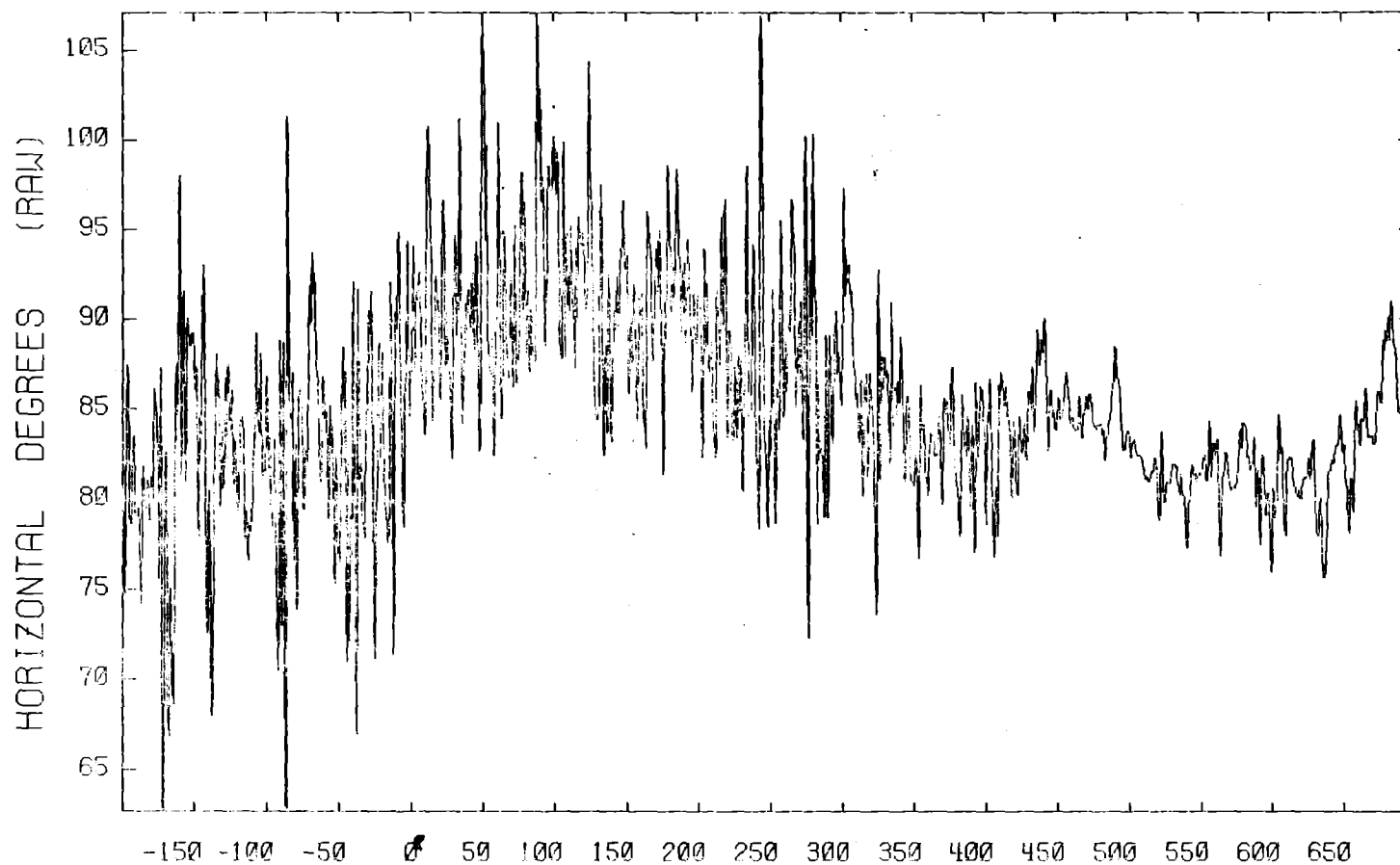
A08
01 METERS

Time(sec)
3-AXIS ANEMOMETER

3-SEP-80
S/N 385

BURR08

T05



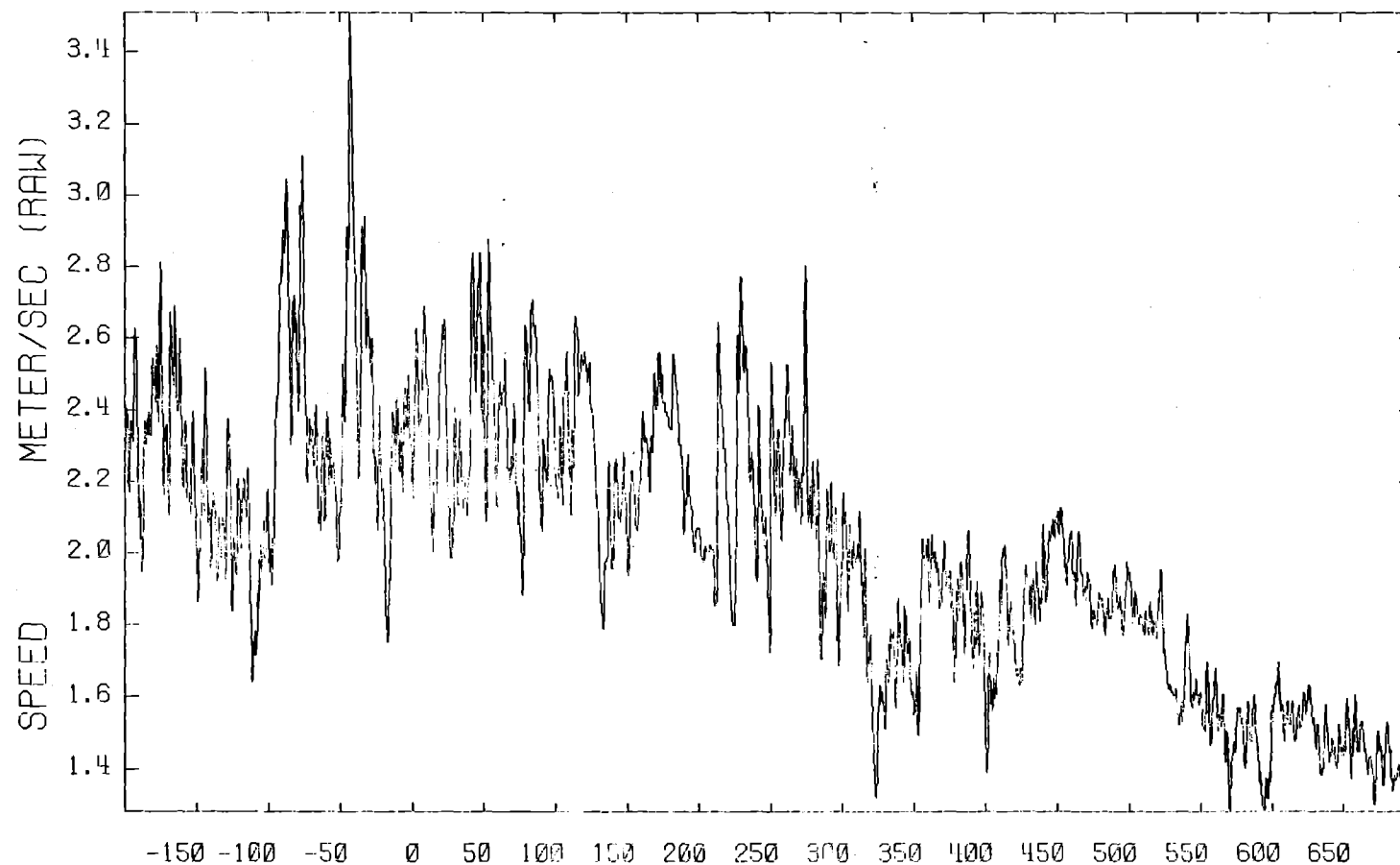
A09 .
03 METERS

3-AXIS ANEMOMETER

3-SEP-80
S/N 374

BURR08

T05



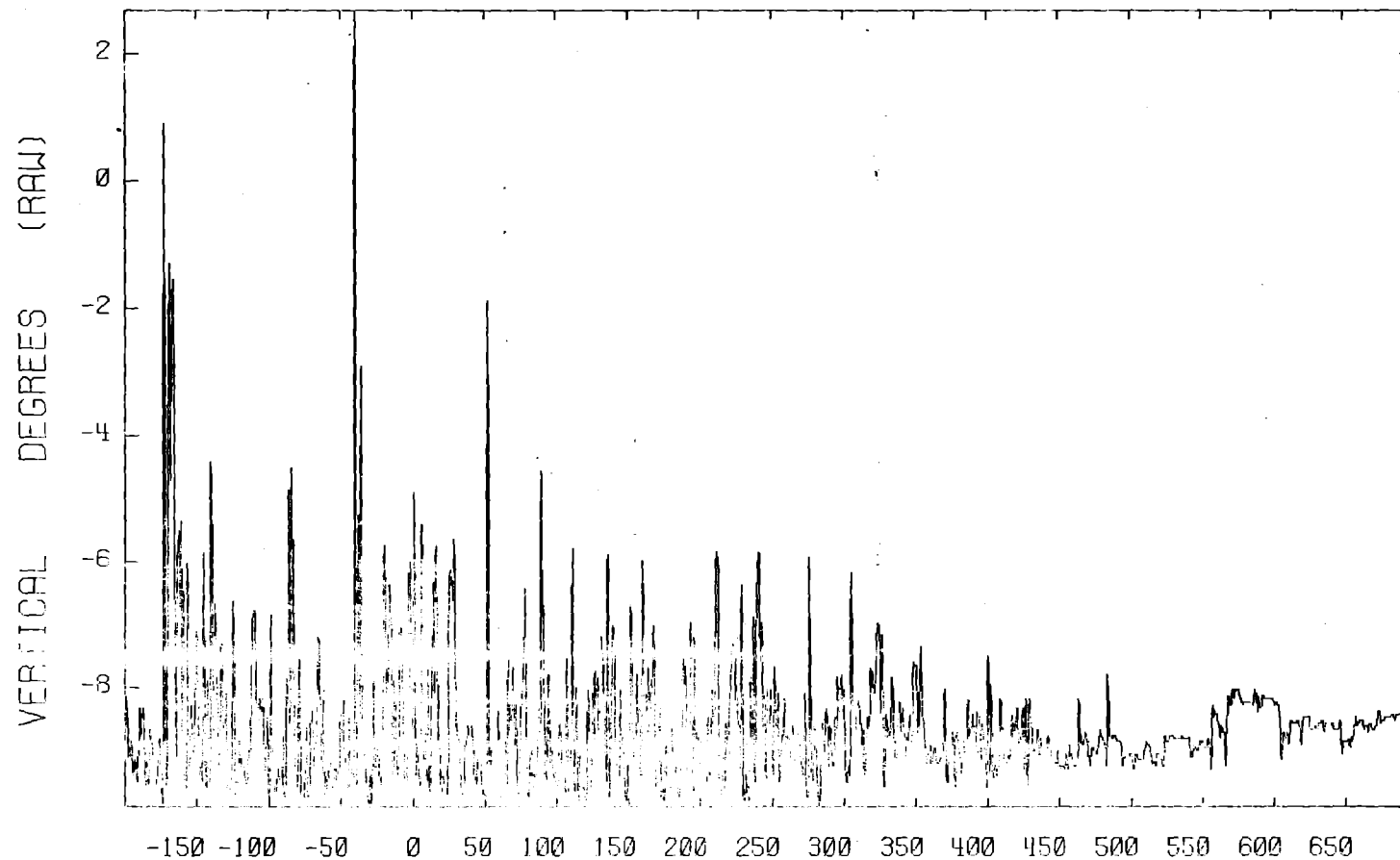
A10
03 METERS

Time(sec)
3-AXIS ANEMOMETER

3-SEP-80
S/N 374

BURR08

T05



A11

03 METERS

Time(sec)

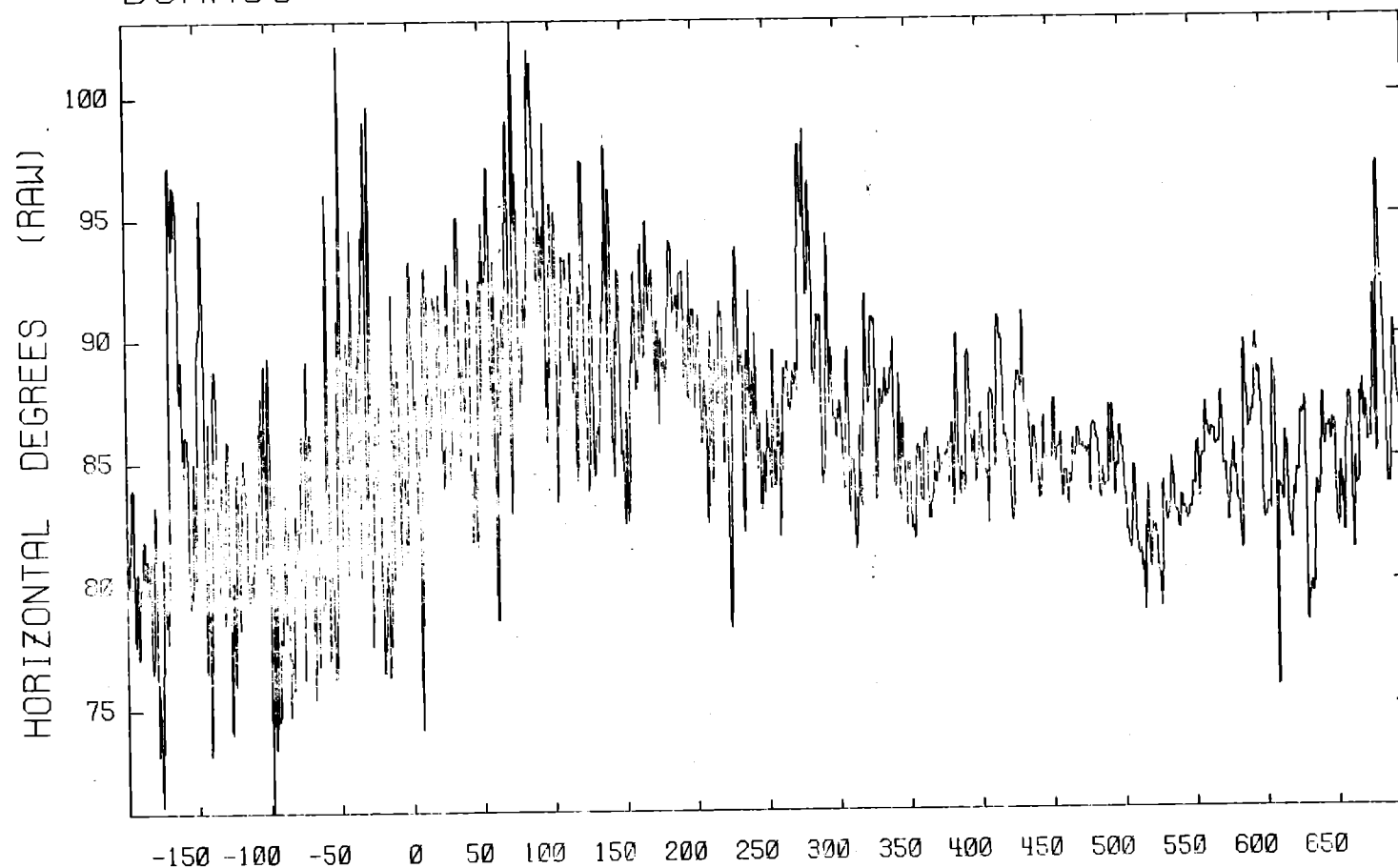
3-AXIS ANEMOMETER

3-SEP-80

S/N 374

BURR08

T05



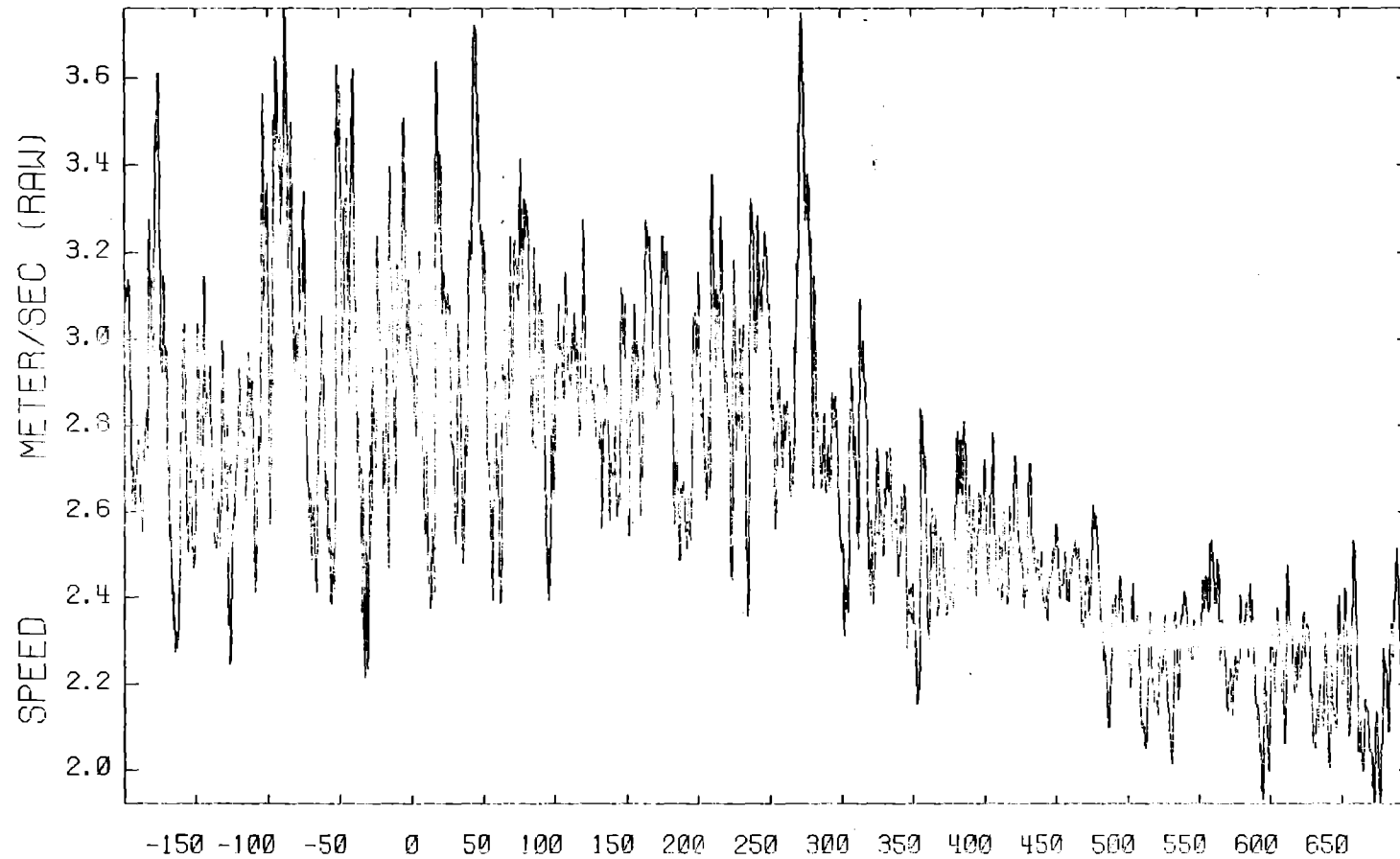
A12
08 METERS

Time(sec)
3-AXIS ANEMOMETER

3-SEP-80
S/N 390

BURR08

T05



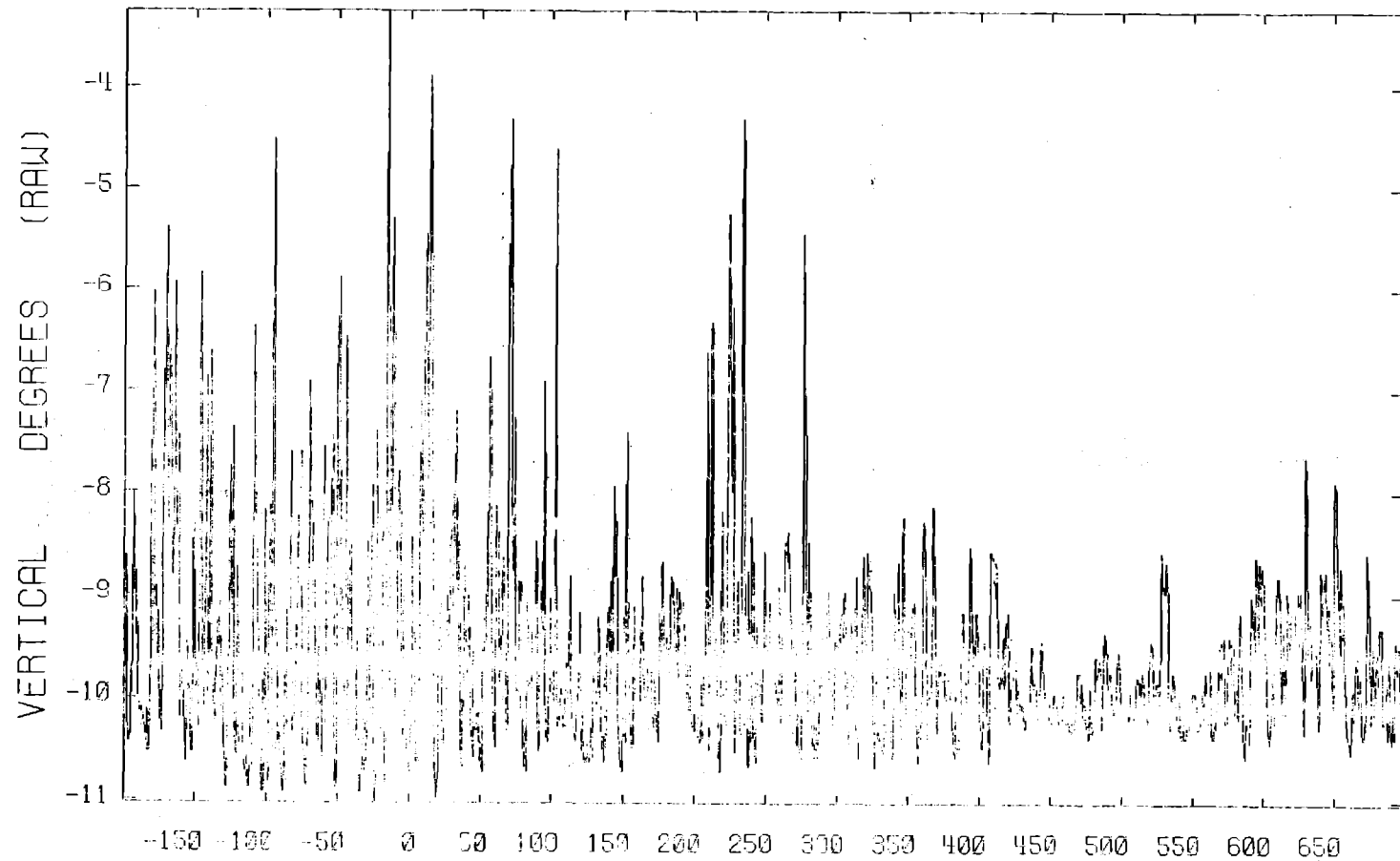
A13
08 METERS

Time(sec)
3-AXIS ANEMOMETER

3-SEP-80
S/N 390

BURR08

T05



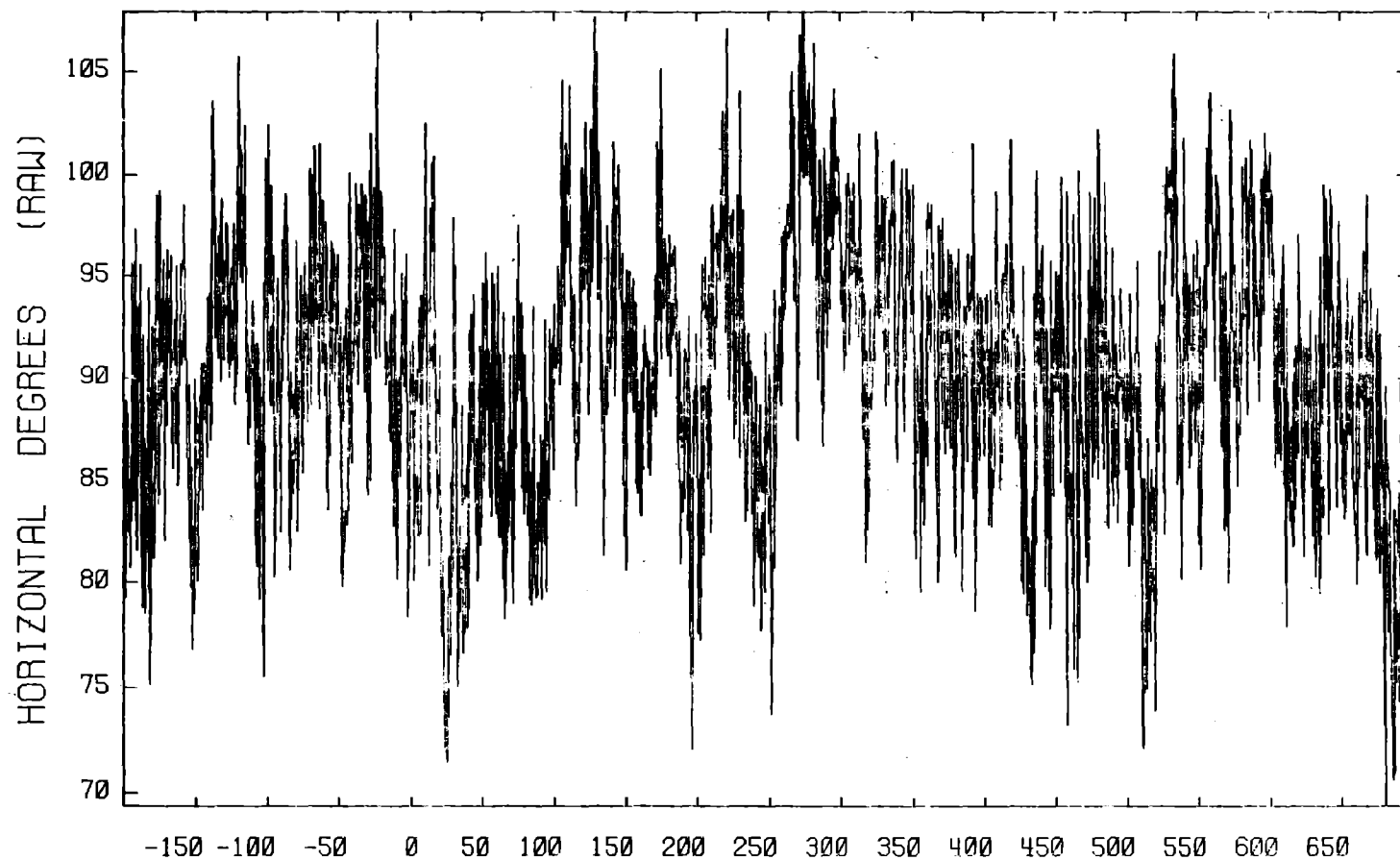
A14
08 METERS

Time(sec)
3-AXIS ANEMOMETER

3-SEP-80
S/N 390

BURR09

T01



A06

01 METERS

Time(sec)

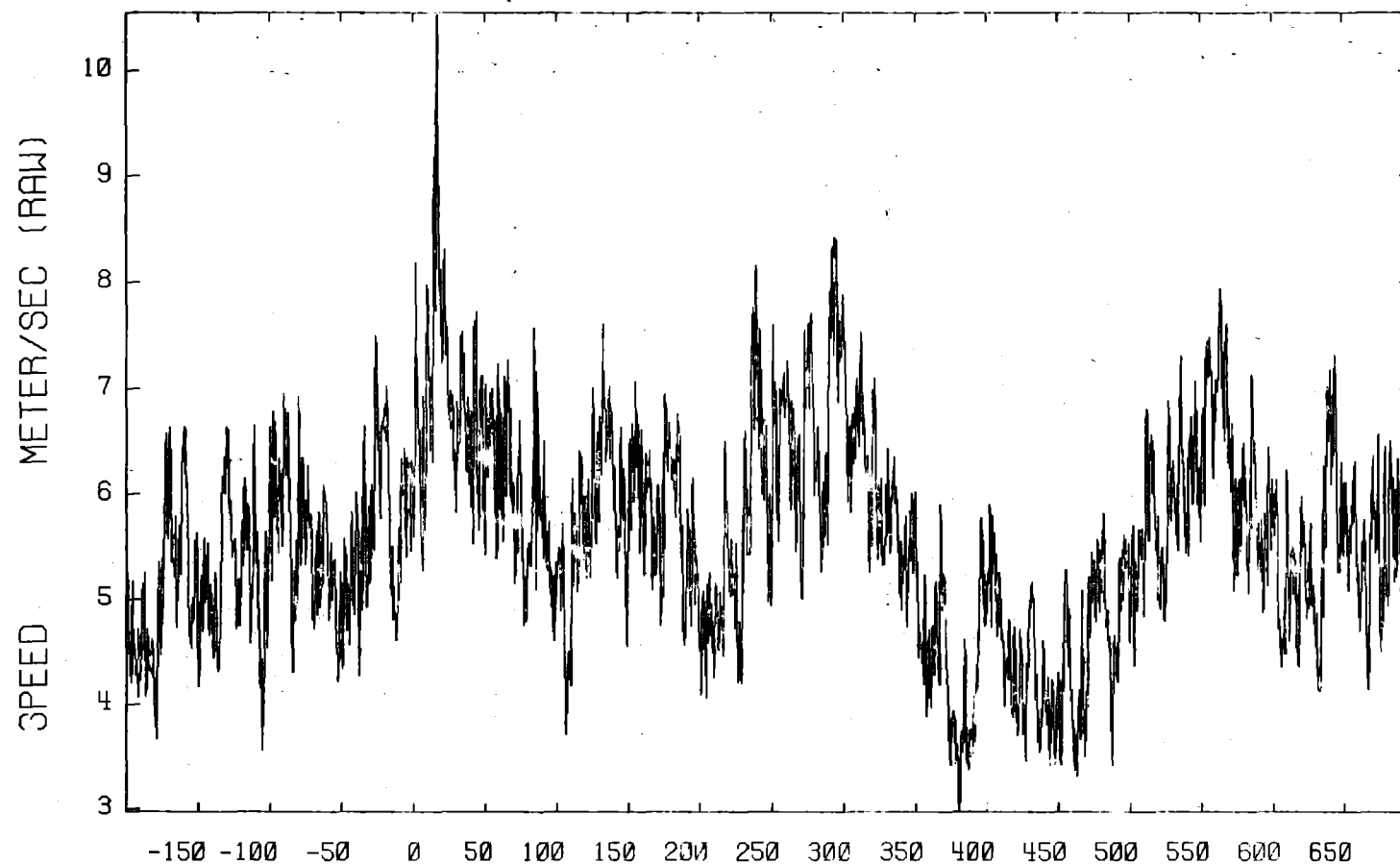
3-AXIS ANEMOMETER

17-SEP-80

S/N 384

BURR09

T01



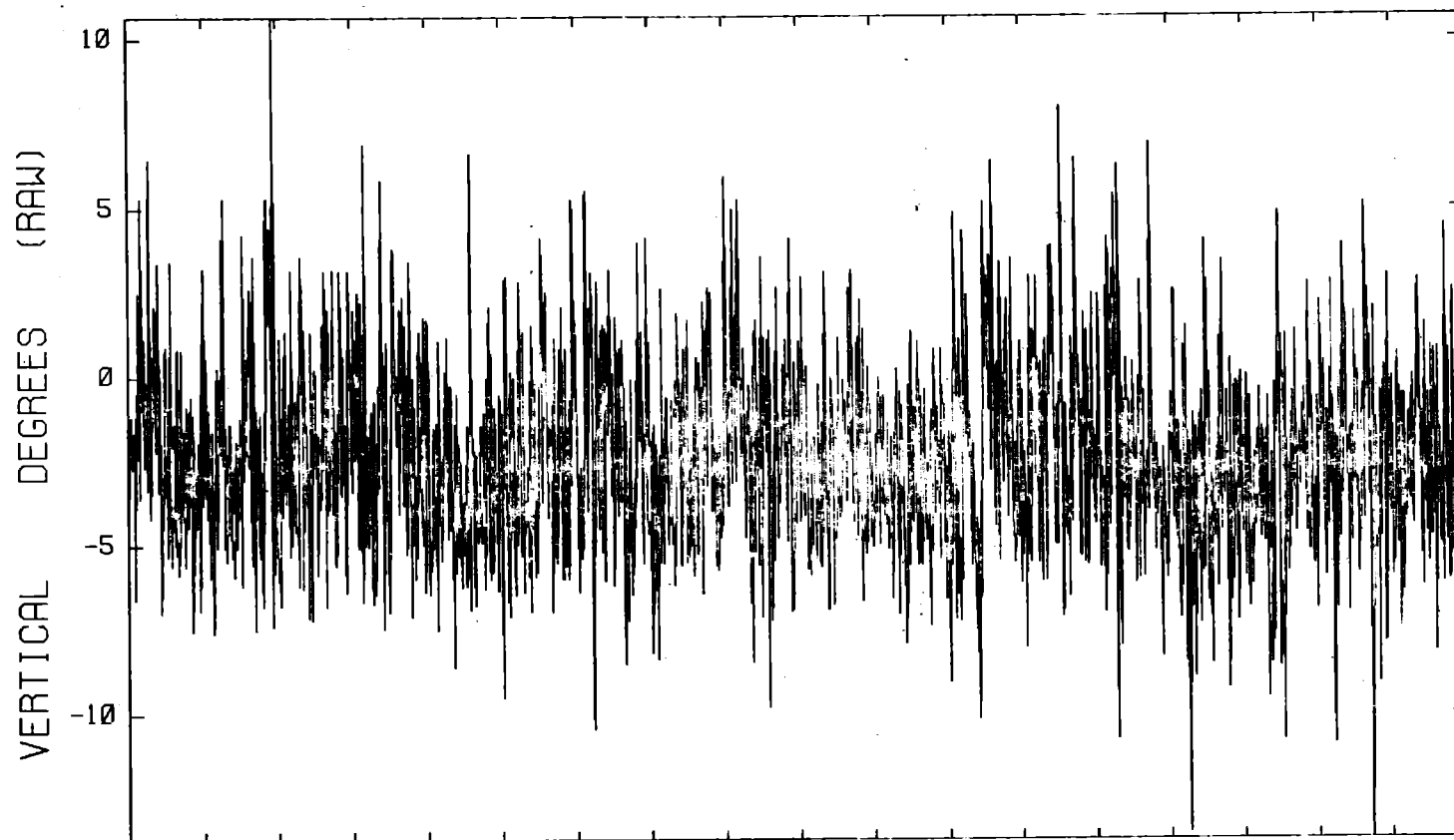
A07
01 METERS

Time(sec)
3-AXIS ANEMOMETER

17-SEP-80
S/N 384

BURR09

T01



A08

01 METERS

Time(sec)

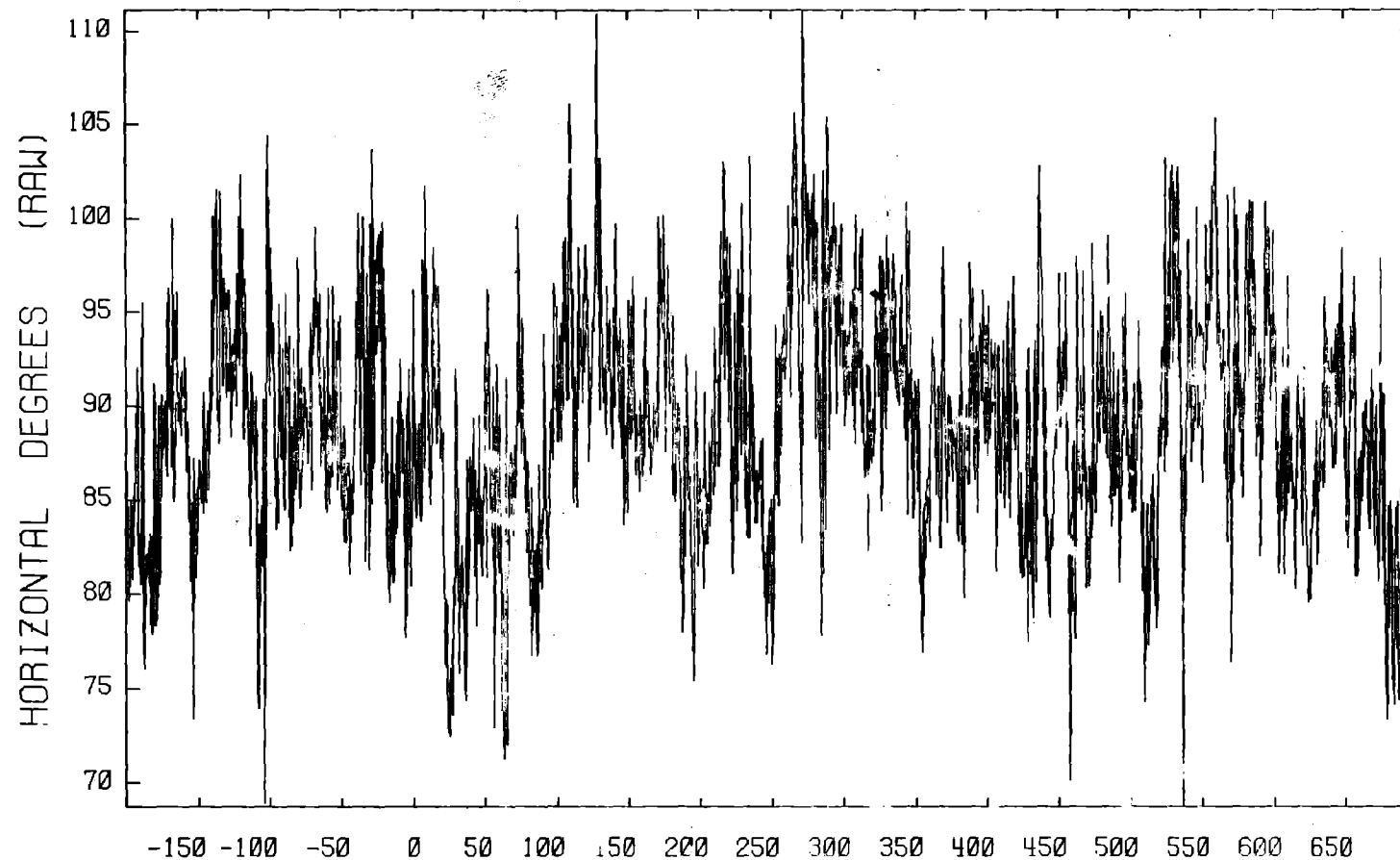
3-AXIS ANEMOMETER

17-SEP-80

S/N 384

BURR09

T01



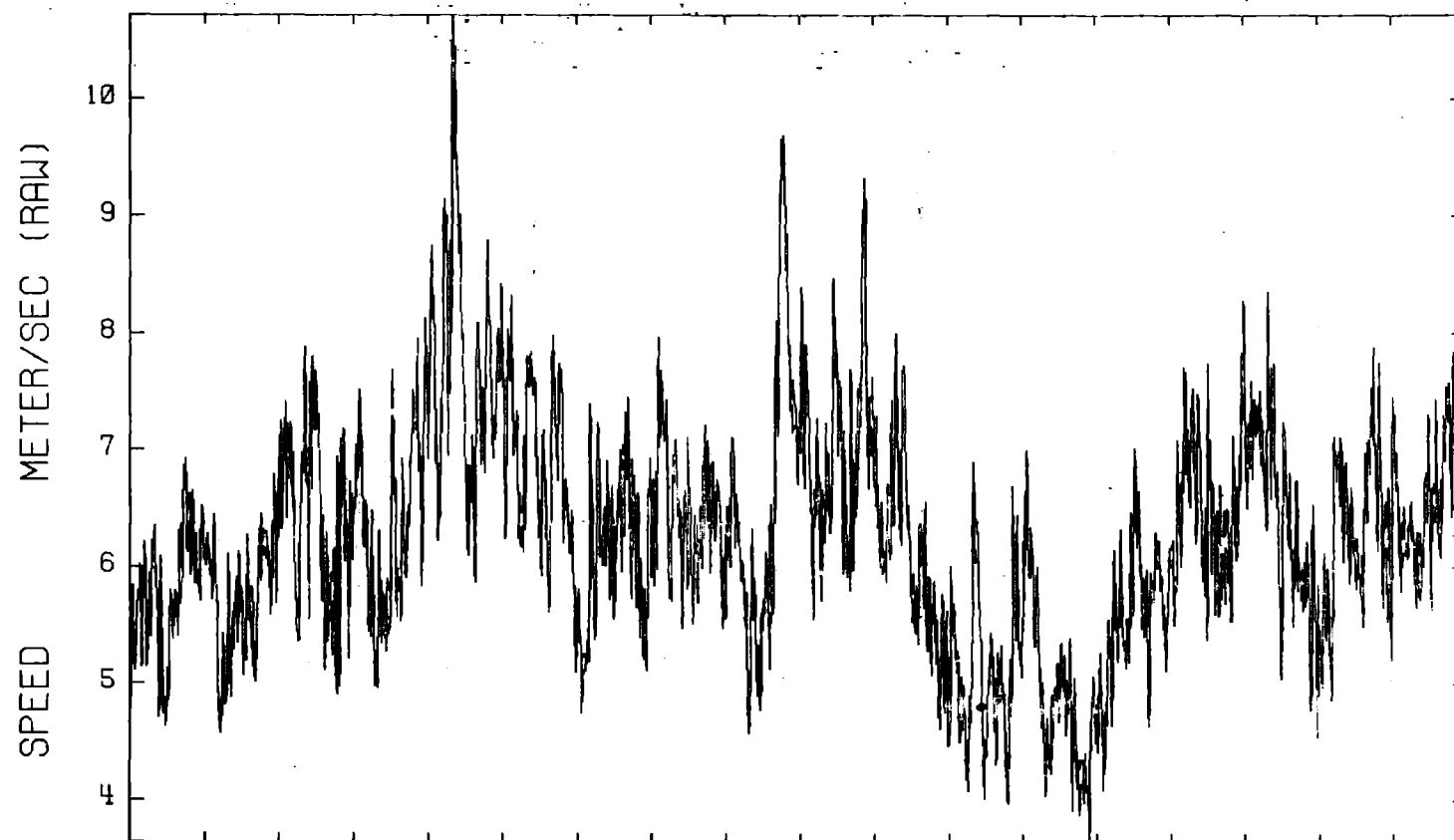
A09
03 METERS

Time(sec)
3-AXIS ANEMOMETER

17-SEP-80
S/N 387

BURR09

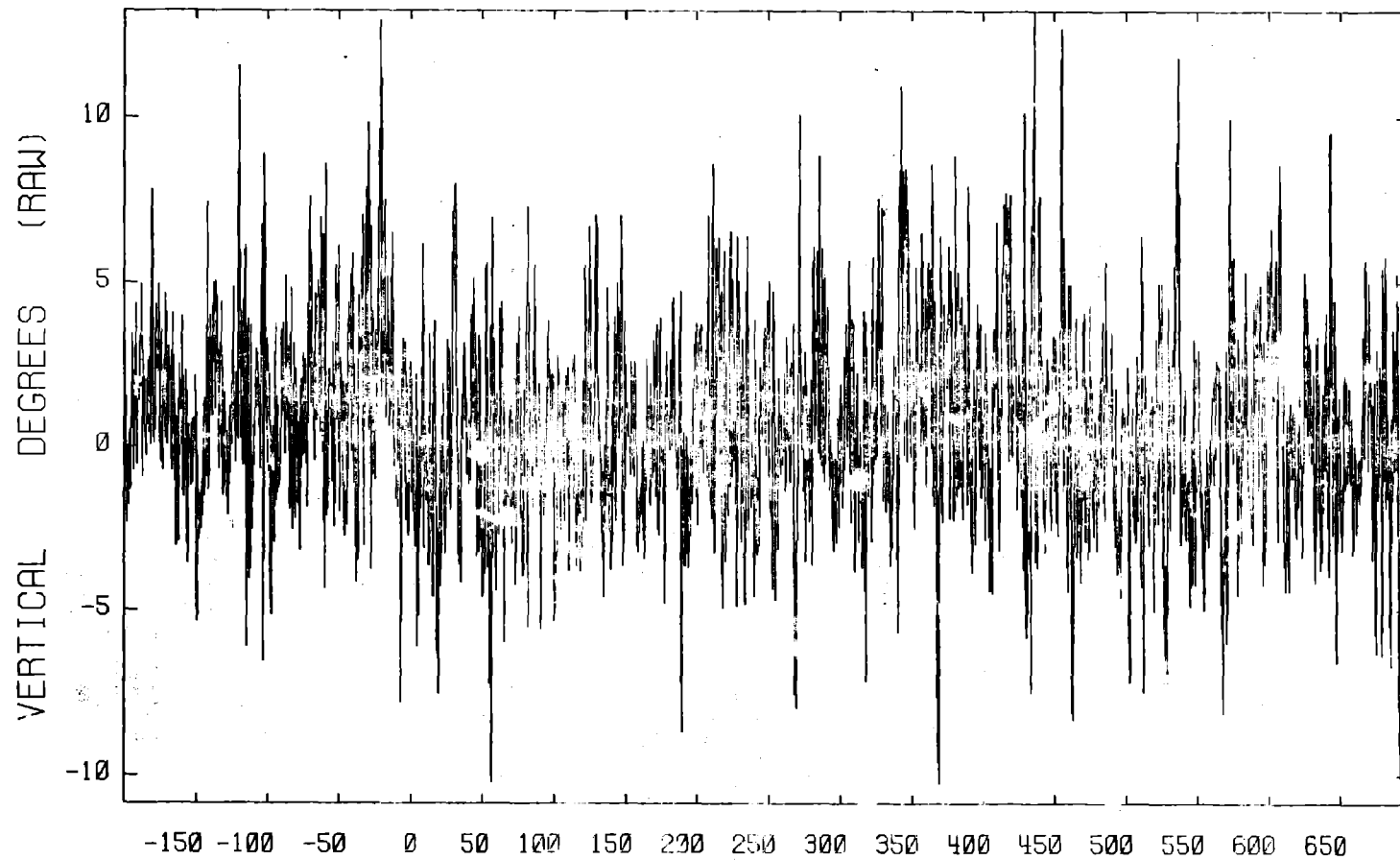
T01



A10
03 METERS
Time(sec)
3-AXIS ANEMOMETER
17-SEP-80
S/N 387

BURR09

T01



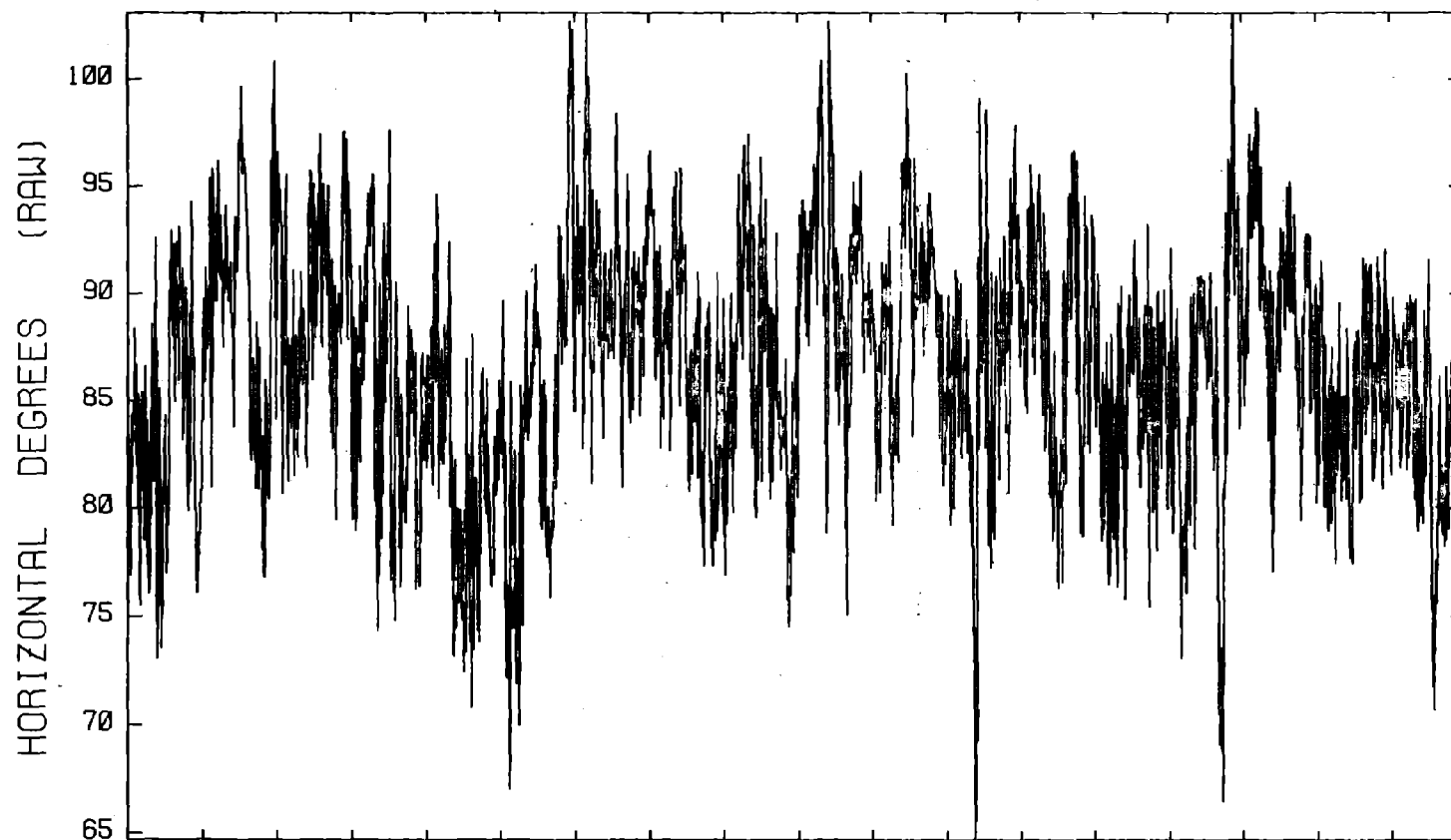
A11
03 METERS

3-AXIS ANEMOMETER

17-SEP-80
S/N 387

BURR09

101



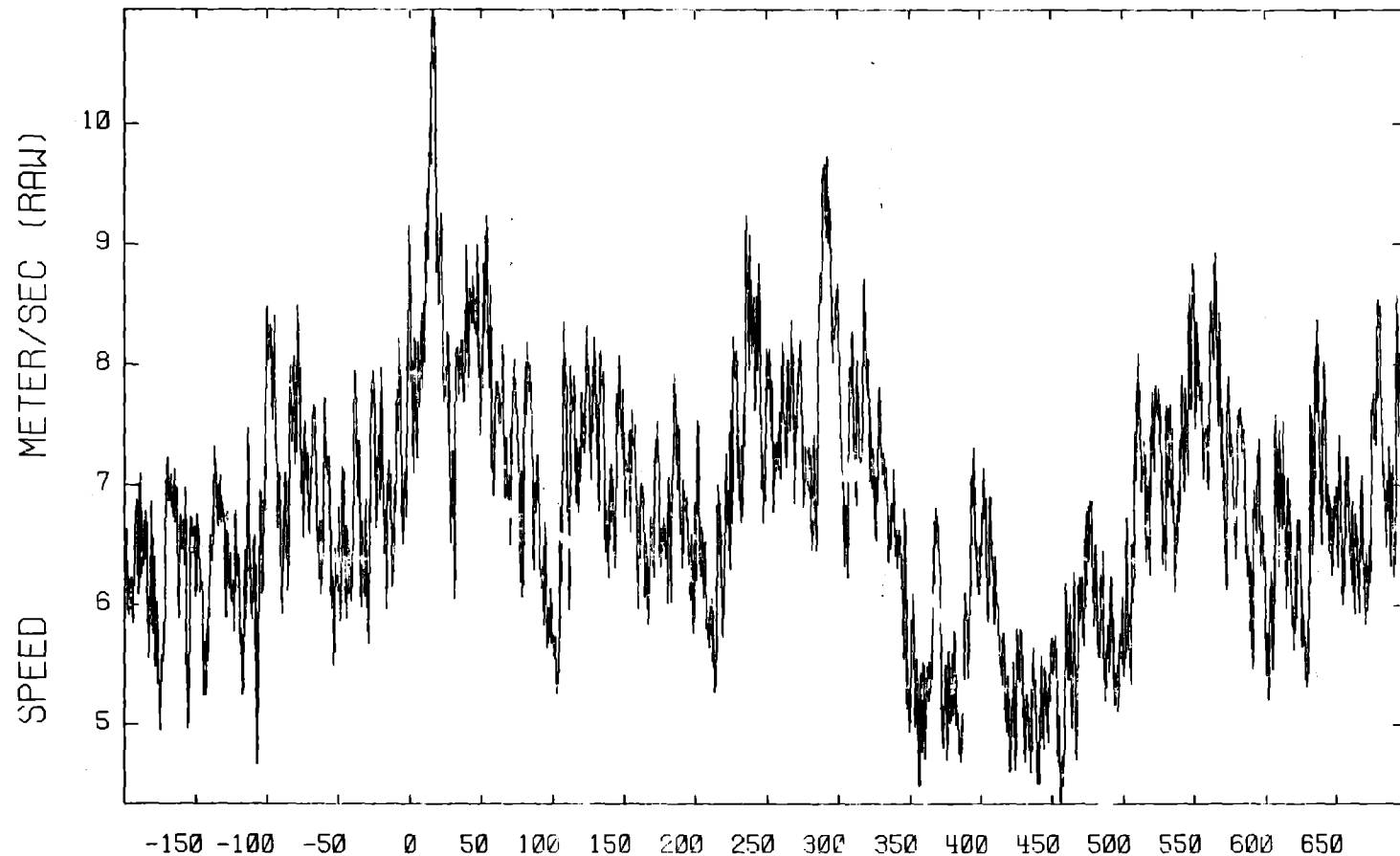
A12
08 METERS

Time(sec)
3-AXIS ANEMOMETER

17-SEP-80
S/N 376

BURR09

T01



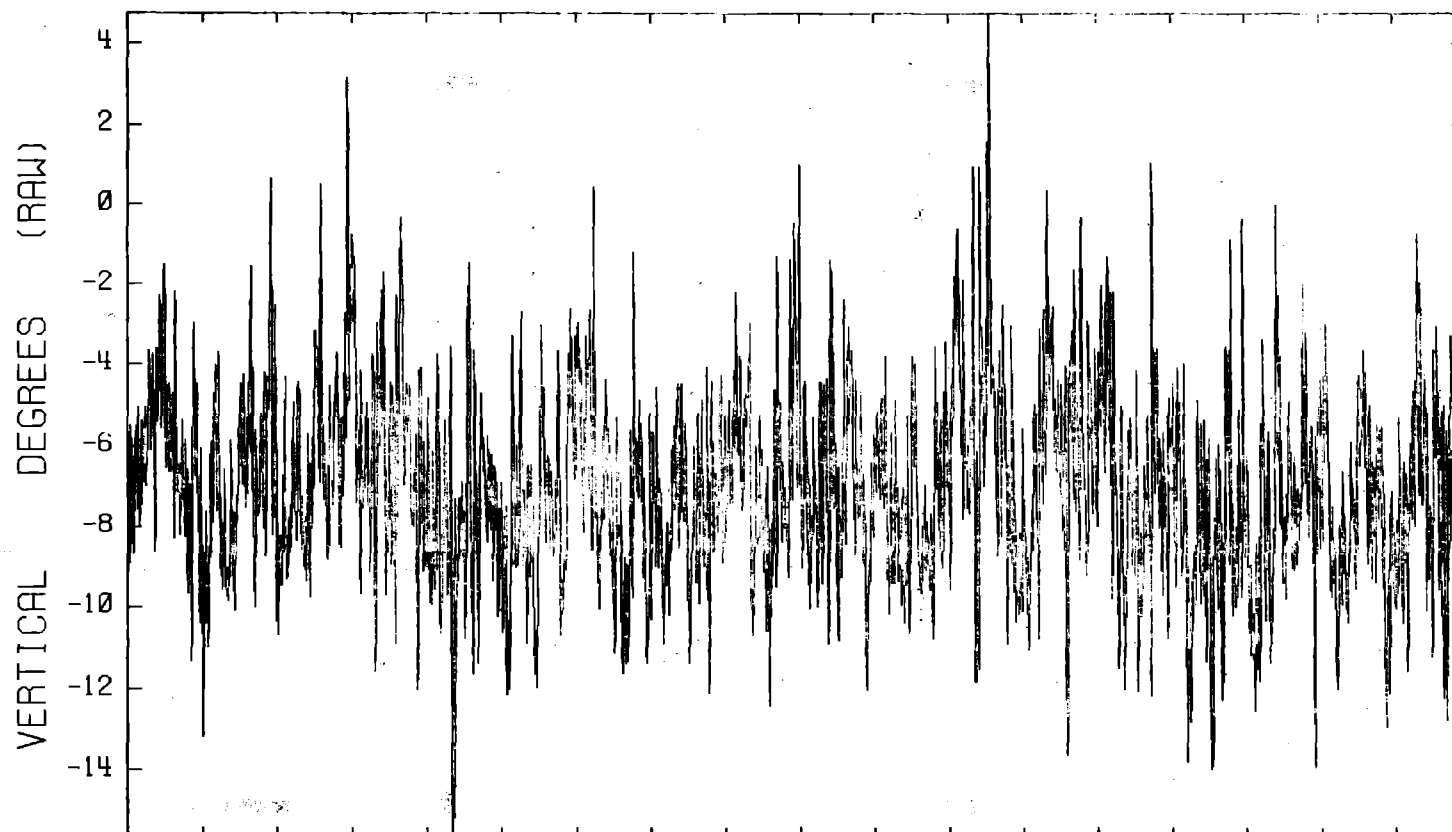
A13
08 METERS

Time(sec)
3-AXIS ANEMOMETER

17-SEP-80
S/N 376

BURR09

T01



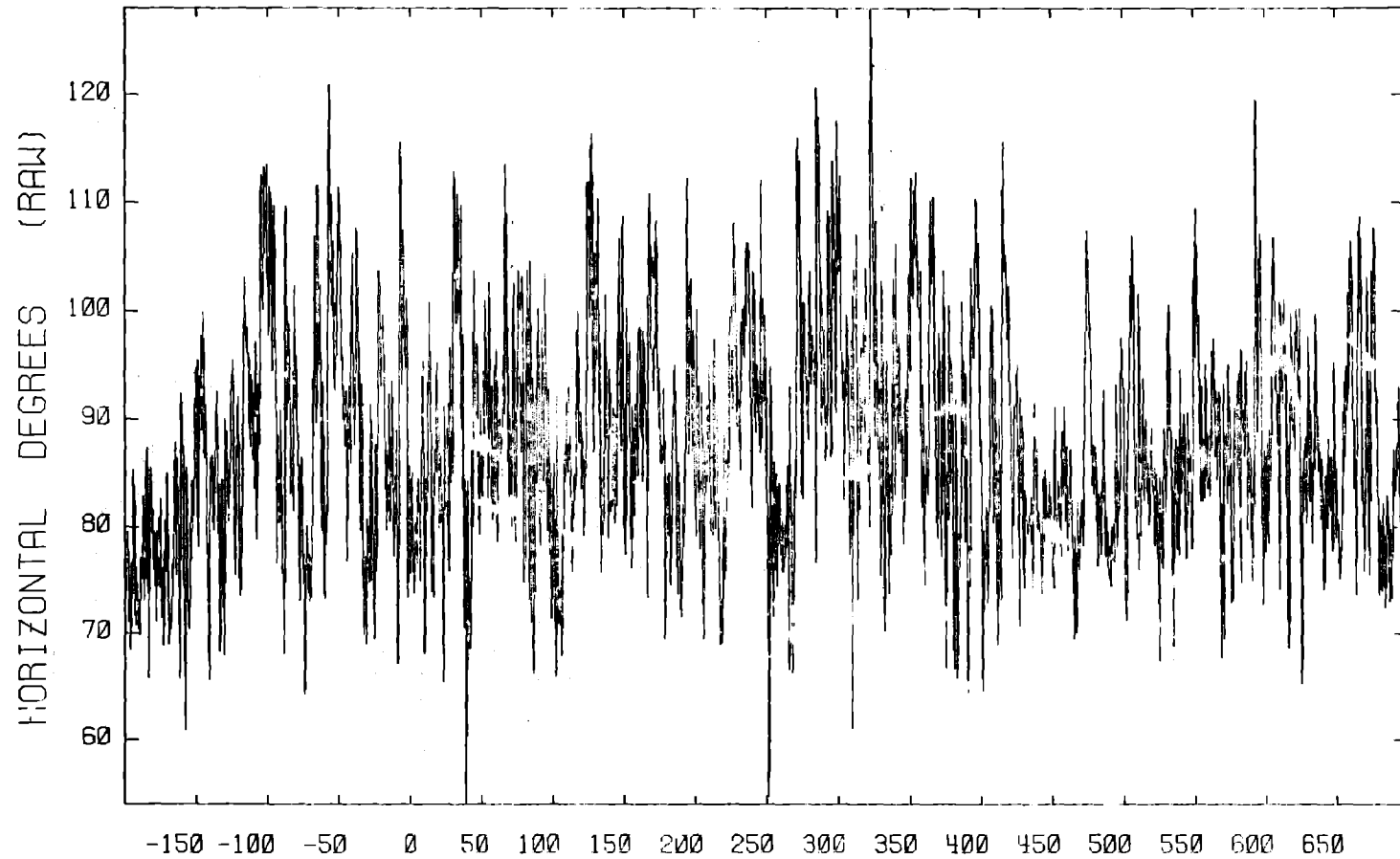
A14
08 METERS

Time(sec)
3-AXIS ANEMOMETER

17-SEP-80
S/N 376

BURR09

T02



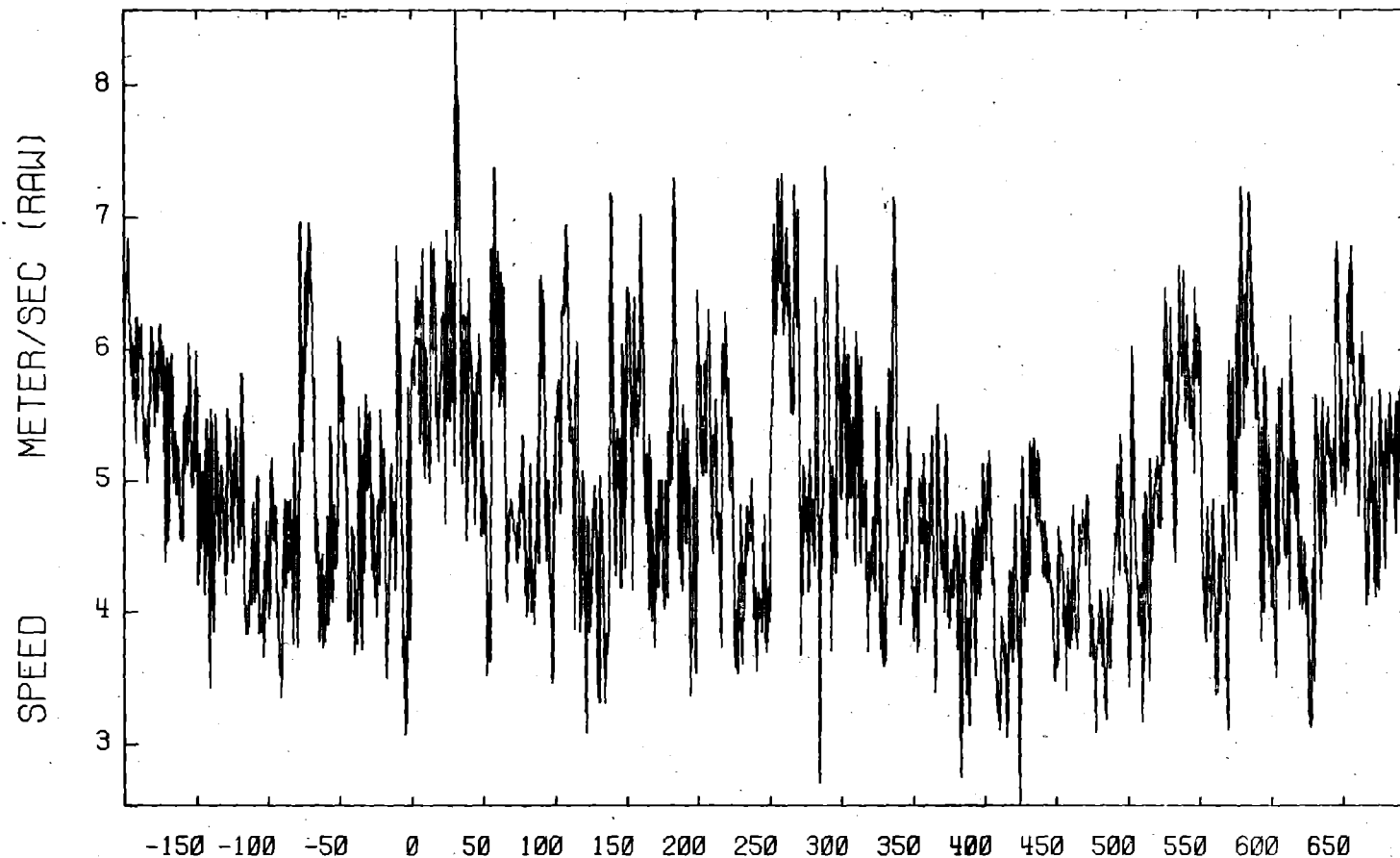
A06
01 METERS

Time(sec)
3-AXIS ANEMOMETER

17-SEP-80
S/N 386

BURR09

T02



A07

01 METERS

Time(sec)

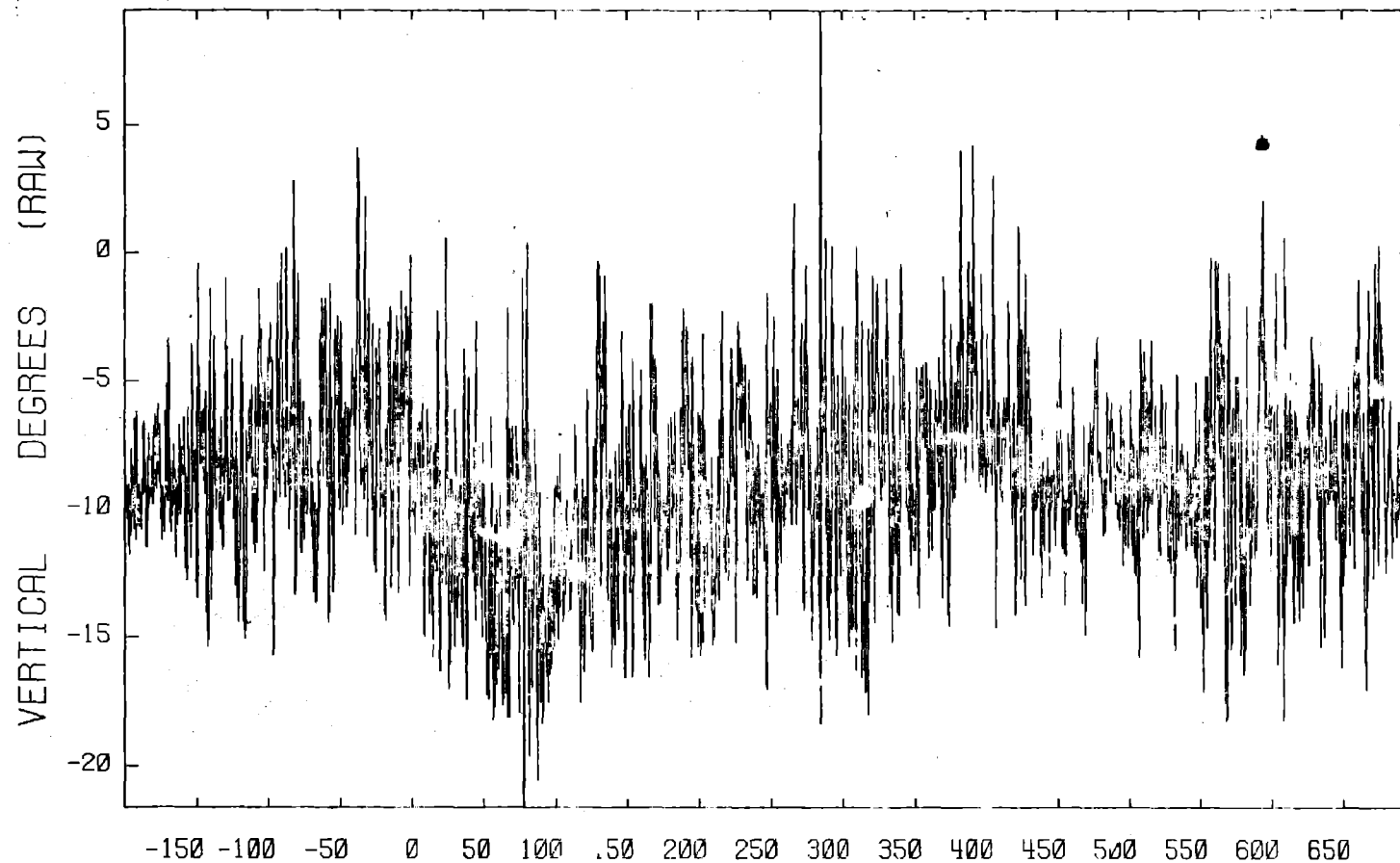
3-AXIS ANEMOMETER

17-SEP-80

S/N 386

BURR09

T02



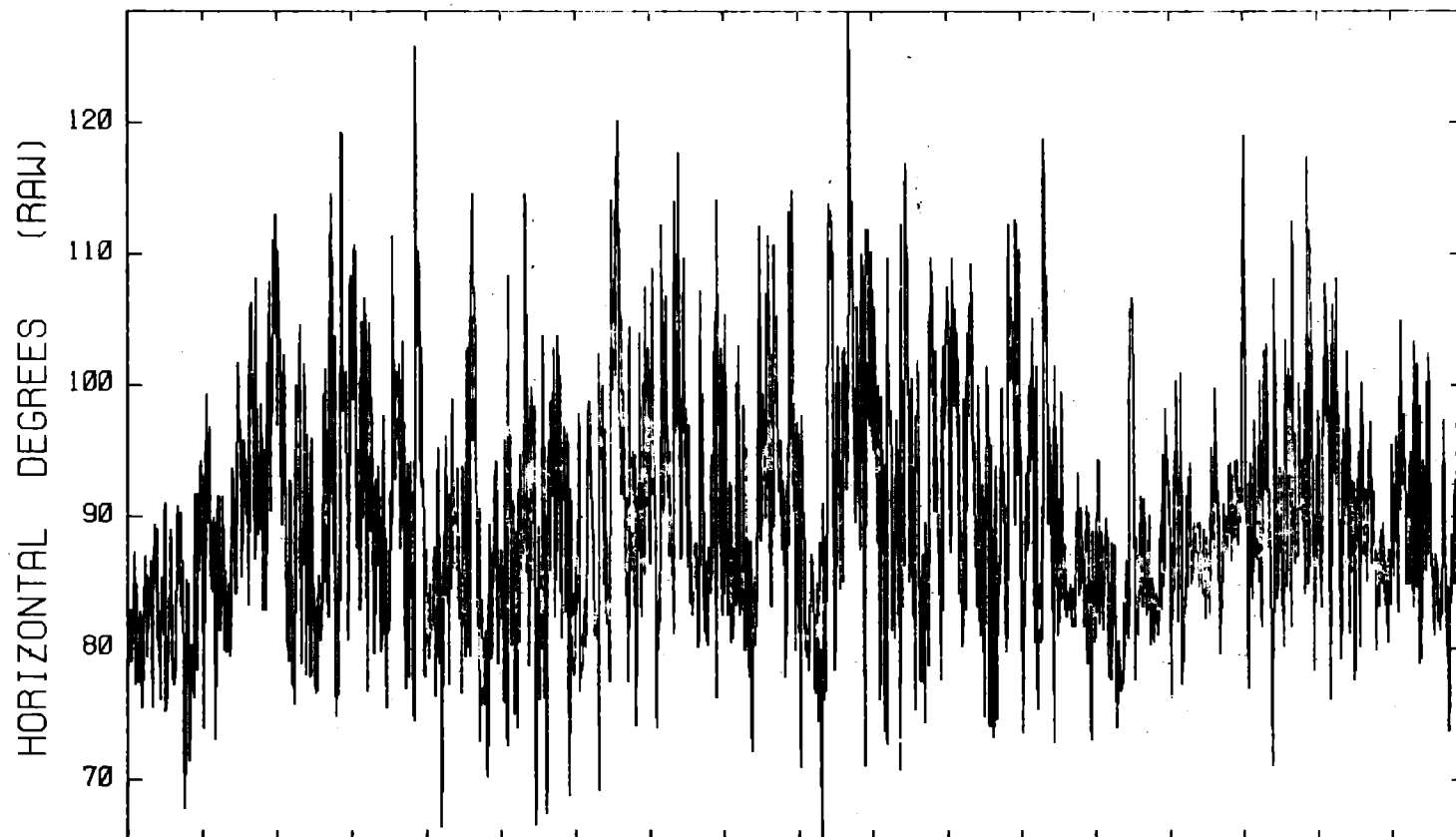
A08
01 METERS

Time(sec)
3-AXIS ANEMOMETER

17-SEP-80
S/N 386

BURR09

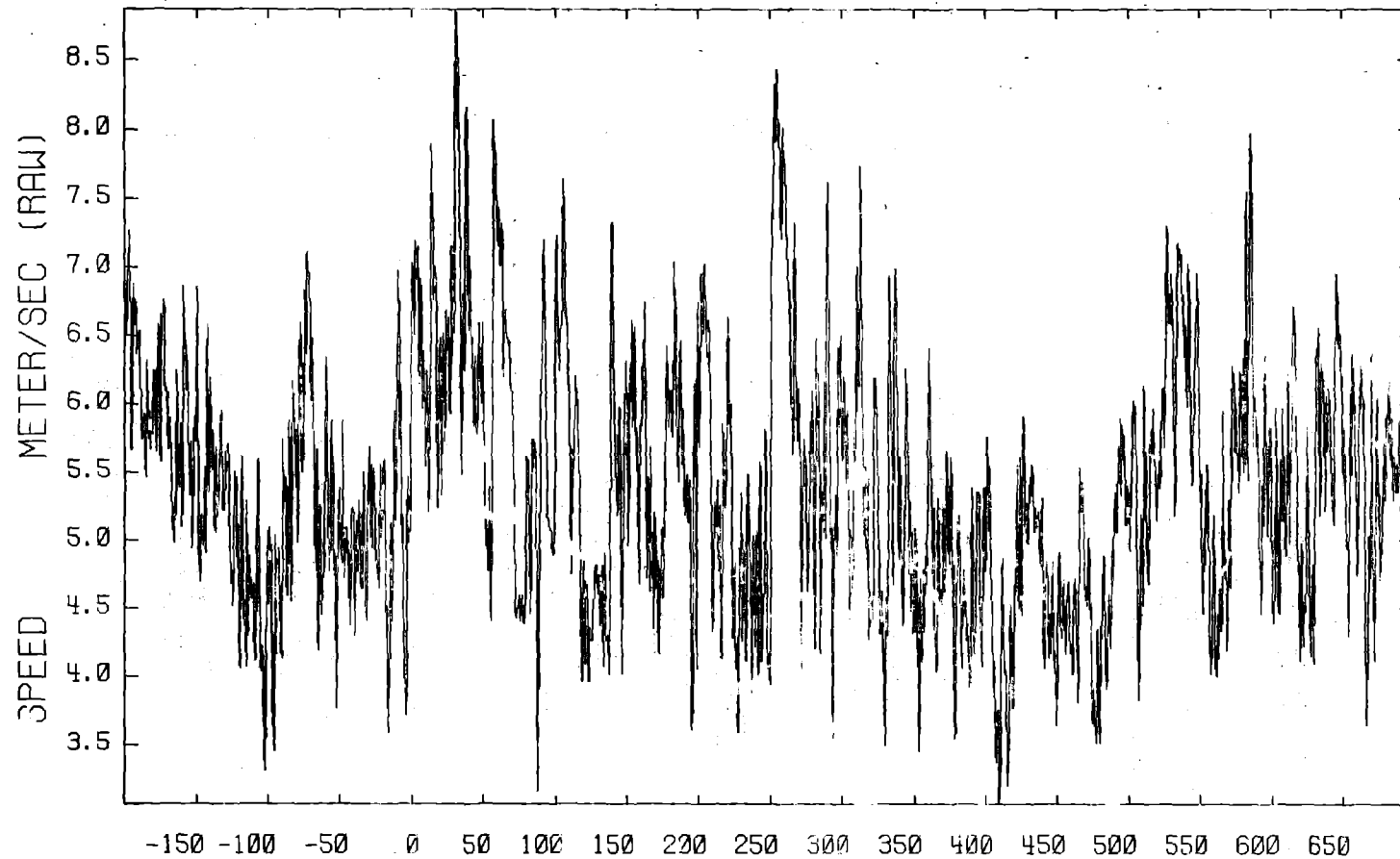
T02



A09
03 METERS
Time(sec)
3-AXIS ANEMOMETER
17-SEP-80
S/N 381

BURR09

T02



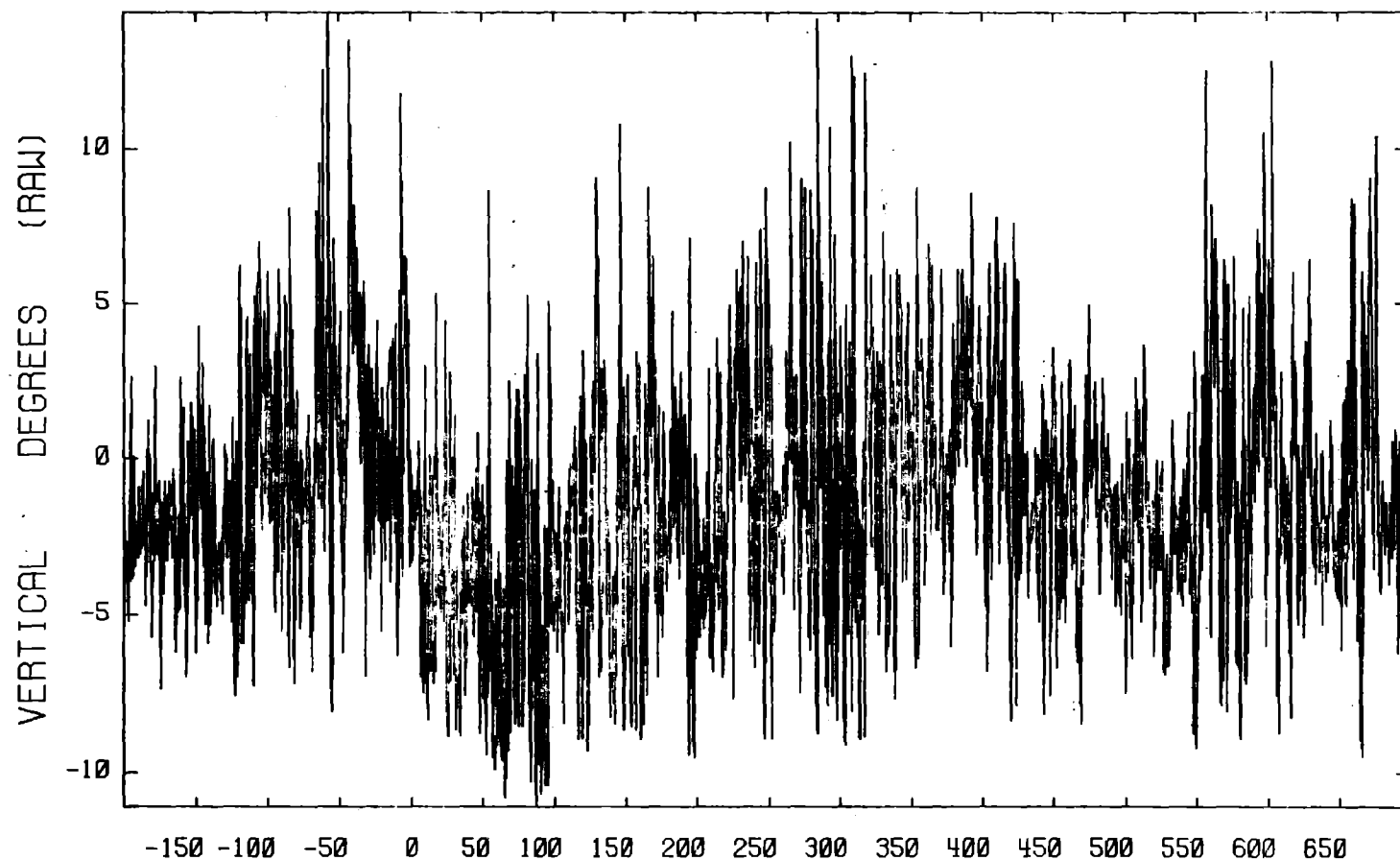
A10
03 METERS

Time(sec)
3-AXIS ANEMOMETER

17-SEP-80
S/N 381

BURR09

T02



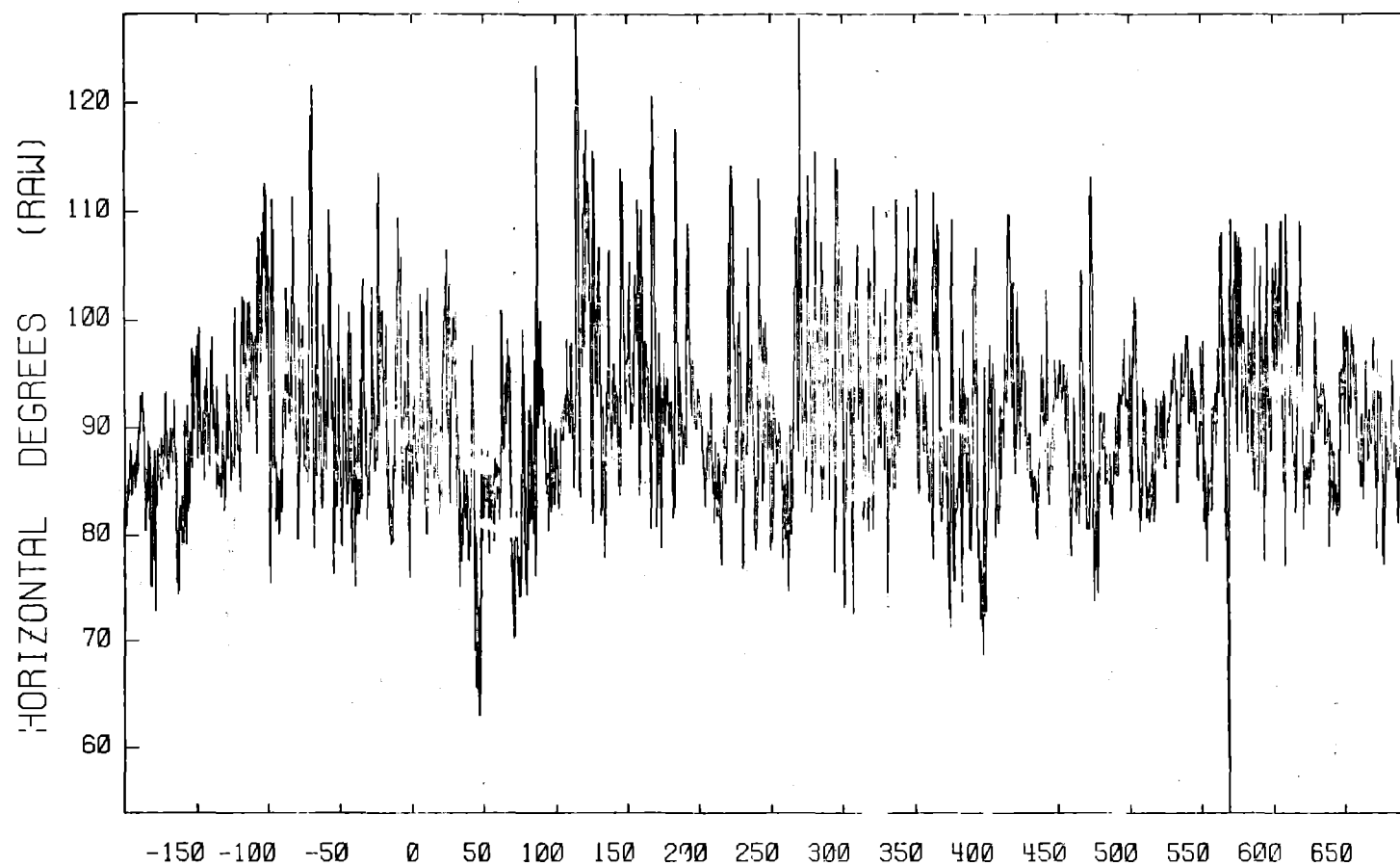
A11
03 METERS

Time(sec)
3-AXIS ANEMOMETER

17-SEP-80
S/N 381

BURR09

T02



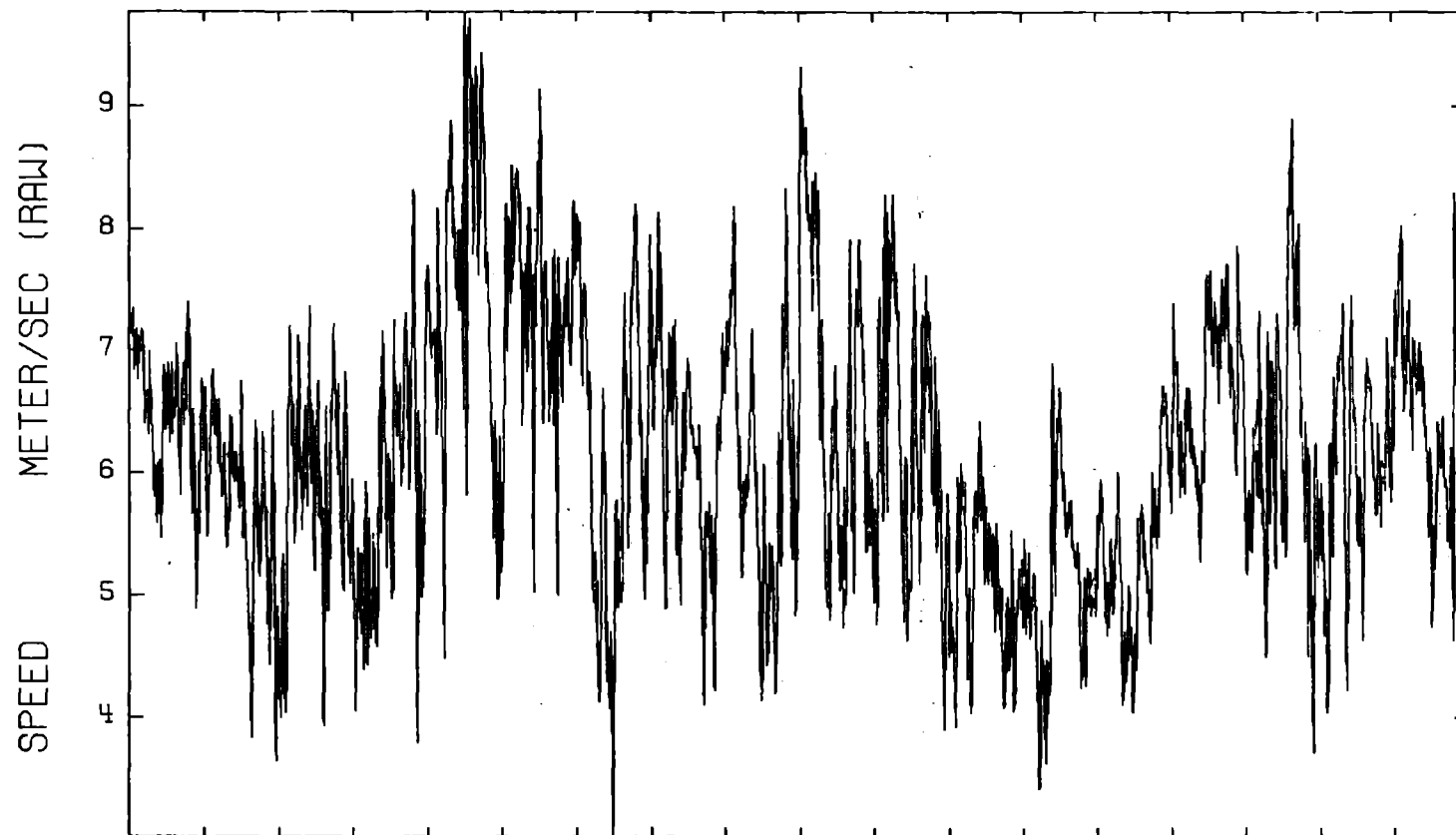
A12
08 METERS

3-AXIS ANEMOMETER

17-SEP-80
S/N 380

BURR09

T02



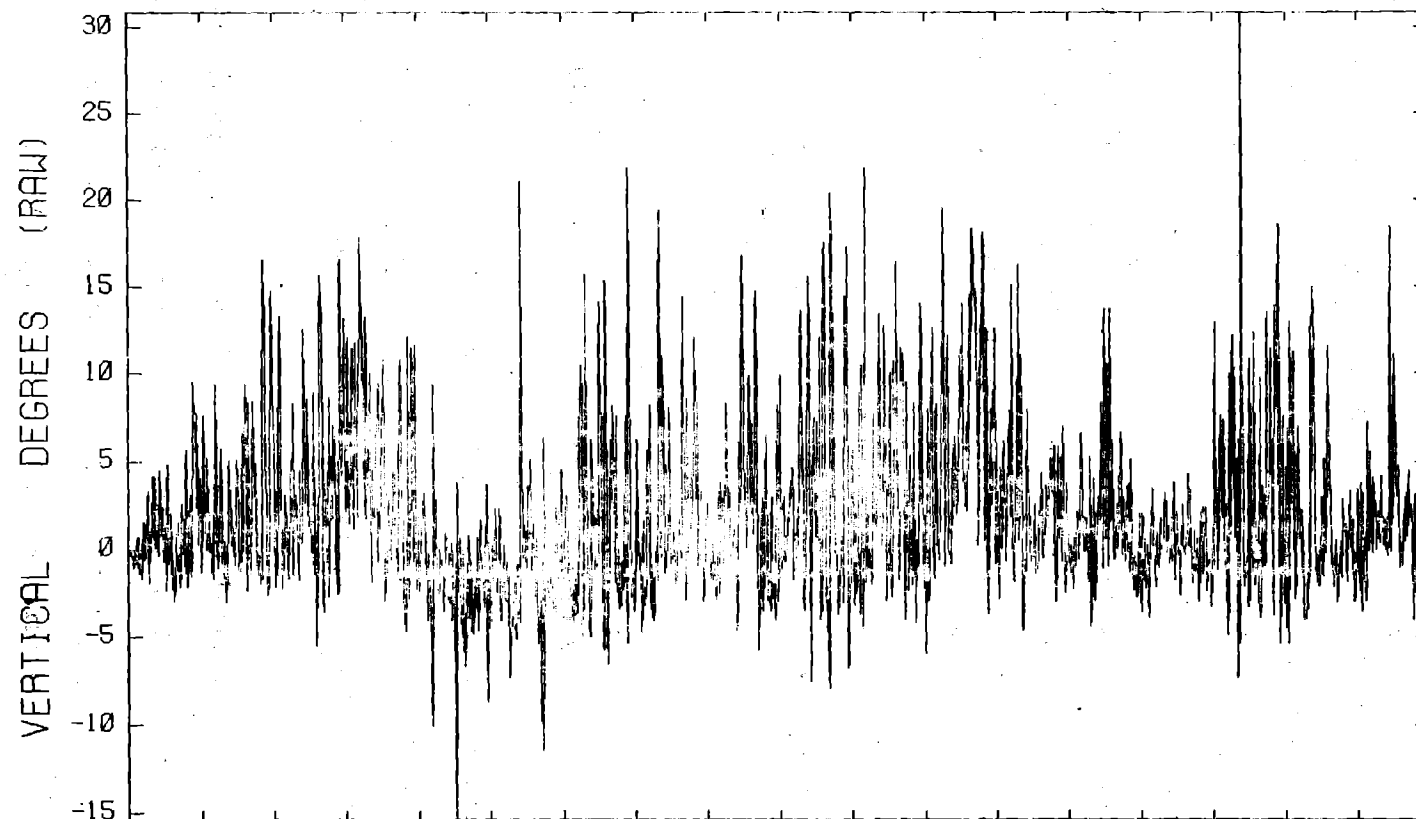
A13
08 METERS

Time(sec)
3-AXIS ANEMOMETER

17-SEP-80
S/N 380

BURR09

T02



A14
08 METERS

Time(sec)
3-AXIS ANEMOMETER

17-SEP-80
S/N 380

F. HUMIDITY AND HEAT FLUX DATA

Humidity

Absolute humidity values, in grams of water per cubic metre, have been plotted for stations in the 57-m and 140-m rows. Table 4 shows, for each test, the stations where there were detectable amounts of gas and an operational humidity sensor.

Absolute humidity values were calculated from measured values of relative humidity and ambient temperature, using the Magnus formula (Eq. (1)) for saturation vapor pressure and then obtaining absolute humidity by the equation of state (Eq. (2)):

$$e_s = 6.108 \exp [17.42 T / (T + 239.7)], \quad (1)$$

and

$$\rho_v = \frac{(r/100)e_s}{R_v(T + 273.16)} , \quad (2)$$

where T is ambient temperature in degrees C, e_s is saturation vapor pressure in millibars, r is relative humidity in percent, R_v is the appropriate gas constant ($4.615 \times 10^{-3} \text{ mb m}^3 \text{ g}^{-1} \text{ deg}^{-1}$), and ρ_v is the absolute humidity in g/m^3 .

As a reference point, for a typical temperature of the desert operating environment (i.e., 38° C), the absolute humidity at saturation (100% relative humidity) is 46 g/m^3 . Thus it can be seen how dry the ambient conditions were (i.e., about 10% relative humidity for ambient values of 5 g/m^3).

To provide a reference to the presence of the LNG vapor cloud, total hydrocarbon concentrations in volume percent have also been plotted (the dotted line). These values were estimated for the humidity sensor height

(2 m) by averaging the measured values at 1 m and 3 m. It can be seen that in general the absolute humidity increases in proportion to the increase in gas concentration. Analyses are in progress to further clarify and quantify this phenomenon.

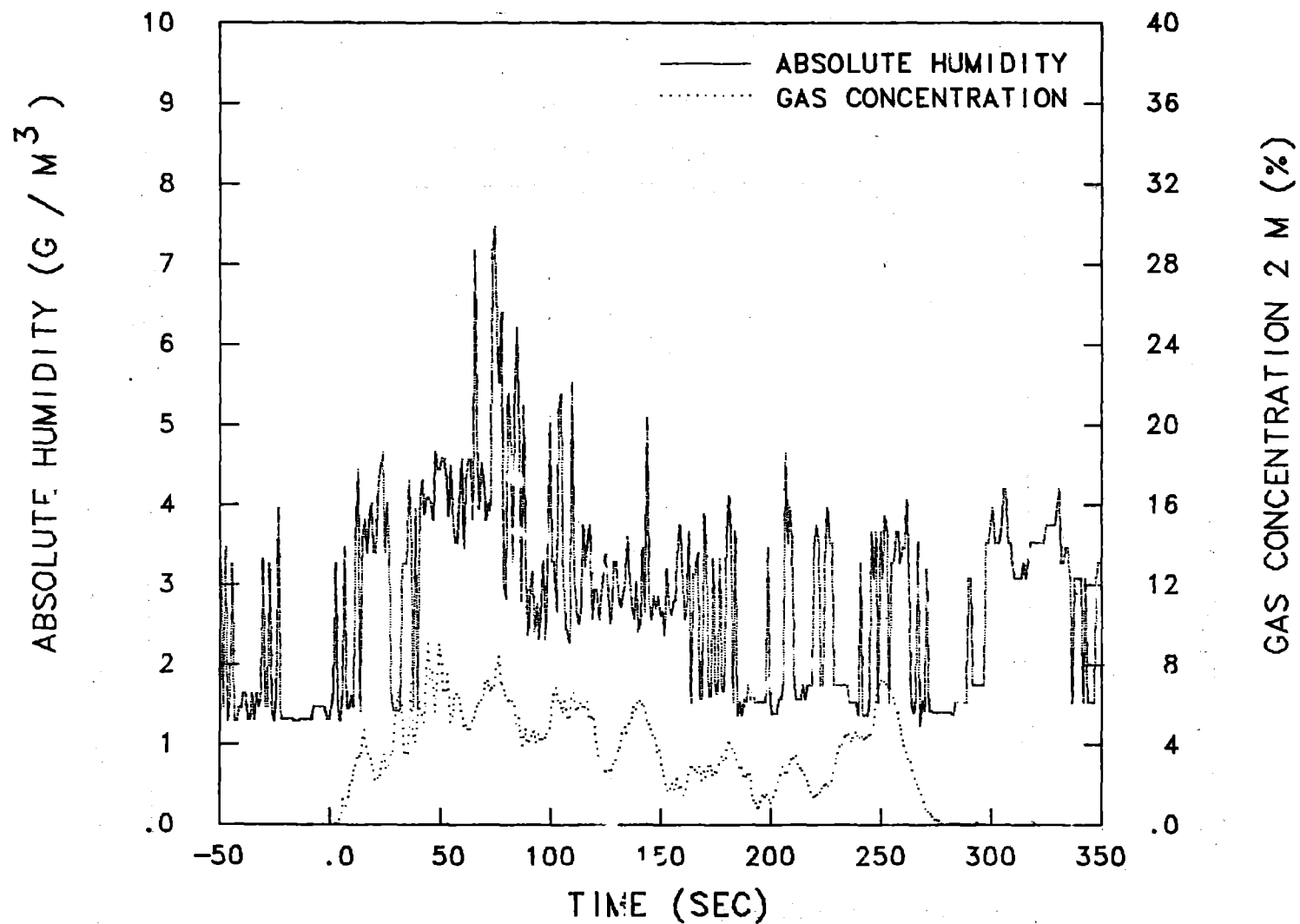
TABLE 4. Summary of Humidity Plots

Burro Experiment No.	Stations		
	G4 (57 m, left)	G5 (57 m, right)	G6 (140 m, center)
2	X		X
3	X		X
4			
5	X ^a		X ^a
6	X	X	X(RPT) ^b
7	X		
8	X		X
9	X(RPT) ^c	X(RPT) ^c	X

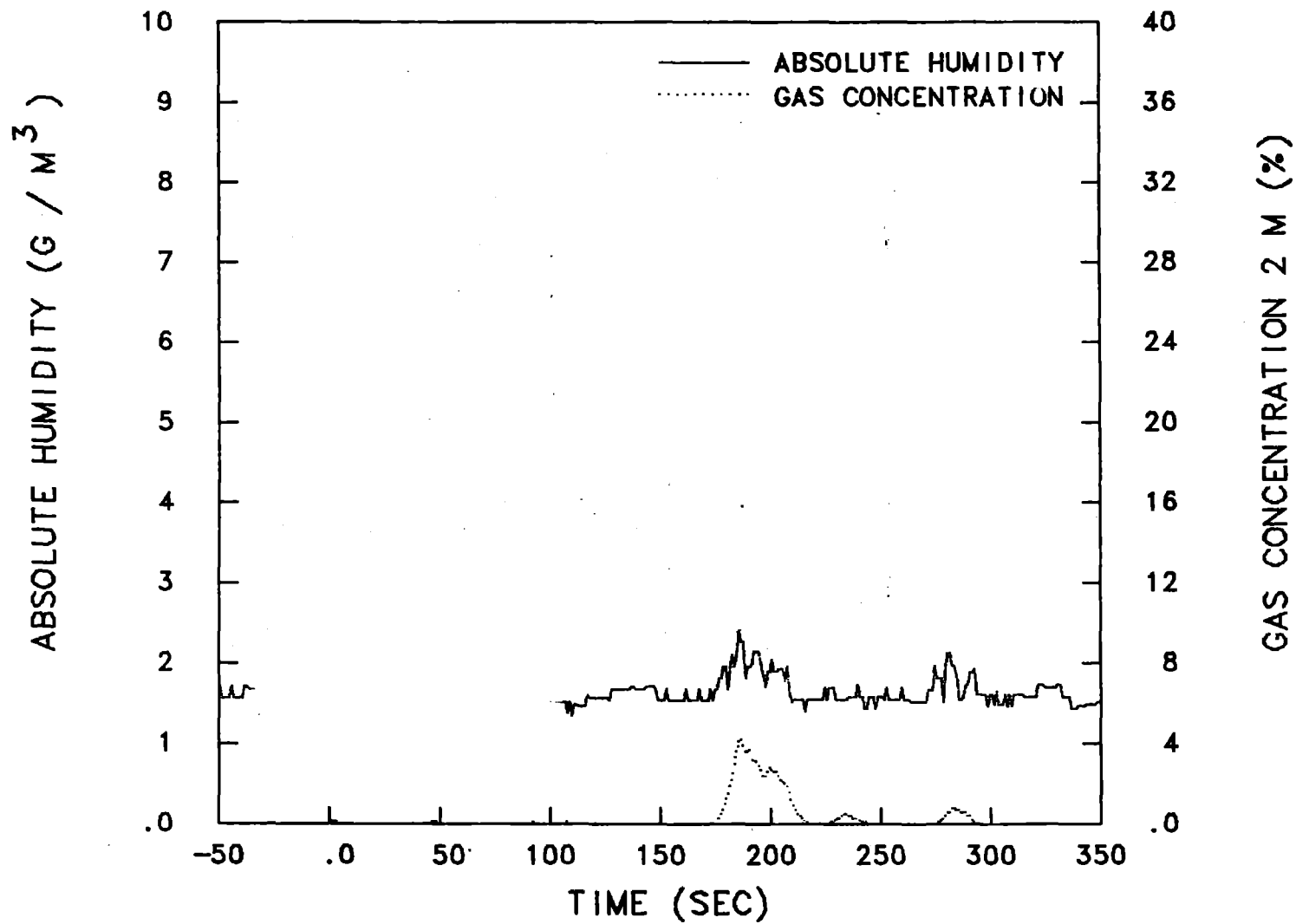
^a Gas sensors inoperative.

^b RPT refers to humidity data perturbations due in part to ejections of pond water during rapid phase transitions.

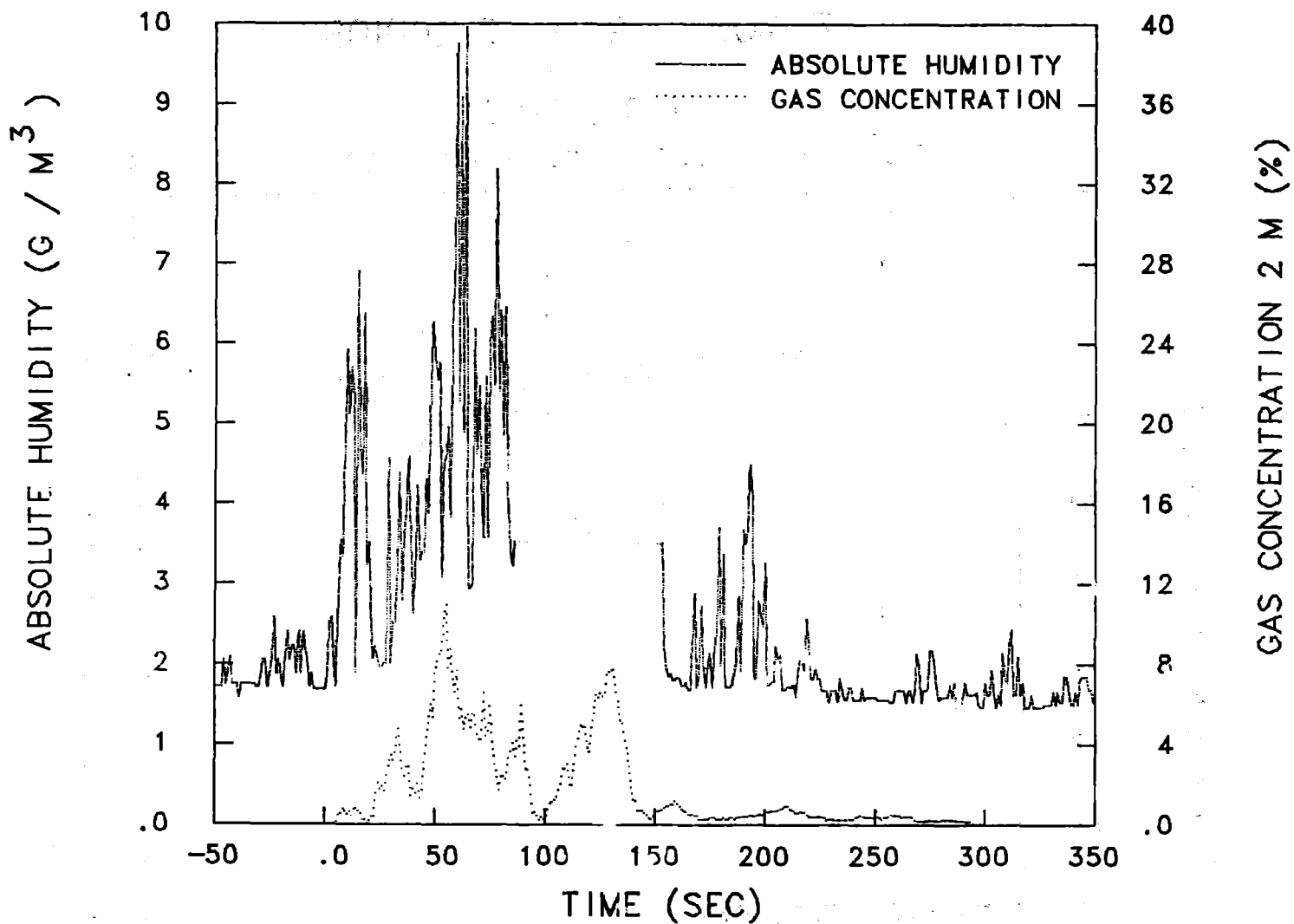
^c Humidity increases were so large that the scale was doubled compared to other plots. Gas sensor data unreliable in Row 1 due to RPT effects.



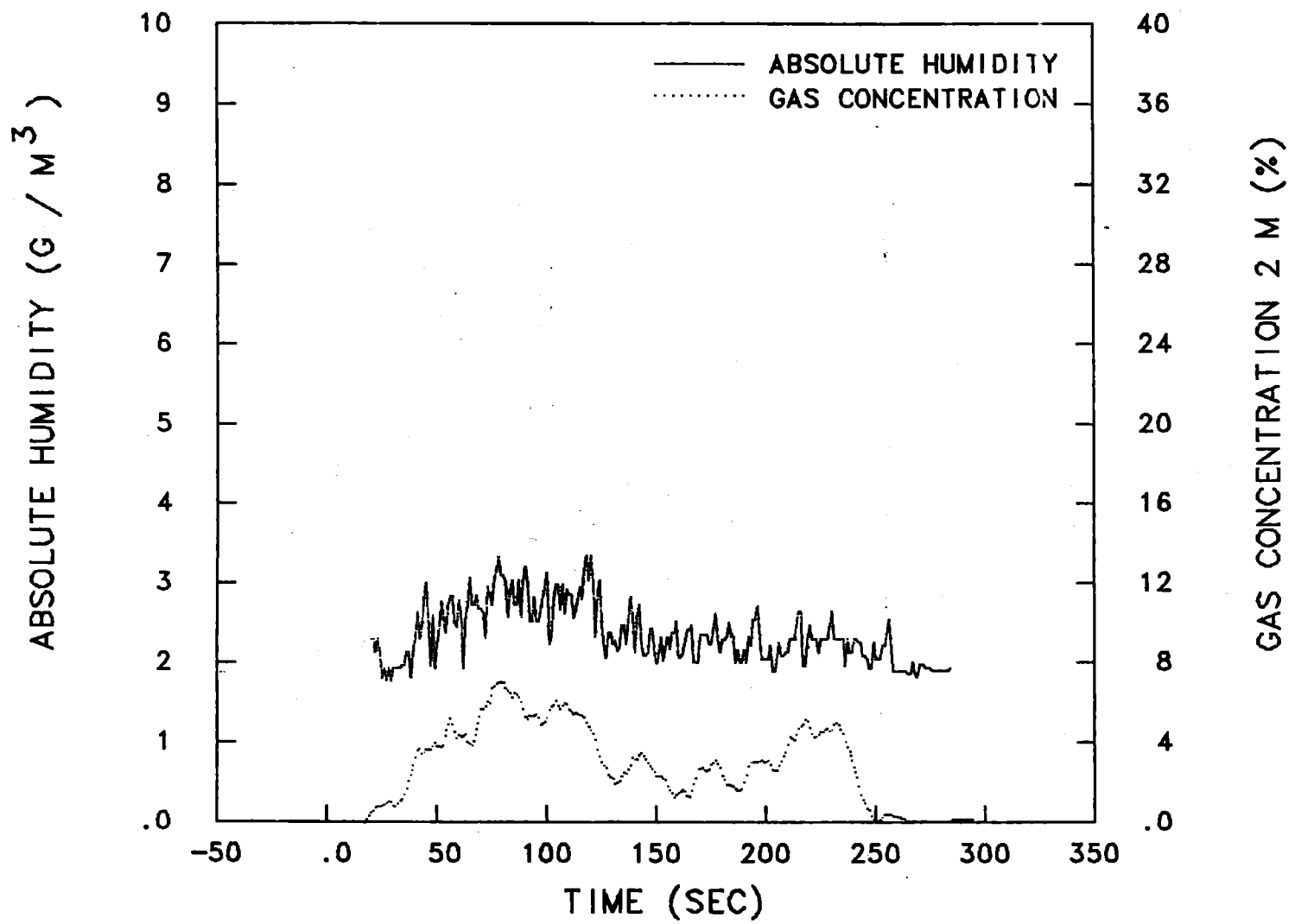
BURRO 2 G-4 ROW 1



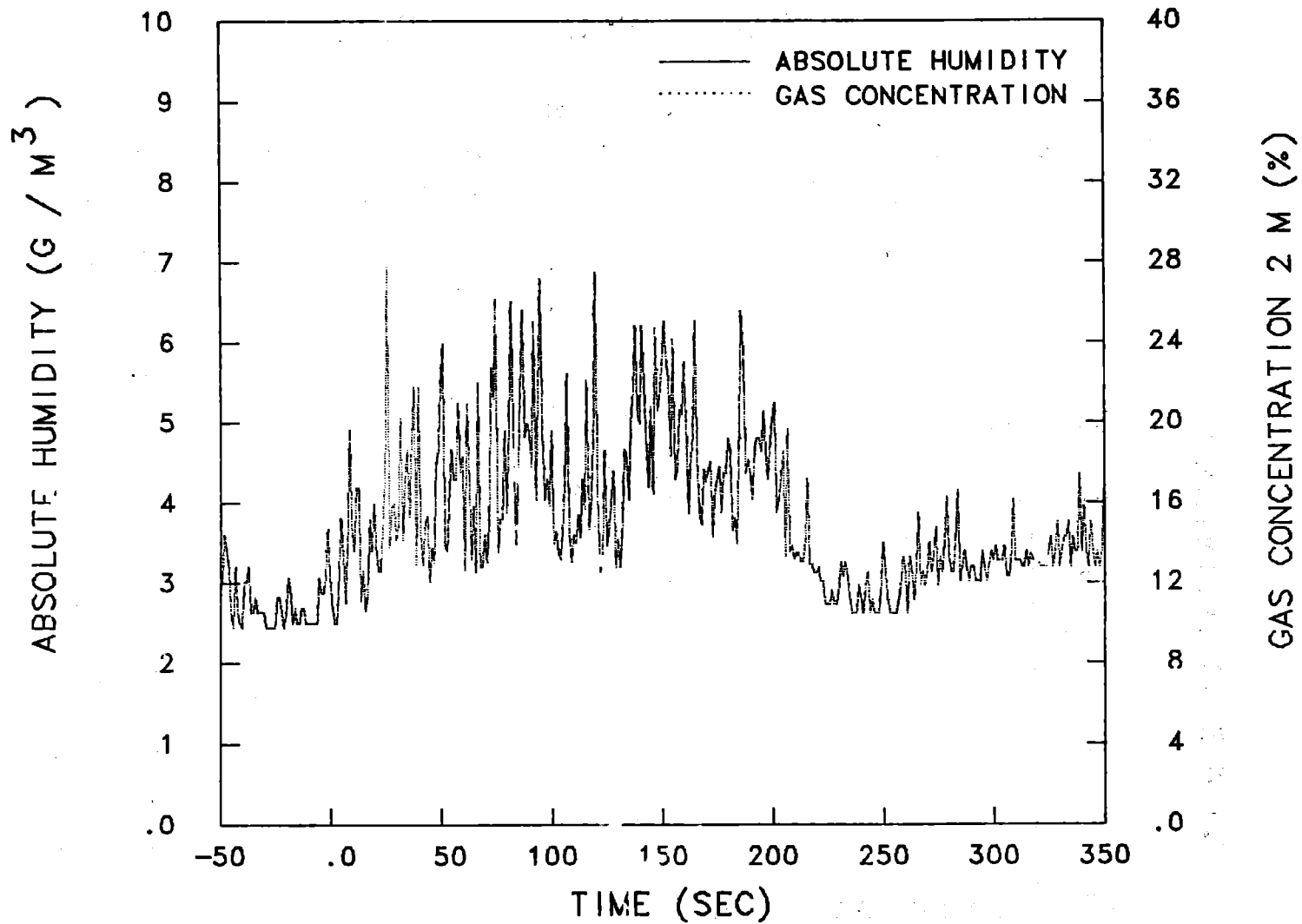
BURRO 2 G-6 ROW 2



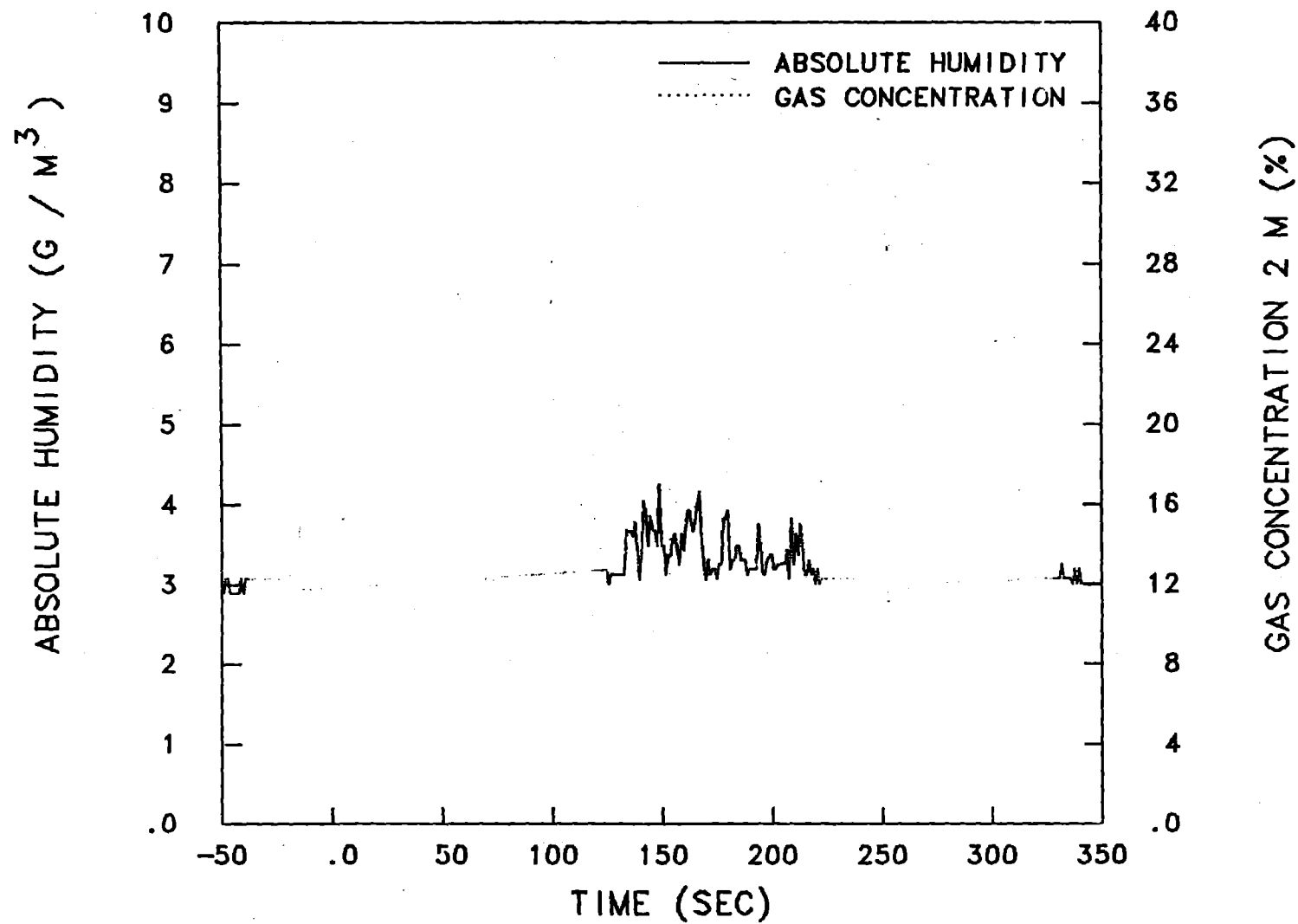
BURRO 3 G-4 ROW 1



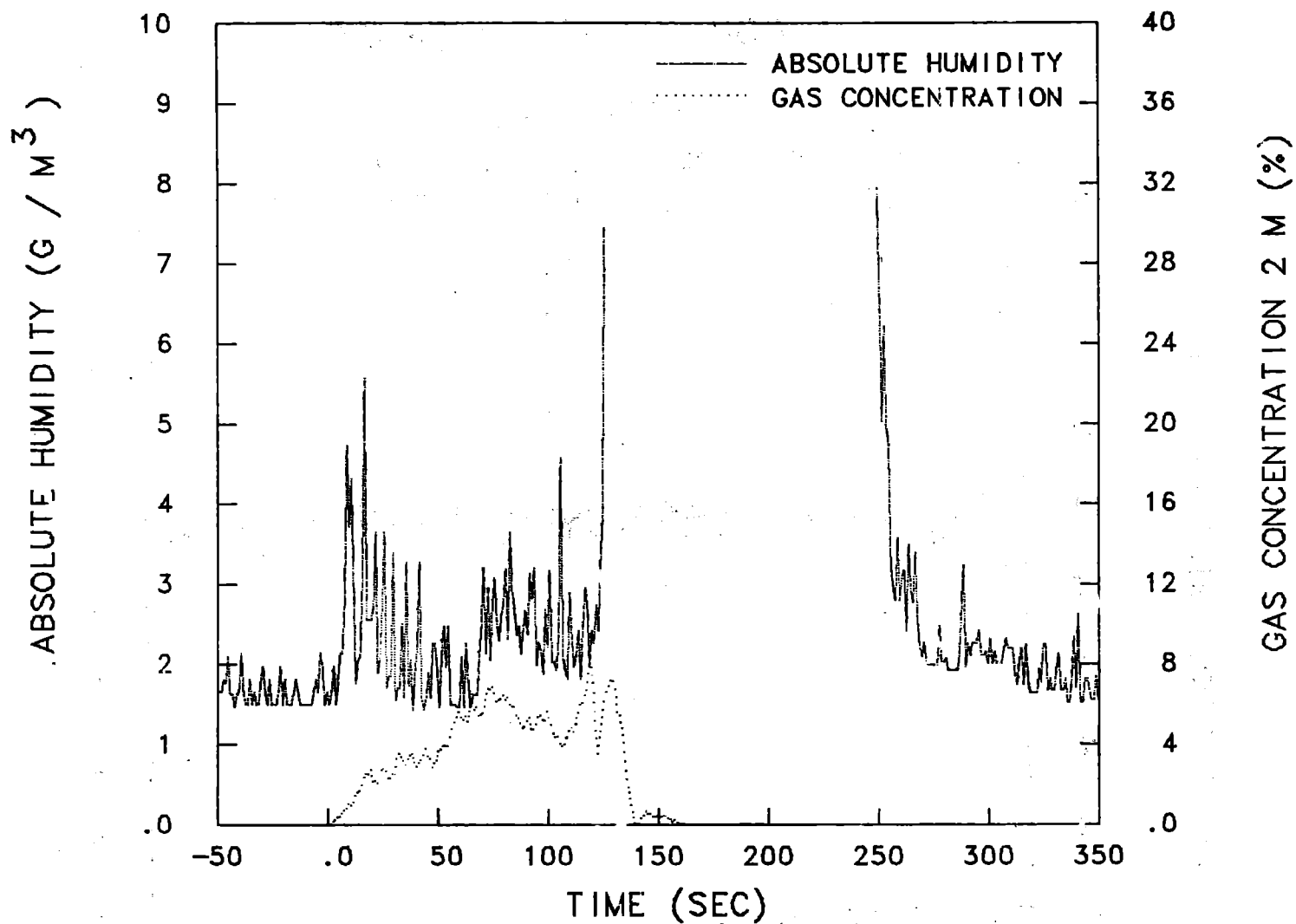
BURRO 3 G-6 ROW 2



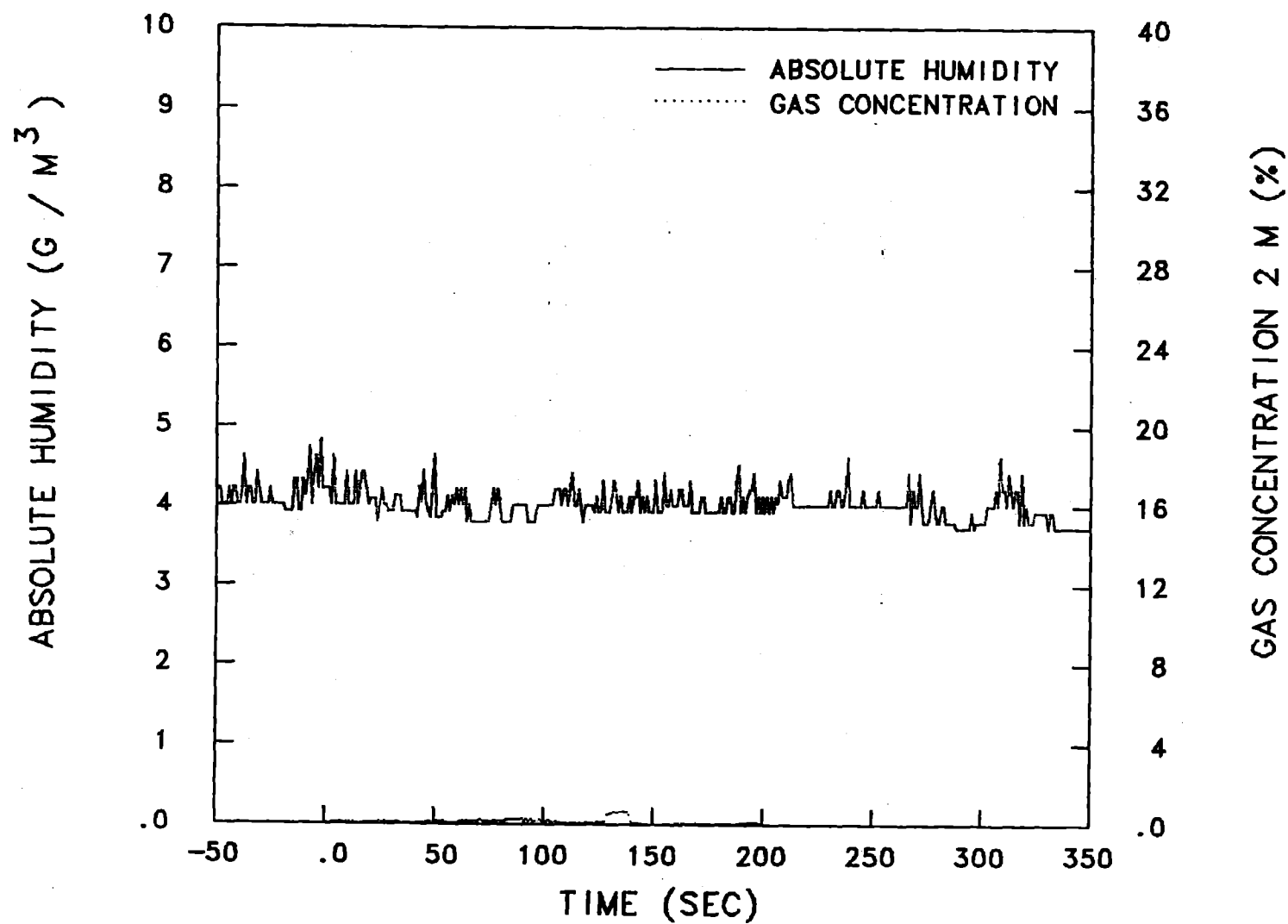
BURRO 5 G-4 ROW 1



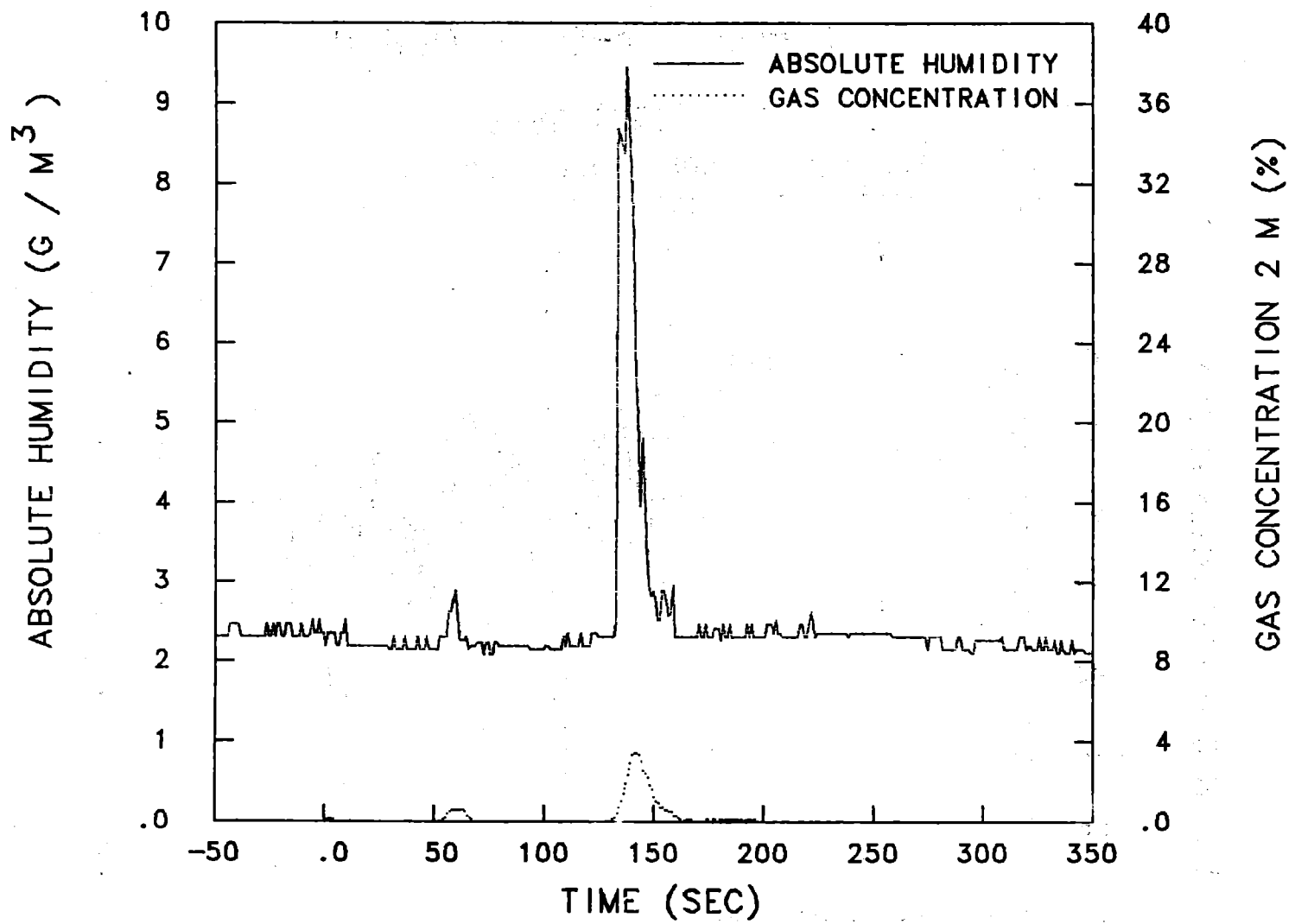
BURRO 5 G-6 ROW 2



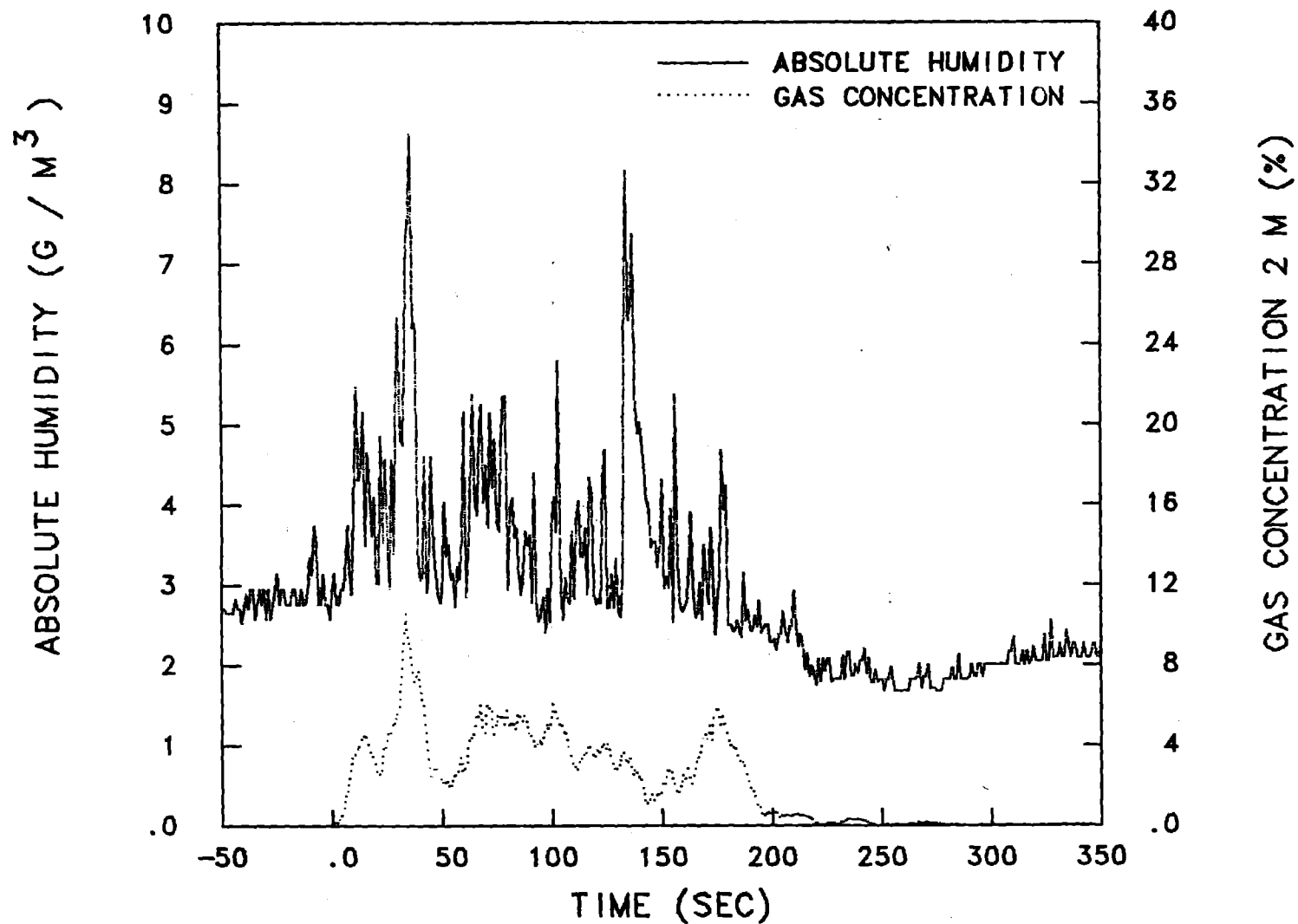
BURRO 6 G-4 ROW 1



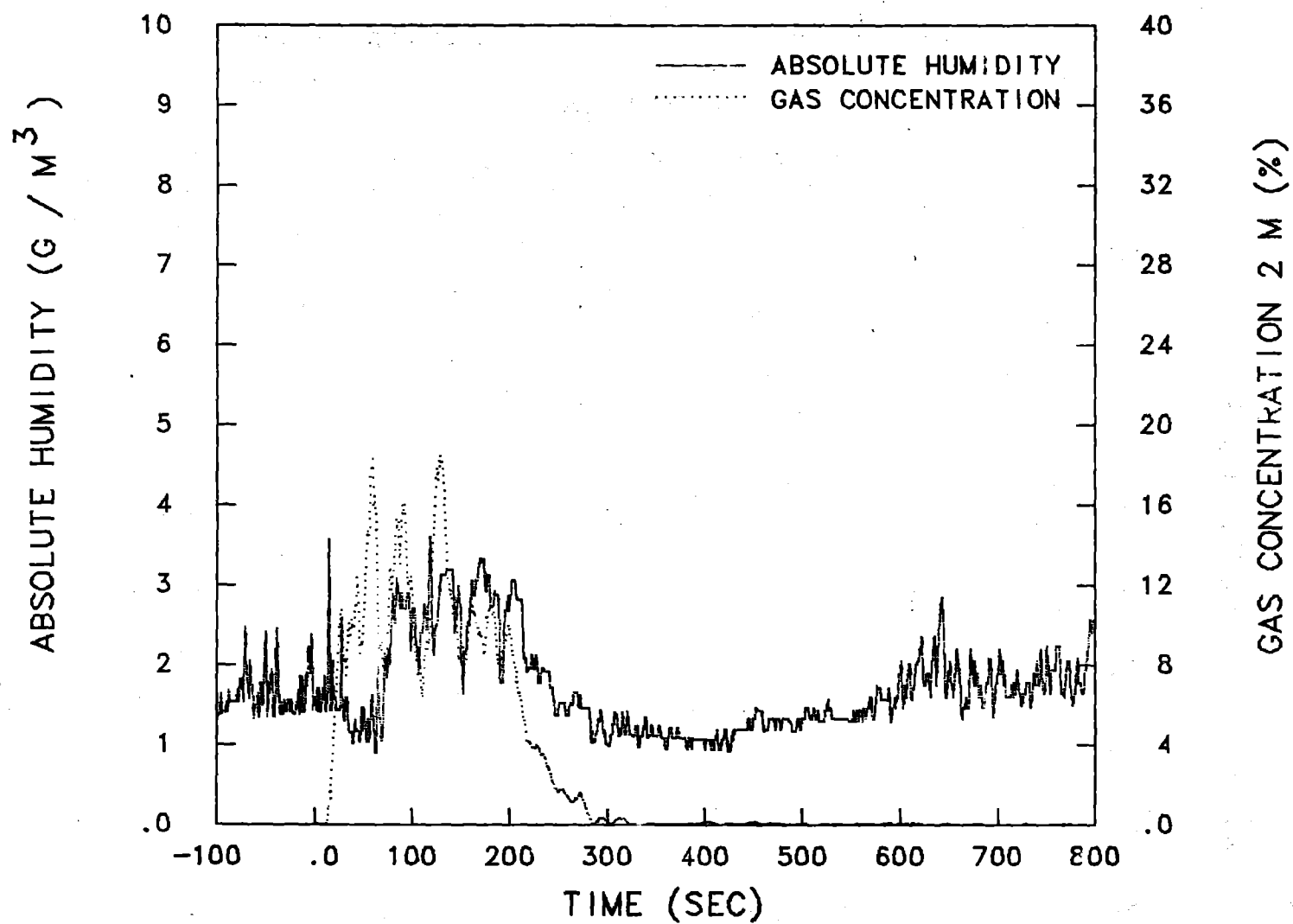
BURRO 6 G-5 ROW 1



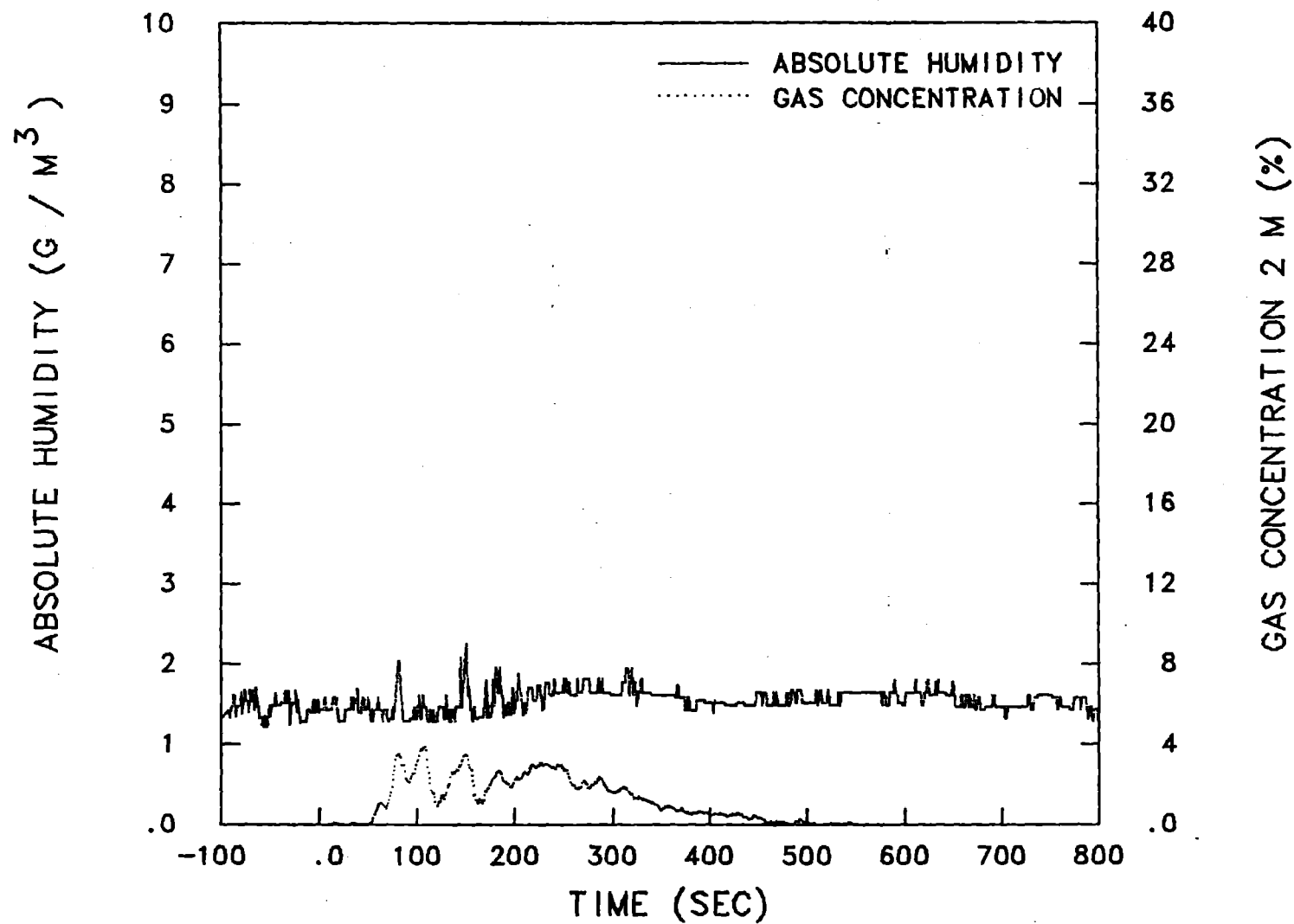
BURRO 6 G-6 ROW 2



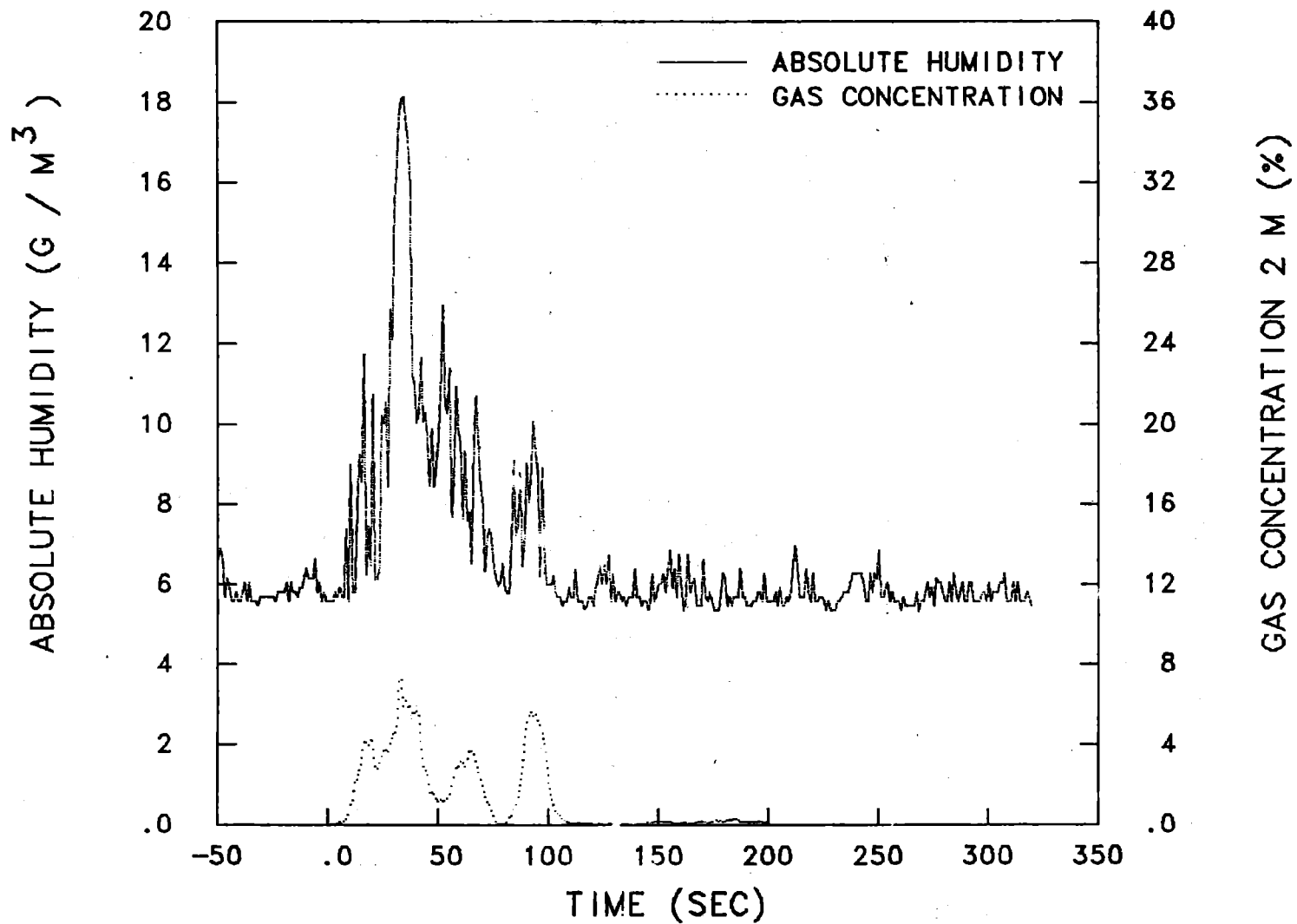
BURRO 7 G-4 ROW 1



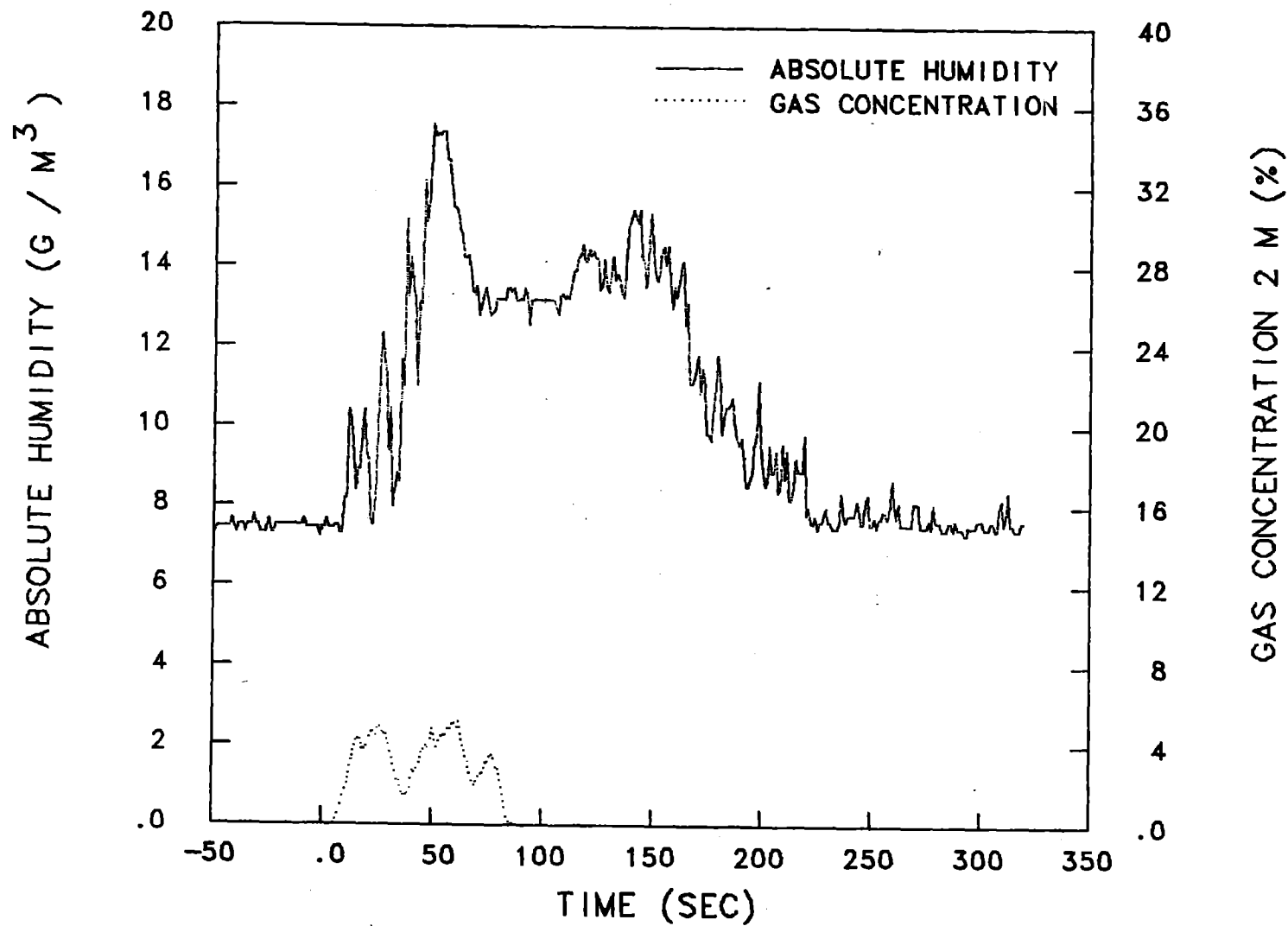
BURRO 8 G-4 ROW 1



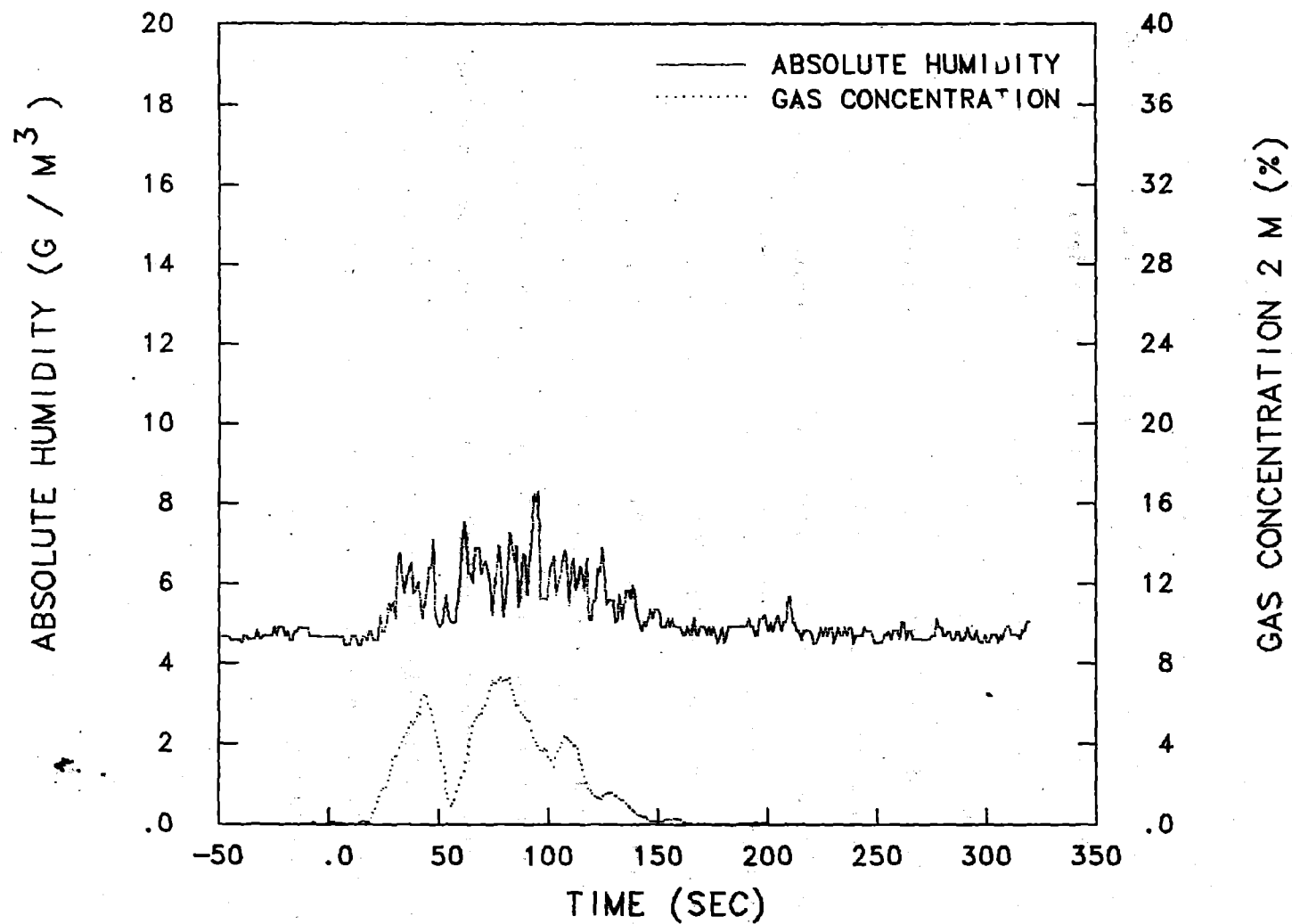
BURRO 8 G-6 ROW 2



BURRO 9 G-4 ROW 1



BURRO 9 G-5 ROW 1



BURRO 9 G-6 ROW 2

Heat Flux

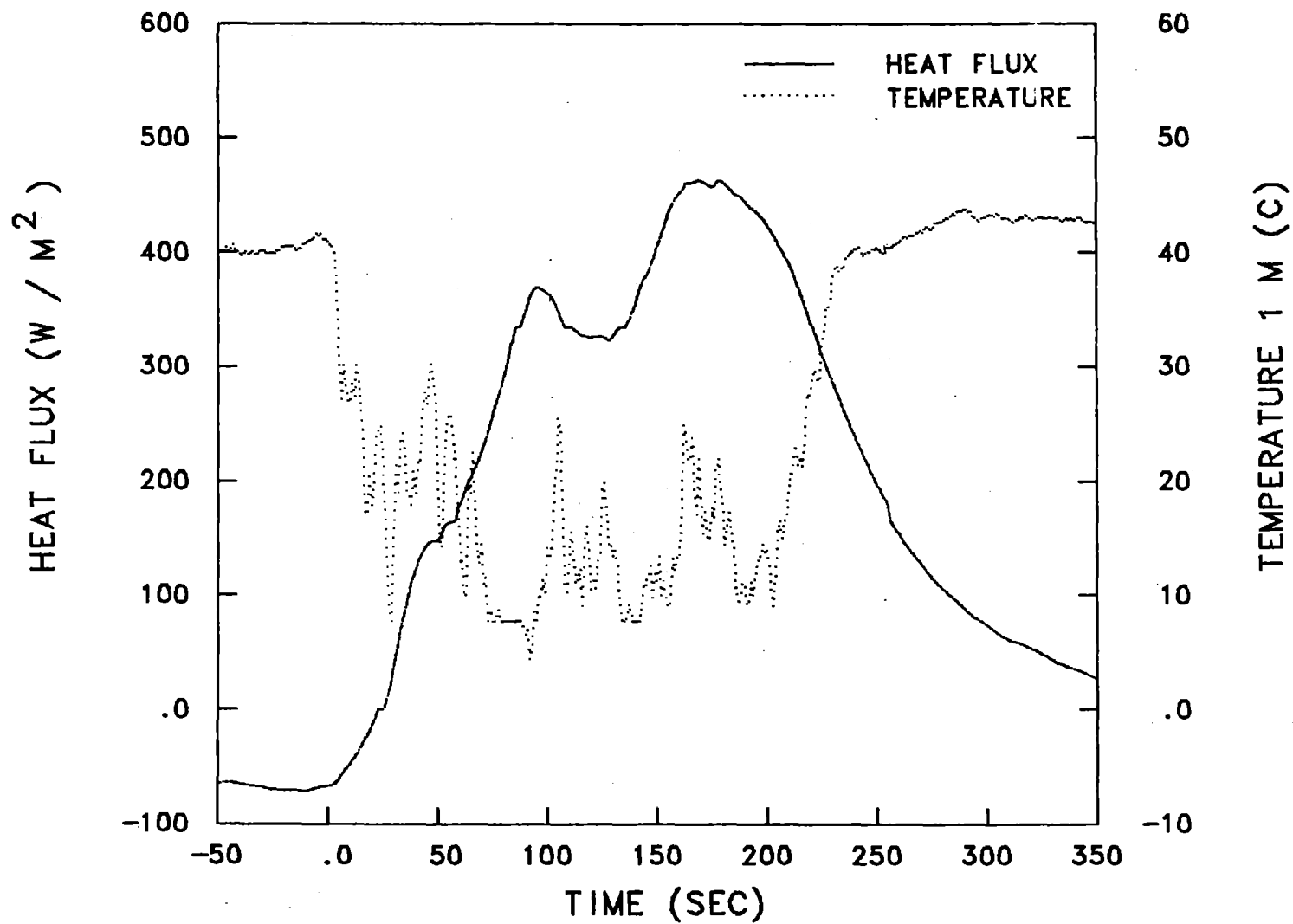
What follows is a series of plots describing the effect of the LNG vapor cloud on the heat flux at the ground surface. The heat flux data acquisition network was fully implemented by the time of the Burro 5 test. Table 5 summarizes the stations which saw sufficient amounts of the LNG vapor cloud to show a perturbation in the ground heat flux. Data are shown for the first 350 seconds of the spill except for Burro 8, where an 800-second data period was appropriate due to the low wind speed. In two instances (Burro 6, G4 and Burro 9, G5), rapid phase transition (RPT) explosions expelled water out past the 57-m row. This significantly altered the ground surface conditions so that the heat flux values went off scale and did not return to the prespill value during the time we were recording data. Plots are included for all other stations marked in the table.

Temperature at 1 m is also plotted (the dotted line) to provide a reference to the presence of cold vapor. The measured rise in the heat flux is not as rapid as the drop in air temperature. This is due to the thermal inertia of the thin layer of soil covering the sensor, which increases the response time of the measurement. Similarly, after the cloud passes and the air temperature rises to its original value, the ground heat flux displays a much longer recovery time. This recovery is approximately an exponential function of time and is governed by the soil properties.

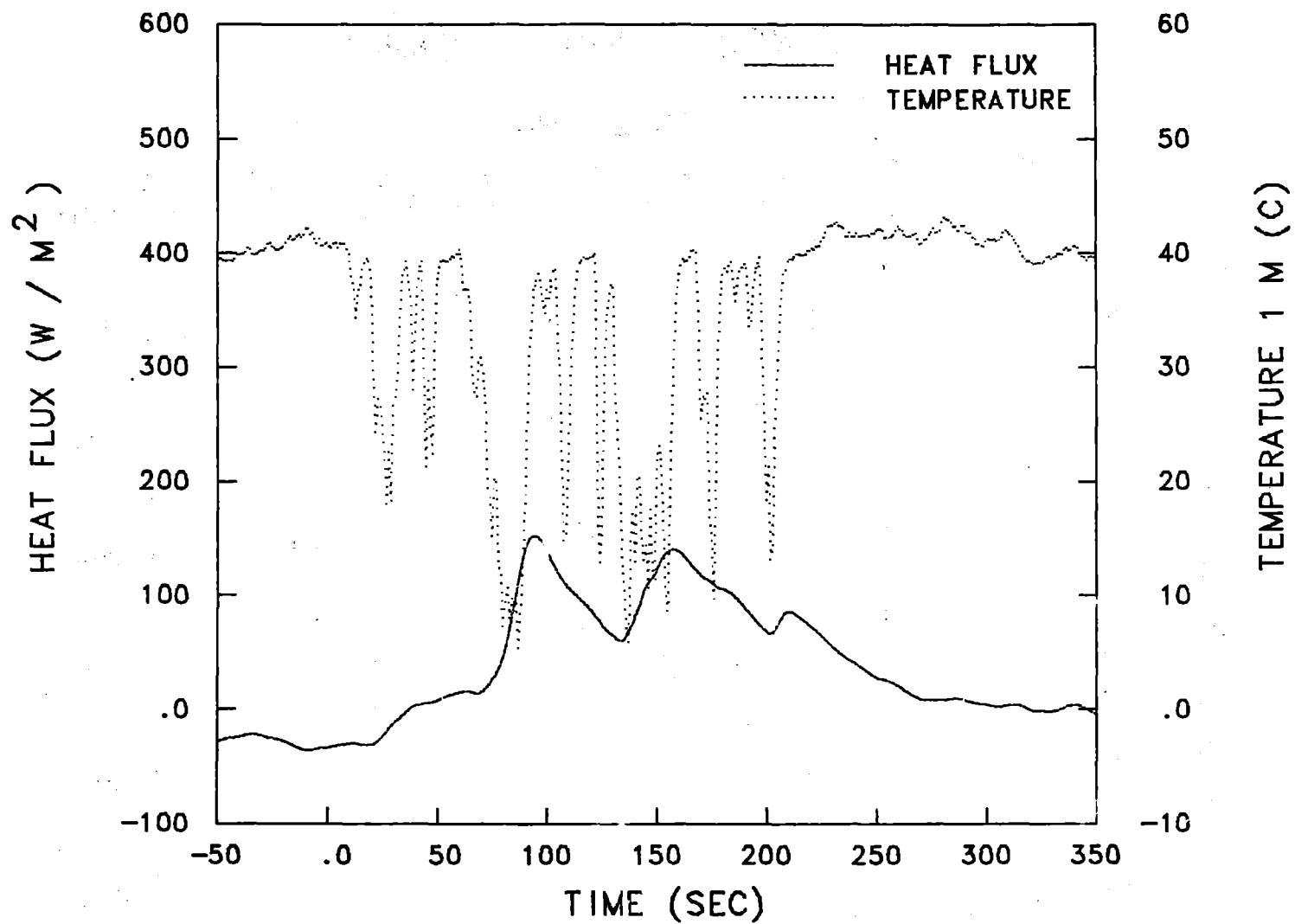
TABLE 5. Summary of Heat Flux Plots

Burro Experiment No.	Stations		
	G4 (57 m, left)	G5 (57 m, right)	G6 (140 m, center)
5	X	X	X
6	RPT		X
7	X		
8	X		X
9	X	RPT	X

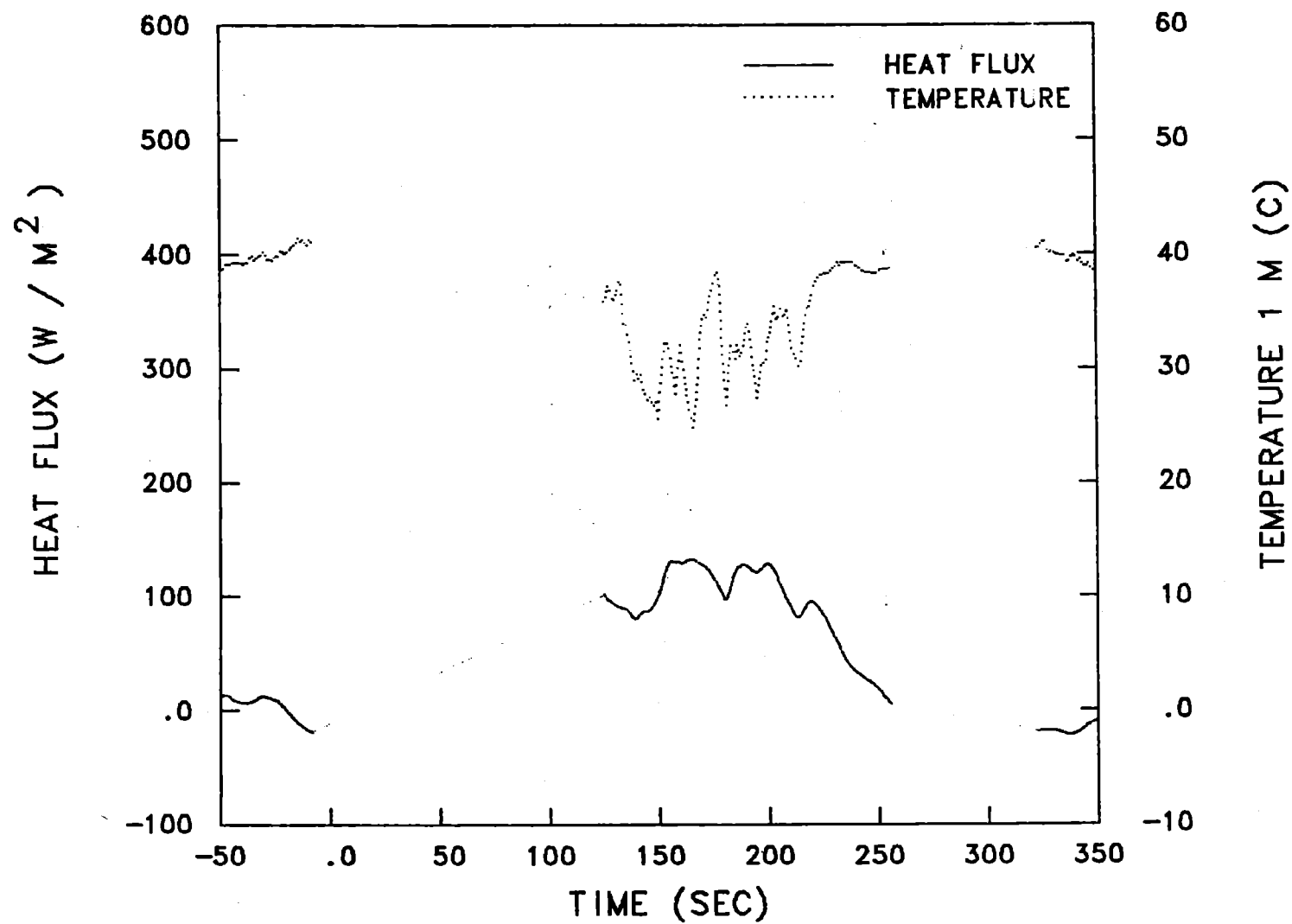
Data is shown for the first 350 seconds of the spill, except for Burro 8 where an 800-second data period was appropriate due to the low wind speed.



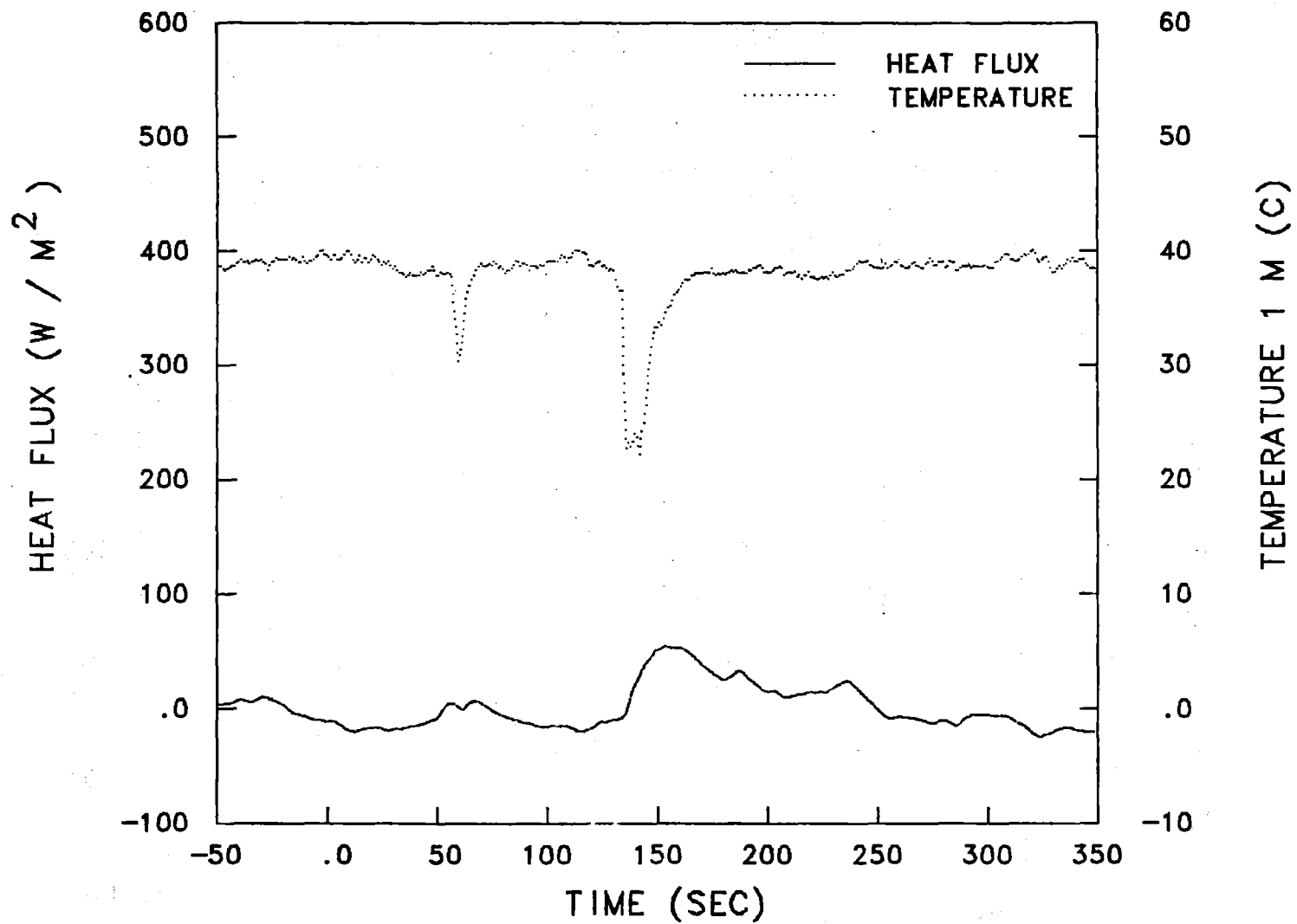
BURRO 5 G-4 ROW 1



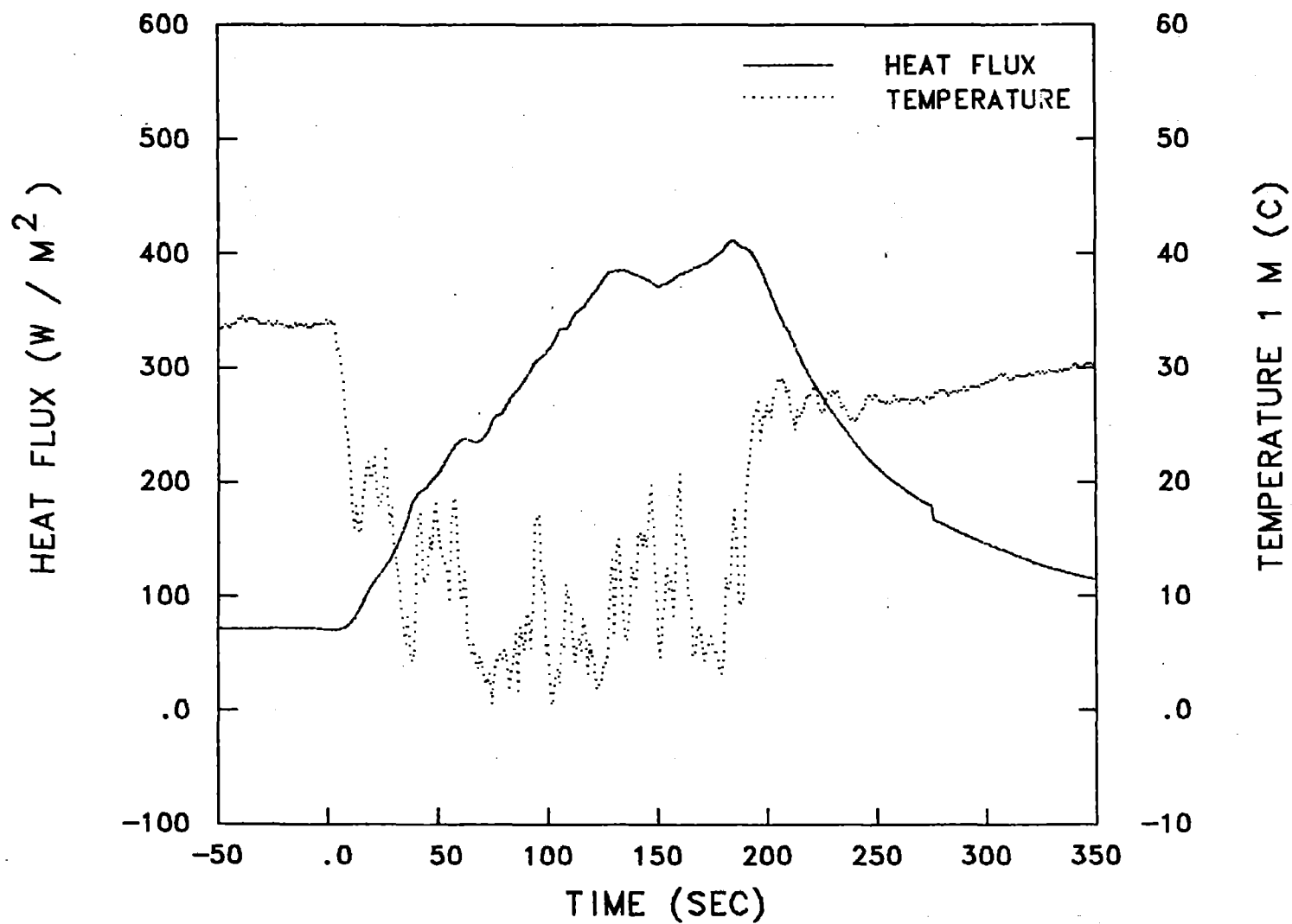
BURRO 5 G-5 ROW 1



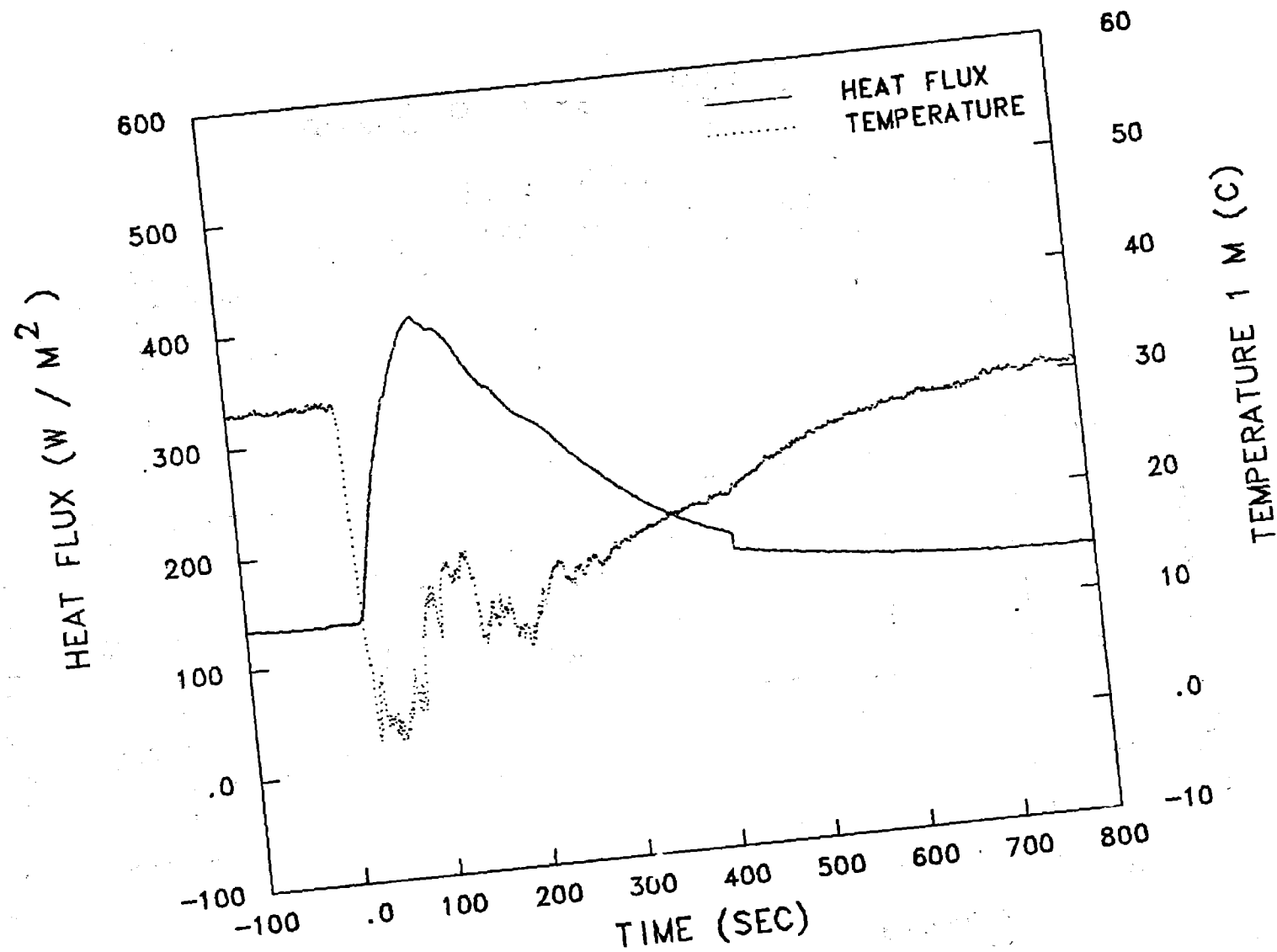
BURRO 5 G-6 ROW 2



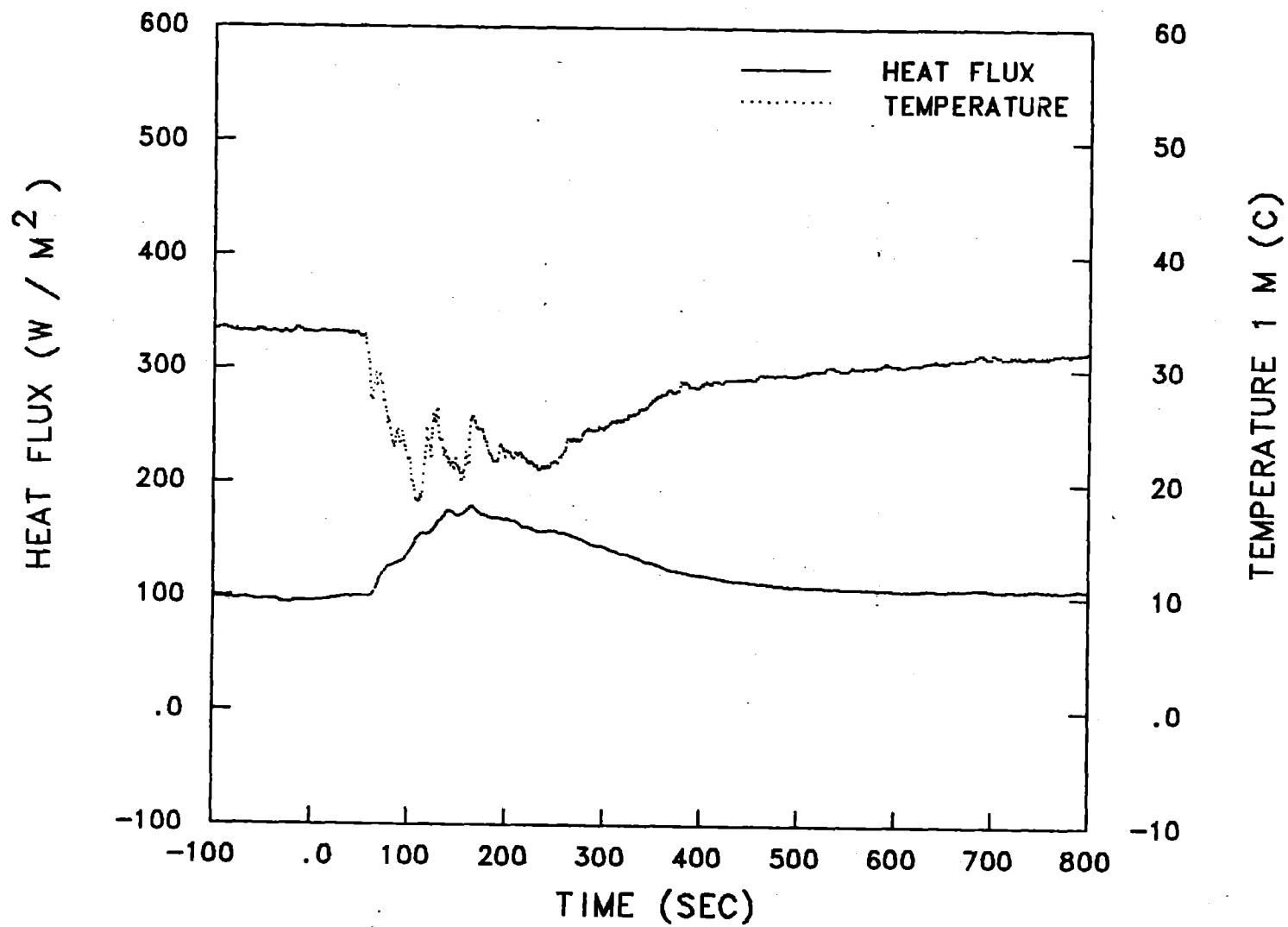
BURRO 6 G-6 ROW 2



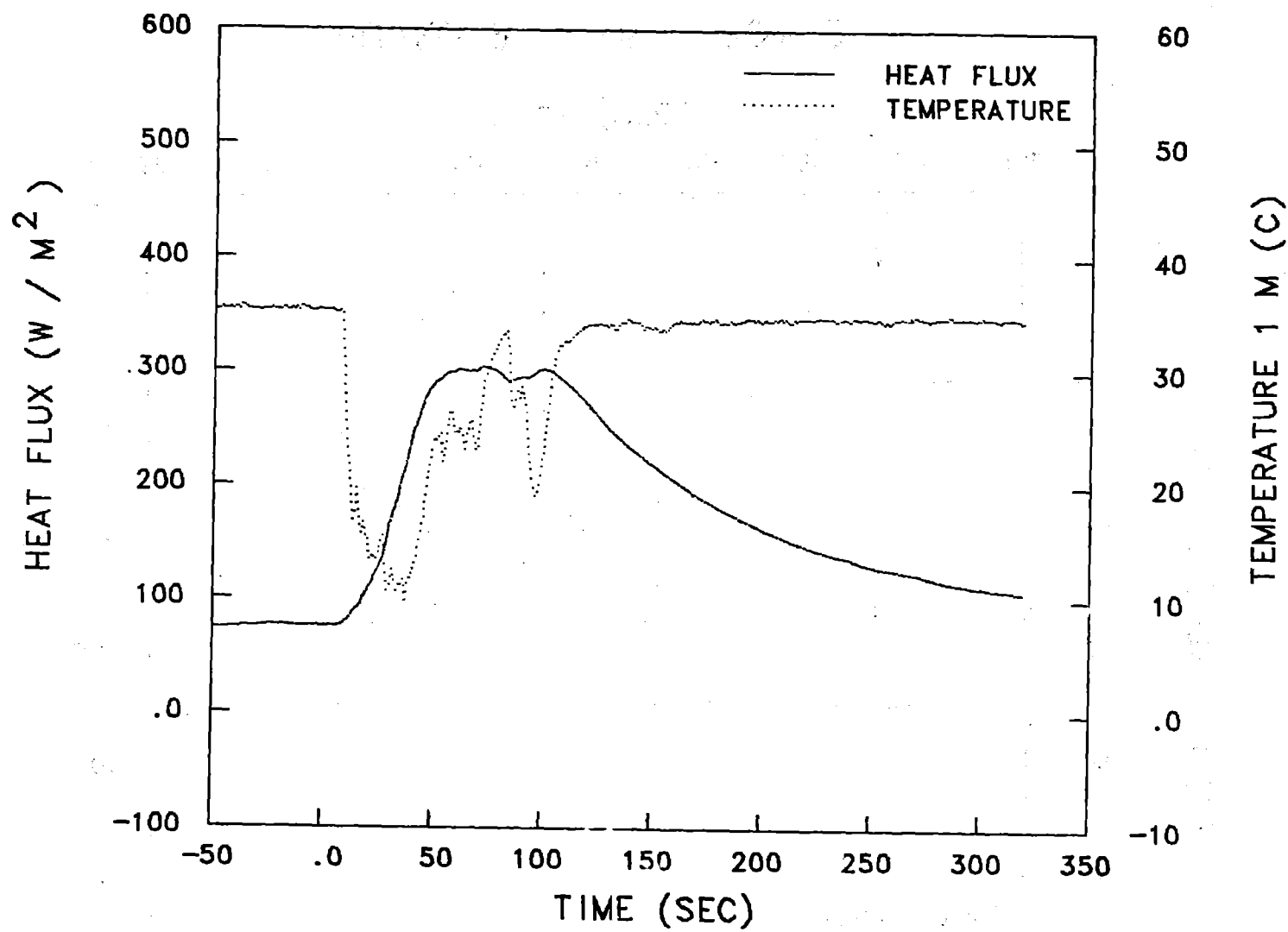
BURRO 7 G-4 ROW 1



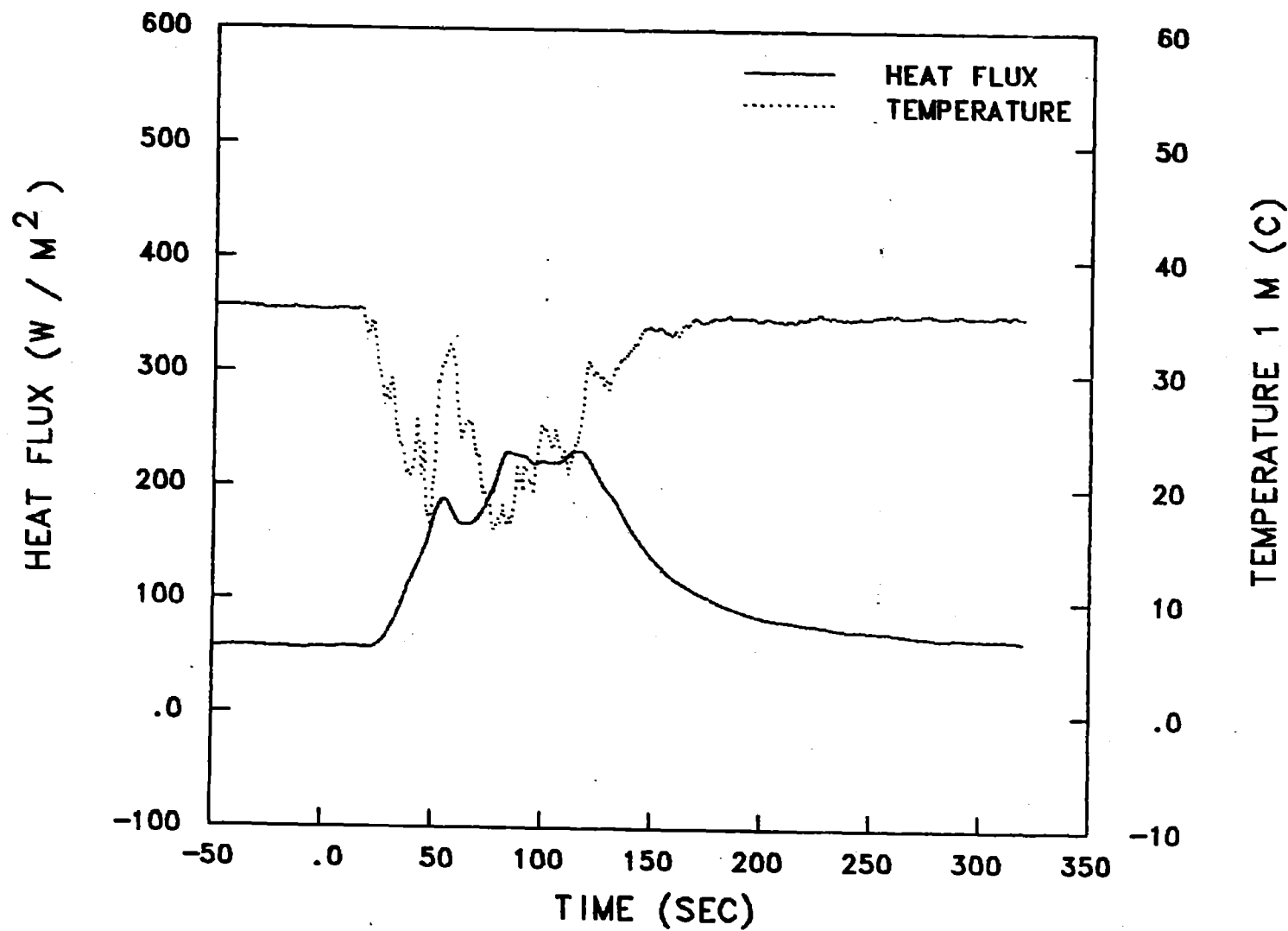
BURRO 8 G-4 ROW 1



BURRO 8 G-6 ROW 2



BURRO 9 G-4 ROW 1



BURRO 9 G-6 ROW 2

G. GAS CONCENTRATION DATA

The data presented in this section are of two types: (1) plots of gas concentration vs time and, (2) plots of gas concentration contours. The gas concentration contours are discussed in this section but, because of the large number of plots involved, are presented in Appendices 2 and 3. The concentrations for both types of data presented are of total hydrocarbons, consequently the LLNL IR methane and ethane-plus-propane data have been combined to yield total hydrocarbons. Also, the data from the faster responding instruments have been smoothed so that all of the data presented here have approximately the same 10-s time constant.

The gas concentration data are presented first as plots of gas concentration versus time from each operational gas sensor for each test. The data have been examined and corrected for all known errors. Because of the large amount of data, we have chosen to display the data from a whole row of stations on one figure, for all tests except Burro 8. Because of the large width of the Burro 8 gas cloud, this form of display became too confusing, consequently separate figures have been produced for the left and right halves of the gas cloud. The key to the identity of the traces is given in the upper right hand corner. If a sensor is not operational for a particular test, it is not listed in the key. During Burro 2, station G8 in the 57-m row failed at 135 s into the test. Data from that station are included, but the indication of zero values after 135 s does not mean that no gas was present at that station.

In some tests and at some locations, the IST sensors experienced high concentrations of gas (above ~ 18%) causing them to saturate. These traces are obvious because of their flat tops. The IST sensors also showed varying degrees of sensitivity to ethane and propane and the correction for these species causes the saturation cut-off to decrease at the end of the spill when the ethane and propane concentrations increase.

A summary of the stations closest to the vapor cloud centerline for the entire Burro Series is given in Table 6. The Burro 2 spill occurred before the entire sensor array was erected, hence, there were only two centerline stations operational for this test. For tests in which the cloud centerline went between stations, both stations are listed. Centerline stations which were not operational are marked with an asterisk in Table 6. The G-5 data of Burro 9 is of questionable accuracy because of the large RPTs which occurred during this spill, a subject which is discussed in more detail later in this section. Note that the cloud centerline, as determined by the wind field, does not coincide with the maximum gas concentration for Burro 8 as it does in the other tests.

The concentration contours are in two forms: horizontal slices at 1-m and 3-m heights, and vertical slices at the array row locations, shown in Appendices 2 and 3. The vertical contours show the gas concentration at the specified row as it would appear to an observer facing the pond from the downwind side. The height and time of the horizontal contour calculation are indicated on each plot in the lower left corner. The height is the vertical distance above the local ground level at each gas station. Horizontal contours at 3-m are shown only for Burro 8 where peak concentrations occurred at this level. For all other tests they are shown only for the 1-m level. Station position, including height above sea level, is given in Table 1. The value of each contour level in percent concentration of total hydrocarbons is indicated on the plots.

Several different interpolation schemes were tried for creation of the horizontal contours. Because of the long distances between rows of gas sensors in the downwind wind direction, and the transient nature of the LNG spills, there were problems with each interpolation scheme. Linear inter-

TABLE 6. Gas plume centerline stations as determined by the wind flow lines.

Burro Experiment No.	Centerline Stations			
	57 m	140 m	400 m	800 m
2	G-4	G-3	G-10*	G-21*
3	G-5	G-6	T-5*/G-15	T-6*/G-21
4	G-4	G-3/T-3*	G-14	G-20*/G-21
5	T-2	G-6*/T-3	T-5*	G-22*
6	G-4	T-3	G-17*	G-21*
7	G-4	G-3	G-14	G-18
8	T-2	G-6	G-15	G-23
9	G-5(RPT)	T-4	G-15	G-22

*Station not operational or data lost.

polation of gas concentration with downwind distance generally produces an overestimate of the concentration between rows. For a steady state gas plume it has been well established that logarithmic interpolation, i.e., linear interpolation in log concentration-log distance space, is the procedure which best represents the dispersion process. If we look at our maximum concentration versus downwind distance data, shown in Fig. 10, for Burro 8, this behavior is well substantiated at least out to the 400 m row. However, because of the transient nature of these gas clouds and the long distances between rows of sensors, logarithmic interpolation tends to underestimate the concentration between rows. This is demonstrated by the gas concentration at 200 seconds, also shown on Fig. 10. The sensor showing the maximum concentration at the 140 m row saturated (as did the sensor at the 57 m row showing the maximum reading at 200 s.) The 57 m and 400 m sensors were used to establish the straight line shown on the figure. We believe that the 140 m sensor would have fallen on the line had it not saturated. Examples of contours generated using linear interpolation and logarithmic interpolation for both Burro 8 and Burro 9 are shown in Figs. 11 and 12.

Having examined the time-dependent behavior of the data, it is our judgement that the linear interpolation scheme best represents the actual gas clouds for the Burro series experiments.

At the beginning of each test shown in Appendices 2 and 3, is a plot of the operational sensors used to generate the contours. An example for the Burro 9 test is shown in Fig. 13. Only the first three arcs of sensors are shown so that attention may be more easily focused on the concentration contours near the flammability limits. Sensors from the 800-m arc are not shown, but their data were used to generate the contours. A similar plot of operational sensors in an arc is shown at the beginning of each set of vertical contours. An example of this is shown in Fig. 14 for the 140-m row for the Burro 8 test.

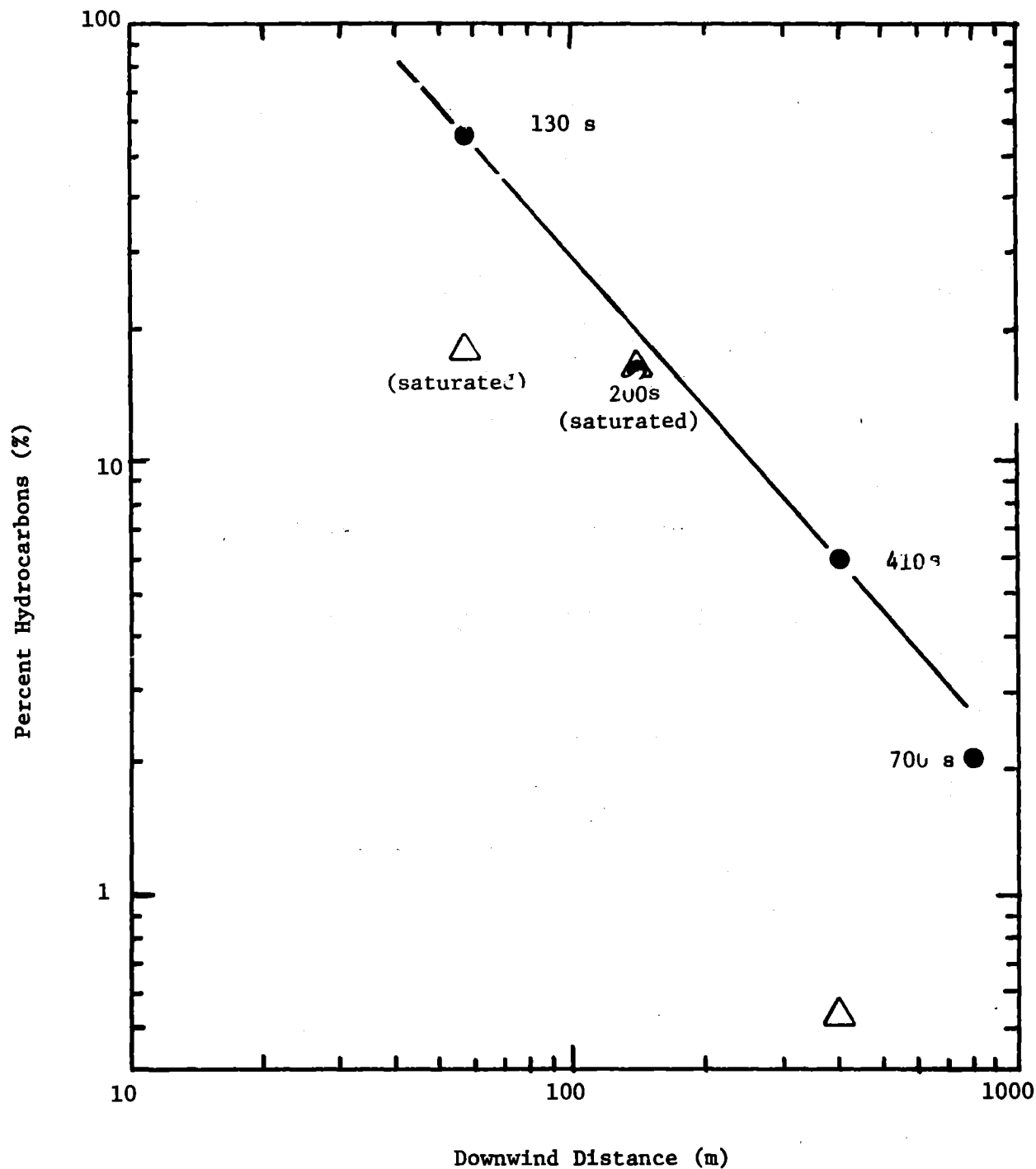


Figure 10. Peak plume centerline concentration versus downwind distance for Burro 8 is shown by ●. The △ shows the concentration at the various rows at 200 seconds.

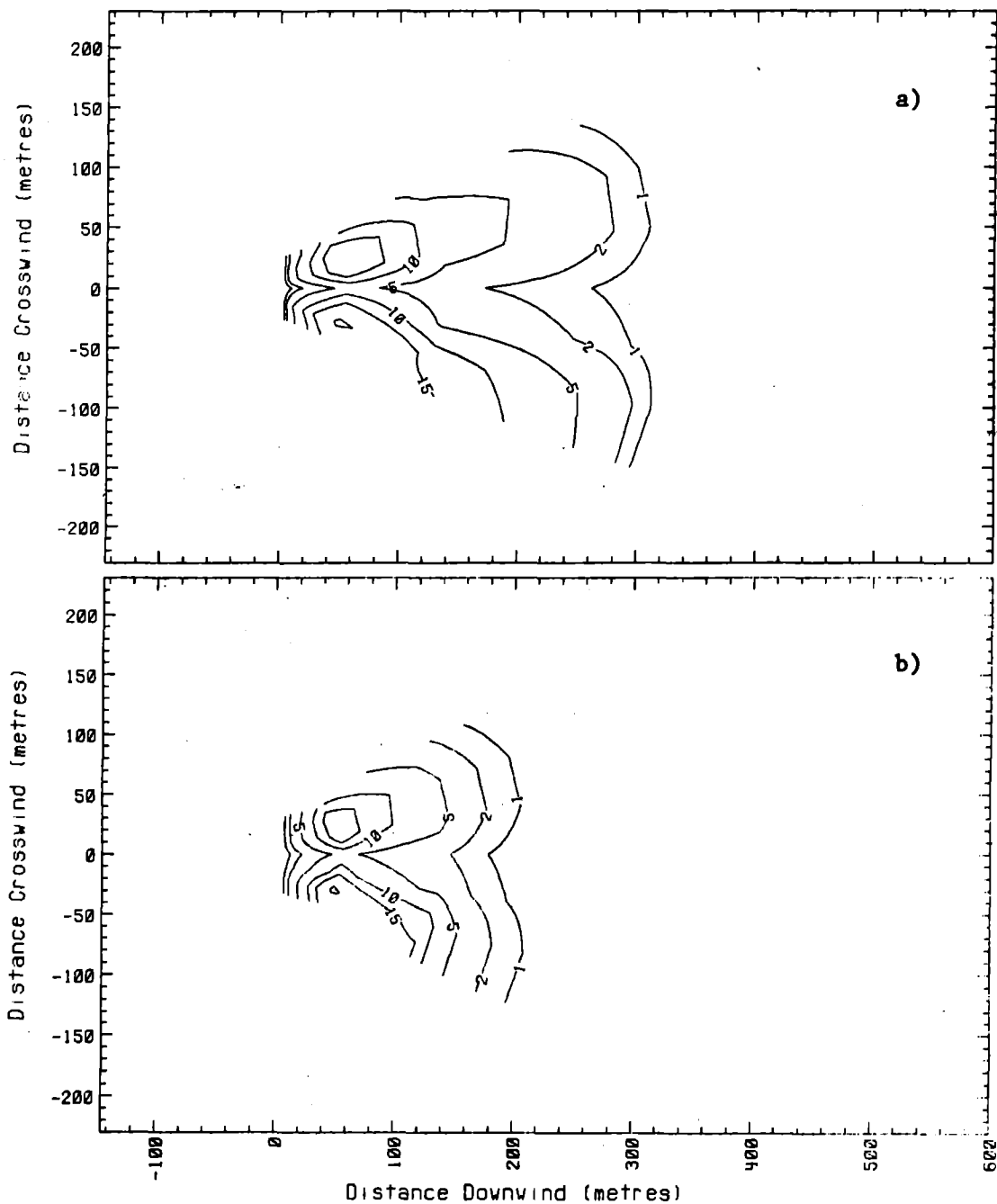


Fig. 11 Horizontal gas concentration contours at 1 m above ground level for Burro 8 at 160 sec. into the spill for both a) linear interpolation and b) logarithmic interpolation.

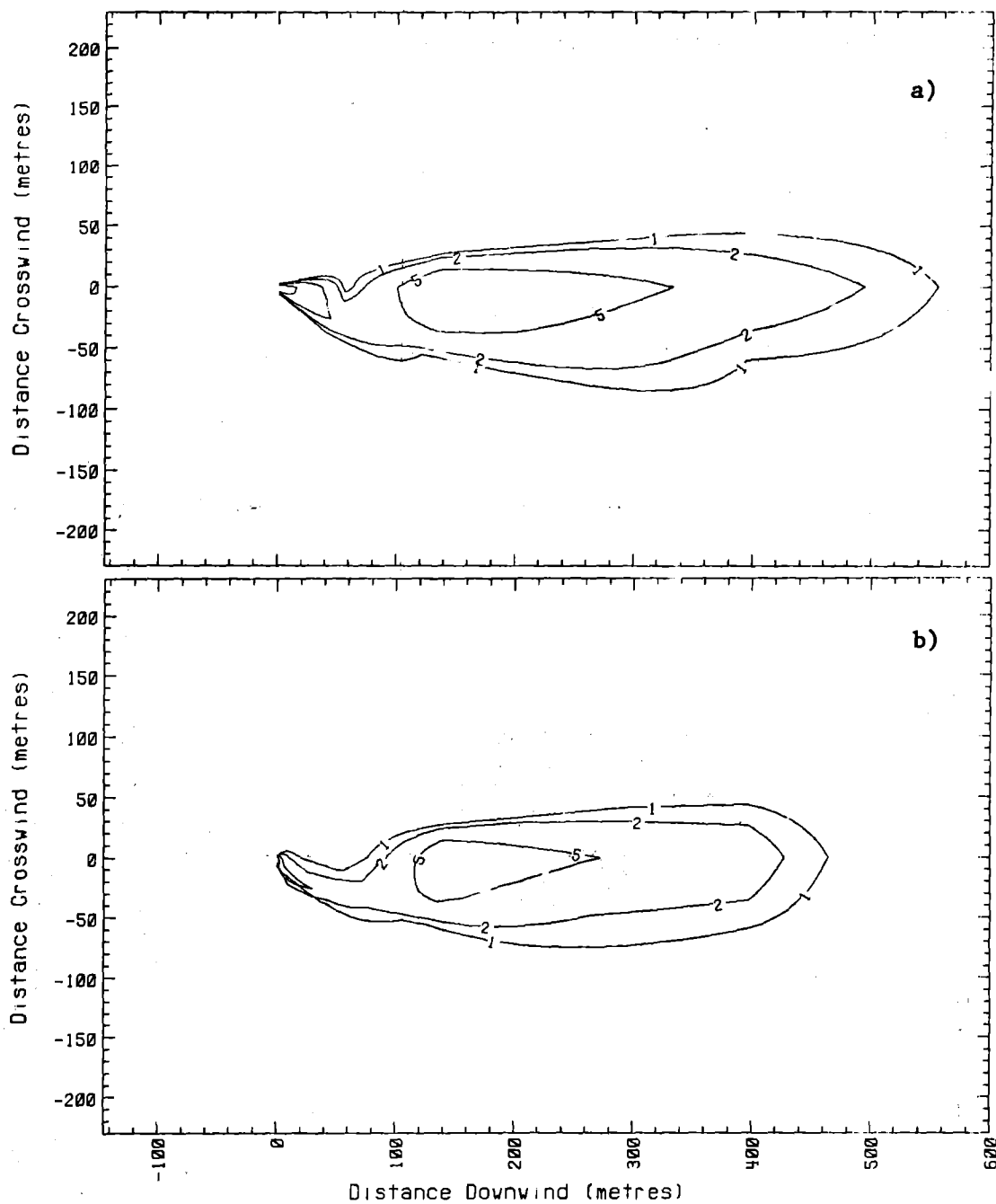
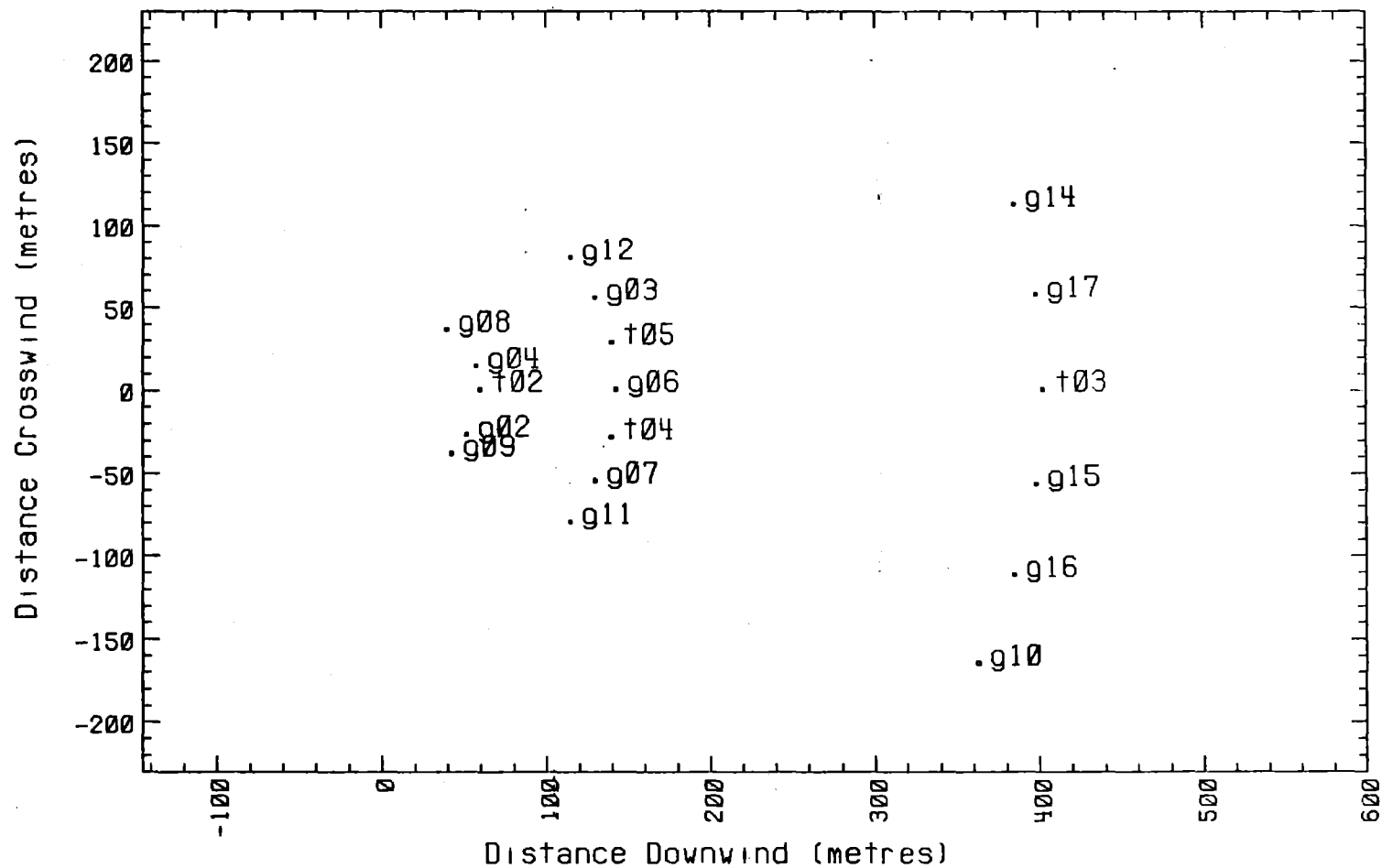


Fig. 12 Horizontal gas concentration contours at 1-m above ground level for Burro 9 at 80 sec. into the spill for both a) linear interpolation and b) logarithmic interpolation.

04/04/83r 16:17:50
04/06/83 10:47:05

Horizontal grid



Burro 9 . LNG 80

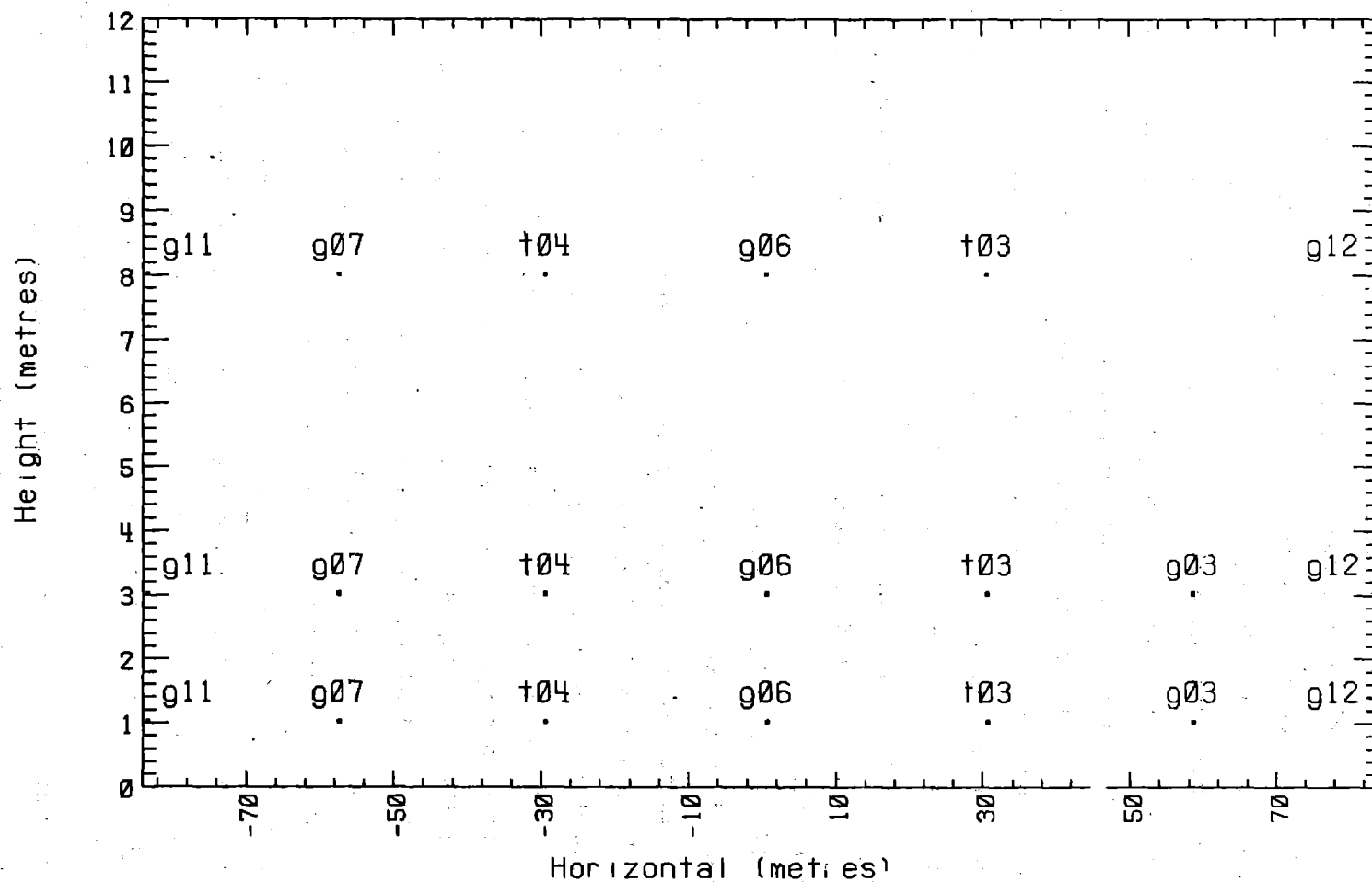
Windvel - 5.700 m/s

edge coefs - 11.620 7.457 0.001

Fig. 13 Station positions for Burro 9. Only operational sensors in the first three arcs are shown. The 800-m arc is not shown.

01/10/83 15:56:50
01/11/83 14:51:09

Vertical Grid



Burro 8 LNG 80
140m

Fig. 14 Operational gas snesors in the 140-m row.

Several other points concerning the contour displays should be mentioned. In the case of the horizontal contours, a line source of LNG vapor has been introduced at the origin in order to close the contours in this region. The source is 20 m in length along the y axis (except for Burro 8) and has a hyperbolic concentration distribution over this distance. For Burro 8, the vapor source length was taken as 50 m due to the large degree of gravity spreading during this spill. The peak concentration value of the vapor source distribution is always at least one contour interval greater than the highest measured concentration at the particular height (1 m, 3 m, or 8 m) of the displayed contour series. The source distribution is constant in time from $t = 0$ to the time of the spill valve closure. It then decreases linearly to zero concentration at a time determined by noting the time of the last measurable concentration at of the 57-m row of sensors and subtracting the time required for the cloud to travel 57 m at the average wind speed for that particular spill.

An artificial row of zero concentration, originating at the pond and moving downwind at the maximum wind speed, has been superimposed on the contours. This technique keeps the downwind interpolation distances to a minimum as the cloud is forming, and avoids the appearance that the cloud is leaping forward as it passes each row of stations.

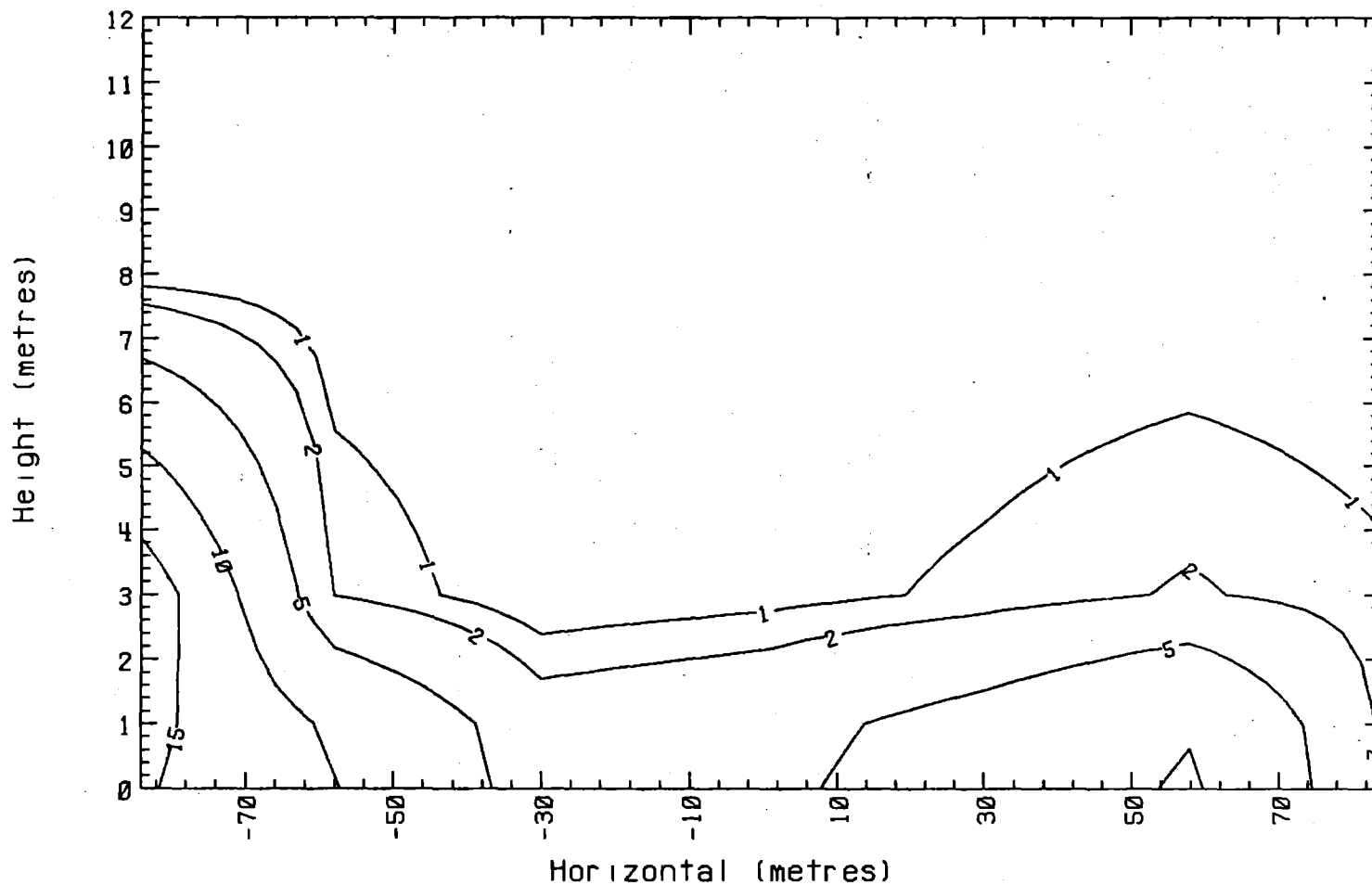
Linear interpolation in both concentration and y and x directions is used for the vertical concentration contours. This is justified since the interpolation distances for these contour calculations are much smaller than those in the downwind direction and there is no evidence to indicate that any other scheme would be better. For all of the vertical contours displayed in Appendix 3, the gas concentration was assumed to be zero at a height of 12 m. Two techniques were used to extrapolate the vertical concentration data to the ground level ($z = 0$). If the 3-m concentration at a station was less than the 1-m value, the ground level concentration was determined by using a quadratic curve through the 3-m and 1-m values whose slope (concentration gradient) is zero at $z = 0$. For cases where the 3-m concentration was greater than the 1-m value, the ground level concentration was determined by a linear extrapolation of these two values to $z = 0$. An example of the vertical contours shown in the Appendix is given in Fig. 15 for the 140-m row for Burro 8. As with the horizontal contours, for cases where the vapor cloud moved off the array of instruments, the vertical contours have been truncated at the edge of the array.

A large RPT occurred at about 124 s into the Burro 6 test, spraying pond water and debris on the sensors in the 57-m arc and causing Lind to terminate the test. This RPT is the reason for terminating the contour plots for Burro 6 at this time. RPTs also occurred throughout the Burro 9 test, and a summary of the resulting shockwave overpressure measurements made by Lind is given in Table 7. The water, debris, and shock waves from these explosions caused severe problems with the IR sensors in the first row. A considerable amount of time and effort was spent trying to salvage this data. Unfortunately the effort was not very successful, and the data from the first row of sensors are not very reliable for this test.

As an example, the 1-m horizontal contours for Burro 9 at 70 and 80 seconds are shown in Fig. 16. As can be seen, there is an apparent indentation in the vapor cloud which alternates from one side to the other during this 10-second interval. This phenomenon is not real and is due to the effect of RPTs on the gas sensors. Attempting to correct for these effects by applying baseline shifts to the data causes underestimates of the vapor cloud concentrations at the 57-m row, while choice of the exact time of the baseline shift produces the apparent oscillation from one side to the other. The actual cloud contours are probably more like the dashed line contours drawn in Fig. 16. There was only a small effect from the RPTs on the second row of sensors (140 m), and the concentration contours downwind of the 57-m row are believed to be accurate for Burro 9.

04/04/83r 16:17:50
04/04/83 16:46:27

Vertical Concentration Contours



Burro 8 LNG 80

Contours:

Time - 200 sec

140m row

1%, 2%, 5%, 10%, 15%, 25%, 35%

Fig. 15 Vertical gas concentration contours for Burro 8, 140-m row at 200 seconds.

TABLE 7. Rapid phase transition (RPT) explosions generating overpressures of 0.10 psi or more on the Burro-9 (LNG-34) test.

Time (s)	Static Pressure (psi)	TNT Equivalent (g)
6.5	0.12	65
7.1	0.15	115
9.2	0.27	530
21.4	0.57	3400
35.1	0.72	6300
43.2	0.10	41
46.0	0.12	65
54.1	0.12	65
54.9	0.13	80
66.9	0.19	215
72.7	0.12	65

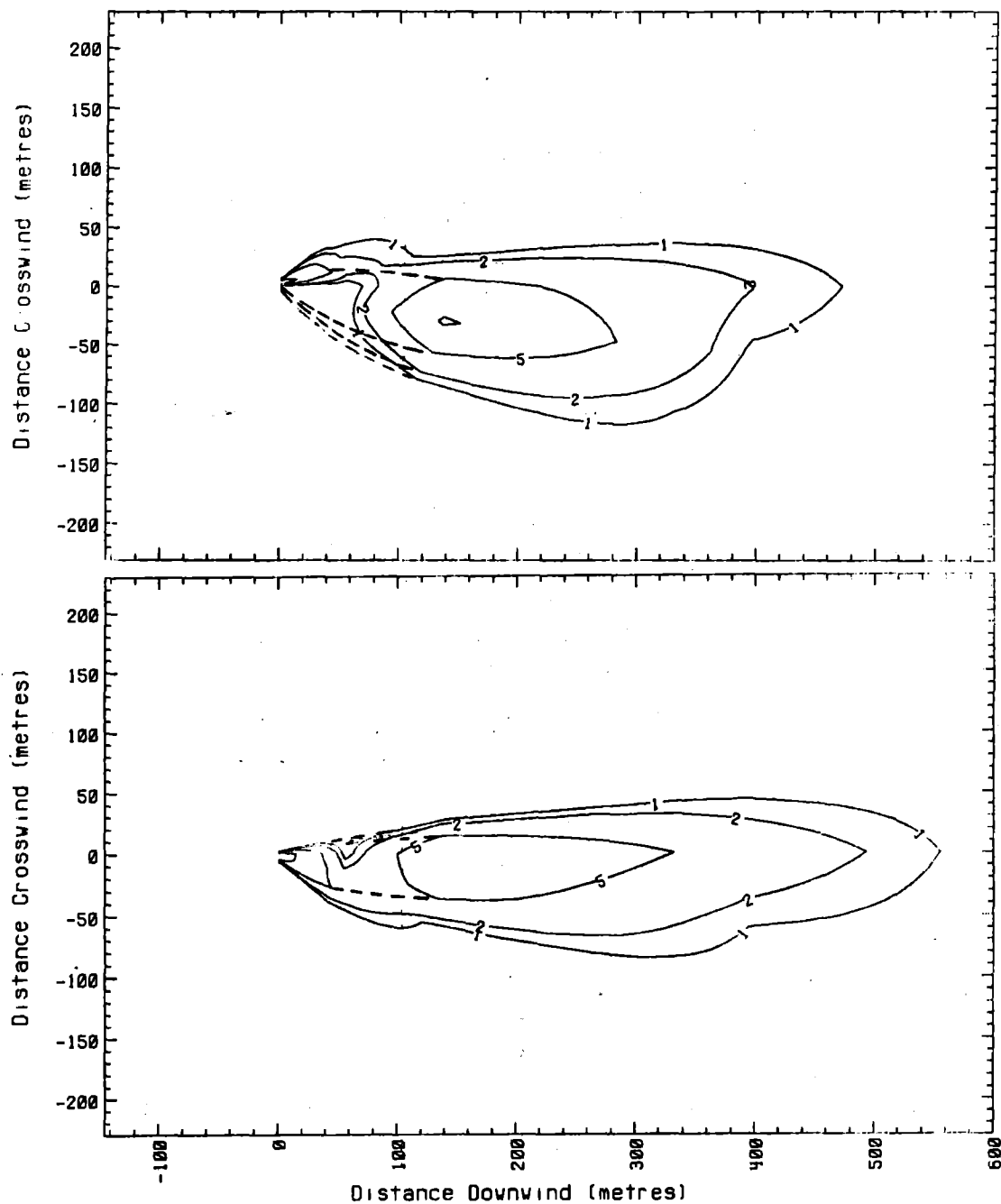
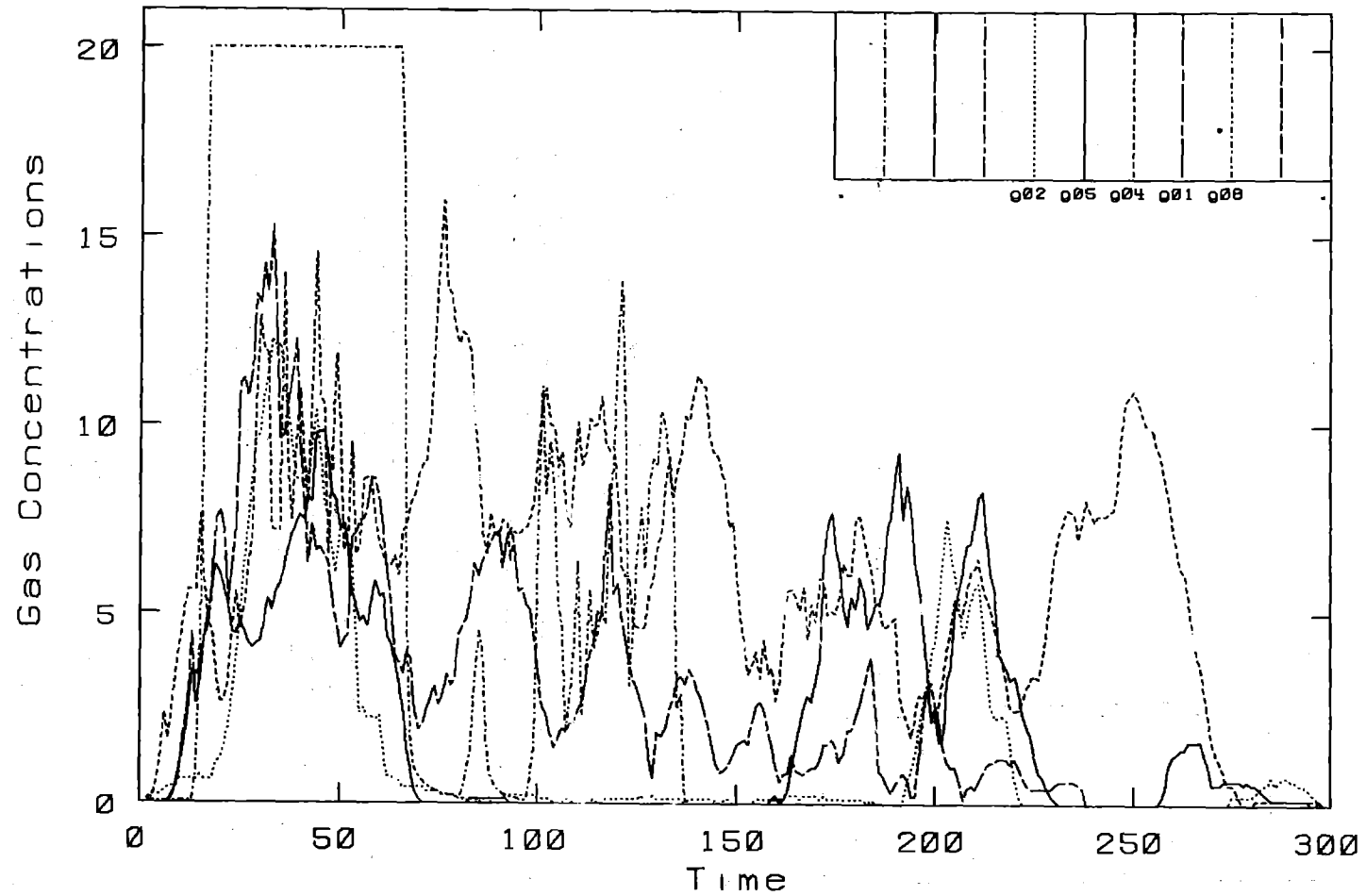


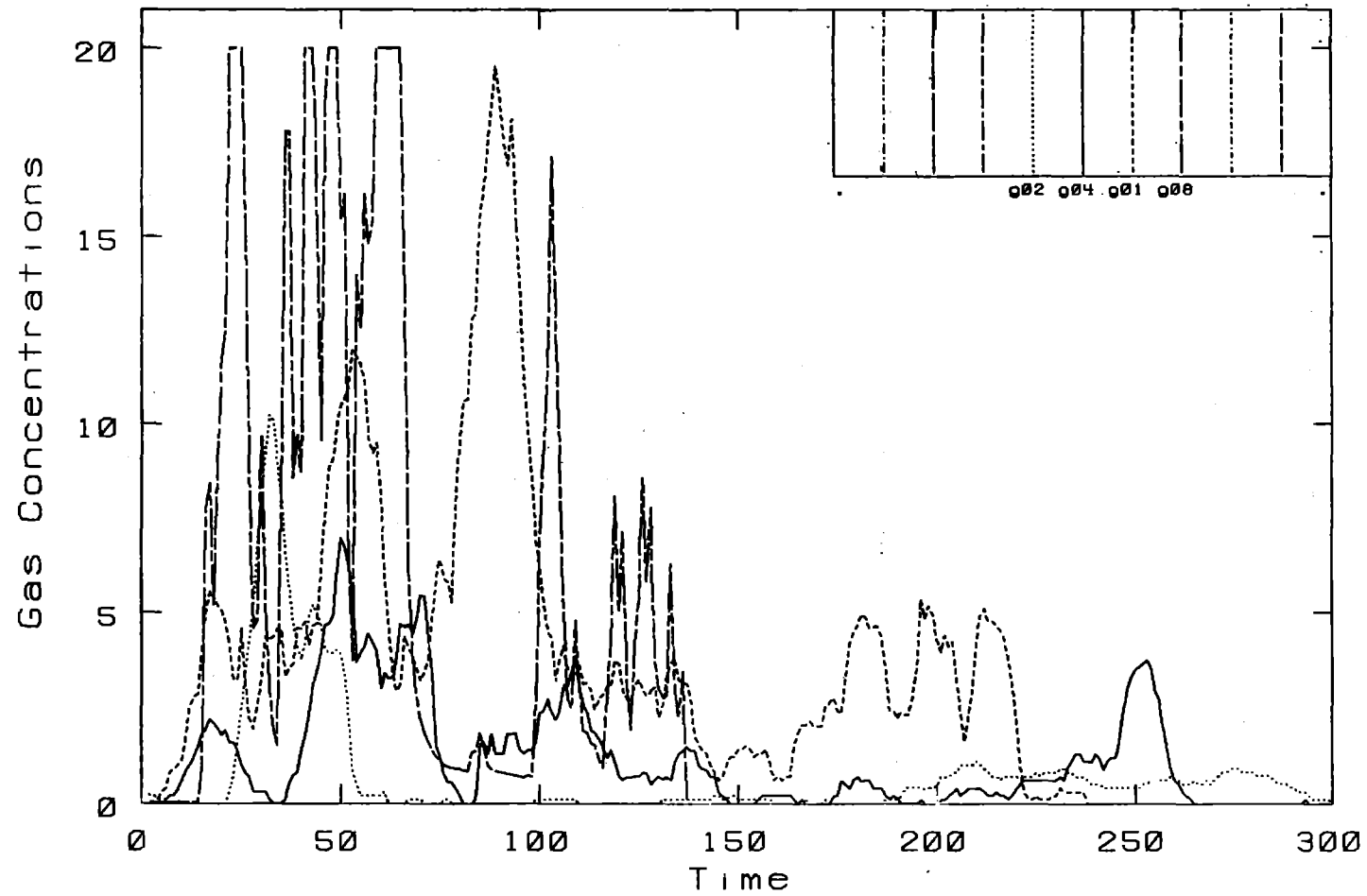
Fig. 16 Horizontal gas concentration contours at 1-m for Burro 9 at a) 70 sec. and b) 80 seconds showing the effects of the RPT on the 57-m arc of gas sensors.

Burro Row Stations



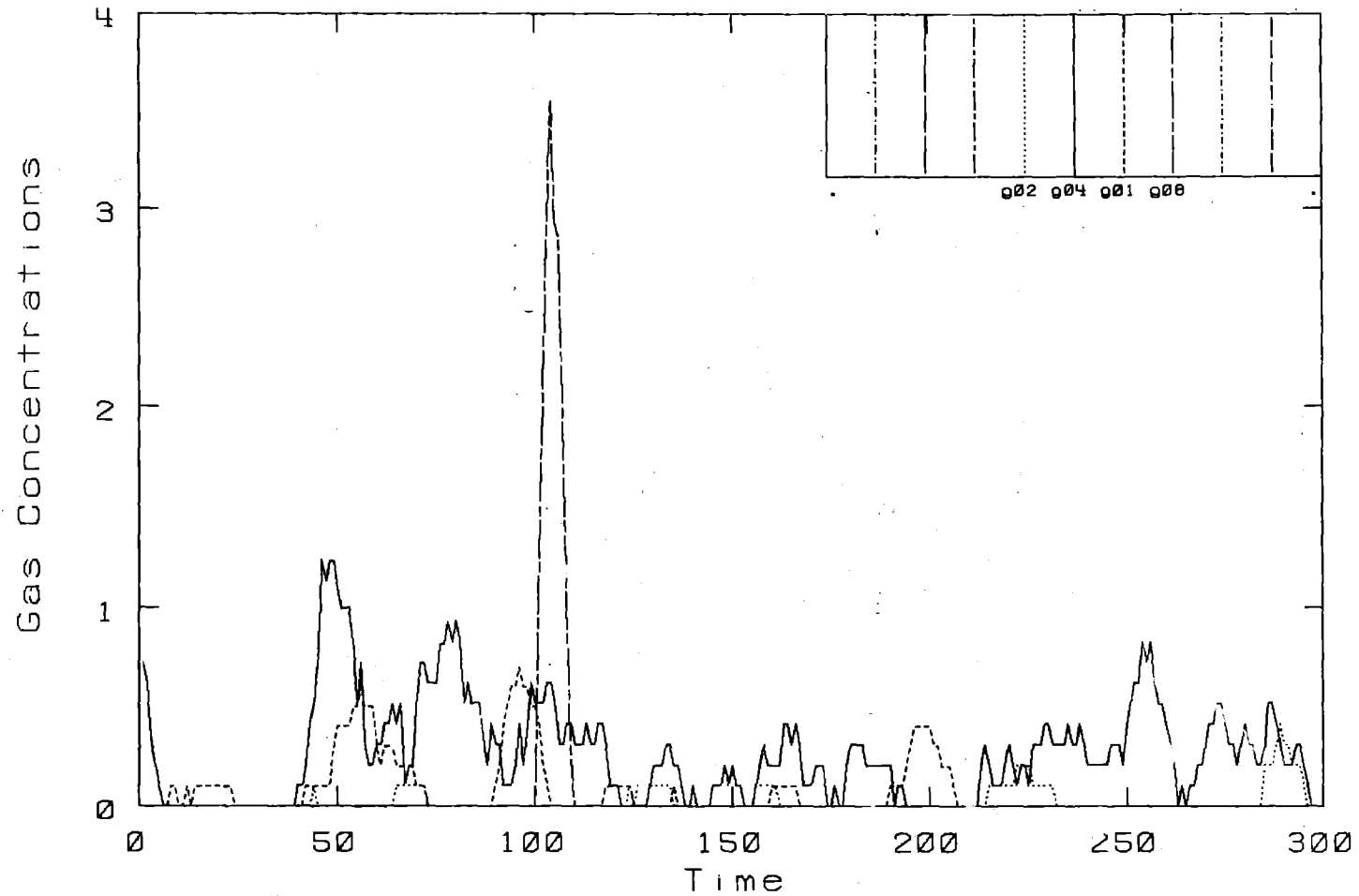
Burro 2. Row: 57 M. - Height: 1 M.

Burro Row Stations



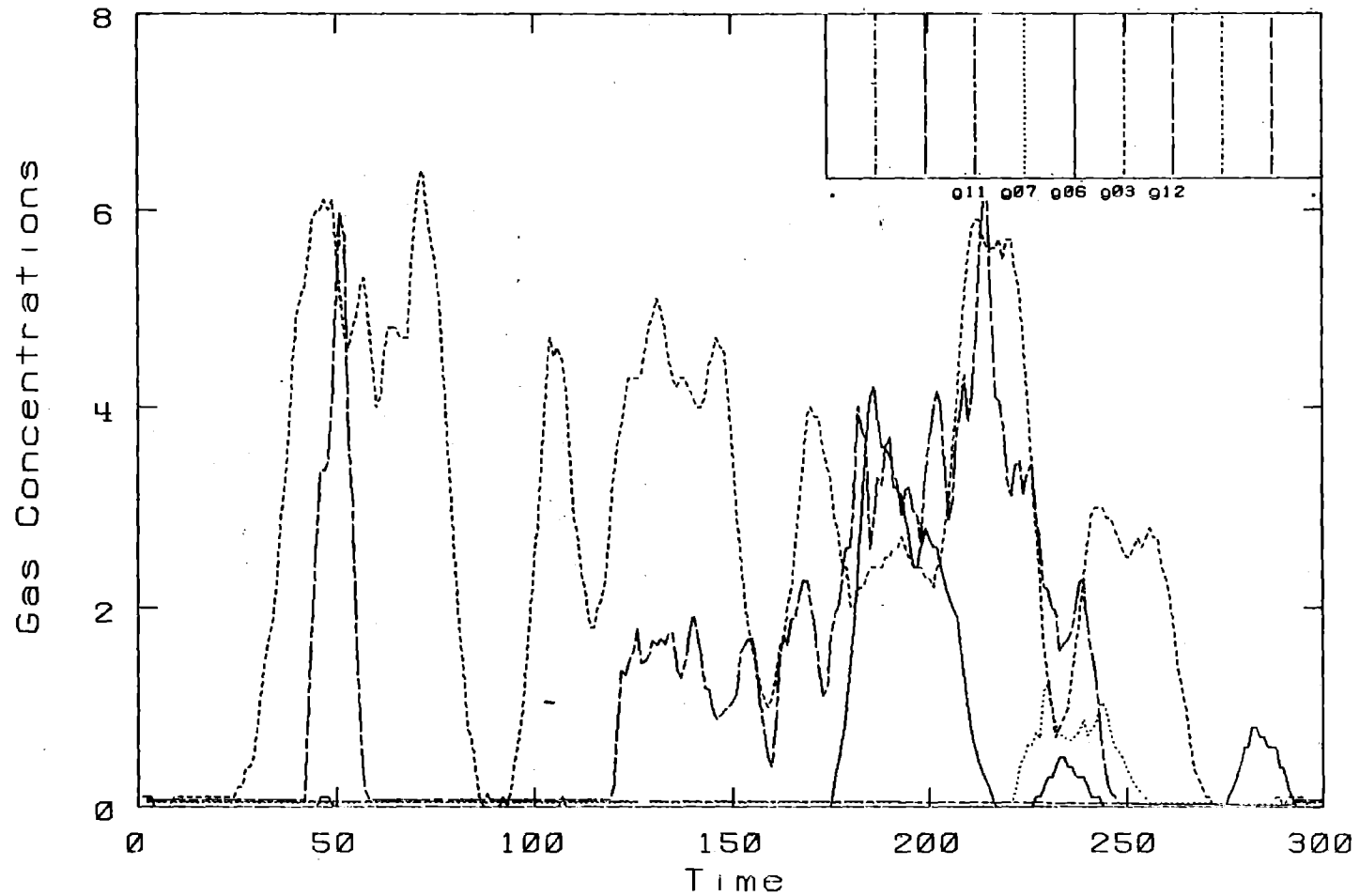
Burro 2. Row: 57 M. - Height: 3 M.

Burro Row Stations



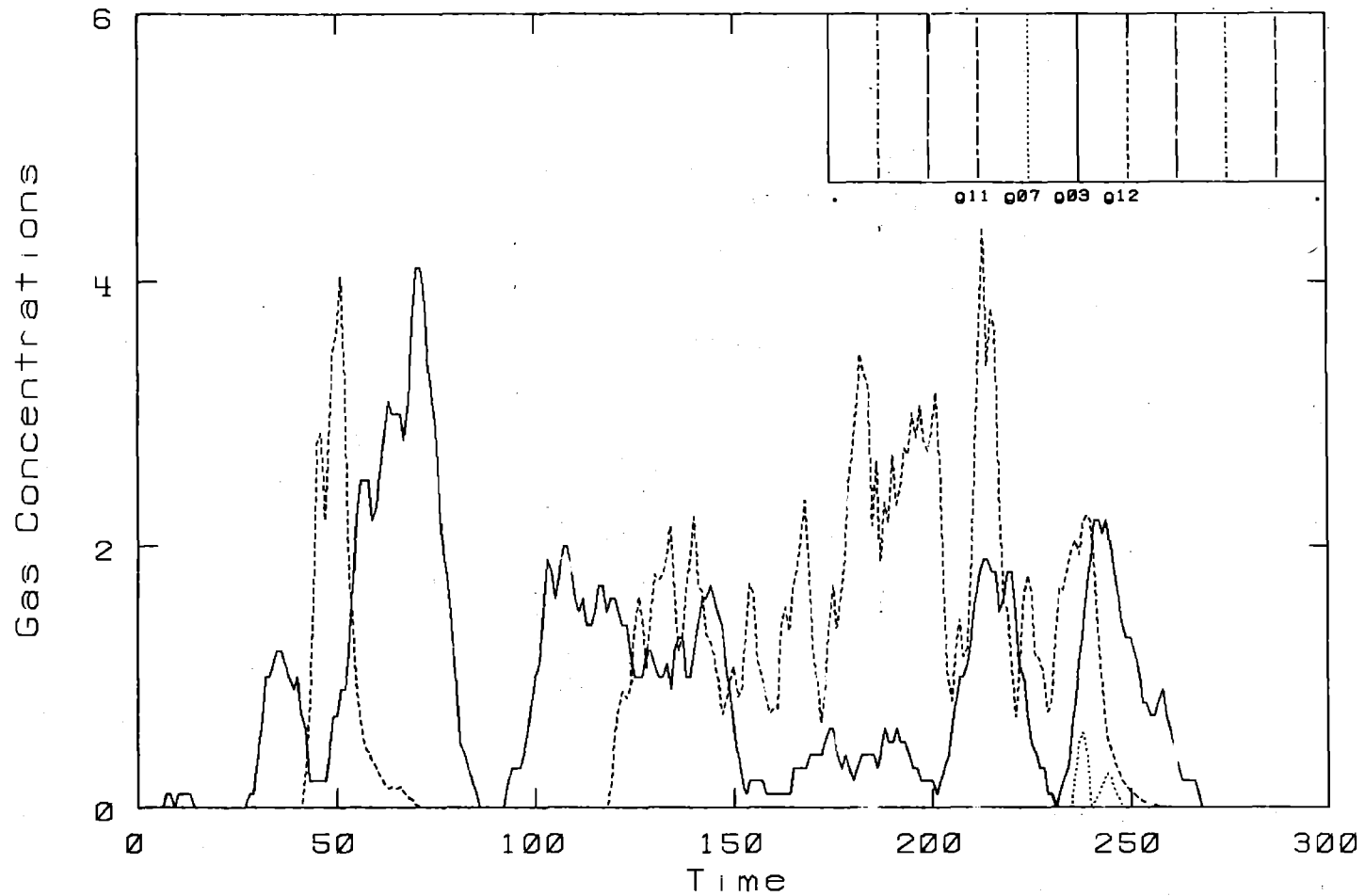
Burro 2. Row: 57 M. - Height: 8 M.

Burro Row Stations



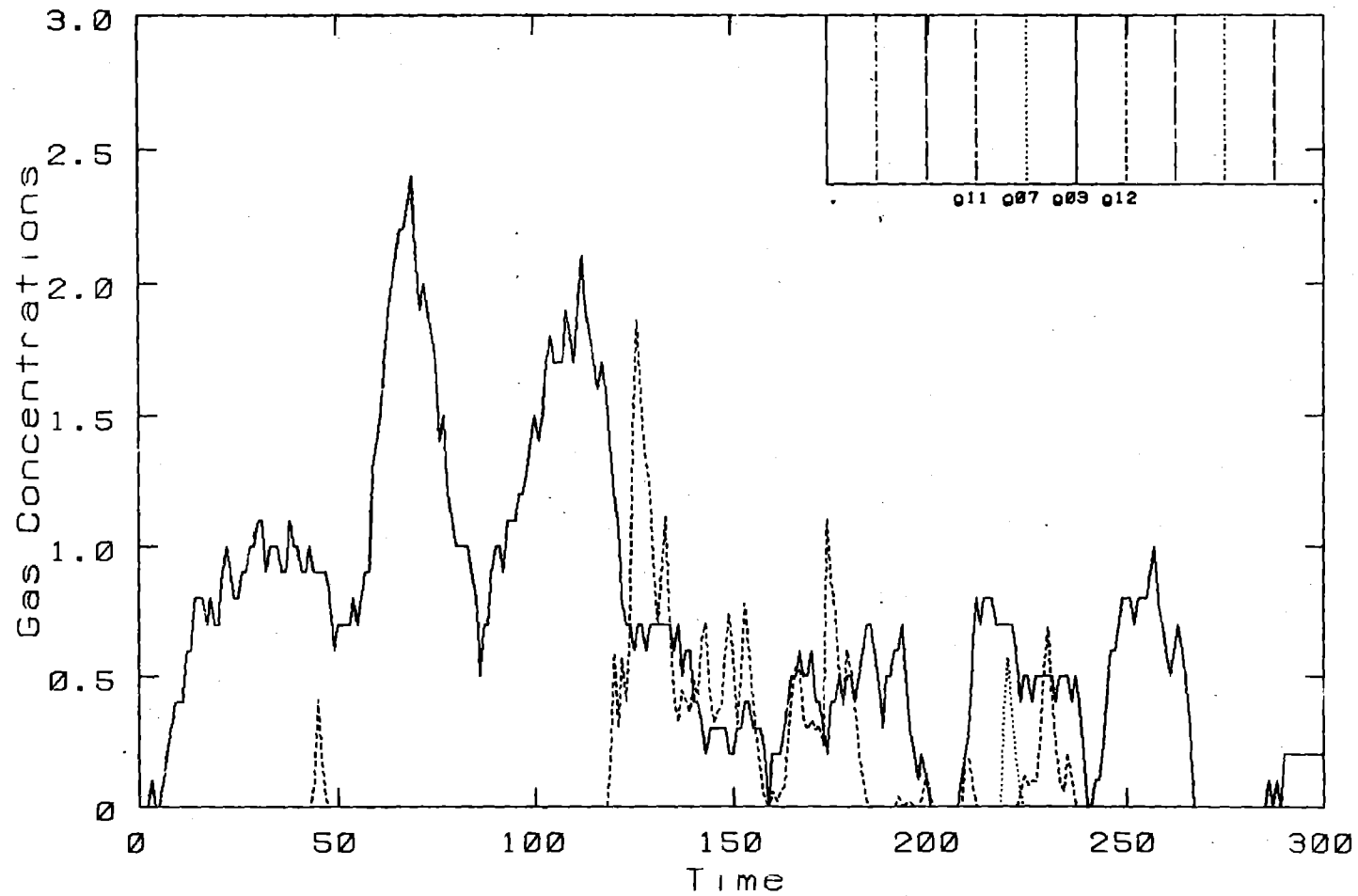
Burro 2. Row: 140 M. - Height: 1 M.

Burro Row Stations



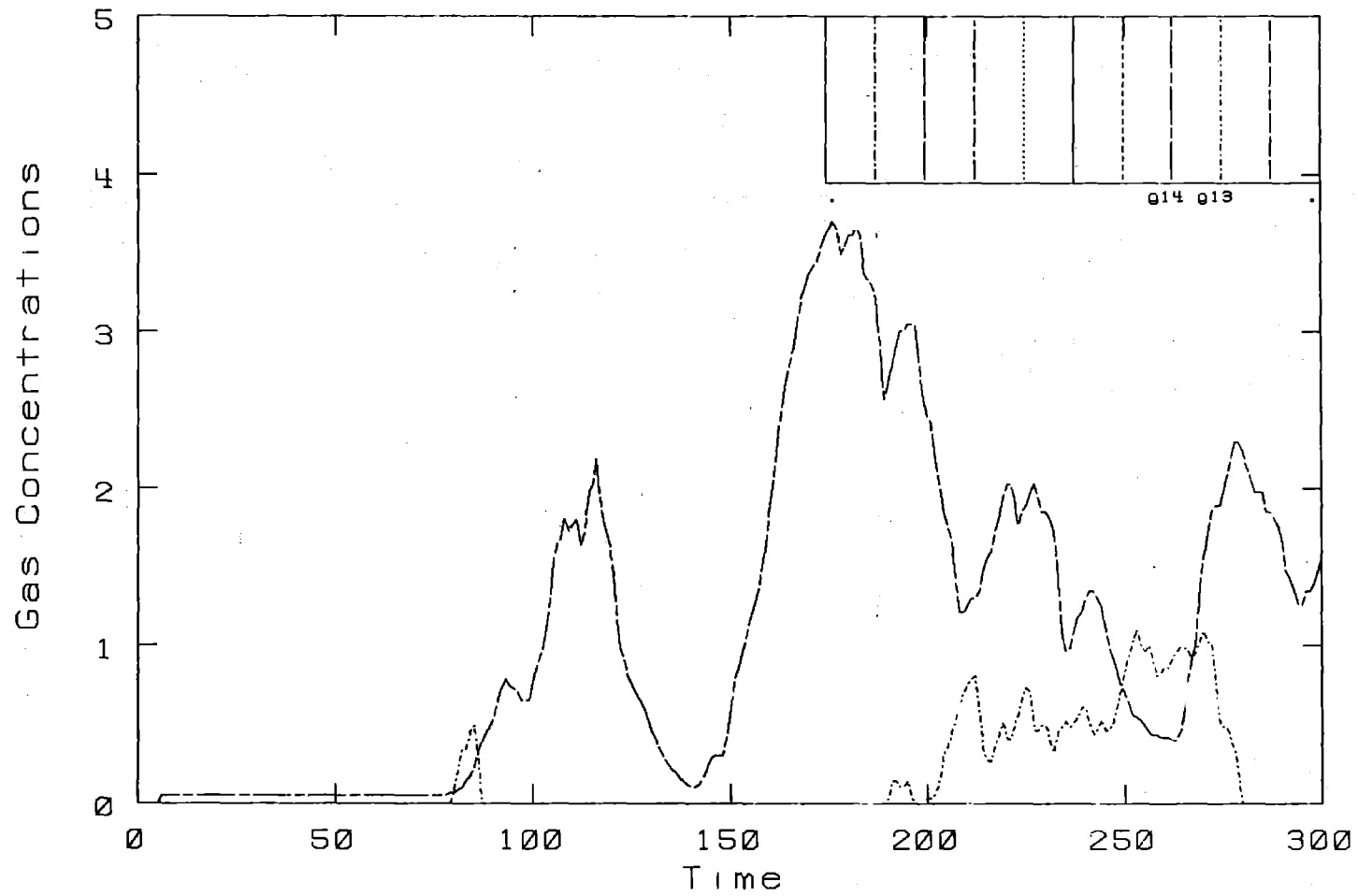
Burro 2. Row: 140 M. - Height: 3 M.

Burro Row Stations

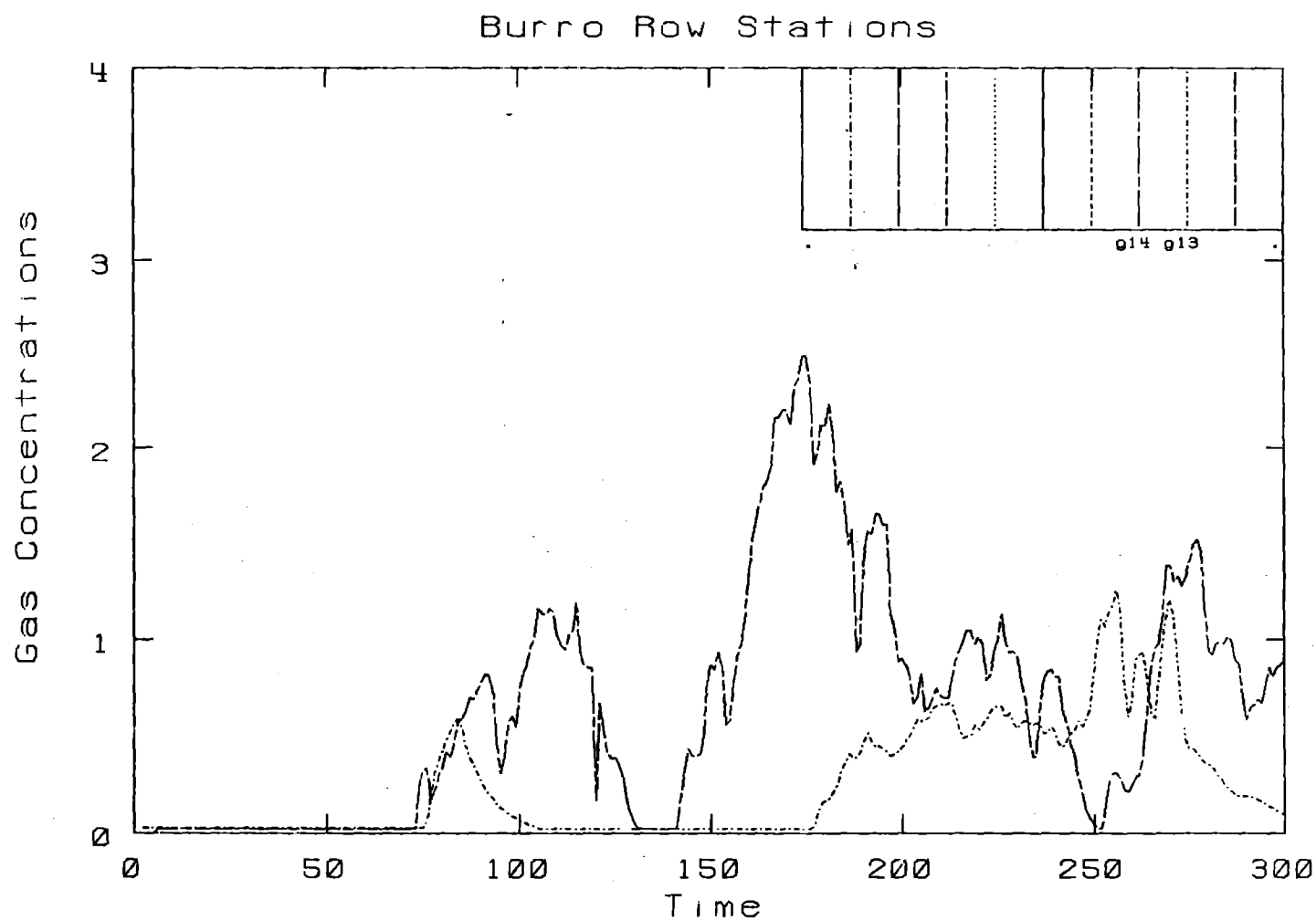


Burro 2. Row: 140 M.- Height: 8 M.

Burro Row Stations

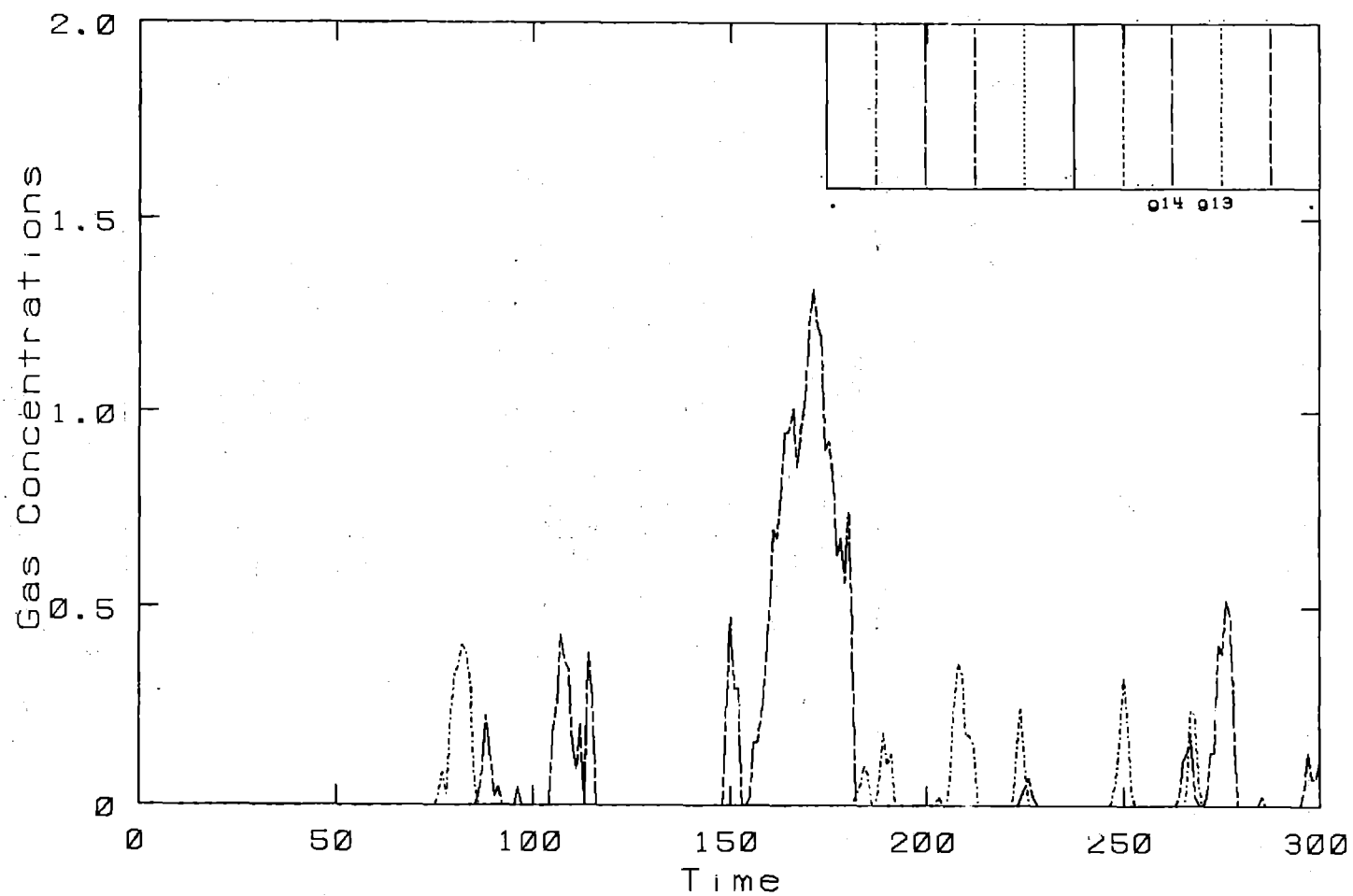


Burro 2. Row: 400 M.- Height: 1 M.



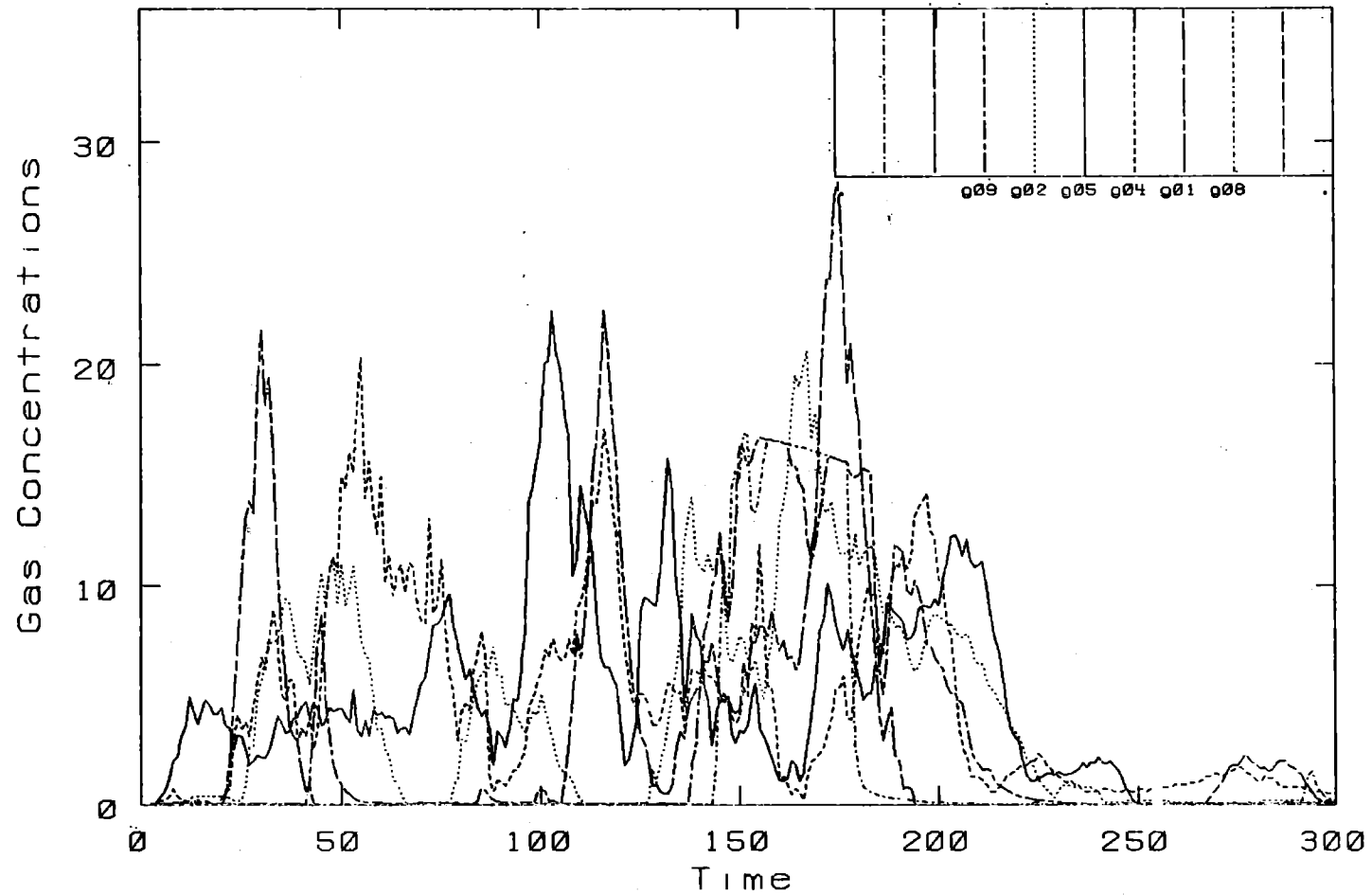
Burro 2. Row: 400 M.- Height: 3 M.

Burro Row Stations



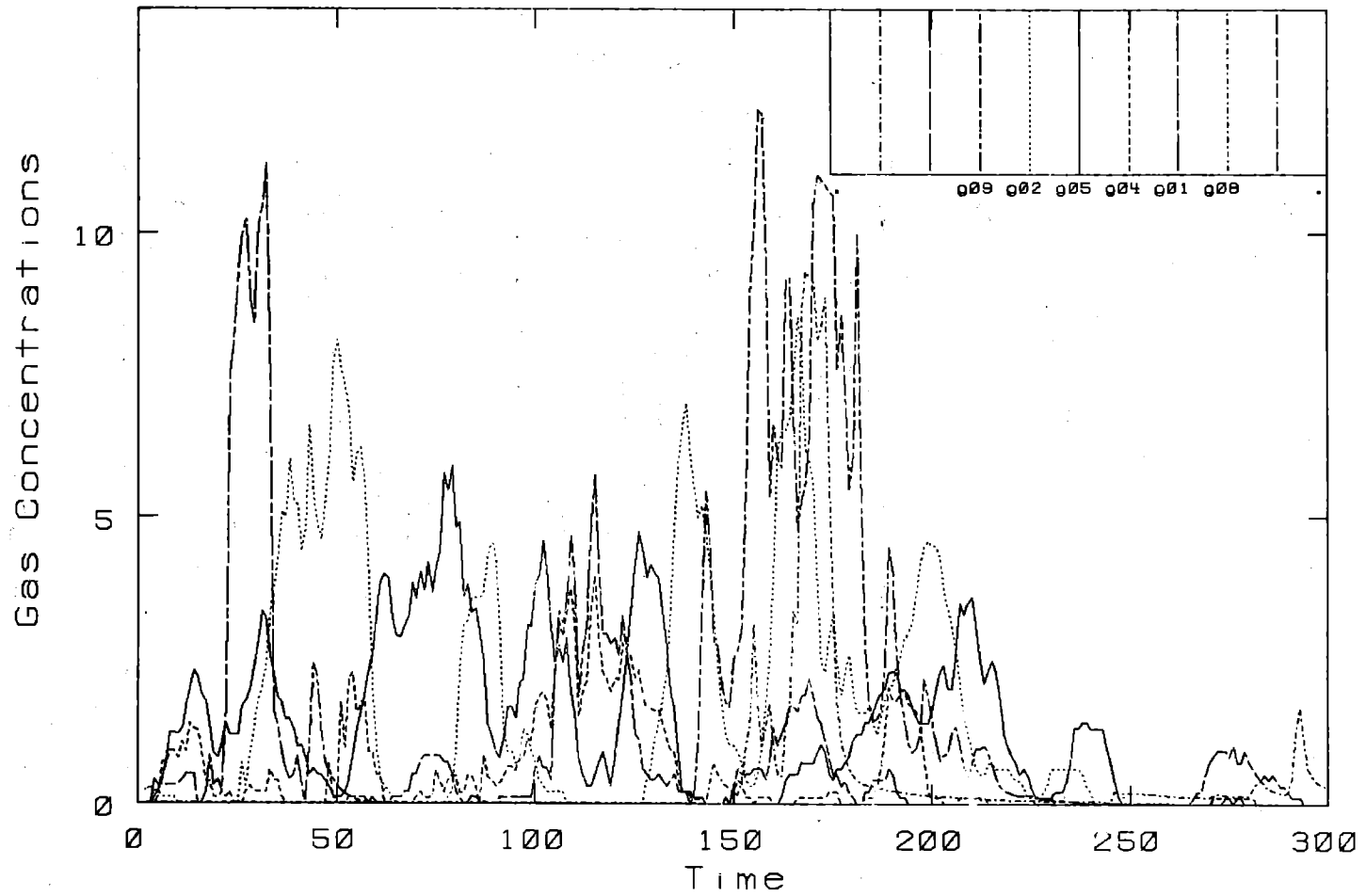
Burro 2. Row: 400 M. - Height: 8 M.

Burro Row Stations



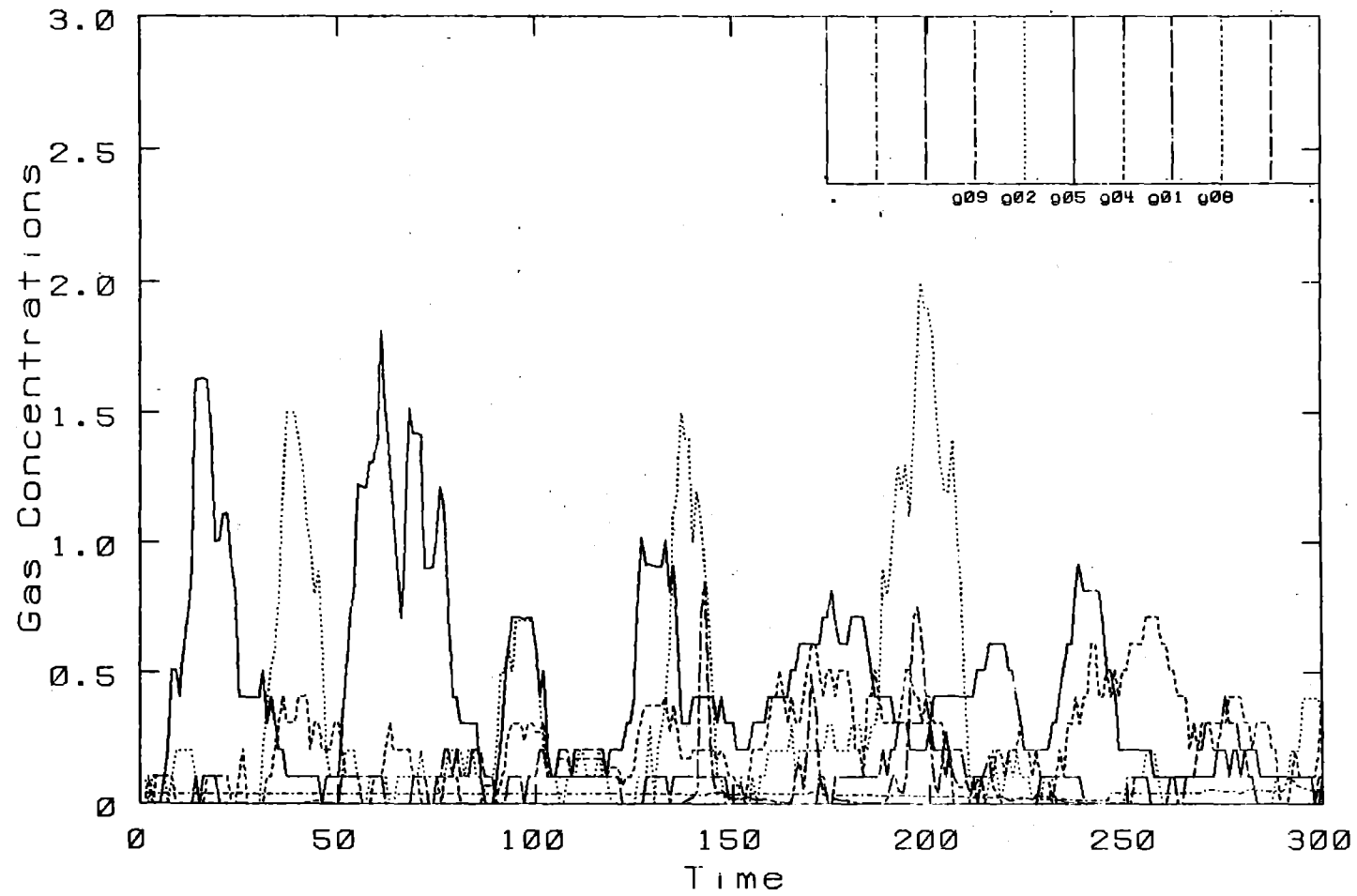
Burro 3. Row: 57 M. - Height: 1 M.

Burro Row Stations



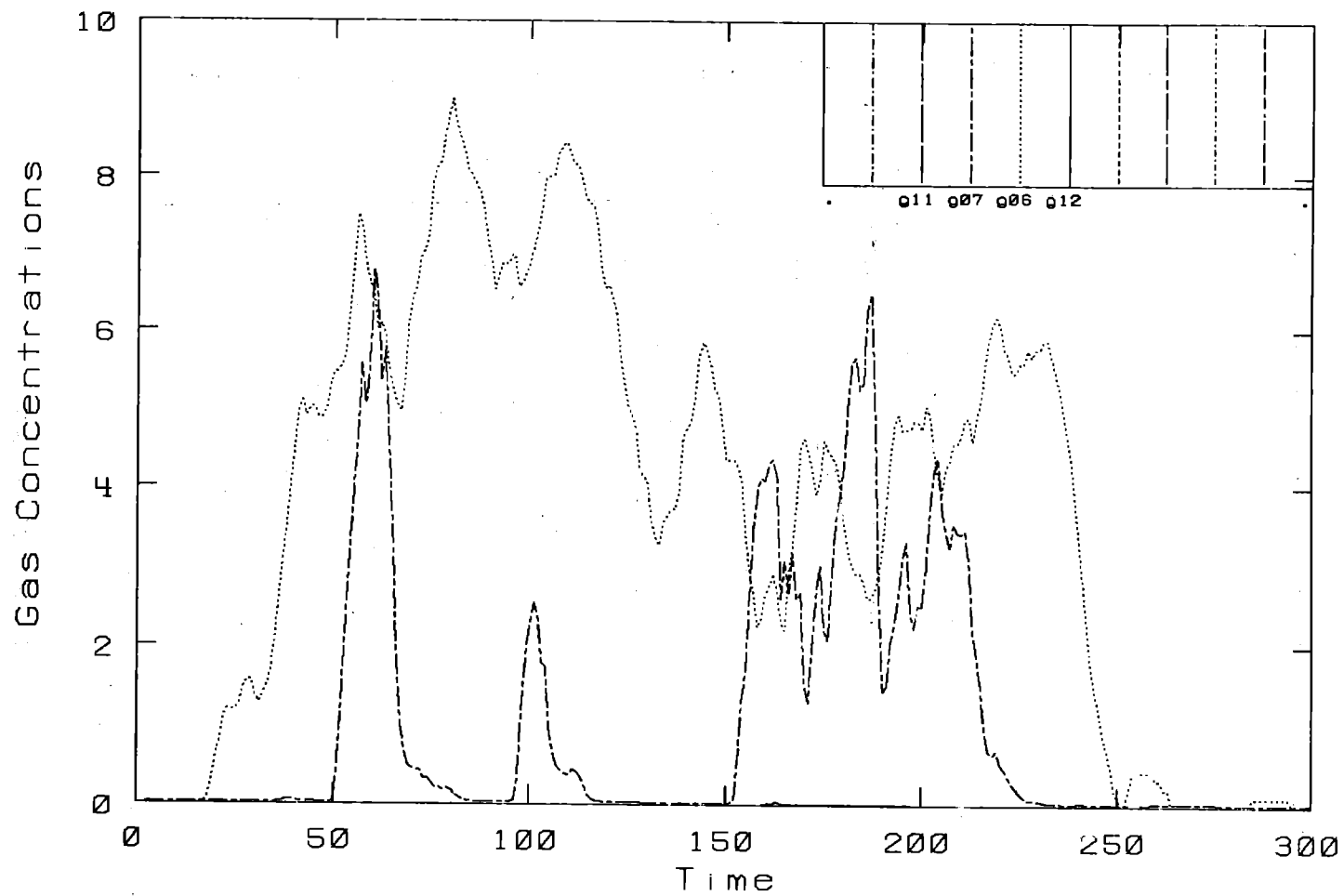
Burro 3. Row: 57 M. - Height: 3 M.

Burro Row Stations



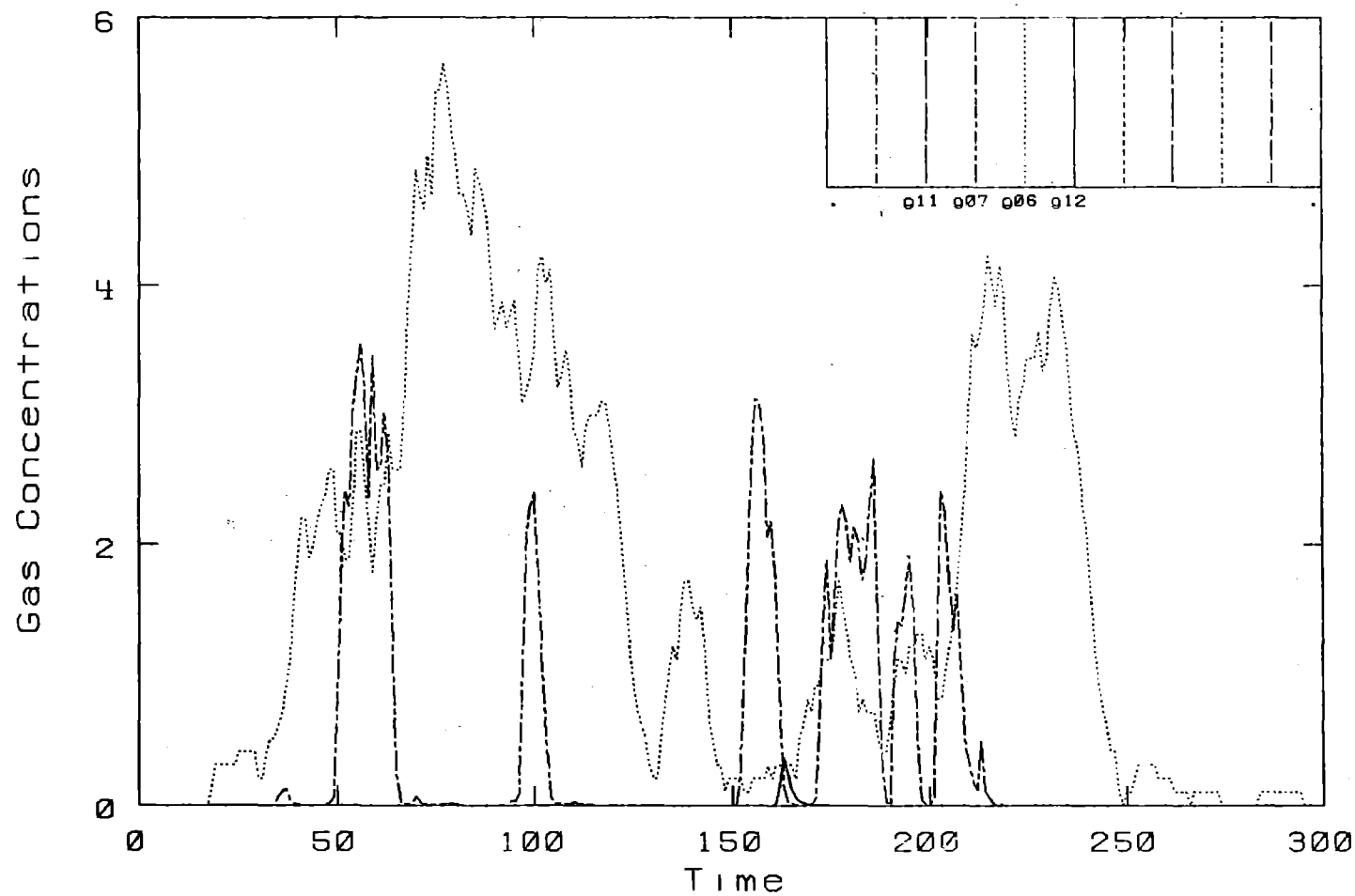
Burro 3. Row: 57 M. - Height: 8 M.

Burro Row Stations



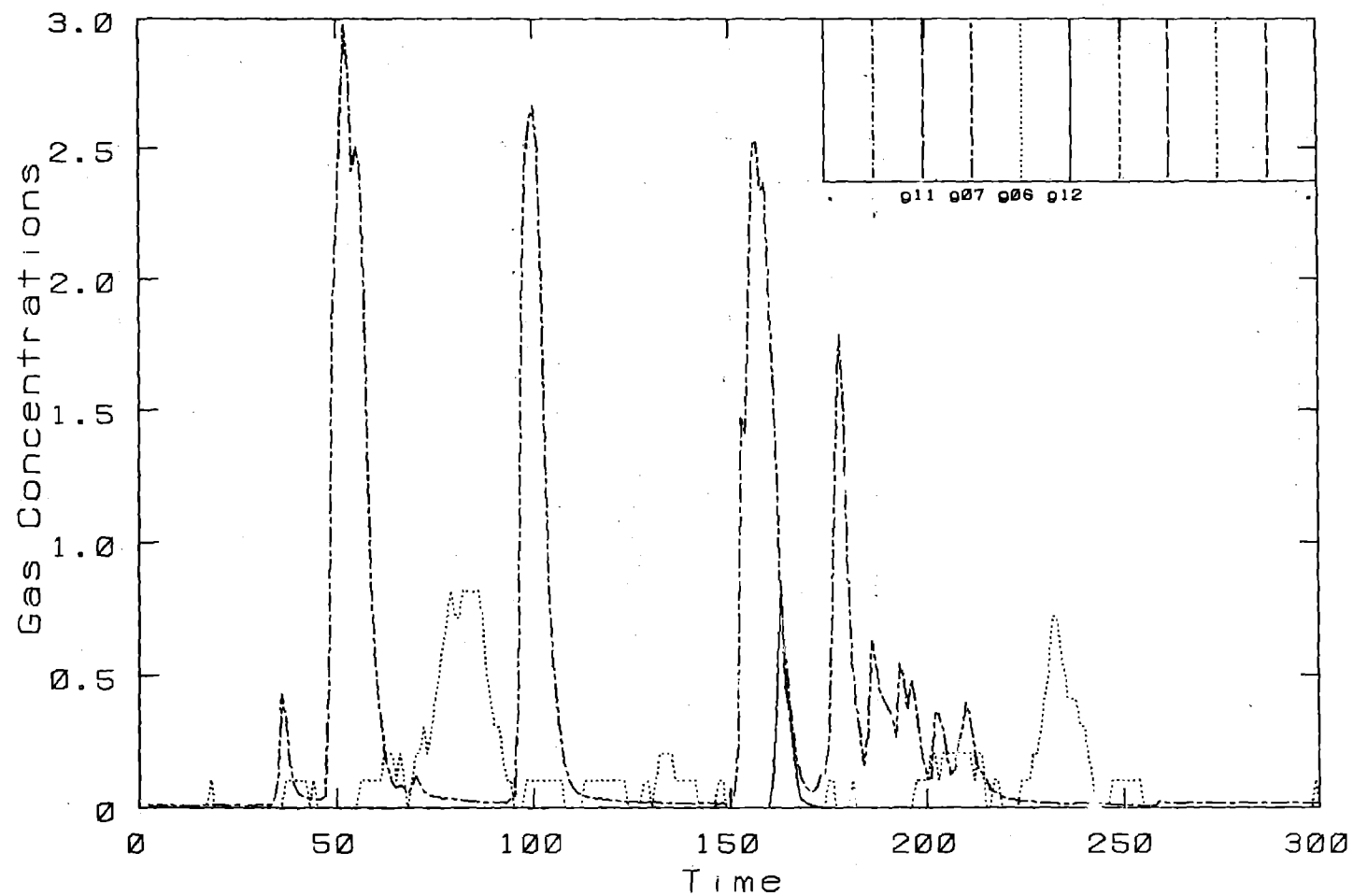
Burro 3. Row: 140 M.- Height: 1 M.

Burro Row Stations



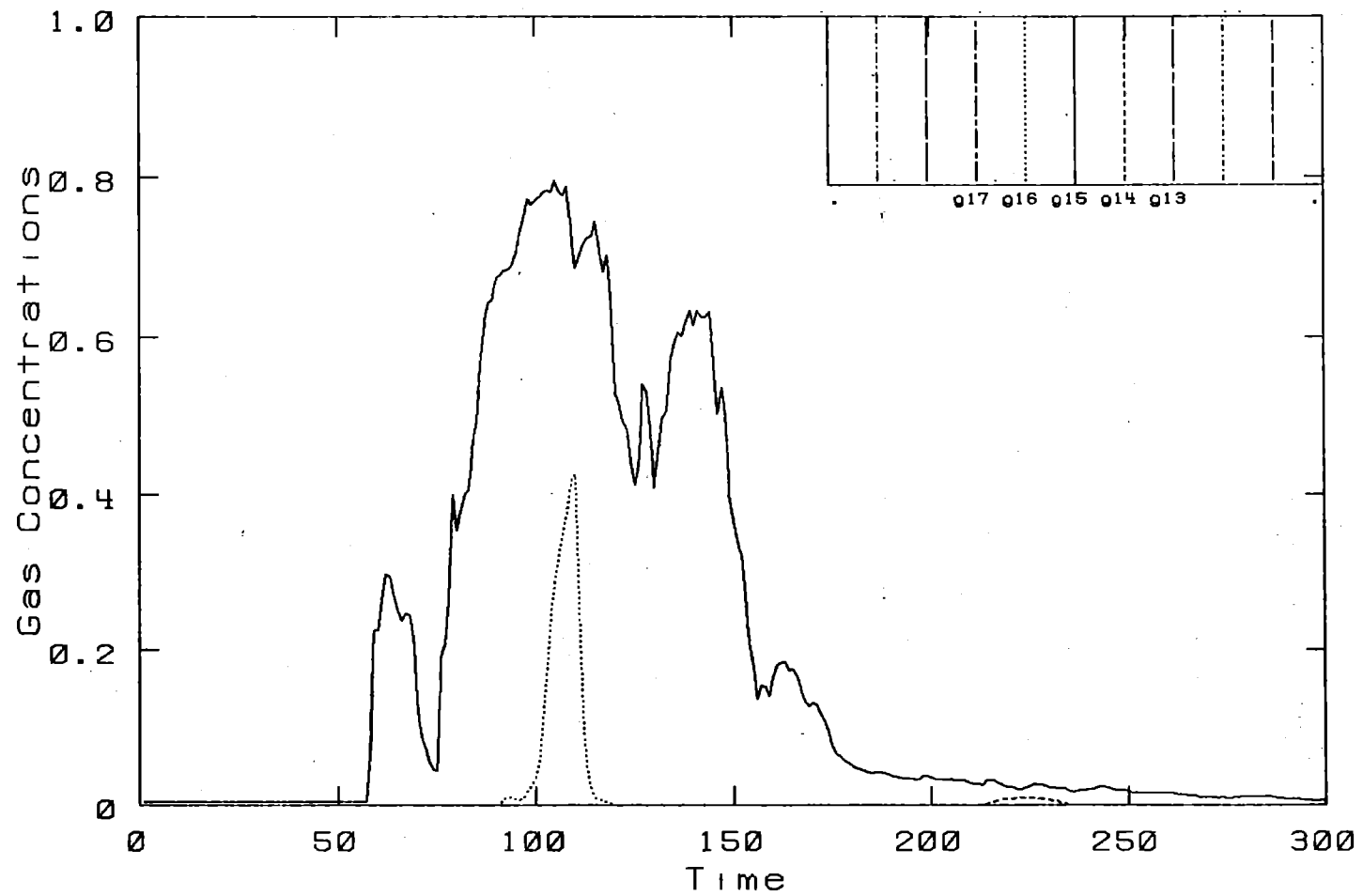
Burro 3. Row: 140 M.- Height: 3 M.

Burro Row Stations

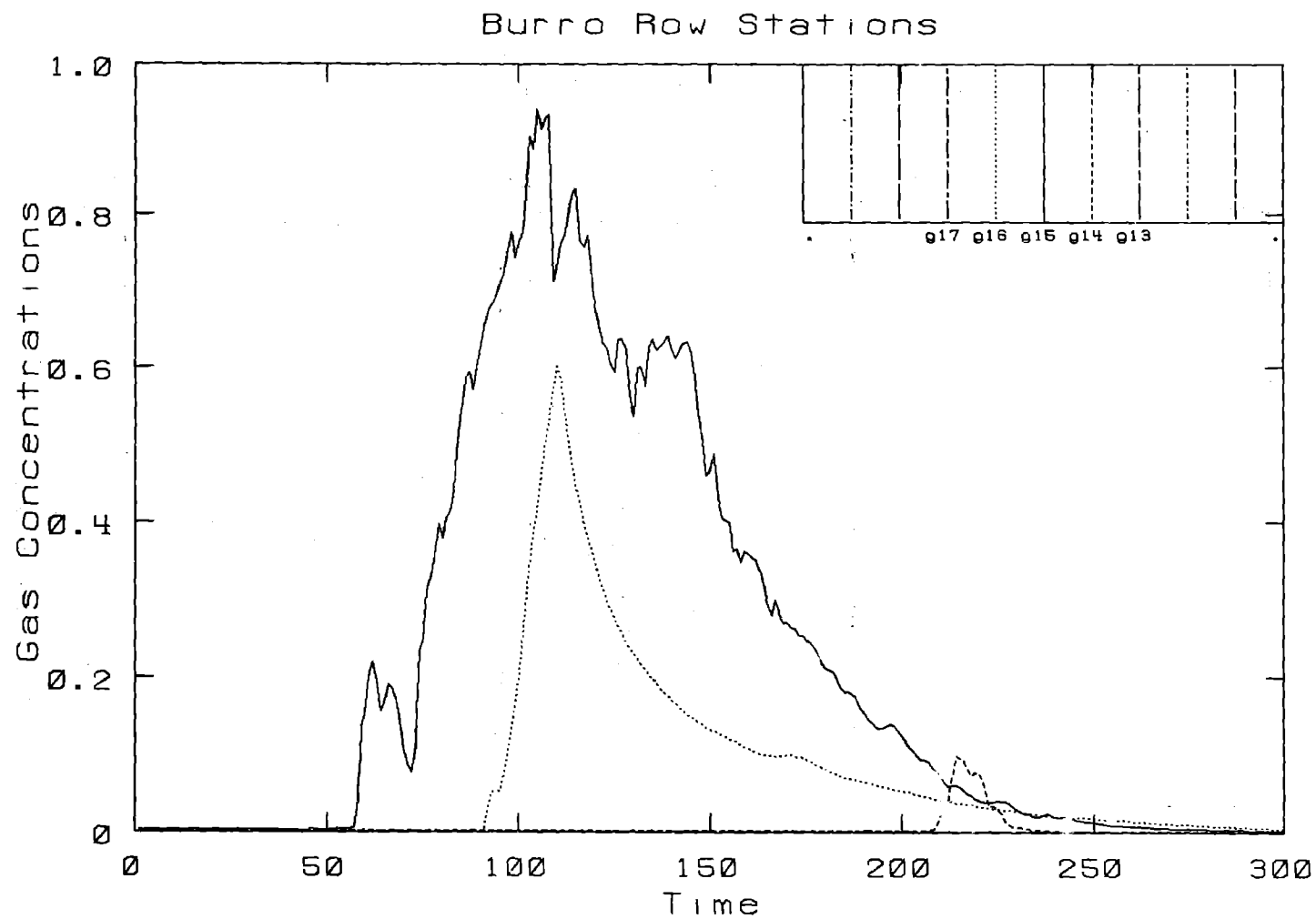


Burro 3. Row: 140 M. - Height: 8 M.

Burro Row Stations

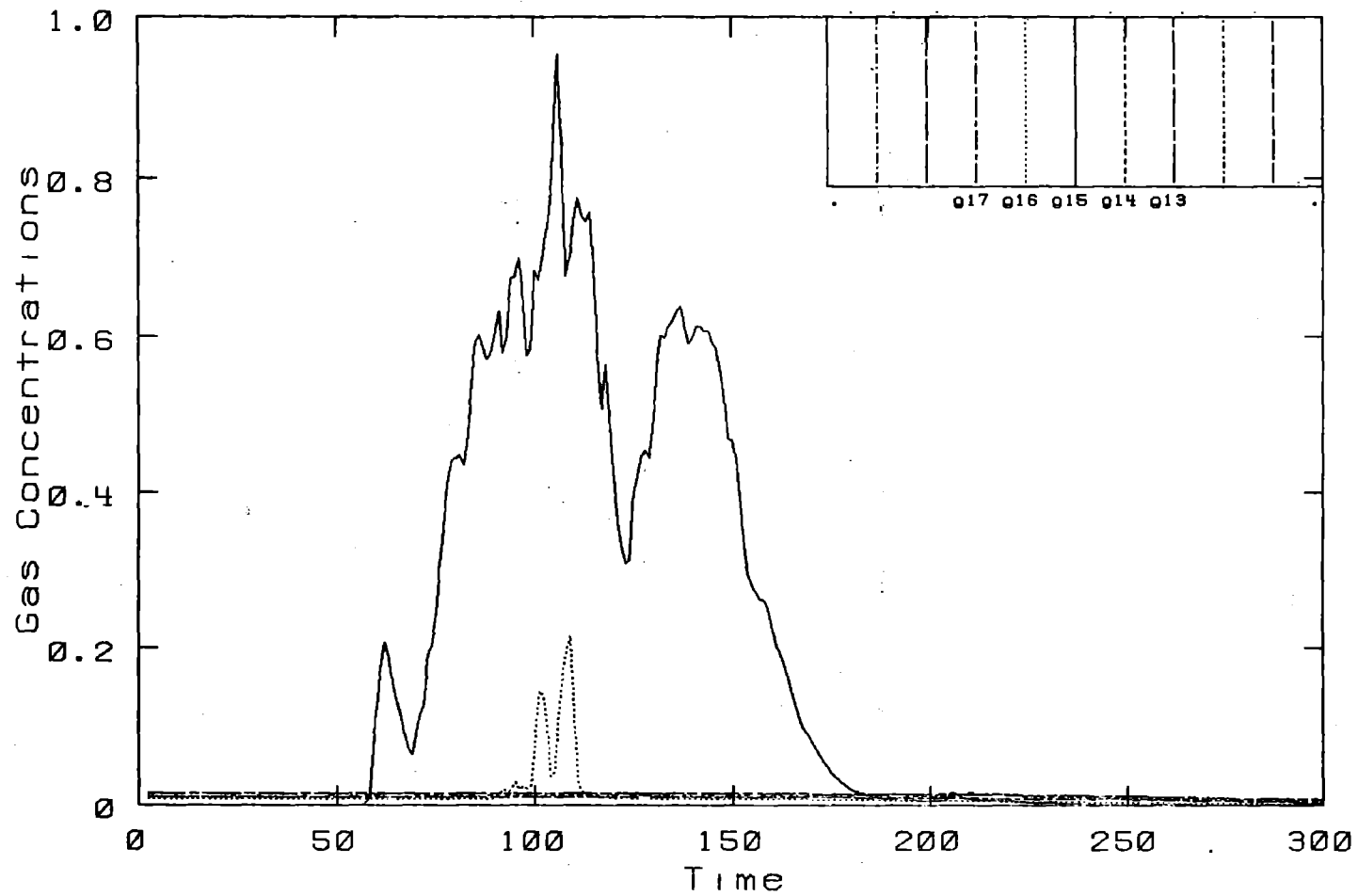


Burro 3. Row: 400 M. - Height: 1 M.



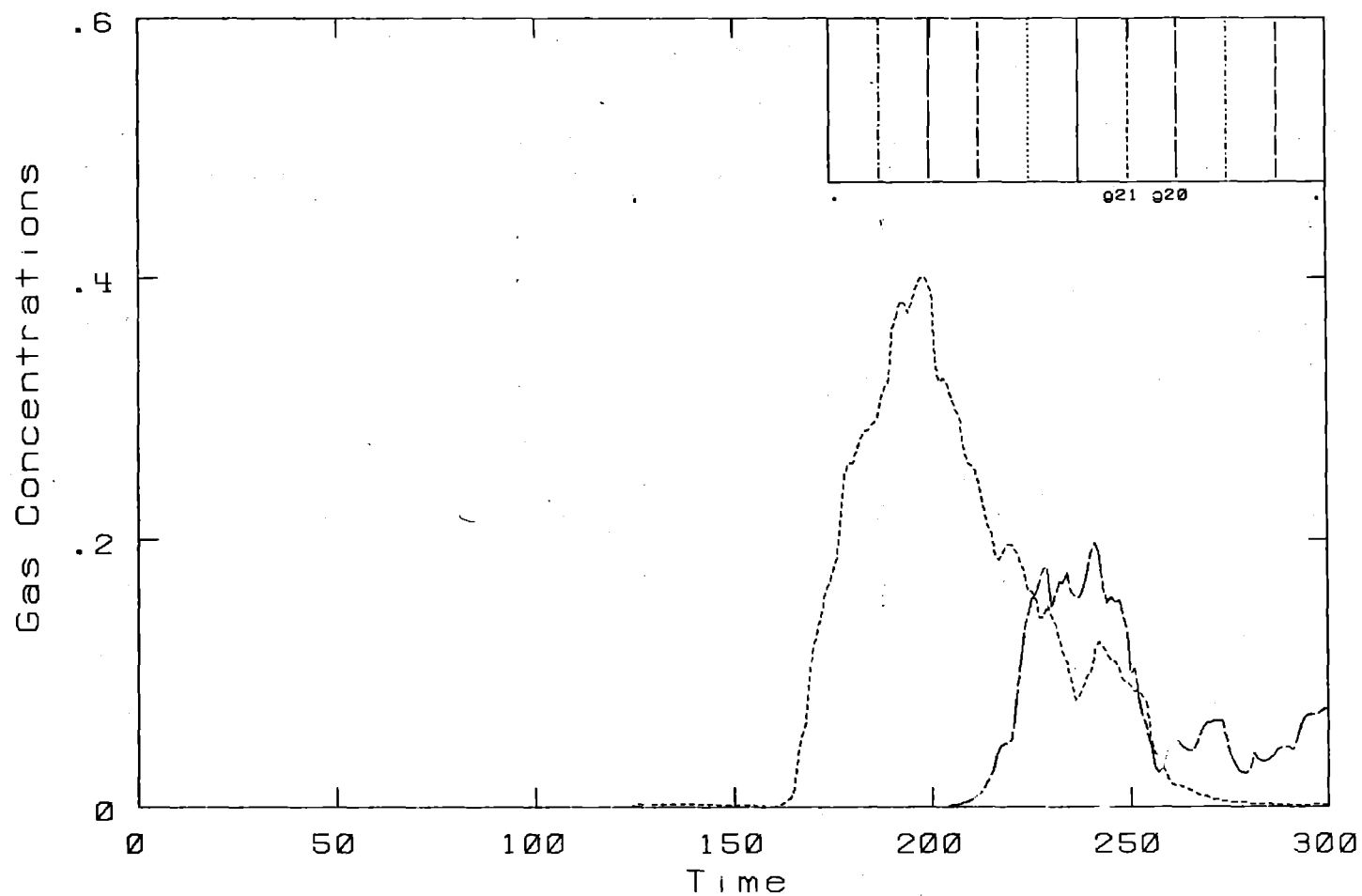
Burro 3. Row: 400 M. - Height: 3 M.

Burro Row Stations



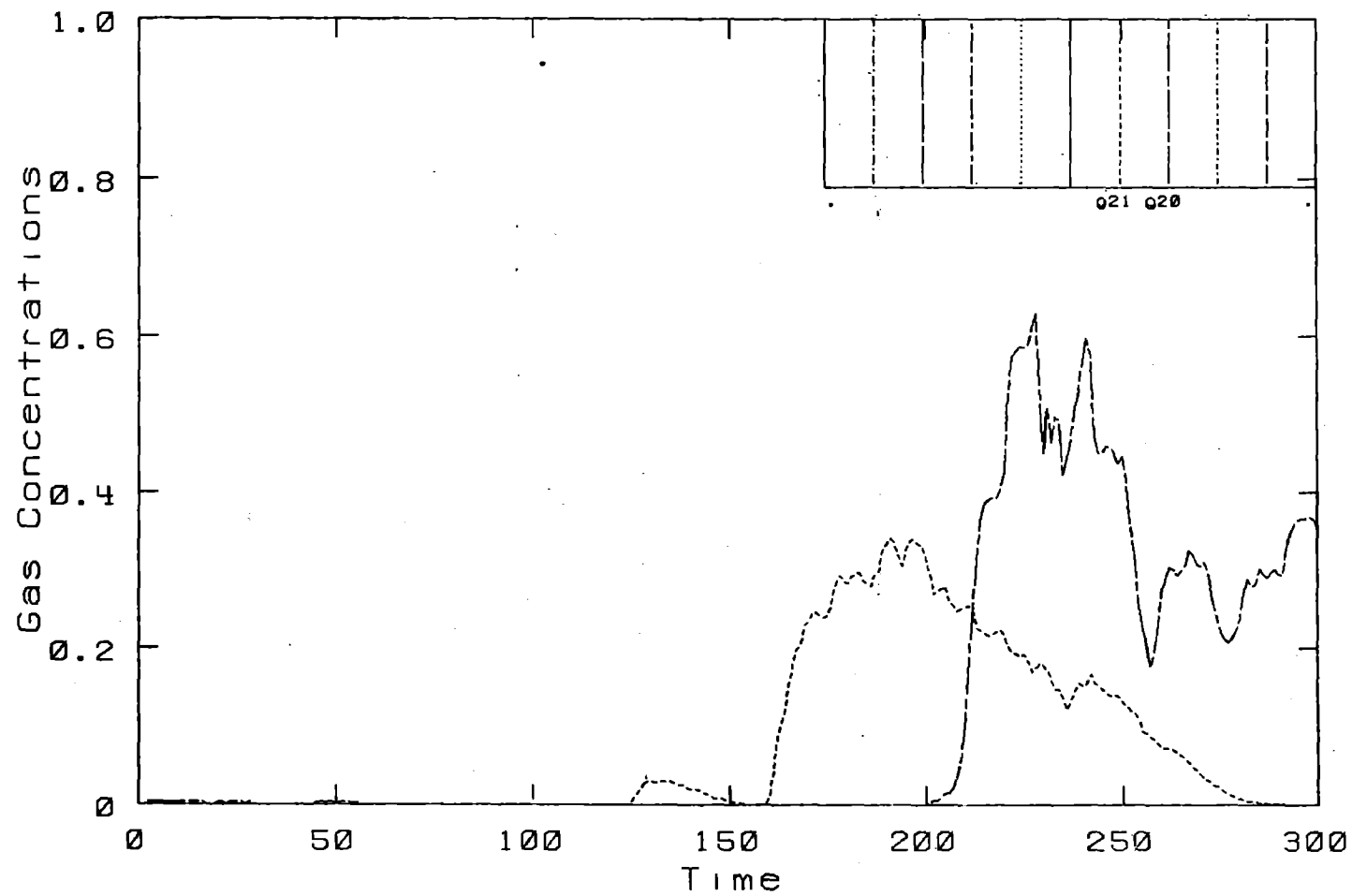
Burro , 3. Row: 400 M. - Height: 8 M.

Burro Row Stations



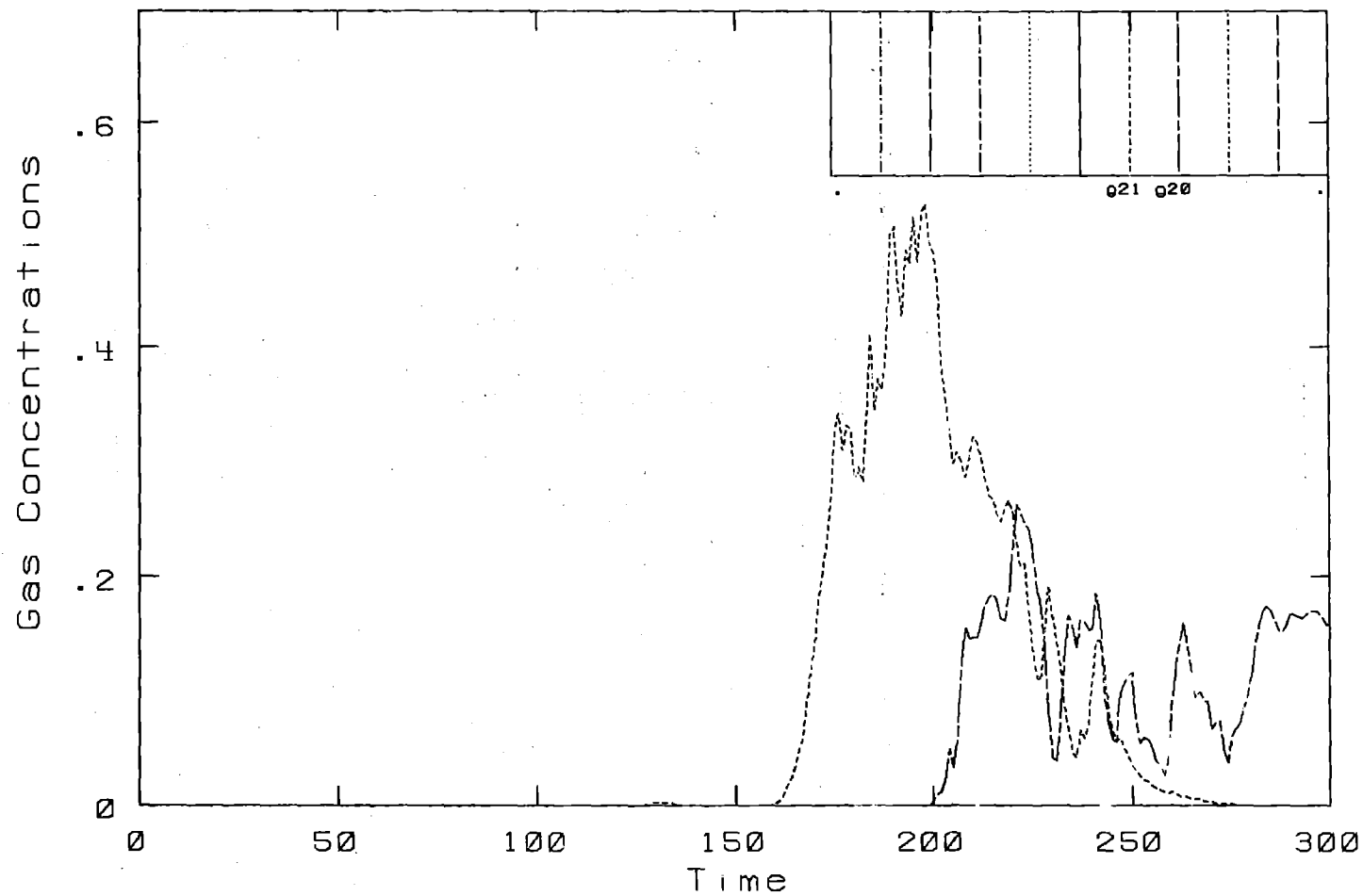
Burro 3. Row: 800 M. - Height: 1 M.

Burro Row Stations

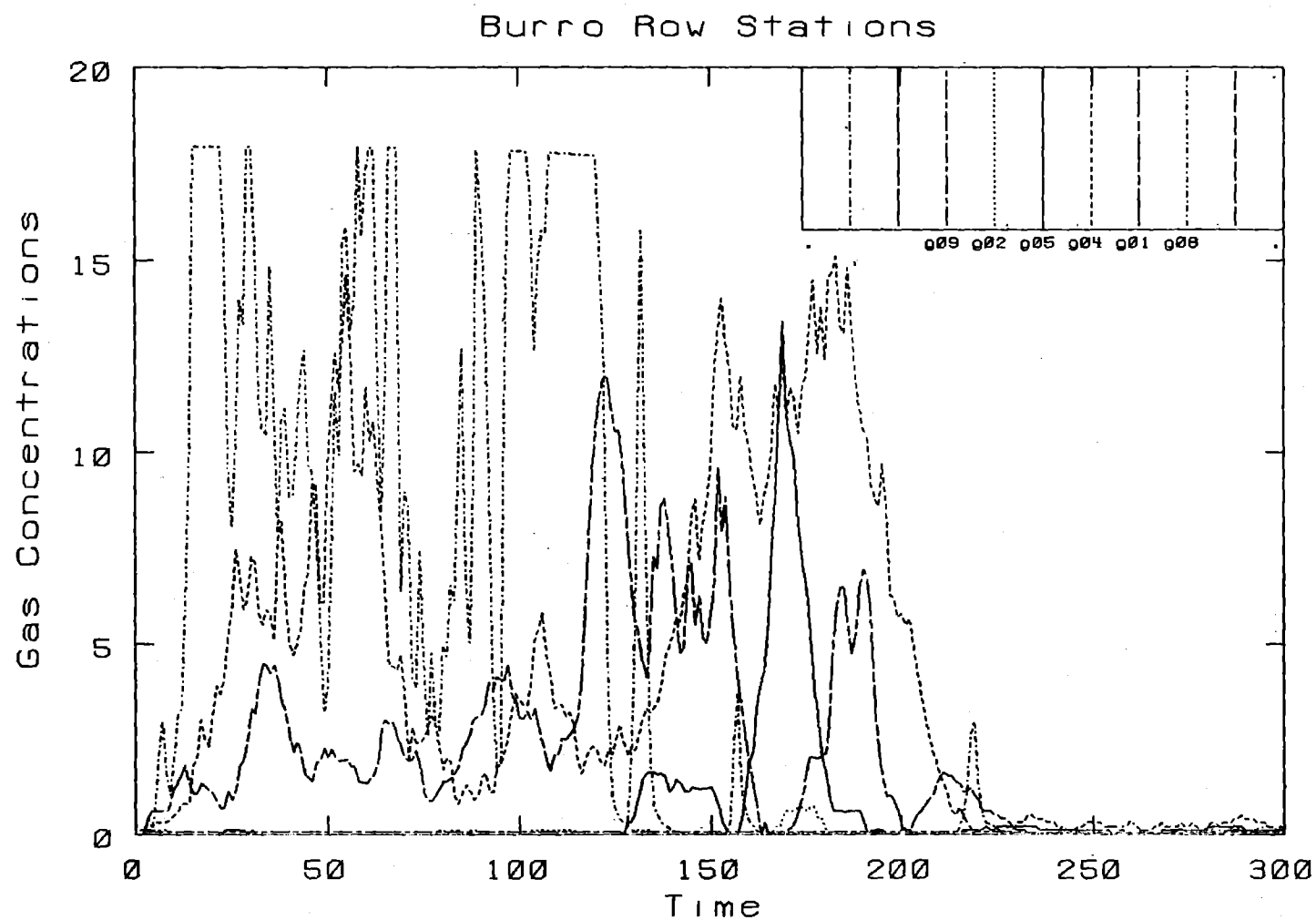


Burro 3. Row: 800 M. - Height: 3 M.

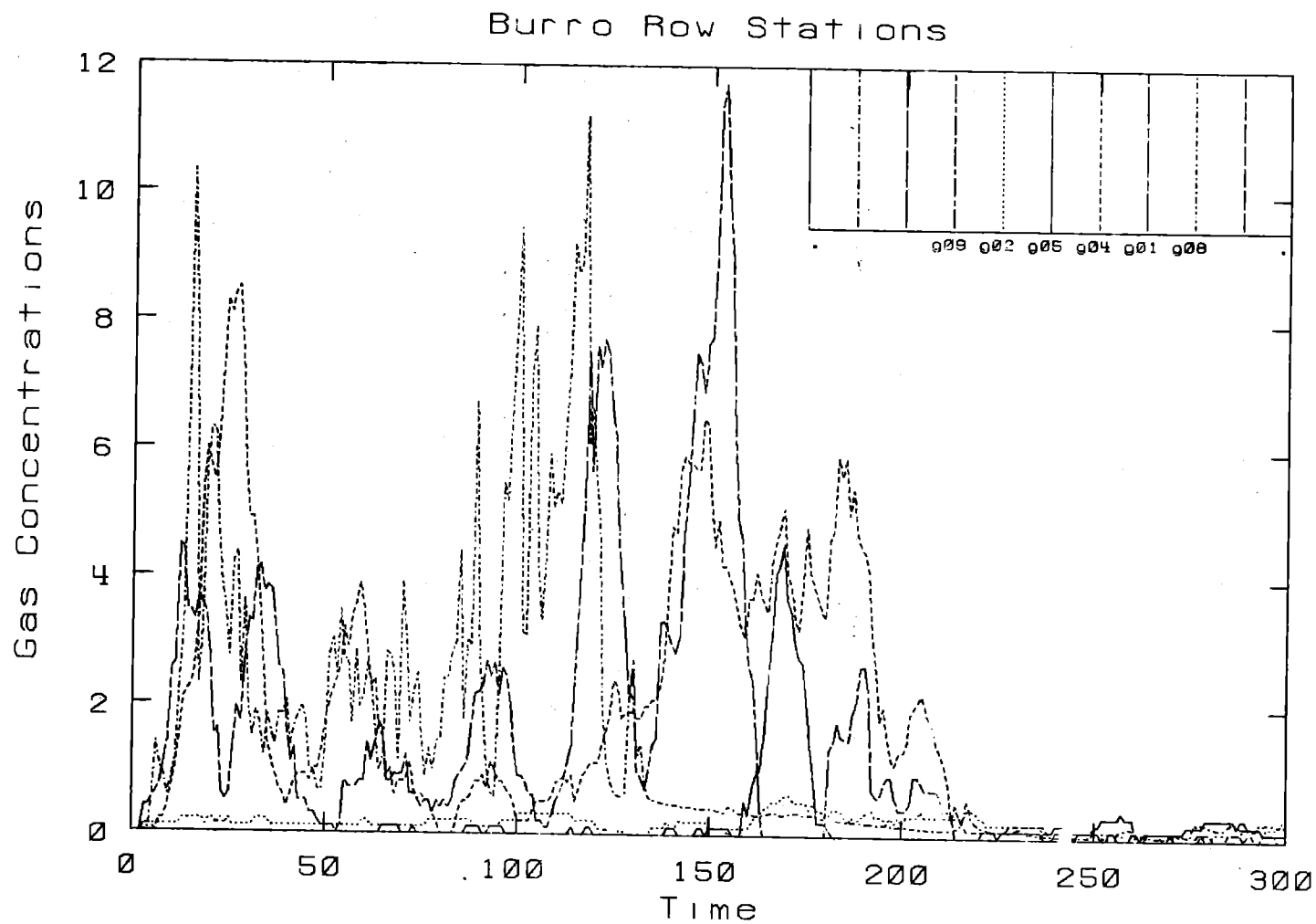
Burro Row Stations



Burro 3. Row: 800 M.- Height: 8 M.

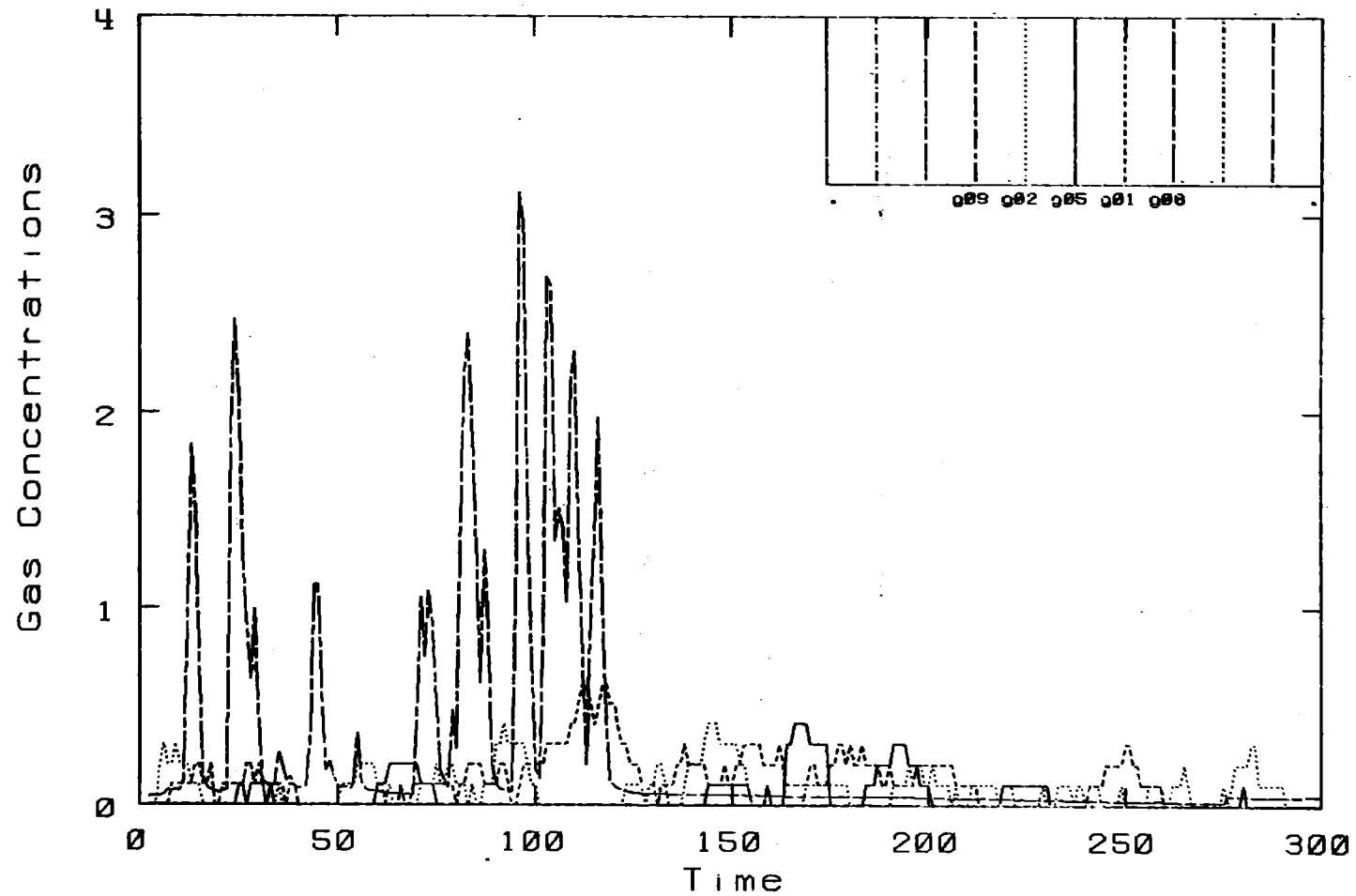


Burro 4. Row: 57 M. - Height: 1 M.



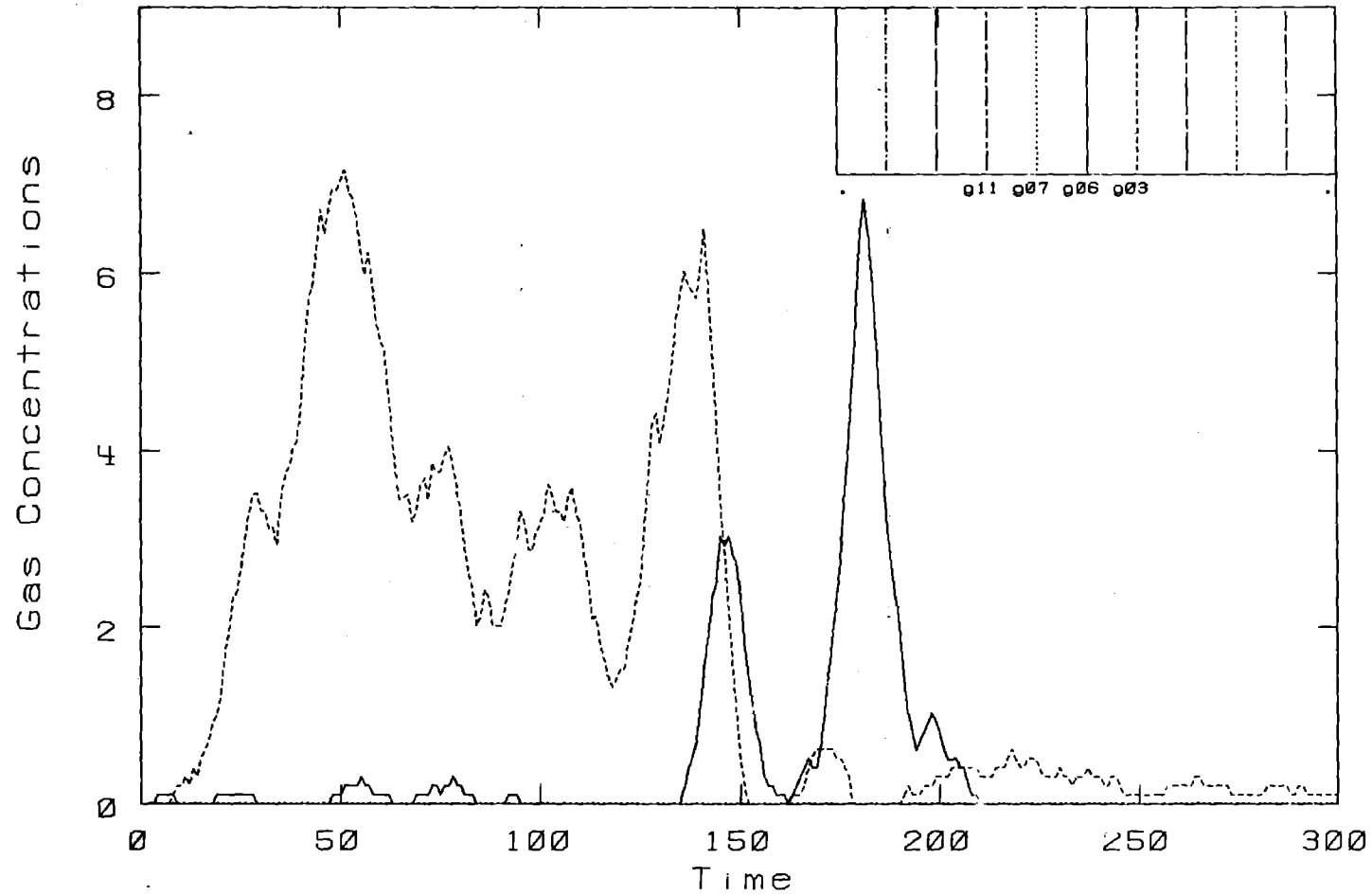
Burro 4. Row: 57 M. - Height: 3 M.

Burro Row Stations



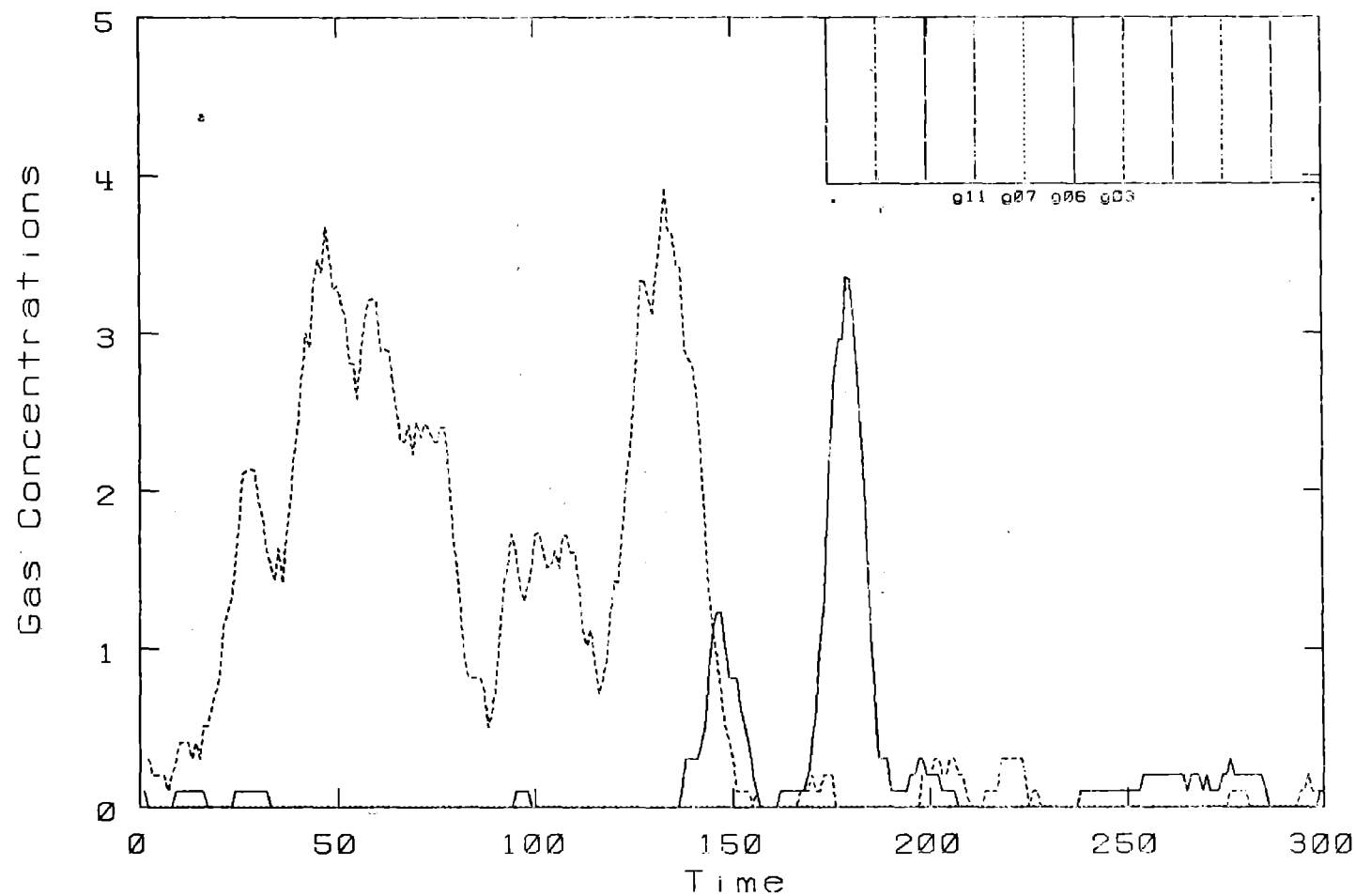
Burro 4. Row: 57 M. - Height: 8 M.

Burro Row Stations



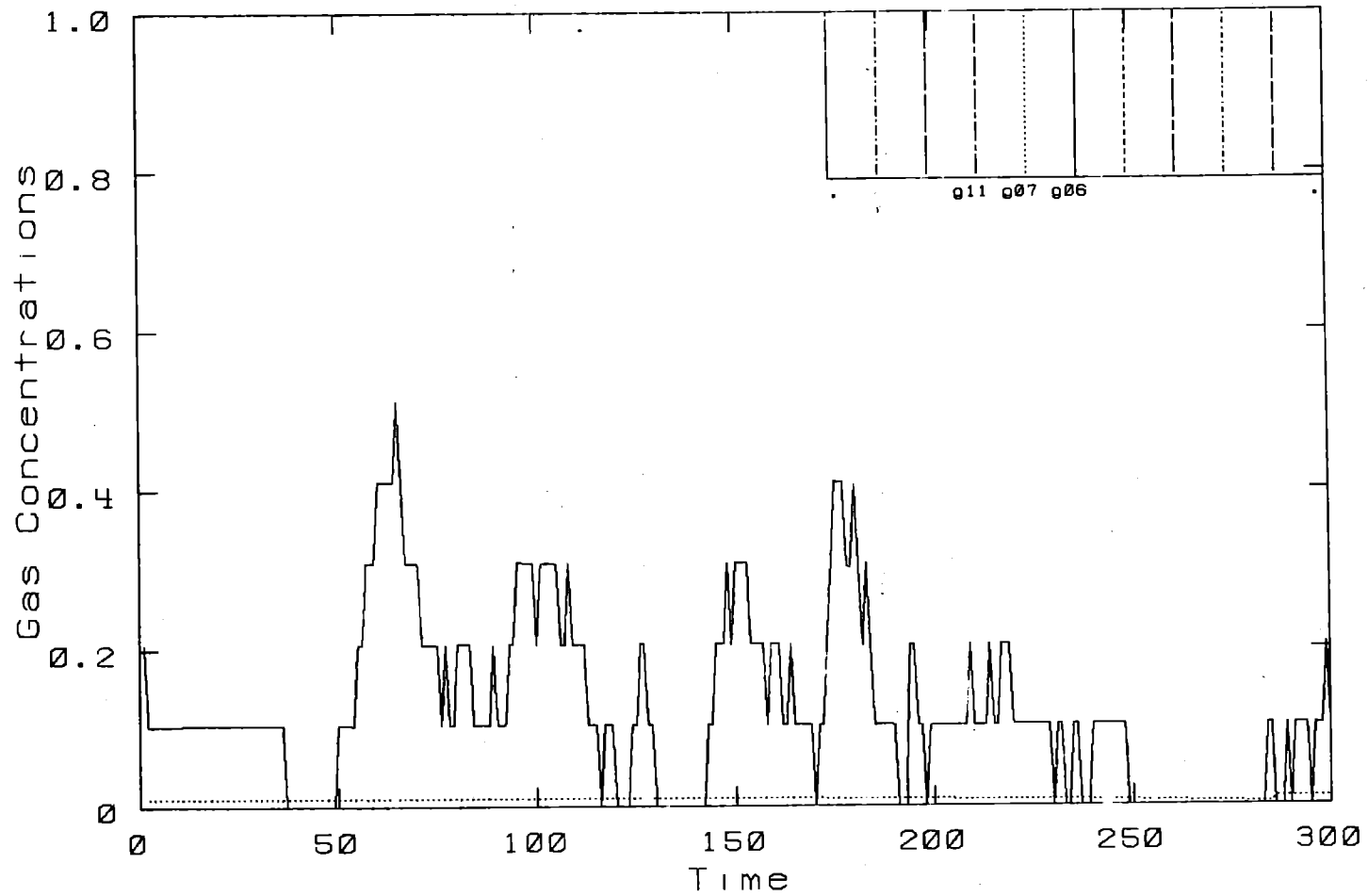
Burro 4. Row: 140 M.- Height: 1 M.

Burro Row Stations



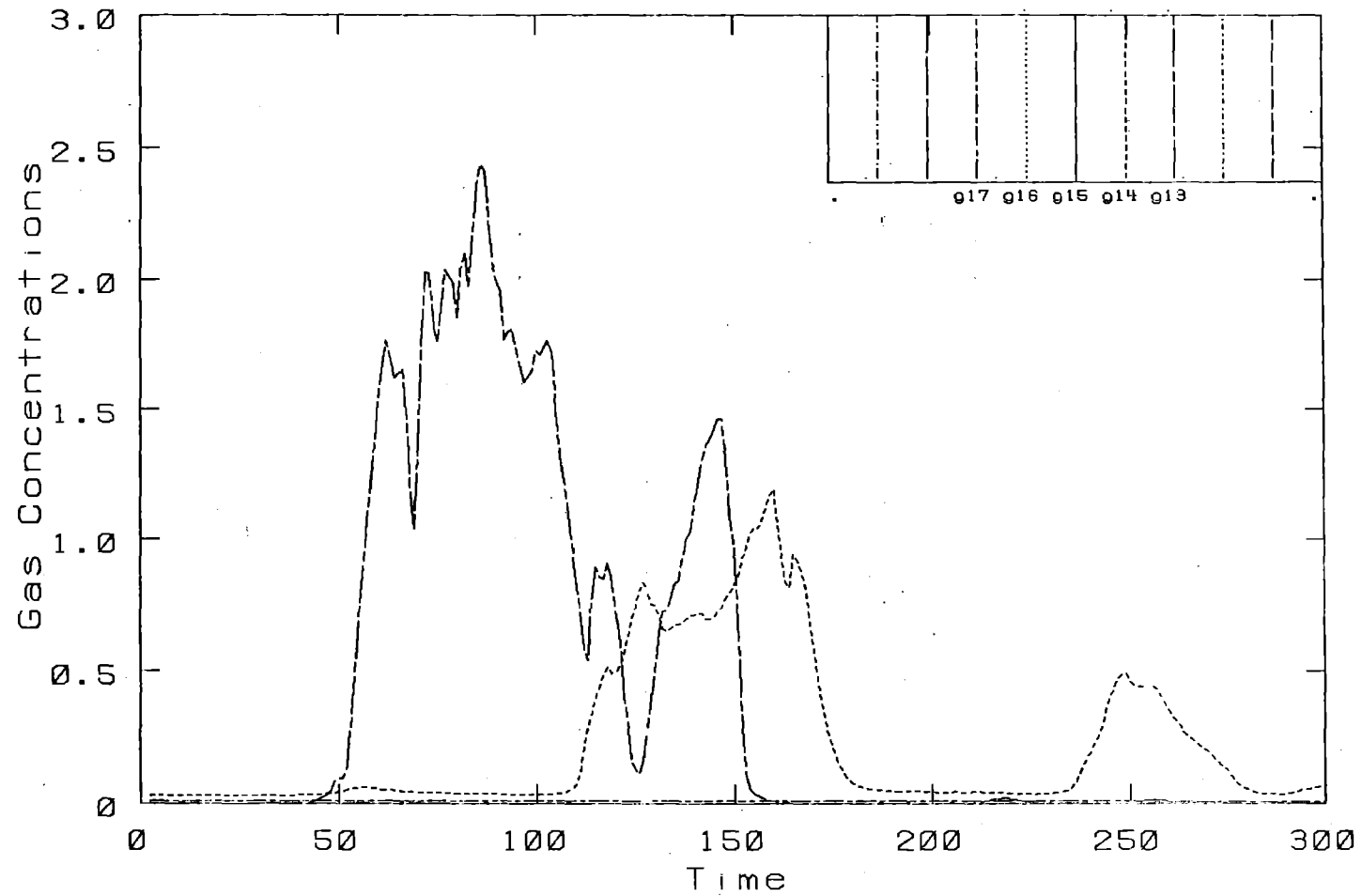
Burro 4. Row: 140 M. - Height: 3 M.

Burro Row Stations

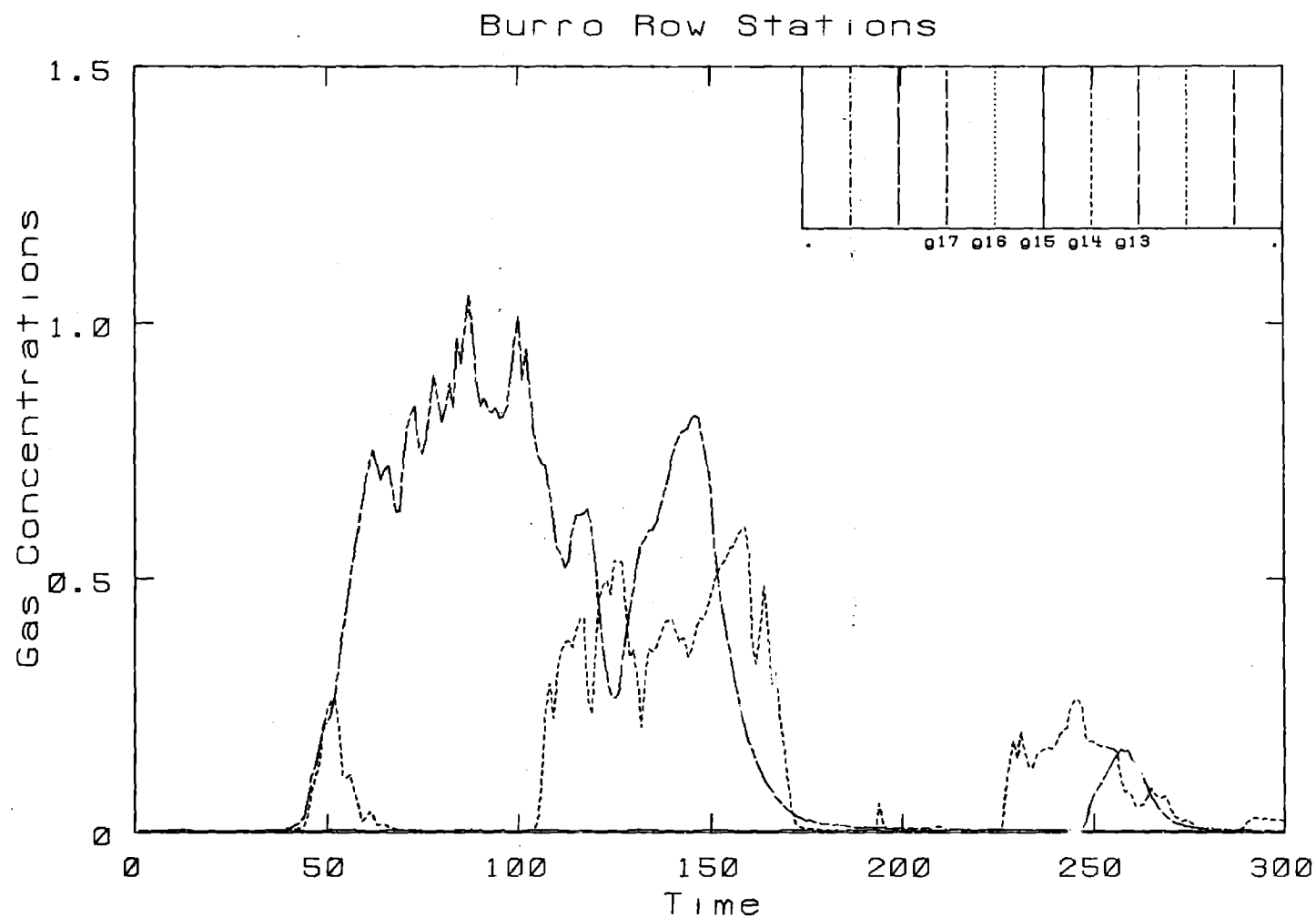


Burro 4. Row: 140 M. - Height: 8 M.

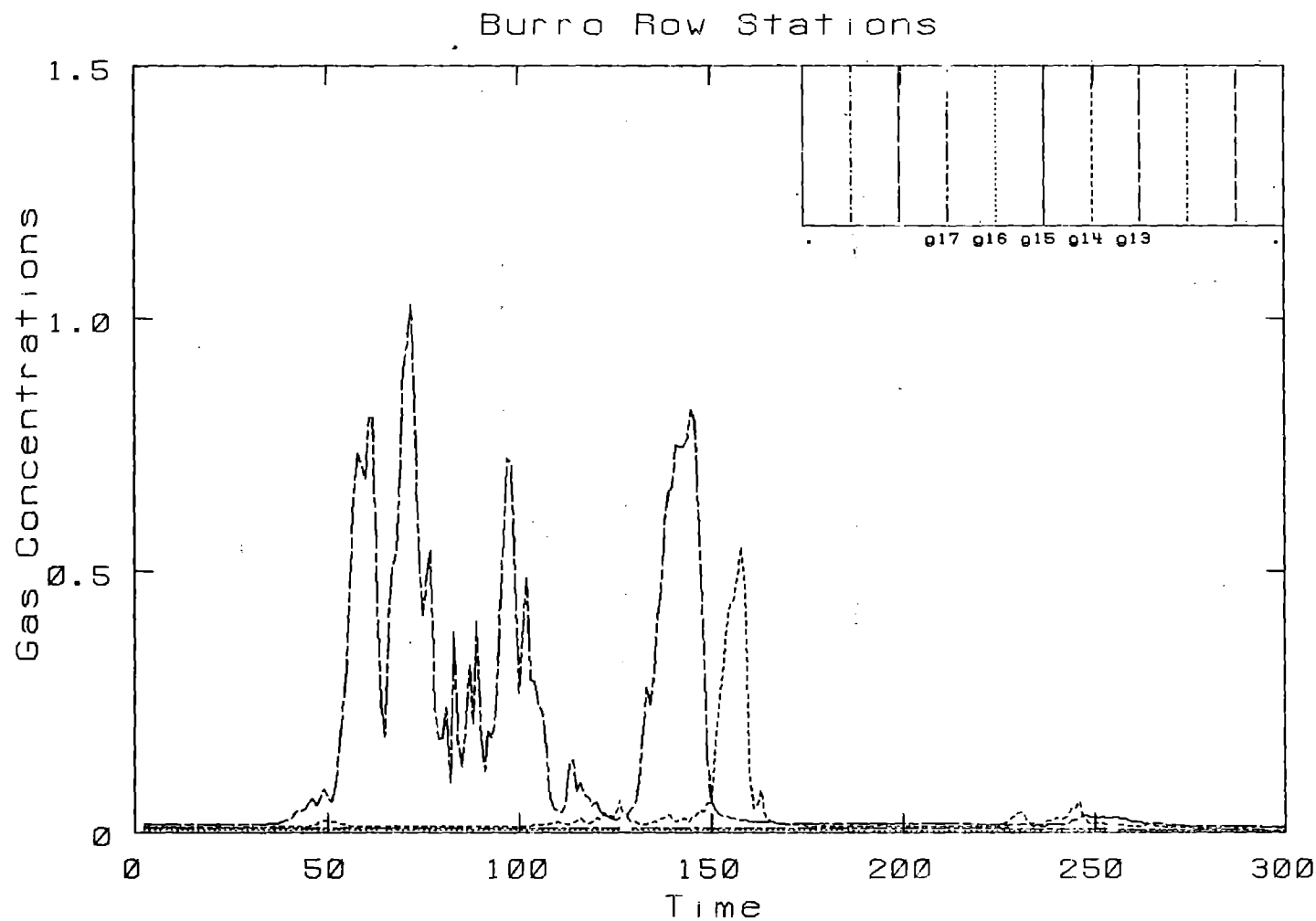
Burro Row Stations



Burro 4. Row: 400 M. - Height: 1 M.

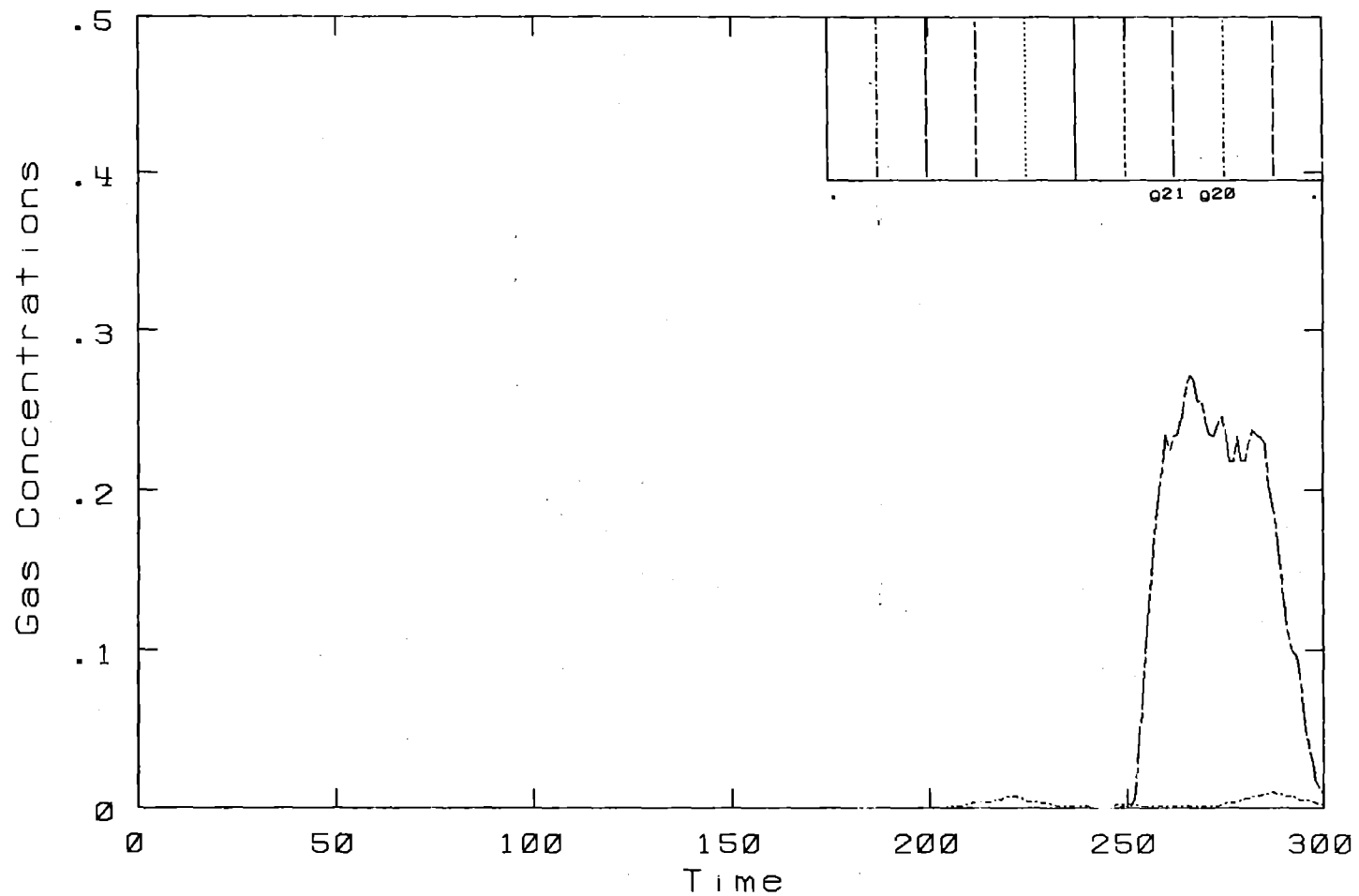


Burro 4. Row: 400 M. - Height: 3 M.



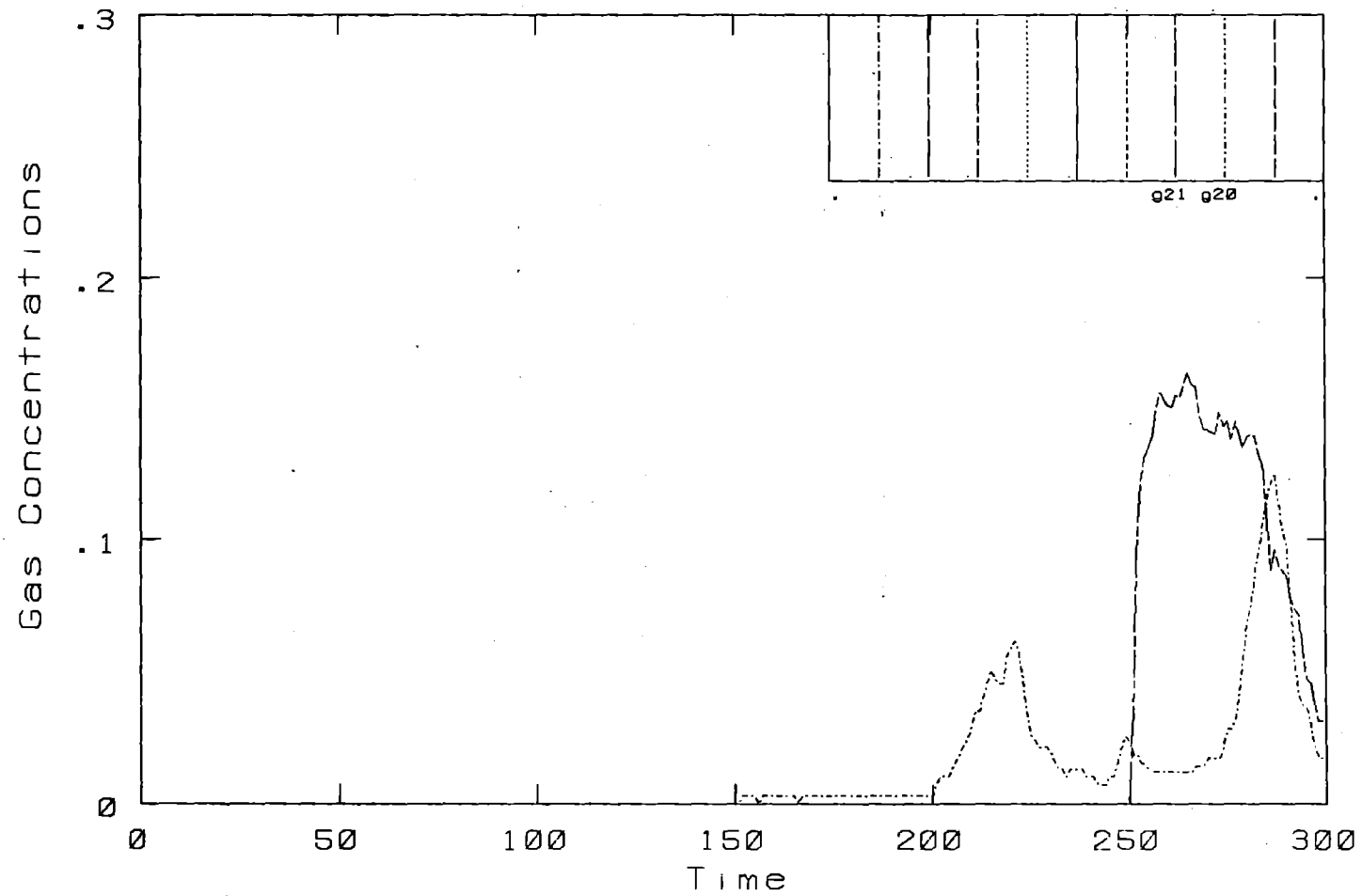
Burro 4. Row: 400 M. - Height: 8 M.

Burro Row Stations



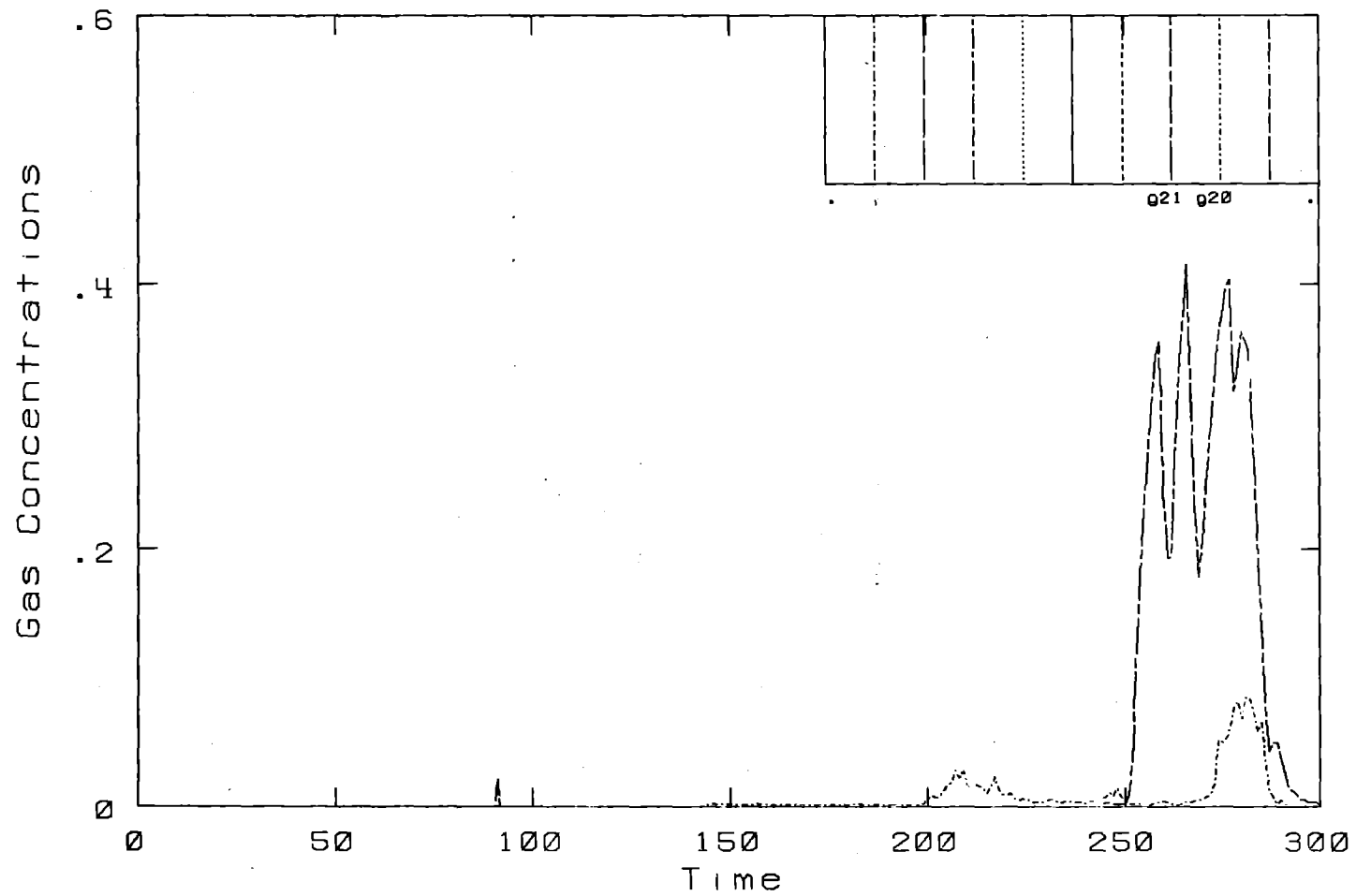
Burro 4. Row: 800 M. - Height: 1 M.

Burro Row Stations



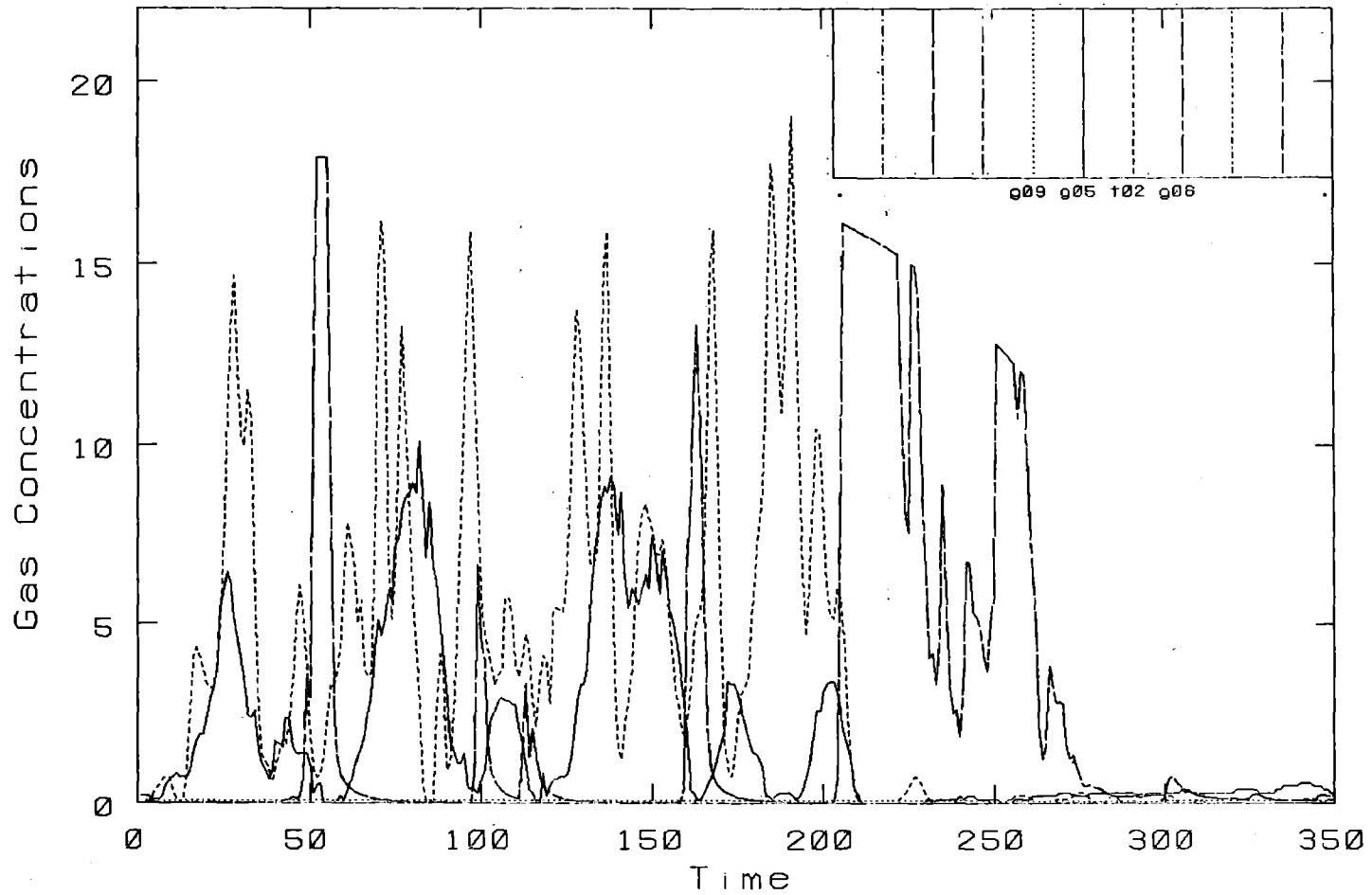
Burro 4. Row: 800 M. - Height: 3.M.

Burro Row Stations



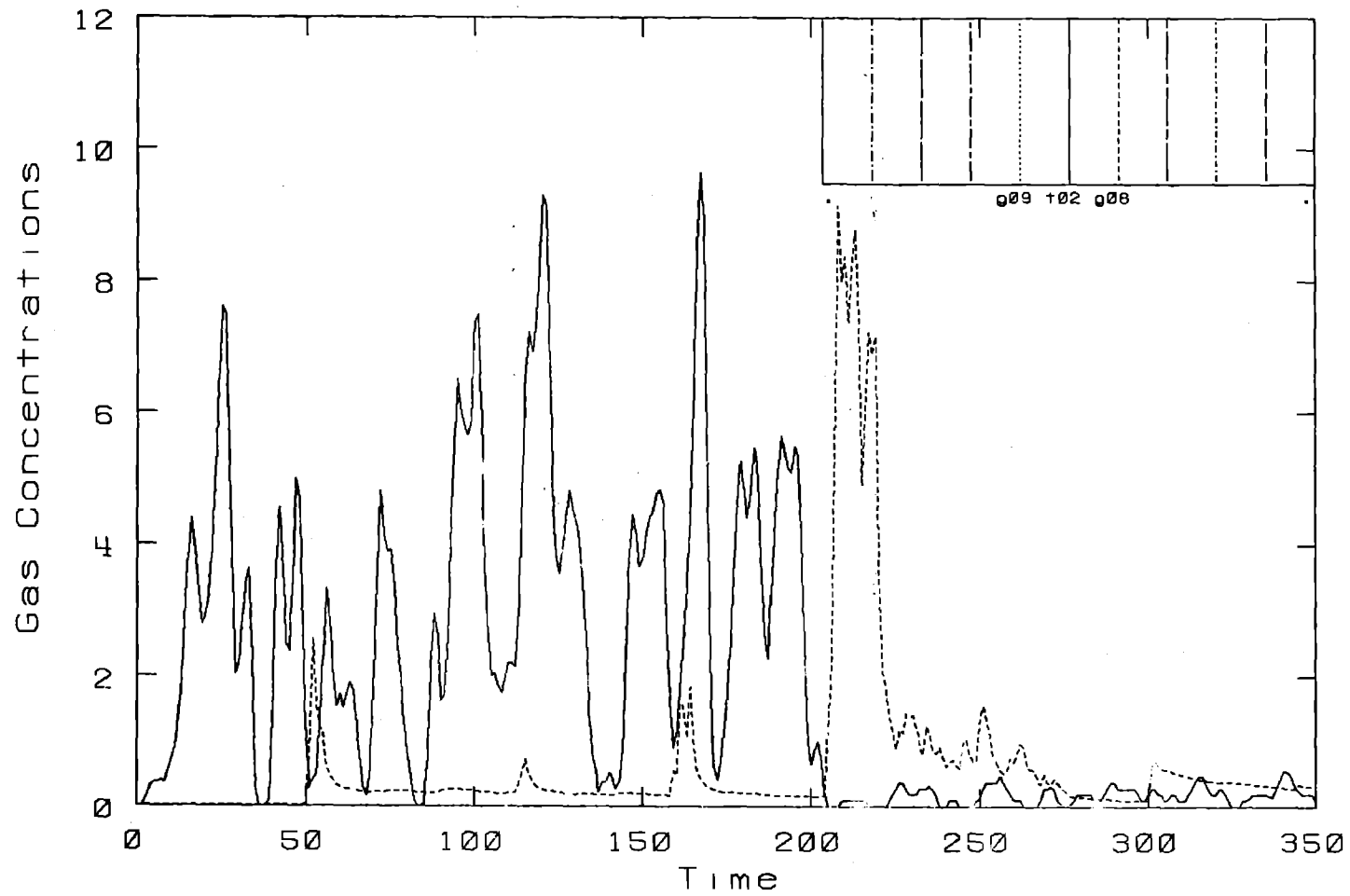
Burro 4. Row: 800 M. - Height: 8 M.

Burro Row Stations



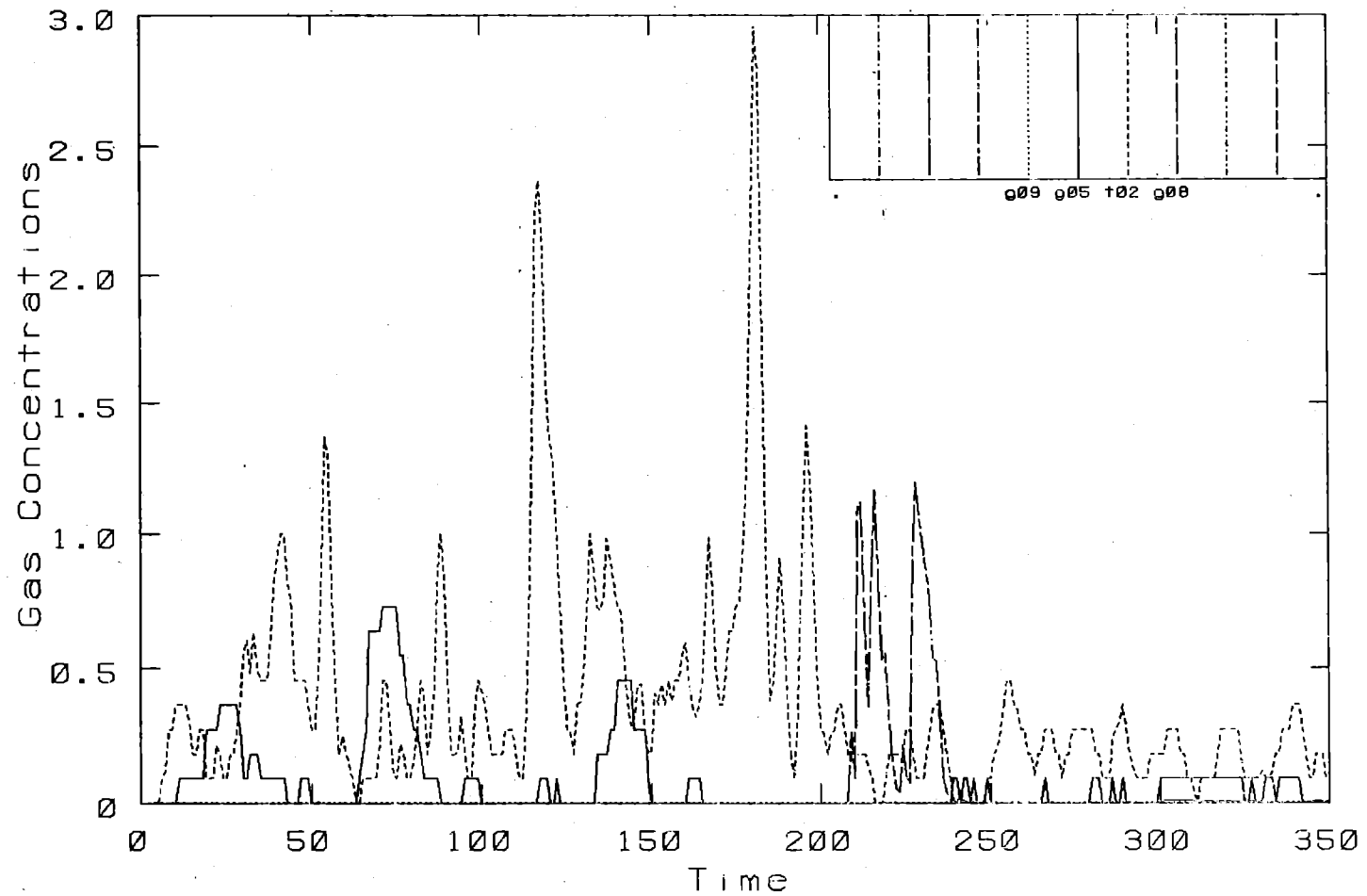
Burro 5. Row: 57 M. - Height: 1 M.

Burro Row Stations



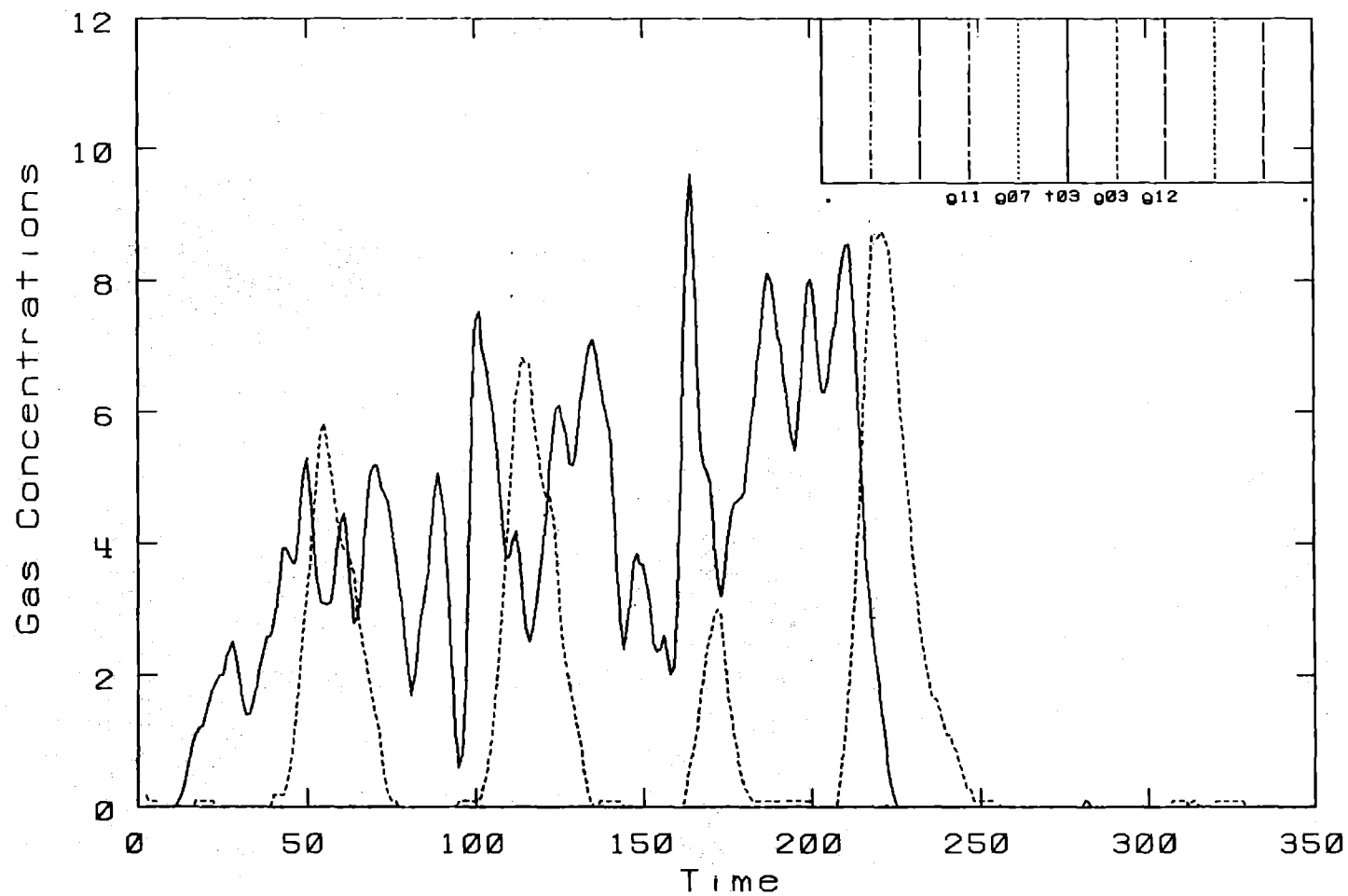
Burro 5. Row: 57 M. - Height: 3 M.

Burro Row Stations



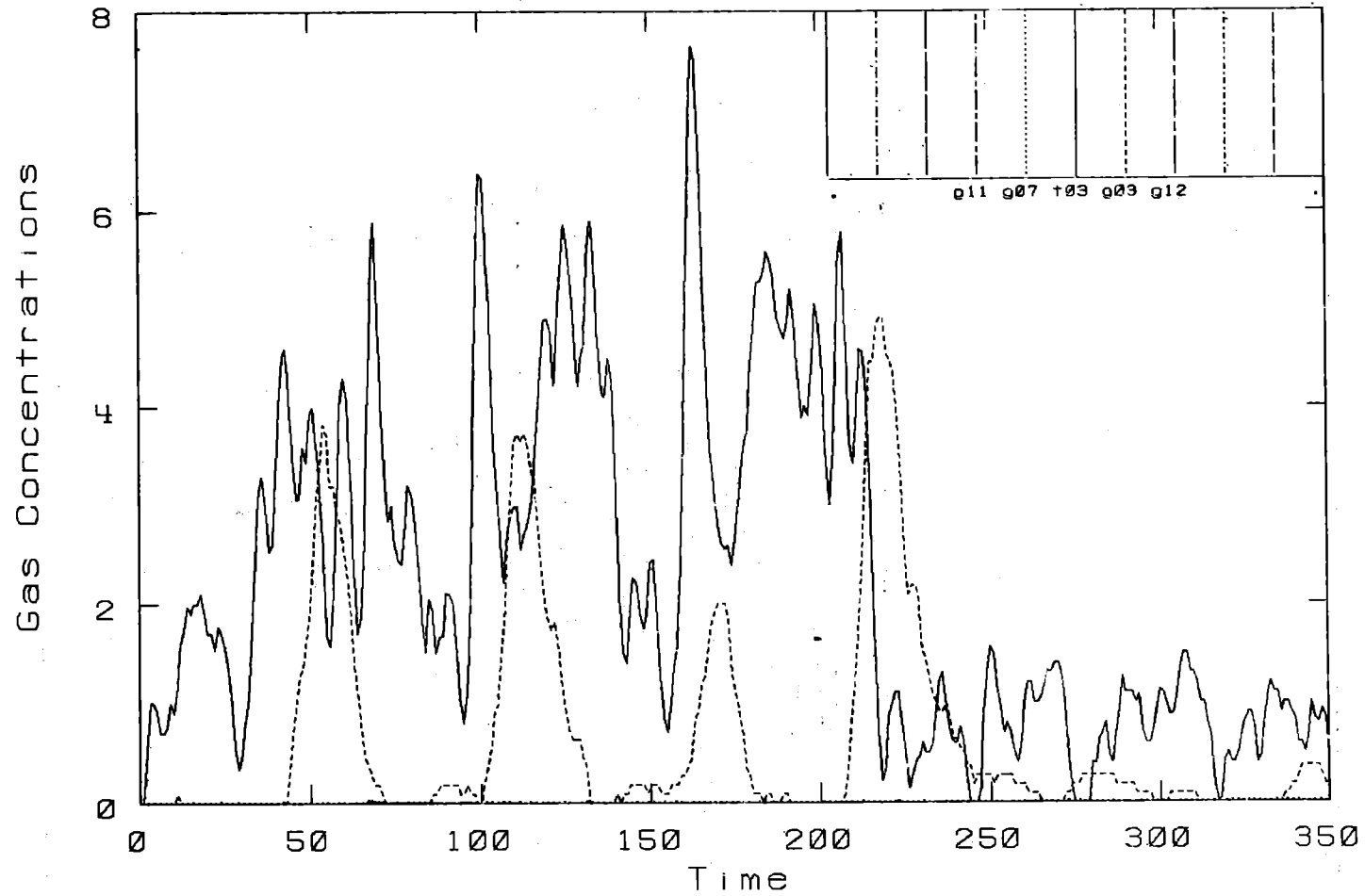
Burro 5. Row: 57 M. - Height: 8 M.

Burro Row Stations



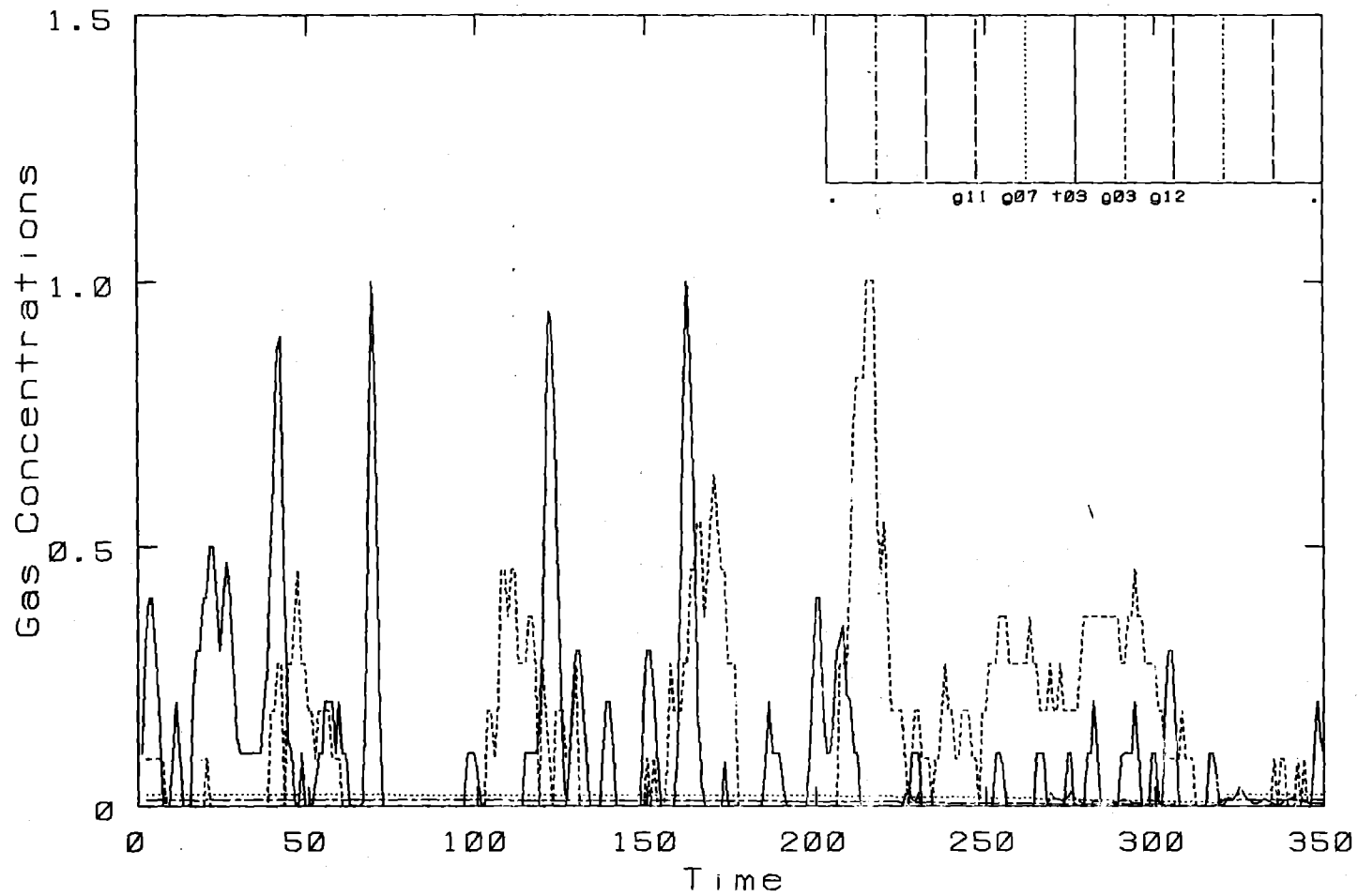
Burro 5. Row: 140 M.- Height: 1 M.

Burro Row Stations



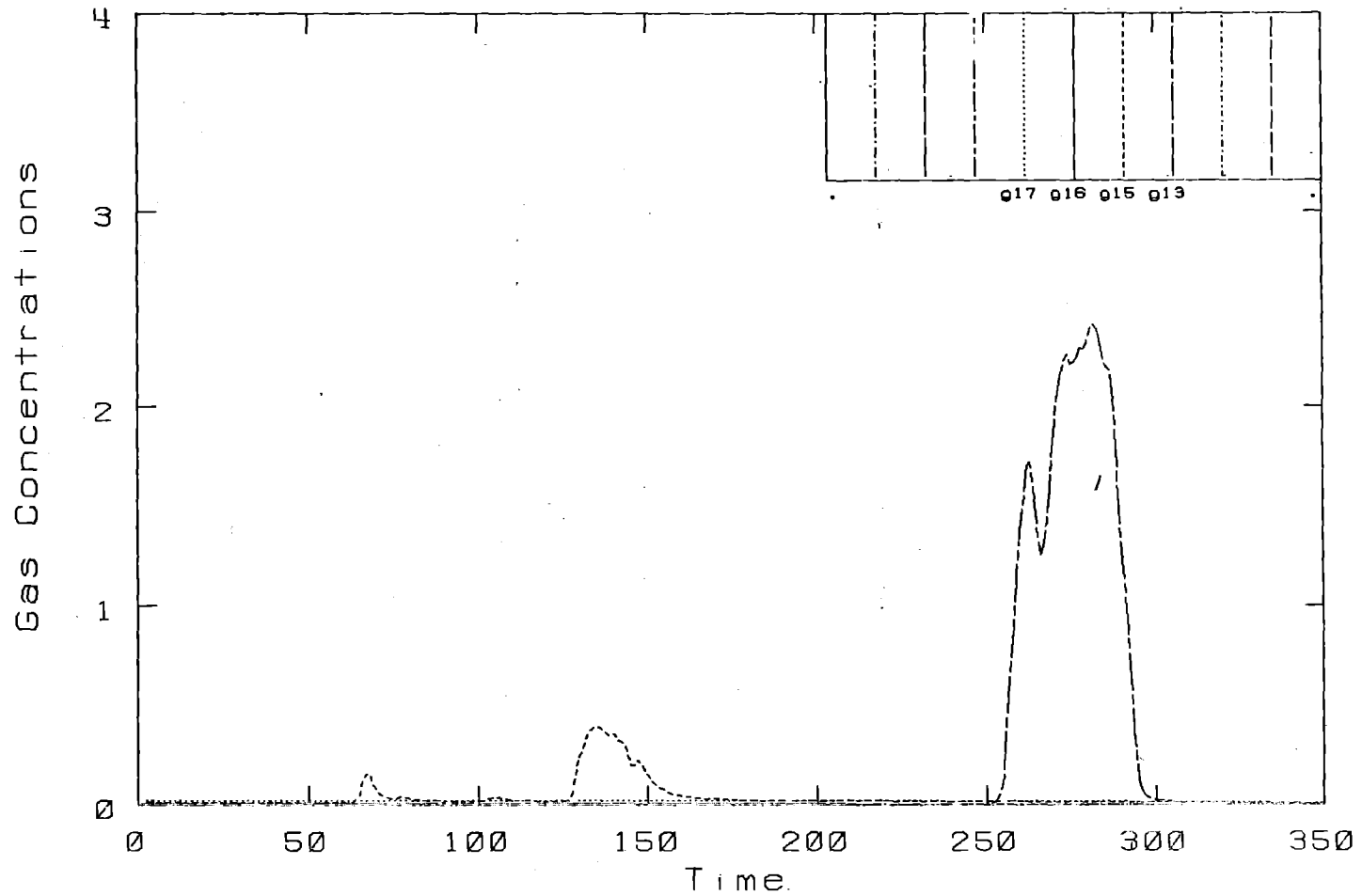
Burro 5. Row: 140 M.- Height: 3 M.

Burro Row Stations



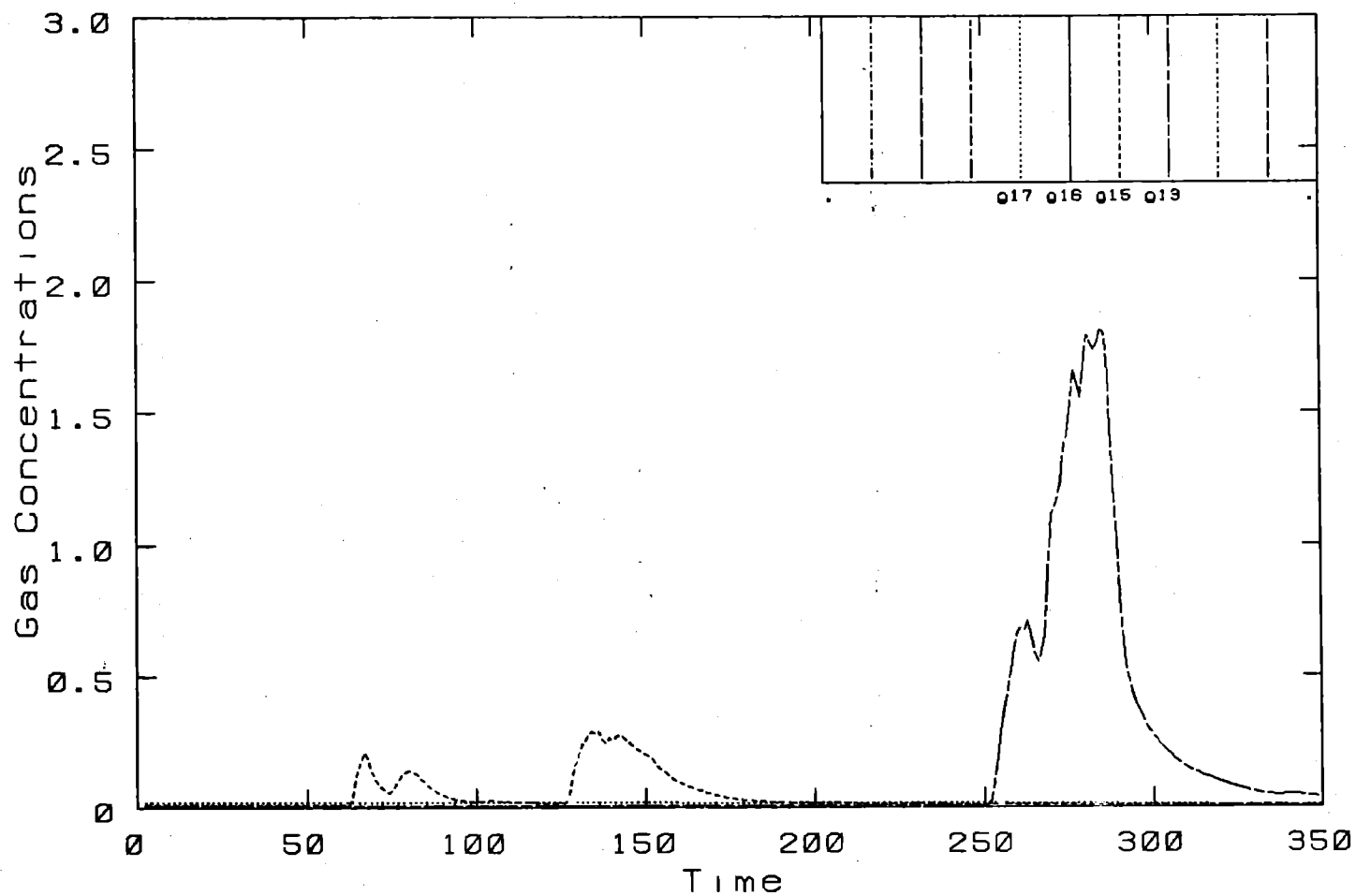
Burro 5. Row: 140 M. - Height: 8 M.

Burro Row Stations

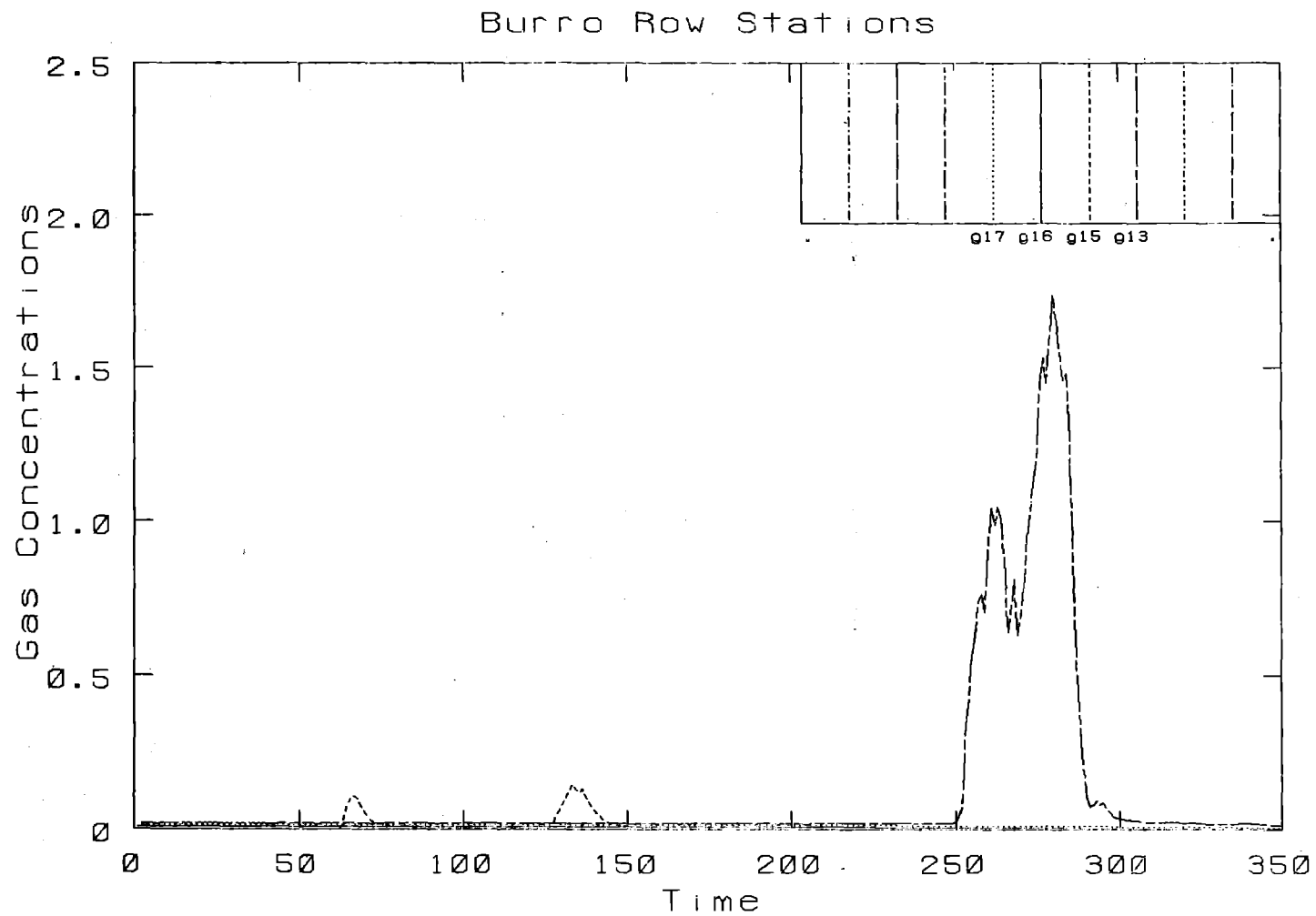


Burro 5. Row: 400 M.- Height: 1 M.

Burro Row Stations

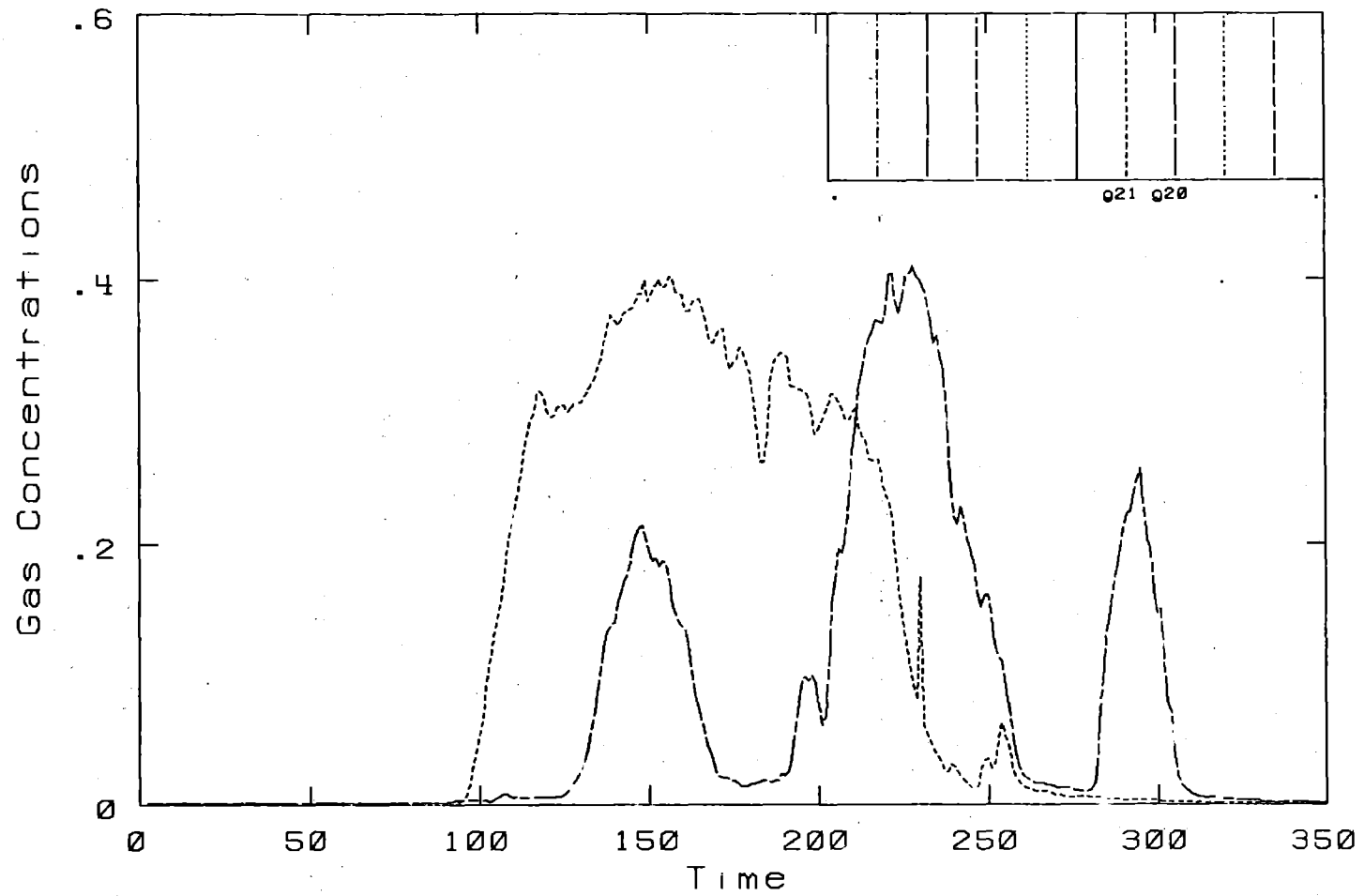


Burro 5. Row: 400 M. - Height: 3 M.

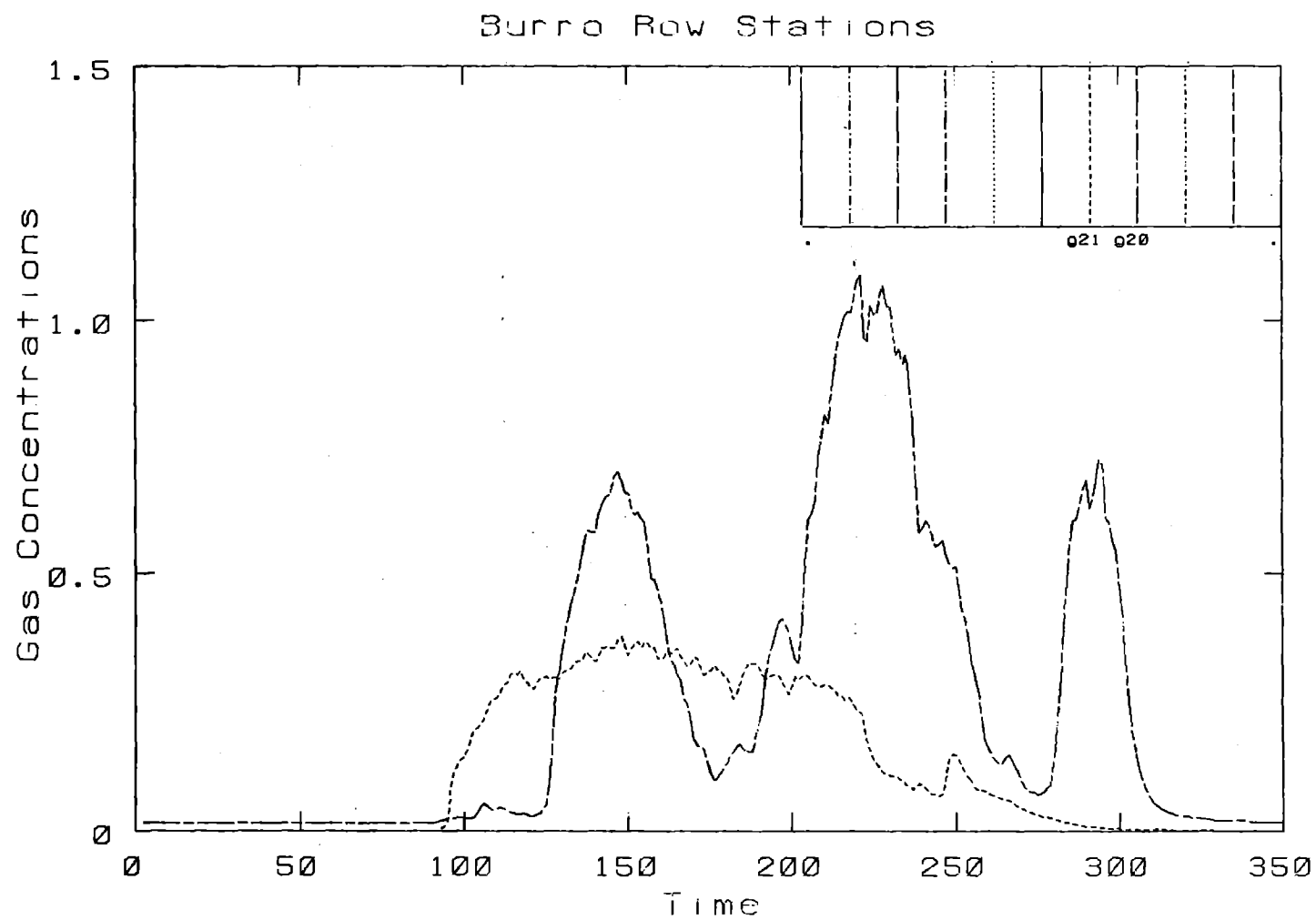


Burro 5. Row: 400 M.- Height: 8 M.

Burro Row Stations

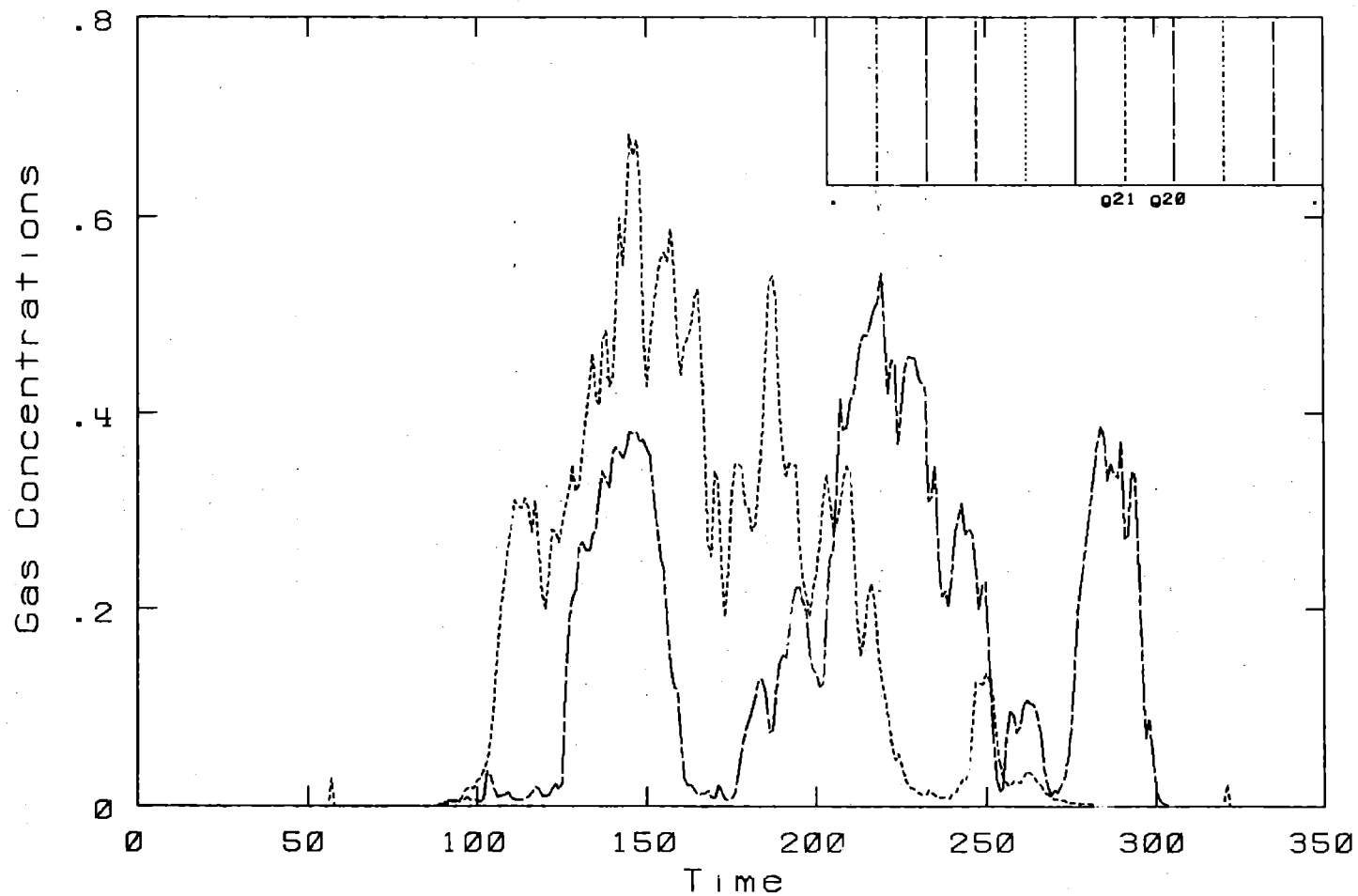


Burro 5. Row: 800 M.- Height: 1 M.



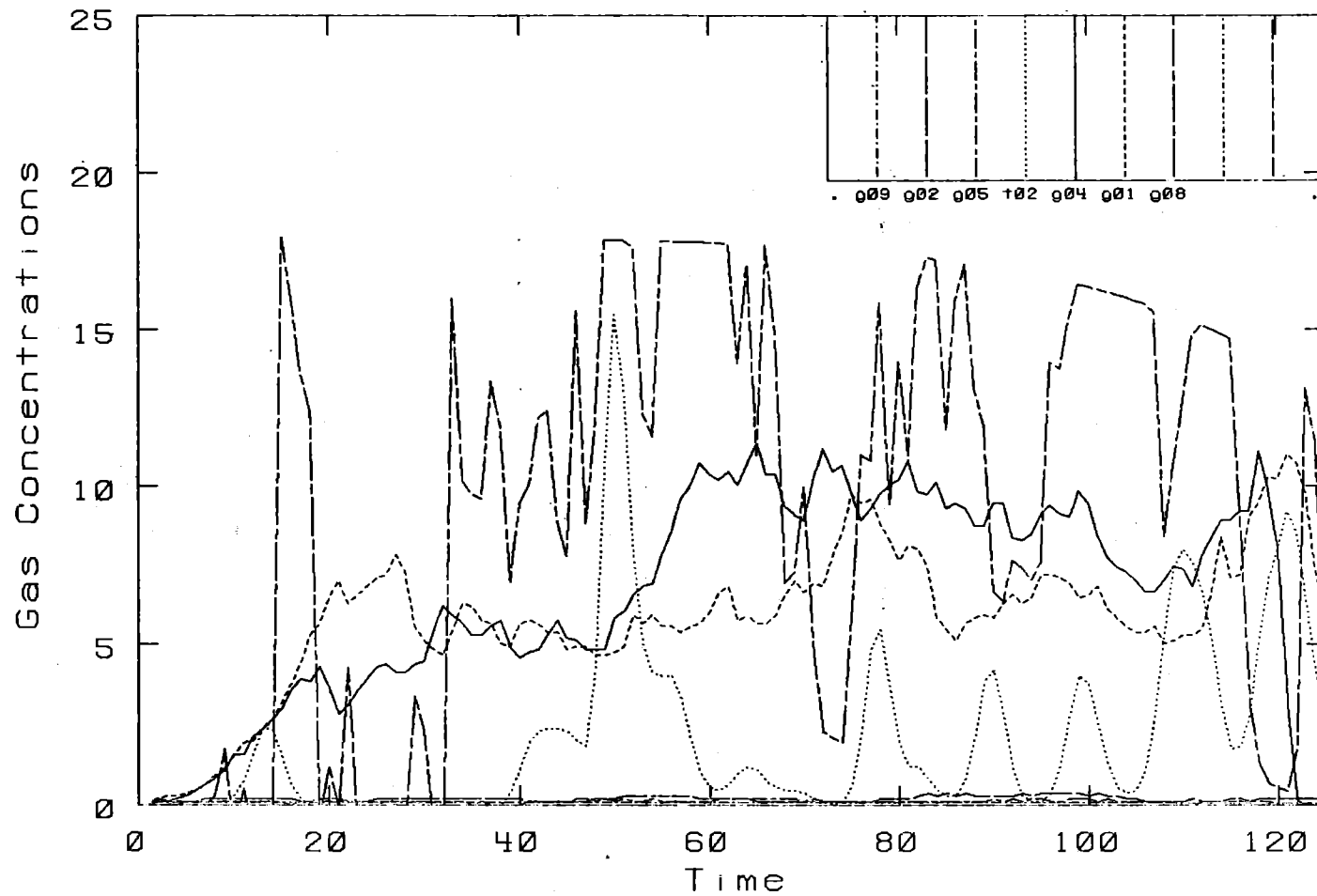
Burro 5. Row: 800 M. - Height: 3 M.

Burro Row Stations



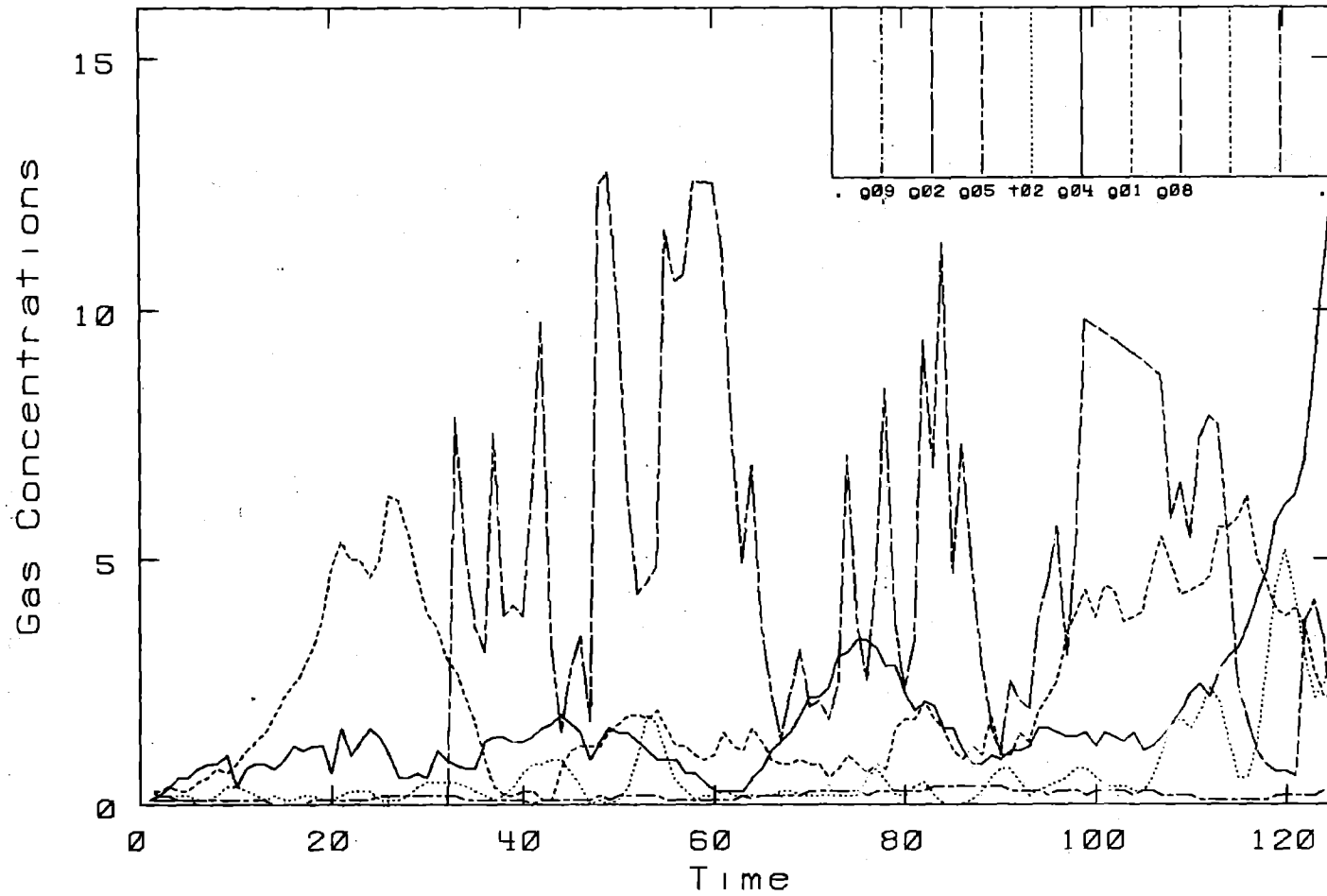
Burro 5. Row: 800 M.- Height: 8 M.

Burro Row Stations

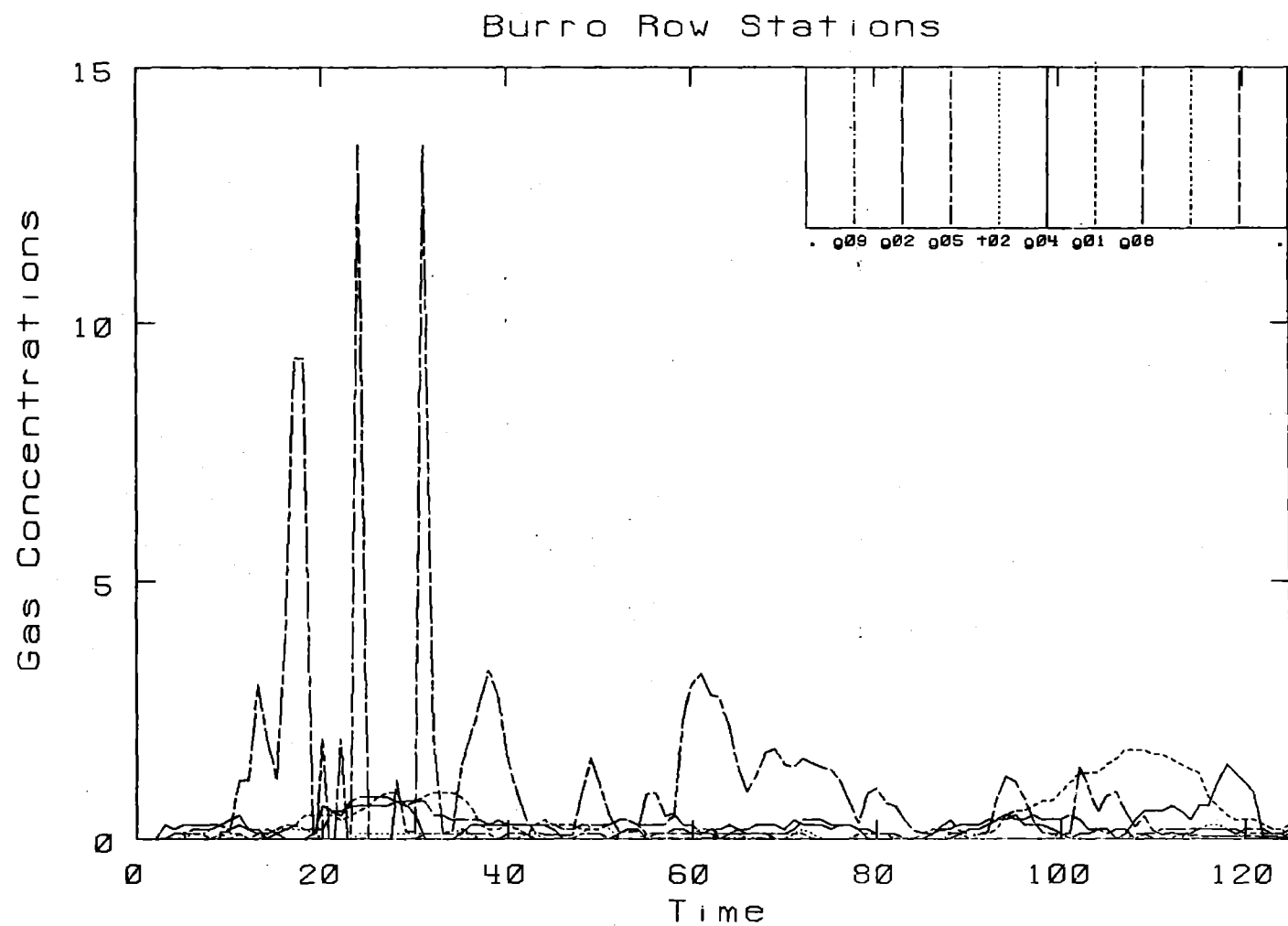


Burro 6. Row: 57 M. - Height: 1 M.

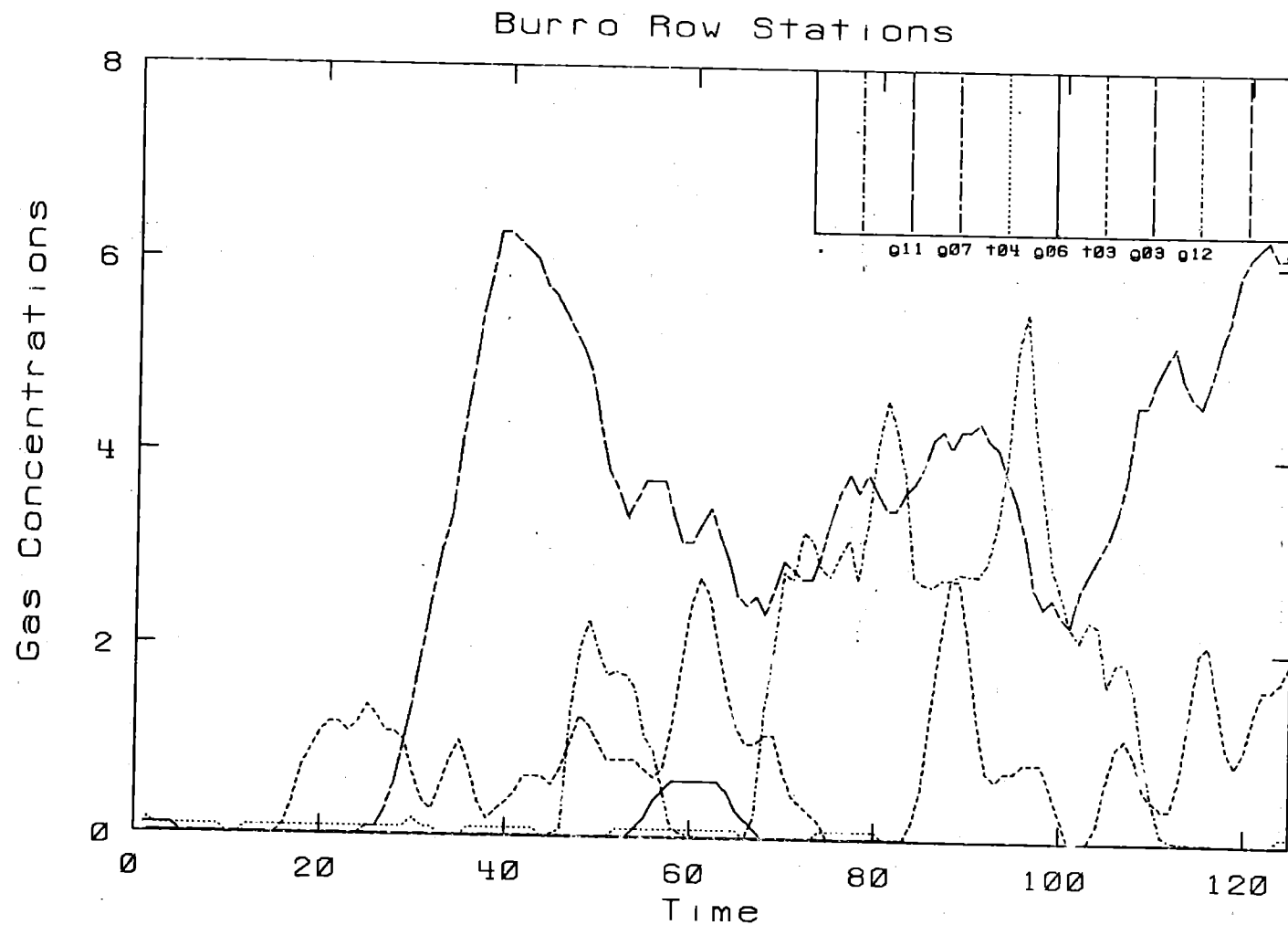
Burro Row Stations



Burro 6. Row: 57 M. - Height: 3 M.

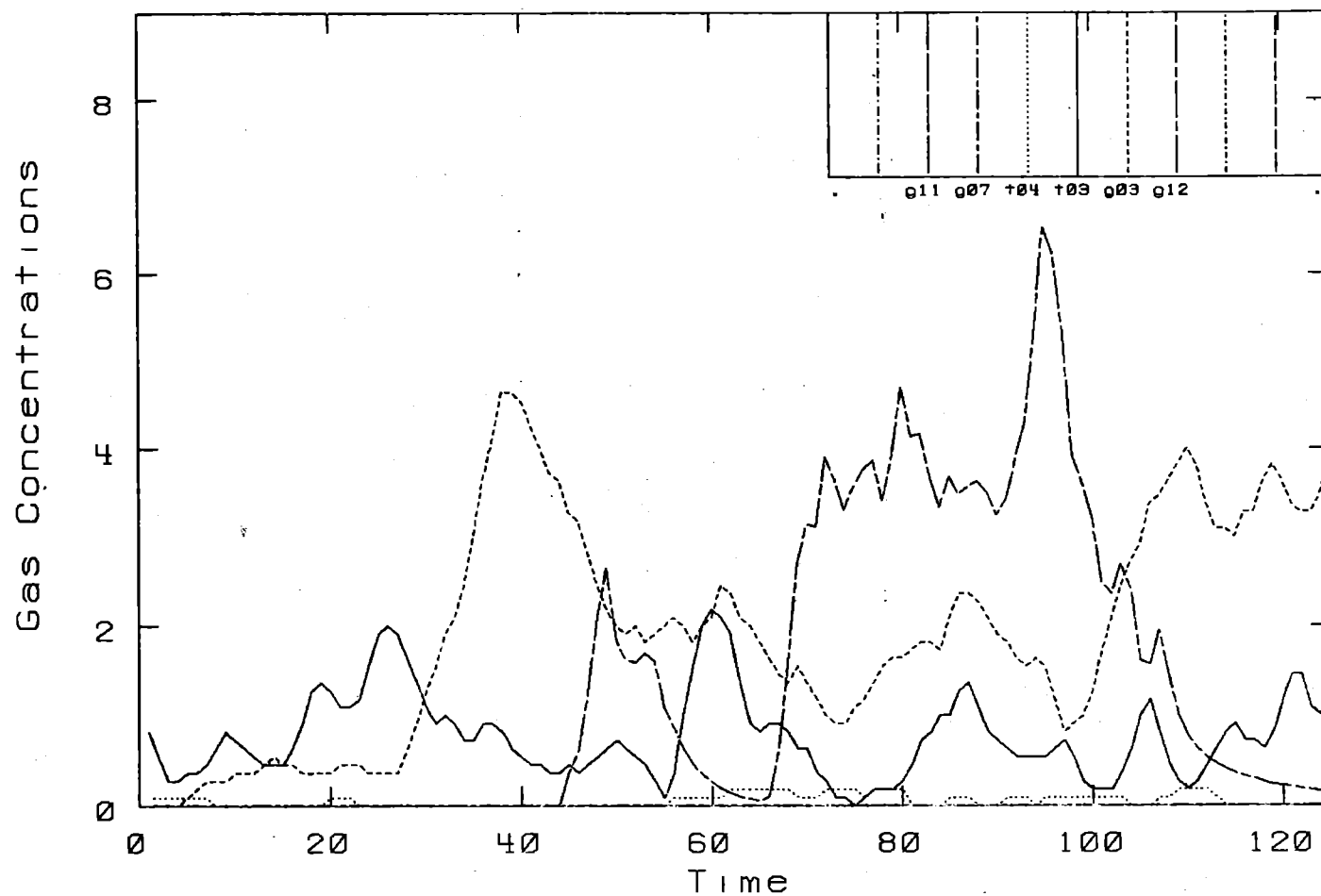


Burro 6. Row: 57 M. - Height: 8 M.



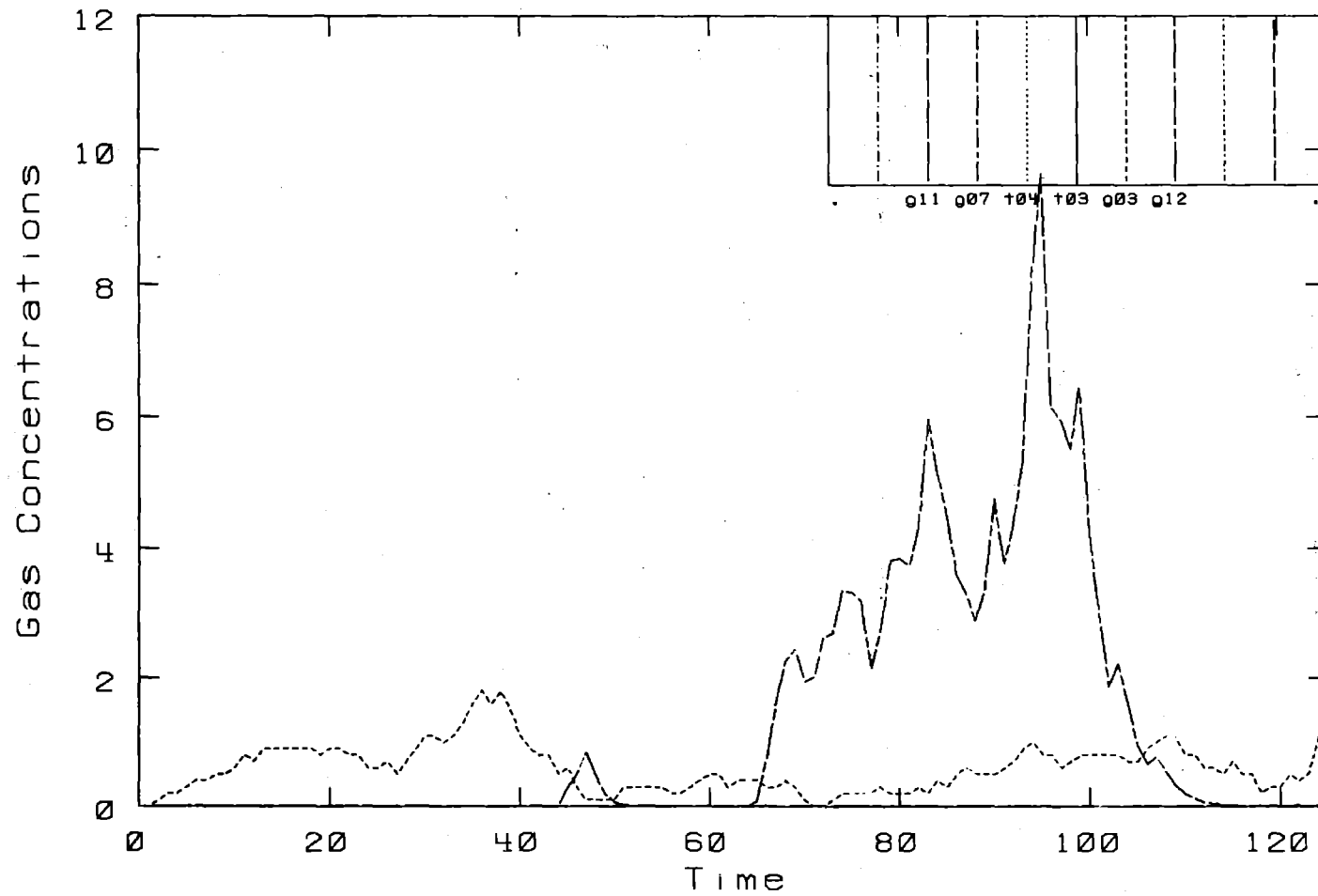
Burro 6. Row: 140 M. - Height: 1 M.

Burro Row Stations



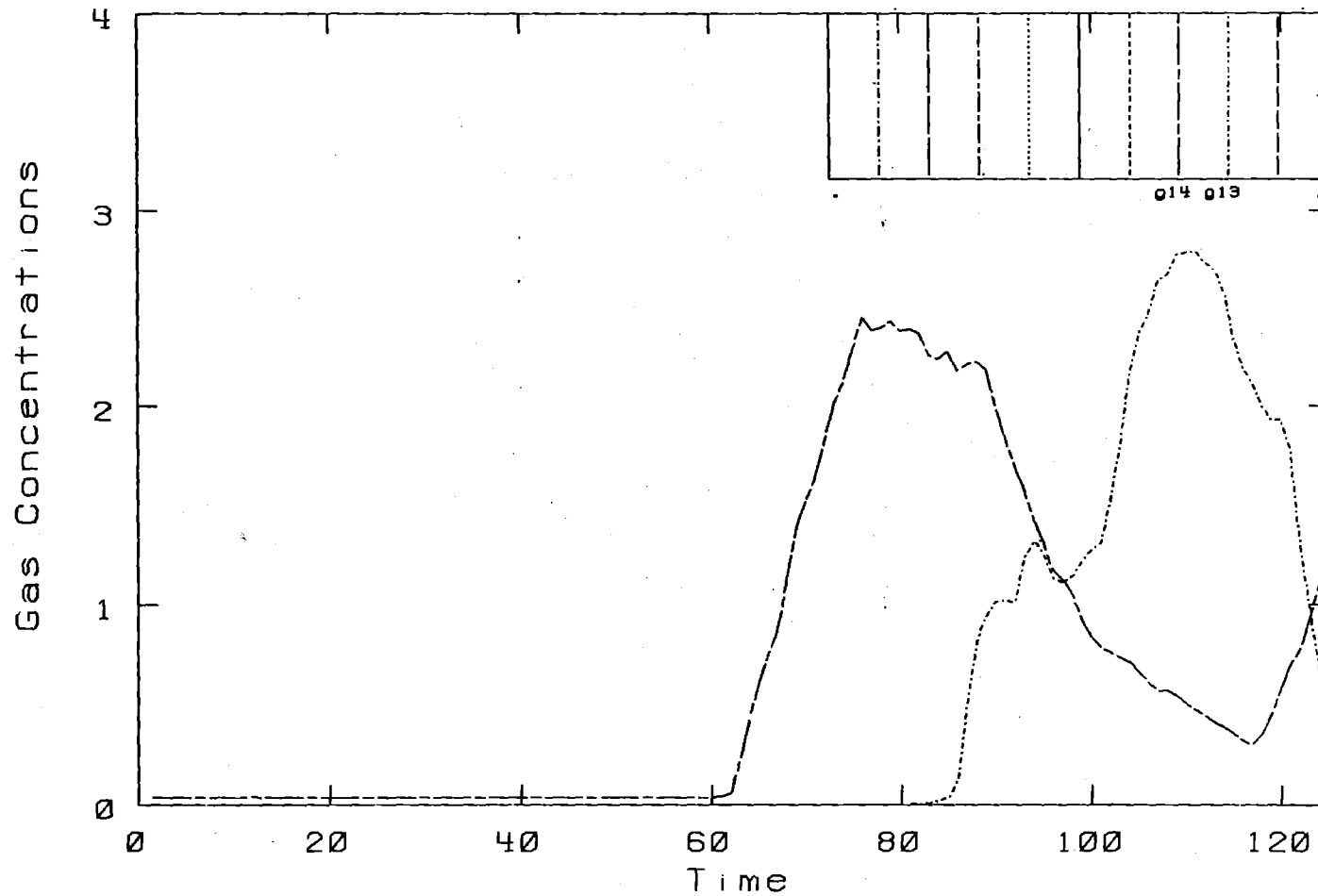
Burro 6. Row: 140 M. - Height: 3 M.

Burro Row Stations



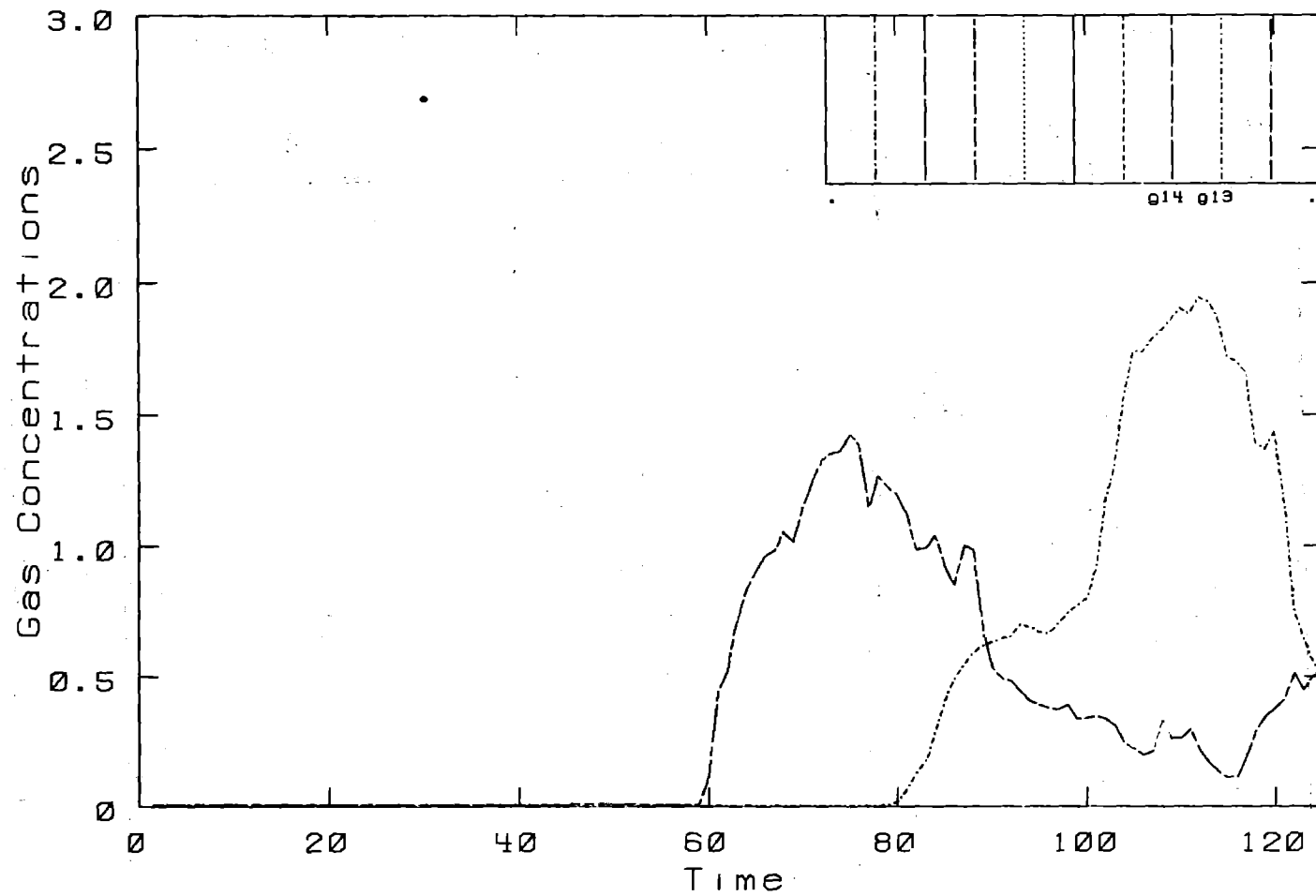
Burro 6. Row: 140 M. - Height: 8 M.

Burro Row Stations

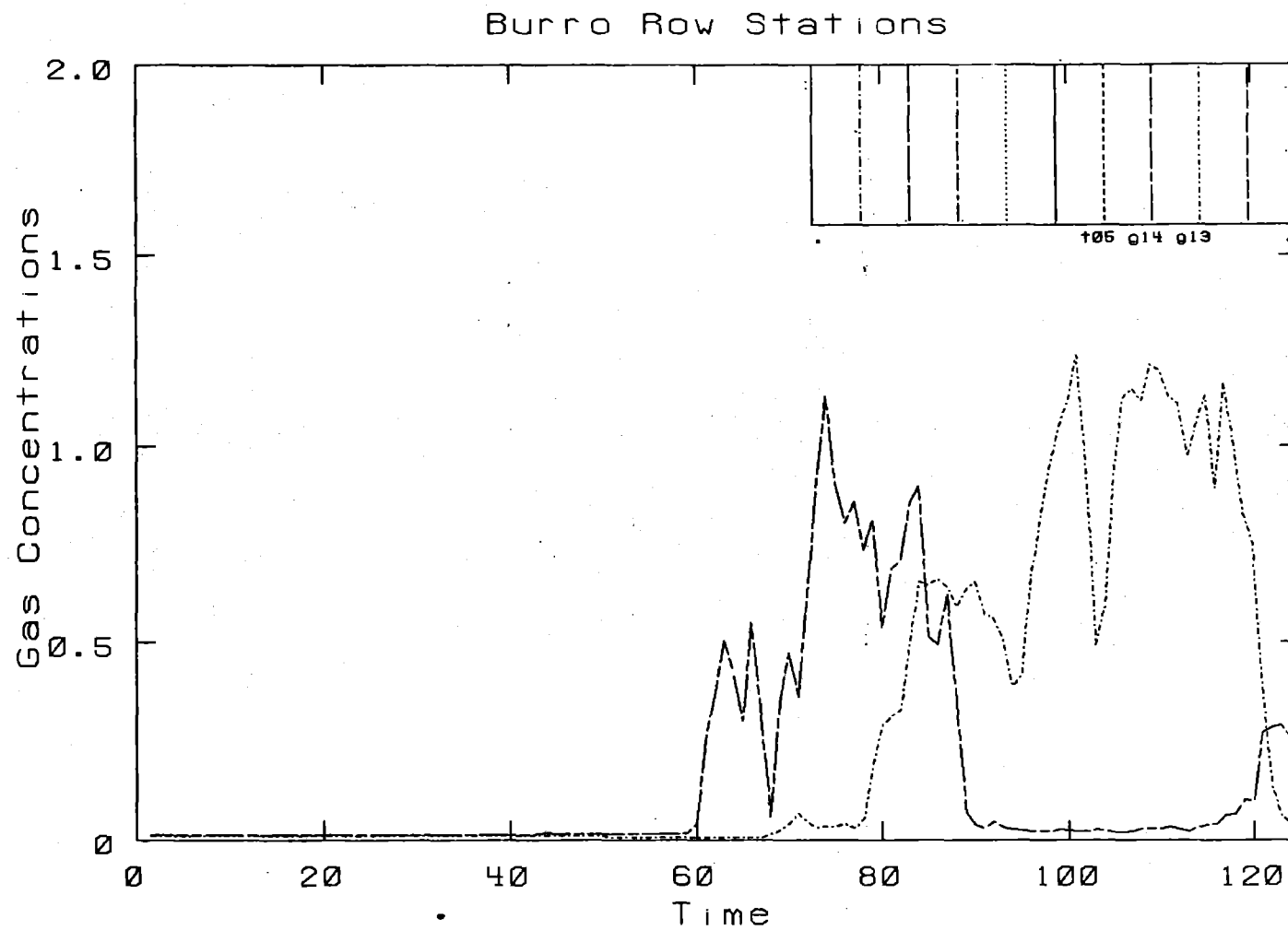


Burro 6. Row: 400 M.- Height: 1 M.

Burro Row Stations

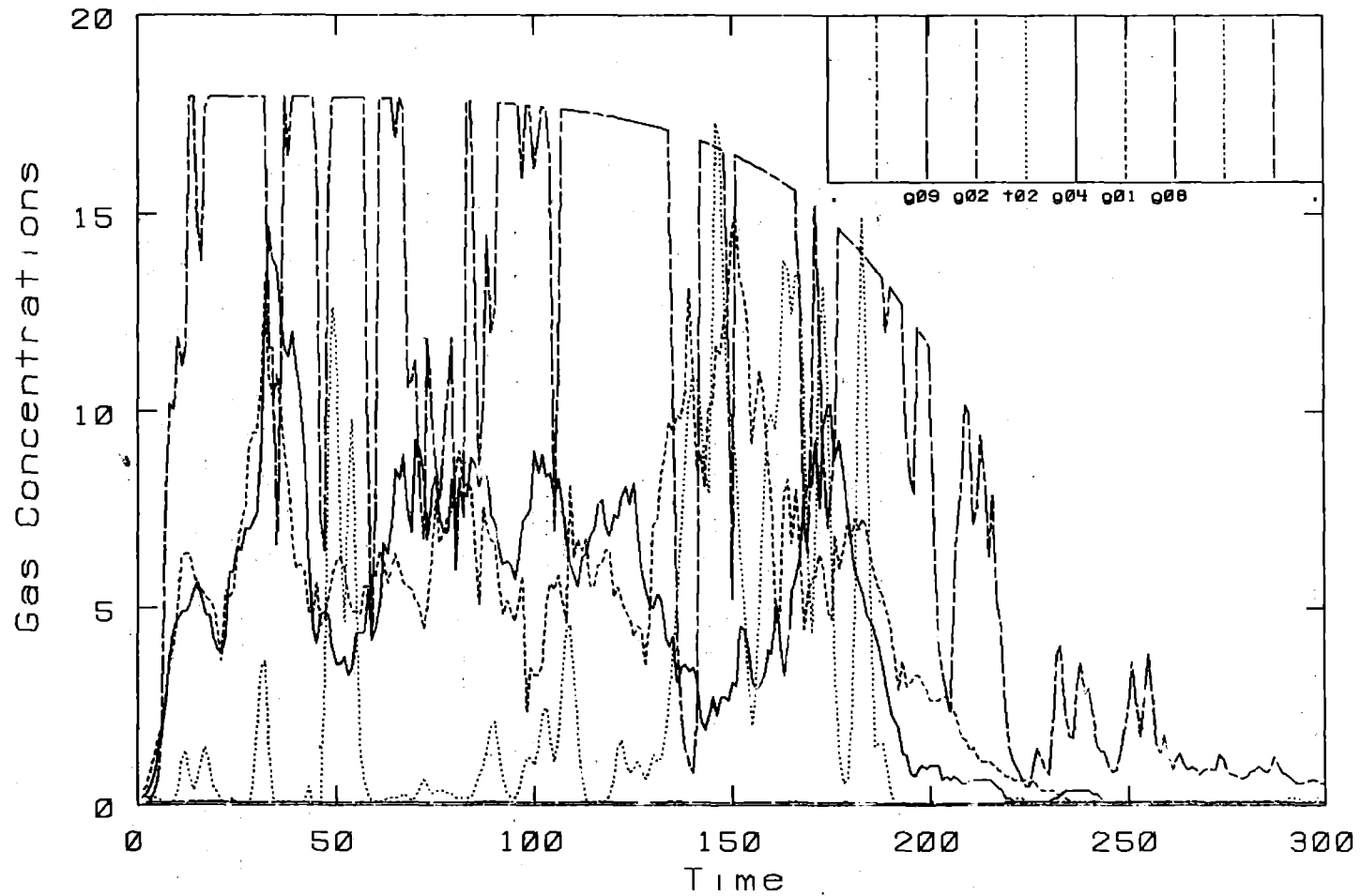


Burro 6. Row: 400 M.- Height: 3 M.



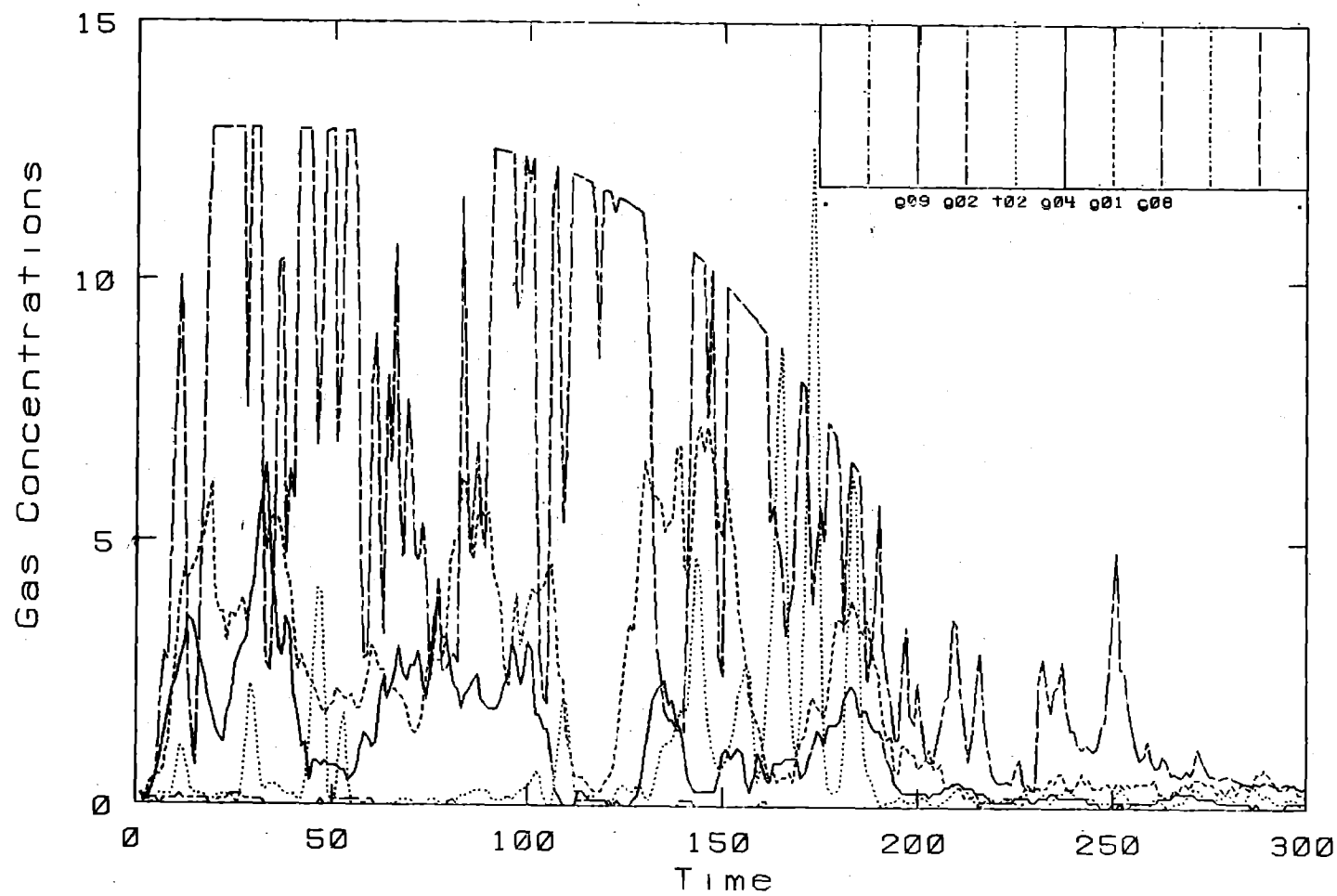
Burro 6. Row: 400 M. - Height: 8 M.

Burro Row Stations



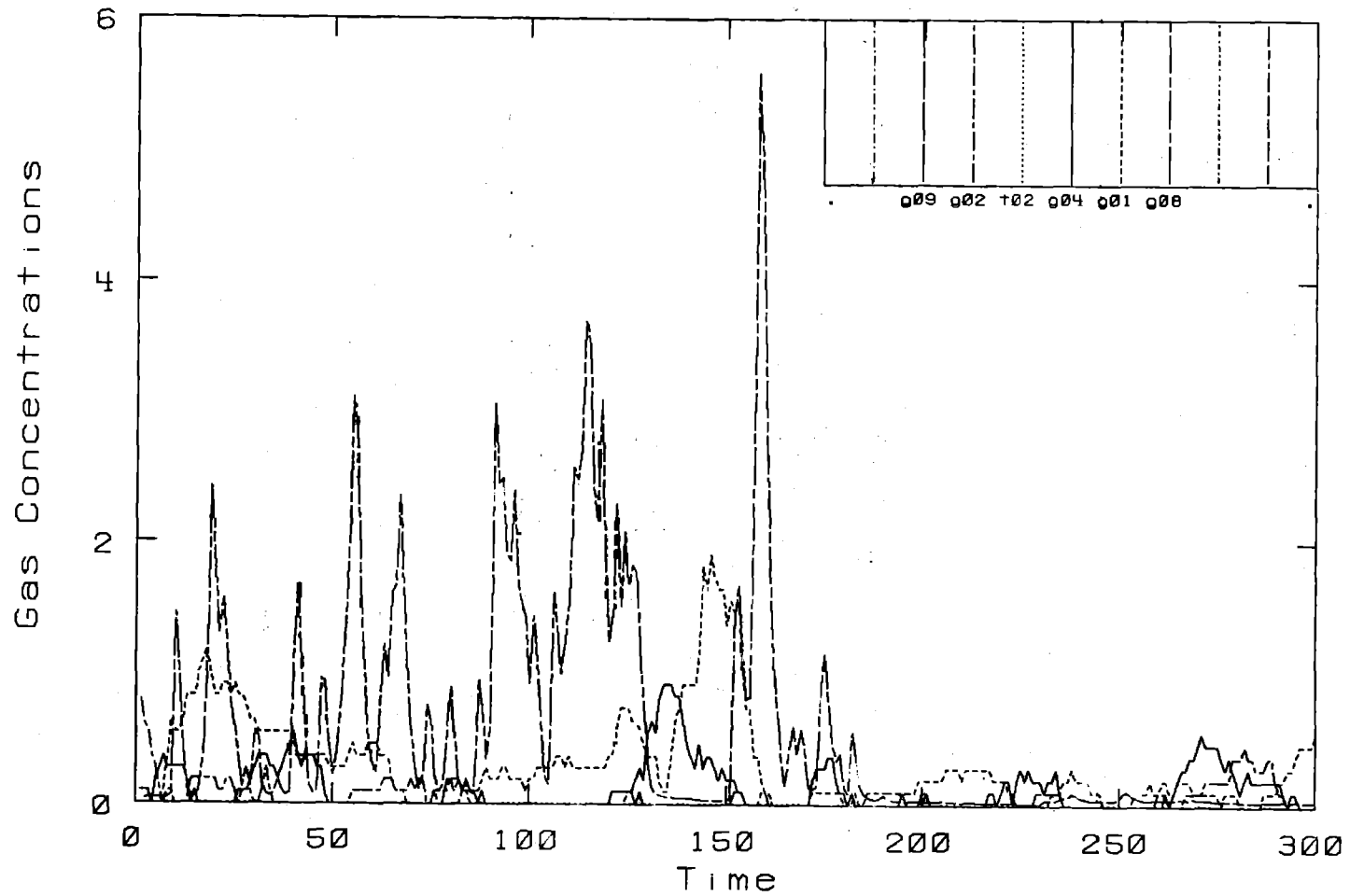
Burro 7. Row: 57 M. - Height: 1 M.

Burro Row Stations



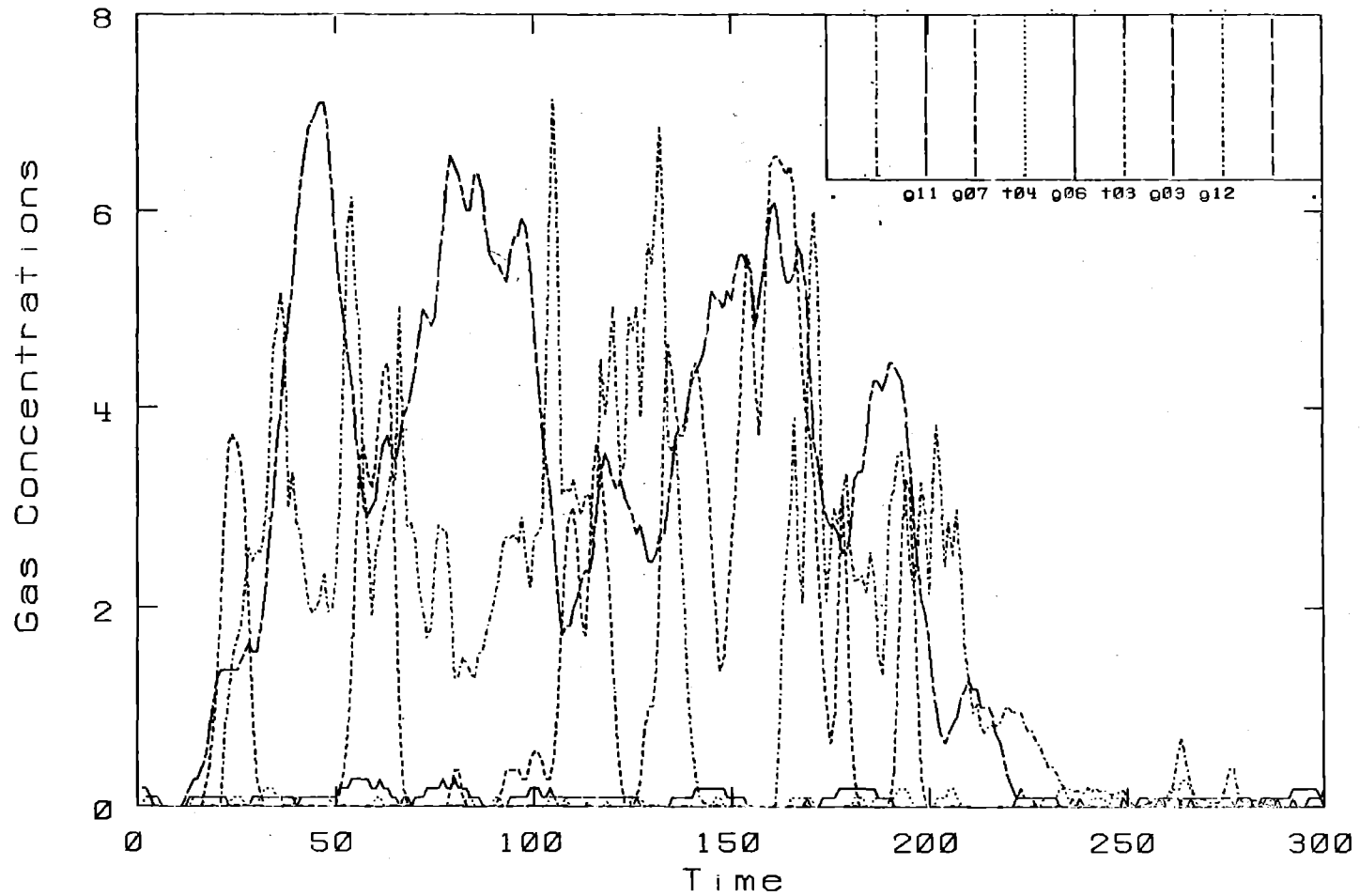
Burro 7. Row: 57 M. - Height: 3 M.

Burro Row Stations

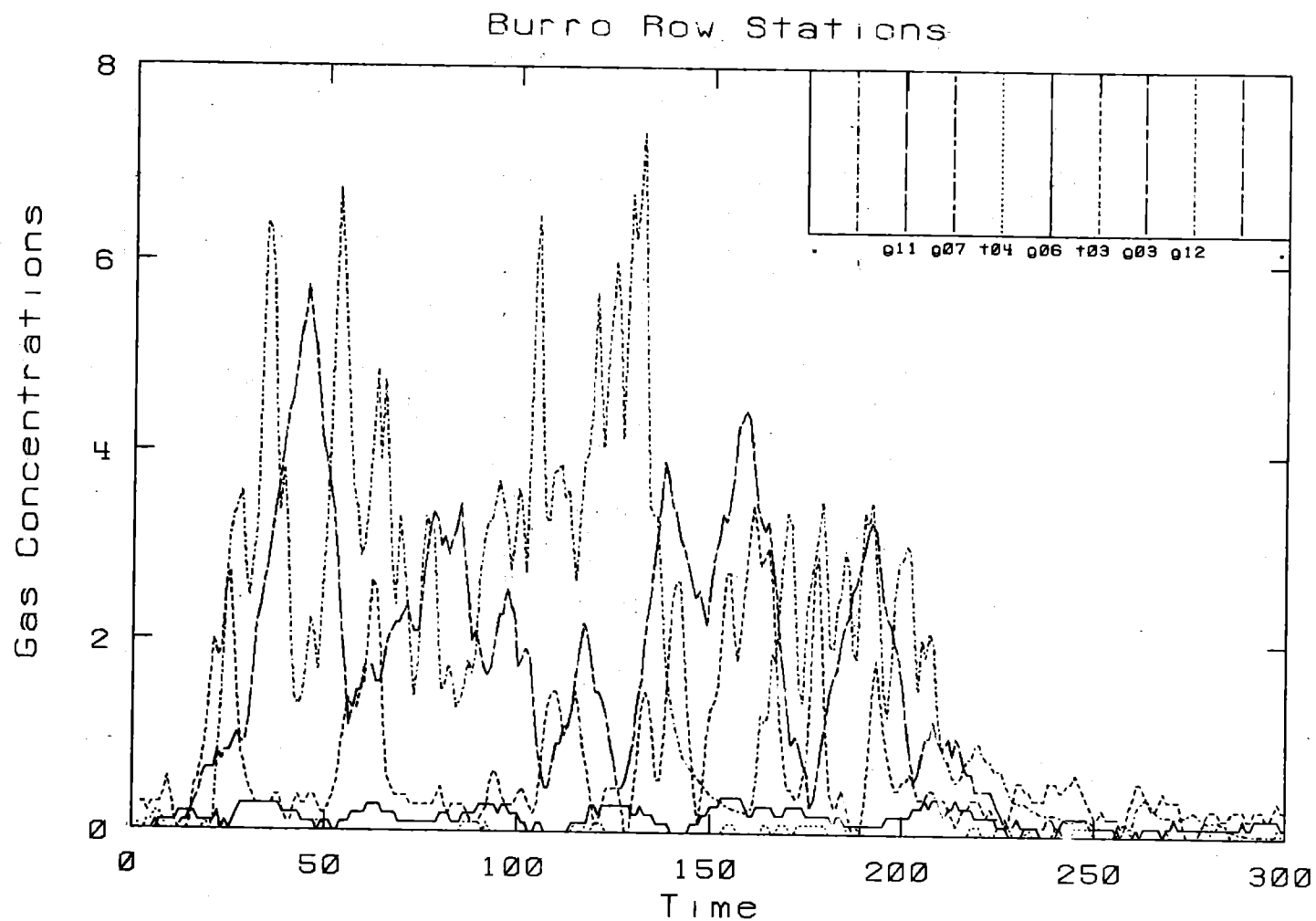


Burro 7. Row: 57 M. - Height: 8 M.

Burro Row Stations

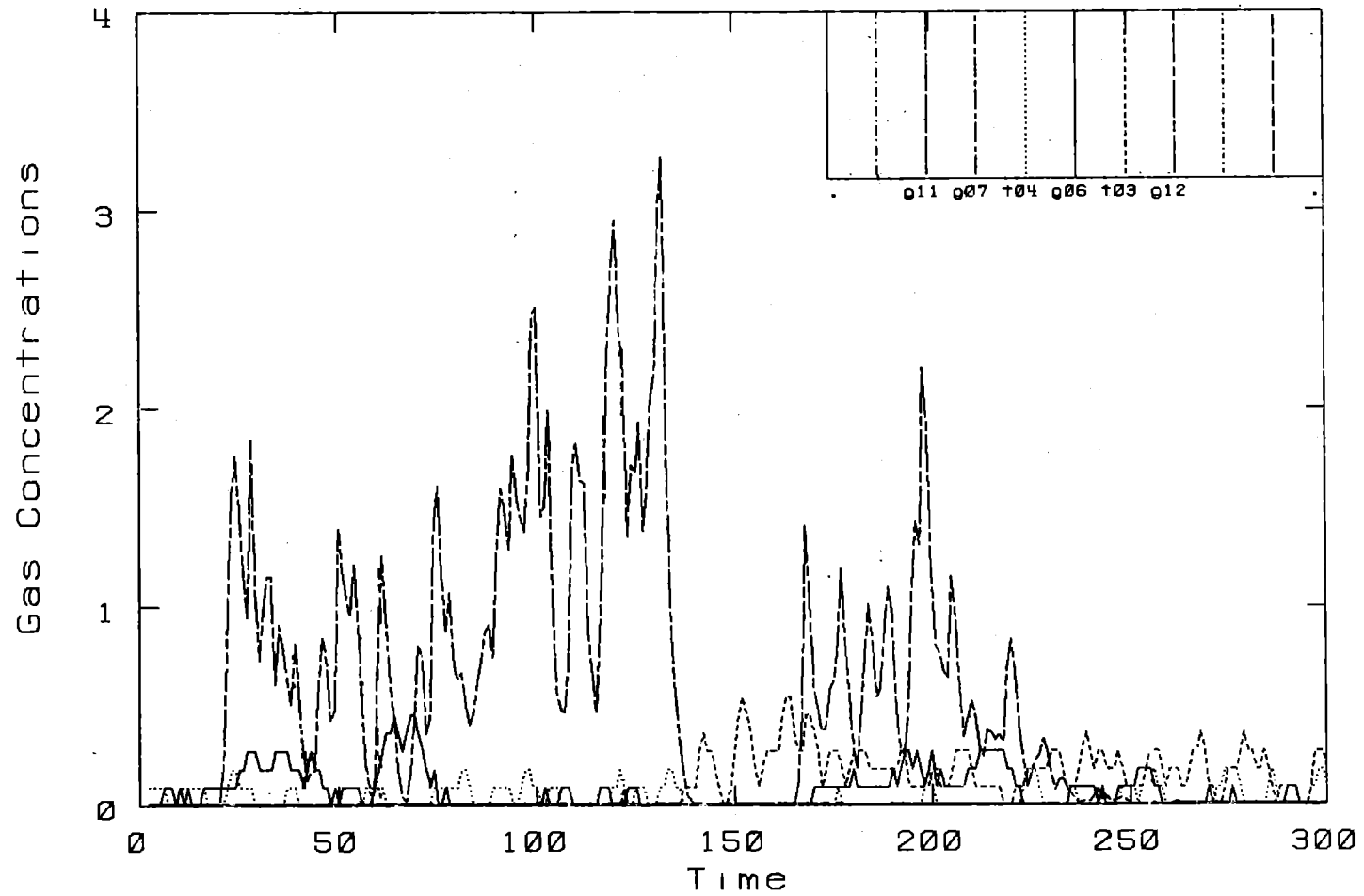


Burro 7. Row: 140 M.- Height: 1 M.

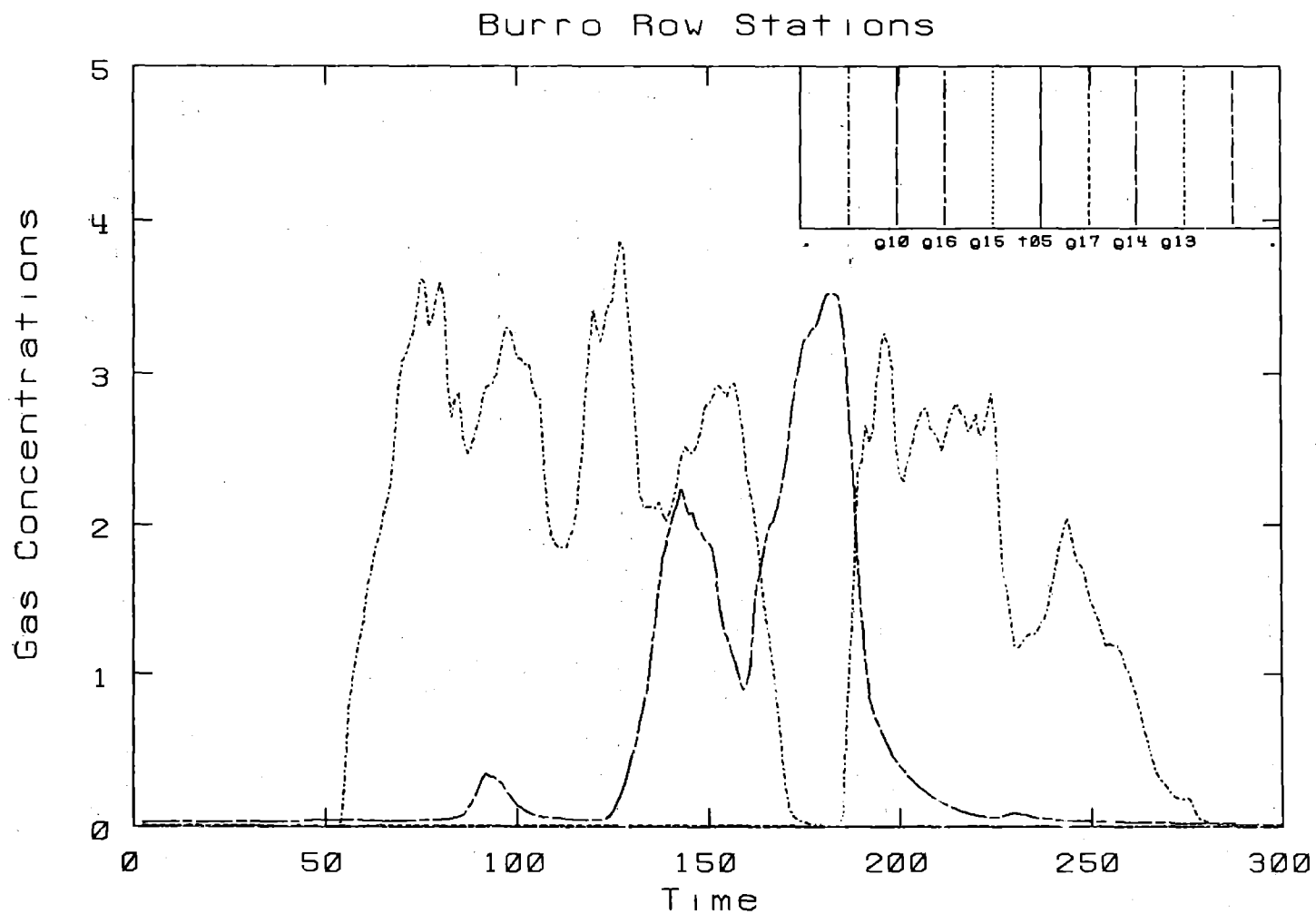


Burro 7. Row: 140 M. - Height: 3 M.

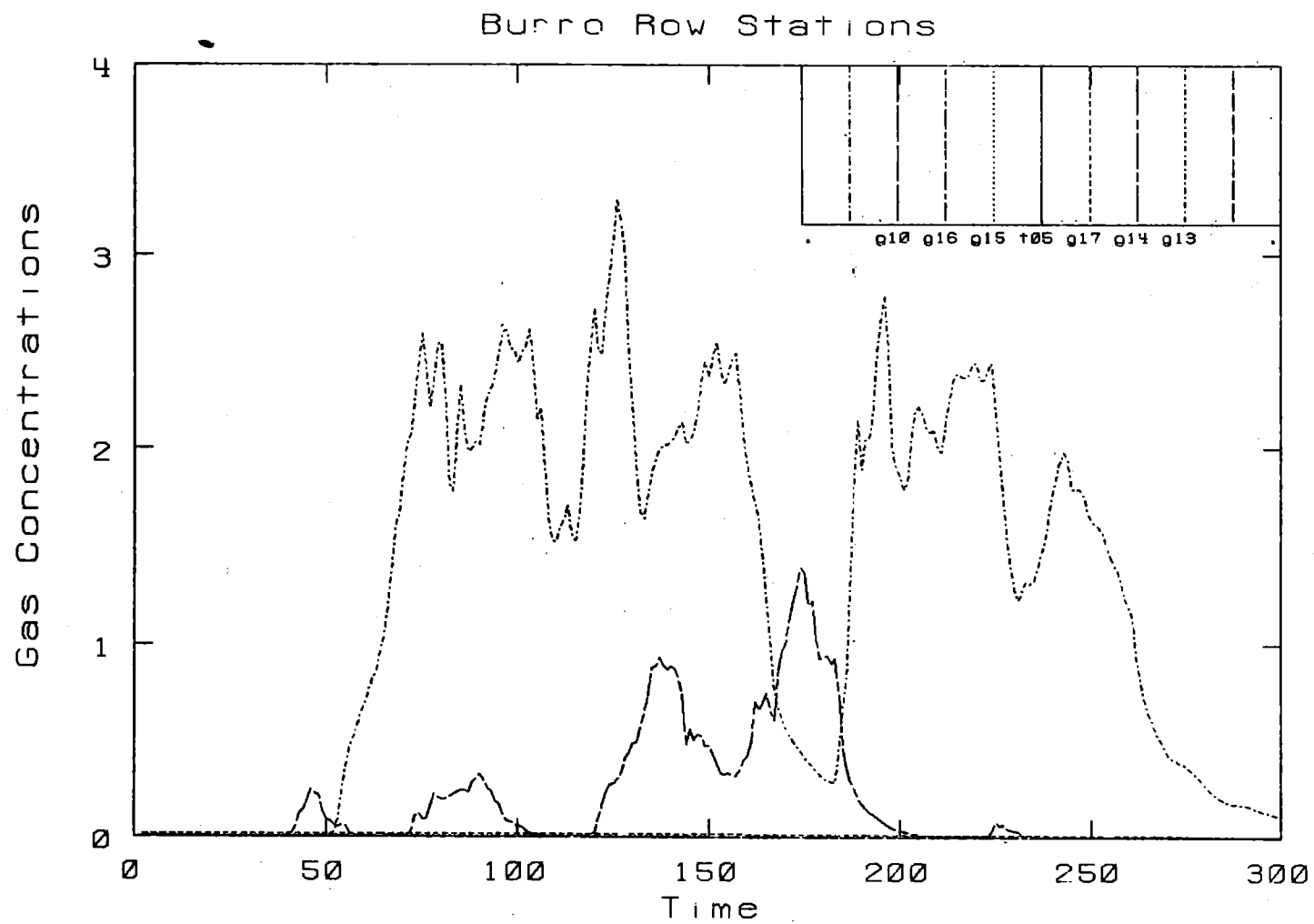
Burro Row Stations



Burro 7. Row: 140 M. - Height: 8 M.

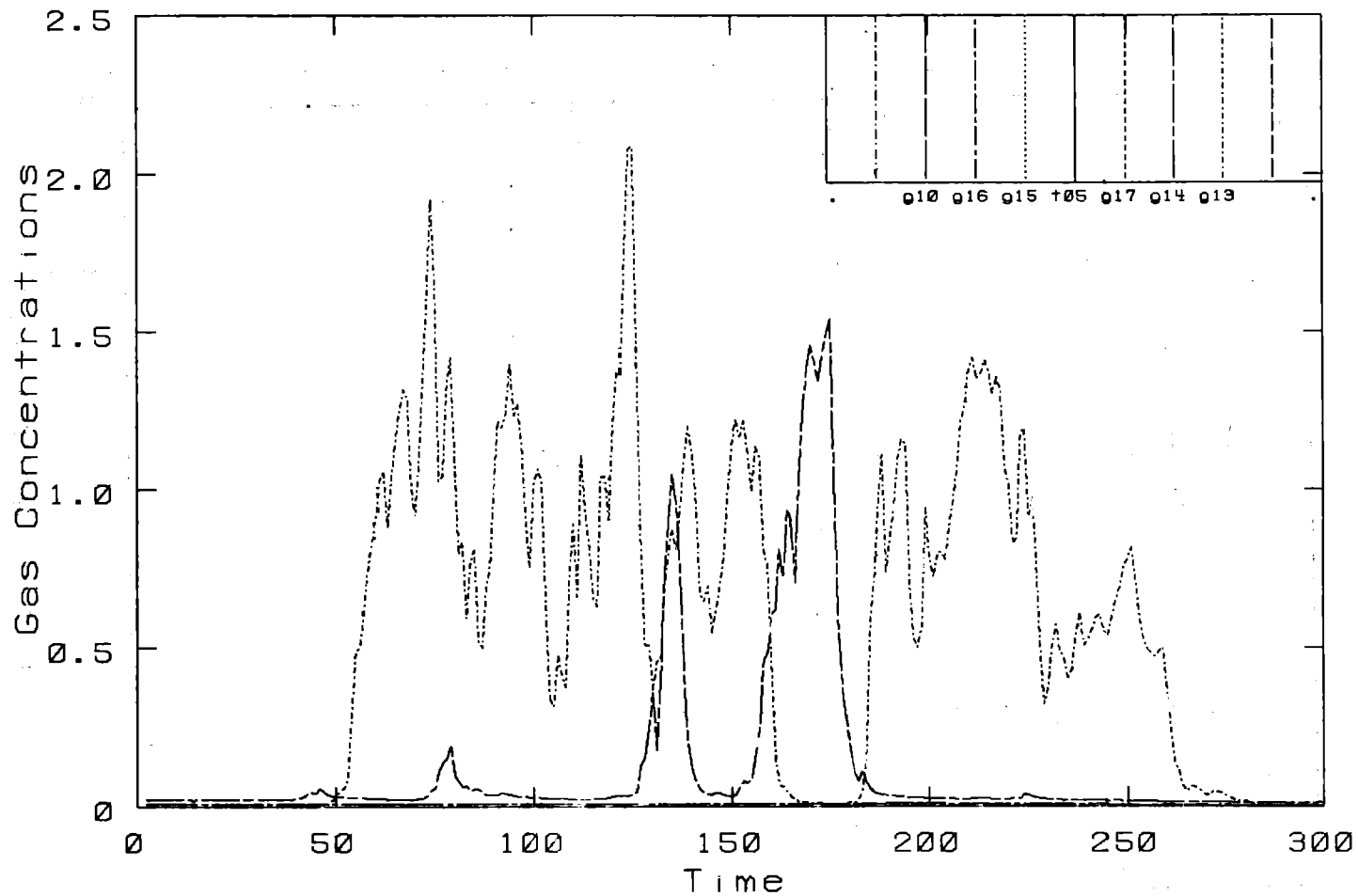


Burro 7. Row: 400 M.- Height: 1 M.



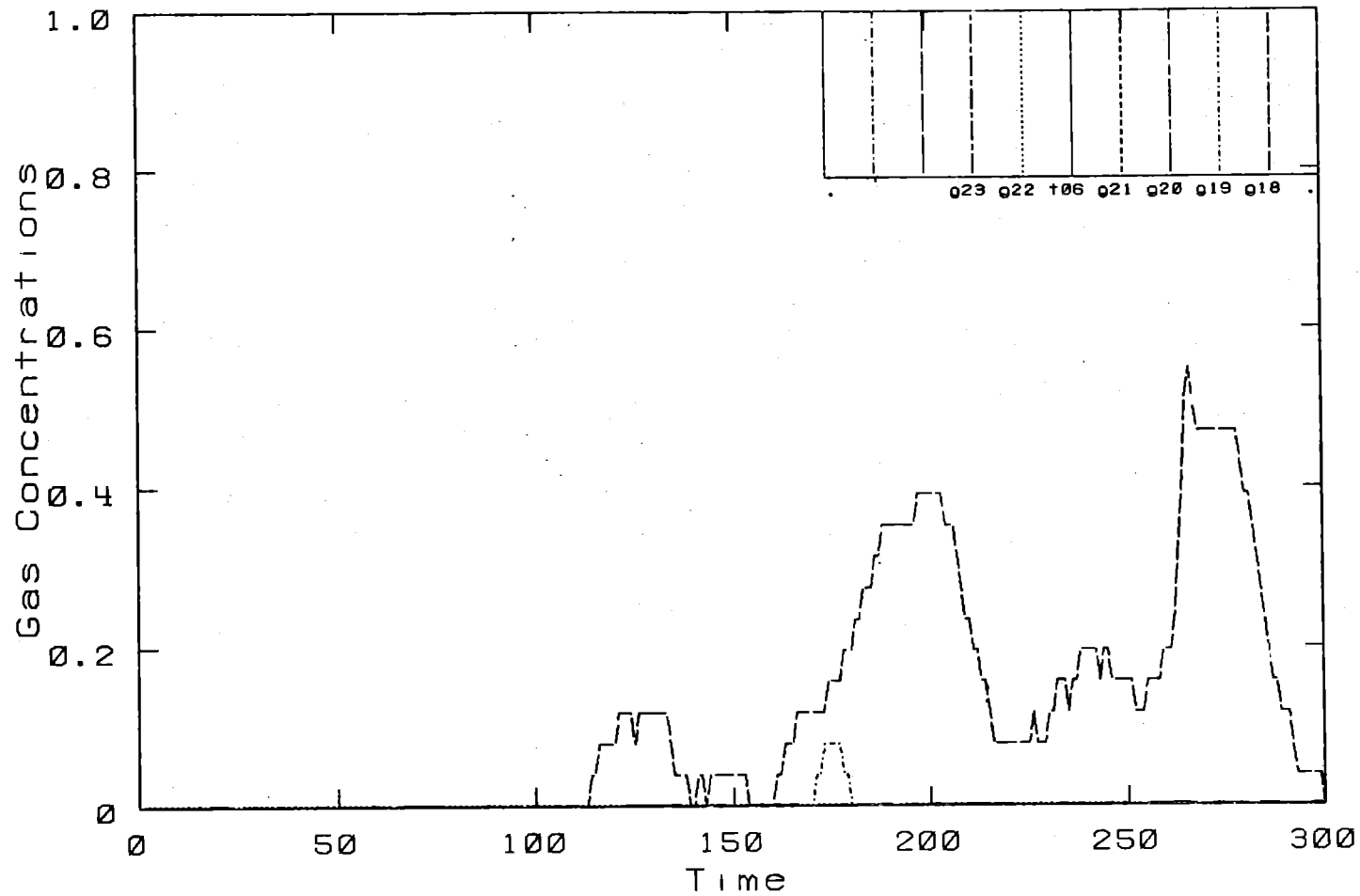
Burro 7. Row: 400 M. - Height: 3 M.

Burro Row Stations



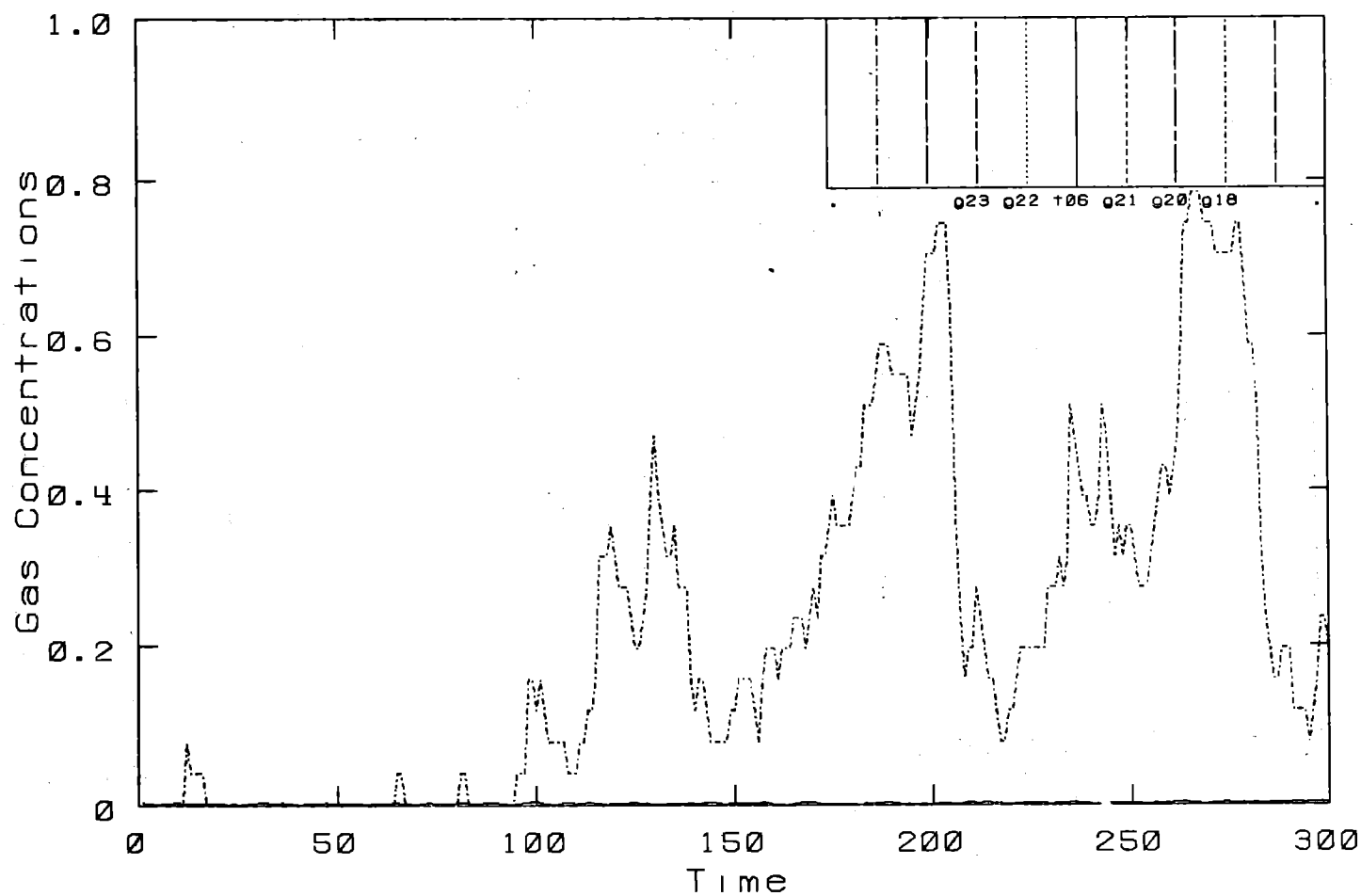
Burro 7. Row: 400 M. - Height: 8 M.

Burro Row Stations



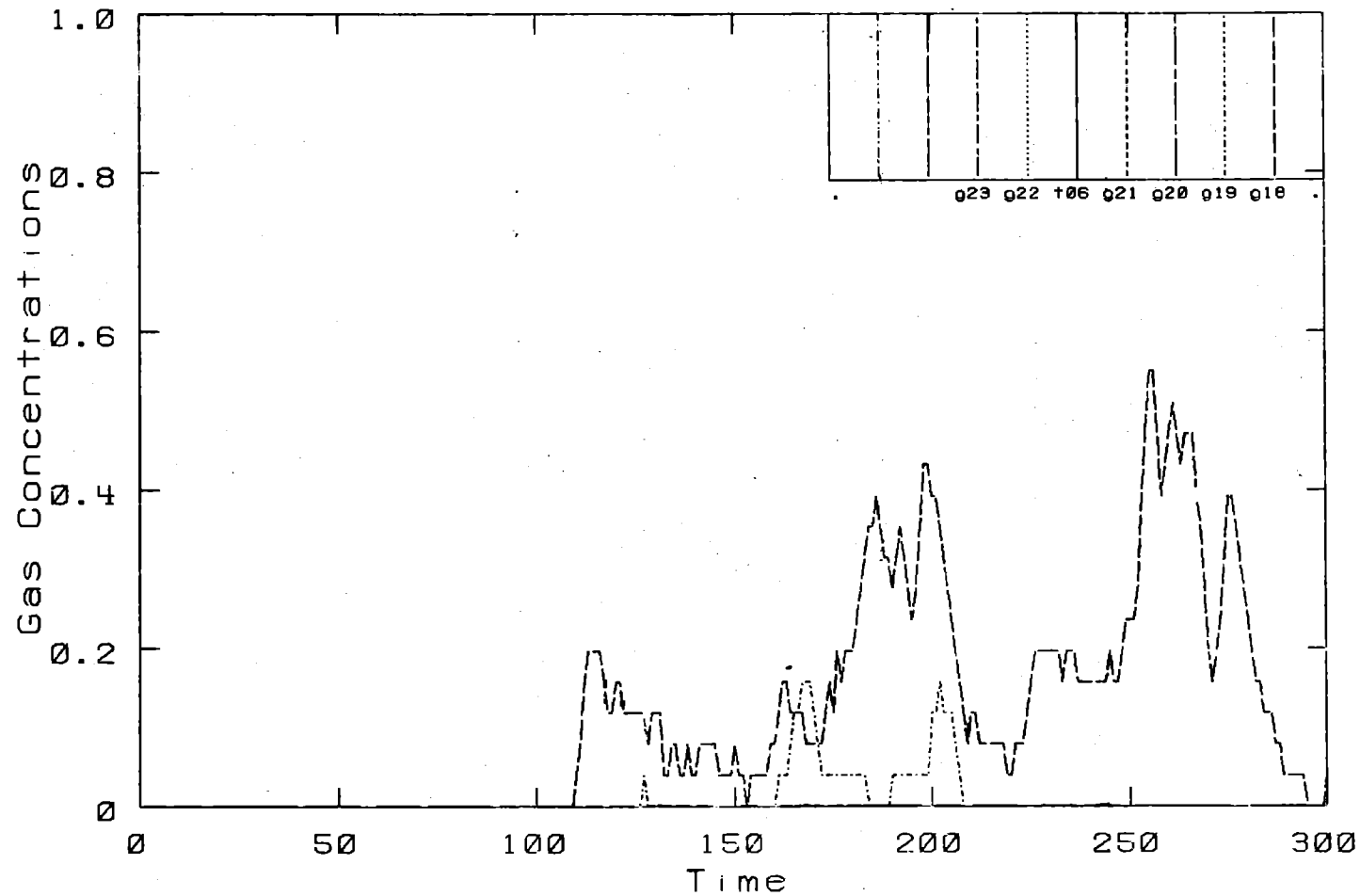
Burro 7. Row: 800 M.- Height: 1 M.

Burro Row Stations



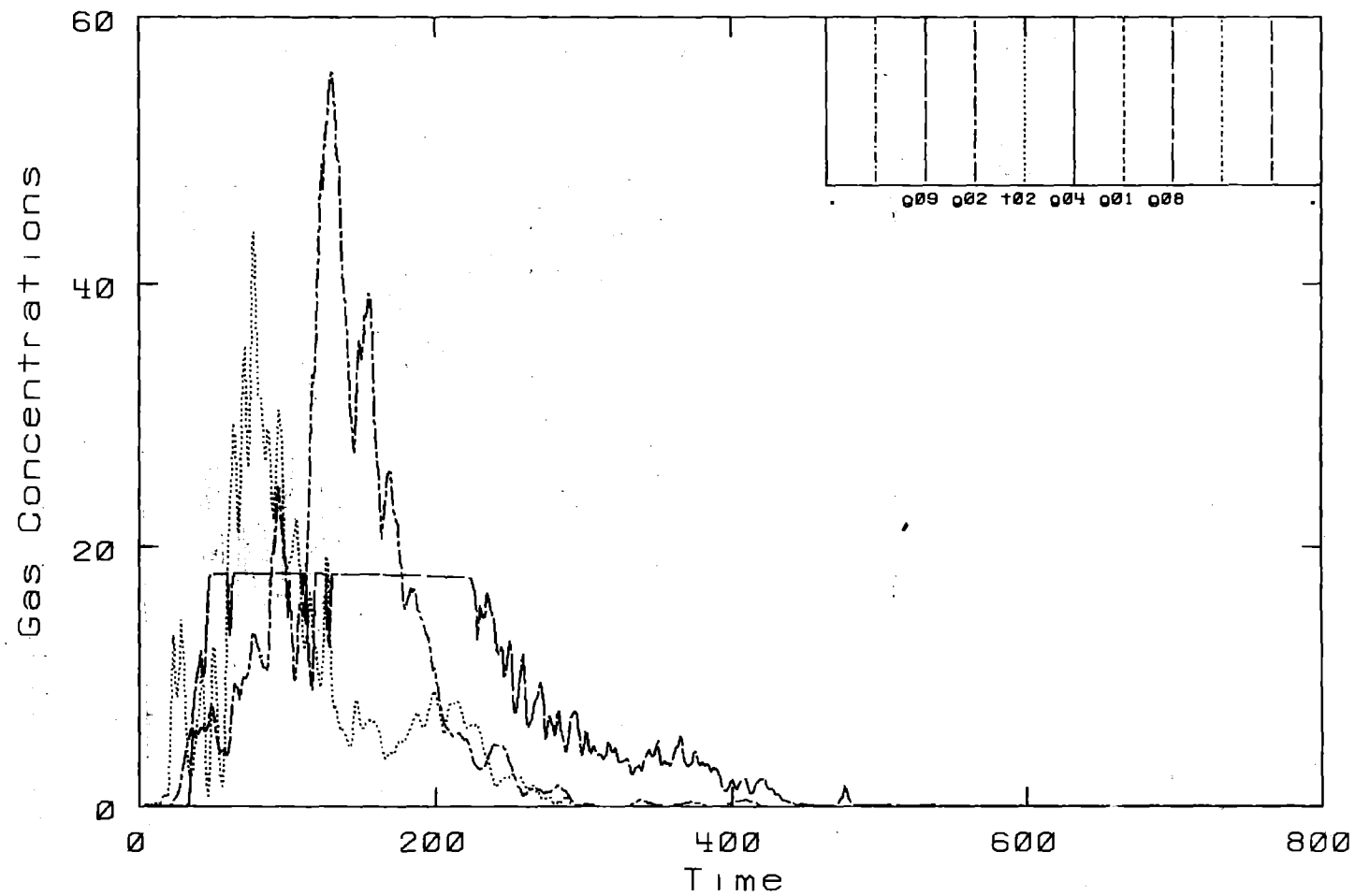
Burro 7. Row: 800 M. - Height: 3 M.

Burro Row Stations



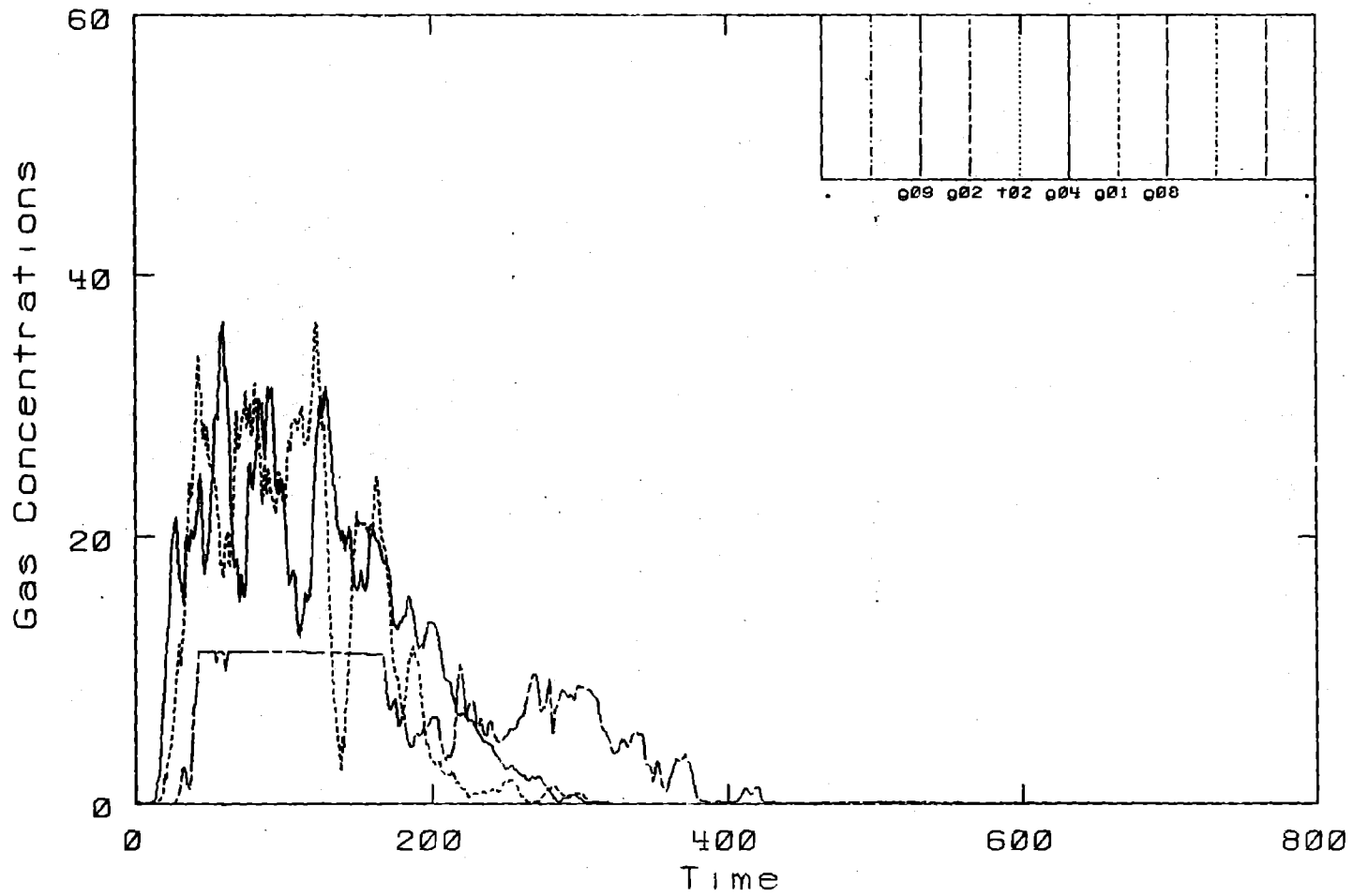
Burro 7. Row: 800 M.- Height: 8 M.

Burro Row Stations



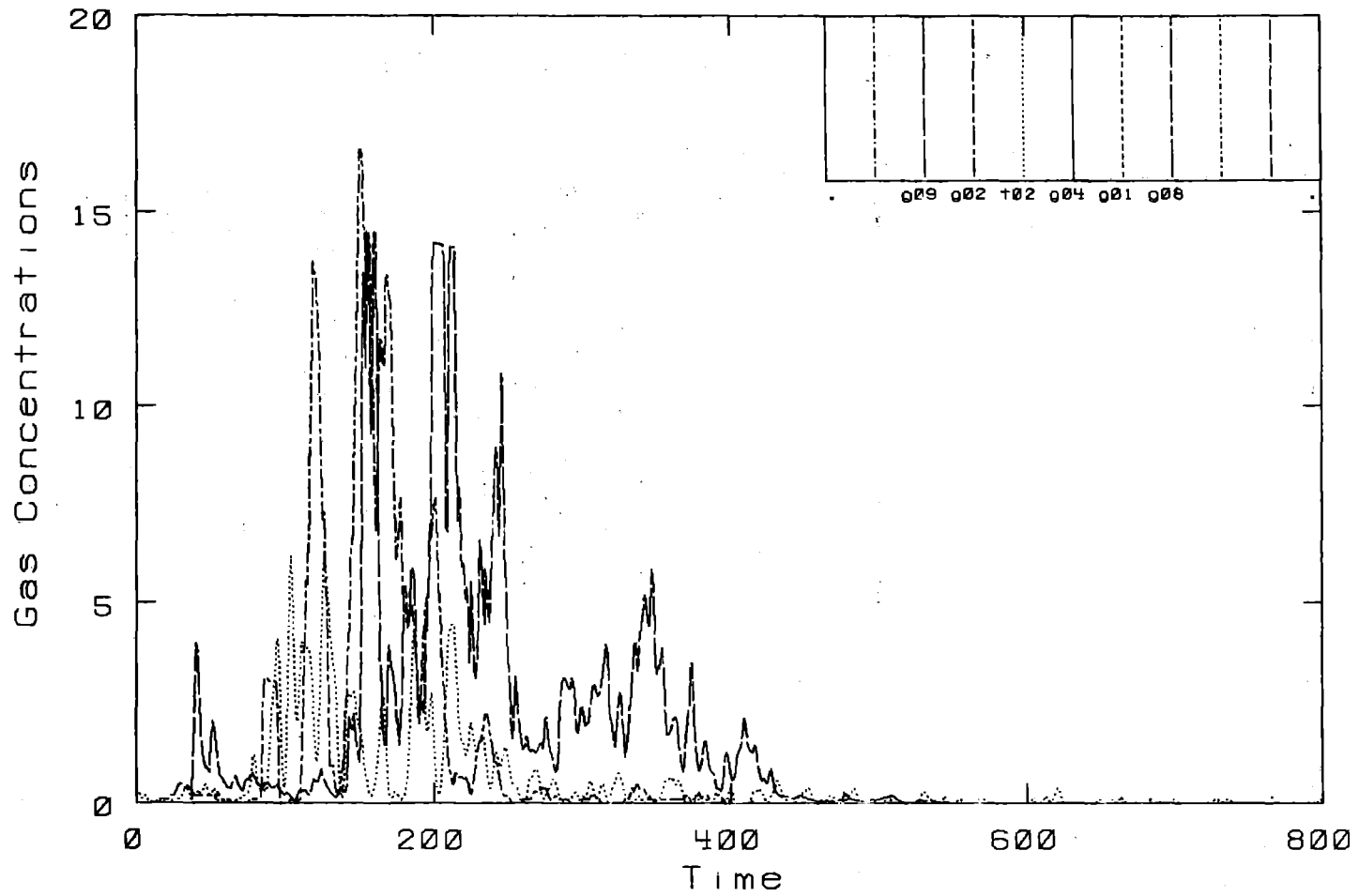
Burro 8. Row: 57 M. - Height: 1 M.

Burro Row Stations

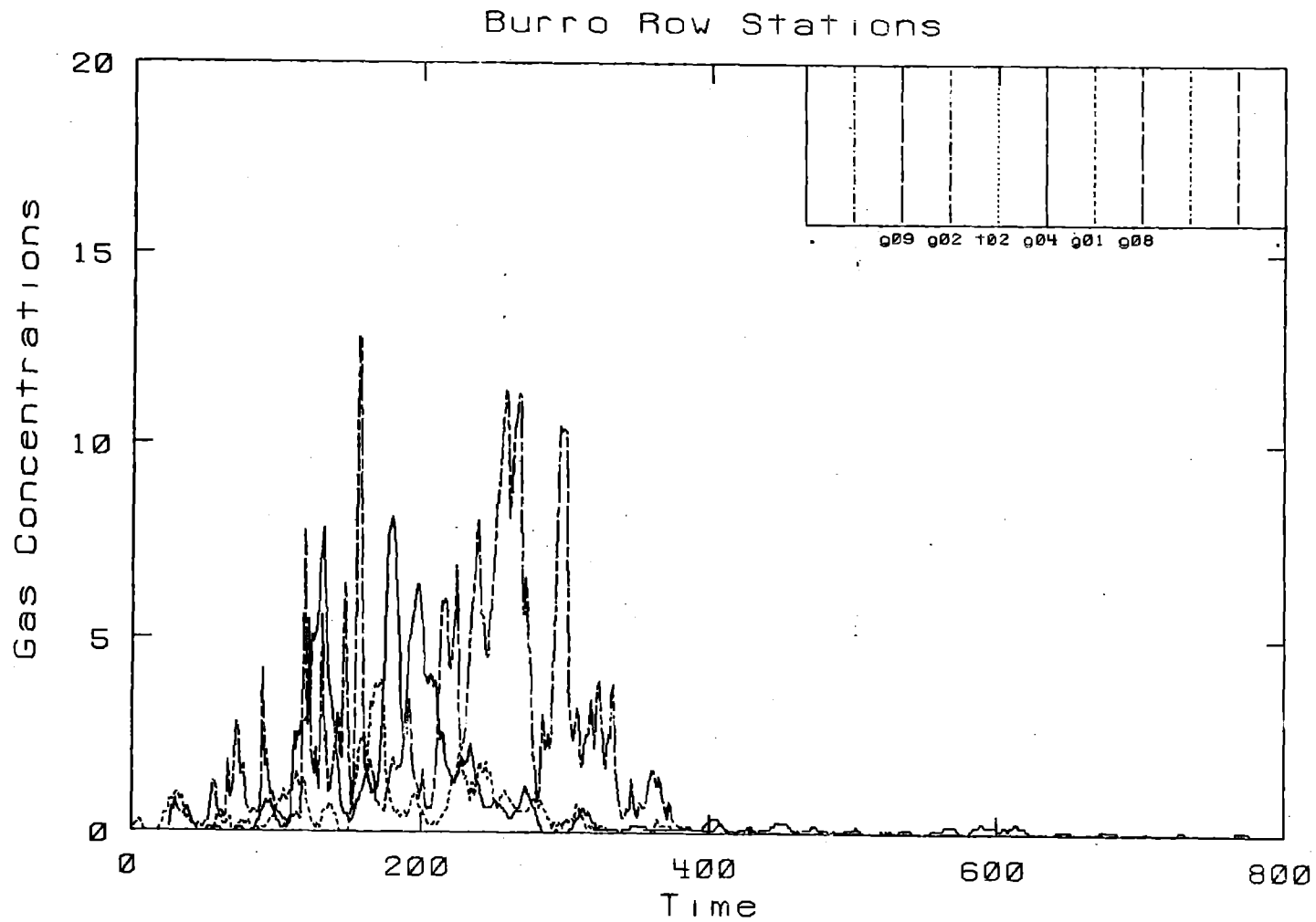


Burro 8. Row: 57 M. - Height: 1 M.

Burro Row Stations

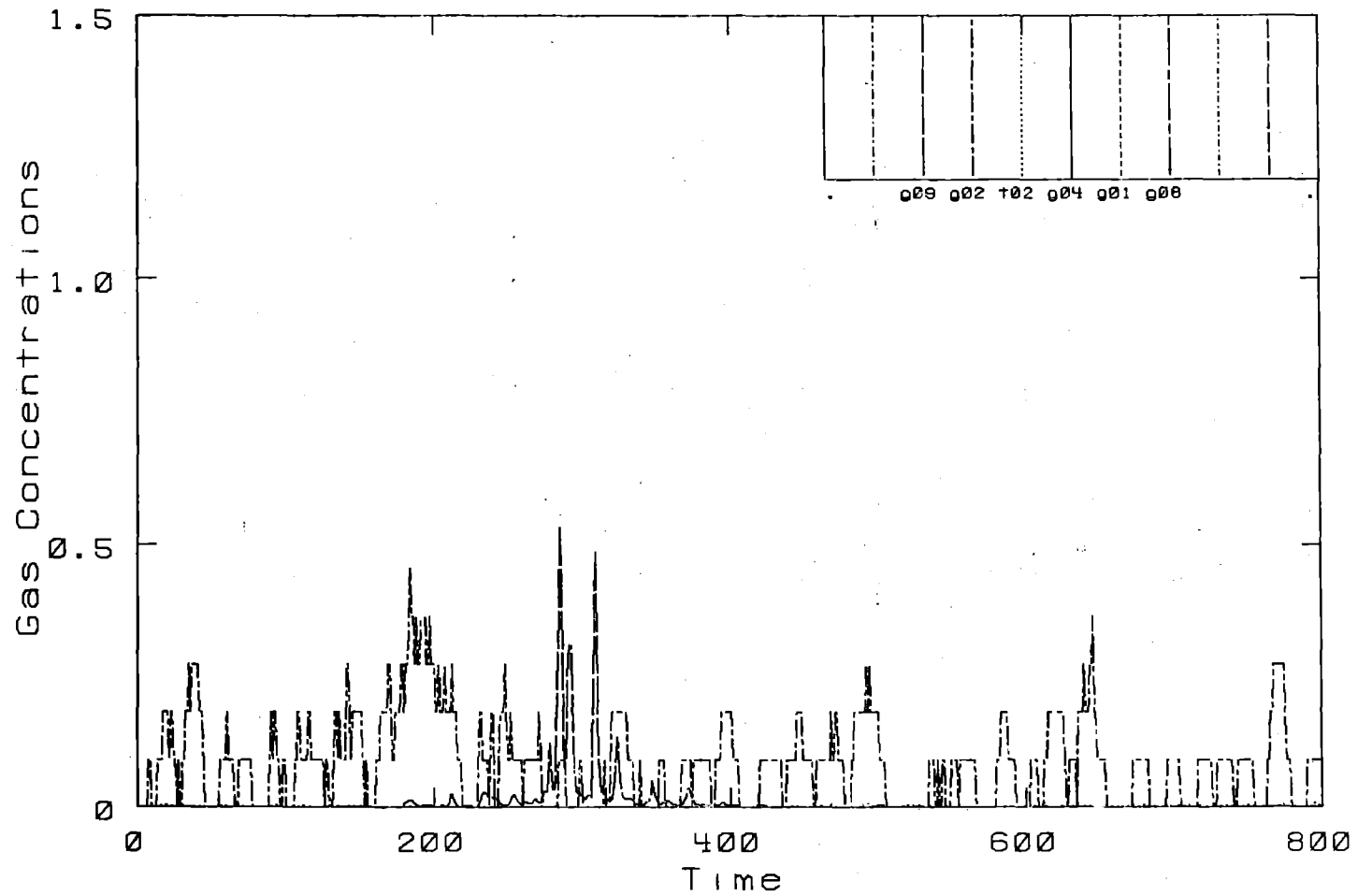


Burro 8. Row: 57 M. - Height: 3 M.



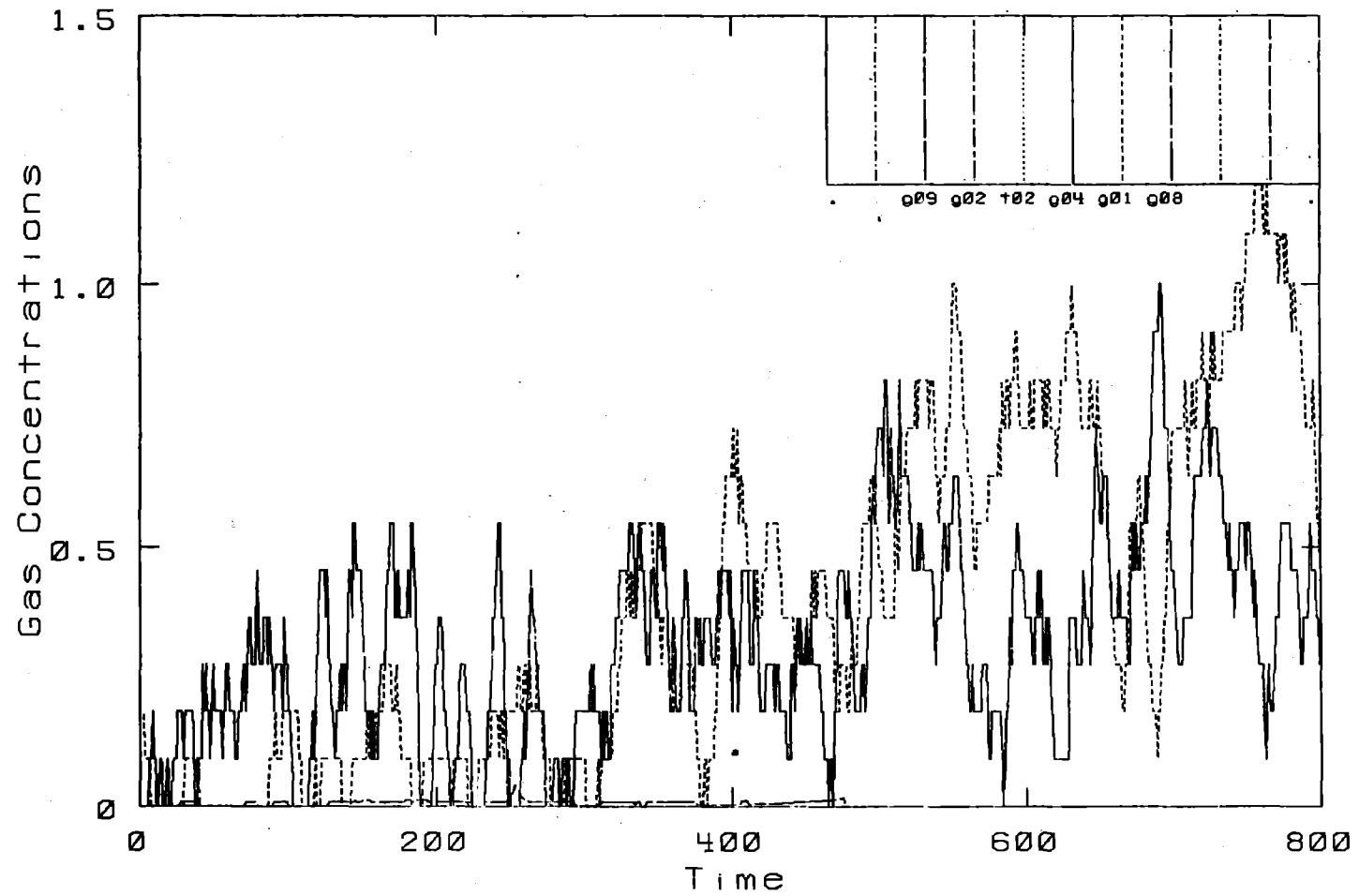
Burro 8. Row: 57 M. - Height: 3 M.

Burro Row Stations



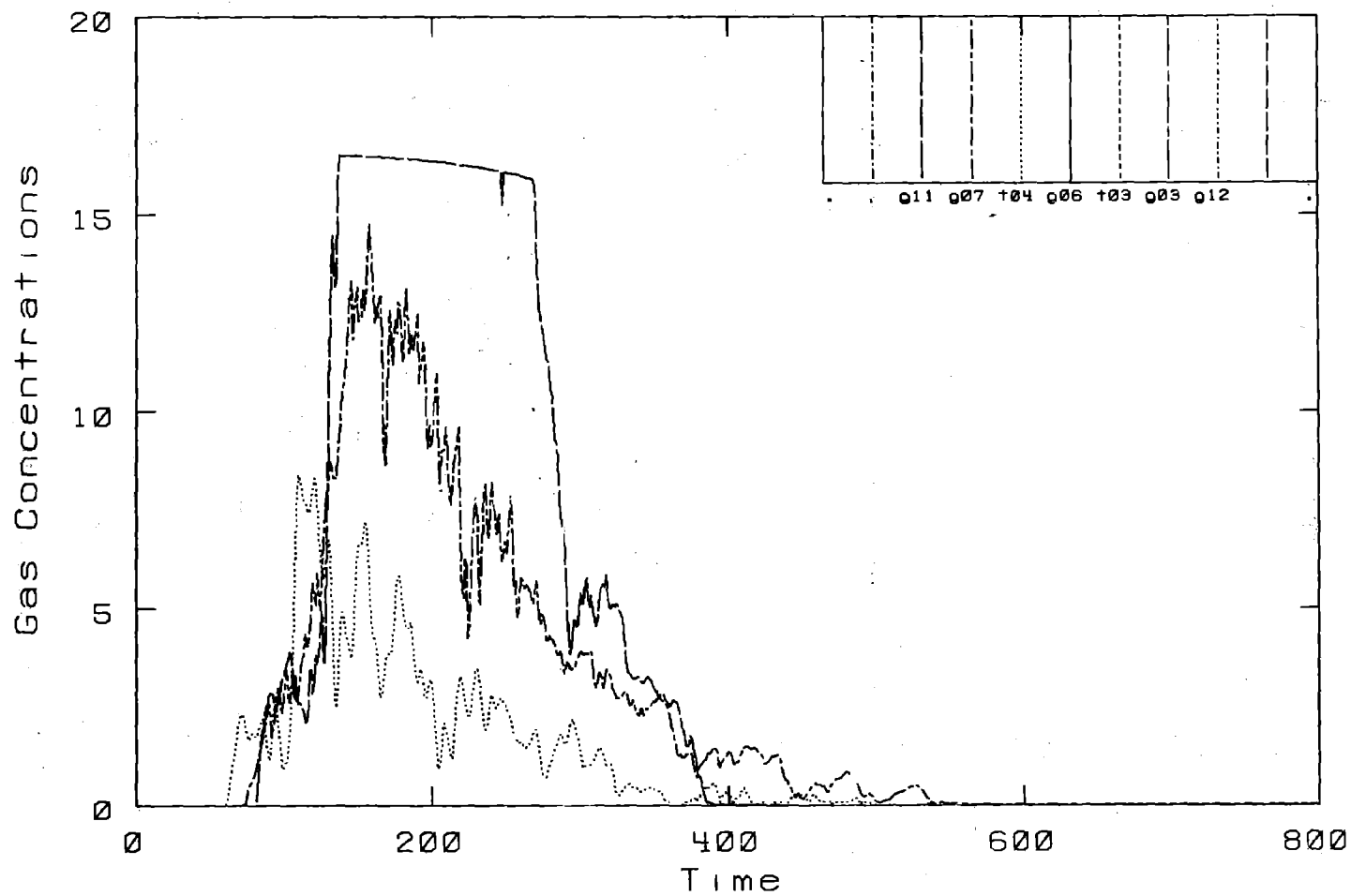
Burro 8. Row: 57 M. - Height: 8 M.

Burro Row Stations



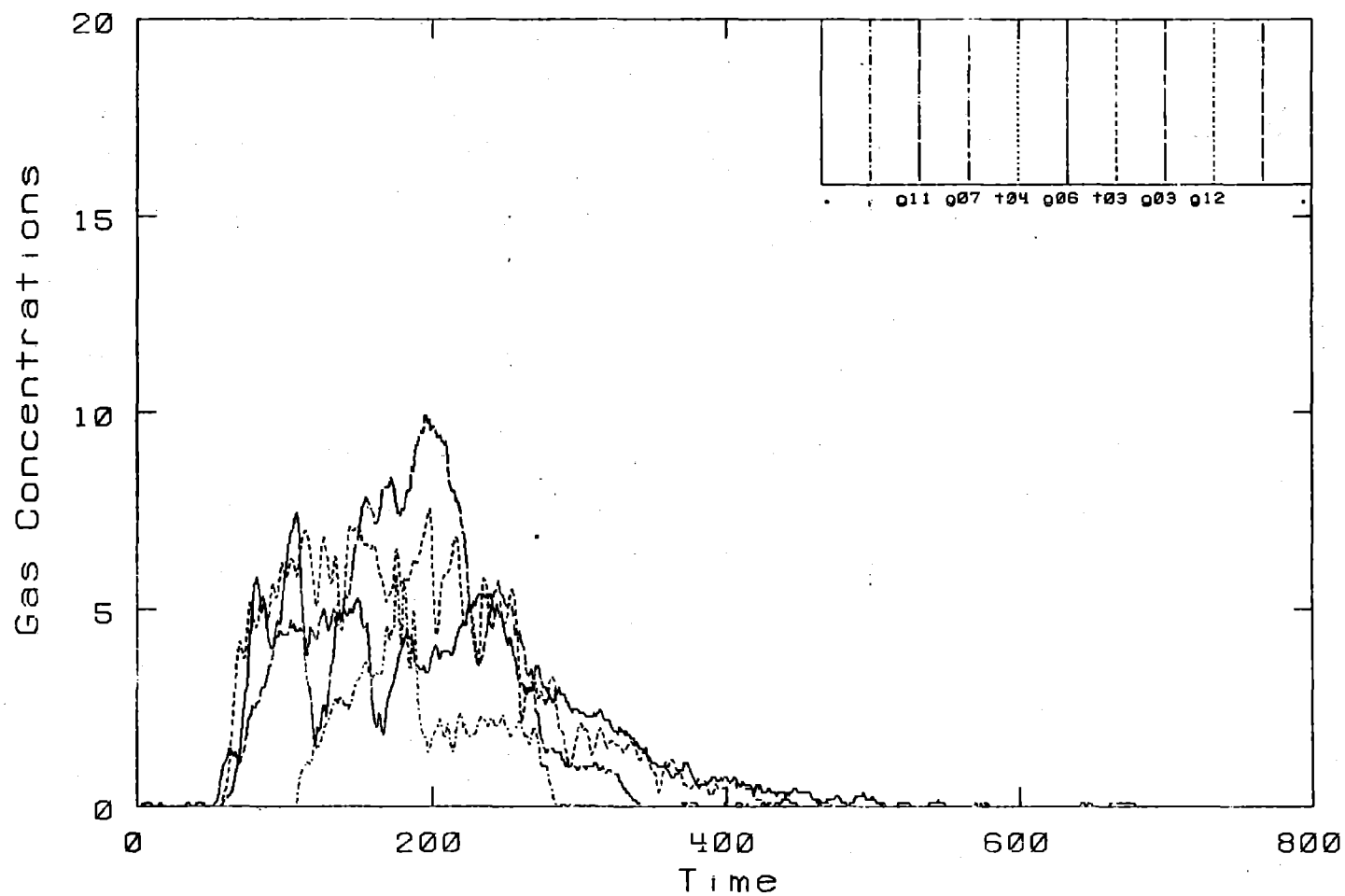
Burro 8. Row: 57 M. - Height: 8 M.

Burro Row Stations

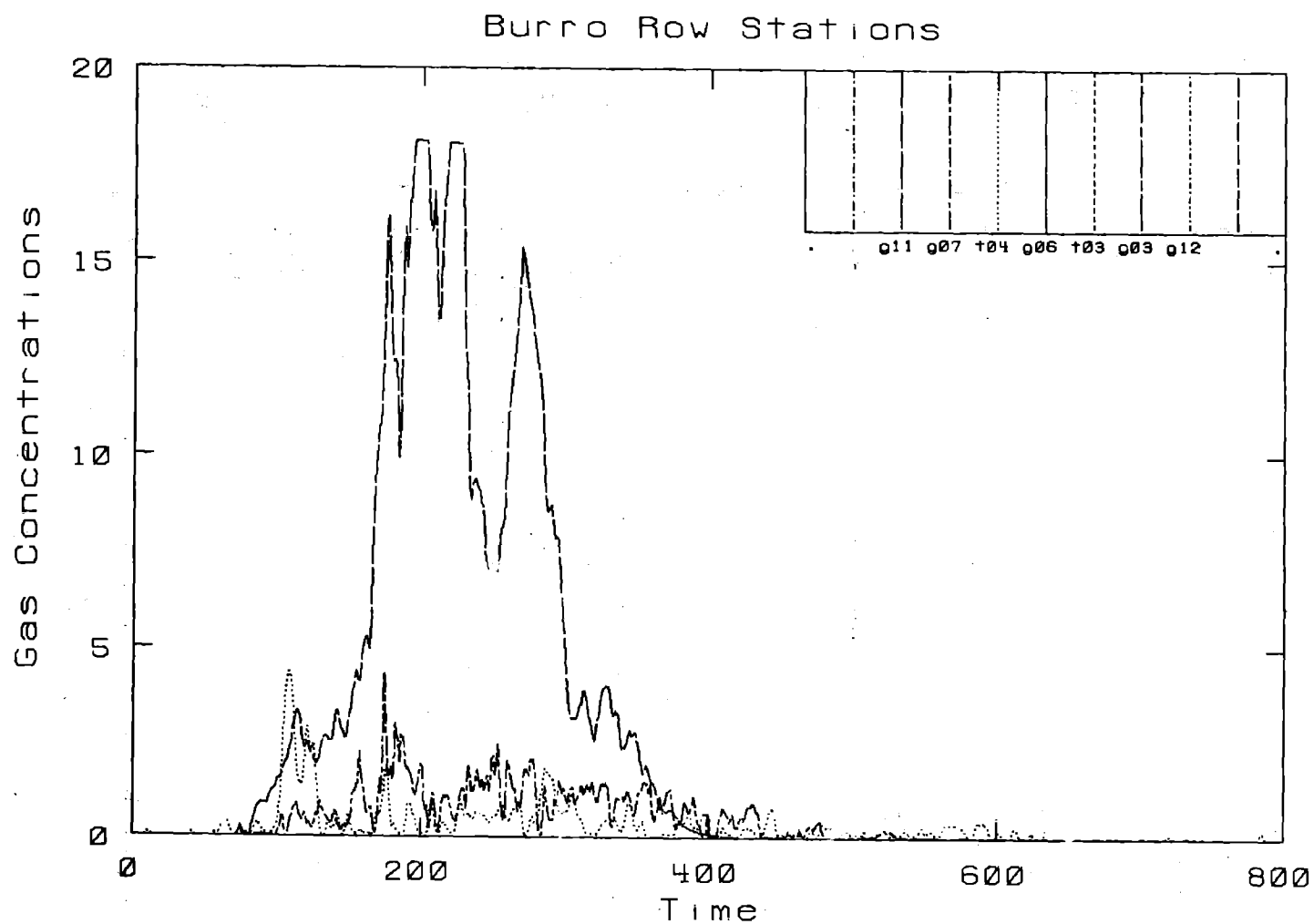


Burro 8. Row: 140 M. - Height: 1 M.

Burro Row Stations

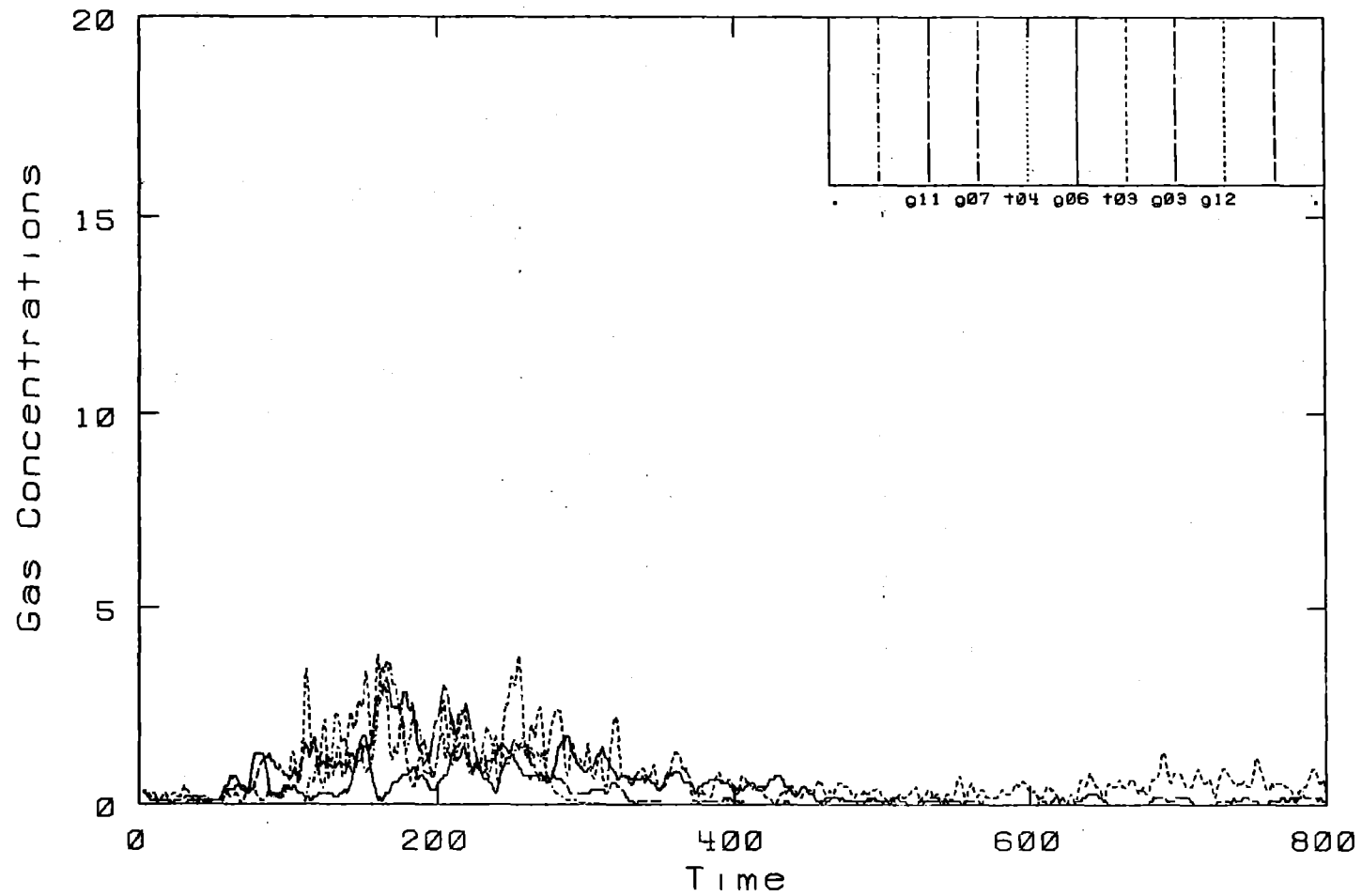


Burro 8. Row: 140 M. - Height: 1 M.



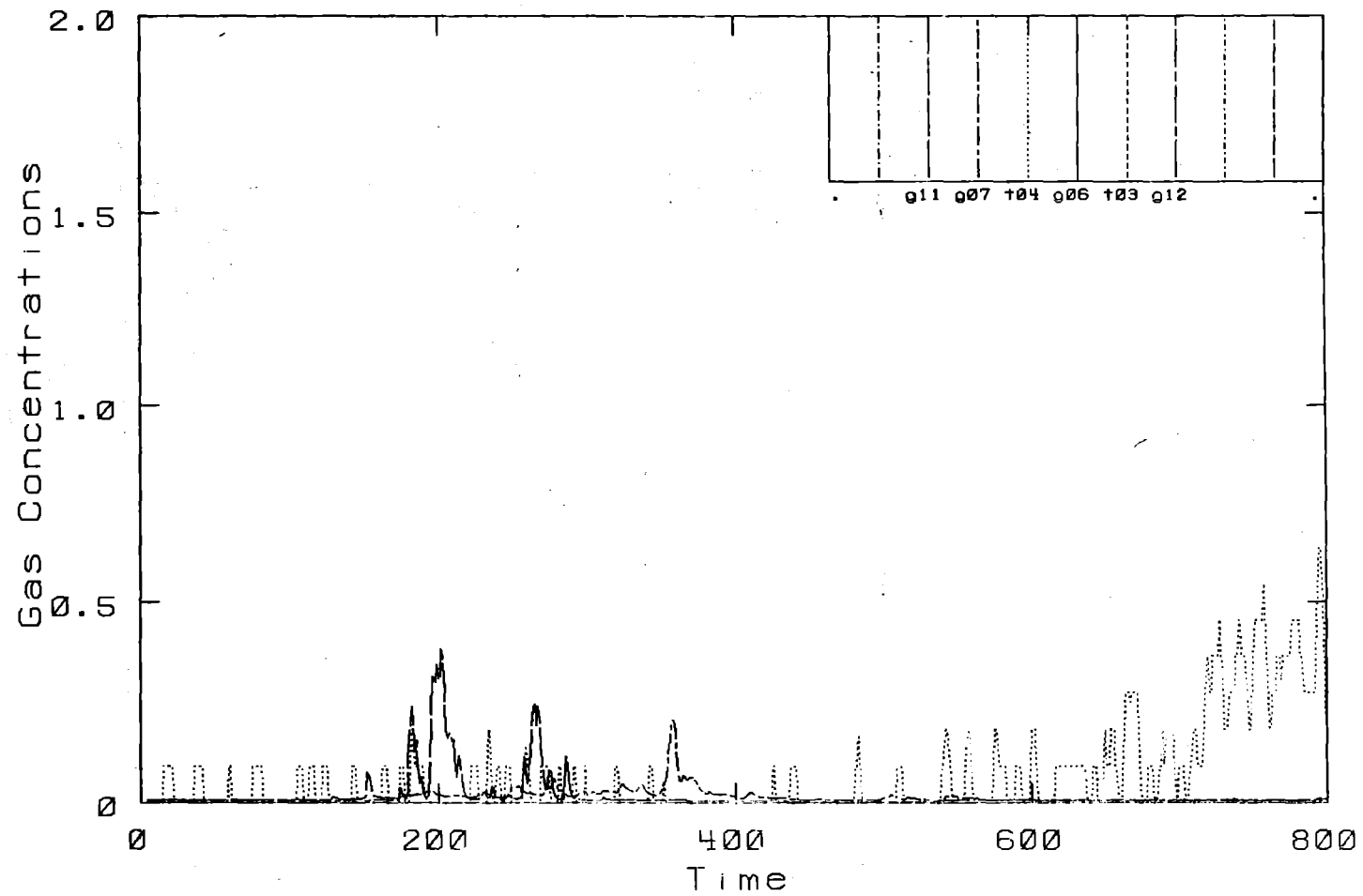
Burro 8. Row: 140 M. - Height: 3 M.

Burro Row Stations



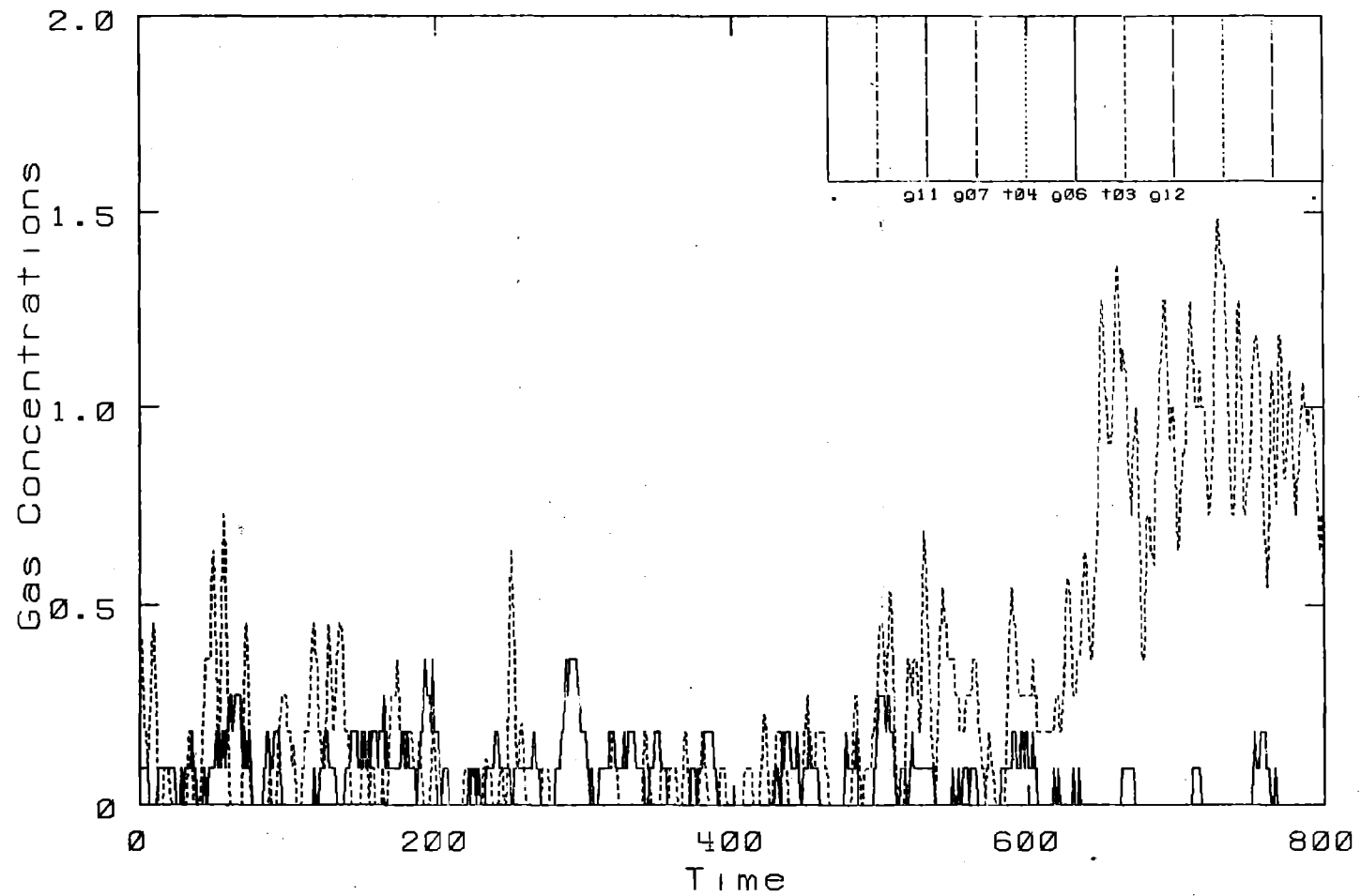
Burro 8. Row: 140 M.- Height: 3 M.

Burro Row Stations



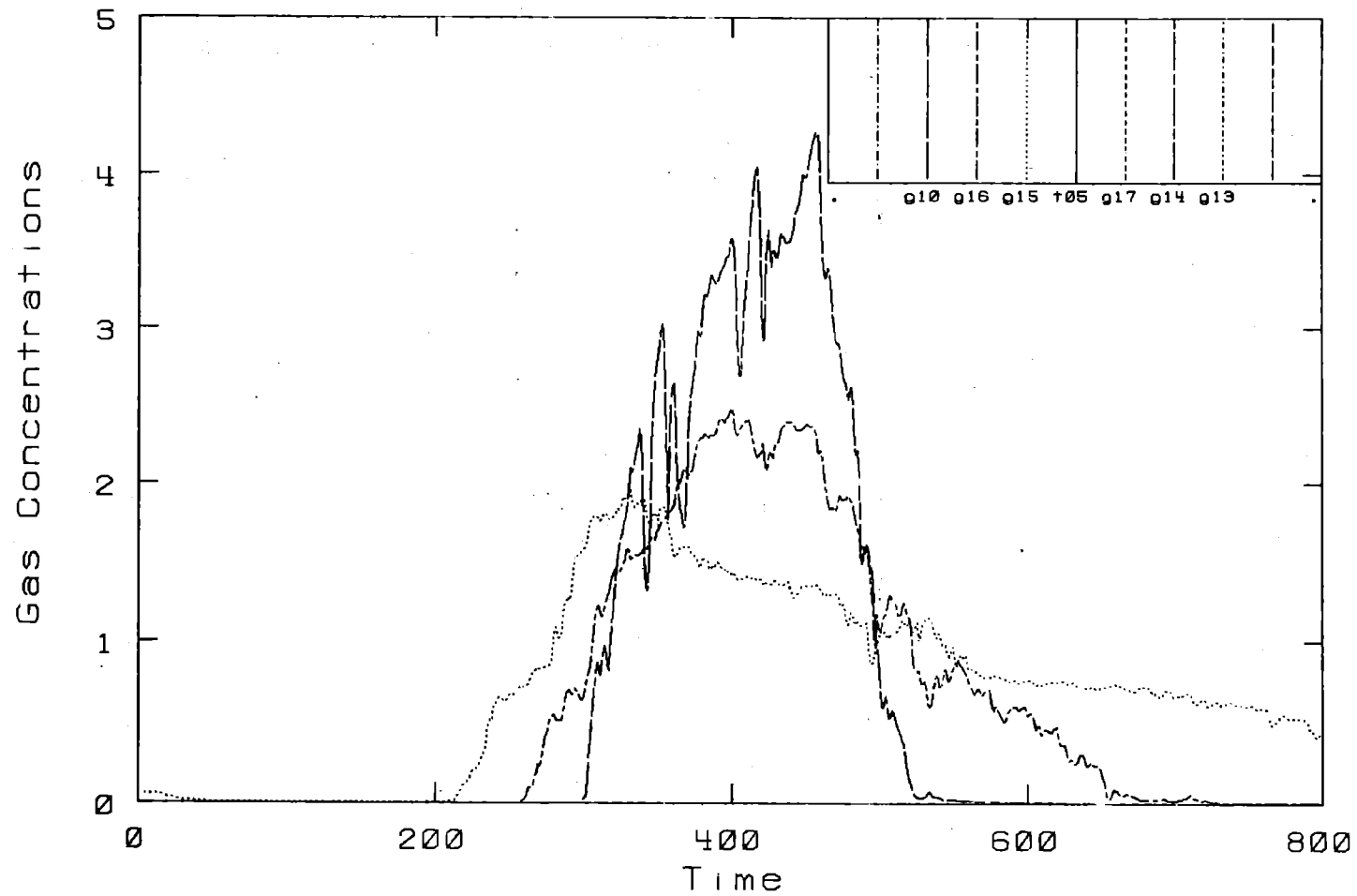
Burro 8. Row: 140 M. - Height: 8 M.

Burro Row Stations

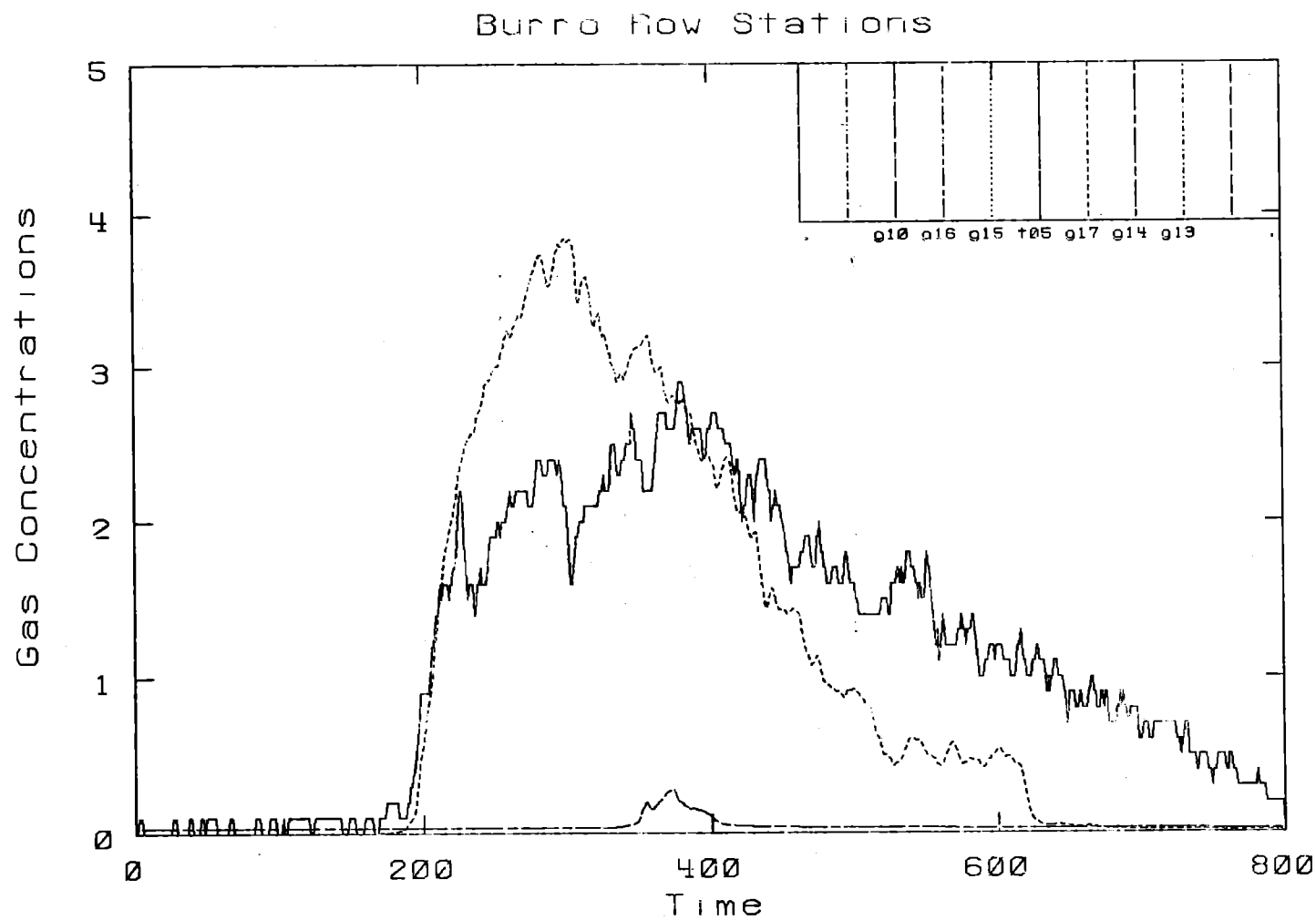


Burro 8. Row: 140 M. - Height: 8 M.

Burro Row Stations

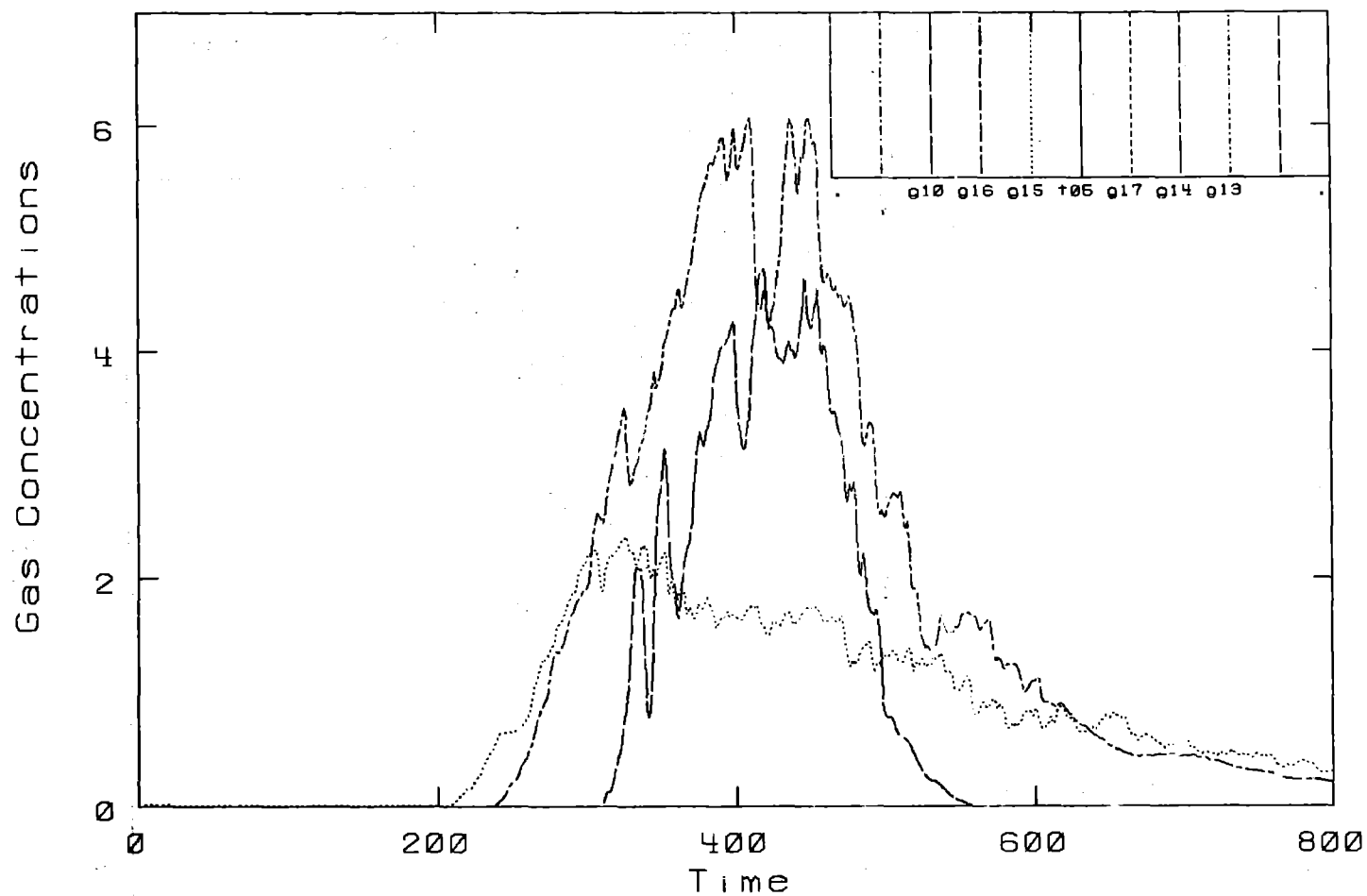


Burro 8. Row: 400 M. - Height: 1 M.



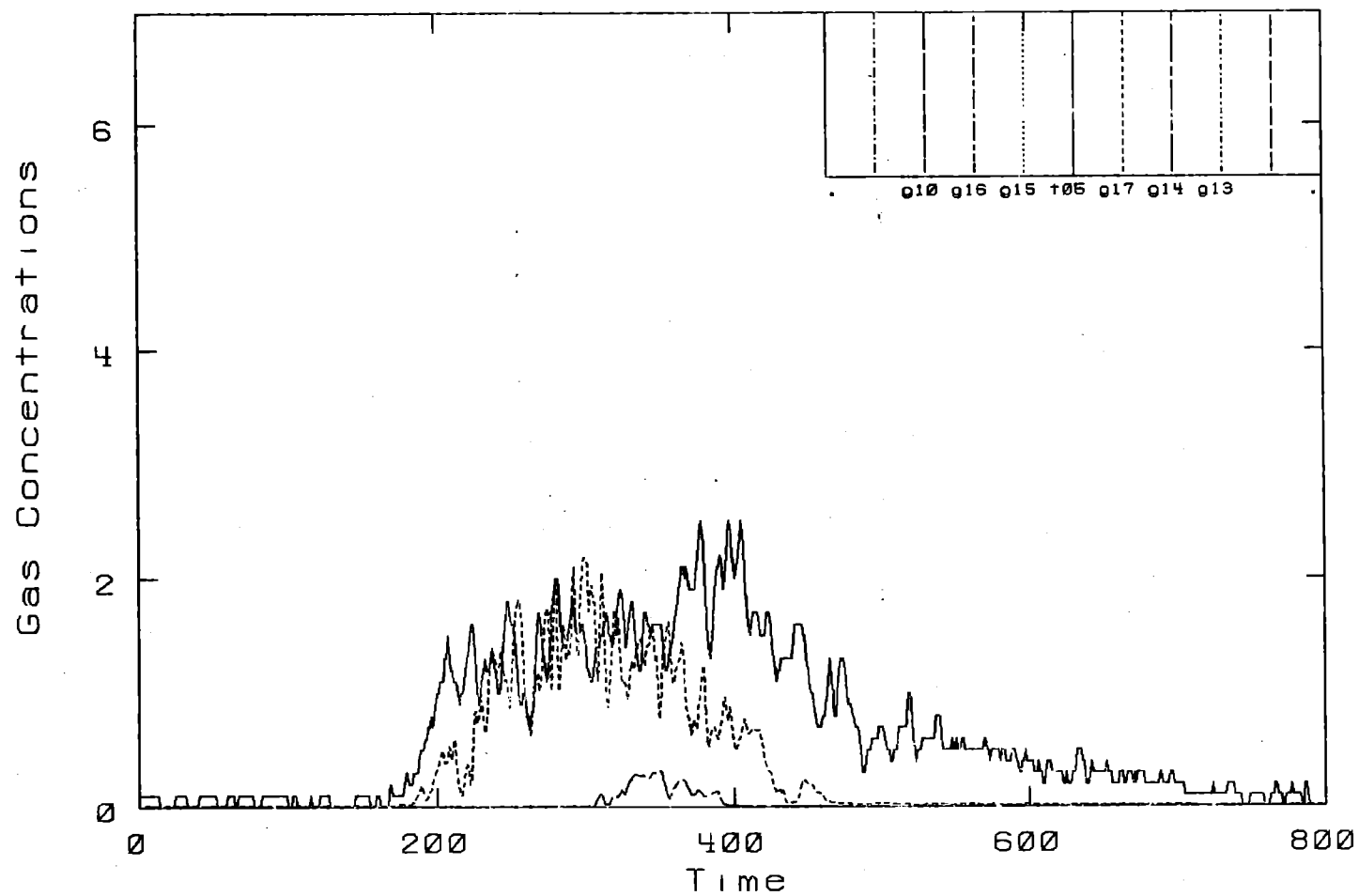
Burro 8. Row: 400 M. - Height: 1 M.

Burro Row Stations



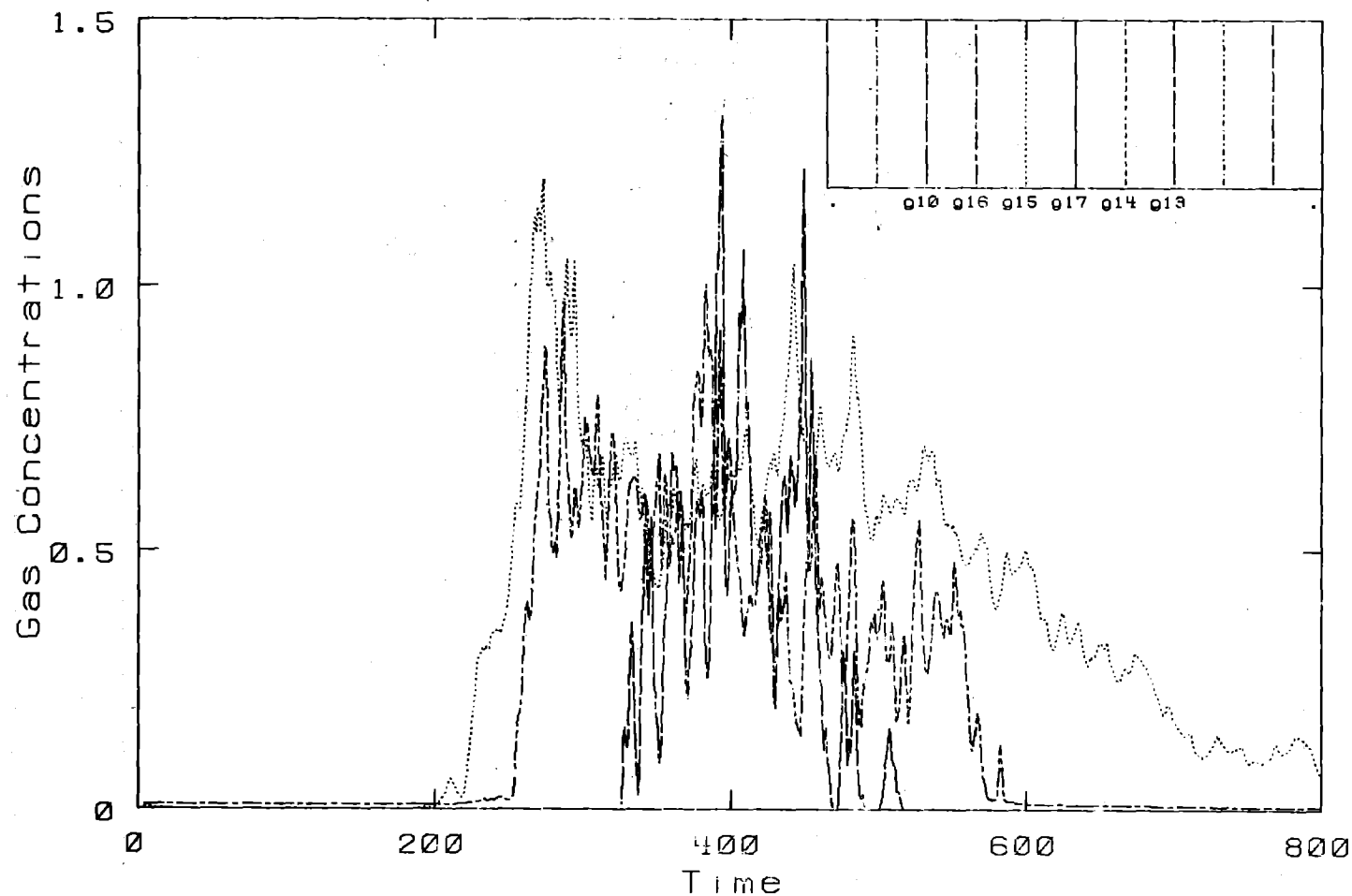
Burro 8. Row: 400 M. - Height: 3 M.

Burro Row Stations



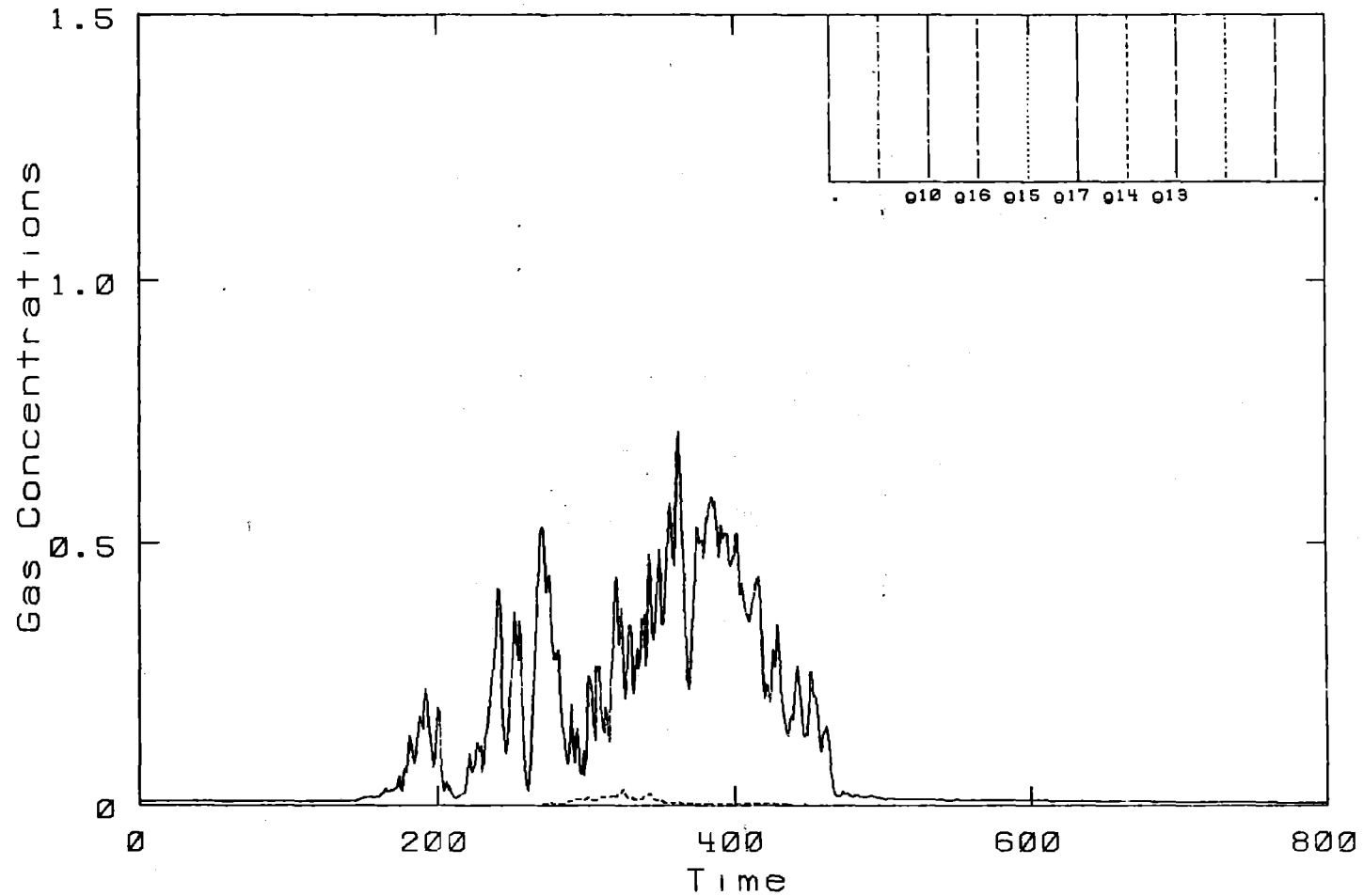
Burro 8. Row: 400 M. - Height: 3 M.

Burro Row Stations



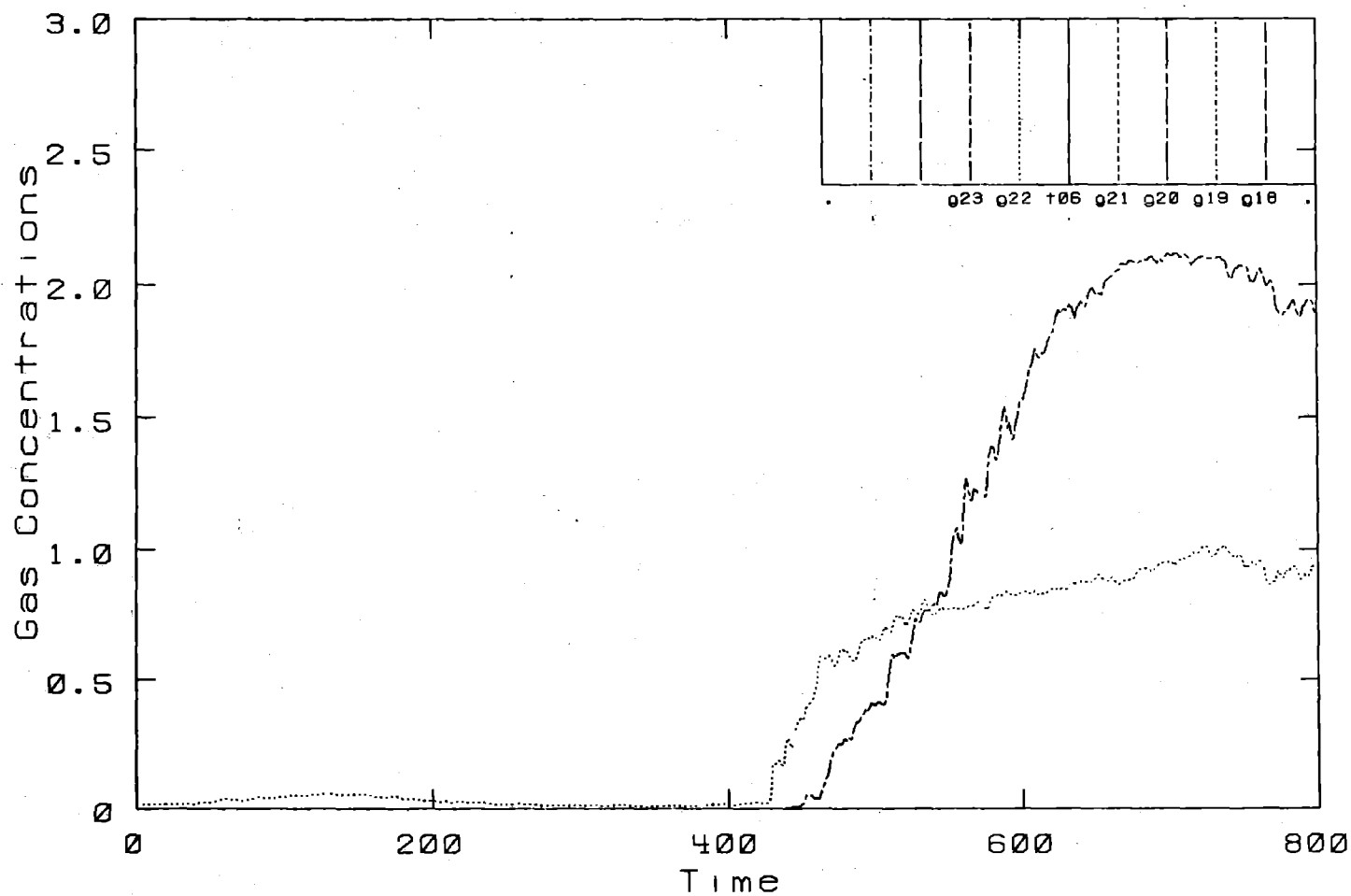
Burro 8. Row: 400 M. - Height: 8 M.

Burro Row Stations



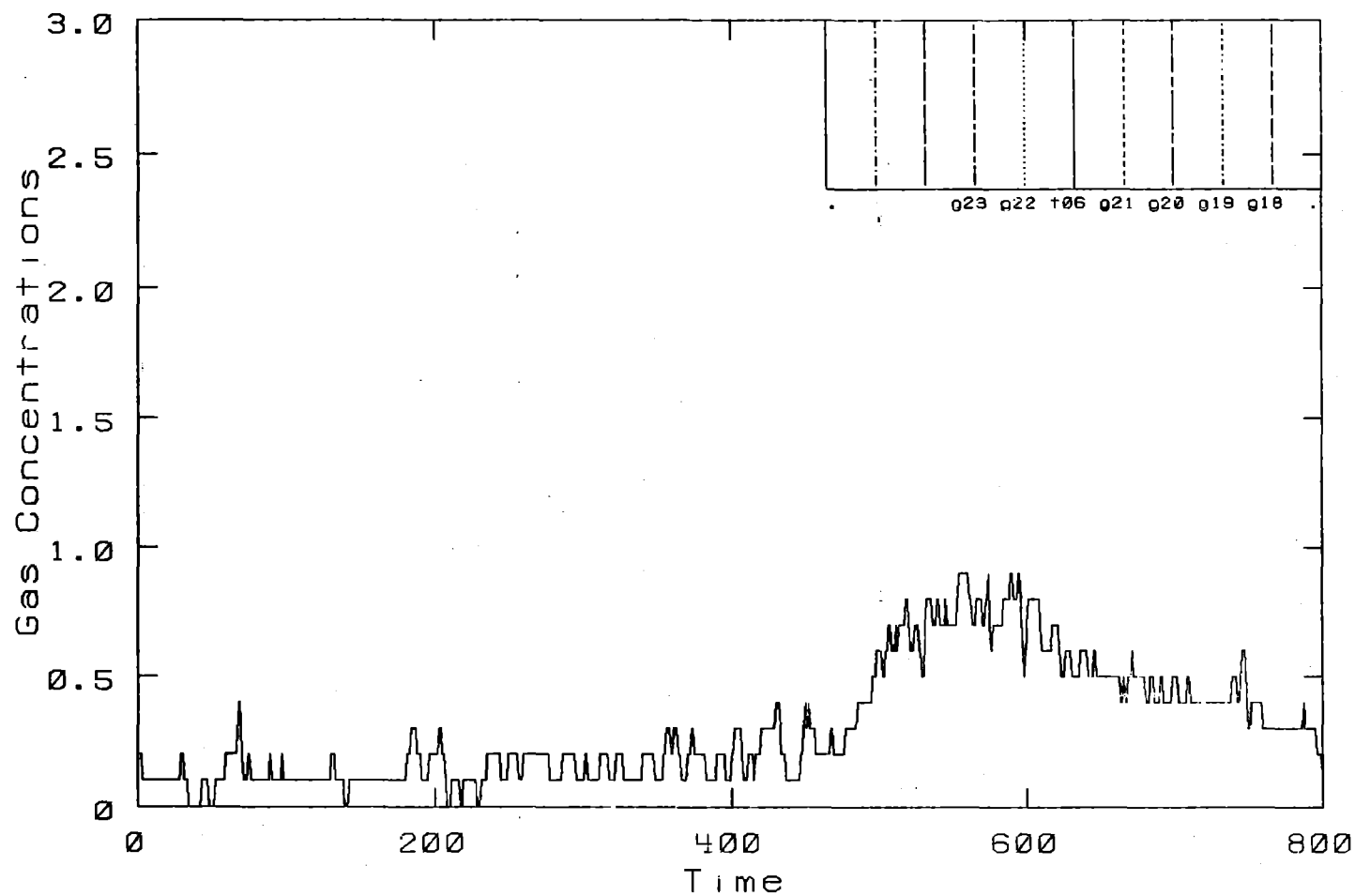
Burro 8. Row: 400 M.- Height: 8 M.

Burro Row Stations



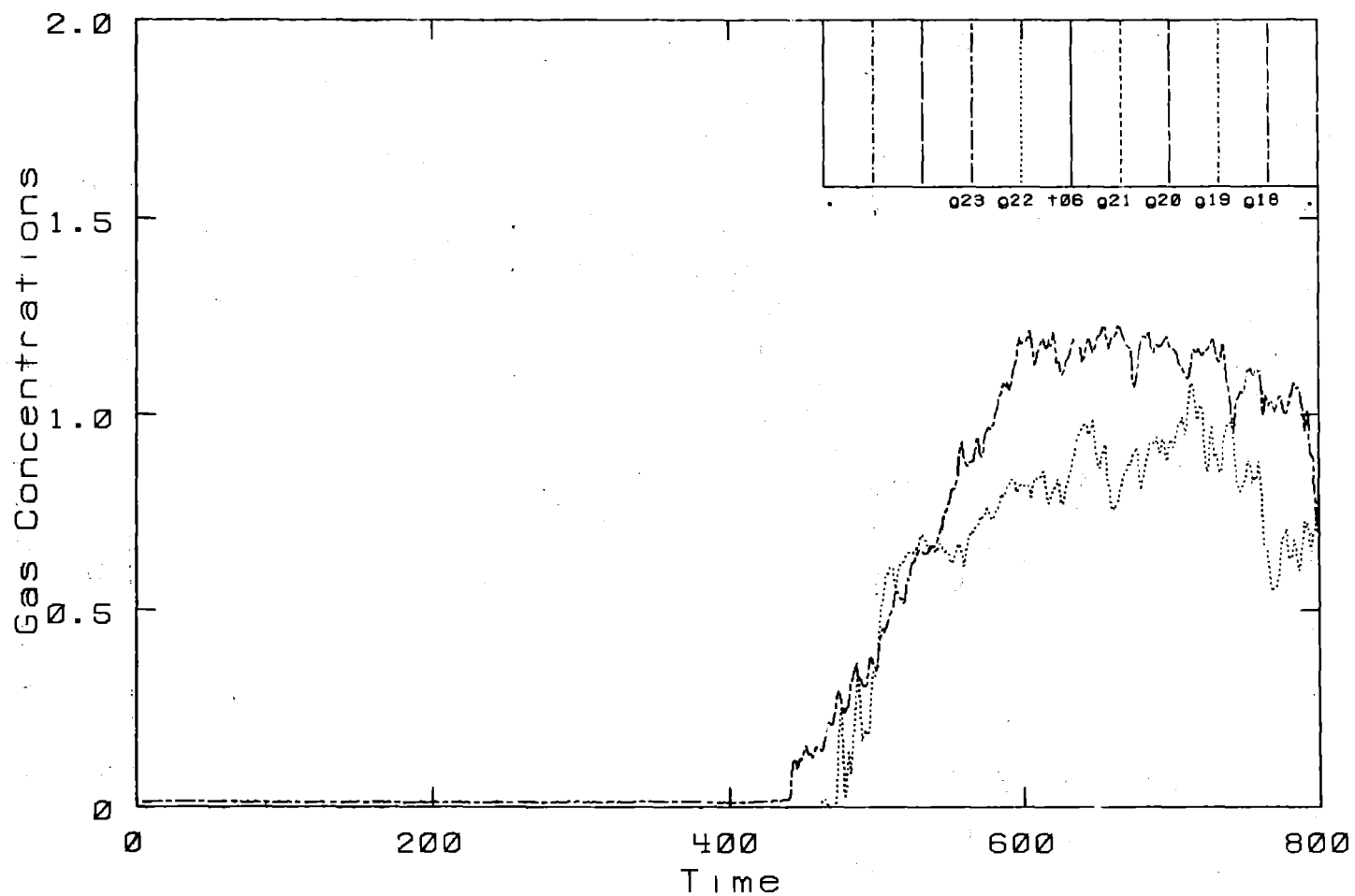
Burro 8. Row: 800 M.- Height: 1 M.

Burro Row Stations



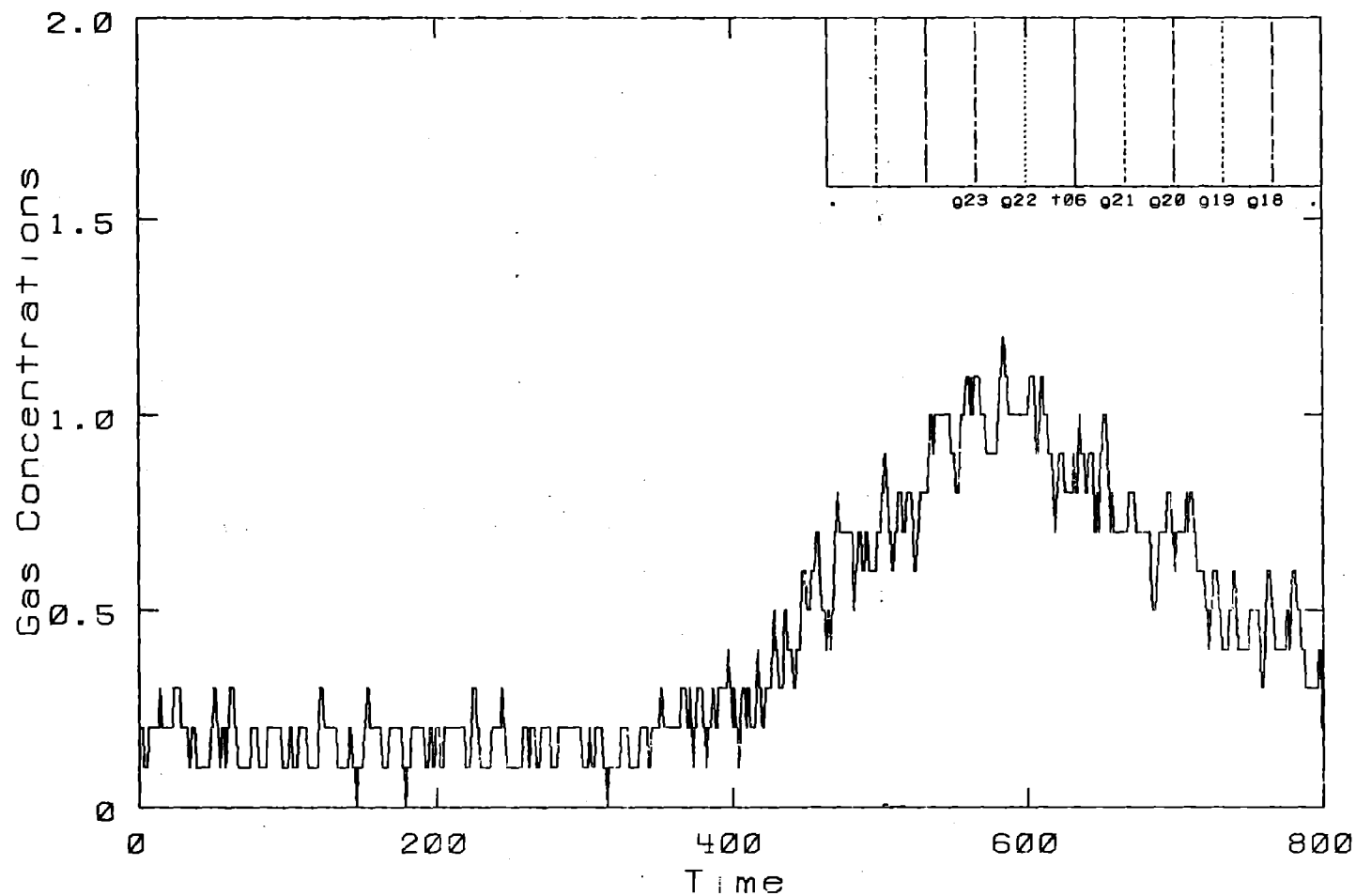
Burro 8. Row: 800 M.- Height: 1 M.

Burro Row Stations



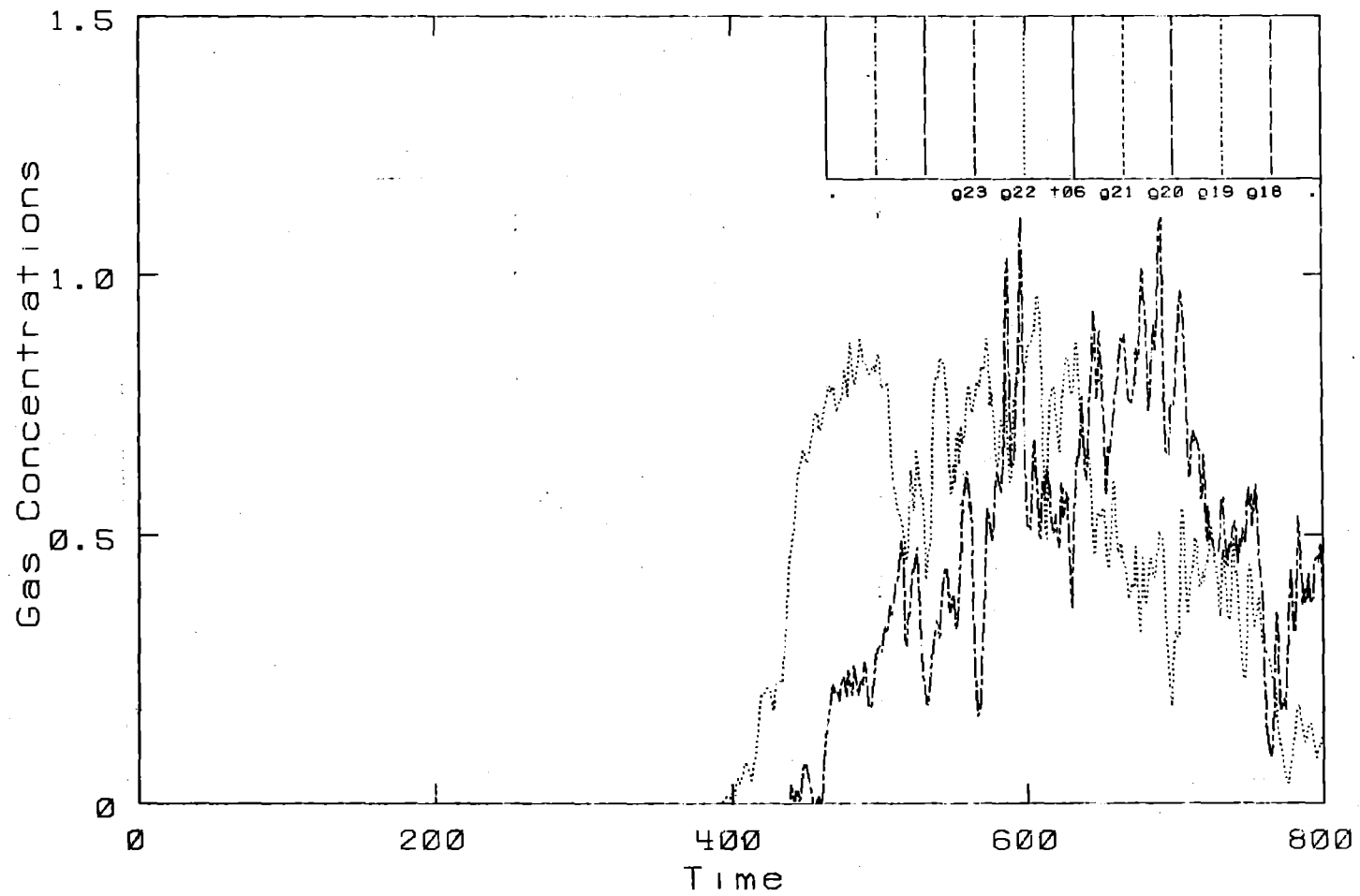
Burro 8. Row: 800 M.- Height: 3 M.

Burro Row Stations



Burro 8. Row: 800 M. - Height: 3 M.

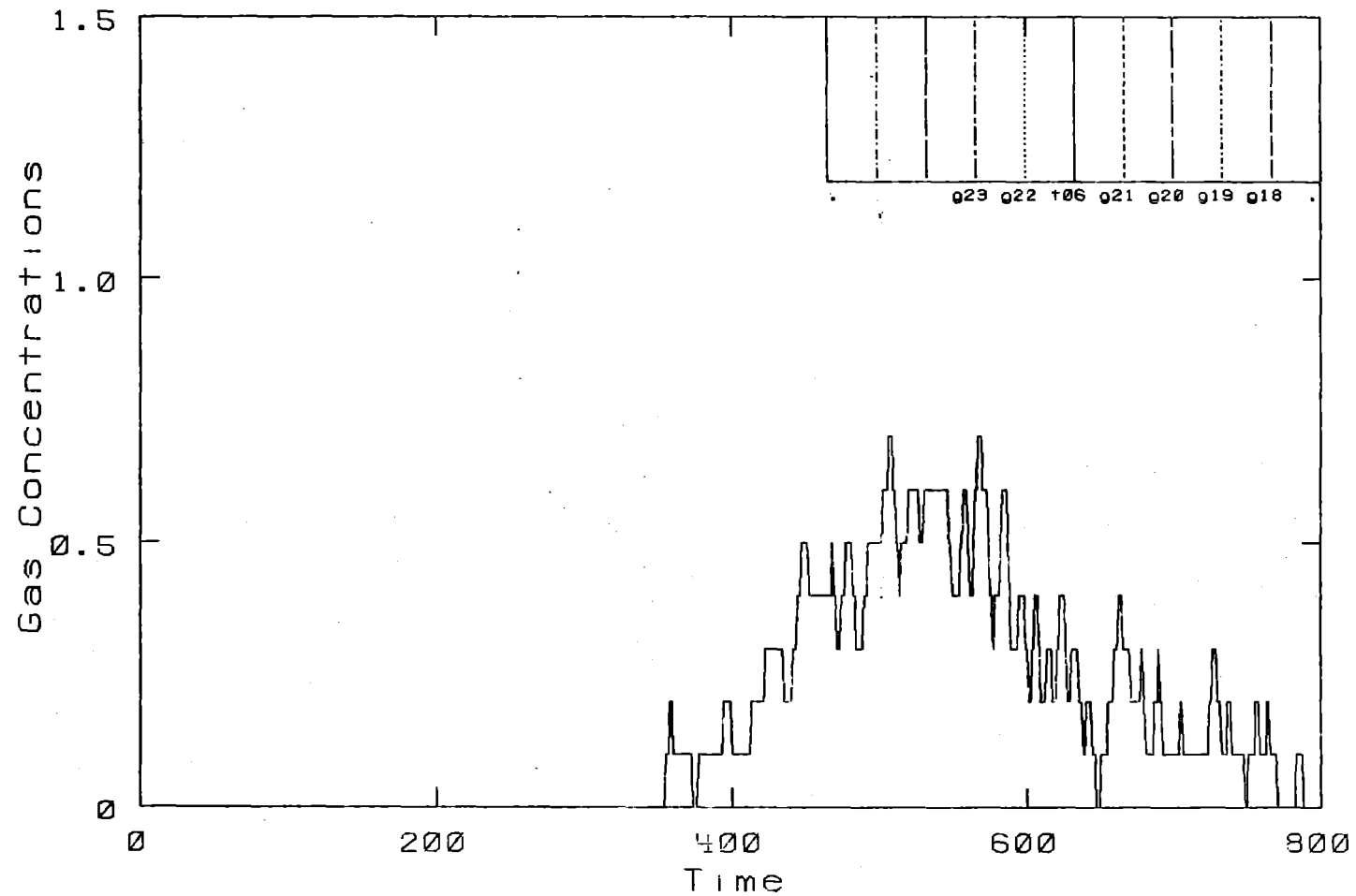
Burro Row Stations



Burro 8.

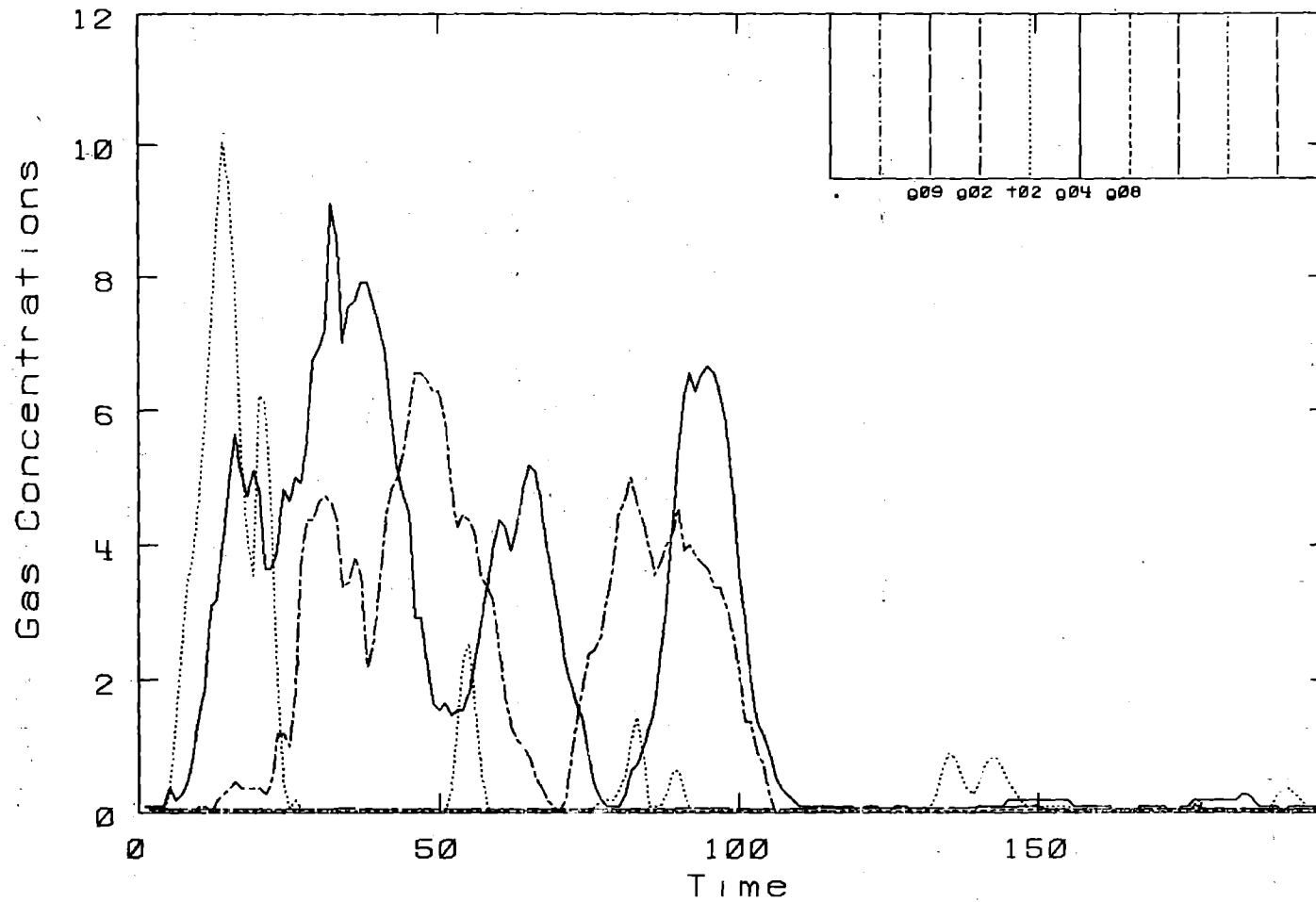
Row: 800 M. - Height: 8 M.

Burro Row Stations



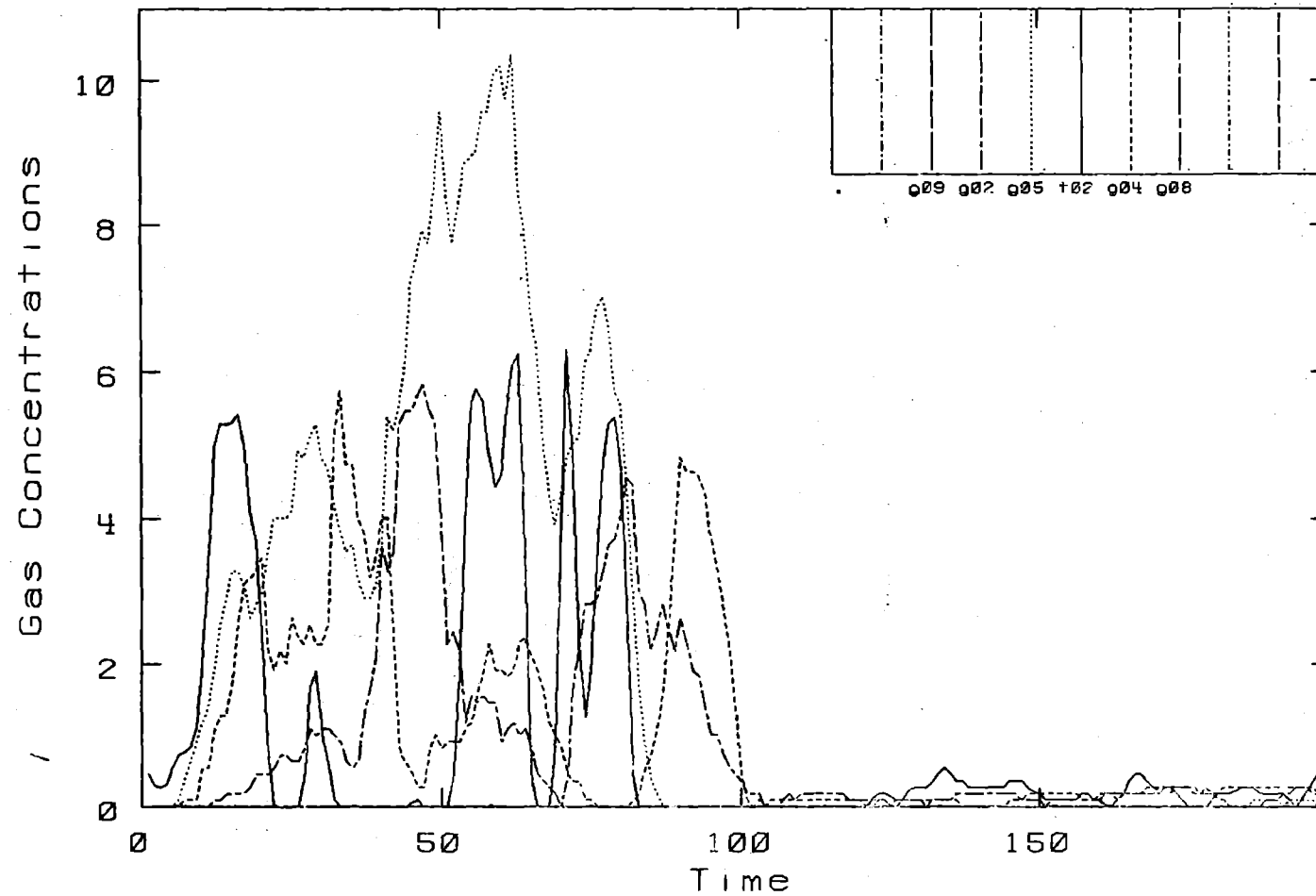
Burro 8. Row: 800 M.- Height: 8 M.

Burro Row Stations



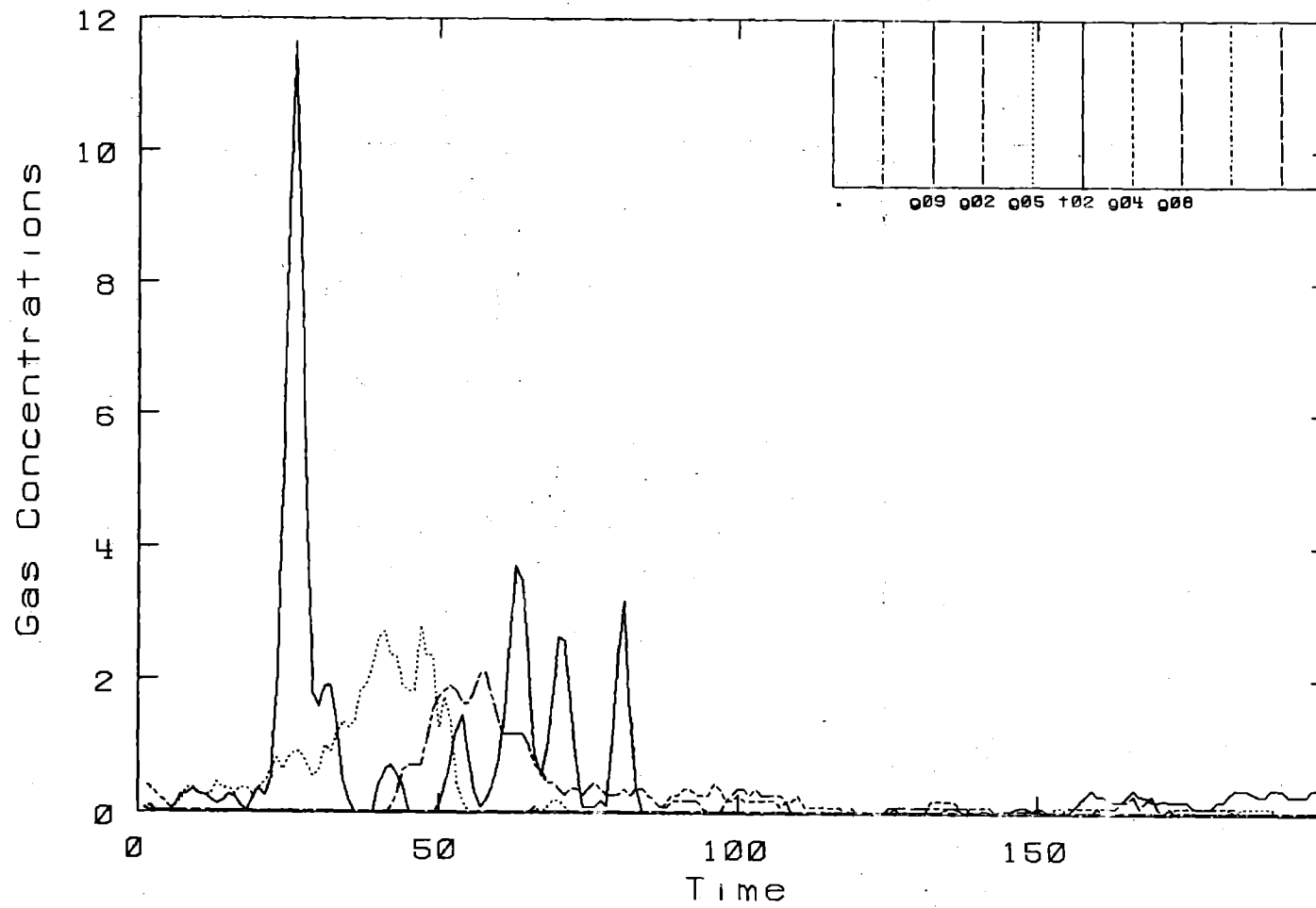
Burro 9. Row: 57 M. - Height: 1 M.

Burro Row Stations

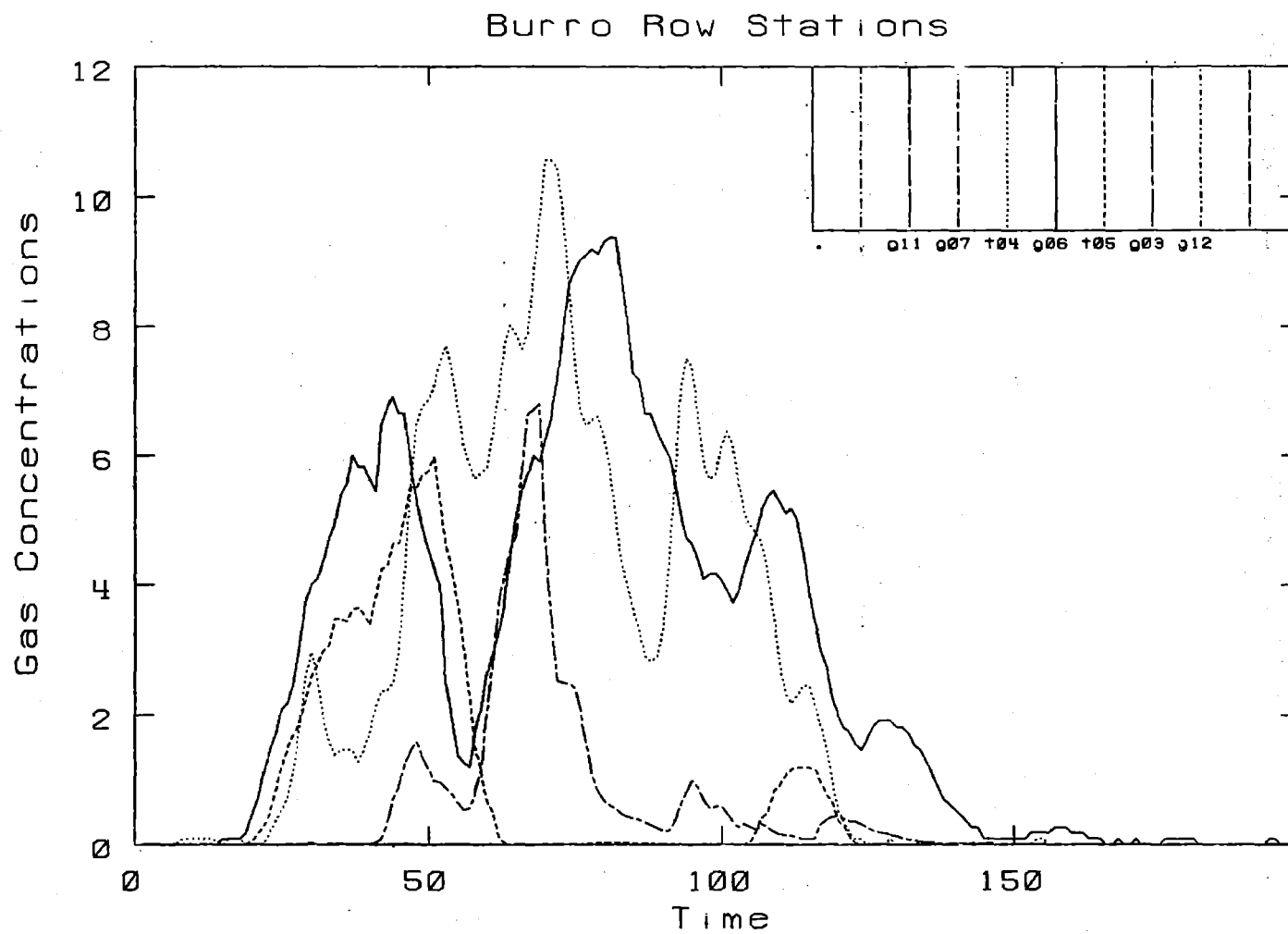


Burro 9. Row: 57 M. - Height: 3 M.

Burro Row Stations

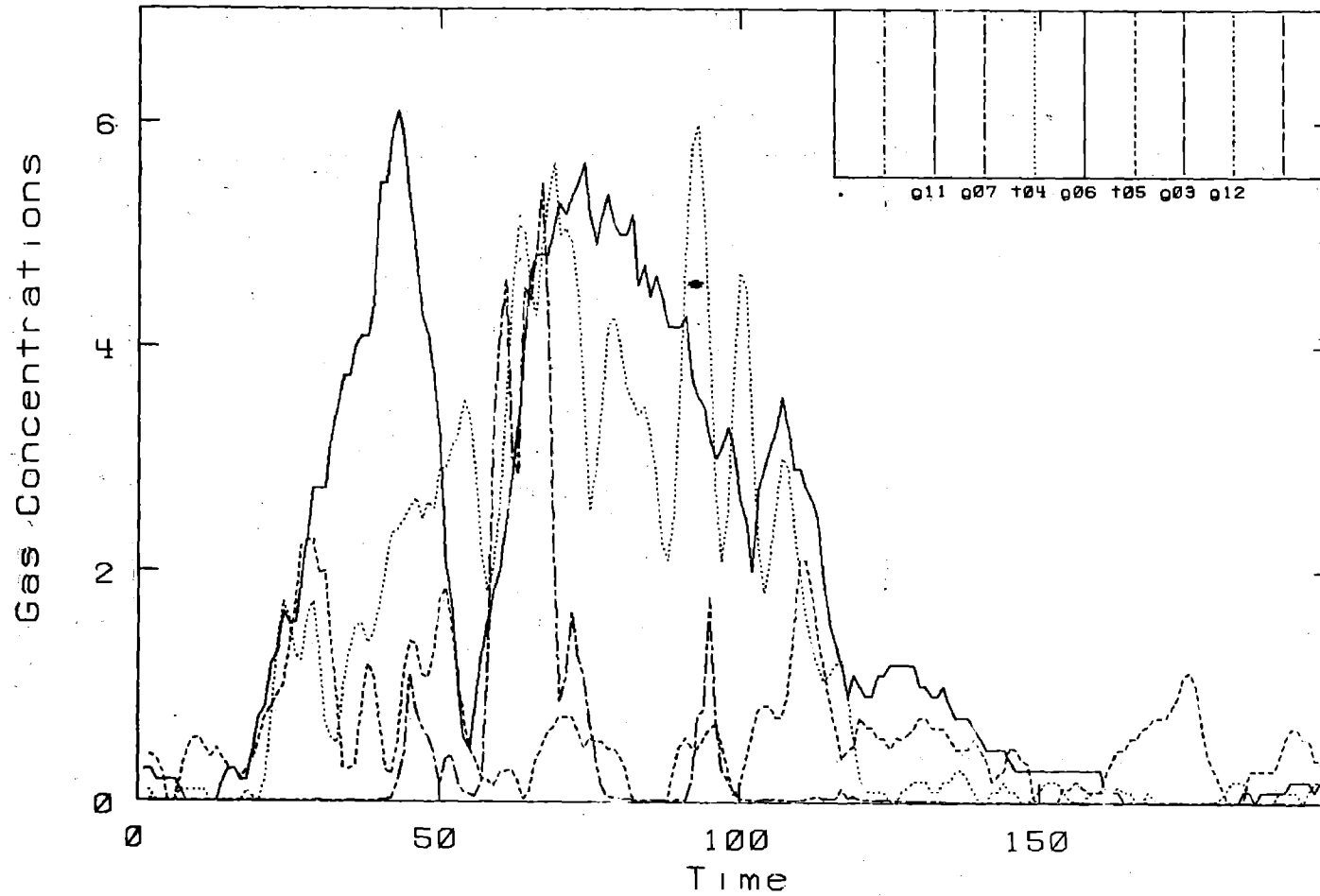


Burro 9. Row: 57 M. - Height: 8 M.



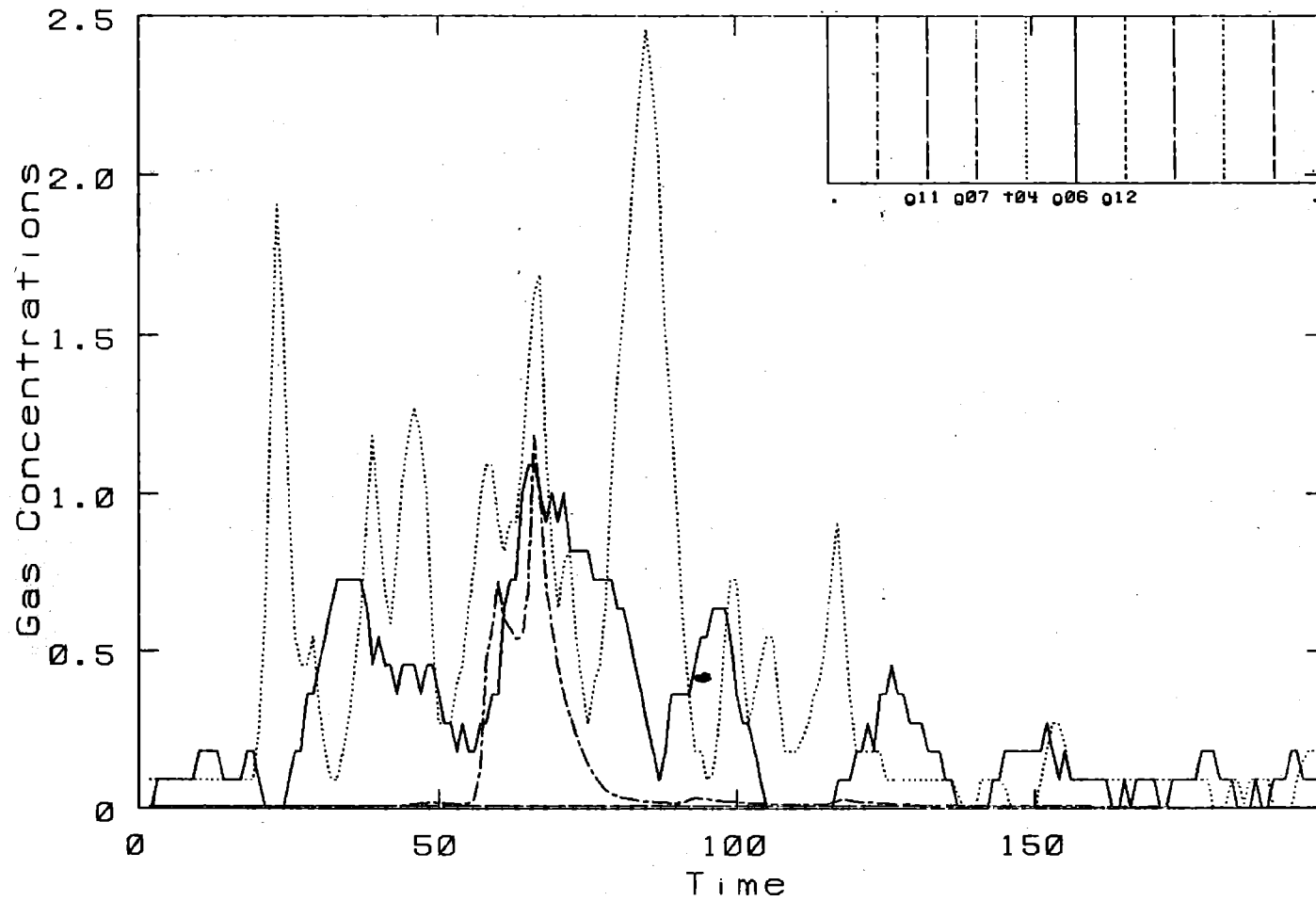
Burro 9. Row: 140 M. - Height: 1 M.

Burro Row Stations



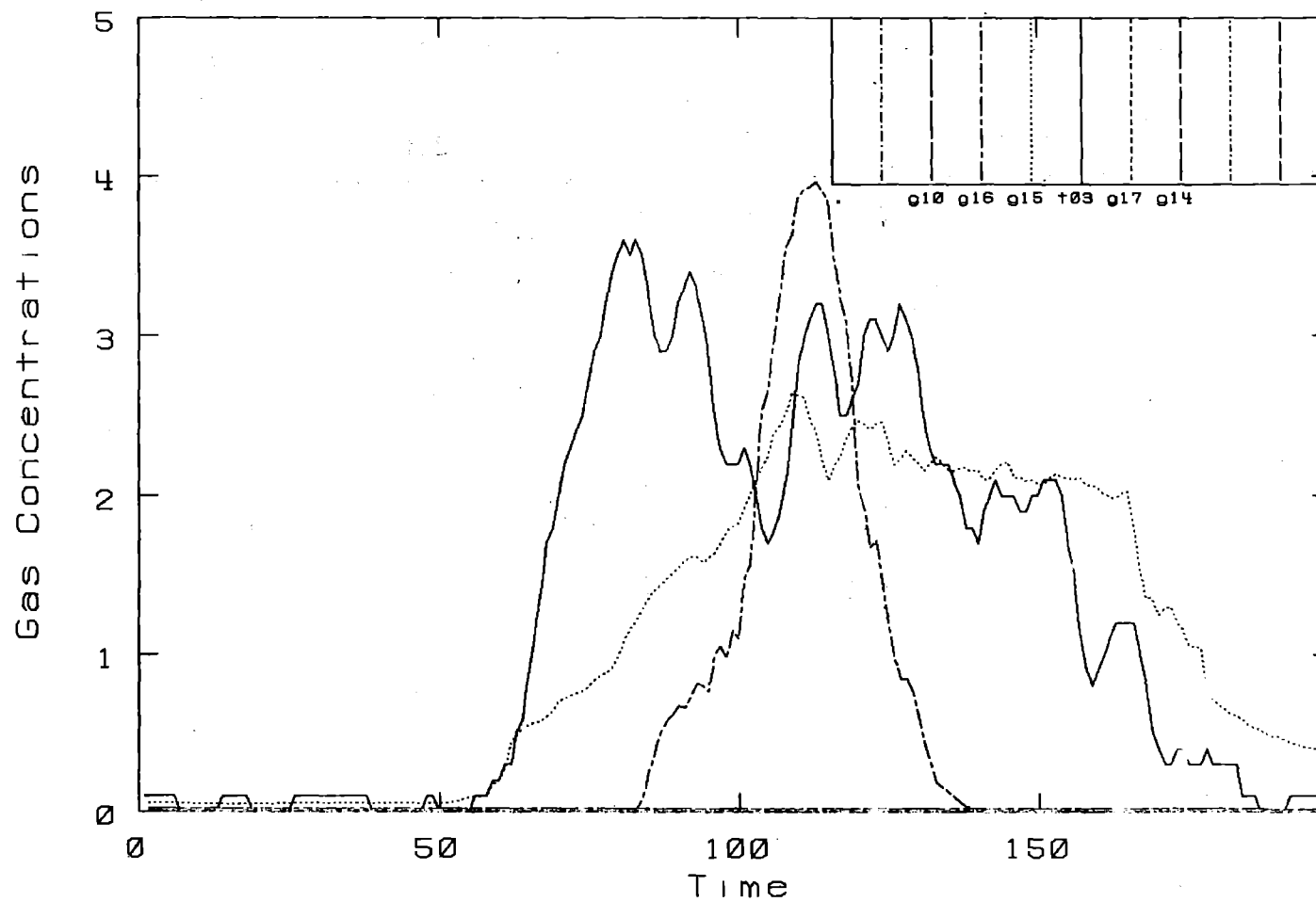
Burro 9. Row: 140 M. - Height: 3 M.

Burro Row Stations

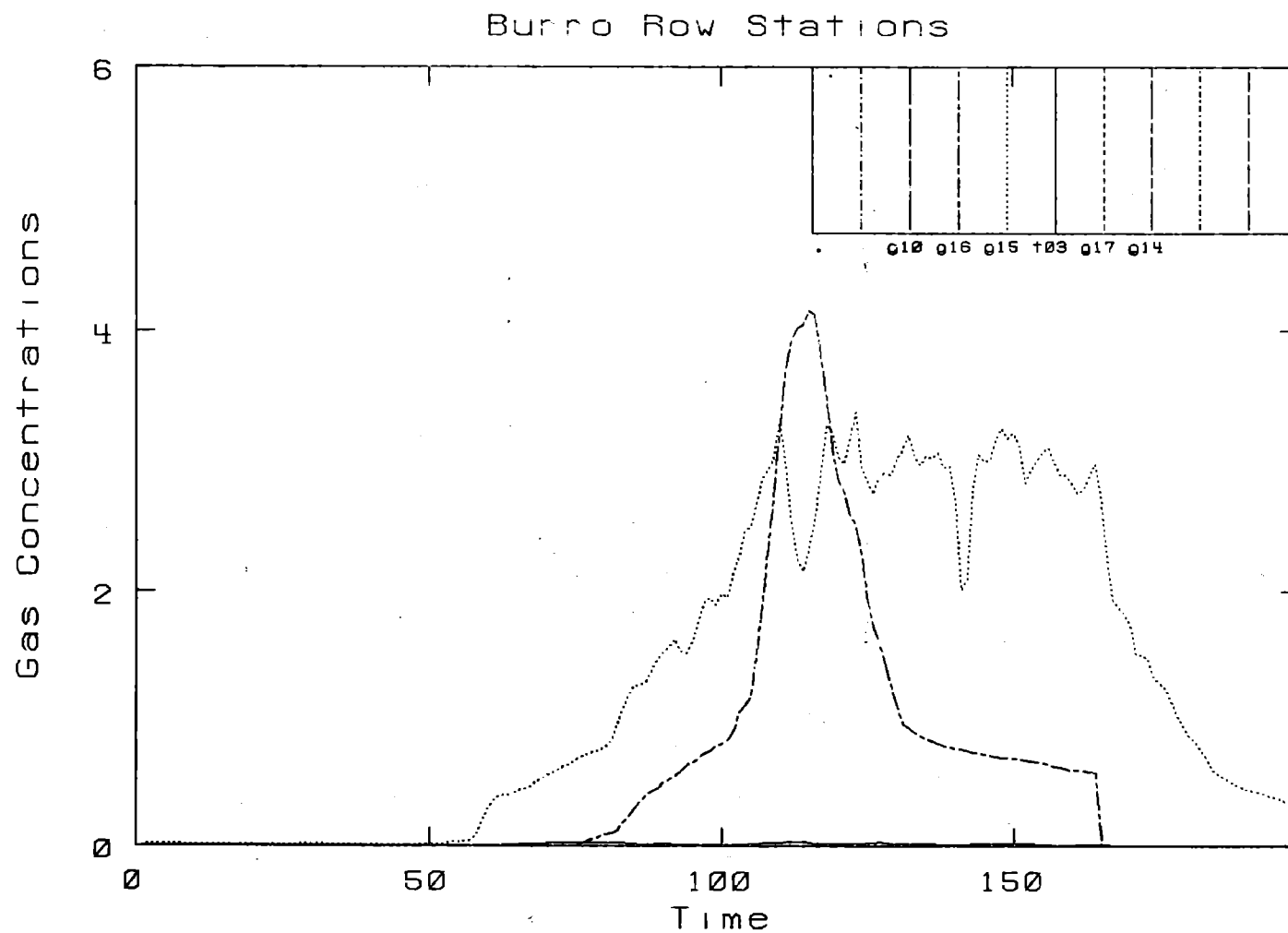


Burro 9. Row: 140 M.- Height: 8 M.

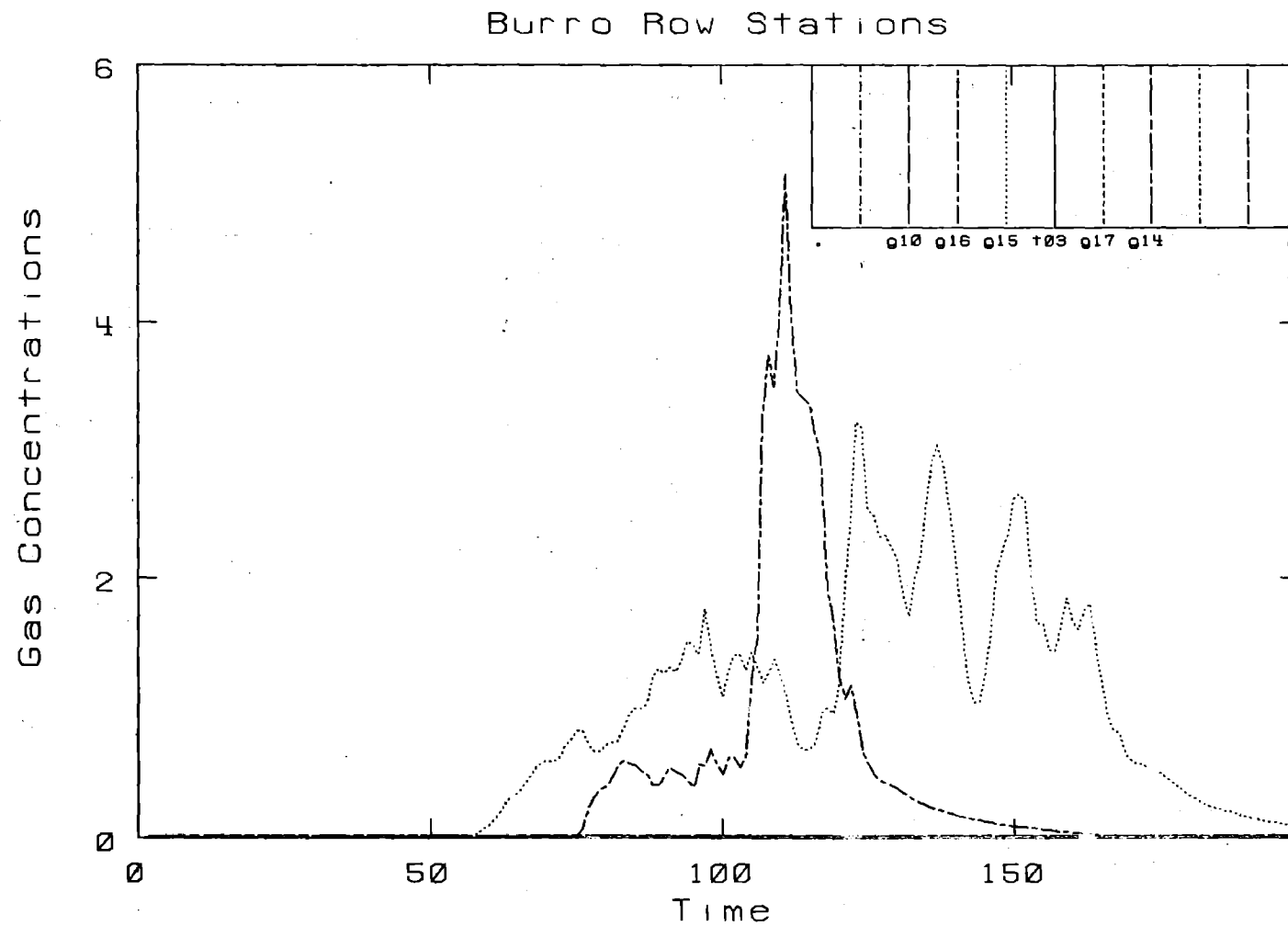
Burro Row Stations



Burro 9. Row: 400 M. - Height: 1 M.

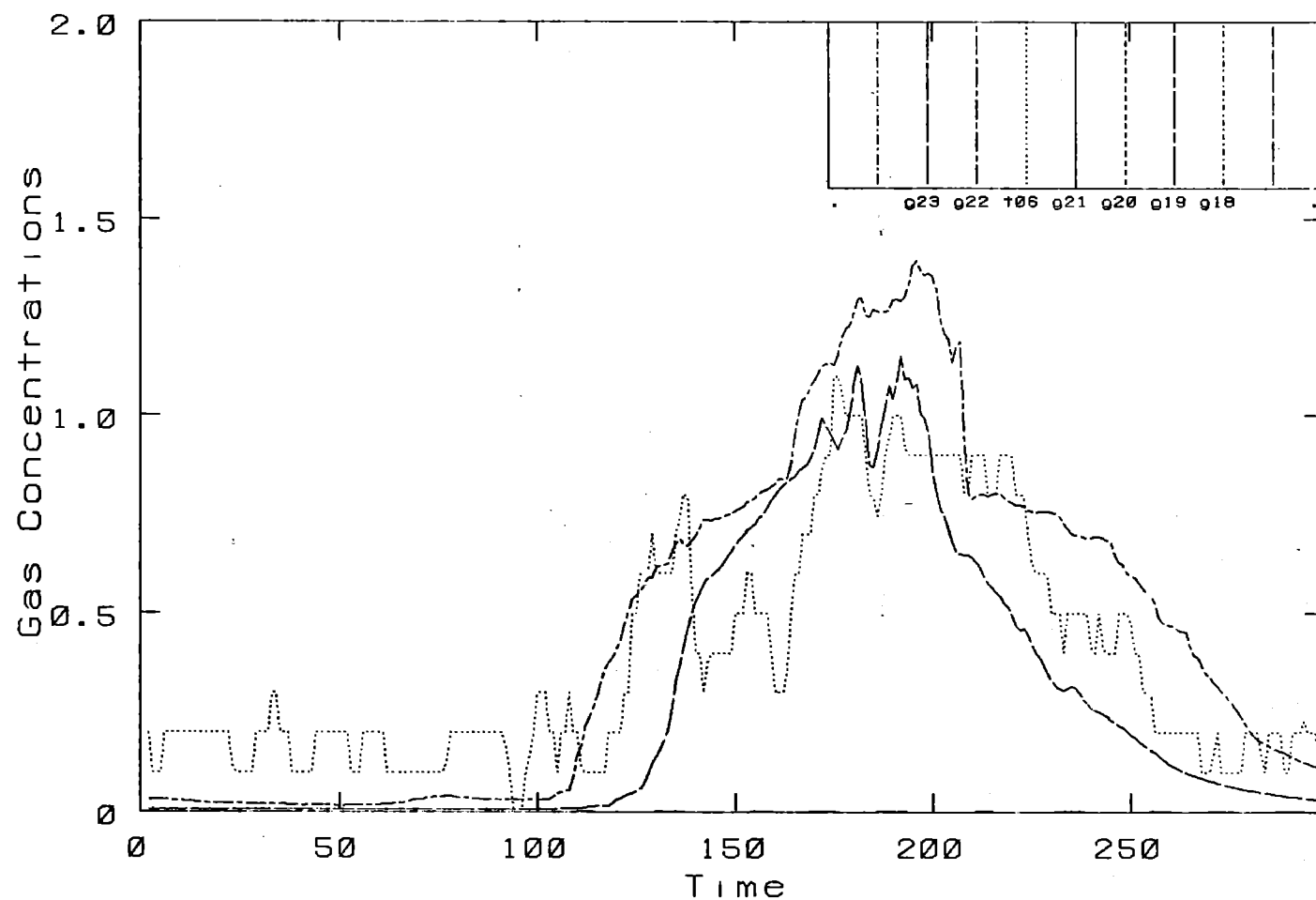


Burro 9. Row: 400 M. - Height: 3 M.



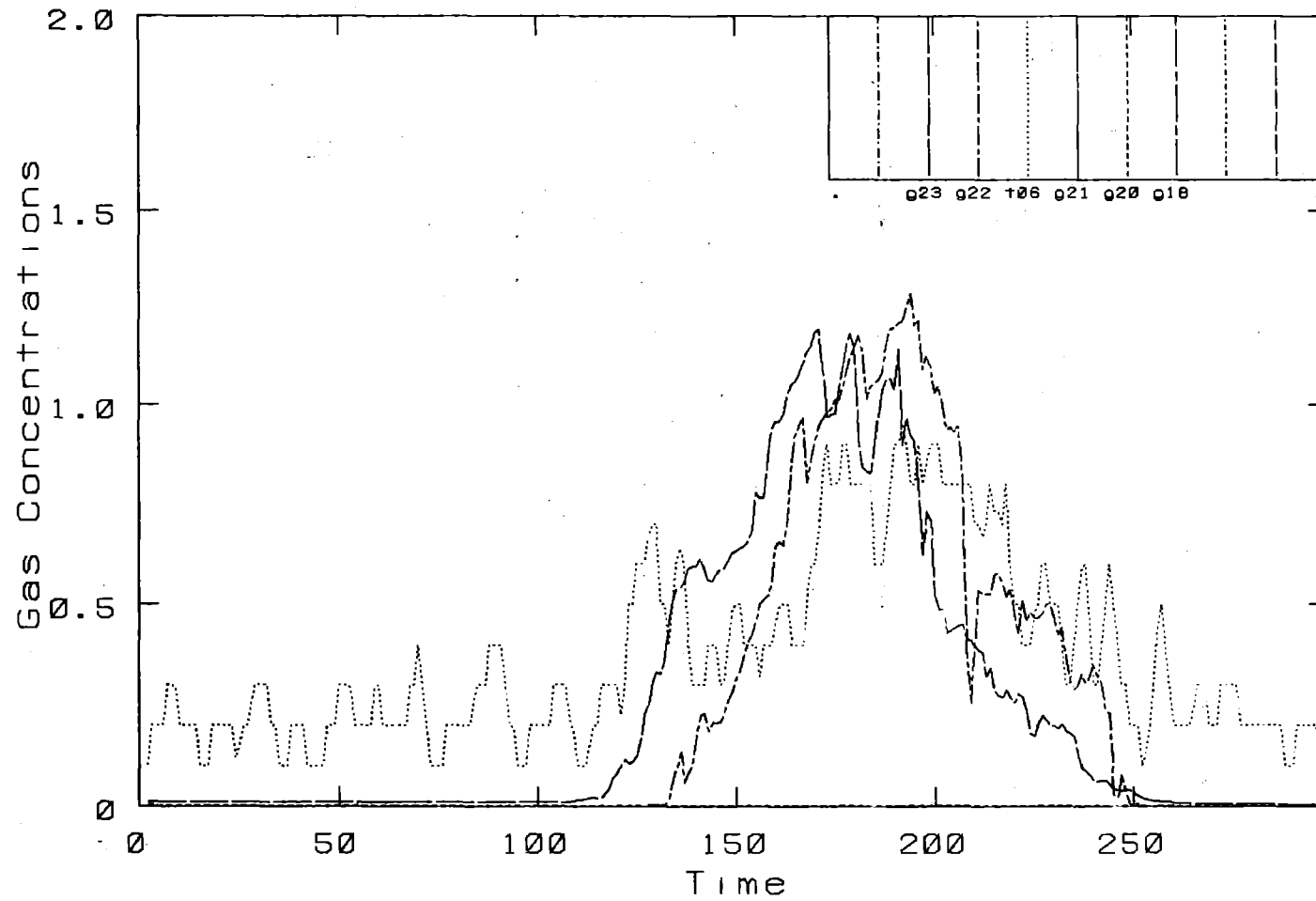
Burro 9. Row: 400 M. - Height: 8 M.

Burro Row Stations



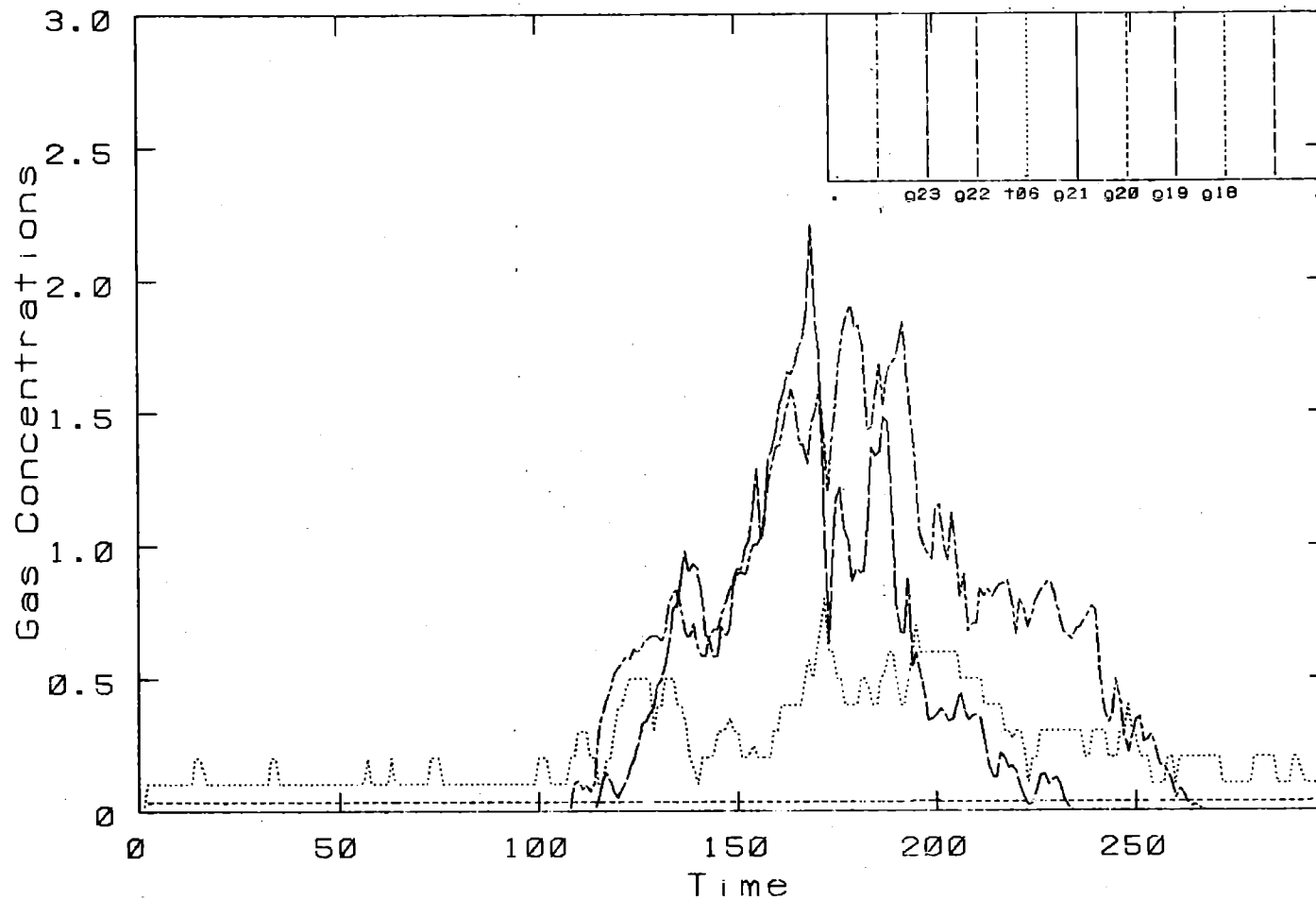
Burro 9. Row: 800 M.- Height: 1 M.

Burro Row Stations



Burro 9. Row: 800 M.- Height: 3 M.

Burro Row Stations



Burro 9. Row: 800 M. - Height: 8 M.

H. CONCLUSIONS

The data shown in this report are unique in that they represent an attempt to measure quantitatively both the size and character of the dispersing gas cloud and, simultaneously, all those phenomena affecting the dispersion, such as wind field, humidity, and heat flux from the ground. This approach allows the systematic study of the effects of these phenomena on cloud dispersion via numerical models as well as the extraction of information on the basic physics involved in dense gas dispersion in the atmosphere. This data represents the first step toward verifying the scaling laws which will eventually allow meaningful predictions concerning the consequences of a large-scale accidental spill of LNG.

Dispersion data were obtained under a variety of different meteorological conditions with wind speeds from 1.8 to 9 m/s and a range of stability conditions. Burro 8 was a uniquely interesting test in which the wind speed was very low, the atmosphere slightly stable, and gravity effects on the dense gas clearly observable.

The data have been extensively checked and cross-checked, but because of the quantity (6×10^6 words), it is difficult to catch every problem. We believe that all serious problems with the data have been found and that the data can be used without reservation. Nevertheless, we encourage users of this data to report any anomalies to us so that we might investigate and correct them.

The fast-response gas concentration data presented in this report have been averaged in time so that all concentration data have approximately the same time constant. The original, unaveraged fast-response data are available upon request and will be used for further analysis.

The data acquisition system and the sensors used to obtain the data worked very well by the end of the test series. However, considerable effort was required, during the tests, to get this new and complicated system operational. Consequently, there are gaps in the data from stations which were not operational until late in the test series. Analysis of the data is being concentrated on the last two experiments where the data sets are most complete and where the experimental conditions are most interesting. The analysis of the data will be covered in subsequent reports.

Gas concentration contours have been produced from the data but should be used with care. They give a very good qualitative overview of the behavior of the gas cloud as a function of time but should, in general, not be used for detailed quantitative information. There are better ways, for instance, to determine the maximum downwind distance to the LFL (5%), such as that shown in Fig. 10. Because of the long distances between arcs, and the short spill duration, linear interpolation produces a better representation of the actual cloud behavior than does logarithmic interpolation.

The LLNL IR sensor performed reliably during the test series and yielded high quality data, particularly outside of the dense fog. The sensor also worked well in the fog, but uncertainties in the ethane-plus-propane data are much higher there. The IST sensor did not work as well as expected, showing generally high sensitivity to ethane and humidity. The concentration data have been corrected for these effects and the uncertainties determined. The other sensors worked reliably and produced high quality data.

I. REFERENCES

1. C.D. Lind and J.C. Whitson, Liquefied Gaseous Fuels Safety and Environmental Control Assessment Program: Second Status Report, DOE/EV-0085, Report R (October 1980).
2. R.P. Koopman, Liquefied Gaseous Fuels Safety and Environmental Control Assessment Program: Second Status Report, DOE/EV-0085, Report Q (October 1980), and Lawrence Livermore National Laboratory, Livermore, CA, UCID-18585 (1980).
3. R.P. Koopman, Liquefied Gaseous Fuels Safety and Environmental Control Assessment Program: A Status Report, DOE/EV-0036, Report K (May 1979).
4. R.P. Koopman, B.R. Bowman, and D.L. Ermak, Liquefied Gaseous Fuels Safety and Environmental Control Assessment Program: Second Status Report, DOE/EV-0085, Report P (October 1980), and Lawrence Livermore National Laboratory, Livermore, CA, UCRL-52876 (1980).
5. G.E. Bingham, R.D. Kiefer, C.H. Gillespie, T.G. McRae, H.C. Goldwire, and R.P. Koopman, A Portable, Fast-Response Multiwavelength Infrared Sensor for Methane and Ethane in the Presence of Heavy Fog, Lawrence Livermore National Laboratory, Livermore, CA, UCRL-84850 (1980). To be published.
6. J.M. Conley, J.J. Simmonds, R.A. Britten, and M. Sinna, Liquefied Gaseous Fuels Safety and Environmental Control Assessment Program: Second Status Report, DOE/EV-0085, Report L (October 1980).
7. P. DuBois, J. Fletcher, and M. Richards, Livermore Time-Sharing System: Chapter 4, Files, Lawrence Livermore National Laboratory, Livermore, CA, Computer Information Center, CIC LTSS-4 Ed. 2, Rev. 1 (February 6, 1976).

8. S.E. Jones and D.R. Ries, A Relational Data Base Management System for Scientific Data, Lawrence Livermore National Laboratory, Livermore, CA, UCRL-80769 (1978).
9. G. Peterson and A.B. Budgor, "The Computer Language MATHSY and Applications to Solid State Physics," Communications of the ACM 23 (8), 466-474 (August 1980).
10. C.A. Paulson, "The Mathematical Representation of Wind Speed and Temperature Profiles in the Unstable Atmospheric Surface Layer," Journal of Applied Meteorology 9 857-861 (December 1970).
11. A.J. Dyer, "A Review of Flux-Profile Relationships," Boundary-Layer Meteorology 7, 363-372 (1974).
12. H.H. Lettau, "Wind and Temperature Profile Prediction for Diabatic Surface Layers Including Strong Inversion Cases," Boundary-Layer Meteorology 17, 443-464 (1979).
13. D.L. Ermak, R.A. Nyholm, and R. Lange, ATMAS: A Three-Dimensional Atmospheric Transport Model to Treat Multiple Area Sources, Lawrence Livermore National Laboratory, Livermore, CA, UCRL-52603 (November 1978).
14. John Baker, "The LGF Data Acquisition System", Lawrence Livermore National Laboratory, Livermore, CA, UCID-19431, (July 1982).